THE UNIVERSITY
of EDINBURGH

The Porosity and Permeability Relationships of the Lekhwair and Lower Kharaib Formations

Peter A. Cox

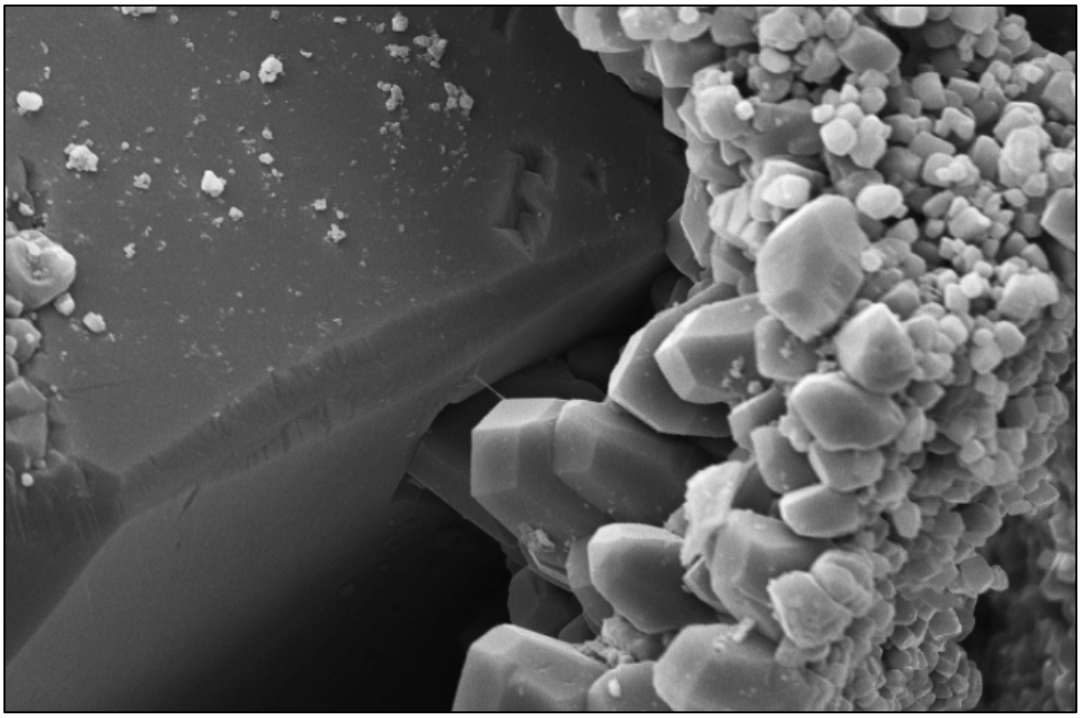

Ph.D.

Supervisors:

Dr. Rachel Wood

Prof. Stuart Haszeldine

Dr. Tony Dickson

Prof. Patrick Corbett

Presented in 2010

Declaration

I declare that the research and the undertakings for this project, along with the writing and composition of this thesis, are my own work, and were completed by me, the Author: Peter A. Cox. This work has not been submitted for any other professional qualification.

17th April 2011

Peter Cox

Contents

ACKNOWLEDGMENTS

The author would like to thank ADNOC and ZADCO managements and Schlumberger Cambridge Research for permission to publish this thesis. Discussions with Ewart Edwards, Mohamed Braik Al Amri, Donatella Astratti and Olaf Schoenicke during the project were greatly appreciated. Help from Ali Ajjawi and his team of assistants at the Mussafah core facility were greatly appreciated. Mike Hall (Thin sections), Nicola Cayzner (SEM), Johnathen Naden (oil inclusion petrography), Colin Chilcott (Mass spectrometer) and John Craven (NERC Ion Microprobe Facility) all supplied considerable technical support. We acknowledge the support from the Scottish Funding Council for ECOSSE which is a part of the Edinburgh Research Partnership in Engineering and Mathematics (ERPem).

Abstract: Up to 60% of the World's oil is now within carbonates, with over 50% in the Middle East. Many existing carbonate fields have very low oil recoveries due to multiple scales of pore heterogeneity. To secure better recoveries the controls from deposition and diagenesis towards the origin of carbonate pore heterogeneity needs better understanding. To provide good sample support, three High frequency Cycle's were sampled (2 from the Lekhwair Formation and the third being the Lower Kharaib Formation) from an offshore field (Abu Dhabi) along a southwest-northeast transect, encompassing the oil leg, transition zone, water leg, the field crest and two opposing flanks.

With respect to deposition, the 4th order Sequence Boundaries' (hardgrounds) and the Maximum Flooding Surface's were correlated across the field, within the sequence stratigraphic framework, showing that each HFC, of the Lekhwair Formation, contains laterally continuous reservoirs (4th order HST's) which are compartmentalised above and below by impermeable seals (4th order TST's). The Lower Kharaib Formation shows significant shoaling producing the shallowest platform (prolonged 3rd order TST) and the best connected reservoir facies.

With respect to diagenesis, $\delta^{18}O$ isotopes trends, from calcite cement zones within macrocements from the water and oil legs, in comparison with oil inclusion abundances suggest that oil charge reduced cementation in the crest macropores. Stylolitisation in the water leg at deep burial provided solutes for new cement nucleation causing near complete macropore occlusion.

The most open micropore networks coincide with the highest porosity/permeability relationships at the mid-late HST's of each HFC. Considering these areas could be lower grade reservoirs, and that pore characterisation by Lucia (1999) does not include identifying and quantifying micropores, a new 'Micropore model' (using elements from the Petrotype atlas method) is devised. This new method highlights micropore-dominated areas alongside macropore-dominated areas within specific reservoir horizons. This provides information of pore heterogeneity at several scales within a carbonate reservoir and may determine the method for oil extraction and increase oil recovery from both the Lekhwair and Lower Kharaib Formations.

Chapter 1

Introduction

In 1970, out of 187 giant oil fields constituting a minimum oil recovery of 638.77 billion bbl, 58% were associated with siliciclastic formations, and 42% associated with carbonates (Halbouty et al. 1970). Today, between 50-60% of remaining oil reserves are within carbonates (Ramakrishnan et al. 2001, Sayers 2008). Over half the World's oil reserves are within the Middle East, within Saudi Arabia, Iran, Iraq, Kuwait, U.A.E., Oman and Qatar producing roughly 18.54 million barrels per day in 2002 (Vahidy & Fesharaki 2003). Although controversial, peak oil production has been suggested to have already occurred in many prolific oil producing areas: 1972 in Texas, 1985 in North America, 1999 in U.K. and 2001 in Norway (Hirsch 2006). With the rising cost of oil, and increasing demand for further oil exploration, attention is needed now to manually enhance oil recovery from known carbonate reservoirs within the Middle East. Within a single oil field 500sq mile in size, offshore Abu Dhabi, it is estimated that 1.95×10^9 stock-tank m^3 are housed within just one Lower Cretaceous Thamama zone (Zone IV) (Hassan & Wada 1979; 1981). The carbonate formations of the Thamama Group clearly house significant quantities of oil and therefore are important carbonate porosity and permeability systems to study.

Carbonate pore systems can be very heterogeneous and difficult to predict. Consequently many past attempts at tapping these reservoirs result in low oil recoveries. For instance, a giant carbonate field, offshore Abu Dhabi, has three porous oil producing Zones (Zones 2-4) within the Thamama Group. Zone II which amounts to 70% of the entire field oil production has a present recovery of 5% (Lutfi et al. 2001). While Zone IV has produced 102.8×10^6 m^3 of oil, in comparison with

1.95 x 10^9 stock-tank m^3 predicted reserves, which only amounts to 5.3% recovery between the years 1967-1978 (Hassan & Wada 1981).

However more recent attempts at enhanced oil recovery have yielded better results. Studies from Al-Hadhrami (2001) on matrix blocks from the Ghaba North field in Oman used stream/hot water to induce a wettability change within the pore system, making the samples water wet. This has increased oil recovery from 2% to ~30%. Similar studies from Xie et al. (2004) have completed experiments on carbonate samples by adding a cationic surfactant to make the pore system water wet. After the initial spontaneous expulsion of oil at elevated temperatures, the result from fifty samples was 0-35% oil recovery, which was enhanced by another 5-10% by adding a cationic surfactant.

When comparing these recovery factors with siliciclastic reservoirs, such as the Cano Limon Field in Colombia; oil recovery from the deltaic sands is 58% (Ellison & Ahumada 1995). Therefore, although recovery factors within carbonates are improving, further work is required in understanding the pore complexities of carbonates, at different scales, to match recoveries from siliciclastic reservoirs

1.1 Carbonate pore systems

Now that the importance of reviewing carbonate reservoirs is established the reasons for why carbonates have complex porosity/permeability relationships is outlined; starting with the complexity of carbonate pores systems, followed by the complexity and determining factors of carbonate permeability, and concluding with quantifying the porosity and permeability relationships of carbonate reservoirs.

1.1.1Carbonate pore heterogeneity

Pore space is defined as the empty space that exists within a solid. Highly porous rocks can uptake fluids such as gas, water and oil. The ability to effectively predict the amount of pore space within a given rock volume will provide a volume of oil reserve potentially available for extraction.

Carbonates can form very complex pore systems that range in size, over several orders of magnitude from micron-sized pores to centimetre moulds, to metre sized

karsts and cave systems. Carbonate pore types are complex in shape and can be fabric or non-fabric selective: i.e. the pore distribution can be determined by the matrix fabric (interparticle pore space in-between packed micrite grains: fabric selective) or be determined by processes that effect all areas of the matrix (dissolution of the matrix creating new pore space: non-fabric selective) (Choquette & Prey 1970).

Most carbonate production occurs on tropical shallow marine platforms by biological skeletal growths (Moore 2001). For example, the porosity within a reef is highly variable and can form framework porosity which is composed of intra-skeletal pores ranging in size from several millimetres to metres in diameter. In comparison, several large foraminifera and algae (Banner et al. 1991, Hottinger 1997, Jones et al. 2004, Simmons & Hart 1987, Schmid & Leinfelder 1996) contain open internal chambers that are millimetres in size, which adds to the intra-skeletal porosity of a carbonate. Burrowing and boring organisms on the sea bed can also add porosity to a carbonate. The settling and stacking of micrite grains and ooids on the sea bed can form interparticle pore spaces ranging in size from millimetres to centimetres in diameter, which either remain open or can be filled with micrite. The micrite grains, ooids and bioclasts can also contain intraparticle porosity.

Diagenesis can act to enhance and destroy the depositional porosity, or a previous diagenetic overprint of the depositional porosity, producing a completely different porosity system with no relationship to the surrounding lithology. The actions of diagenesis through carbonate dissolution and cementation can open or occlude pores and pore throats. Cementation can reduce porosity but simultaneously it can form new intercrystalline pore spaces that can exist in-between newly formed cement crystals. Mineral stabilisation on the sea floor, along with later burial compaction and pressure solution, forming stylolites, can all reduce the porosity within a carbonate.

Oil charge is proposed to completely inhibit cementation (Neilson et al. 1996; 1998), or to slow cementation until a ‘critical oil saturation’ is reached (Heasley et al. 2000), within the crest of a field. Oil charge can also bring acidic porewaters (carbonic and carboxylic acids) which may cause widespread dissolution throughout carbonate pore systems (Lambert et al. 2006). Aragonitic bioclasts, which are

metastable, can also dissolve out to leave enhanced moulds. The dissolution of carbonate creates vugs that can amalgamate with other vugs to form larger pore spaces, potentially reconnecting a pore system previously occluded by cement.

Carbonate grains such as micrite grains, ooids, and bioclastic fragments can all develop microporosity, a feature described as having a chalky texture, as it resembles the micron-sized pores between coccoliths within chalk (Moshier 1989b). This is defined by Cantrell & Hagerty (1999) as pore space <10µm in diameter. Carbonate microporosity has been attributed to both depositional processes (Kaldi 1989) and almost every diagenetic process that occurs during burial: early mineral stabilisation (Lasemi & Sandberg 1984, Moshier 1989a, Steinen 1982), dissolution due to meteoric water circulation (Ahr 1989, Budd 1989, Perkins 1989), shallow-intermediate burial (Al-Aasm & Amzy, 1996), to deep burial (Dravis 1989) and carbonate dissolution due to oil charge (Lambert et al. 2006, Moshier 1989a).

There are many types of micropores within carbonates. However there is a distinction between the microporosity within Chalk, which is derived from the micron sized pore spaces between coccoliths (depositional origin) and the formation of microporosity within most carbonates during diagenesis.

Many skeletal fragments may contain micropores before any diagenetic alteration, as micron sized pores can exist between the aragonite needles within the aragonitic portions of bioclasts. Diagenetic alteration, through mineral stabilisation, can form microspars of LMC and intraparticle porosity (micropores) within ooids (Ahr 1989, Dravis 1989), micrite grains (Cantrell & Hagerty 1999) and bioclasts (Kaldi 1989). These primary micropores can be further solution enhanced to form secondary micropores (Moshier (1989b) such as micromoulds (Dravis 1989) and microvugs. Many grains can also develop microfractures that can be enhanced by corrosive fluids through dissolution, to form secondary micropores and micro channels (Al-Aasm & Amzy 1996, Kaldi 1989). The progressive cementation of macropores through meteoric and/or shallow-deep burial cementation can create intercrystalline micropores that exhibit several different shapes depending on the habits of the surrounding forming microspar (Cantrell & Hagerty 1999).

Therefore, carbonate pore heterogeneity is not limited to the macropore realm, but also the micropore realm. Carbonates can have significant reservoir heterogeneities at several scales regarding its pore system. To understand the porosity/ permeability relationships of carbonates, carbonate reservoir heterogeneity needs better understanding on the macro/micropore scale. Detailed understanding is required of the depositional and diagenetic processes, attributed to pore type formation and distribution, throughout a carbonate pore system (Fig 1.1) before any accurate assessment is attempted on the reservoir quality of a carbonate (Fig. 1.1).

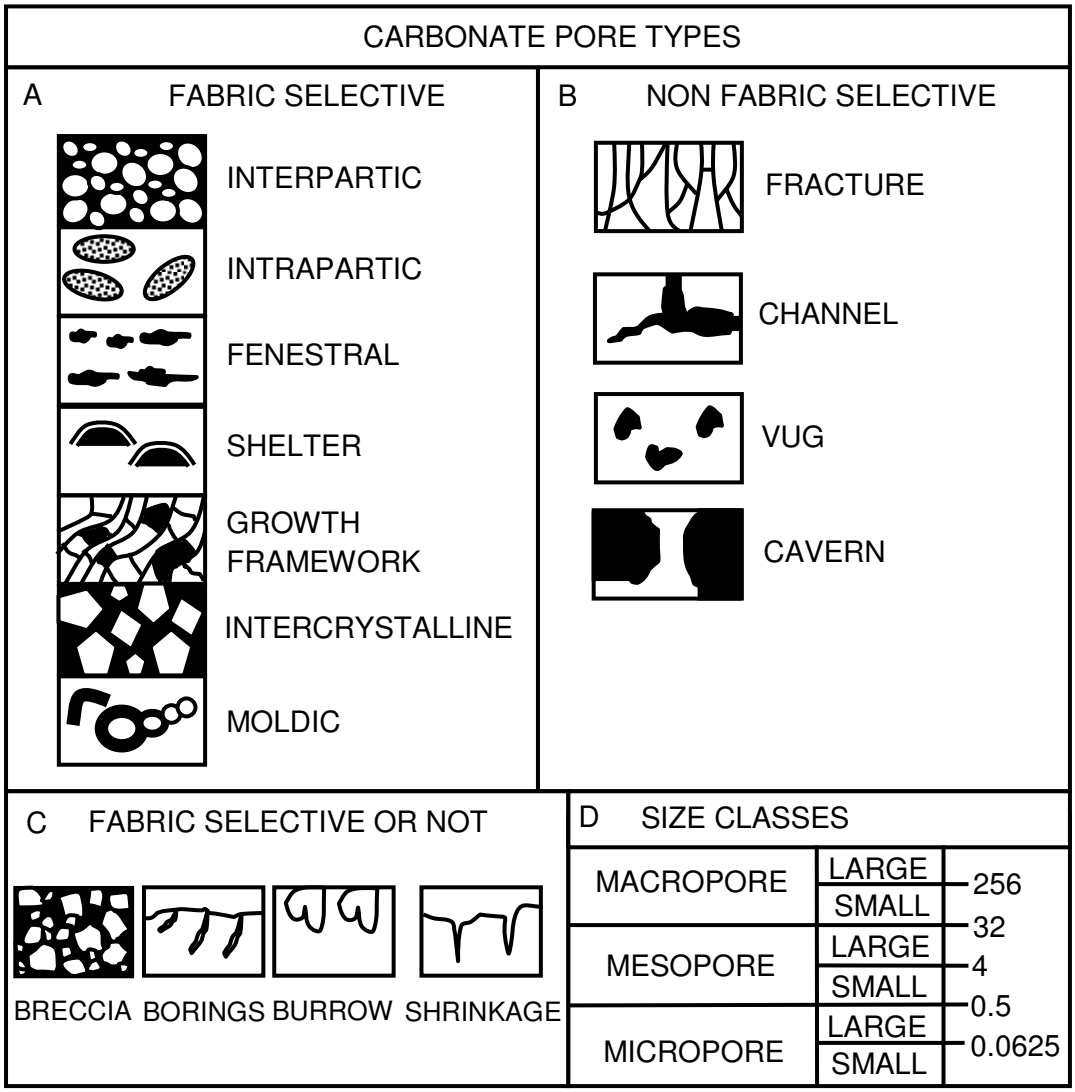

Figure 1.1: Ranges in pore shape, size and heterogeneity within carbonates. A) Fabric selective types of porosity that form primarily from deposition, with the exception of intercrystalline pores. B) Non-fabric selective pore types formed by diagenetic processes C) Pores that can be either fabric selective or non-fabric selective. D) Size ranges for pore types. The cavern pore type is present on a metre scale (redrawn from Choquette and Prey 1970).

1.1.2 Pore-pore throat ratios in carbonates: effective permeability

For oil to permeate a solid rock effectively, all the pore spaces need to be well connected by open pore throats. If a significant oil volume is trapped within a deeply buried reservoir and cannot permeate out under pressure, the reservoir cannot be exploited successfully. Therefore determining factors on reservoir permeability are the amount, and distribution of open pore throats, but also a low pore/pore throat ratio. The difference in ratio between pore sizes and adjoining pore throats determines the flow potential of the pore system. Modelling the pressure required for mercury to effectively permeate a pore system from Toledo et al. (1994) shows that the pressure increases when fluid permeates through narrow pore throats (Fig. 1.2A).

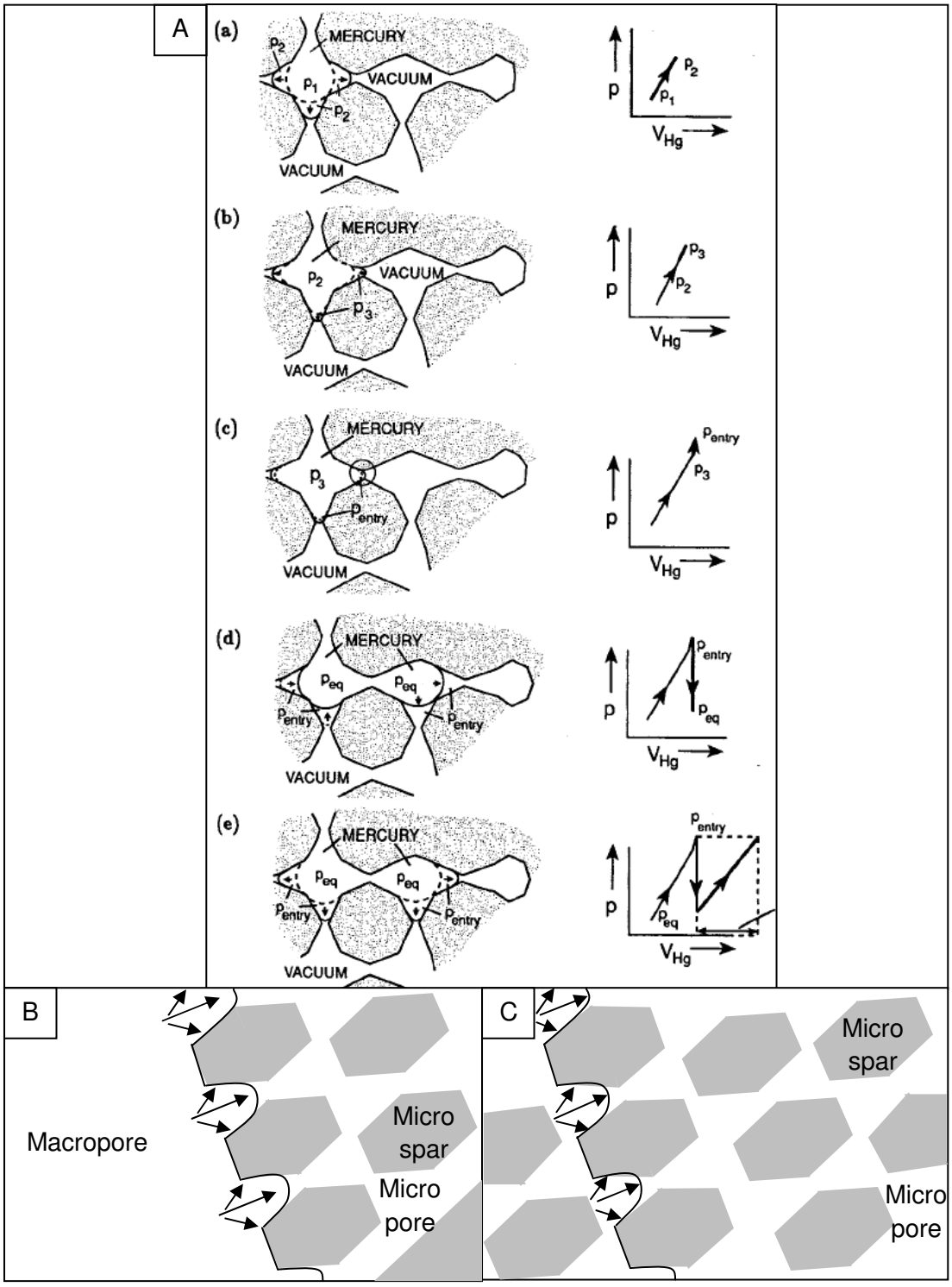

Figure 1.2: the step process of pressure change modelled by Toledo et al. (1994) of mercury permeating through a pore system. A) Pressure spikes when a fluid permeates through narrower pore throats. B) For a macropore system connected by micropores, after complete macropore flooding, the pressure required entering the micropores dramatically increases. C) A micropore system connected by similar sized pore throats will require a higher initial entry pressure, but will produce more prolonged sustained oil recovery.

Therefore the larger ratio between the pores and pore throats will require greater entry pressures to permeate a fluid through the system. For instance a macropore system linked together by smaller narrower micropore throats (micropores >10µm: (Cantrell & Hagerty 1999) with a macropore measuring one centimetre), could have a pore/pore throat ratio of 10,000/1 and will require high entry pressures to push the oil through the system (Fig. 1.2B). Considering the initial recovery is high, as the oil is evacuated from the larger macropores, the recovery tails of considerably when reliant on pushing oil through these narrow connecting pore throats (Fig. 1.3), making it harder to extract oil from the micropores.

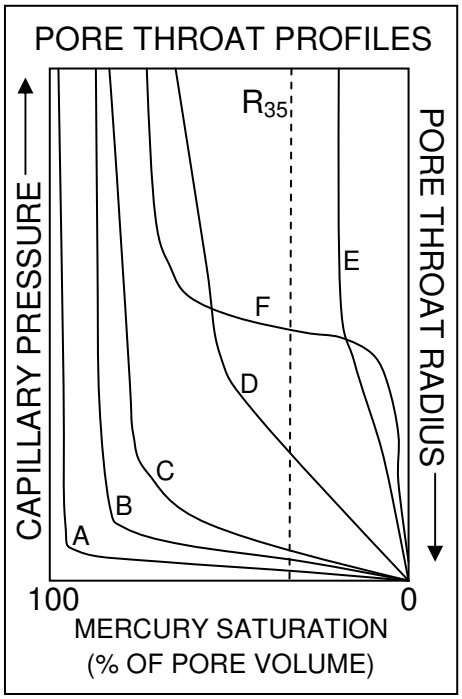

Figure 1.3: Theoretical mercury saturation curves for samples dominated by different pores. A) Represents a homogenous pore system with a low pore-pore throat ratio, B) represents mainly intercrystaline pores, C) represents heterogeneous over sized pores and intercrystaline pores, D) represents a dual pore system of microporosity and interparticle macroporosity, E) represents alternating laminations of two pore sizes whereas F) represents a heterogeneous mix of variable sized pores and isolated vugs (Beiranvand et al. 2003). This indicates that a sharp cut off at 90% mercury saturation for (A): increasing amounts of pressure are required to drive fluids form the remaining micropores, as opposed to (D) where a more sustained flow of fluid is achieved through the micropore system.

In comparison with a micropore system the micropores will always be connected by similar sized pore throats (average pore ratio of 10/1), due to the small nature of

the pores (Fig.1.2C). Therefore, although the volumetric amount of oil is lower in comparison with macropore systems and the initial oil recovery is much lower, because the pore/pore throat ratio is lower there is no dramatic tail off in productivity (Fig. 1.3). This information becomes very important when regarding the effective permeability of carbonate reservoirs containing both macropore and micropore dominated pore systems; which pore systems should be targeted first?

The effective permeability is considered the measure of a single fluid to permeate through the pore systems of a rock when another fluid is already present. An example of this is when CO_2 is pumped into a reservoir to push out remaining oil. If CO_2 is injected through the macropore systems, although a large amount of oil is extracted initially, the pressure required to push out all the remaining oil within the connected surrounding micropore system is large, and is therefore near impossible. Consequently there is a large reduction in oil recovery after a short time period (Fig. 1.3A). However if the micropore system is targeted first, the oil within the micropore system can be used to push out the oil from the surrounding macropores. Although a higher initial entry pressure is required, and may result in a smaller initial oil recovery, oil is recovered at a steady rate over a longer term (Fig. 1.3D). Therefore being able to determine the extent and relationships between macropore and micropore-dominated reservoir sections within a carbonate, will determine the method of oil extraction.

1.1.3 Carbonate porosity and permeability relationships

Now the issues of carbonate porosity and permeability are established, a final area to outline is (once all the depositional and diagenetic information is gathered) quantifying the porosity and permeability relationships of a particular carbonate reservoir. Unlike porosity, (commonly measured using mercury injection) which can be physically defined within core plugs, the permeability is a more difficult physical parameter to measure effectively. Therefore many oil prospectors have turned to using the porosity values to predict the permeability. A siliciclastic rock can have a very uniform porosity and permeability relationship (Fig 1.4B) and therefore extrapolating and up-scaling the porosity and permeability data set to encompass unexplored areas of a particular field can yield relatively accurate porosity and

permeability values. However, unlike a siliciclastic rock, the porosity of a carbonate can often bear no relationship to permeability (Fig. 1.4A). In addition, both the actions of deposition and diagenesis can produce a pore network so complex, that several different porosity and permeability relationships can exist within single lithologies or lithofacies. Predicting the permeability from the porosity within a carbonate can be very difficult.

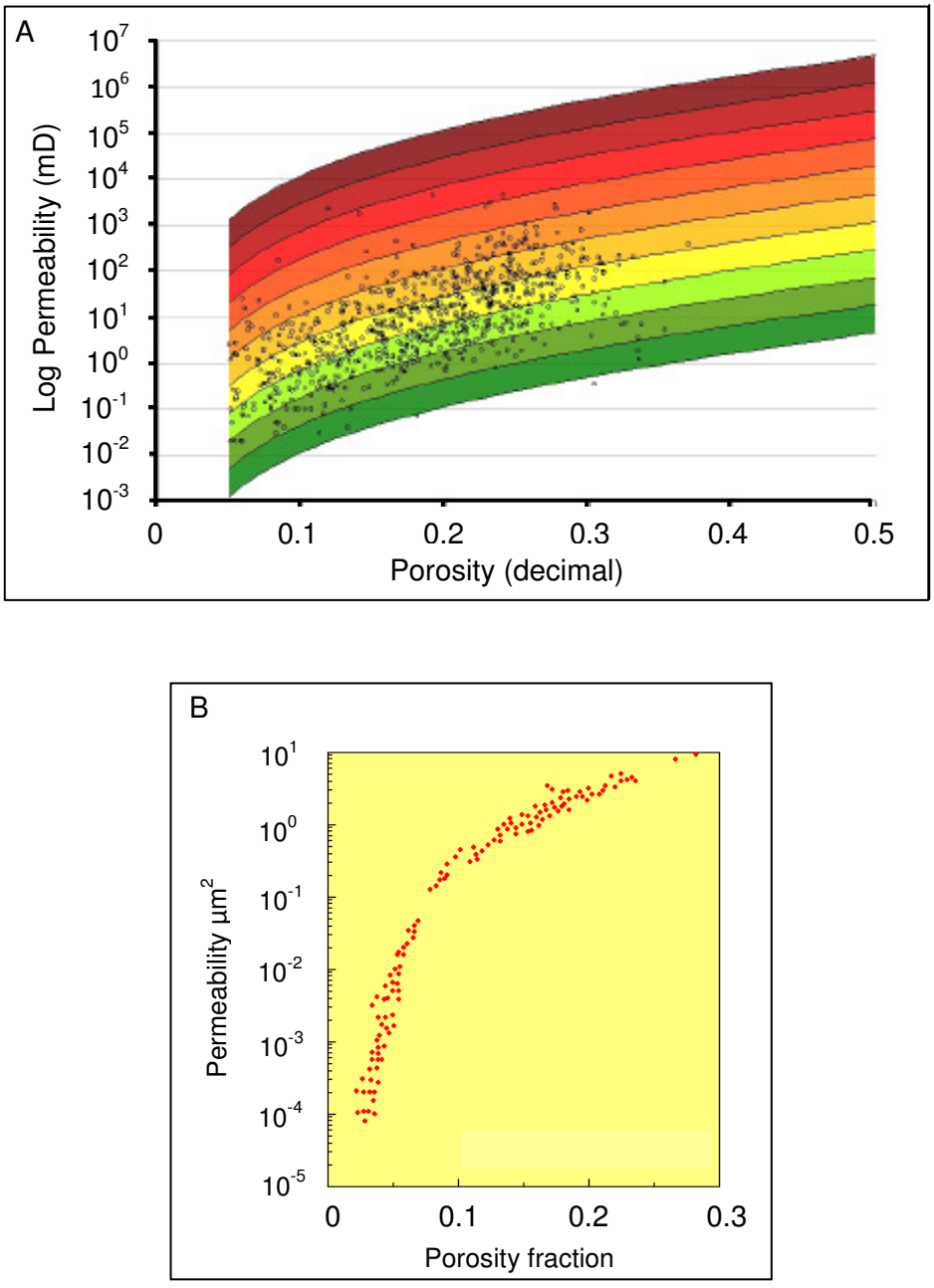

Figure 1.4: Porosity and permeability relationships of A) a carbonate which shows very little correlation making any extrapolation of the dataset difficult (Corbett & Potter 2004) while B) data from a siliciclastic reservoir shows correlation and the porosity can be effectively used to extrapolate permeability (Bourbie & Zinszer 1985).

Many studies have focused upon understanding porosity and permeability relationships within carbonates (Amaefule et al. 1993, Choquette & Prey 1970, Corbett et al. 2009, Gomes et al. 2008, Gunter et al. 1997, Lønøy 2006, Lucia 1999, Moore 2001, Shenawi et al. 2009, Svirsky et al. 2004). Three main methods exist:

1: Lucia model: This method separates out the highest porosity and permeability relationships into three separate classes based on the size, the amount and sorting of grains, which determines the size and distribution of the surrounding interparticle pores (Fig. 1.5) (Lucia 1999).

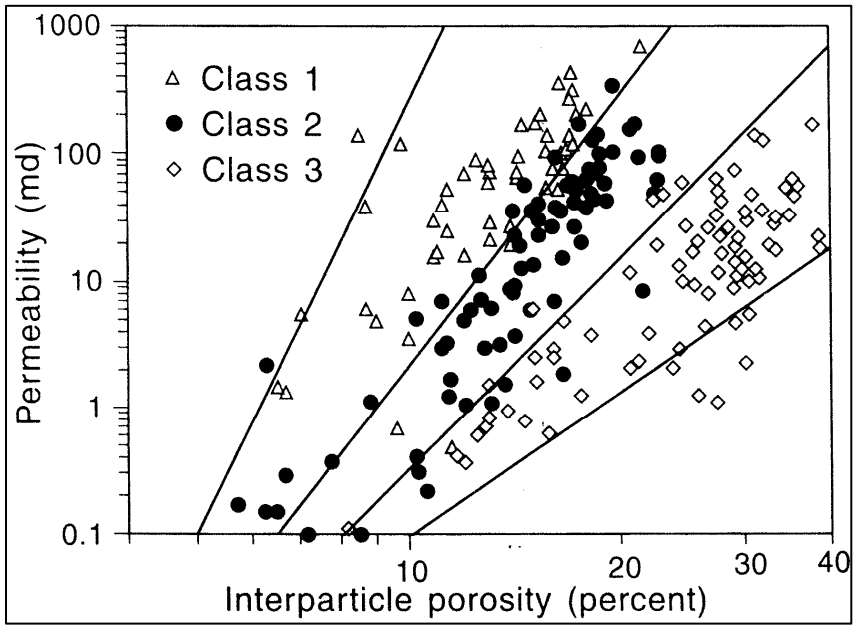

Figure 1.5: The Lucia (1999) method separates the data into three main classes using the size and sorting of the grains, which determines the size and distribution of the surrounding interparticle pores

2: Lønøy model: This method clarifies carbonates according to pore types (Fig. 1.6) instead of grain type (Lucia 1999). This separation shows that if 1mD is considered the critical flow parameter, the cut-off for porosity in microporous mudstones is 31% whereas for macromouldic pore types it is 13% (Lønøy 2006). This method shows how pore type can control the reservoir quality and the flow capability of a carbonate reservoir.

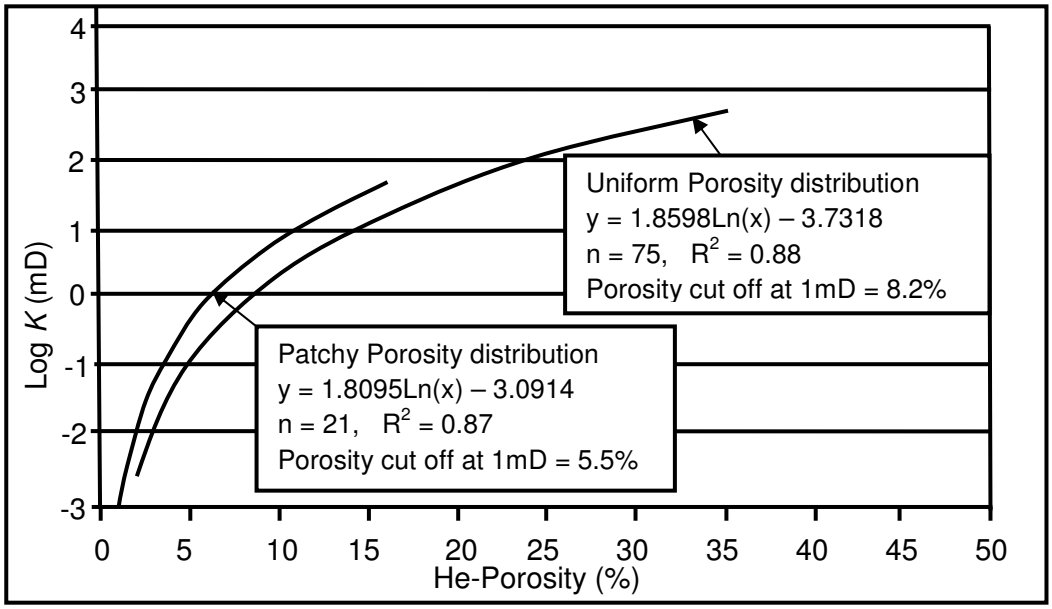

Figure 1.6: Two regression lines outline the distribution of patchy (black line) and uniform (dotted black line) macro interparticle pore dominated reservoirs (redrawn from Lønøy 2006).

3: Petrotyping method: This method is based on the Kozey/Lorenz Equation and the Reservoir Quality Index (RQI) (RQI defined as permeability divided by the amount of porosity: Equation 1.1). Dividing the RQI by Φz (pore volume to grain volume ratio: Equation 1.1), a Flow Zone Indicator (FZI) can be established (where ø is porosity and k is permeability). The data is then separated into classes (Hydraulic Flow Units: HFU's) defined by FZI's (Amaefule et al. 1993, Gunter et al. 1997, Shenawi et al. 2009, Svirsky et al. 2004). For the Petrotype atlas method (Fig. 1.7) the data is ordered into bands (GHE: Global Hydraulic Elements: Corbett & Potter 2004) centred on lines (i.e. FZI's).

Equation 1.1: $FZI = RQI/\Phi z = (0.0314(\sqrt{k}/ø))/(ø/1-ø)$

(Corbett & Potter 2004)

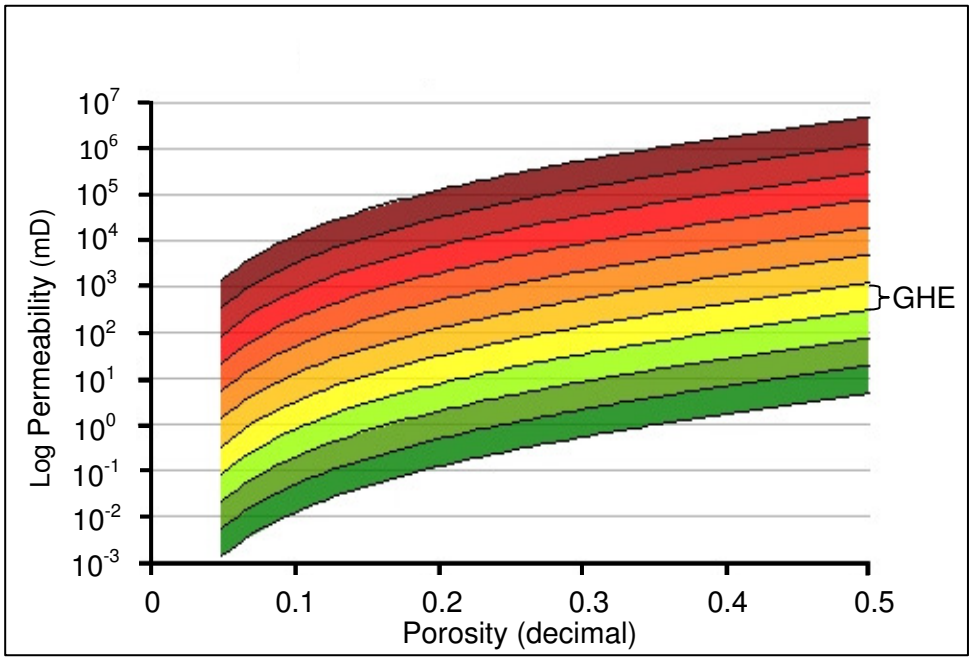

Figure 1.7: The Petrotype atlas method: The data is separated out using the GHE bands (redrawn from Corbett & Potter 2004).

This method shows that several distinctive rock types and lithofacies can all share similar GHE's. The Petrotype atlas method allows for more detailed reservoir characterisations, and for better extrapolation of lithofacies during up-scaling. That is, all the internal reservoir components can be up-scaled together to enable better estimations of reservoir quality on larger scales outside the dataset. This method also demonstrates that flow properties of the rock are not necessarily solely controlled by pore types and lithofacies, but also by diagenesis.

1.2 Thesis Aims

This study concentrates on the Lekhwair and Lower Kharaib Formations within one of the largest offshore fields within the Arabian Gulf. The field is located 70km northwest, offshore Abu Dhabi, and it covers an area roughly 500sq kilometres in size (relates to Zone IV): Hassan & Wada 1979). The structure (at the oil-water contact) is 40km in length, and 23.5km wide, with structural closure of roughly 1000ft (Hassan & Wada 1979). The field is dipped to the east and north by 2.5-2.8° and to the west by <1° (Hassan & Wada 1979).

For sampling purposes five wells were selected along a southeast to northwest transect encompassing the water leg, transition zone, oil leg, the field crest and two opposing flanks. The distances between the five wells are very large; Well 1-Well 2: 9km, Well 2-Well 3: 8.5km, Well 3-Well 4: 2km and Well 4-Well 5: 9.25km (Table 1.1). The transect encompasses the water leg on the south western field margins (Well 1), the transition zone on the south western flank (Well 2), the crest of the field and the oil leg (Wells 3 & 4), and the transition zone of the north eastern flank (Well 5) (Fig 1.8 & Table 1.1).

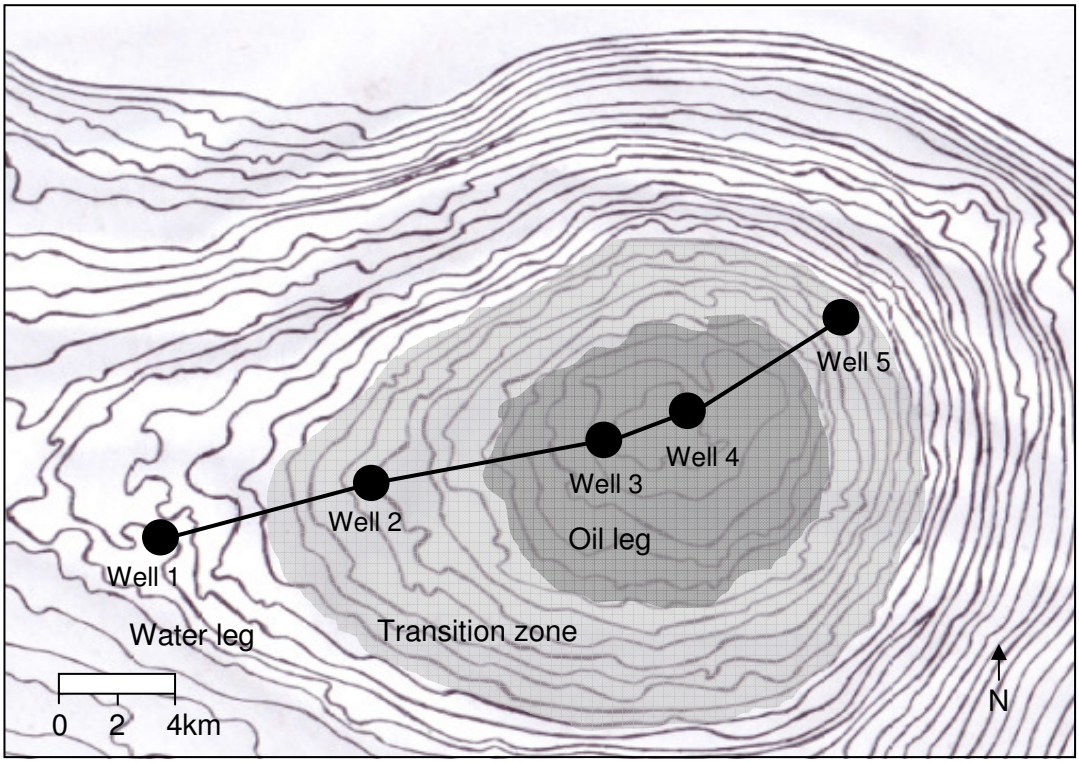

Figure 1.8: The positions of the five wells across the offshore field. Well 1 is in the water leg, with Wells 2 and 5 in the transition zone and Wells 3 and 4 in the oil leg. The specific position of the oil water contact is not known so it was placed roughly between Well 1 which is known to be in the water leg and Well 2, which is known to be in the transition zone. The contour level is then traced around the field. The same principle was applied to the oil leg transition zone contact.

	Well 1		Well 2		Well 3		Well 4		Well 5	
Cycles	A	B	A	B	A	B	A	B	A	B
C	35		44		46		Near vertical		42	
1	65	65	n/a	n/a	93	480	85	460	9	403
2a	n/a	n/a	n/a	n/a	32	387	n/a	n/a	47	394
2b	n/a	n/a	n/a	n/a	52	355	n/a	n/a	42	347
3	n/a	n/a	n/a	n/a	67	303	n/a	n/a	58	285
4a	n/a	n/a	47	242	40	236	37	212	39	227
4b	n/a	n/a	21	195	25	196	26	175	19	188
5	n/a	n/a	39	174	37	171	40	149	40	169
6	n/a	n/a	39	135	39	134	30	109	41	129
7a	n/a	n/a	41	96	53	95	42	79	47	88
7b	n/a	n/a	55	55	63	42	47	37	48	41

Table 1.1: A) Individual 4th order HFC thicknesses (feet), B) the cumulative thickness (feet) of all the 4th order HFC's and C) shows the deviation of each well in degrees (Fig. 1.13 for well positions). The overall thicknesses for each well are the cumulative values at the top of the columns labelled B. The row highlighted in grey represents the only 4th order HFC in the Lower Kharaib Formation (Cycle 1). The remaining 4th order HFC's (2a-8) are within the Lekhwair Formation.

The controlling factor to low oil recovery from carbonates appears to be pore heterogeneity at several scales; i.e. metre, millimetre and micron. Before a thorough investigation of pore heterogeneity can be achieved, along with a method devised to understand heterogeneity for the Lekhwair and Lower Khariab Formations, several areas of study regarding the deposition and the diagenesis are addressed first. The flow chart in Figure 1.9 summaries the areas of study, and the order they are addressed within this thesis, before the final chapter is reached where the comprehensive study on pore heterogeneity will take place, and a new model is proposed to tackle carbonate pore heterogeneity.

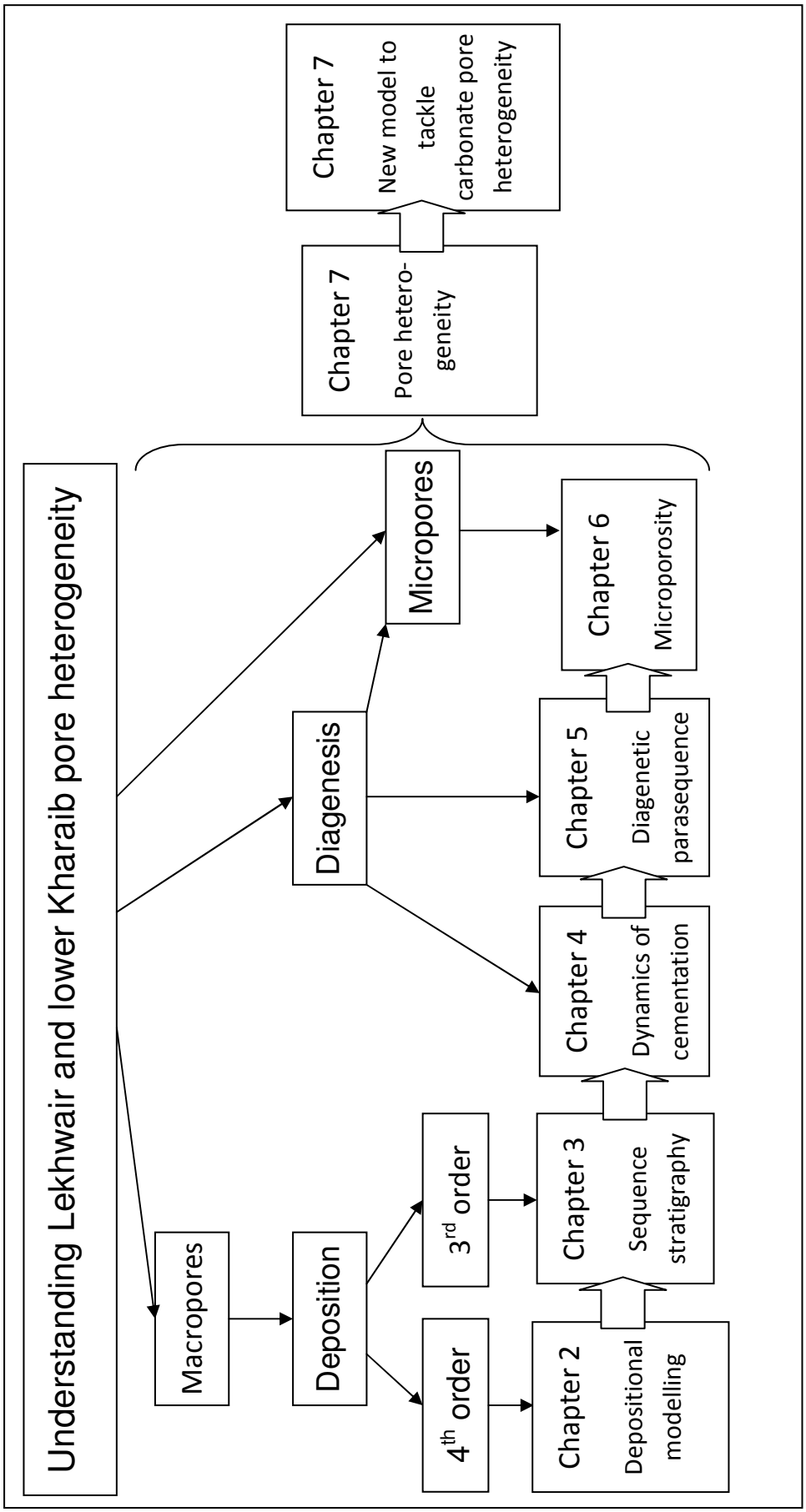

Fig. 1.9: The work flow, showing the structure of this thesis, listing the aims, and the elements of study in the order they are presented within this thesis.

The next section lists the aims of this thesis (as outlined in Fig. 1.9), the importance behind these aims, followed by the methodology solving the key issues for each aim. A list of key terms is shown for each Section within the Glossary at the end of the thesis. The aims and methodologies are ordered into the sequence they are presented within this thesis. Therefore this section also outlines the sequence and the contents of each Chapter.

Chapter 2

Aim 1: The formation of depositional models for the Lekhwair and Lower Kharaib Formations. For understanding the depositional controls on pore heterogeneity, and the porosity/permeability relationships of the Lekhwair and Lower Kharaib Formations, detailed petrographic information is gathered. Lithofacies are generated and ordered relative to their occurrence; this provides an understanding of palaeoenvironment change (occurrence of macro and microfossils), and the vertical occurrence of the coarsest reservoir lithologies. Specific palaeoenvironments can be associated with specific pore systems: for instance which environment produces the coarsest lithology and the best connected macropore systems?

Aim 1: Methodology: From each well, four 4th order HFC's were sampled: one from the base (Cycle 7a), two from the middle (Cycles 4a & 4b) of the Lekhwair Formation, with a fourth constituting the Lower Kharaib Formation (Cycle 1). This provides a good overview of the entire Lekhwair Formation in relation with the Lower Kharaib Formation. Ten core samples were collected from each 4th order HFC, including the HST's and TST's. Each core sample had a 2" by 3" thin section cut, for petrographic analysis. The depths for samples within Wells 2-5 were calculated using Cycle 8 hardground (SB) as the base of the scale, whereas for Well 1 the depths were calculated using the base of the core (Cycle 2a SB) for the base of the scale. The individual fossils were counted; a fossil diversity was taken (Appendix 1A-1E). The counts were used to track changes in individual fossil abundance throughout the Lekhwair and Lower Kharaib Formations. More detailed observations on the lithologies and fabrics were also noted alongside. Combining the lithological information with the fossil counts, 20 lithofacies were created. These lithofacies were

used to create depositional models of the base, and the top of the Lekhwair Formation, along with a third depositional model for the Lower Kharaib Formation.

Chapter 3

Aim 2: Developing a sequence stratigraphic framework for the Lekhwair and Lower Kharaib Formations. The depositional information gathered previously needs ordering into a framework, to collectively compile the depositional architecture for each 4th order HFC, within the Lekhwair and Lower Khariab Formations, to produce a 3rd order stacking pattern. The coarsest lithofacies, and the reservoirs, can then be correlated across the offshore field, determining their lateral extent. The coarsest lithofacies/reservoirs can also be related to relative sea level change and carbonate production. Information regarding the diagenesis and the porosity/permeability relationships can then be applied to this framework for correlation with the depositional architecture.

Aim 2 methodology: To create a sequence stratigraphic framework that encompassed a good cross section throughout the entire offshore field, extensive core logging encompassed five wells (including the field crest and two opposing flanks) along a southwest-northeast trajectory was completed (Fig 1.13).

For the logging, Dunham's classification (Dunham 1962) was used to determine the lithology and grain size (Appendix 2A-2E). Additional observations, where possible, included identifying the macrofossils with the large foraminifera. The oil staining, the types of grains present, the burrows, stylolites and compaction seams were also recorded. The 3rd and 4th order TST's and HST's were added to the logs along with the 3rd and 4th order MFS's and SB's. A sequence stratigraphic framework was then established using the 3rd and 4th order SB's and MFS positions. The Lekhwair and Lower Kharaib Formations, and their broad lithologies were then correlated across the entire structure.

Chapter 4

Aim 3: Assessing the dynamics of cementation and oil charge within the Lekhwair and Lower Kharaib Formations. The affects of diagenesis (cementation) towards the porosity/permeability relationships of the Lekhwair and Lower Khariab Formations is assessed. Instead of using a hand pick to extract the youngest, largest, and most easily accessible cement zone, to provide a $\delta^{18}O$ value for temperature/burial depth proxies, this study will employ a new technique. A combination of Cathodoluminescence (providing images of cement zone thicknesses) and the Ion Microprobe (where specific spots are ablated from carbonate samples to provide $\delta^{18}O$ values) detailed transects are established from the oldest-youngest cement zones, that can be compared between the water and oil legs to understand relative cement growth histories across the offshore field.

For the first time, within this study, depositional (amount of pore types) and diagenetic (amount of open/occluded pores) information is presented on the Lekhwair and Lower Kharaib pore systems. This is an appropriate place to compare both sets of data to the commercially measured porosity/permeability data. With reference to the sequence stratigraphic framework, the controlling factors from deposition and diagenesis towards the Lekhwair and Lower Khariab pore systems is established.

Aim 3 methodology: Two samples were selected from Cycle 1 (Lower Kharaib Formation); one is from the water leg (Well 1) while another is from the oil leg (Well 4). Three samples were taken from Cycle 4a; two from the transition zone (Well 2) and another from the oil leg (Well 3). The samples from Cycle 1 are rudist and Orbitolinidae packstone and grainstone, the samples from Cycle 4a are rudist and *Lithocodium/Bacinella* wackestone and packstone. LMC cements precipitated in marine and meteoric waters are found in these rocks but only LMC macrocements (>10μm diameter) that crystallized from formation waters during burial are considered here. These LMC macrocements occur in every sample and volumetrically dominate the cementation of these rocks. The amount of open pore space and fully occluded (cemented) pore space was manually counted from the

same epoxy impregnated 2" by 3" thin sections used for petrography (Appendix 3A). The amount of pore types was also counted from the same thin sections (Appendix 3B). The pores types were: small vugs, large vugs, intra-skeletal pores, small moulds, large moulds, interparticle pores and fracture porosity. Porosity and permeability data of the oil and water leg was measured commercially from adjacent petrophysical plugs, by mercury injection and by air injection, respectively.

The samples were cut into 22mm diameter rounds and were highly polished in preparation for the Cathodoluminescence. LMC macrocements displaying syntaxial overgrowths upon echinoid fragments were selected. These LMC macrocements contain the most complete cement sequences with the earliest cement zones and final zones abutting against open pore space (confirming the final, youngest cement growth). A Cathodoluminescence cold cathode CITL 8200 MK3A was used to identify cement zones separated by differing luminescence (Habermann et al. 1996; 1998; Mason 1987, Mason and Mariano, 1990). This formed the basis for establishing a cement stratigraphy for the water leg and oil leg (Braithwaite 1993). The Cathodoluminescence is however only a fabric tool as the cement zones only represents changes, in Mg and Fe quenching luminescence, and Mn enhancing luminescence. These zones bear no relation to $\delta^{13}C$ and $\delta^{18}O$ isotope data, and are therefore not used to correlate zones across the field.

The same samples selected for the Cathodoluminescence were searched for oil inclusions. A Leitz Metallux Leica 3 microscope, with a 100w Hg HBO 103 W/2 bulb, with a blue filter creating UV light with a waveband of 440-490nm, was used to locate oil inclusions. Inclusions were recognised by the presence of a mobile vapour bubble. This combined with green luminescence under UV light of the fluid portions indicated an oil inclusion. Any oil inclusion found is related to an individual cement zone and to the nearest $\delta^{18}O$ value. Any oil inclusions next to a fault, fracture or cleavage plane were disregarded as the oil may have been emplaced through fractures or faults and not by the trapping of oil upon a surface of a growing LMC macrocement. The relative timing of oil emplacement with respect to cementation is therefore uncertain, and these oil inclusions are not used. Any string of aligned oil inclusions along a straight line may also have been formed along a fracture and fault; these inclusions were also disregarded.

Samples were gold coated and placed within the Cameca 1270 Ion Microprobe to gain in situ $\delta^{18}O$ measurements for individual cement zones. A 10-15µm diameter Cs Ion beam was used to ablate 10-15µm spots from the sample. The internal precision for each spot ranges between 0.009 and 0.015 (% Standard Error). The external precision was estimated to 0.4‰ that was determined by consecutive analysis of a UWC (University of Wisconsin Calcite) standard that was assessed to be homogenous.

All analysis were standardised against the UWC preceded within a separate holder. This decreases the accuracy of the method, but relative variations are believed to be precise to 0.4‰ (external precision of the UWC). Therefore all Ion Microprobe data is displayed to 1 decimal place.

Chapter 5

Aim 4: Using separated component stable isotope analysis for constraining the timing of diagenetic events within the Lekhwair and Lower Kharaib Formations. Other diagenetic processes are taken into account to enable a full understanding of the effects of diagenesis upon the pore systems of the Lekhwair and Lower Kharaib Formations. A relative time frame is established for all diagenetic events.

Aim 4 methodology: The same 2" by 3" thin sections used for petrographic analysis were also stained with Alizarin Red Solution and Potassium Ferricyanide, for separating Fe-LMC and Fe-dolomite, using the staining method outlined by Dickson (1965). Staining helps to identify dolomite over LMC for sampling purposes of $\delta^{13}C$ and $\delta^{18}O$ isotopes. The staining only reveals the presence of LMC and the amount of Fe present within both the LMC and dolomite. Staining only provides limited information about the cement zones and therefore the cement growth history, associated with the amount of Fe present. The cement sequence highlighted by staining, along with cross-cutting relationships of other features (i.e. borings, stylolites) determined petrographically, are used to develop a relative sequence of diagenetic events (paragenetic sequence) during the burial of the Lekhwair and Lower Kharaib Formations.

Powders of sample size 0.03-0.2mg were also extracted for isotope analysis from the 2" by 3" thin sections (the same thin sections used for petrography) using a steel needle under a Leica 240 microscope. Powders were dissolved at 25°C with 100% phosphoric acid followed by conventional mass spectrometry using a Thermo Delta+ Advantage. Results are reported as deviations from VPDB standard (‰) and precision was measured at a level better than 0.1‰ for $\delta^{13}C$ and $\delta^{18}O$.

All the thin sections used for petrography have $\delta^{18}O_{VPDB}$ and $\delta^{13}C_{VPDB}$ values taken from the bulk micrite, LMC cements and dolomite cements (Appendix 4). For sampling the bulk micrite, areas of micrite lacking in bioclasts of other grains were targeted to limit contamination from bioclasts and intraclasts. The relative sequence of data relating to the increasing negativity of $\delta^{18}O$ values (increasing burial depth) are considered for use in constraining the paragenetic sequence of diagenetic events within the Lekhwair and Lower Kharaib Formations, created earlier from petrographic observations.

Chapter 6

Aim 5: Understanding the origins of microporosity within the Lekhwair and Lower Kharaib Formations. Microporosity can be responsible for part of effective permeability within a carbonate pore system. It therefore seems important to include the distribution, the size and shape of open micropores when considering the reservoir quality of any carbonate. As microporosity, (other than chalk microporosity; not relevant for this study) is considered a product of diagenetic alteration; mainly diagenetic processes will be studied to determine the history of micropore formation within the Lekhwair and Lower Kharaib Formations. An outcome would be to establish whether the microporosity was formed and altered (enhanced or occluded) by the same diagenetic processes that have affected the macropore systems. An understanding of pore heterogeneity can then be established at the macropore and the micropore scales.

Aim 5 methodology: To quantify the amount of microporosity within each 2" by 3" sample analysed petrographically, the method employed by Cantrell & Hagerty (1999) was used (Appendix 5). The amount of total porosity, as a percentage of the

core plug volume, was measured commercially by mercury injection. Photographs taken of the blue epoxy impregnated 2" by 3" thin sections were analysed using Adobe Photoshop for the percentage of blue pixels within the entire image. The percentage of blue was taken as the amount of visible macroporosity within each sample. Therefore the percentage of blue was subtracted from the total porosity volume of the core plugs. The difference was attributed to the amount of open microporosity. However, for some samples this method did not work for three reasons: 1) the thin sections are not of the core plugs: the percentage of pore space analysed commercially did not always correspond to the amount of blue within the thin sections, 2) comparing a flat thin section to a cylindrical core plug is problematic and 3) impregnation of the thin sections, in some cases, caused a blue film of resin to form over the slides, making them contain more blue than open pore space. These reasons are why some samples are not displayed in Section 6.3.1 as the porosity difference calculated was negative.

Rock chips were broken from the same core samples cut for thin sections for analysis on the Lower and Upper Lekhwair Formation and for the Lower Kharaib Formation. These rock chips ranged from 4-12mm: they were placed on 11mm diameter metal stubs, cleaned with a sonic bath for 5 minutes and gold coated. These stubs were placed into Phillips XL30CP Scanning Electron Microprobe. A 20Kv, 6μm diameter electron beam was used to image at 120x magnification and reduced to 4μm in diameter at 1950x magnifications, to maintain good image resolution.

Secondary Electron images were taken of the micropore fabrics. The micro and macrospars were noted along with the micro and macroporosity. Secondary Electron images taken of the core samples also provided information on the micropore systems, how the microporosity forms and where the most interconnected micropore systems are within the Lekhwair and Lower Kharaib Formations.

Chapter 7

Aim 7: The location of the highest porosity and permeability relationships within the Lekhwair and Lower Kharaib Formations. This objective involves directly comparing the porosity and permeability relationships, for every foot of core, on the

4th and 3rd order scales. The specific points with the highest porosity permeability relationships can be directly related to lithofacies, and be associated with specific points within the 3rd order cycle stacking pattern within the sequence stratigraphic framework. The effects of diagenesis and the areas containing the most connected micropores systems are added. Pore heterogeneity can then be collectively understood on the 3rd order scale, the 4th order scale, the macropore scale, and the micropore scale.

Aim 7 methodology: This Chapter is mostly reliant on the porosity and permeability data (shown as % and milli-Darcies (mD), respectively) which was measured commercially from 2" diameter core plugs taken from every foot interval throughout the five wells selected (Appendix 6). The amount of porosity was measured by mercury injection from adjacent core plugs in relation to the samples taken. The permeability was measured horizontally (with respect to the core) by air injection. The permeability data chosen to compare with the porosity data is the horizontal permeability rather than the vertical permeability measurements. This horizontal permeability data is more relevant to this study as the 'layer cake' nature of the field, with many impermeable transgressive muds, may have prevented most vertical fluid flow.

Using the depositional models, the distribution of cements, the paragenetic sequence of diagenetic events and the distribution of microporosity within a sequence stratigraphic framework, the porosity and permeability relationships for the Lekhwair and Lower Kharaib Formations are established.

Plotting the porosity and permeability data alongside the depositional and diagenetic information on the 4th order scales highlights which parts of each 4th order HFC commonly have the highest porosity and permeability relationships. This information is also applied to the 3rd order scale to show where the highest porosity and permeability relationships exist within the offshore field between the Lekhwair and Lower Kharaib Formations. Certain lithologies and pore types are associated with the highest porosity and permeability relationships on the 4th and 3rd order scales. The effects of diagenesis are also attributed to where the highest porosity and permeability relationships on the 4th and 3rd order scale.

Aim 7: Comparing rock typing methods for identifying micropore-dominated reservoir pore systems. To address the issue of carbonate pore heterogeneity at several scales within single reservoirs, this study will provide a new method for identifying several different reservoir components. This new method provides a means to evaluate the amount of open micro and macroporosity, and also the contribution both have on effective permeability, which could aid in determining the method of oil extraction.

Aim 8 methodology: Porosity and permeability data is plotted up on a Lucia plot (Lucia 1999), on a Lønøy plot (Lønøy 2006) and on a Petrotype atlas plot (Corbett & Potter 2004). These three methods are used as a basis to form a new method for plotting porosity and permeability data for carbonate pore systems, which is able to highlight the best pore systems (macropore-dominated pore systems) alongside the lower grade pore systems (micropore-dominated systems), both capable of producing oil. By combining information on the micropore and macropore systems a better understanding of the different scales of reservoir heterogeneity can be achieved within each reservoir horizon. The seemingly poor porosity/permeability relationships for a specific reservoir horizon can be ordered into internal flow units (micropore dominated, macropore dominated, non reservoir), which may help in further porosity/permeability extrapolation when up-scaling these single internal reservoir units. By knowing the reservoir heterogeneity at different scales will determine the method of oil extraction (Section 1.1.2) which may ultimately maximise oil recovery from the Lekhwair and Lower Kharaib Formation reservoirs, and potentially other carbonate reservoirs across the globe.

Chapter 2

Regional context

This short section covers four main topics: 1) the Cretaceous, 2) the regional tectonic history of the Arabian plate, 3) the oil habitats of the Arabian plate, and 4) sequence stratigraphy, which involves a more in depth analysis of the Thamama Group Stratigraphy regarding the offshore field. The section should provide background knowledge to support the following chapters regarding deposition, sequence stratigraphy, diagenesis, microporosity and porosity/permeability relationships.

2.1 The Cretaceous

The Cretaceous had a very different climate to modern day along with very different ocean chemistries. Therefore marine diagenesis operated differently; it is important to understand how syn-depositional diagenesis occurred in the Cretaceous in comparison with modern day.

Lower Cretaceous seawater was also LMC producing, with a molar Mg to Ca ratio of near 1 to 1, in comparison with 5 to 1 for today's aragonite seas (Hardie 1996). Consequently HMC and aragonite grains on the sea bed were readily dissolved and redistributed as LMC cements. Consequently Cretaceous oceans are labelled as calcite seas (Hardie 1996) (Fig. 2.1).

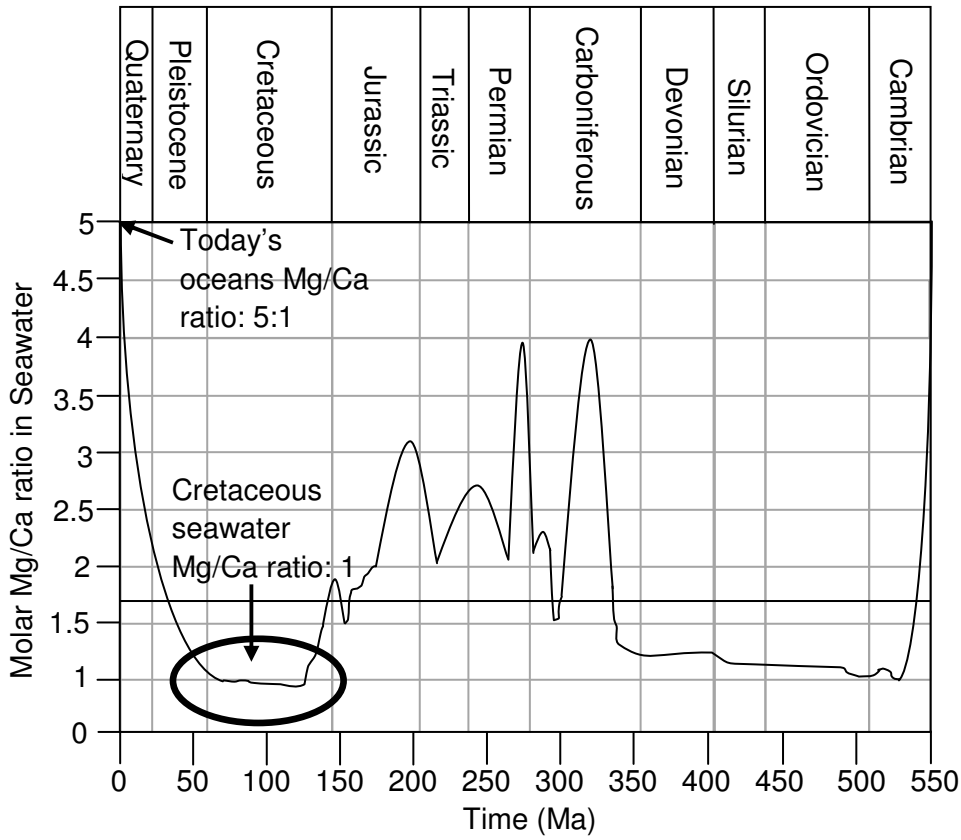

Figure 2.1: The prediction of secular variation of non-skeletal marine carbonates of Mg to Ca. In comparison with today's ratio of 5 to 1, Lower Cretaceous seawater had a ratio of almost 1 to 1. Cretaceous seawater is considered calcite seas in comparison with today's 'aragonite seas' (redrawn from Hardie 1996).

The Lower Cretaceous (145 to 99Ma: Gradstein & Ogg 1994, Walker & Geissman 2009) was a period of sea level highstand (Matthews & Frohlich 2002), with higher sea level of 100m (±50m) in comparison with the present day (Miller et al. 2005), larger global oceanic coverage and higher atmospheric pCO_2 (3-12 times higher than modern (pre-industrial) day (Berner 2001): i.e. an 900-3300p.p.m.v. increase: (Kuypers et al. 1999)) leading to a warmer global climate (Hallam 1985). An increase in seafloor spreading in the Pacific caused oceanic plateaus to form through flood basalt volcanism along the Pacific ridge crest (Larson 1991) (Fig. 2.2). Global seafloor spreading rates between the Aptian and Albian were ~3.3 x $10^6 km^3$/Myr in comparison with today's global seafloor spreading rate of ~1.8 x $10^6 km^3$/Myr: seafloor spreading rates were 50-75% higher than normal during the Lower Cretaceous (Larson 1991) (Fig. 2.2). More basaltic volcanism would have increased the ocean coverage and the amount of atmospheric CO_2 out gassing across

the globe. The increase in greenhouse gasses created a warmer climate elevating sea level, causing widespread continental flooding, larger oceanic processes and continental erosion (Föllmi 1993, Föllmi et al. 1994).

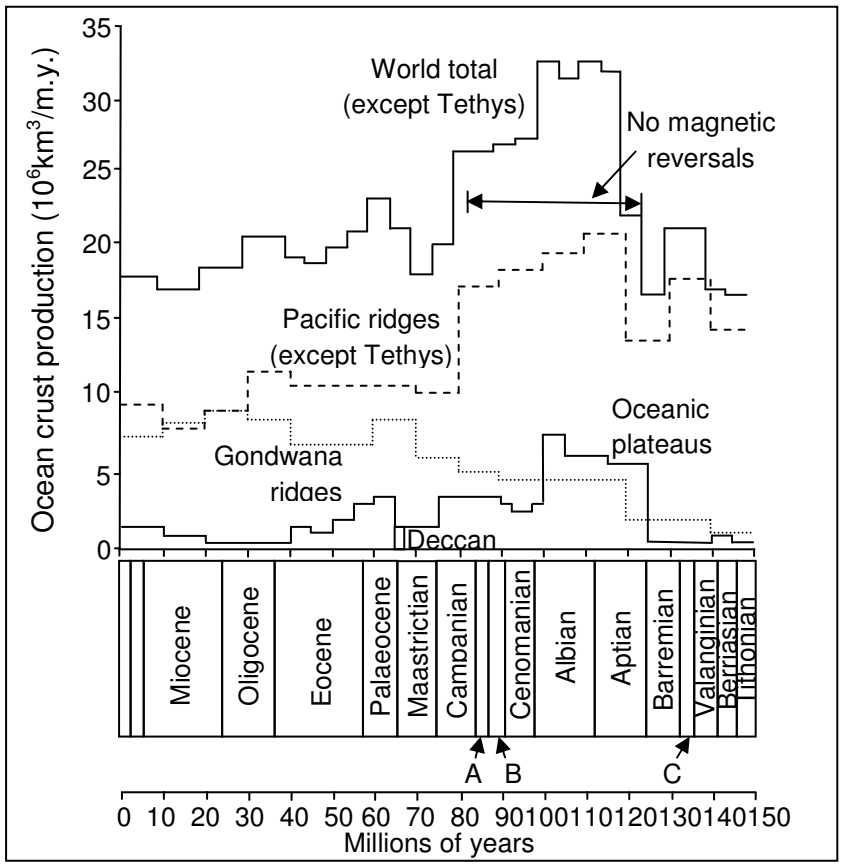

Figure 2.2: There has been an increase in oceanic crust production at the Mid pacific ridges during the Lower-Mid Cretaceous (Larson 1991). On the x-axis A represents the Santonian, B represents the Turonian and C represents the Hauterivian.

However the Cretaceous has had some climate variability. Studies from Matthews & Frohlich (2002) explain a link between long term eccentricities (400ky. duration) with sequence stratigraphy (in particular 3rd order cyclicity). 'Times of relatively high eccentricity, combined with precession and tilt maxima at times of summer solstice at perihelion' are suggested by Matthews & Frohlich (2002) to melt polar ice caps over several thousand years. By modelling the amount of ice volume at the poles provides an estimation of sea level change; three sea level peaks occur; one at 117.7Ma, 121Ma and 122,6Ma suggesting the Lower-mid Cretaceous had varied.

More specifically, studies from Steuber et al. (2005) of the Early Cretaceous has identified several cooler periods. By using the $\delta^{18}O$ variation from planktonic foraminifera the seasonality is determined: between 10-20°N the maximum temperatures were 35-37°C with a variability of <12°C, whereas in the cooler periods the variability was near 18°C (Steuber et al. 2002).

Studies from Price et al. (2000) have used $\delta^{18}O$ from belemites to predict warmer temperatures for the early Valanginian of 15-16°C, for the earliest Hauterivian temperatures were cooler of <9°C. The amount of kaolinite and smectite, which represents humid and arid climate phases correlates with the warm and cold periods

Studies from Melinte & Mutterlose (2001) suggest that shifts between abundances of *Nannoconus spp.* in the Mid-Upper Berrisian and the Upper Valanginian, coupled with abundance of *Watznaueria spp* in the Lower Berrisian and the Upper Berrisian-Lower Valanginian, represent shifts in climate. *Watznaueria spp* is thought to represent periods of cooler humid conditions whereas *Nannoconus spp.* reflect more stable surface waters.

In the late Cretaceous a similar variability has been suggested by Li & Keller (1999). During the late Campanian-Maastrictian (70-73Ma), sea surface temperatures decreased by 4-5°C whist intermediate waters decreased by 5-6°C (Li & Keller (1999). While just before the Cretaceous-Tertiary boundary sea surface temperatures warmed by 3-4°C (Li & Keller 1999).

2.2 Regional setting

Across the Arabian plate, the late Jurassic corresponds to sea level rise and stacked shoaling upward cycles, showing the transition from intertidal carbonates (Arab Formation) into supratidal and arid evaporites (Hith Anhydrite) (Zeigler 2001). In the early Jurassic the Neo-Tethys began subduction along its northern Iranian margin, which created a strong slab pull, which added to the break-up of Pangaea in the west (Stampfli & Borel 2002). This rifting created the Atlantic Ocean which began at 149Ma (Sharland et al. 2001); this is marked in offshore Kuwait by a major sedimentary hiatus (Valanginian-Early Hauterivian age) (Ziegler 2001). The

opening of the Atlantic Ocean inevitably led to the convergence of the Neo-Tethys northeast of the Oman passive margin (Lippard et al. (1986), Robertson & Searle 1990). Consequently between 149-92Ma, and the Valanginian-Santonian, the mid-ocean ridge of the Tethys became subducted under the North Iranian margin (Stampfli & Borel 2002).

The Berriasian-Valanginian (144-132Ma) (Fig. 2.3) marks the first early Cretaceous 2nd order sequence (AP8: Sharland et al. 2001) and is associated with high, but falling eustatic sea level (Haq et al. 1987). The western Arabian plate margin was undergoing uplift and erosion while the eastern Arabian plate margin was subsiding, and protruded into the Neo-Tethys. The combination of both processes caused the Arabian plate to tilt towards the northeast (Sharland et al. 2001). Consequently accommodation space was generated along the eastern Arabian plate margin allowing for extensive shallow marine shelf accretion (Fig. 2.3).

Sediments were deposited within shallow intra-shelf basins which were surrounded on the north, east and south by passive margins (Sharland et al. 2001, Zeigler 2001). Consequently there is a shift from terrigenous sandstones in the east, through shallow marine carbonates in the central plate and deepwater marls and muds in the east (Fig. 2.3). More specifically in the north-western portion of the Arabian plate a siliciclastic environment dominated (Helez sandstones) which marks the uplifted portions of the plate, while in the northern Arabian plate (in the former Gotnia Basin) argillaceous limestones of the Sulaly/Makhul Formations, along with peloidal mud supported limestones of the Ratawi Formation were deposited (Ziegler 2001).

In the central eastern portion of the Arabian plate the Yamama carbonates were deposited whereas within the interior of Oman, at the eastern edge of the Arabian plate, the cherty lime mudstones of the Rayda Formation. These deposits represent deep marine basin fill, representing the plate tilt towards the east and increasing amounts of accommodation space (Fig. 2.3). The Habshan Formation formed at the eastern portion of the Arabian plate representing the first sediment fill within the Rayda Basin between 143Ma and 129Ma (Sharland et al. 2001) and the extensive drowning and incursion of the deep shelf towards the west (landward) (Scott 1990).

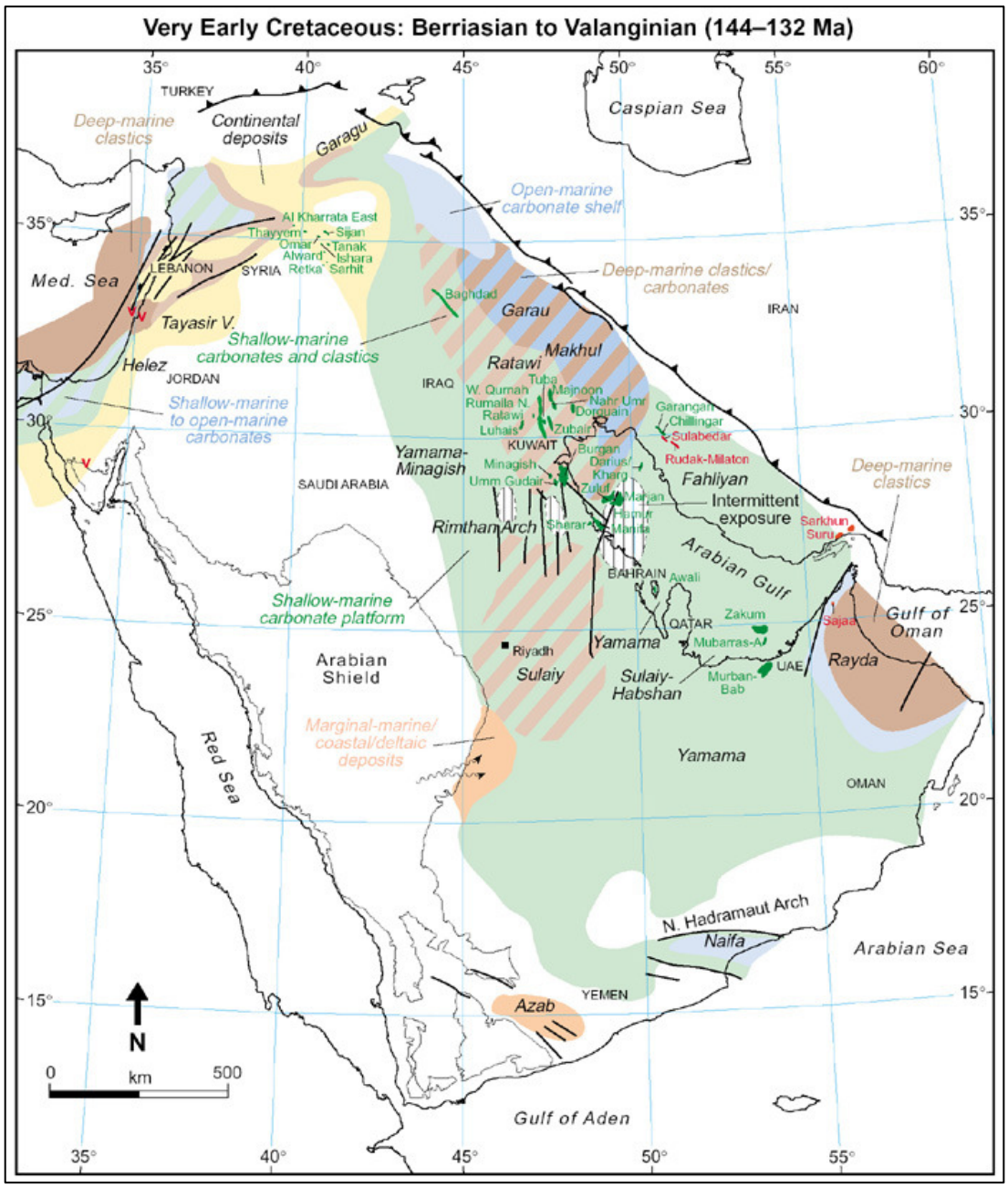

Figure 2.3: The regional geology of the Arabian plate showing the carbonate ramps that prograded to the east during the Berriasian-Valanginian (Ziegler 2001).

After a short lowering of sea level, from the early Valanginian, sea level rose to a Mesozoic-Cenozoic peak in the Early Turonian: Therefore the Hauterivian-Barremian period (132-121Ma) (Fig. 2.4) is associated with progressive sea level rise (Haq et al. 1987). Continental deposits are inter-bedded with volcanics in Lebanon confirming uplift of the north eastern margin of the Arabian plate (Zeigler 2001).

The Gotnia basin is defined by deeper water argillaceous mudstone with pelletal bioclastic mudstone, the same is found at Qatar. The northern plate was covered by shales and sabkhas of the Areban, Cheriffe and Mdarej Formations which change towards the north east into sandy limestones with low biodiversities, suggesting restricted marine conditions (Ziegler 2001: Fig. 2.4). Sea level rise is marked by the Gulf basin deposits changing from continental fluvial systems and shallow marine sand bars/subtidal shales, to carbonate ramp systems (Biyadh-Buwaib-Zubair Formations) (Ziegler 2001). The palaeocoastline migrated further east and existed east of Riyadh but west of Abu Dhabi during the Lower-mid Barremian (Murris et al. 1980, Zeigler 2001: Fig 2.4).

At Abu Dhabi the Lekhwair/ Kharaib Formation represent shoaling upwards cycles (Scott 1990) consisting of peliodal rudist grainstones representing carbonate ramp systems (Fig. 2.4). These shallow water carbonate ramps prograded towards the east into the Neo Tethys (Murris et al. 1980, Shebl & Alsharhan 2000). These carbonate ramps were very broad, low angle slopes that expanded for over 500km (Murris 1980, Ziegler 2001). Both the Lekhwair and Kharaib Formations form a stacked 'layer cake' repeated assemblage of 4^{th} order High Frequency Cycles (HFC's). The lateral extent and the 'layer cake' nature of these 4^{th} order HFC's indicates deposition may have occurred on a near horizontal platform or ramp (Alsharhan 1989). Each HFC has a reservoir assemblage comprised of packstone and grainstone capped by the transgressive mud of the next 4^{th} order HFC. Between 129Ma and 123Ma (Sharland et al. 2001) the Lekhwair (Alsharhan 1989; 1995, Alsharhan & Nairn 1986, Alsharhan & Kendall 1991), Kharaib Formations were deposited forming the lower half of the Thamama Group (Thamama Zones IV, III, IIIA & II: offshore Abu Dhabi units).

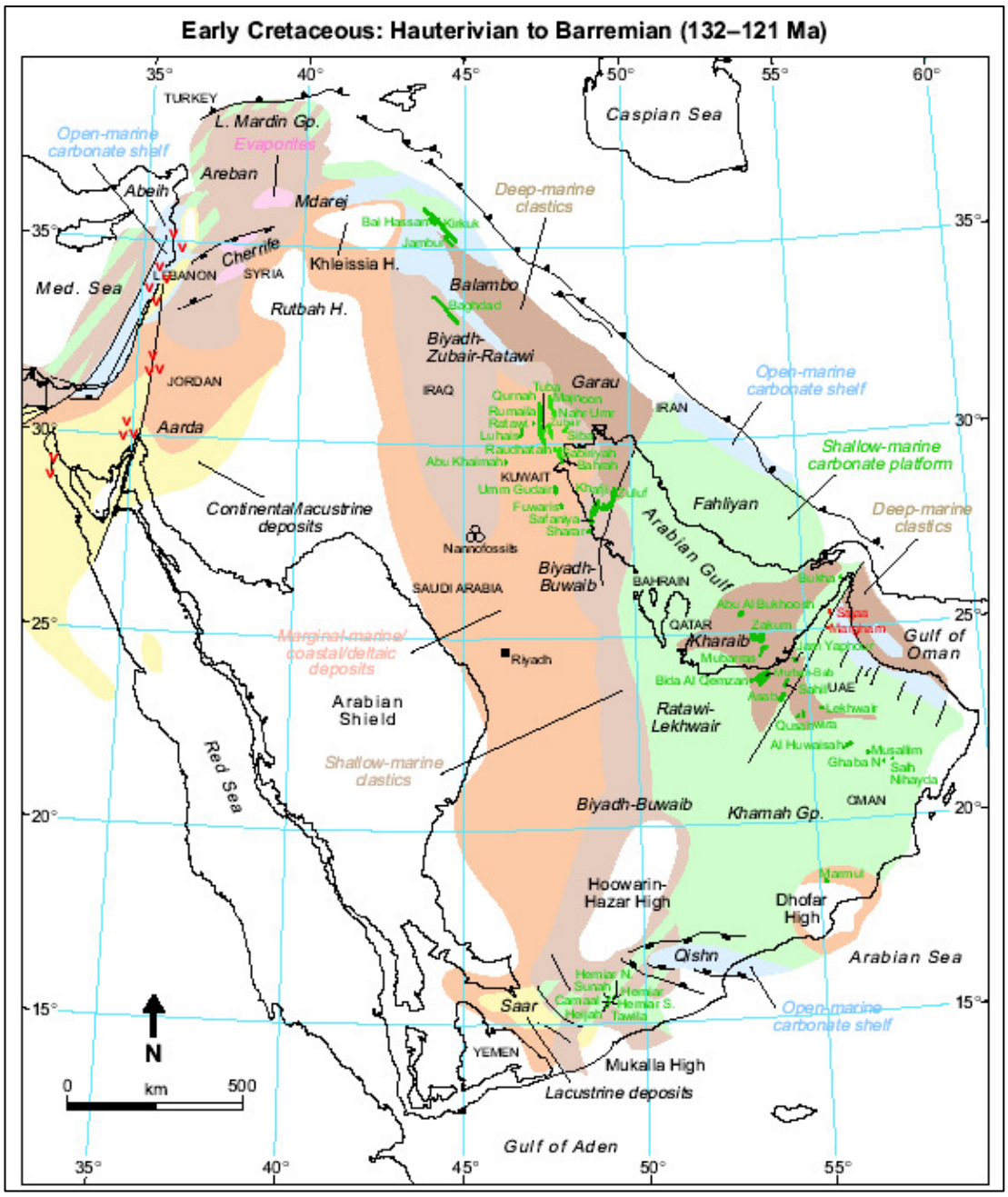

Figure 2.4: The regional geology of the Arabian plate showing the carbonate ramps that prograded to the east during the Hauterivian-Barremian (Ziegler 2001).

The Aptian-Albian sequence (121-98.9Ma) (Fig. 2.5) represents sea level rise (Haq et al. 1987), followed by the Albian unconformity (111Ma: Sharland et al. 2001). The eastern Arabian plate is represented by organic rich shales and argillaceous limestones (Kazhdumi & Balambo Formations), representing the eastern intrashelf basins of Iran and Iraq (Ziegler 2001). The Aptian Shu'aiba Formation shows a general shoaling from deepwater limestones, to rudist rimmed platforms, to

back-bank and then lagoonal deposits at the Rub' Al-Khali Basin (Hughes 2000, Ziegler 2001) (Fig. 2.5). The Shu'aiba formation (Alsharhan 1987; 1989, Al-Silwadi et al.1996, Aziz & El-Satter 1997, van Buchem et al. 2002, Granier et al. 2000; 2003/05, Hughes et al. 2002b, Pittet et al. 2002, Strohmenger et al. 2006a and Yose et al. 2006) was deposited between 123-111Ma (Sharland et al. 2001) and forms Thamama Zone I (offshore Abu Dhabi units) constituting the remainder of the Thamama Group. The Shu'aiba has an intrashelf basin in the southern Arabian Gulf (Bab Basin) which is represented by an increase in sediment thickness and hemipelagic deposition (Alsharhan 1995). Although the Bab basin is considered the basinal equivalent of the Shu'aiba, much of its deposition is younger in the late Aptian (Scott 1990). Overall, the deposition of the Lekhwair-Kharaib-Shu'aiba Formations (Thamama Group) lasted from about 18Ma (Scott 1990, Sharland 2001).

The Thamama Group is capped by the Nahr Umr Formation, which lasted for 22Ma and contains four shoaling upward cycles (Scott 1990), and forms the lower portion of the Wasia Group (Sharland et al. 2001, Shebl & Alsharhan 1993): this is shown in the Shaybah field the Shu'aiba Formation shows weathering and invasion of the Nahr Umr Formation shales (Hughes 2000, Ziegler 2001) (Fig. 2.5). The base of the Nahr Umr Formation is a 2nd order SB, and represents the transition between the Aptian-Albian (dated at 112Ma by Gradstein & Ogg 2004).

In Saudi Arabia, the Sallah Member (top Biyadh Formation) represents the end of the Aptian; it is comprised of shallow sands/shales representing a MFS (Ziegler 2001). These continental sands and conglomerates change northwards to littoral shallow marine pro delta environments in Kuwait (Aptian Zubair Formation-Albian Burgan sands) (Ziegler 2001) (Fig. 2.5). On the north-eastern Arabian plate margin the Kazhduni shales were deposited with open marine planktonic foramimifera (Zeigler 2001).

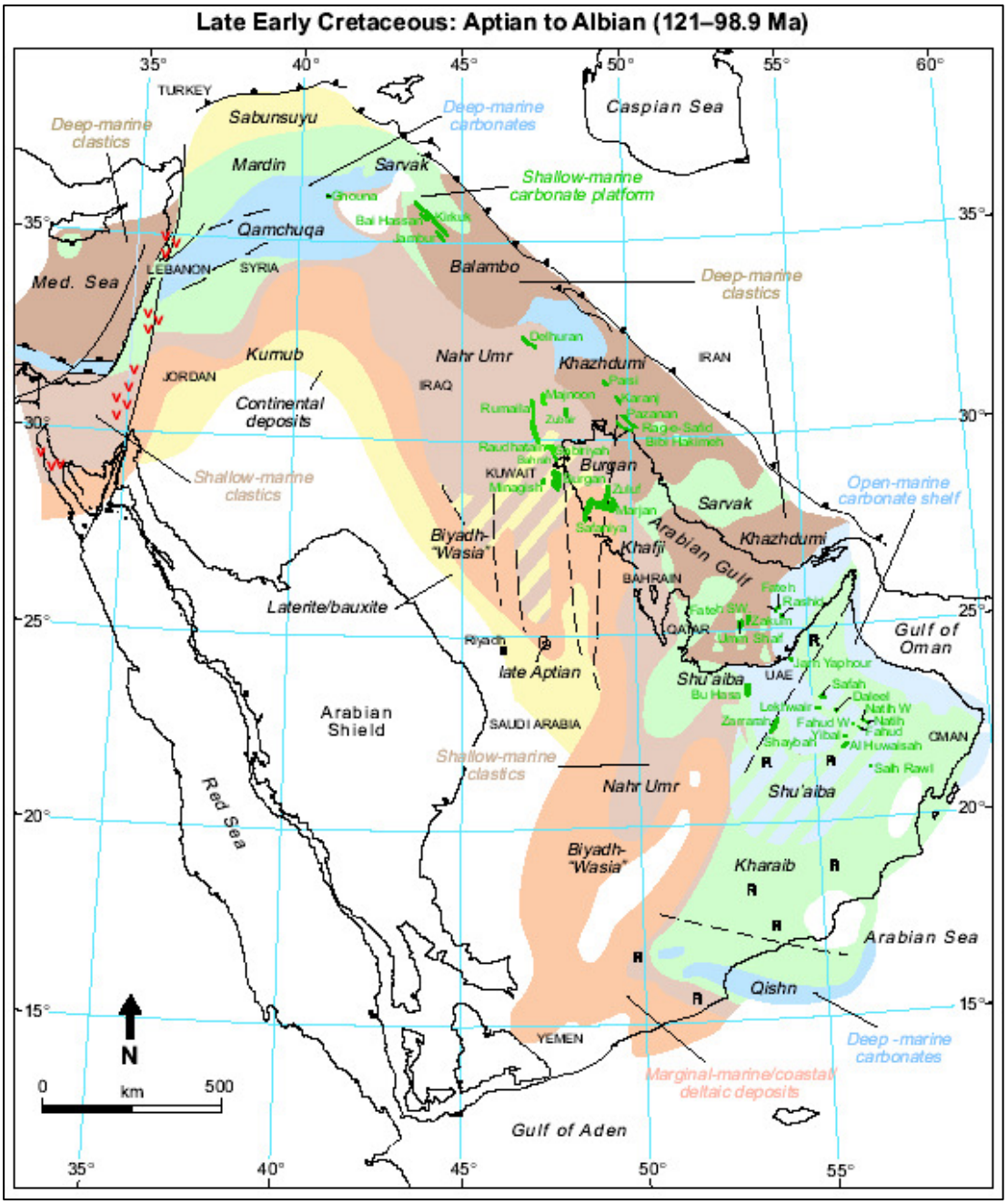

Figure 2.5: The regional geology of the Arabian plate showing the carbonate ramps that prograded to the east during the Albian-Aptian (Ziegler 2001).

The Lekhwair and Lower Kharaib Formation sediments were progressively buried until 92Ma when the Semail Ophiolite obducted on to the eastern Arabian Plate margin (Sharland et al. 2001). Prior to this, during the Cenomanian (99.6-93.5Ma: Gradstein & Ogg 2004), the Mishrif Formation was deposited representing widespread carbonate shallow marine platform accretion, and represents a reduction in terrigenous input in comparison with the Wasia Formation below (Ziegler 2001).

The Mishrif Formation is overlain by the Ruwaydha carbonates at Abu Dhabi of late Cenomanian-Early Turonian age (Turonian is dated at 93.5-89.3Ma: Gradstein & Ogg 2004). These carbonates are overlain by a hiatus until the early Campanian which extends to the southwest Arabian plate (Saudi Arabia) (Sharland et al. 2001). The hiatus is the Late Turonian unconformity (92Ma), the base of AP9 and the Aruma Group (Sharland et a. 2001), and also represents the Wasia-Aruma Gap which is regionally significant and extensive (Glennie 1974, Robertson & Searle 1990) and measures a gap of 2.5Myr in Oman (Scott 1990).

Sea levels are suggested to have been slowly lowering from the Early Turonian into the Cenozoic (Haq et al. 1987) (93.5-65.5Ma; Gradstein & Ogg 2004). Above the hiatus only in the northeast Arabian plate, more towards the marine shelf, are the Laffan and Halul Formations representing erosion, truncation and onlap in the southwest (Christian 1997, Koop & Stonely 1982). Into the Campanian (83.5-70.6Ma: Gradstein & Ogg 2004) there was a reduction in exposed landmass, on the western Arabian plate, as a broad shallow marine shelf developed forming the Aruma Formation (Christian 1997, Ziegler 2001) (Fig. 2.6). On the eastern Arabian plate margin a narrow NW trending fore-deep developed in response to ophiolite nappe emplacement along the North western Arabian plate margin and the Zagros margin in Oman, Iran and the Troodos Mountains of Cyprus; in particular the overthrusting and emplacement of the Sumeini, Hawasina and the obduction of the Semail nappes occurred along the leading edge of the Semail Ophiolite (Searle 1988, Robertson & Searle 1990, Ziegler 2001) (Fig. 2.6 & 2.7). The oceanic crust which eventually became the Semail nappes/ophiolite are suggested to have been generated between 98-93Ma (Tilton et al. 1981: Robertson & Searle 1990), which has resulted in the Wasia-Aruma unconformity; dated at 92Ma (Sharland et al. 2001).

Compression in the north western plate created many en-echelon structures in the north-western Arabian plate such as the Euphrates Graben complex (Sharland et al. 2001, Walley 1998, Zeigler 2001) (Fig. 2.7). Several thrust faults are present 30km west from the obduction, within the carbonate shelf deposits, which are truncated by Tertiary carbonate sediments, confirming they formed in the Late Cretaceous (Dunne et al. 1990, Robertson & Searle 1990). The Suneinah forebulge developed folding the

Lekhwair and Kharaib Formations in response to obduction (Sharland et al. 2001) (Fig. 1.13) causing extensive erosion of the Wasia Group in Oman (Glennie 1974, Scott 1990). In comparison, the east and the Oman margin underwent down-flexing creating a foreland basin resulting in submergence and transgression (Ziegler 2001). Rapid subsidence in the east, coupled with uplift and erosion in the west, lead to increased eastward sediment fluxes and to the deposition of 1000ft of hemipelagic mudstones of the Fiqa Formation as flysch within the fore deep (Gurpi Basin) (Koop & Stonely 1982, Ziegler 2001) (Fig. 2.6 & 2.7). Continued erosion in the west, of the Suneinah fore-bulge, deposited the deep marine Maastrictian Simsima (Aruma Formation) and Shiranish Formations overlying the Fiqa Formation (Sharland et al. 2001, Ziegler 2001).

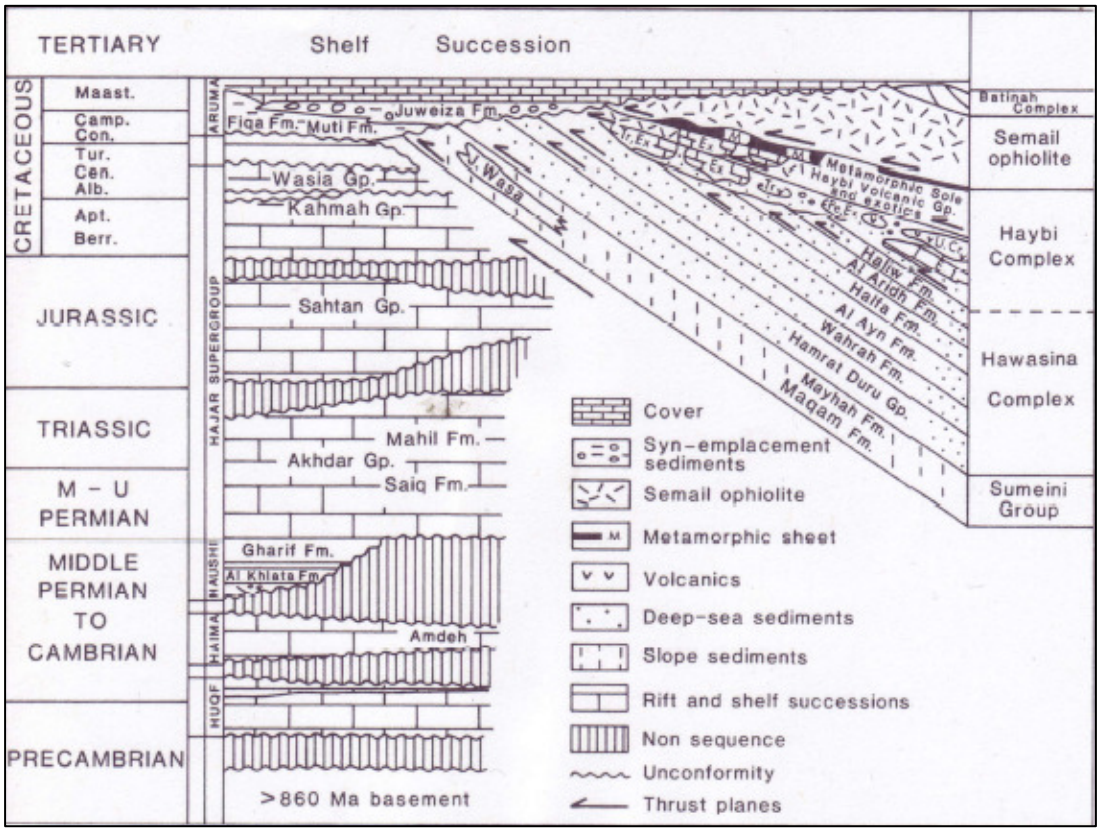

Figure 2.6: The stratigraphy of the Arabian plate at the Oman Mountains from the PreCambrian to the Late Cretaceous (Glennie 1974: Robertson & Searle 1990).

In comparison, from the east close to the Zagros thrust, sands and silts formed the Amiran and Tanjero flysch sediments which represented erosion from the folding and uplift in the east (Ziegler 2001). Cessation of orogenic activity is represented by the transgression of the Qahlah detrital clastics over the Semial ophiolite and the

onlap of the Simsima Formation onto the allocthon of the Oman Mountains (Nolan et al. 1990, Ziegler 2001). This is overlain by another major hiatus which is dated to 63Ma, the Danian, and marks the top of AP9 (Sharland et al. 2001) (Fig.2.7).

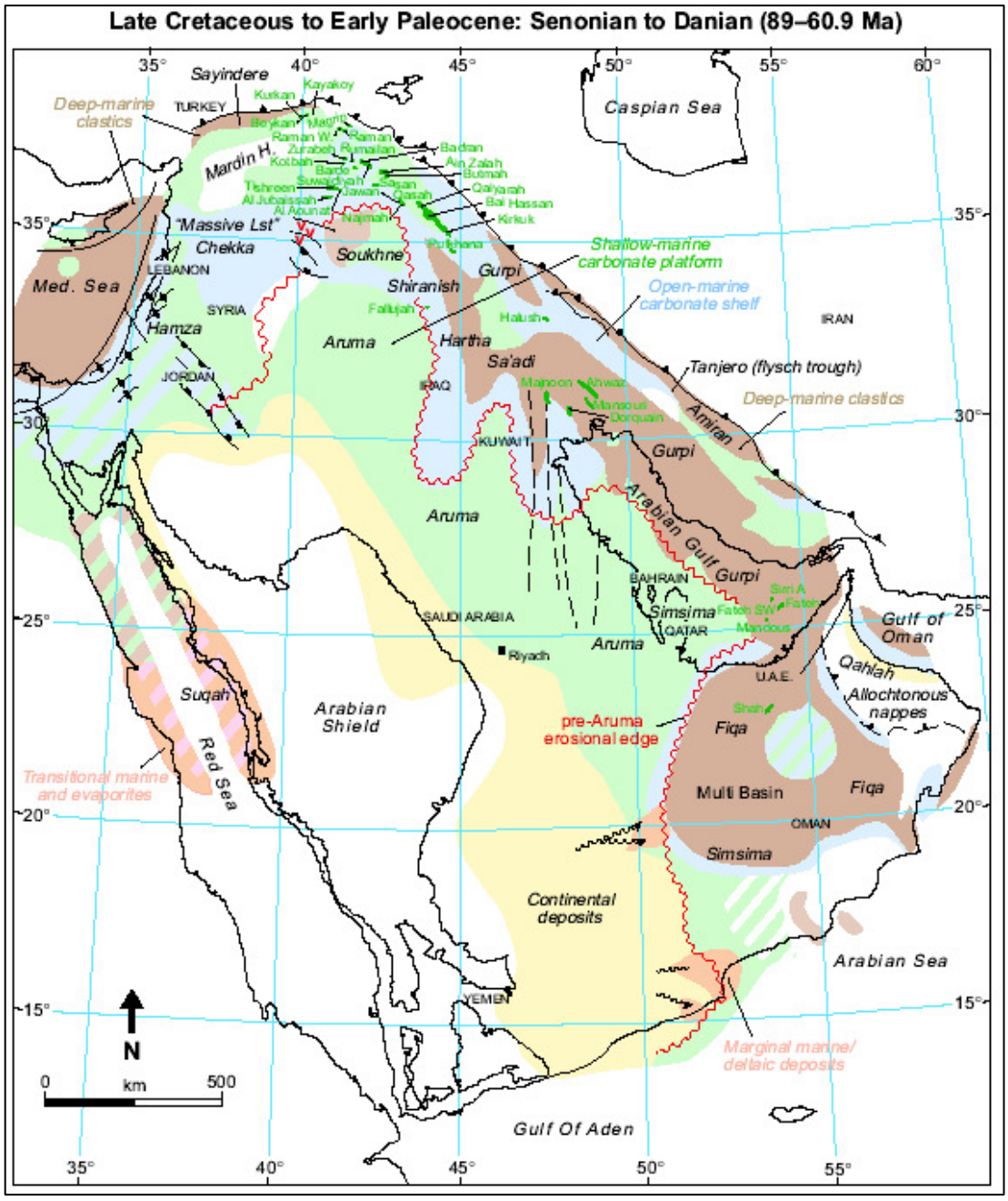

Figure 2.7: The regional geology of the Arabian plate showing the carbonate ramps that prograded to the east during the Senonian-Danian (Ziegler 2001).

With respect to compression on the Arabian plate, due to the Semail ophiolite obduction, studies by Al-Barwani & McClay (2008) have suggested the PreCambrian

Ara salt layers have undergone halokinesis and influenced the structures of oil fields in South Oman (Alsharhan 1985, Alsharhan & Nairn 1986). At a giant offshore field, Abu Dhabi, the same suggestion is proposed by Hassan & Wada (1979) where the Cambrian Hormuz Salt Series had diapered beneath the Cretaceous stratigraphy. The same suggestion is proposed by Edwards et al. (2006), that salt diapirs had exploited the eastern portion of the anticlinal trap (Fig. 2.8). Consequently the offshore field shows an asymmetric profile towards the East (Edwards 2006, Edwards et al. 2006). Halokinesis does not appear to have effected trap formation during the deposition of the Fiqa Formation in the Campanian (85-63Ma: At Al-Huwaisah, Oman: Sharland et al. 2001), but has influenced the structure post-Fiqa times. This is the reason behind why salt doming is constrained to after the formation of the Oman Mountains and to the Semail Ophiolite obduction at 92Ma. The combination of tectonics and halokinesis caused the formation of several hydrocarbon traps that today determine the positions of onshore and offshore fields around Abu Dhabi (Fig. 2.8).

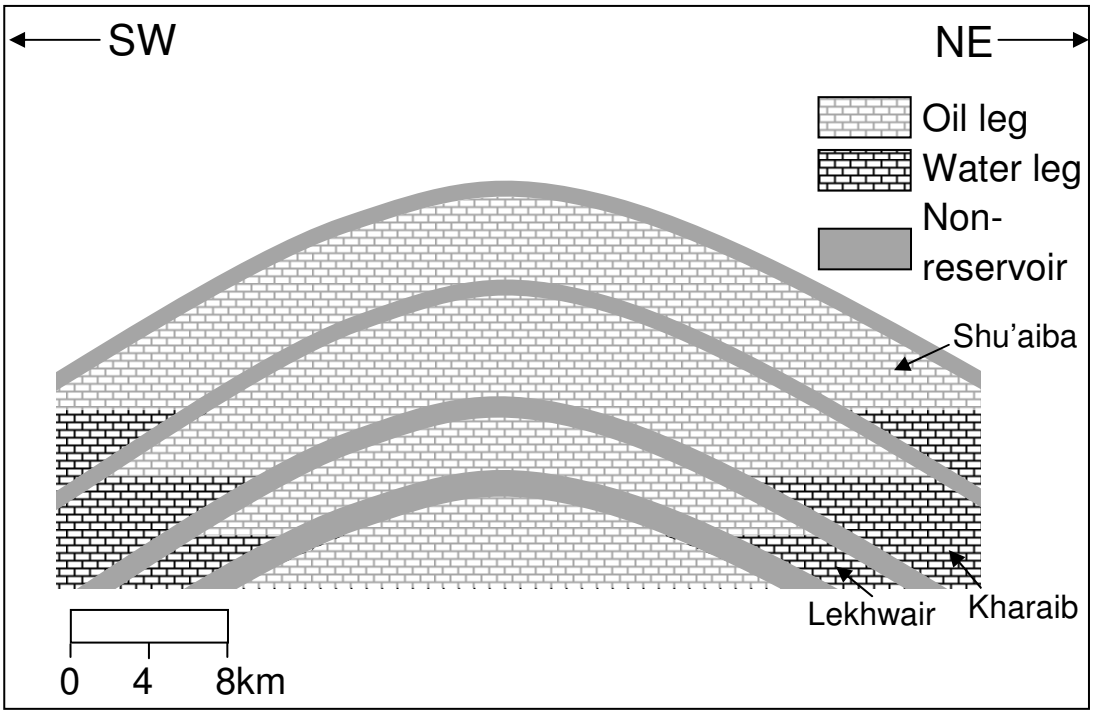

Figure 2.8: a typical oil field formed from tectonics and salt diapirism. The different oil water contacts for the Shu'aiba, the Kharaib and the Lekhwair Formations (Based on Grötsch et al. 1998).

The offshore field is overprinted by a rhombohedral fault array, which is composed of two sets of faults (one trending NE-SW and the other trending NW-

SE), which have been caused by basement movements related to mountain building events (Oman Mountains, Zagros orogeny) (Edwards et al. (2006): i.e. these faults have opened during uplift and the formation of the anticlinal trap.

2.3 Oil charge

There are three main oil charge models that can be applied to this offshore field and to the Lekhwair and Lower Kharaib Formations: 1) the migration of oil from the east and the Bab Member into the offshore field, 2) the migration of oil from the Jurassic below and 3) an internal source for oil. Each possibility will be outlined and then critically reviewed:

1) The first suggestion is that oil charge had entered these fields during trap formation (Gumati 1993, Taher 1997). This suggestion also presumes that oil had migrated great distances from the Bab Member (basinal Shu'aiba Formation) in the East into many traps within the Abu Dhabi region (Gumati 1993, Milner 1998, Taher 1997). This suggestion is based upon where the most likely sources for oil would have been generated (in 'thermal kitchens'), by the thermal maturation of oil, through progressive burial. The geothermal gradient was calculated by Gumati (1993) by using 116 bottom hole temperatures, from core wells, to yield an average of 36°C/km. Combined with the Thamama Group formation ages, the Lekhwair Formation had not reached the oil generation threshold until 40Ma in the Eocene (Gumati 1993). A similar conclusion was reached by Taher (1997) by also using present day reservoir temperatures. A geothermal gradient of 1.5-2.3°F/100ft was calculated and the burial histories of the Shu'aiba, Zakum and Diyab Formations were plotted (Taher 1997). This shows the Bab Member source rocks could not have entered the oil window before the Eocene (55Ma). Main oil charge is therefore constrained by Taher (1997) to the Eocene, after trap formation. The oil would have migrated from the East into the offshore field (Fig. 2.9). Thamama Zone B (Upper Kharaib Formation) would be a good carrier bed for oil (Taher 1997). The Bab Member as a source rock seems a good possibility considering its size and capability of producing a significant quantity of oil capable of filling the structure of the studied offshore field. However a major issue with this model is the distance that the oil is required to migrate from the Bab Basin towards the offshore field, which is in excess

of 150km (Taher 1997). Although, migration could have easily occurred over several million years, it still seems a long way for the oil to travel to become specifically trapped within this offshore field (Fig. 2.9).

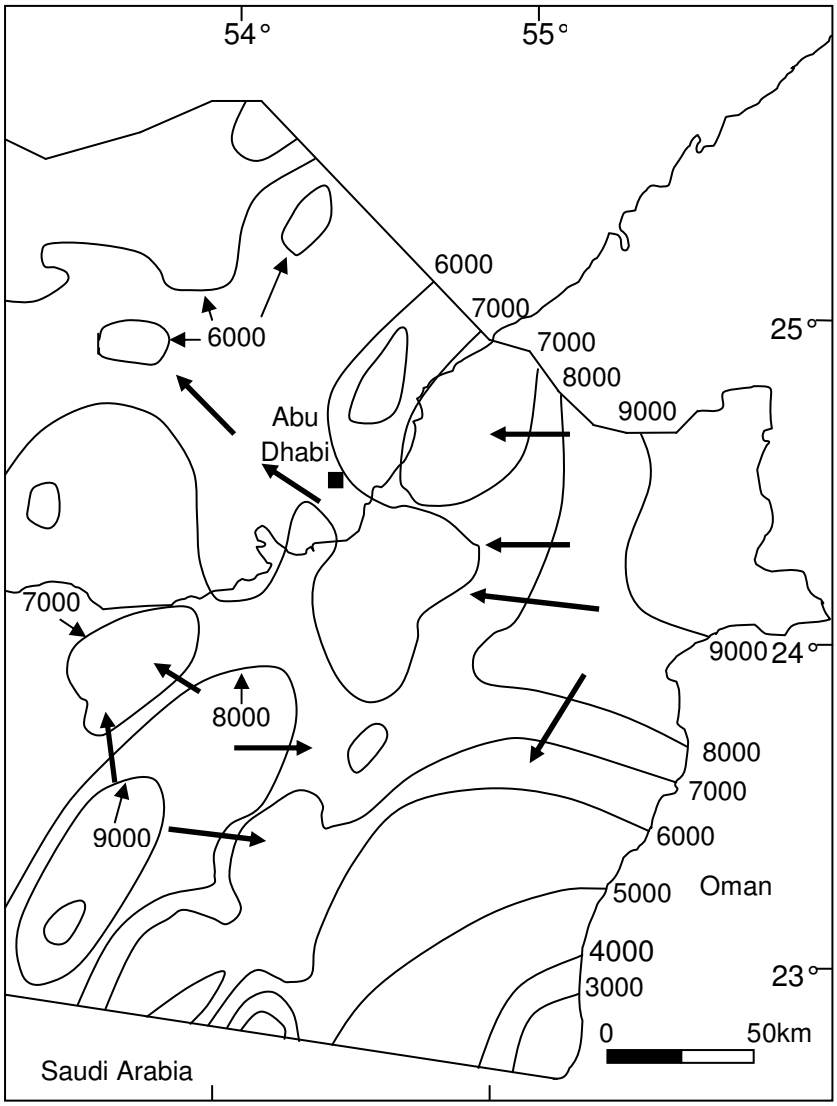

Figure 2.9: The Lower Cretaceous Thamama Zone B (Upper Kharaib Formation) during the Eocene. The oil could have migrated eastwards into many offshore fields (Redrawn from Taher 1997).

2) Within Qatar, and the Diyab Formation, the stacked assemblage of the Hanifa argillaceous limestones, overlain by the Jubaila limestone, followed by the Qatar and Hith Anhydrites, comprises the largest source-reservoir-seal sequence within the Middle Eastern region (Murris 1980). The amount of oil predicted within this sequence was at least 100 x 10^9 bbl of oil of recoverable reserves (Murris 1980). The

area of the source rock (Hanifa Formation) is predicted to cover over 300km from Saudi Arabia, Qatar, U.A.E., and into the Arabian Gulf (Milner 1998). Considering the top of the source rock, the Hanifa Formation, is roughly 400-450m below the base of the Thamama Group (Sharland et al. 2001), in comparison with the migration from the Bab Member, this is a much shorter distance. However the Hith Anhydrite seals the Jurassic source and reservoirs; the Anhydrites need to be broken for the oil to migrate through up into the Lower Cretaceous Thamama Group. However another, more established route is the lateral migration to the north east, into the present day position of the Arabian Gulf (Taher 1997: Fig. 2.10). The oil migrates under the Hith Anhydrite seal until it thins out allowing for the vertical migration up into the Thamama Group (Taher 1997) (Fig. 2.10). The earliest point for oil maturation for the base of the Diyab Formation (Early Oxfordian ~160Ma: Sharland et al. 2001) is 85-90Ma and the Early Turonian-Coniacian (Gumati 1993, Taher 1997): oil migration could have occurred just prior to the Semail Ophiolite obduction at 92Ma.

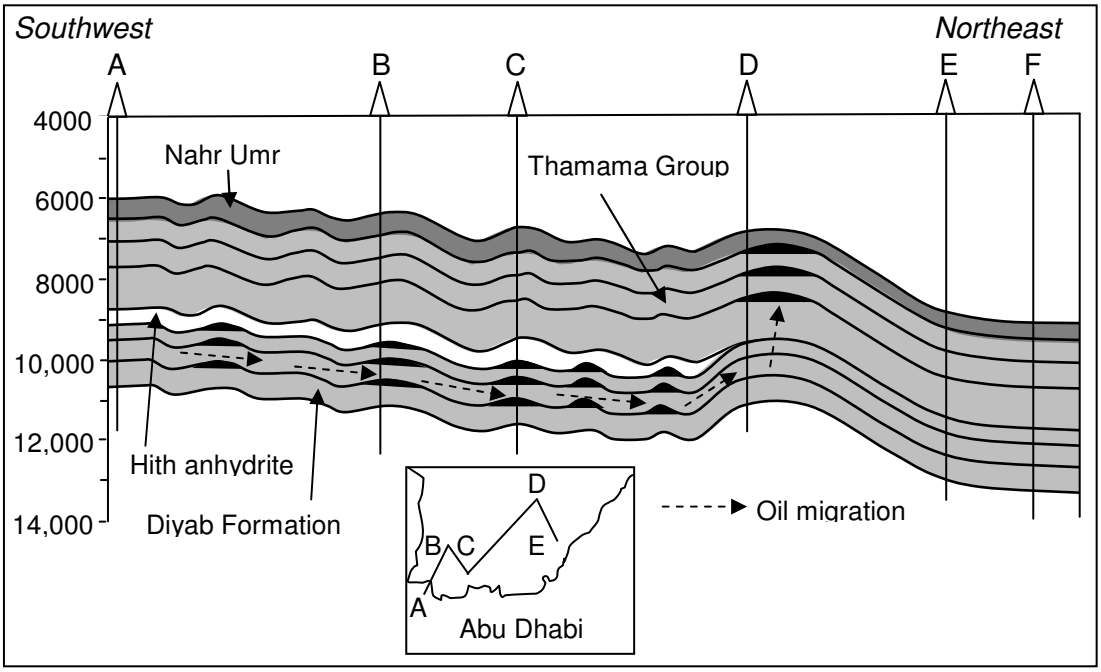

Fig. 2.10: The lateral migration of hydrocarbons from the Jurassic Hanifa Formation under the Hith Anhydrite to the point where the seal disappears allowing for vertical migration up into the Thamama Group (Taher 1997).

3) A review of many oil fields globally, by Wilson (2005), shows the migration of hydrocarbons into traps would be difficult considering that traps are surrounded by impermeable barriers. For traps to work, and keep oil within their structures, the

impermeable barriers need to be unbroken: this would also prevent any fluid from entering the structure. For example, many fields that lie in succession along oil migration pathways are water-bearing: the Katy gas field near Houston is adjacent to later formed San Felipe and Hockley domes that are both water-bearing (Wilson 2005). Another example in the Middle East shows an absence of hydrocarbons over the Qatar Arch, which separates two oil kitchens. The timing of structural formation clearly determines an oil field: once the trap has formed it is impermeable to any future hydrocarbon migration (Wilson 2005). Within the Piper field in the North Sea, and the Northeast Thompsonville field on the Texas Gulf Coast, cementation had sealed the porosity below the oil and gas water contacts (Wilson 2005). Further oil migration into this structure, after cementation, would therefore seem impossible: the oil could not migrate through the impermeable cemented flanks. Wilson (2005) therefore suggests the majority of oil is most likely sourced locally, within the trap. There is one major issue with this suggestion and that the offshore field does not appear to have a significant accumulation of a source rock for the volume of oil trapped within the structure; i.e. it does not have an expanse equivalent to the Bab Member in the east and the Jurassic source rocks below.

With respect to the timing of oil charge, within the Thamama Group, oil charge was relatively early in comparison with the majority of burial spar formation and stylolitisation (Neilson et al.1998). This relationship lead Neilson et al. (1996) to suggest that initial oil charge within the Thamama Group had occurred in the Upper Cretaceous, which supports studies by Alsharhan (1989) and Burruss et al. (1985). There is evidence to show that oil was emplaced before the maturation and migration of oil in the Bab Member from the East. Other Thamama Group reservoirs, including the Kharaib Formation around Abu Dhabi, show burial cements devoid of oil inclusions: oil charge could have occurred later after burial spar formation in the Early Tertiary (Neilson et al. 1996; 1998), which supports studies by Gumati (1993) and Taher (1997). Another possibility presented by Neilson et al. (1998) is oil charge arrested all cementation, preventing any burial cements forming, and therefore no oil inclusions were trapped within any cements. Therefore there may have been at least two main phases of oil charge in the Arabian Gulf; initial oil charge within the Late Cretaceous and main oil charge within the late Eocene (Neilson et al. 1996).

2.4 Chronostratigraphy: Facies verses time on the Arabian plate

Compiling a chronostatigraphic chart involves many techniques, including lithostratigraphy, biostratigraphy, radiometric dating and sequence stratigraphy. Lithostratigraphy is a technique that divides the stratigraphy according to rock type and faunal successions. The major issue with this technique is lithostratigraphic units can contain many packages of sediments representing different events. In other words lithostratigraphy does not necessarily define single isochronous sediment packages.

Biostratigraphy is a technique used to determine a relative age of a lithology or lithofacies when particular taxa occurrence overlaps surfaces defining sedimentary units (SB's/MFS's). This occurrence may overlap a particular surface at many locations across a terrane; the taxa inception and extinctions (Biozones) are used to correlate the surface. However, the inception and extinction of particular taxa may occur at different points in the substratum. To solve this issue the position with the most constrained taxa inception/extinction is used as a tie point (Fig. 2.11). The age range at this location is then correlated to all other occurrences across the terrane.

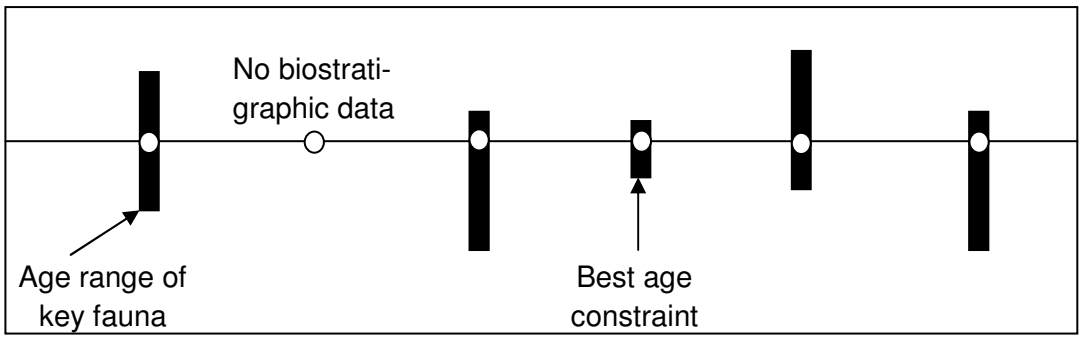

Fig. 2.11: Using tie points to correlate the relative age of a particular surface across a terrane (redrawn from Sharland et al. 2001).

However there can be many issues when creating a biostratigraphic sequence involving information from previous literature; 1) the taxa may be wrongly identified, 2) fossils may be given an incorrect age estimate based on lithological correlation, 3) there may be problem sequences that have little taxa providing fine

enough age resolution and 4) previous literature may not have good enough taxa descriptions to allow for relative age estimates.

Absolute ages are defined by radiometric dating on tuffs, ash beds, intrusives and glauconites. These beds need to intersect well constrained biozones. This technique is reliant on volcanic beds or glauconite being present within the stratigraphy, and within well constrained relatively aged biozones (Fig. 2.12). The age estimates may also not always correspond to the relative ages. Radiometric dates from glauconites tend to provide younger ages, in comparison with dates from volcanic and intrusives (Harland et al. 1990). For this reason Davis et al. (2002) and Sharland et al. (2001) has not used radiometric dates from Haq et al. (1987), who has included glauconites, but instead used Grastein & Ogg (1996) who has only used igneous sourced radiometric dates.

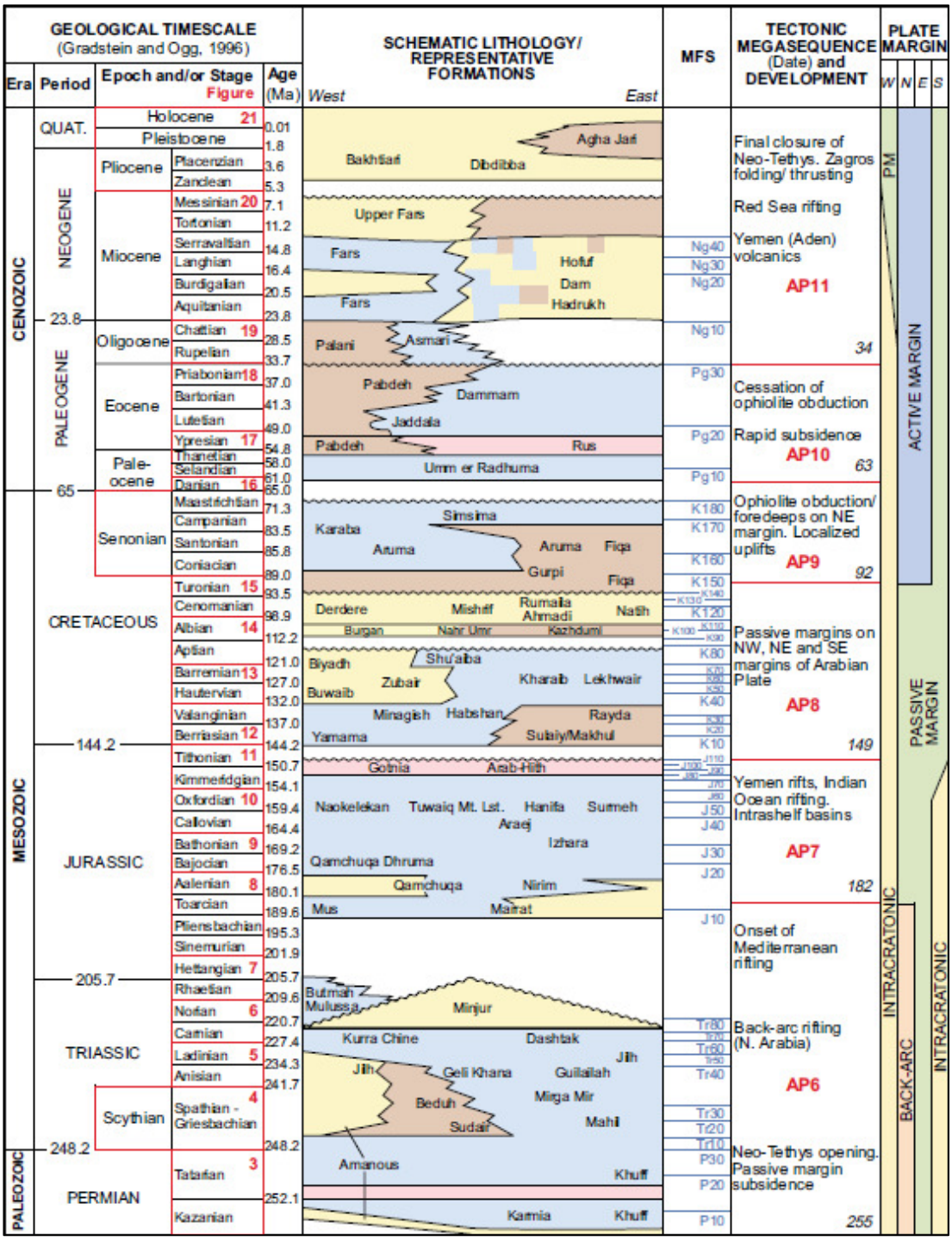

Figure 2.12: Chronostratigraphic chart of the Arabian plate from the Permian to Modern day showing the compilation of lithostratigraphy and radiometric dating. The Thamama Group is the lower half of AP8 (Zeigler 2001).

Sequence stratigraphy is the grouping of sediments into packages that define eustatic changes in sea level/ subsidence/sediment supply, providing information

about accommodation space. Unlike lithostratigraphy, Sequence stratigraphy involves the correlation with time equivalent units to define isochronous sediment packages. There are two main ways for correlating the stratigraphy using sequence stratigraphy: 1) using SB's and 2) using MFS's.

Studies by Vail et al. (1977) have used SB's to define 'depositional sequences' because: 1) these surfaces define packages of sediment representing continuous deposition, 2) they can be easily recognised in the stratigraphy of rift basins and passive margins (on seismic profiles; Sharland et al. 2001) and 3) can be used to determine the bathymetric geometry of a sedimentary basin. However SB's represent a time gap at proximal locations; in many cases the actual surface is eroded away. Therefore dating a sequence boundary is problematic; the surface will range in age from the older incised sediments beneath and the overlying younger sediments. This also means that due to deposition still occurring in the deep basin, many SB's (with its correlative conformity) are diachronous.

Galloway (1989) has used MFS's to define Genetic Stratigraphic Sequences (GSS). The reasons are; 1) the MFS represents a period of non-deposition, 2) it represents the maximum flooding surface at all points in the basin, and therefore is isochronous, 3) marks the point of major sediment reorganisation in the basin (Galloway 1989) and 4) MFS's can be easier to date: includes the combination of Gamma ray log Maxima, condensed strata, signs of non deposition (bioturbation) and a narrow range of deep water pelagic foraminifera. However an issue using MFS's is the GSS's will contain SB's and unconformities and therefore do not represent continuous deposition. However by using MFS's to define GSS's, the time gaps can be added as empty space, between the sediment packages within a sequence stratigraphic framework; and will therefore provide better estimates of the time gap extents. This cannot be accurately achieved using the method by Vail et al. (1977).

2.4.1 Chronostratigraphy for the Thamama Group

Considering that many chronostratigraphic markers are related to major changes in sea level, Simmons et al. (2007) suggests there is a nature link of sequence stratigraphy with chronostratigraphy. This possible link becomes very useful with the

stratigraphy of the Arabian plate at Abu Dhabi, considering the cyclic nature reservoir and non reservoir units are results of sea level change. These links have been demonstrated by Sharland et al. (2001), Davis et al. (2002); they have correlated major shifts in sea level (3rd order MFS's) with absolute ages. These absolute ages are referenced to the timescale outlined by Gradstein & Ogg (2004). The dates are based on radiometric dating which are integrated with the biozones, and magnetic polarity reversals (Gradstein & Ogg 2004). The benefit of using MFS horizons is they can be biologically calibrated in terms of age (with respect to their reference section) and they were laterally extensive (Fig. 2.11) (Sharland et al. 2004). Studies from Sharland et al. (2001), which are updated by Davies et al. (2002) and Sharland et al. (2004), have divided the Arabian plate stratigraphy into Genetic Stratigraphic Sequences (GSS): i.e. the stratigraphy is separated into distinct isochronous units, which all contain progradational, aggradational and retrogradational sequences, that are genetically related across the Arabian plate (Galloway 1989). The main reason for using this technique (in comparison with SB's) is the 'layer cake' geometry of the majority of sediments across the Arabian plate makes the identification of SB's difficult on seismic lines. Work form Sharland has been updated by Davis et al. (2002) which is displayed in Figure 2.13.

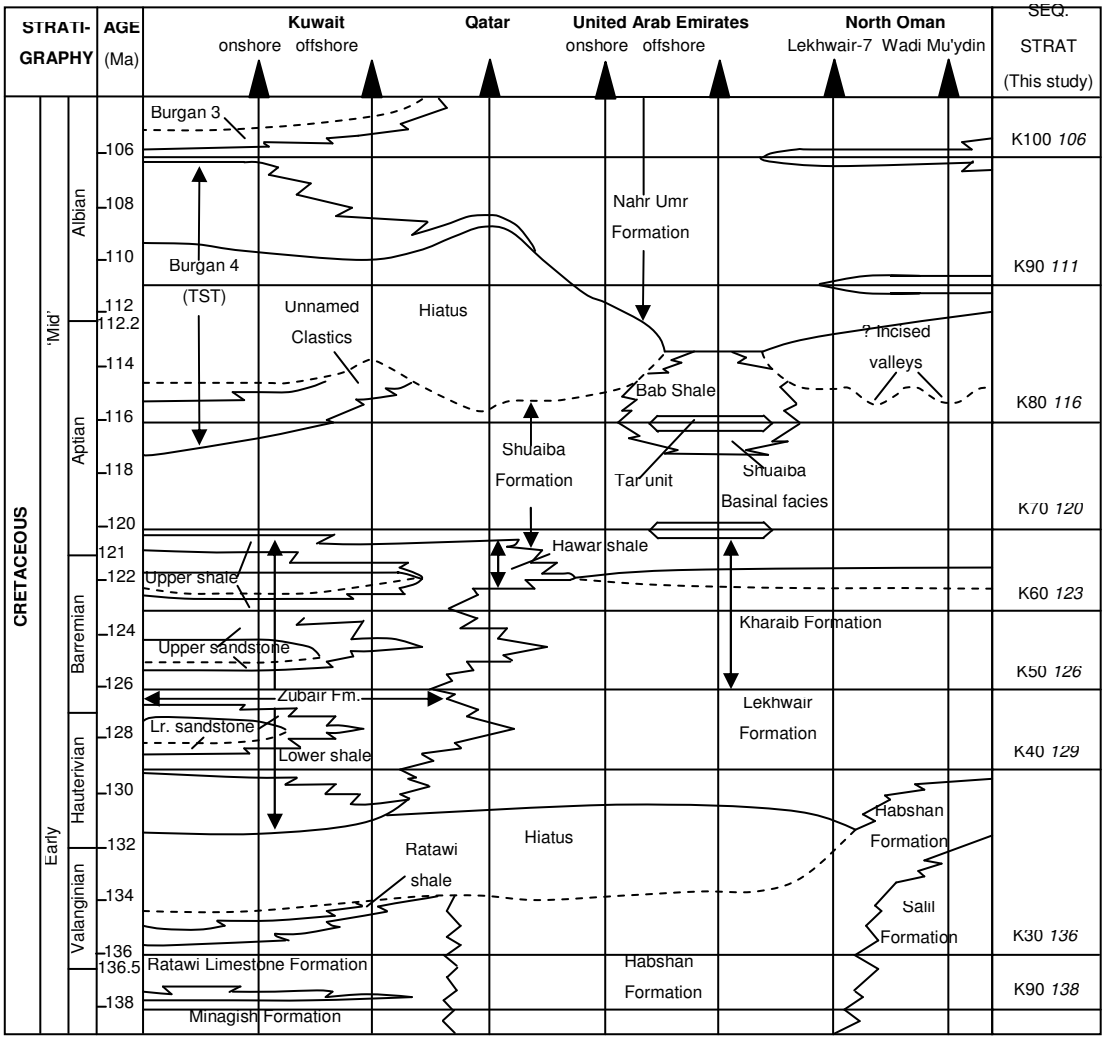

Fig. 2.13: A chronostratigraphic chart of the Lower Cretaceous between Kuwait and North Oman (dashed lines represent unconformities (redrawn Davis et al. 2002)

There are six Maximum Flooding Surfaces (MFS's) that are correlated across the Arabian plate which relate to 3rd order MFS's and are termed K40 (129Ma), K50 (126Ma), K60 (123Ma), K70 (120Ma), K80 (116) and K90 (111Ma) (Davis et al. 2002, Sharland et al. 2001) (Fig. 2.13). Therefore the Kharaib and Lekhwair Formations at Abu Dhabi were deposited between the Upper Hauterivian to Lower Barremian (124-120Ma: Davis et al. 2002, Sharland et al. 2001) and the mid Valanginian to Upper Hauterivian (129-124Ma: Davis et al. 2002, Sharland et al. 2001), respectively (Fig. 2.13).

Chapter 3

Depositional modelling

The Thamama Group is 'layer cake' comprising of laterally continuous High Frequency Cycles (HFC's) within the giant offshore field, Abu Dhabi. This is also demonstrated in Fig. 3.1 from another giant onshore field, within U.A.E. (Strohmenger et al. 2006) which has the Lekhwair and Kharaib reservoirs highlighted. All reservoirs are continuous and have uniform thickness across the structure (Strohmenger et al. 2006). Each HFC contains a transgressive (argillaceous mudstone/burrowed wackestone) and highstand (rudist and *Lithocodium/B.* pack-grainstone) component; the lowstand portions are missing from each HFC.

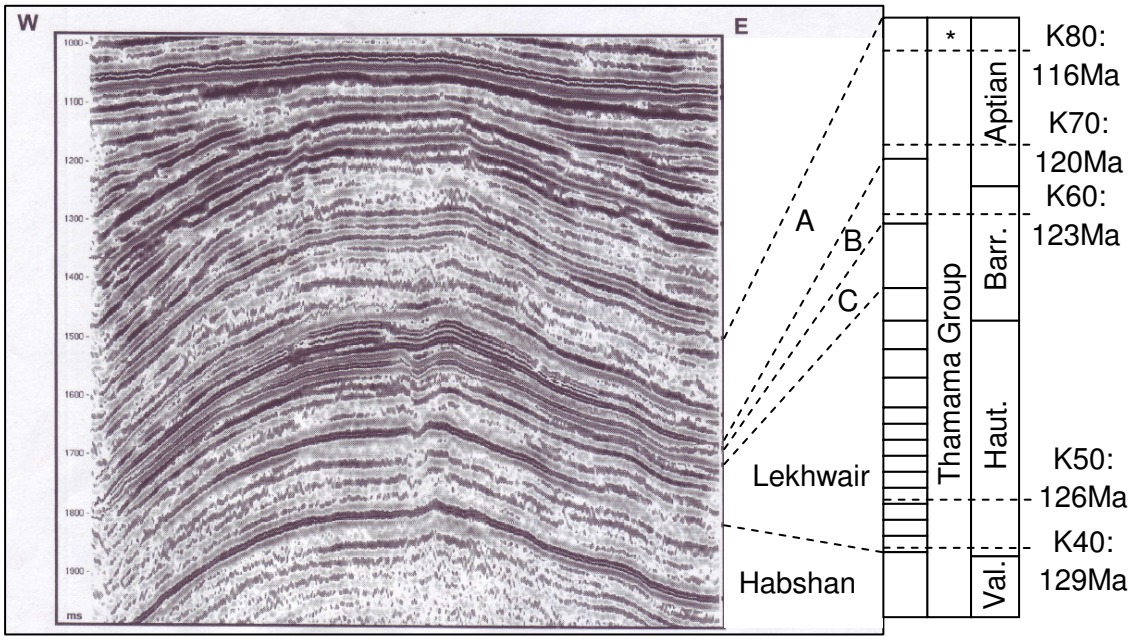

Figure 3.1: The layer cake stratigraphy of the Thamama Group across a giant onshore field, U.A.E (Strohmenger et al. 2006). The dates and stratigraphy on the right are from Davis et al (.2002). A represents the Shu'aiba Formation, B represents the Upper Kharaib Formation and C represents the Lower Kharaib Formation. * represents the column for 4th order HFC's

Now the Thamama Group architecture is established, the next step is to identify the boundaries of each HFC: i.e. the Sequence Boundaries, followed by the MFS's, to form a sequence stratigraphic framework. As this framework will only stretch for 20km, and is restricted to one particular field, determining the sequence boundaries/MFS's on seismic can be difficult (Sharland et al. 2001) and therefore seismic profiles have not been used. For the level of detail required for this study, only core information is regarded; consequently the sequence boundaries are easily recognised from the transition from rudist rich pack-grainstone overlain by argillaceous muds and shale. A further discussion is present in Sections 4.3 regarding the SB and MFS placements, which includes using the fossils, the lithologies and the sedimentary features within the upper and lower most portion of each HFC to pin point the SB's.

Outlining the general architecture of the Thamama Group provides the reader with a preamble to the HFC cyclicity, so the context of lithological description and macro/microfossils abundances, within each HFC can be understood. This Chapter therefore assumes the 'layer cake' nature of the Lekhwair and Lower Kharaib Formations, and the SB and MFS placements outlined in Section 4.3, and involve constraining the detailed lithological and faunal/floral descriptions within each HFC. This Chapter describes the lithological and biodiversity changes within each HFC. Patterns and repeatability of both lithology and biodiversity are established. The highstand and transgressive components are associated with particular lithologies and fossil abundances, providing an understanding of the changing environment within each 4^{th} order HFC.

Considering that, to some extent, the pore heterogeneity of the Lekhwair and Lower Kharaib Formations are a product of their depositional environment (and the resulting sediments being deposited within that environment), this chapter will also associate particular lithologies, biodiversities, and palaeo-environments, with the most open pore systems of the Lekhwair and Lower Kharaib Formations. In order for future understand the porosity and permeability relationships, regarding diagenetic overprints of the depositional pore systems, a detailed account of the lithological

successions is also required within the water leg, transition zone, and the oil leg, across the entire offshore field.

Debate exists about specific fossils and their preferred environments of habitation. Several species are reported to represent many different environments: *Lithocodium/Bacinella* and *Palorbitolina lenticularis* are attributed to both shallow and deep water environments by separate authors. To solve this issue, an assessment of Thamama Group biostratigraphy, along with a list of key fossils and their suggested habitats within the Lower Cretaceous, is presented.

The Lower Kharaib Formation was studied previously within the literature. The Lekhwair Formation has received little attention regarding its deposition and fossil successions: this is the first detailed study focused on both these aspects. Observations are compared with previous depositional models for the Lekhwair, Kharaib and Shu'aiba Formations to provide a state-of-art detailed understanding of the depositional environments attributed with both the Lower Kharaib and Lekhwair Formations.

Sample coverage includes five wells along a single southwest to northeast transect and the water leg, transition zone, and the oil leg, from the giant oil field, offshore Abu Dhabi, U.A.E. (Section 1.2). Detailed petrographic information was gathered from sections cut from core samples. Manual counting of fossil abundances is the main dataset supporting the biota successions through each 4^{th} order HFC (Appendix 1A-1E). For each sample, information on the lithology and the fossil abundance are used to develop an environment of deposition: constituting a lithofacies. These lithofacies are then ordered with respect to their position found within the succession and to the 3^{rd} and 4^{th} order HST's and TST's. This provides a relative sequence of environment change through each 4^{th} order HFC. The environments of deposition for many species including *Lithocodium/B.* and *P. lenticularis* are therefore based upon the bounding lithological units and fossil successions. The succession of lithofacies is used to develop three separate depositional models for the Lower Lekhwair, Upper Lekhwair and the Lower Khariab Formation. For further information on the application of 4^{th} and 3^{rd} order HST's and TST's, within the Lekhwair and Lower Kharaib Formations, see Sections 4.2, 4.5 & 4.6: Figs. 4.7-4.11, 4.13 & 4.14.

3.1 'Thamama Group' Biostratigraphy

The biostratigraphy, presented by Simmons (1994) for the Kahmah Group in the Central Oman Mountains, is based on the graphical correlation technique initially outlined by Shaw (1964). The method plots two outcrop sections (x/y plot), with one being the Composite Standard Reference Section (CSRS) (on the x axis) against another section (y axis). The CSRS is then equally divided into Composite Standard Time Units (CSTU's). The inceptions and extinction points of the taxa are plotted and the Line of Correlation (LOC) is then determined graphically through these data points, by making sure that the taxa inceptions lie to the left and the taxa extinctions lie to the right (i.e. creating a 'line of best fit'). The LOC must also cross time significant sedimentological features (hardgrounds) and isochronous events (ash beds). The CSTU'S of the CSRS are then correlated across to the other outcrop section on the y axis via the graphically determined LOC. The two outcrop sections used to compile the biostratigraphy of the Central Oman Mountains (Fig 3.2) are Wadi Mi'Aidin section (CSRS) against the Jebel Madar section (Simmons 1994). The determined range between the taxa inceptions and their extinctions forms the biozones seen in Figure 3.2 (Simmons 1994).

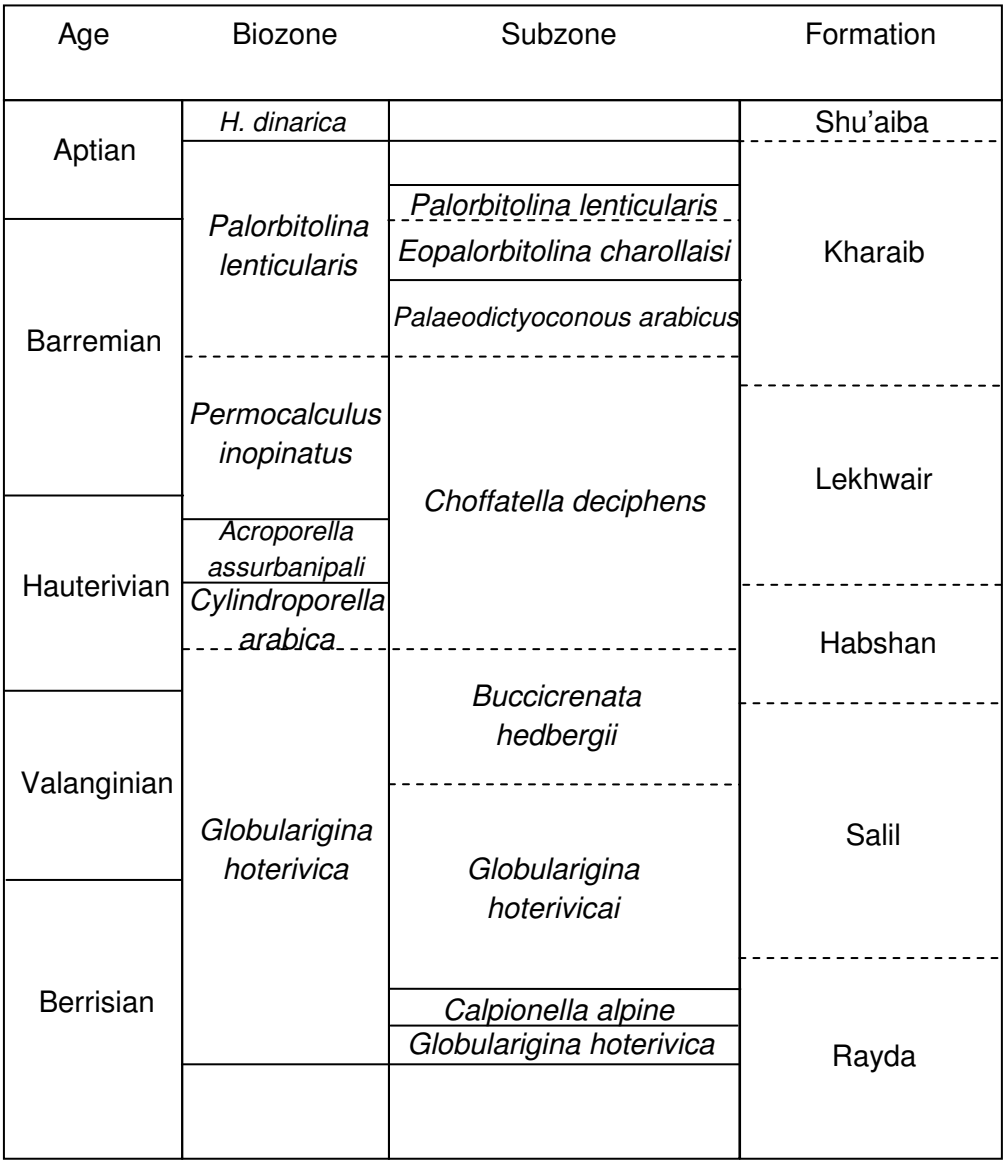

Figure 3.2: The biostratigraphy of the Thamama Group of the Central Oman Mountains. The Lekhwair Formation is defined by three species of algae, while the Kharaib Formation is defined by Orbitolinidae; especially P lenticularis and C deciphens H. dinarica stands for Hensonella dinarica *(Redrawn from Simmons 1994).*

The 'Thamama Group' biostratigraphy includes many species of dasycladacean algae (Simmons 1994). The Lower Lekhwair is dominated by the dasycladacean algae *Accroporella assurbanipali* while the Upper Lekhwair is dominated by *Permocalculus inopinatus* (Fig. 3.2) (Simmons 1994). The Lower Kharaib Formation is dominated by the benthic foraminifera *Palorbitolina lenticularis* (Fig. 3.2) (Simmons 1994).

3.2'Thamama Group' biota

Glossomyphorus Costatus

The dominant species of rudist present within the Lekhwair and Lower Kharaib Formations is *Glossomyphorus costatus*. Immenhauser et al. (2005) associates *G. costatus* with nutrient rich conditions: this is based on the assumption that rudists, unlike scleractinian corals, did not have a symbiotic relationship with photosynthetic algae and instead filter-fed on phytoplankton that thrived during mesotrophic conditions (Johnston et al. 2001, Mutti & Hallock 2003). However there is no evidence to support this claim. *G. costatus* is a caprotinid and is labelled by Gilli et al. (1995) as an elevator rudist. Rudists are considered by Gili et al. (1995) as sediment dwelling sessile aclonal suspension feeders. Within coral associations, several coral species bind together for stability, towards waves and current action, to form a framework (superstratal growth fabric), whereas rudist associations have growth fabrics that develop at the same rate as sedimentation ('*constratal*' growth fabric) (Gili et al. 1995). Their presence in the Cretaceous is therefore not necessarily determined by nutrient fluxes, but by the availability of sediment for elevator rudists to anchor themselves into the sea bed (Gilli et al. 1995). Unlike coral reefs, lithosomes of rudists such as *G. costatus* do not produce frameworks and therefore should not be labelled as 'reefs of the Cretaceous' (Gilli et al. 1995).

G. costatus is associated with *Palorbitolina lenticularis*, *Debarina hahounerensis*, *Praechrysallidina infracretacea*, *Vercosella arenata*, *Lithocodium/aggregatum*, *Coptocomplyloden lineolatus* and *Salpingoporella dinarica* in the Shu'aiba Formation within the Saybah Field, Saudi Arabia (Hughes et al. 2000a). This association is used by Hughes (2000b) to suggest a depth range of 5m-20m (Banner & Simmons 1994) within shallow water, bathymetric highs on the sea bed, within lagoons and protected back- barrier environments for *G. costatus* (Skelton 1997).

Lithocodium/Bacinella

The association of *Lithocodium/Bacinella* is still not fully understood. As there are no direct modern day analogues and there is ambiguity about *Lithocodium/Bacinella*.

One suggestion considers *Lithocodium/ Bacinella* as an association of at least two different species (Leinfelder et al. 1993): *Lithocodium aggregatum* being the surrounding lofusiid foraminifera (the alveolar wall structure of *L. aggregatum* is similar to other lofusiid foraminifera: i.e. *Pseudocyclammina lituus* and not codiacean algae), and *Bacinella irregularis*: a benthic foraminifera (Immenhauser et al. 2005, Schmid & Leinfelder 1996). The *L. aggregatum* can display internal dissolution features representing partially dissolved shells: therefore Schmid & Leinfelder (1996) suggests that *L. aggregatum* encrusts shells and uses them as a basal wall. *L. aggregatum* shows its internal chambers increasing in size from the centre towards the outer walls of the organism, along with the chambers themselves arranged in a coiled fashion (similar to lofusiid foraminifera: i.e. *Pseudocyclammina lituus*) (Schmid & Leinfelder 1996). Therefore Schmid & Leinfelder (1996), suggest in the juvenile stage the *L. aggregatum* grows into a coiled structure and irregular shape giving the organism potential to form oncoids and crusts, and uncoils into the adult growth stage. An epiderm of alveolar structures represents *L. aggregatum* and the adult form of the lofusiid foraminifera, which is thought to support photoautotrophic symbionts (Fig. 3.3). The phrenotheca structures cross-cutting *L. aggregatum* are thought to belong to *Bacinella irregularis*: the presence of the phrenotheca determines the association *Lithocodium/B.* (Schmid & Leinfelder 1996) (Fig. 3.3).

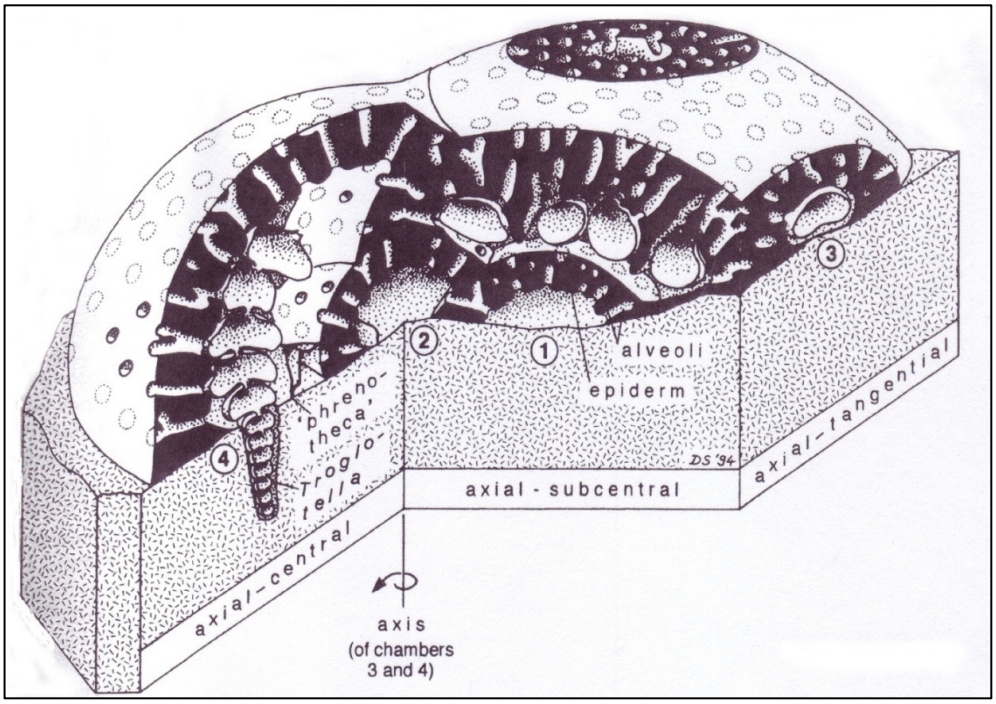

Figure 3.3: The structure of the Lithocodium/Bacinella *(Schmid & Leinfelder 1996).*

Another alternative by Banner et al. (1990) suggests that *Lithocodium/Bacinella* initially grows and encrusts sponge skeletons and other objects such as *Rivularia sp.* and grew in stages, forming several cortices and medullas. The final thickest outer wall covers poorly calcified "vacuolated" medullas (Banner et al. 1990). Due to it not showing any erosion or abrasion, suggests no transport had occurred after formation: i.e. it has been sufficiently buried by the surrounding sediment to prevent reworking (Banner et al. 1990). The *Lithocodium* lacks a filamentous medulla while the *Bacinella* also lacks any cortical structures and is instead formed of irregular arranged "medullary" filaments (Banner et al. 1990). This may be a consequence of only partial calcification of the skeleton; i.e. parts of the skeleton are completely dissolve and missing (Banner et al. 1990). *Lithocodium/B.* is found within the reservoirs, and not the non-reservoir intervals; this has implications as the internal chambers of the *Lithocodium/B.* add to the intra-particle porosity and may determine primary reservoir quality in Thamama Group carbonates (Banner et al 1990).

Preferred habitat of Lithocodium/Bacinella

Lithocodium/B. has been readily observed within micritic matrices suggesting that it preferred lower water turbidity's and palaeo-currents sufficient to allow for argillaceous material to be deposited; i.e. *Lithocodium/B.* would have formed in waters deeper than inner-shelf settings (Banner et al. 1990). Combined with the lack of association with shallow water Codiacea (*Salpingoporella*) suggests *Lithocodium/B*, prefers "warm, fully marine, well oxygenated, calcium carbonate rich, mid-shelf seas" (15-60m) (Banner et al. 1990).

Studies by Banner & Simmons (1994) and Jones et al. (2004) have revised the palaeodepth estimates for *Lithocodium/B.* of 2.5-40m water depth with algae such as *Permocalculus sp*. These palaeodepths are based on modern day photosynthetic algae, and the known amounts of light they require in the water column to survive.

Within the Lower Aptian sediments of Oman, *L. aggregatum* and *Lithocodium/ Bacinella* are present: both bind the lithology forming irregular stromatolite and thrombolite nodules that alternate with rudist rich deposits (Immenhauser et al. 2005). A shared assumption of Immenhauser et al. (2005), Johnson et al, (2001) and

Mutti & Hallock (2003) is rudists filter-fed on phytoplankton which flourished under mesotrophic conditions. Conversely an increase in phytoplankton in the water column would reduce the light conditions required for corals with algal symbiotic relationships. Therefore the absence of corals with *Lithocodium/B.* suggests that these 'algal-foraminiferal reefs' prefer mesotrophic-eutrophic conditions (Immenhauser et al. 2005). The reason for Immenhauser et al. (2005) identifying an algal component to *L. aggregatum* and *Lithocodium/B.* is unclear.

In the Barremian-Aptian Lower Shu'aiba Formation of Oman, *Lithocodium/B.* is also observed by Pittet et al. (2002). Schmid & Leinfelder (1996) suggest that *Lithocodium* readily agglutinates detritus, and can display many incorporated siliciclastic grains. This suggests that *Lithocodium/B*. can tolerate siliciclastic input, but not direct clay input (Pittet et al. 2002, Leinfelder et al. 1993, Schmid 1996). This association is interpreted by Pittet et al. (2002) to represent well oxygenated, shallow water, mesotrophic environments. *Lithocodium/B.* is also associated with slightly deeper subtidal-intertidal environments in front of the rudist wave-influenced shoals (Pittet et al. 2002).

Studies on the Shaybah Field, Saudi Arabia from Hughes et al. (2000b) generally place *L. aggregatum* in lagoonal facies behind the main shoals of *G. costatus*. However there are local areas of *L. aggregatum* with microsolenid corals. Hughes (2000b) associates the microsolenid corals to heterotrophic feeding, reduced light levels and deeper waters. These associations may represent localised deeper water conditions or areas affected by episodic debris brought in from storms, which is consistent Pittet et al. (2002) view that *Lithocodium/B.* can tolerate siliciclastic input (Pittet et al. 2002).

Palorbitolina lenticularis

The Orbitolinidae family are large benthic foraminifera with their earliest appearance of *Palorbitolina lenticularis* in the Upper Barremian (Simmons et al. 2000). This family diversifies through the Cretaceous (Simmons et al. 2000). The *Palorbitolina l.* structure is described in detail and consists of discoidal chambers, each separated into fine chamberlets that fan radially about a central complex, and

the megalospheric embryonic apparatus at the top of the organism (Simmons et al. 2000) (Fig. 3.4).

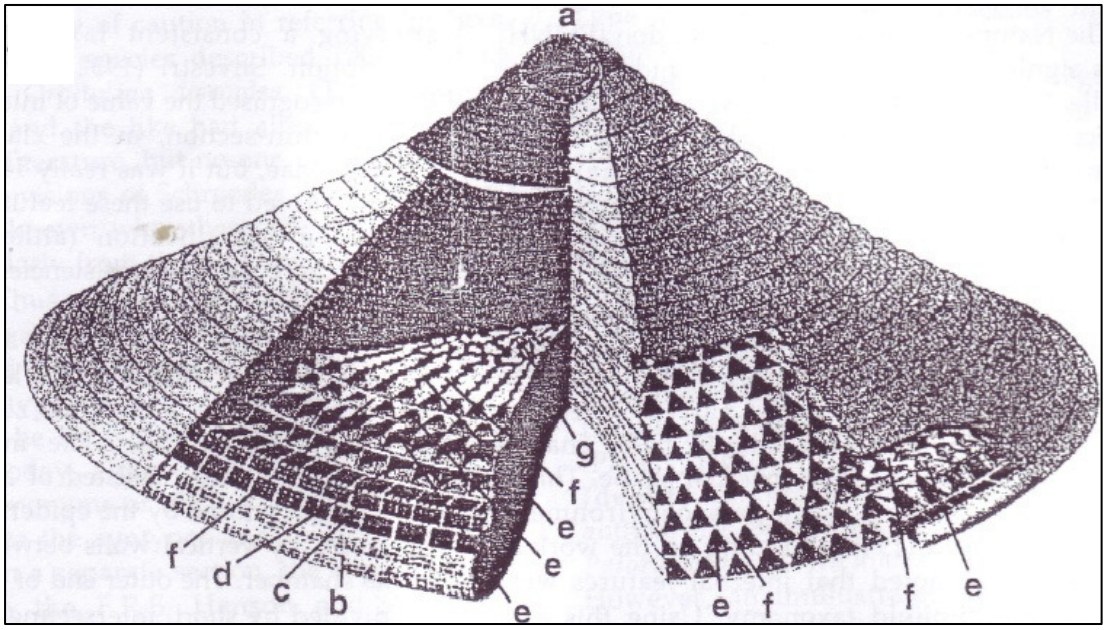

Figure 3.4: structure of Palorbitolina lenticularis*: with a) the megalospheric embryonic apparatus, b) exposed cellules, c) the marginal zone, d) the exposed chamberlets, e) the chamber passages of the radial zone, f) the zigzag partitions of the radial zone and g) the central complex (Simmons et al. 2000).*

The habitat of Orbitolinidae

Many authors regard Orbitolinidae foraminifera to deeper water environments as they exist within dense argillaceous marls, muds and wackestone intervals (Alsharhan 1995, Masse et al. 1997; 1998, Vilas et al. 1995). Within the Lower Kharaib Formation, the appearance of Orbitolinidae in argillaceous limestone, coupled with the intense bioturbation represented by *Thallassinoides,* are the main factors for Pittet et al. (2002) to suggest that large flat Orbitolinidae are representative of low sediment accumulation rates.

Orbitolinidae are suggested by Hottinger et al. (1997) to contain photosymbionts as these organisms only contains lateral chamberlets on their upper surface which can receive sunlight. Evidence for the presence of photosymbionts, and which environment the Orbitolinidae preferred, is based on a Holocene age rotalid *Baculogypsinoides.* This rotalid survives in shallow water, high energy, oligotrophic

environments, on hard substrates, and also contains similar lateral chamberlets to Orbitolinidae, that Hottinger et al. (1997) call 'symbiont greenhouses'. Algal symbiosis provides a physiology for how larger foraminifera survive on shallow carbonate platforms with minimal seasonal nutrient fluxes (Hallock et al. (1985) and why Orbitolinidae are found readily within argillaceous marls, muds and wackestones (Alsharhan 1995, Masse et al. 1998; 1997, Vilas et al. 1995) during low sediment accumulation rates (Pittet et al. 2002).

Within the Barremian-Aptian of North Oman and the Upper Kharaib Formation, Orbitolinidae occur with miliolids, calcareous algae and intense bioturbation in wackestone and packstone, which Hillgärtner et al. (2003) has defined as a shallow open lagoon, marking steady sea level rise and the start of a long term TST. Similarly, abundant *Palorbitolina* species are found in the Aptian of Southeast Spain, within coastal sediments, with small amounts of siliciclasts during TST, which is the main reason for Vilas et al. (1995) to conclude that *Palorbitolina* are indicative of early TST at the end of a terrigenous period. Orbitolinidae rich sediments are considered to serve as indicators for "major breaks in the temporal and spatial evolution of Mid-Cretaceous carbonate platforms" (Vilas et al. 1995). Higher nutrient levels would favour faster growth rates (Vilas et al. 1995) to produce larger foraminifera. This provides as alternative explanation behind why these Orbitolinidae are so large. Instead of *P. lenticularis* growing and increasing its top surface area, which maximises the capture of sunlight though it's algal relationship in oligotrophic conditions (Hallock et al. 1985 and Hottinger et al. 1997), *P. lenticularis* has grown larger because there are more available nutrients in the water column to utilise (van Buchem et al. 2002, Vilas et al. 1995).

In the Kharaib Formation, Simmons et al. (2000) suggests that *P. lenticularis* are tolerant of low light, clay rich, turbid environments. Simmons et al., (2000) also highlights that *P. lenticularis* changes morphology through a shoaling upward HFC from large flat organisms in marly mudstone and the TST, to small conical organisms within packstone, and beds rich in dasycladacean algae and miliolids in the HST. Therefore, based on the associated fossils and the stratigraphic architecture, Simmons et al. (2000) has suggested the changing environment had a morphological

effect upon the *P. lenticularis,* with the large flat *P. lenticularis* dominating during sea level rise (flattest at the MFS's), and small conical forms dominating during reduction of sea level (Fig 3.5). Immenhauser et al. (1999) has also noted abundance in small conical Orbitolinidae prior to the formation of hardgrounds, to high illuminated environments and to sub-aerial exposure. Immenhauser et al. (1999) also links the larger morphologies to above hardground surfaces and to lower illuminated environments. In the Shu'aiba Formation, the same trend is observed by Hughes (2004) as the smaller forms dominate the shallower back-bank environments while the larger forms dominate the deeper open marine environments. Both Pittet et al. (2002) and Vilas et al. (1995) also acknowledge these morphological changes through shoaling upward HFC's.

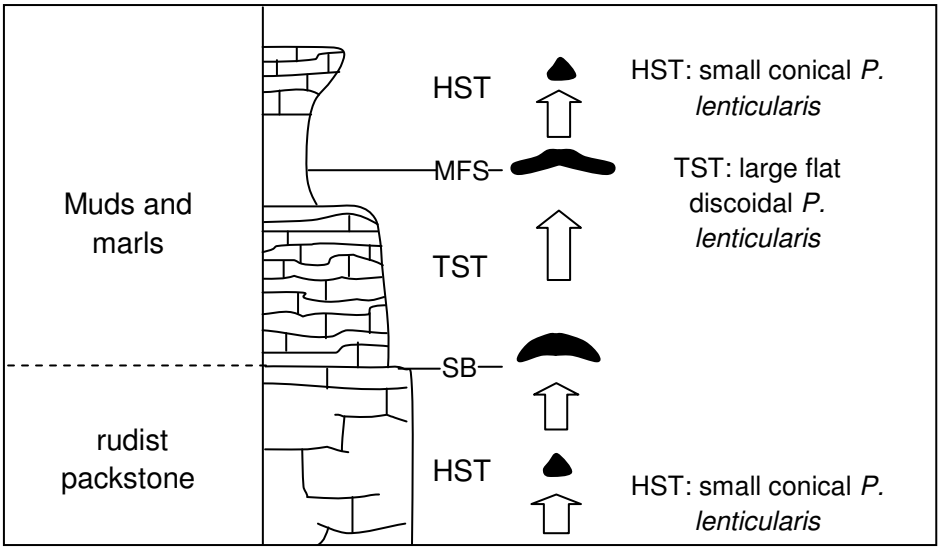

Fig 3.5: A) Abundance of P. lenticularis *morphologies are compared with a 4th order HFC. It shows smaller conical forms dominating within the late HST and larger flatter forms dominating within the TST and early HST within shoaling upward HFC's (redrawn from Simmons et al. 2000).*

Choffatella deciphens

Within the Oman Mountains, at Abu Dhabi, *Choffatella deciphens* is present within the Upper Hauterivian-Barremian and the Kharaib Formation (Simmons & Hart 1987). *C. deciphens* is observed with abundant calcareous green algae in the Upper Lekhwair Formation (Hauterivian-Lower Barremian) which is a reason for

Granier et al. (2003/05) to interpret *C. deciphens* as preferring shallow water environments. However across the Lekhwair-Kharaib boundary and up into the Lower Kharaib Formation, *C. deciphens* is associated with deeper water environments (Barremian) (Granier et al. 2003/05): however Granier et al. (2003/05) does not provide a reason for this conclusion. *C. deciphens* is also associated with deeper water environments (possibly with *D. hahounerensis*, *V. arenata*, *P. infracretacea* and *Lithocodium/a.*) and the TST of the Shu'aiba Formation at the Saybah Field, Saudi Arabia (Hughes 2000b): this is consistent with Jones et al. (2004) associating *C. deciphens* with 20-60m.

Other Foraminifera

The Textulariacea present within the Thamama Group are *Praechrysallidina infracretacea* and *Redmondoides lugeoni*. Both these types of Textulariacea have a conical morphology with the *P. infracretacea* containing several 'broad apatural plate-like flaps' (Banner et al. 1991) to form an internal zigzag pattern when viewed in cross-section, cut down its long axis. The *P. infracretacea* is observed no earlier than the Habshan Formation in Oman (Banner et al. 1991, Simmons & Hart 1987). In the Shu'aiba Formation Hughes et al. (2000a) associates *P. infracretacea* with a deep lagoon because of it was observed with *C. lineolatus, S. dinarica* and *Lithocodium/a.*

The *R. lugeoni* is composed of many internal chambers that are roughly three times broader in comparison with their height (Banner et al. 1991). These chambers become larger upwards and in some cases amalgamate into one large chamber. The first appearance of *R. lugeoni* in the stratigraphic record is the Bajocian (Banner et al. 1991).

Several other benthic foraminifera exist within the Lekhwair and Lower Kharaib Formations, such as *Vercosella arenata* and *Debarina hahounerensis* are attributed by Hughes (2000a) with deep lagoonal environments, whereas *V. arenata*, *D. hahounerensis*, *Bigenerina sp.*, *Nautiloculina brönnimanni* and *Reophax sp.* are associated with lagoonal environments, as they are present within lithologies that cap rudist bank deposits within shallowing upward HFC's of the Shu'aiba Formation (Hughes 2000b). *V. arenata* is also found in the Oman Mountains, by Simmons &

Hart (1987), within Valanginian-Hauterivian lithologies, and within the Upper Lekhwair Formation.

Dasycladacean algae

Key algal species represent specific parts of the stratigraphy in the Kahmah Group, Central Oman Mountains (Simmons 1994). The Mid-Upper Hauterivian (Lower Lekhwair Formation) is dominated by the dasycladacean algae *Acroporella assurbanipali*, whilst the Upper Hauterivian-Lower Barremian (Upper Lekhwair Formation) is dominated by the gymnocodiacid algae *Permocalculus inoptimus* (Fig. 2.1) (Simmons 1994). The Lekhwair Formation also contains smaller amounts of the dasycladacean algae *Cylindroporella arabica* and *Salpingoporella dinarica,* with the latter persisting up into the Kharaib and Shu'aiba Formations (former: Valanginian-Hauterivian, latter: Mid-Valanginian to Aptian) (Simmons 1994, Simmons & Hart 1987). The dasycladacean algae *Salpingoporella pygmaea* is attributed with the Habshan and the Lekhwair Formation (Lower Hauterivian to Mid-Barremian) whereas *Salpingoporella muelbergii* is attributed to the Lower Kharaib Formation (Mid-Barremian) (Simmons 1994). The dasycladacean algae *Coptocomplyloden lineolatus* (constrained by Simmons & Hart 1987 to the Salil Formation, the Lower Kharaib Formation, and the Early Valanginian/Barremian-Late Hauterivian, and constrained by Simmons 1994 between the Habshan-Lower Shu'aiba and the Upper Valanginian) is associated with fore bank deposits, in front of the main rudist banks, whereas *Salpingoporella dinarica* is associated with lagoonal deposits behind the main rudists banks within the Shaybah Field, Saudi Arabia (Hughes et al. 2000b). The dasycladacean algae *Hensonella dinarica* is associated by Simmons et al. (1991) with shallow water environments and the Hauterivian-Upper Aptian.

Borings

The appearance of significant bioerosion from boring bivalves (*Lithophaga*) and cleonid sponges is linked by Hallock & Schlager (1986) to increased nutrient conditions, as boring organisms thrive on plankton components, which in turn thrive in mesotrophic environments. Studies from Wood (1993) explain that low nutrient levels, linked with low dissolution and bioerosion rates, will result in higher net

carbonate production. Whereas with higher nutrient levels, bioerosion increases along with the production of carbonate sediment, which coupled with deposit feeding will increasingly produce carbonate mud (micrite) (Wood 1993).

3.3 Previous depositional models

3.3.1 The Lekhwair Formation

The Lekhwair Formation contains many 4th order HFC's each comprising dense argillaceous lime mudstones at their bases that shoal up into microporous wackestone, porous grainstone, and peloidal packstone, and grainstone (Alsharhan 1989, Alsharhan & Kendall 1991). The environmental interpretations by Alsharhan (1989) and Alsharhan & Kendall (1991) of the 4th order succession are: from deep water subtidal open marine shaley stylolitic micrite (4th order TST's), to open marine shallow water (near wavebase) subtidal, turbulent water, grain rich limestone and to inner shelf lagoons, and intertidal grainstone (4th order HST's) (Alsharhan 1989, Alsharhan & Kendall 1991) (Figure 3.1C). The upper components of each 4th order HFC, within the Lekhwair Formation, are very porous: Alsharhan & Kendall (1991) have attributed pore enhancement with freshwater leaching during sea level fall.

Another interpretation involves the abundance of fragmented dasycladacean algae within the Lekhwair Formation, which indicates Lekhwair Formation deposition to an inner platform environment (Granier et al. 2003/05) or more specifically within a back shoal with some lagoonal channels (Simmons & Hart 1987). Lithofacies concentrated in dasycladacean algae fragments, within the lagoonal facies of the Lekhwair Formation, have been labelled 'algal debris facies' by Granier et al. (2003/05) and Simmons & Hart (1987).

3.3.2 The Kharaib Formation

The base of the Lower Kharaib Formation 3rd order sequence contains muddy, fossil poor deposits, which Hillgärtner et al. (2003) has interpreted as TST deposits, representing an open shallow lagoon. An increase in faunal diversity occurs up into the late TST which represents the development of a deepening, more open, lagoon (Hillgärtner et al .2003). Further up section, the HST contains 'grainy, bioclastic,

rudist and miliolid dominated sediments' representing a shallowing lagoon (Hillgärtner et al. 2003).

In comparison, Strohmenger et al. (2006a) describes the base of the Lower Kharaib Formation as highly bioturbated (*Thallassinoides*) wackestone and packstone, which represents the TST and an open lagoonal environment. The overlying HST comprises algal and skeletal grainstone and rudstone, with rudist fragments and coated grains, which represents tidal influenced high energy bioclastic shoals (Strohmenger et al. 2006a). At the top of the Lower Kharaib Formation, the late HST is composed of peloidal, skeletal, algal, peloidal, miliolid rich float-grain-rudstone, which is interpreted as moderate-high energy miliolid shoals (Strohmenger et al. 2006a). The overall succession represents loss of accommodation and the shallowing of the Lower Kharaib platform environment (Strohmenger et al. 2006a). Generally the rudists and algal formations indicate the water column was nutrient rich, while the presence of *Lithocodium/B.* indicates low water turbidity (Dupraz & Strasser 1999; Immenhauser et al. 2005): although Strohmenger et al. (2006a) does not provide any evidence to support this claim.

The Kharaib Formation has been split into four HFC's instead of two (i.e. Lower and Upper Kharaib Formation) by Granier et al. (2003/05). Therefore the information displayed in Figure 3.6 represents the lowermost HFC that Granier et al. (2003/05) has recognised. The entire HST is associated with an inner ramp environment, with the *C. deciphens* dominating the TST, Orbitolinidae decrease, species of dasycladacean algae *Cylindroporella* and *Carpathoporella* along with benthic foraminifera *Chrysallidina* increase, as the platform shallows up section (Granier et al. 2003/05). Generally the dasycladacean algae dominate the platform top while the Orbitolinidae dominate the deeper water environments (Granier et al. 2003.05) (Fig. 3.6).

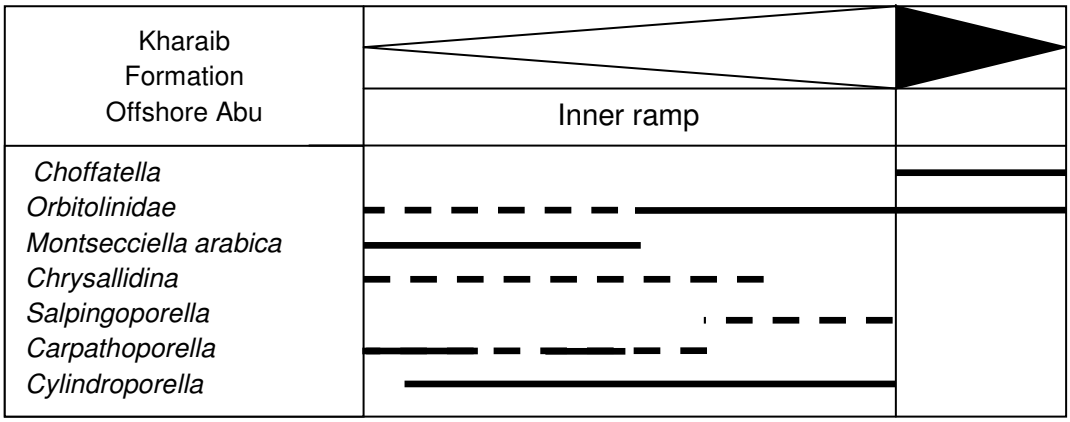

Figure 3.6: association of species with depositional environments of the Kharaib Formation by Granier et al (2003/05). Choffatella *is placed in a deeper environment, with the shallow platform associated with abundant algae (Compiled with data from Granier et al. 2003/05).*

In comparison to the Lower Kharaib Formation, the Upper Kharaib Formation is muddier and highly bioturbated reflecting steady sea level rise during the early part of a long term sea level TST (Hillgärtner et al. 2003). The TST is associated with an open lagoonal environment that becomes deeper: represented by an increase in biodiversity (Hillgärtner et al. 2003) (Fig. 3.7). The HST is associated with bioclastic rudist rich grainstone representing higher energy and a shallowing lagoonal environment (Hillgärtner et al. 2003). The cycle is capped with a miliolid grainstone which is interpreted to represent restricted high energy shoals (Hillgärtner et al. 2003) (Fig. 3.7).

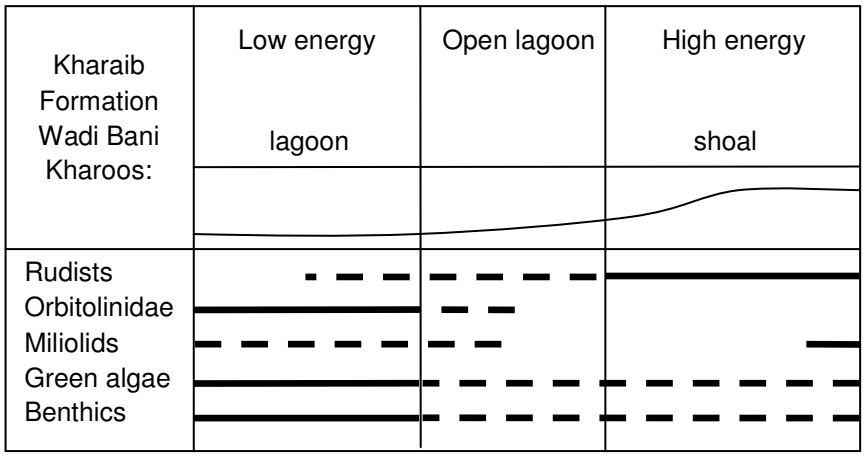

Figure 3.7: Fossil associations of the Upper Kharaib Formation at Wadi Bani Kharoos (complied with data from Hillgärtner et al. 2003).

Alternatively, Strohmenger et al. (2006a) has described the early TST of the Upper Kharaib Formation as Orbitolinidae and skeletal wackestone and packstone, which are heavily bioturbated. The late TST firmgrounds are burrowed by *Thallassinoides* which represent temporary phases of non-sedimentation (Strohmenger et al. 2006a). Peloidal and skeletal wacke-pack-grainstone and float-rudstone rich in miliolids, rudists, algae and coated grains, define the HST. The presence of caprotinid and monopleurid rudists reflects deposition in a shallow environment with moderate-high energy conditions (Strohmenger et al. 2006a). Figure 3.8 shows the lithofacies of the entire Kharaib and Shu'aiba Formations by Strohmenger et al. (2006a).

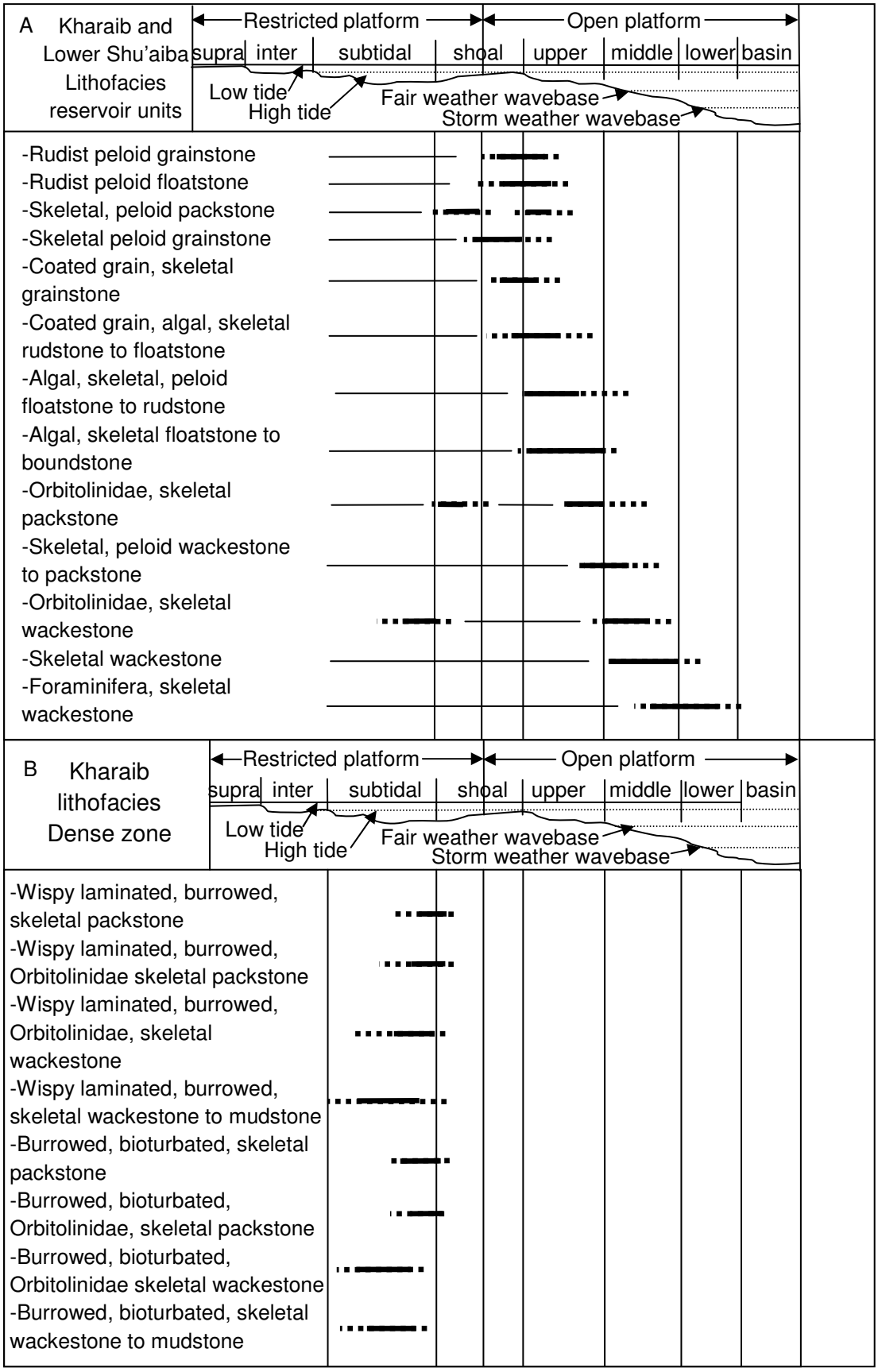

Figure 3.8: Fossil associations of the Kharaib and Lower Shu'aiba Formations: A) the reservoir units and B) the TST (redrawn from Strohmenger et al. 2006).

3.3.3 The Shu'aiba Formation

The Shu'aiba Formation within the Bu Hasa field (Alsharhan 1995) shows a progression from Orbitolinidae and planktonic (*Hedbergella* and *Globigerinelloides*) argillaceous lime mudstone, to coarse grained Orbitolinidae and rudist debris rich packstone and grainstone, to coarse grained Orbitolinidae, caprinid, caprotinid and *Lithocodium/B.* packstone, grainstone and boundstone and finally to highly bioturbated dasycladacean algae, miliolid and Orbitolinidae wackestone (Fig. 3.9). The argillaceous nature of the mudstone is interpreted by Alsharhan (1995) to represent a low energy open marine basin while rudist debris is interpreted as low-moderate energy and an unstable slope representing a barrier foreslope environment (Fig. 3.9). The in situ rudists represent a moderate-high energy rudist barrier and the high amount of bioturbation represents low energy and non-deposition within a shelf lagoon (Alsharhan 1995) (Fig. 3.9).

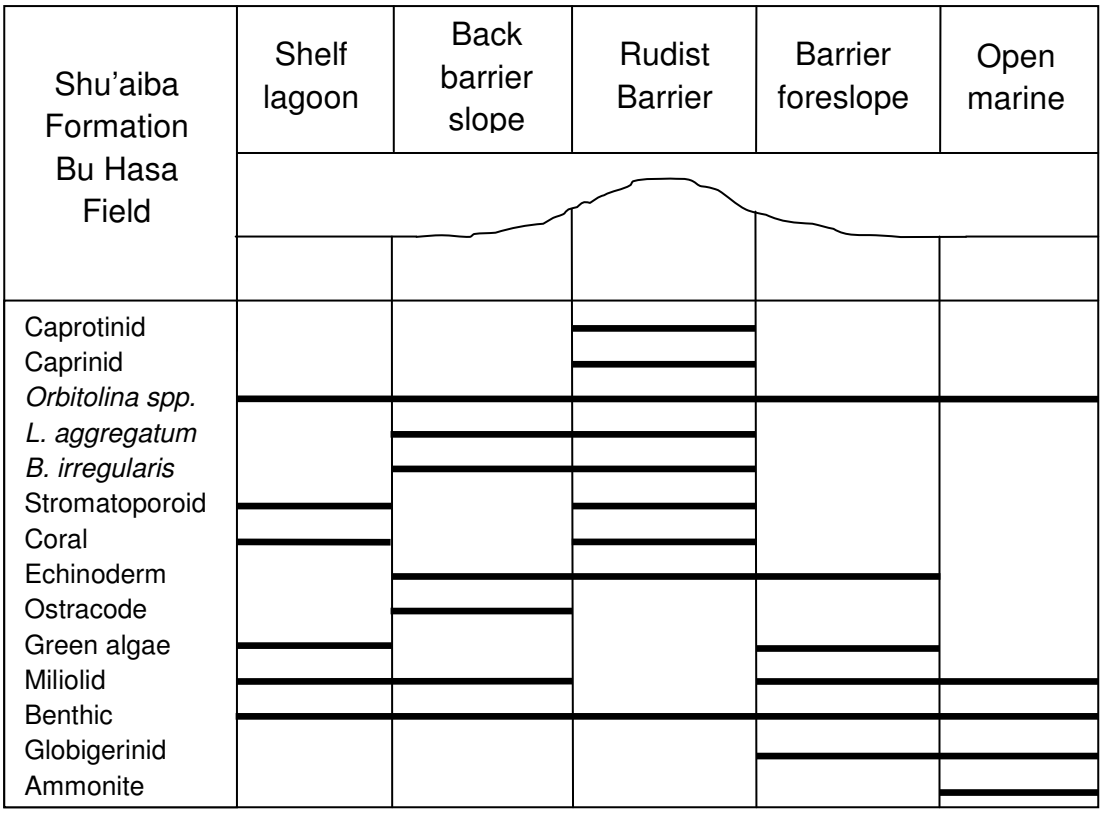

Figure 3.9: association of species to the environments of the Shu'aiba Formation, in the Bu Hasa Field. The benthic foraminifera along with L. aggregatum *are associated more with the back shoal and lagoon environments, while the rudists dominate within the shoals (data collated from Alsharhan 1995).*

A south-north transect from Wada Hammam to Wadi Barakah within Oman and the Shu'aiba Formation displays the lateral transition from '*Bacinella* facies' into '*G. costatus* facies' across the platform towards the basin (Masse et al. 1998) (Fig 3.10). The caprinids form further out on the platform margin with the corals forming on the escarpment (Masse et al. 1998) (Fig. 3.10).

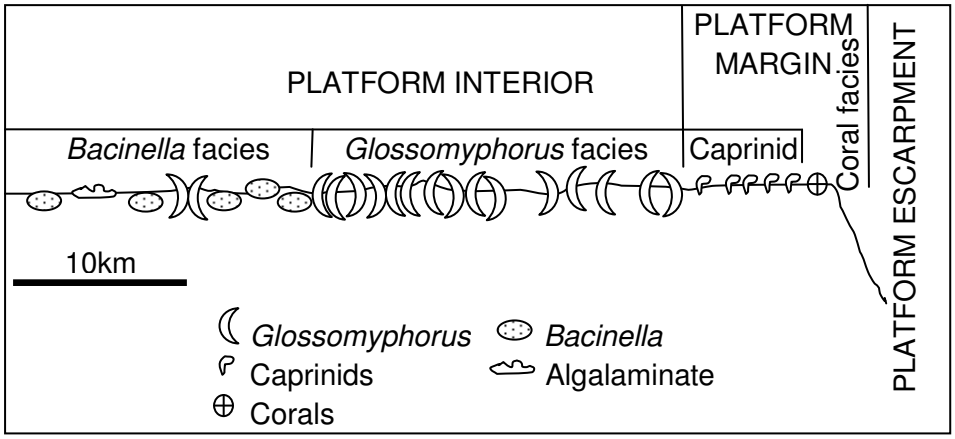

Figure 3.10: association of G. costatus *and* Bacinella *(*B. irregularis*) on the platforms of the Bab Member.* Bacinella *is associated with shallower environments in comparison with several species of rudist (redrawn from Masse et al. 1998).*

In the Shaybah field, Saudi Arabia, for each HFC the base of the TST's are associated with *Hedbergella delrioenss, Debarina hahounerensis,* and *Praechrysallidina infracretacea* (Hughes et al. 2000b) (Fig. 3.11). These develop into *Offneria murgenesis* rudist bank complexes, which develop further into a back-shoal environment dominated by *G. costatus*. This progression ends with algal blanket facies containing *L. aggregatum,* with *Trocholina alpina, Salpingoporella dinarica, P. lenticularis* and *P. infracretacea* of the lagoon (Hughes 2000b) (Fig. 3.11).

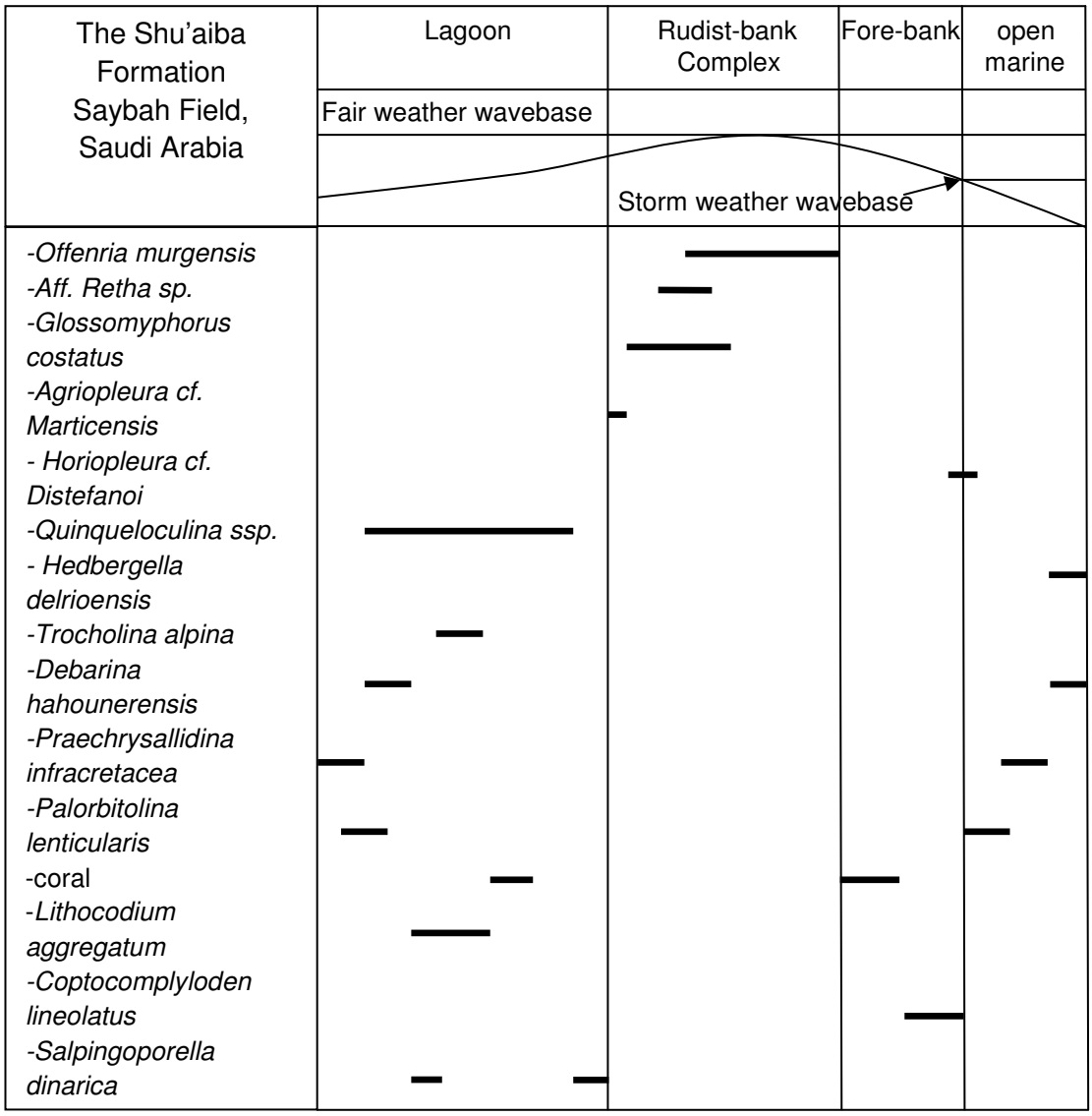

Figure 3.11: association of species to environments within the Shu'aiba Formation at the Shaybah Field. Benthic foraminifera and L. aggregatum *are mostly associated with back-shoal and lagoon environments, while the rudists dominate within a shoal environment (compiled with data from Hughes et al. 2000b).*

The Shu'aiba Formation is described by Granier et al. (2003/05) containing *Palorbitolina* wackestone at its base, which progresses up into mudstone and wackestone containing *Choffatella* and *Lenticulina* (Granier et al. 2003/05) (Fig 3.12). The entire sequence is capped with a condensed unit containing ammonites, suggesting a deepening upward trend; sedimentation could not keep pace with the rate of subsidence (Granier et al. 2003/05). Figure 3.12 shows the general progression of species abundance up through the Shu'aiba Formation (Granier et al. 2003/05).

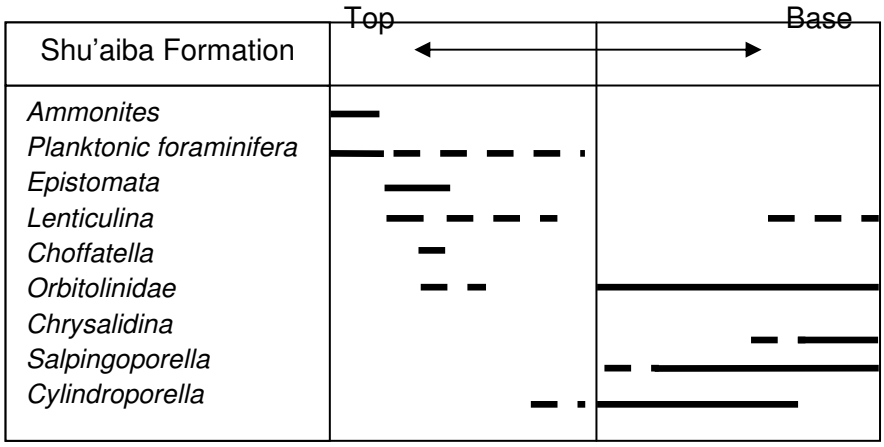

Figure 3.12: association of species to the Shu'aiba platform. The right hand part of the table represents the base whereas the left represents the top of the Shu'aiba Formation. The division has been placed between the disappearance of P. lenticularis *within the basal wackestone and the appearance of* Lenticulina *within upper mudstone and wackestone (complied with data from Granier et al. (2003/05).*

Studies from Pittet et al. (2002) have included both the Kharaib and the Shu'aiba Formations. The rudists are considered by Pittet et al. (2002) as being shallower dwelling species (on tidal/wave bars & channel deposits) compared with the *Lithocodium/B.* (shallow oligotrophic waters) (Fig. 3.13). The *C. deciphens* is related to shallower lagoonal environments above the storm weather wave base while Orbitolinidae are associated within deeper subtidal environments (Fig. 3.13).

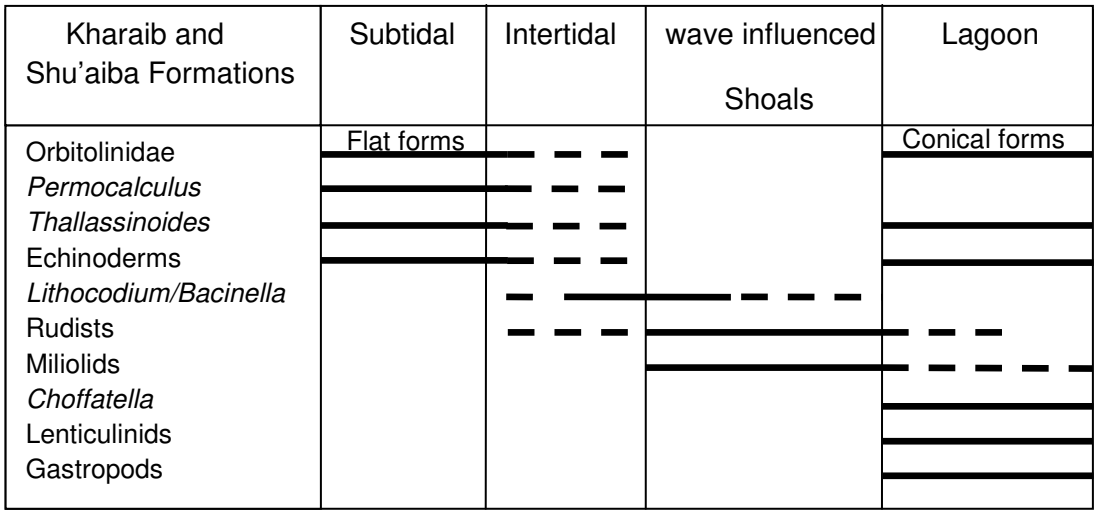

Figure 3.13: association of species to the Kharaib and Shu'aiba Formations. The flat forms and conical forms relate to the Orbitolinidae morphology within the specific environment (compiled with data from Pittet et al. 2002).

3.3.4 Limitations of biostratigraphy

The main way of determining what specific species represent in the lithologies, with respect to palaeoenvironment, is by associating them with a modern analogue with known water depth and environment preferences.

This relies on whether the flora or fauna in the rock are correctly identified; i.e. is it really related to any modern analogues. There are certain species, for instance *Lithocodium/Bacinella*, which has no modern day analogue, and therefore it is difficult to associate it with a preferred environment of habitation via these means. Therefore aspects of the lithologies, housing these particular fossils, can be used to support interpretations of the palaeoenvironment.

The fossil may not be in situ and may have been transported after death across a considerable distance. With the case of the Lekhwair and Lower Kharaib platforms, being very gentle slopes, material could be transported great distances within strong ocean currents.

The fossils seen in thin section rarely provide a detailed view of all parts of a particular flora or fauna; depending on how the section has been cut determines the cross-section through the fossils. Therefore with incomplete information some species may be incorrectly identified.

Can this study provide a high enough resolution by looking at the internal fossil abundance changes within each 4^{th} order cycle to determine changing palaeoenvironment? With this much detail the occurrence of specific species could occur and disappear three of four times within a particular 4^{th} order HST of TST. This could either mean the specific thin sections cut through areas of the rock with abundance of a particular fossil, have transacted small centimetre patches devoid of these fossils, and therefore their disappearance should be disregarded. Or is this cyclicity of importance and does it represent higher order (5^{th} order) trends? The challenge is judging what constitutes sample support and what is an actual change is biodiversity within the rock record. This will be solved by correlation; i.e. any significant shift in biodiversity either across an SB/MFS or within a TST/HST will

be compared with other samples from separate wells to determine its extent, and therefore its importance in palaeoenvironment interpretation.

3.4 Results

This section already assumes the layer cake nature of the Thamama Group and the positions of the 4th order SB's and MFS's (Sections 4.3.1 & 4.3.2). Therefore the aim here is to see if any internal cyclicity is present within the 4th order HFC's and the individual 4th order HST's and TST's. To do this three parts within this section are presented: 1) the lithology from core observation), 2) the biodiversity (from petrography) and 3) the lithofacies (from petrography) of the Lekhwair and Lower Kharaib Formations. These three sections are then summarised to provide a detailed account of the internal biological/lithological changes within the 4th order HFC's from the Lekhwair and Lower Kharaib Formations. Any trends can then be used to determine how the environment of deposition has changed during the deposition of each 4th order HFC and between the Lekhwair and Lower Kharaib Formations.

3.4.1 Lithology (core descriptions)

Each 4th order HFC contains a reservoir and non-reservoir. The non-reservoirs are not constrained to the TST, but include the uppermost HST of the 4th order HFC below: the firmgrounds. The firmgrounds, like the TST, are muddy and are not oil stained (Fig 3.14). The reservoirs are defined as the oil stained areas, within each 4th order HFC, which usually consists of the mid- late HST. However in many cases the base and topmost portions of the HST, corresponding to the reservoir, are oil free. These positions are fully cemented preventing oil from entering the lower-uppermost reservoir (Fig. 3.14). Therefore diagenesis, through cementation, has narrowed the reservoir conduit for housing oil within most 4th order HFC's. Cementation increases away from the crest (oil leg) until the entire reservoir is cemented in the field flanks: this is observed in the water leg, in Well 1, where the entire reservoir is oil free.

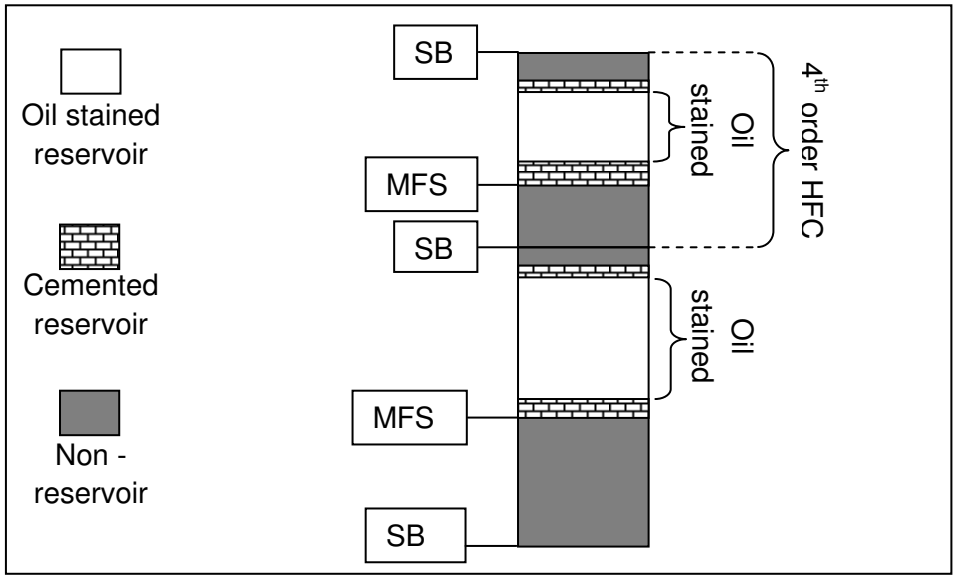

Figure 3.14: The non-reservoirs encompass the firmground assemblage and therefore overlap SB's and are not solely constrained to the TST. The degree of oil staining determines the vertical extent of the reservoirs.

Each 4th order HFC comprises seven general lithologies distinguished in core section (Figs. 3.15 and 3.16). These are not lithofacies, they are broad lithological assemblages observed within each 4th order HFC, in core.

1. Highly friable argillaceous micrite/mudstone (Fig. 3.15 and 3.16A).
2. Pyritised micrite/mudstone, rich in glauconite, compaction seams and compressed burrows (Fig. 3.15 & 3.16B).
3. Orbitolinidae shell hash, highly cemented with LMC, contains pyrite, glauconite and many disarticulated fragmented bivalve and brachiopod shells (Fig. 3.15 & 3.16C).
4. Muddy wackestone concentrated in mottled burrows (can contain *Lithocodium/B.*).
5. *G. costatus* and *Lithocodium/Bacinella* wackestone and packstone concentrated in mottled burrows. The *Lithocodium/B.* is heavily oil stained within the reservoir portions of each 4th order HFC (Fig. 3.15 & 3.16D).

6. *Glossomyphorus costatus* and *Lithocodium/B.* packstone and grainstone. There are sparse coral and sponge fragments, along within mottled burrows, stylolites, bivalve and brachiopod fragments. These areas are heavily oil stained (Fig. 3.15 & 3.16E).

7. *Lithocodium/B.* boundstone. *Lithocodium/B.* binds the rock and bioclasts such as *G. costatus* and microsolenid coral fragments.

8. *Thallassinoides* burrowed firmground (*Glossifungites* assemblage) comprising of muddy wackestone, rich in pyrite and dolomite. There is no evidence within the final 10ft of any 4th order HFC, within both the Lekhwair of Lower Kharaib Formations, for meteoric dissolution or any other features displaying subaerial exposure (Fig. 3.15 & 3.16F).

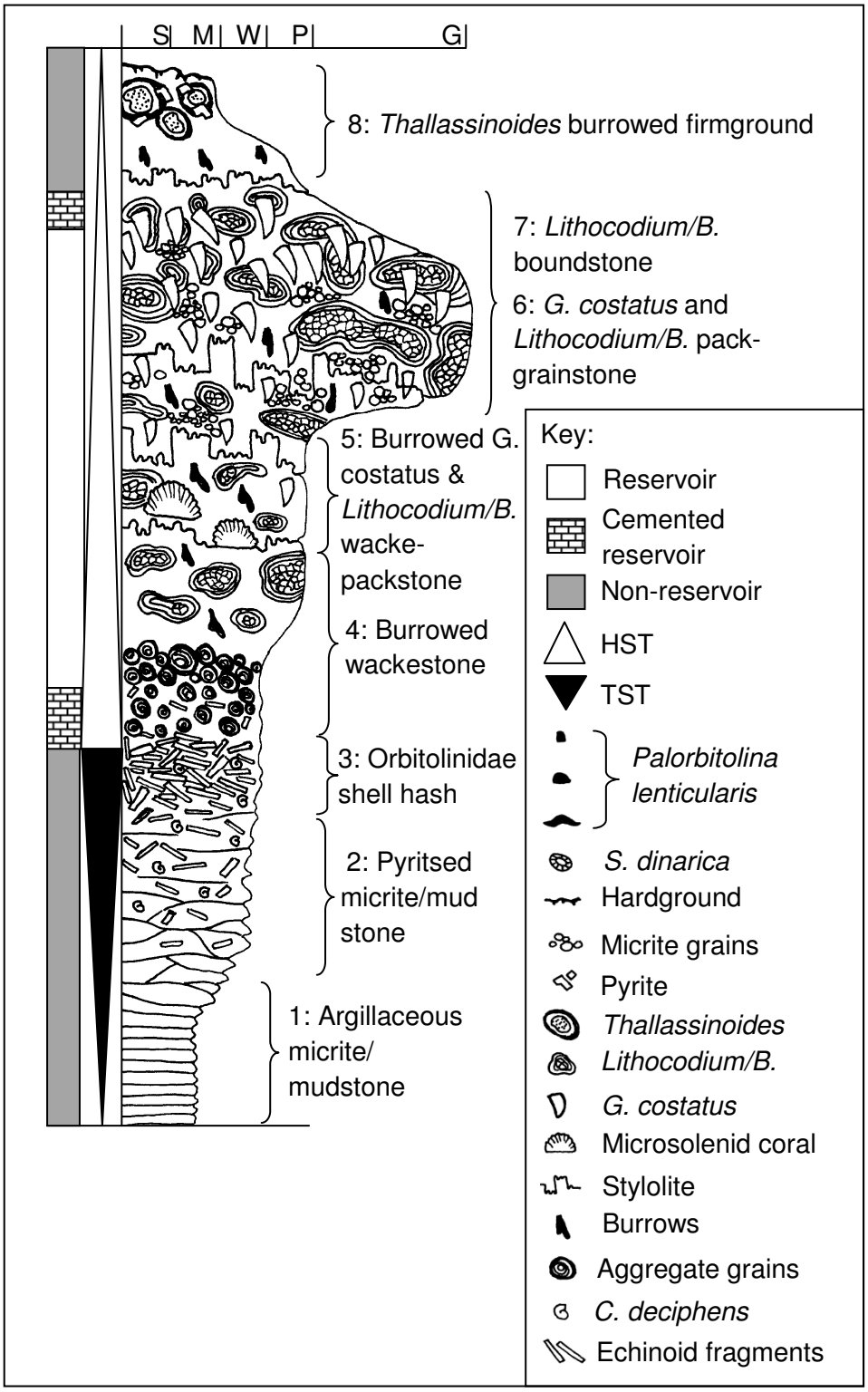

Figure 3.15: The seven broad lithologies observed in core section are associated with a general 4th order HFC. Lithologies 1-3 represent the TST whereas lithologies 4-7 represent the HST. The shell hash and the pyritised micrite/mudstone are not always in this order and can be interbedded with each other. There is no scale, as the HFC drawn is not a single 4th order HFC, but is instead an assemblage of traits seen throughout the five wells.

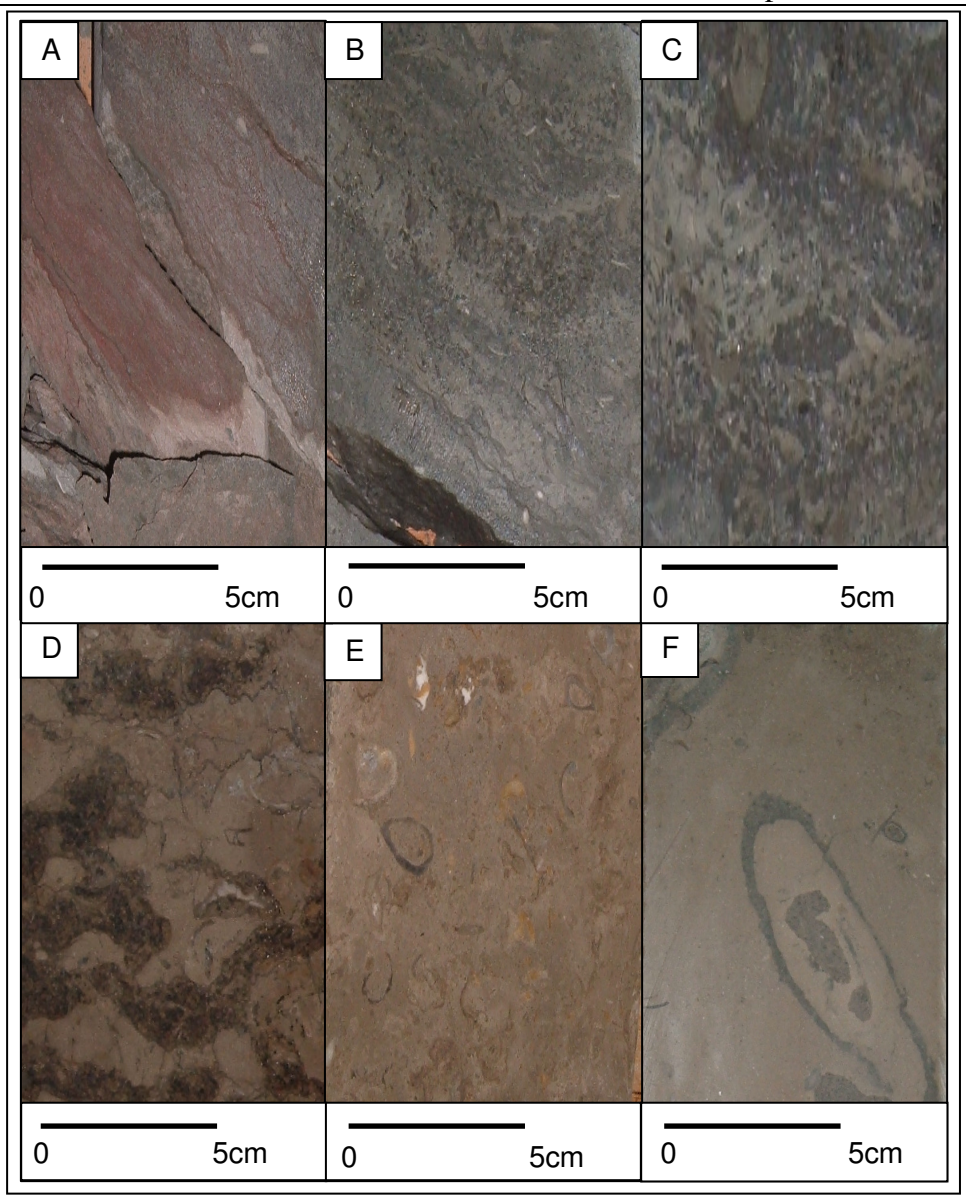

Figure 3.16: a shoaling upward 4th order HFC in the Lekhwair and Lower Kharaib Formations. From the base upwards: A) argillaceous micrite/mudstone, B) pyritised micrite/mudstone, C) Orbitolinidae shell hash, D) G. costatus *&* Lithocodium/B. *wackestone and packstone, F)* G. costatus. *and* Lithocodium/B. *packstone and grainstone and G) the* Thallassinoides *firmground. A representative picture for burrowed wackestone and* Lithocodium/B. *boundstone could not be found.*

3.4.2 Biodiversity

The specific species found within the Lekhwair and Lower Kharaib Formations are displayed in Figures 3.17 (macrofossils) and 3.18 (microfossils and algae).

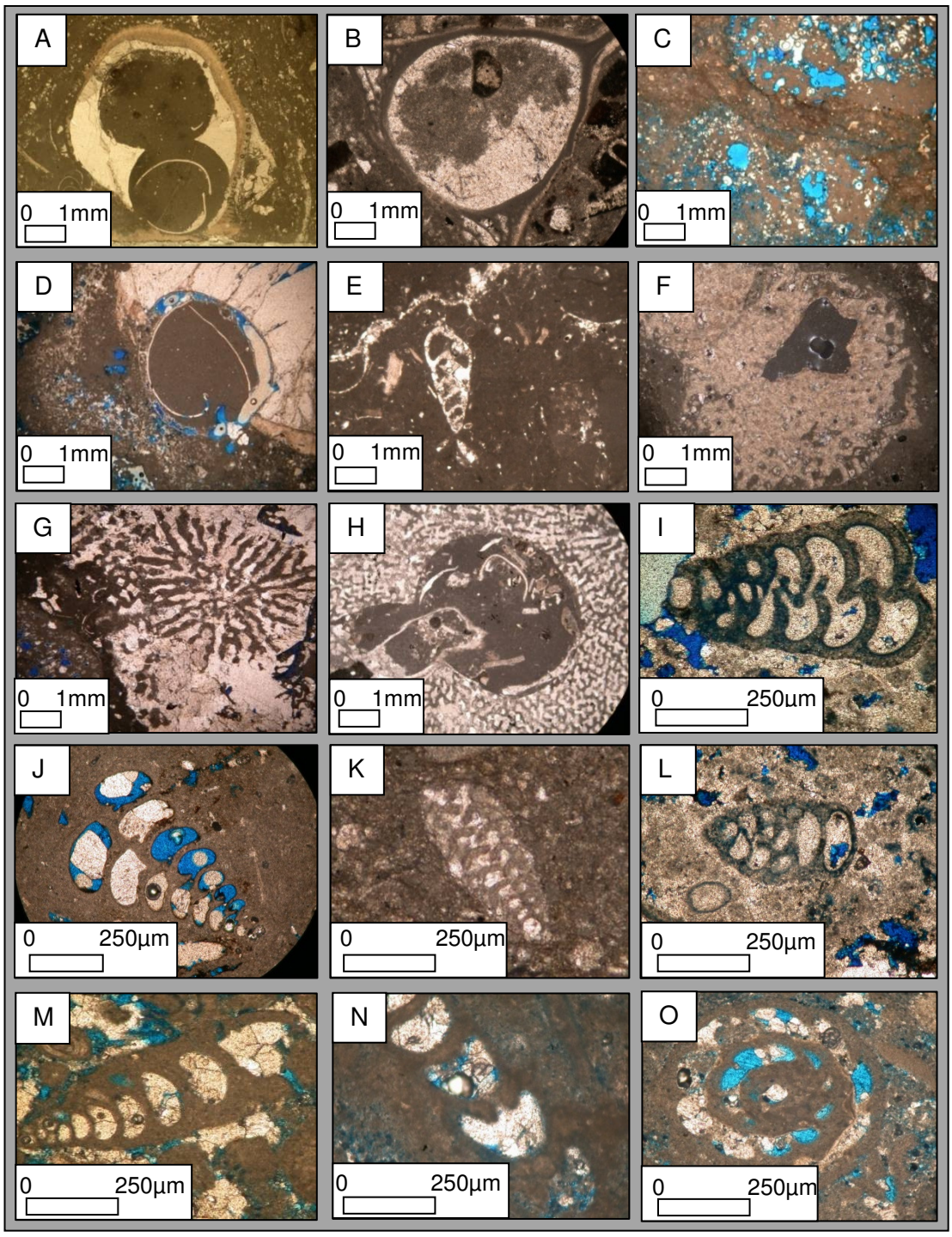

Figure 3.17: macrofossils and benthics of the Lekhwair and Lower Kharaib Formations: A) Glossomyphorus costatus*, B) caprinids, C)* Lithocodium/Bacinella*, D)* Lithophaga*, E)* T small gastropod*, F)* Cladocoropsis*, G) microsolenid coral, H) stromatoporoid, I)* Praechrysallidina infracretacea*, J)* Redmondoides lugeoni*, K)* Textularia sp.*, L)* Bigenerina sp.*, M)* Bigenerina sp.*, N)* Reophax sp. *and O)* Debarina hahounerensis.

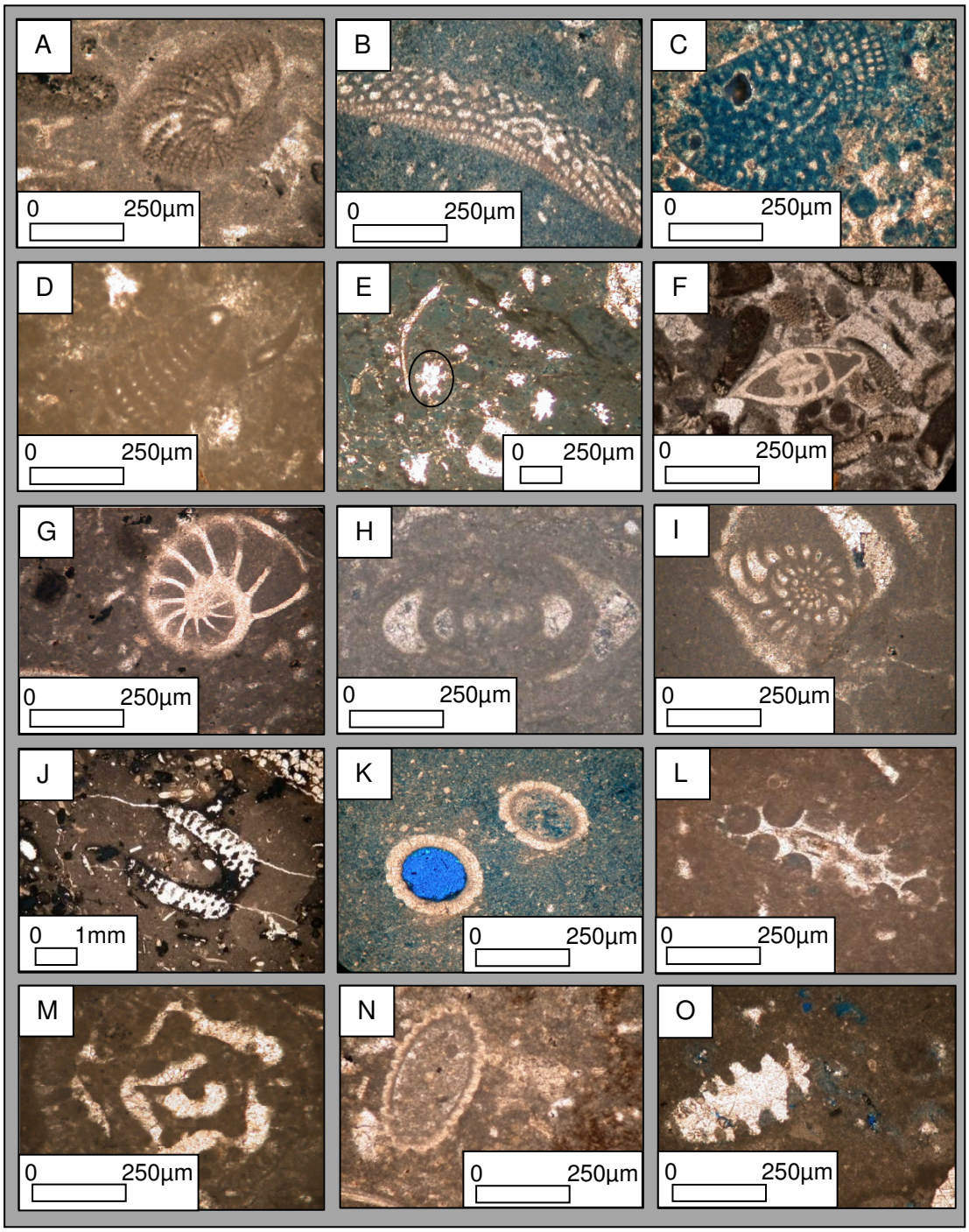

Figure 3.18: *benthics and algae of the Lekhwair and Lower Khariab Formations: A)* Choffatella deciphens*, B) large flat* Palorbitolina lenticularis, C) *small conical* Palorbitolina lenticularis*, D)* Vercosella arenata*,* E) Coptocomplyloden lineolatus*, F)* undifferentiated rotalid, G) undifferentiated rotalid, H) Nautiloculina brönnimanni*, I)* Merlingina cretacea*, J)* Acroporella assurbanipali*, K)* Salpingoporella dinarica*, L)* Cylindroporella arabica*, M)* Buccicrenata hedbergi*, N)* Hensonella dinarica *and O)* Trocholina sp.*. The circle in (E) highlights* C. lineolatus.

The varying abundance of all the species observed within the Lekhwair and Lower Kharaib Formations is achieved through manual counting from the thin sections. This data displayed in Fig. 3.19-3.23 is from the manual bioclastic counts from each thin section. Not every species is plotted on Figures 3.19-3.23: only the abundant fossils are shown (for full list of data see Appendix 1A-1E).

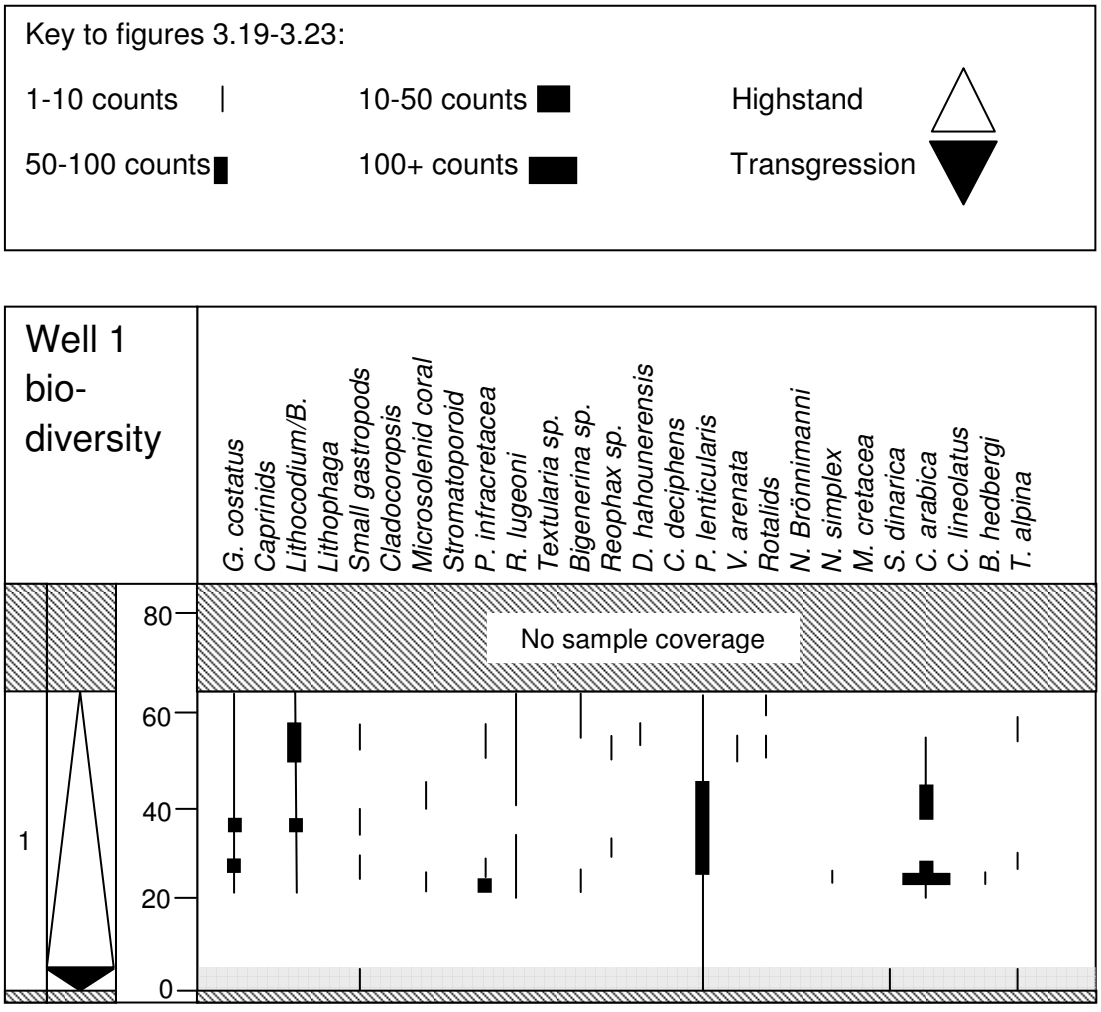

Figure 3.19: macrofossil and microfossil occurrence within Well 1. The depth axis is in feet and is scaled using the core base.

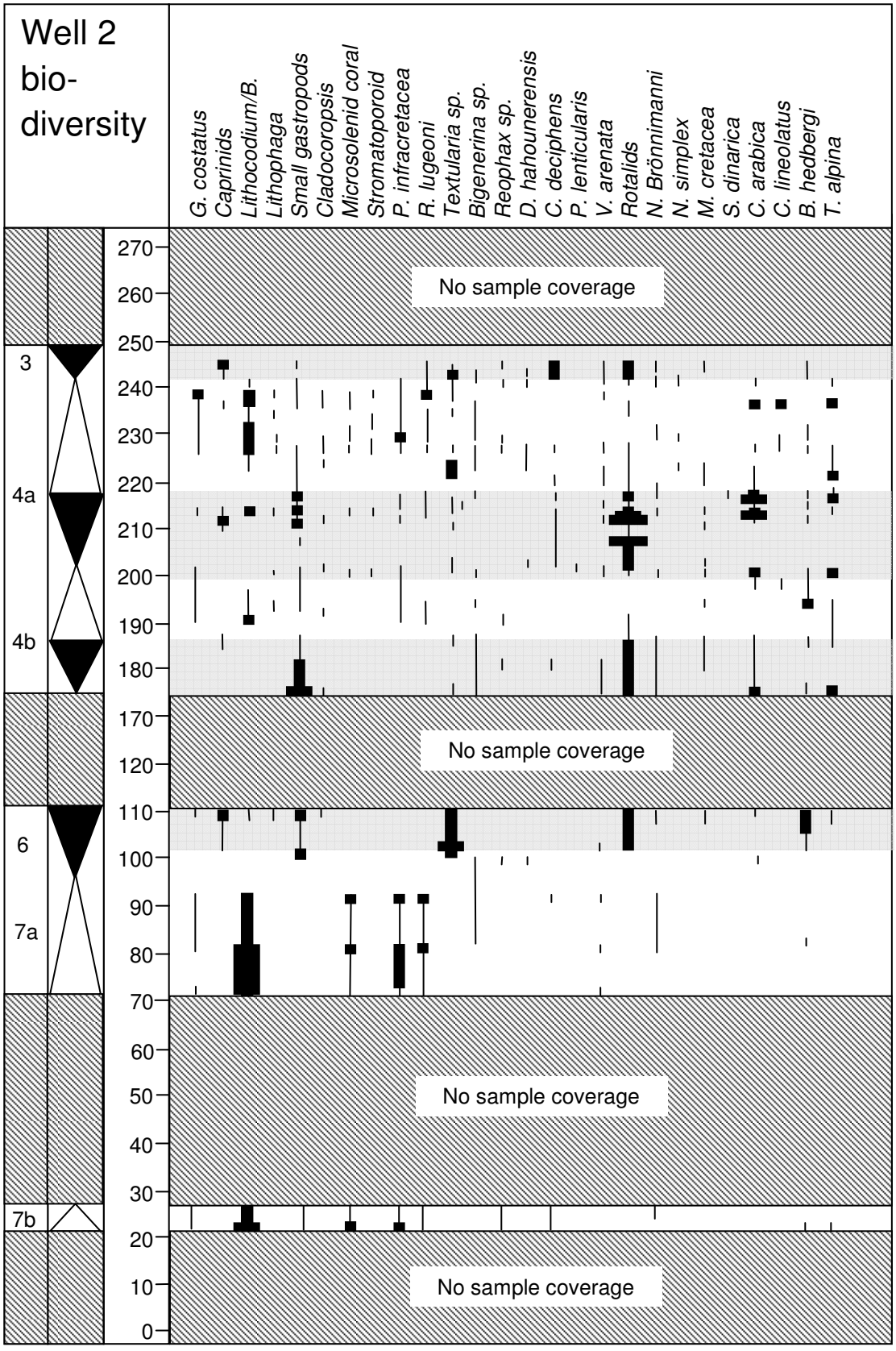

Figure 3.20: macrofossil and microfossil occurrence within Well 2. The depth axis is in feet and is scaled using Cycle 8 SB as the base.

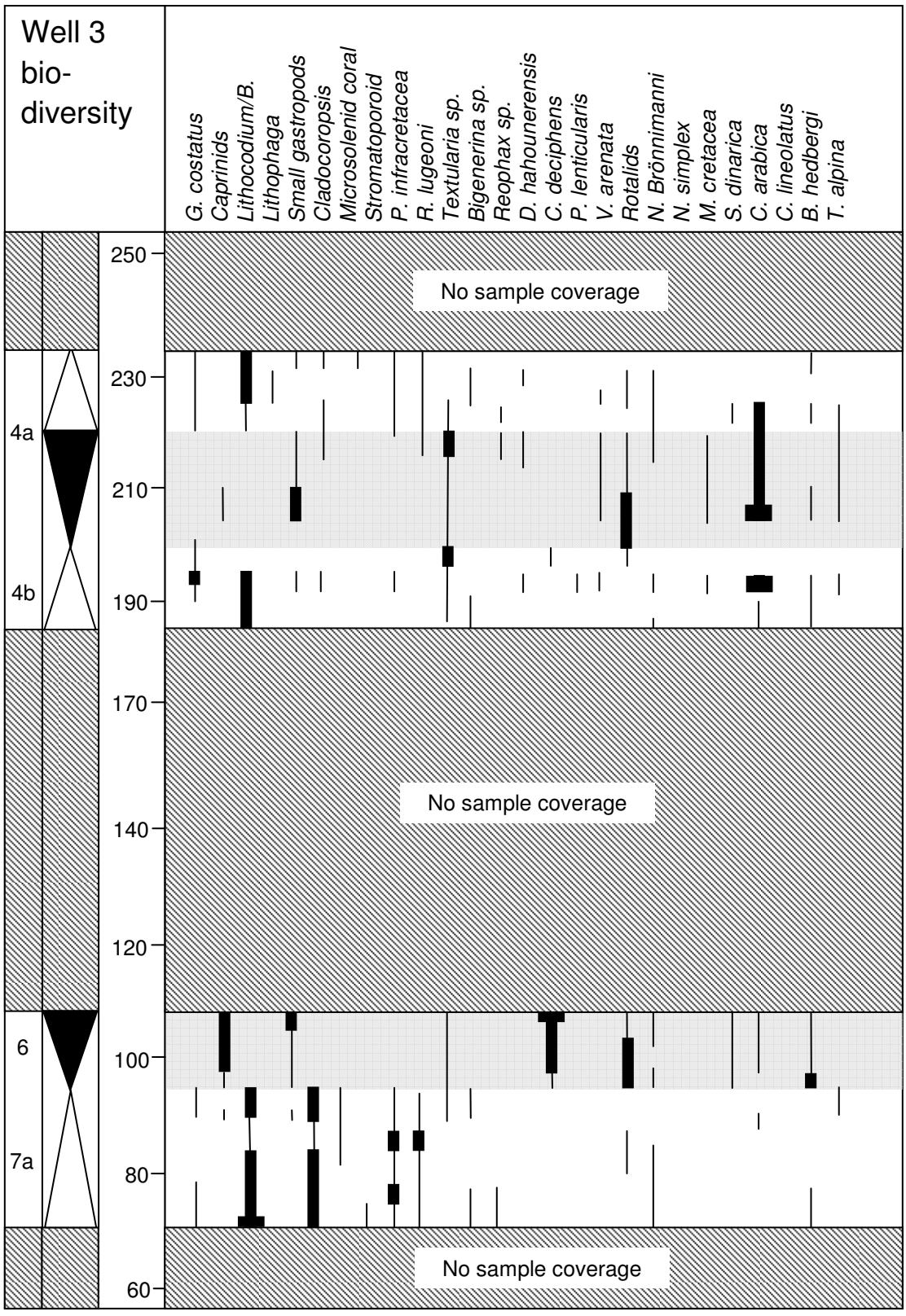

Figure 3.21: macrofossil and microfossil occurrence within Well 3. The depth axis is in feet and is scaled using Cycle 8 SB as the base.

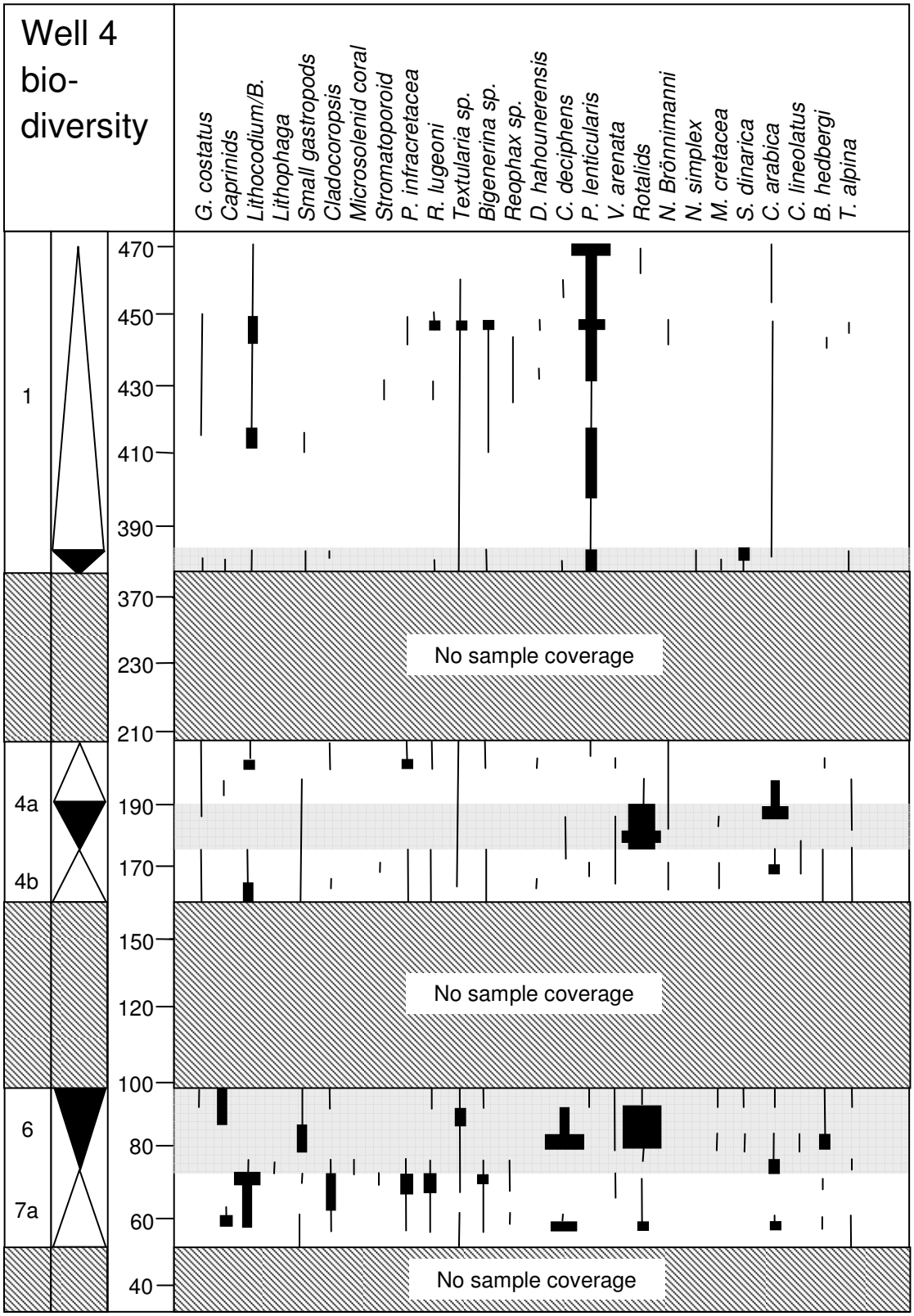

Figure 3.22: macrofossil and microfossil occurrence within Well 4. The depth axis is in feet and is scaled using Cycle 8 SB as the base.

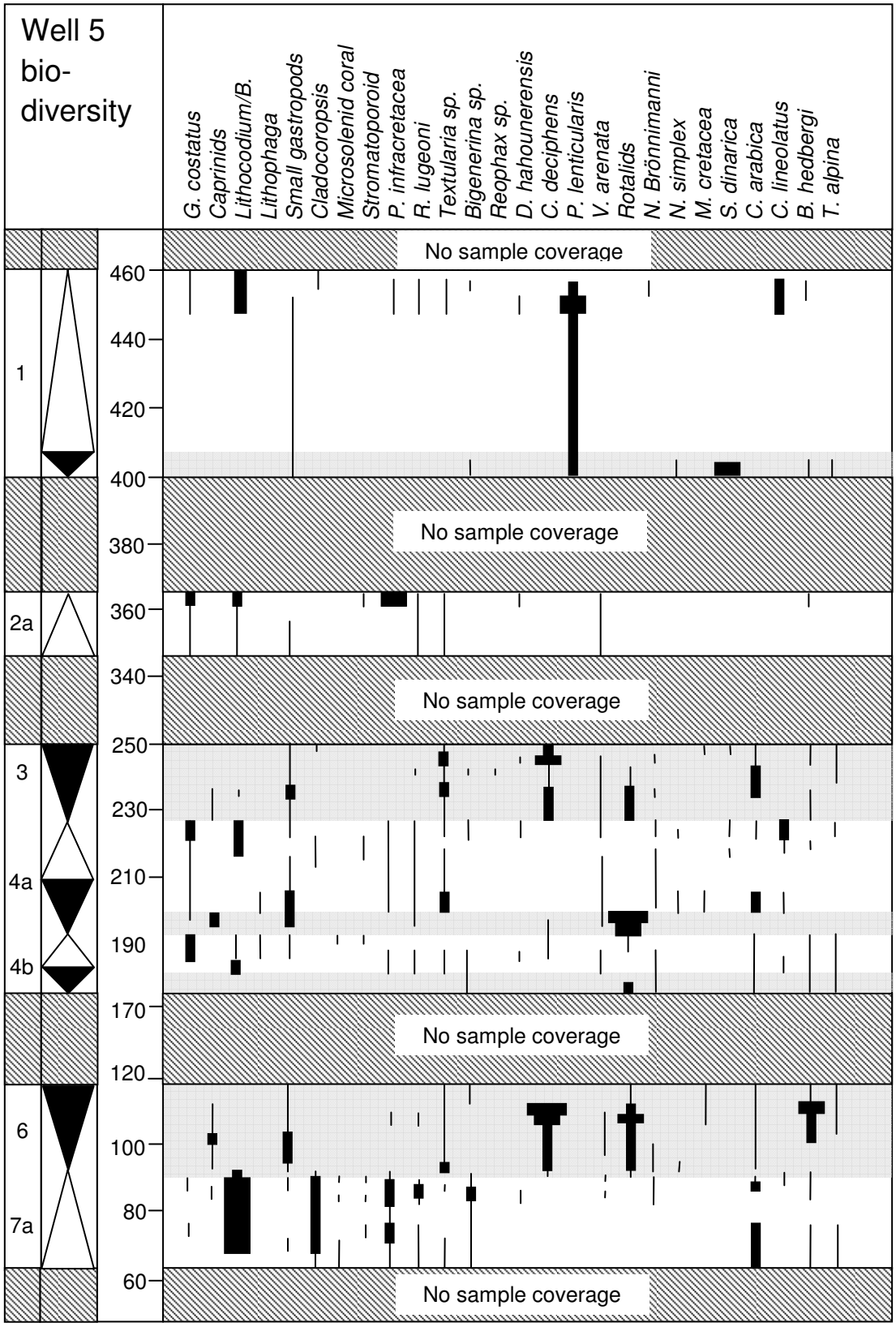

Figure 3.23: macrofossil and microfossil occurrence within Well 5. The depth axis is in feet and is scaled using Cycle 8 SB as the base.

3.4.3 Lithofacies

Using the lithological data gathered from core samples, the biodiversity data from petrography, and extra petrographic information on the lithologies, several lithofacies have been generated. In total, 20 lithofacies are established for the Lekhwair and Lower Kharaib Formations (Figs. 3.24A-T)

Figure 3.24A: Lithofacies 1: Bioclastic micrite/mudstone (cycle top)

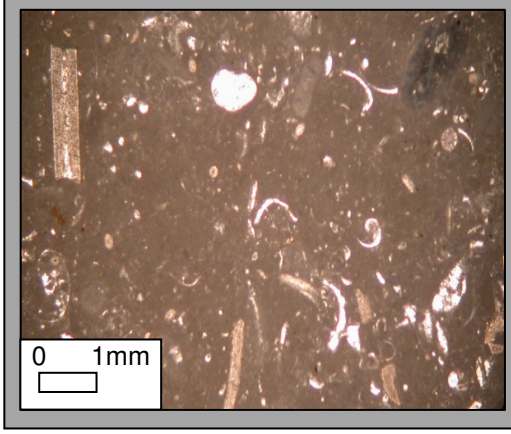

Lithology: *very muddy and contains sparse 100-250µm dolomite rhombs throughout the matrix. There are sparse fragmented 0.5-1mm undifferentiated rotalids,* Salpingoporella muelbergii*,* Trocholina sp.*,* C. arabica *and on occasion 1-2mm* C. deciphens*, 1-2mm* Buccicrenata hedbergi*, 1mm V. arenata and 1-2mm conical* P. lenticularis*. There is relative concentration in 1-2mm gastropods. This lithology has a very high diversity of broken bioclasts and contains relative concentration of small blackened mineralised grains.*

Figure 3.24B: Lithofacies 2: Dolomitised wackestone

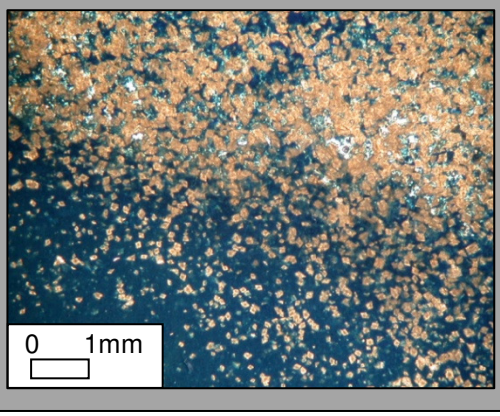

Lithology: *concentrated in 100-250µm dolomite rhombs. It is very muddy and contains a sparse assemblage of 0.5-1mm bioclasts:* C. arenata*,* S. pygmaea*, undifferentiated rotalids,* N. brönnimanni *and on occasion unbroken 0.5-1mm* P. infracretacea*, 1mm* V. arenata*, 1-2mm* C. deciphens*,* B. hedbergi *and conical* P. lenticularis*. There is relative concentration in 1-2mm gastropods. This lithology has high diversity of broken bioclasts.*

Figure 3.24C: Lithofacies 3: *Thallassinoides* burrowed dolomitised wackestone

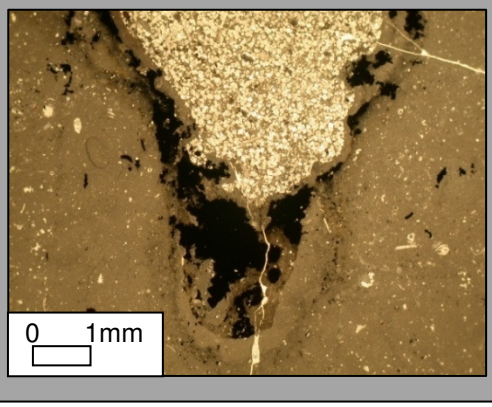

Lithology: *very muddy and is concentrated in 0.5-1cm wide* Thallassinoides *filled with 100-250µm dolomite rhombs. The* Thallassinoides *are surrounded by a 0.5mm thick blackened halo containing 1-5mm framboides of pyrite. The lithology contains a sparse coverage of 0.5-1mm in situ bioclasts:* S. muelbergii, C. arenata, *undifferentiated rotalids,* P. infracretacea, R. lugeoni *along with occasional unbroken 1-2mm* C. deciphens, *1-2mm* B. hedbergi *and 1mm* V. arenata *There is relative concentration in 1-2mm gastropods.*

Figure 3.24D: Lithofacies 4: *P. lenticularis* wackestone

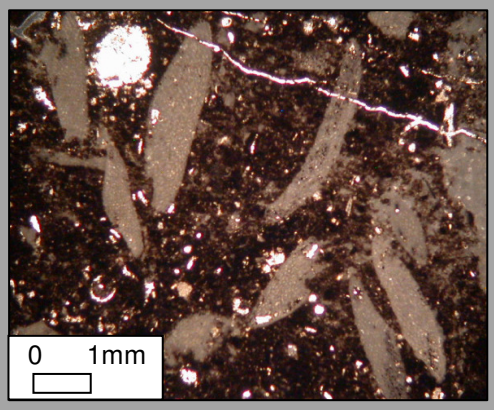

Lithology: *very muddy, has a high concentration of a black dendritic mineral (pyrite?) with a high concentration of 4-5mm sized large flat* P. lenticularis. *There are a few 1-2mm conical* P. lenticularis. *Other than a few echinoid fragments this lithology has a very low biodiversity.*

Figure 3.24E: Lithofacies 5: *G. costatus*, *Lithocodium/B.*, *Cladocoropsis* pack-grainstone

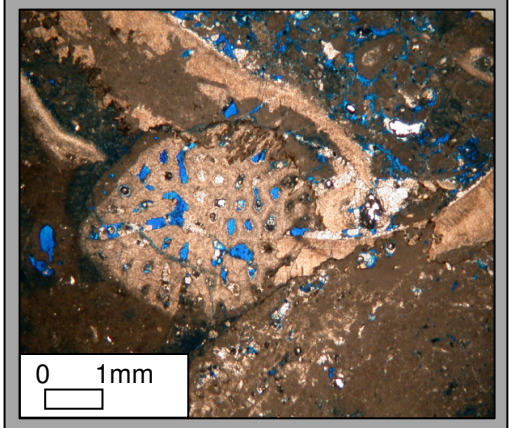

Lithology: *compacted 0.25-0.5mm micrite grains forming packstone. The matrix contains grainstone patches containing 0.25-1mm micrite pellets, either isolated within the matrix, or within* G. costatus *shells. The 1-2cm* G. costatus *shells are intact and are readily encrusted with 0.5-1mm layers of* Lithocodium/B. *There are also 0.5-1cm* Cladocoropsis *fragments encrusted with 0.5-1mm* Lithocodium/B. *The majority of* Lithocodium/B. *forms 1-2cm isolated patches that have either formed independently or have nucleated around* Cladocoropsis *fragments and* G. costatus *shells which are also bored by* Lithophaga *and by cleonid sponges There are some Textulariacea ranging from 3-4mm:* P. infracretacea, R. lugeoni, Bigenerina sp. *and* Textularia sp. *There are also occasionally 1mm* D. hahounerensis, *0.5-1mm* N. brönnimanni *and 1mm* V. arenata.

Figure 3.24F: Lithofacies 6: Rudist, *Lithocodium/ Bacinella* and *P. lenticularis*

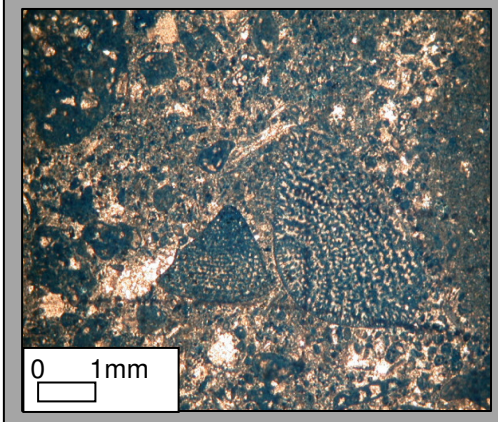

Lithology: *concentrated in 0.25-0.5µm micrite grains. There are intact 1cm* G. costatus *shells, sparse 0.5cm* Lithocodium/B. *patches, 1mm conical* P. lenticularis *(dominant species) and some 3-4mm flat discoidal* P. lenticularis. Lithocodium/B. *is mostly present as 0.5-1mm encrusting layers upon the G. costatus shells.*

Figure 3.24G: Lithofacies 7: microsolenid coral and stromatoporoid grainstone

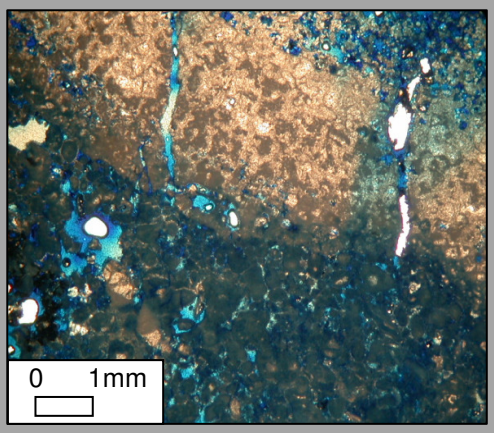

Lithology: *concentrated in 0.25-0.5µm micrite grains containing 1-2cm* G. costatus *shells, 1-2cm* Lithocodium/B. *patches, 1-2cm microsolenid coral fragments and 1-2cm stromatoporoid fragments. The rudist, coral and sponges fragments are readily encrusted by 0.5-1mm* Lithocodium/B. *There are some Textulariacea ranging from 3-4mm:* P. infracretacea, R. lugeoni, Bigenerina sp. *and* Textularia sp. *There are also occasionally 1mm* D. hahounerensis, *0.5-1mm* N. brönnimanni *and 1mm* V. arenata.

Figure 3.24H: Lithofacies 8: *Lithocodium/B.*

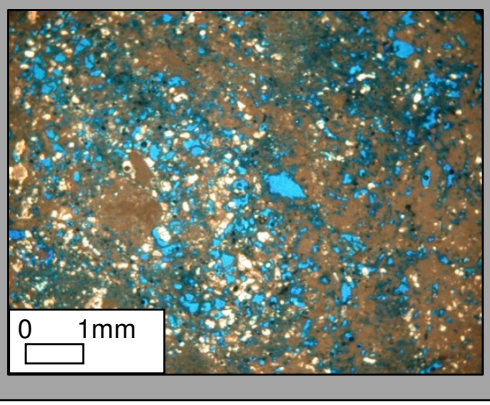

Lithology: *a collection of bounded* Lithocodium/B. *patches engulfing 1-2cm* G. costatus *shells and 1-2cm* Cladocoropsis *fragments. The* Lithocodium/B. *is clearly in situ, whereas the other engulfed fossils may not be in situ.*

Figure 3.24I: Lithofacies 9: *G. costatus* and *P. lenticularis* packstone

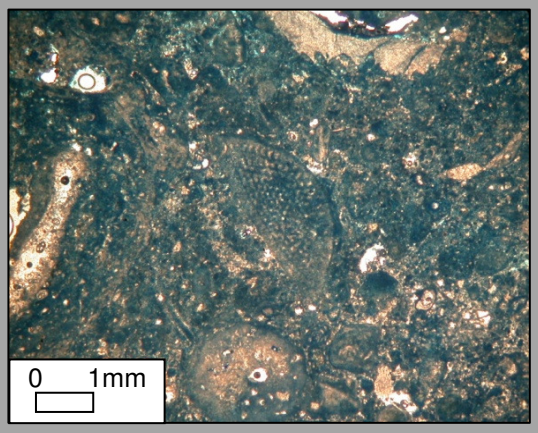

Lithology: *concentrated in compacted 0.25-0.5µm micrite grains forming a muddy packstone. There are many intact 1cm* G. costatus *shells with a concentration of 3-4mm flat discoidal* P. lenticularis *and some 1mm conical* P. lenticularis*. There is some* Lithocodium/B. *present within this lithology, but only as 0.5-1mm encrustaceans upon* G. costatus *shells.*

Figure 3.24J: Lithofacies 10: *G. costatus* and *Lithocodium/B.* packstone

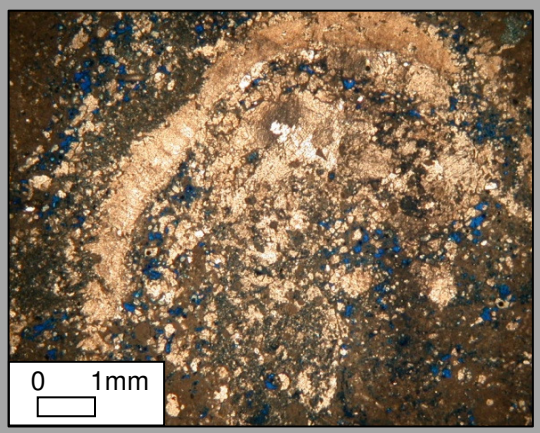

Lithology: *compacted 0.25-0.5µm micrite grains forming muddy packstone. The lithology is abundant in 1-2cm G. costatus shells and encrusted with 0.5-1mm* Lithocodium/B. *The dominant form of the* Lithocodium/B. *is large 1-3cm isolated patches within the matrix. There are some Textulariacea ranging from 1-2mm:* P. infracretacea*,* R. lugeoni*,* Bigenerina sp. *and* Textularia sp. *There are also occasionally 1mm* D. hahounerensis*, 0.5-1mm* N. brönnimanni *and 1mm* V. arenata*.*

Figure 3.24K: Lithofacies 11: *G. costatus*, *Lithocodium/B.* and *Cladocoropsis* pack-wackestone

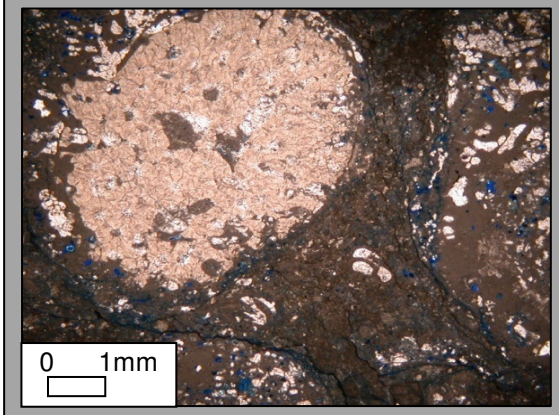

Lithology: *muddy sparse 0.25-0.5µm micrite grains with blackened mineralised grains. The 1-2cm* G. costatus *shells and 1-2cm* Cladocoropsis *fragments are encrusted with 0.5-1mm* Lithocodium/B. *The majority of* Lithocodium/B. *is present as 1-3cm isolated patches within the matrix. There are some Textulariacea ranging from 1-2mm:* P. infracretacea*,* R. lugeoni*,* Bigenerina sp. *and* Textularia sp. *There are also occasionally 1mm* D. hahounerensis*, 0.5-1mm* N. brönnimanni *and 1mm* V. arenata*.*

Figure 3.24L: Lithofacies 12: microsolenid coral and stromatoporoid pack-wackestone

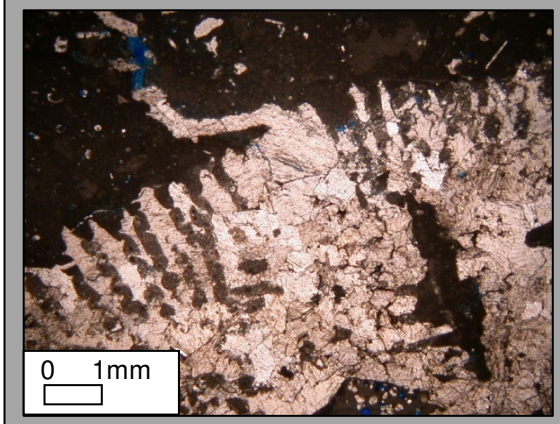

Lithology: *very muddy and contains sparse 0.25-0.5µm micrite grains and blackened mineralised grains. The dominant bioclasts are isolated fragments of 1-2cm microsolenid coral and stromatoporoid. There is also 1-2cm* G. costatus *encrusted with 0.5-1mm layers of* Lithocodium/B. *along with larger 4-3cm* Lithocodium/B. *isolated patches within the matrix. There are some Textulariacea ranging from 0.5mm-1mm:* P. infracretacea*,* R. lugeoni*,* Bigenerina sp. *and* Textularia sp. *There are also occasionally 1mm* D. hahounerensis*, 0.5-1mm* N. brönnimanni *and 1mm* V. arenata*.*

Figure 3.24M: Lithofacies 13: *G. costatus* and *Lithocodium/B.* wackestone

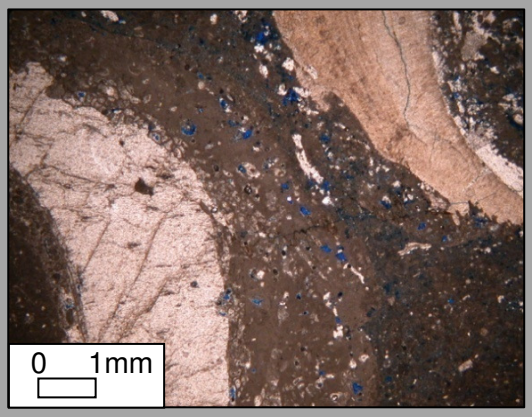

Lithology: *very muddy and concentrated in 1-2cm* G. costatus *encrusted with 0.5-1mm layers of* Lithocodium/B. *The dominant form of* Lithocodium/B. *is large 1-4cm isolated patches within the matrix. There are some Textulariacea ranging from 0.5mm-1mm:* P. infracretacea*,* R. lugeoni*,* Bigenerina sp*. and* Textularia sp. *There are also occasionally 1mm* D. hahounerensis*, 0.5-1mm* N. brönnimanni *and 1mm* V. arenata*.*

Figure 3.24N: Lithofacies 14: *S. dinarica* dolomitised wackestone

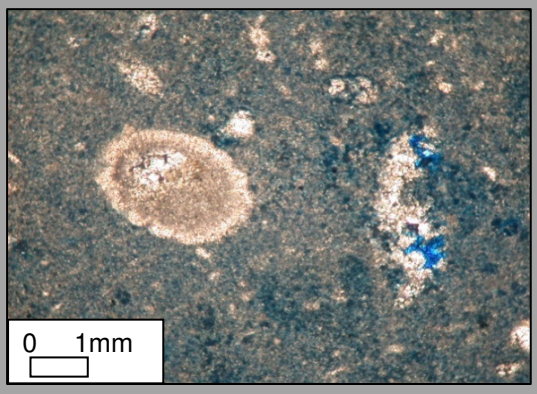

Lithology: *very muddy, is concentrated in 100-250µm dolomite rhombs, echinoid fragments and 0.5mm* S. dinarica *and 0.5mm* C. lineolatus *fragments.*

Figure 3.24O: Lithofacies 15: Mineralised aggregate grain rich algal pack-wackestone

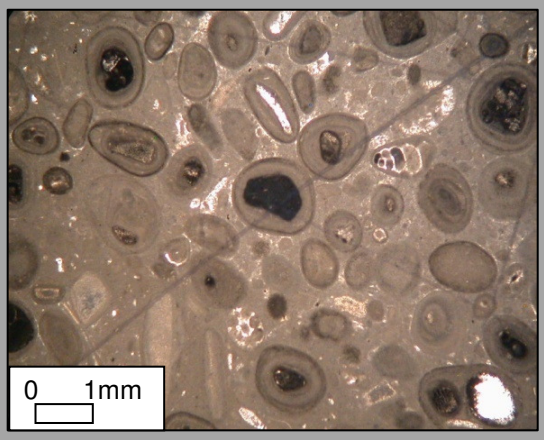

Lithology: *very muddy and concentrated in aggregate grains. The nuclei of the aggregate grains are mostly reworked 0.25-0.5mm* Trocholina sp.*, 1-2mm* C. arabica*, 0.5mm undifferentiated rotalids and 0.5-1mm echinoid fragments that is covered by layers of micrite. The external micrite coat has been blackened and mineralised, to form a black halo. There is also some 1-2mm* C. deciphens *that is reworked and heavily mineralised. There are other sparse fossils such as 0.5mm* Merlingina cretacea*, 1-2mm* B. hedbergi *and 0.5mm* Nezzazata simplex*.*

Figure 3.24P: Lithofacies 16: Cemented algal, rotalids, *C. deciphens* shell hash (grainstone)

Lithology: *dominated by a collection of 0.5mm undifferentiated rotalids, 8-10mm echinoid spines, 1-2mm* C. arenata *fragments, 0.5-1mm* Trocholina sp. *fragments and 0.5-1cm caprinid fragments. These bioclasts are freshly broken and display little reworking. There are also 1-2mm* C. deciphens *and 1-2mm* B. hedbergi *within the shell hash that show little reworking. There are other sparse fossils such as 0.5mm* M. cretacea *and 0.5mm* N. simplex *High level of cementation mainly between the large echinoid spines indicates there was once a high level of interparticle porosity.*

Figure 3.24Q: Lithofacies 17: Coarse algal, rotalid, *C. deciphens* shell hash (pack-grainstone)

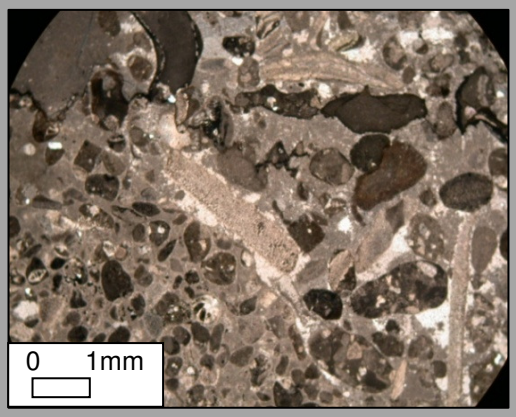

Lithology: *dominated by a collection of 0.5-1mm undifferentiated rotalids, 3-4mm echinoid fragments and spines, 1-2mm* C. arenata *fragments, 0.5-1mm* Trocholina sp. *fragments and 0.5-1cm caprinid fragments. These bioclasts are freshly broken and display little reworking. There are also 1-2mm* C. deciphens *and 1-2mm* B. hedbergi *within the shell hash that show little reworking. There are other sparse fossils such as 0.5mm* M. cretacea *and 0.5mm* N. simplex.

Figure 3.24R: Lithofacies 18: Coarse algal, rotalid, *C. deciphens* shell hash (wacke-packstone)

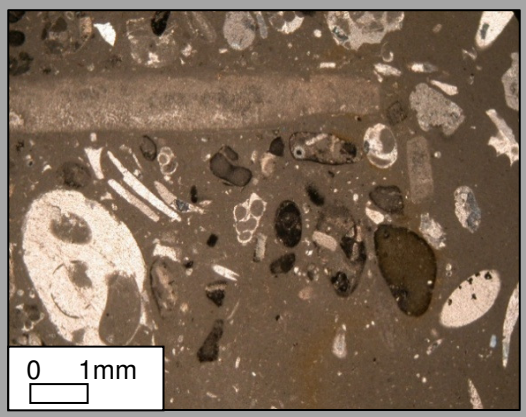

Lithology: *dominated by a collection of 0.5-1mm undifferentiated rotalids, 1-2mm echinoid fragments and spines, 1-2mm* C. arabica *fragments, 0.5-1mm* Trocholina sp. *fragments and 0.5cm-1cm caprinid fragments. These bioclasts are freshly broken and display little reworking. There are also 1-2mm* C. deciphens *and 1-2mm* B. hedbergi *within the shell hash that show little reworking. There are other sparse fossils such as 0.5mm* M. cretacea *and 0.5mm* N. simplex.

Figure 3.24S: Lithofacies 19: Compacted algal and rotalid wackestone

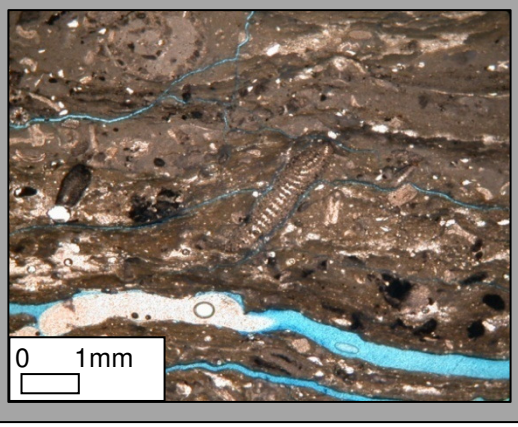

Lithology: *very muddy and concentrated in 0.5-1mm undifferentiated rotalids, 1-2mm echinoid fragments and spines, 1-2mm* C. arenata *fragments, 0.5-1mm* Trocholina sp. *fragments and 0.5-1cm caprinid fragments. There is also sparse 1-2mm* C. deciphens. *The lithology displays compaction from black organic rich seams that may indicate the former presence of organic rich insoluble's. The rock is heavily compartmentalised by the seams to form a very impermeable rock.*

Figure 3.24T: Lithofacies 20: Bioclastic micrite/mudstone (cycle bottom)

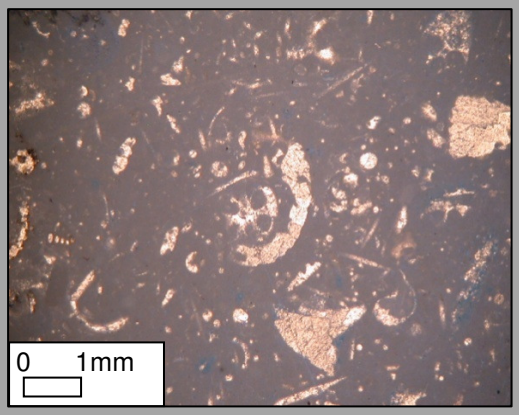

Lithofacies: *very muddy, contains sparse fragmented 0.5-1mm undifferentiated rotalids,* S. muelbergii, Trocholina sp., C. arenata *and on occasion 1-2mm* C. deciphens *There is a large biodiversity of sparse broken bioclasts, coupled with sparse 250-500µm dolomite rhombs and small blackened mineralised grains within a muddy matrix.*

3.4.4 Summary of observations

This section summarises all the detail regarding the biodiversity and the lithologies of the Lekhwair and Lower Kharaib Formations. The positions of the lithofacies are also outlined to show how they fit to the biodiversity and lithological changes, and to the core descriptions.

Using the detailed biodiversity changes from Fig. 3.19-3.23, general changes in biodiversity are compared with the lithologies for the single 4th order HFC's within the Lekhwair during a 3rd order HST and the Lower Kharaib Formation during a 3rd order TST. The lithofacies trends of the Lekhwair Formation outlined below generally agree with studies by Alsharhan & Kendall (1991), as they report that each HFC coarsens upward from argillaceous mudstone into porous wackestone and grainstone.

The Lekhwair Formation

The fossil successions are similar within the 4th order TST's for Cycles 7a, 7b, 4a and 4b. They start with bioclastic micrites/mudstone which grades upward into compacted micrites/mudstone and wackestone (L20 & L19, respectively) (Figs. 3.24S, 3.14T & 3.15). The bioclastic micrites/mudstones are overlain by algal rich debris deposits. The dasycladacean algae present are *Trocholina sp.* (Fig. 3.18O), *C. arabica* (Fig. 3.18L) and *A. assurbanipali* (Fig. 3.18J), along with the foraminifera *C. deciphens* (Fig 3.18A), *M. cretacea* (Fig. 3.18I), *B. hedbergi* (Fig. 3.18M), undifferentiated rotalids (Fig. 3.18F & 3.18G) and caprinid fragments (3.17B) (Fig. 3.19-3.24 & Appendices 1B-1E for biodiversity data). The bioclastic debris is graded: the finest material is present at the base with the coarsest material present at the top forming 1-2mm interparticle pore spaces (L18 (finest)-L16 (coarsest): Figs. 3.24P, 3.24Q, 3.24R & 3.25). These interparticle pores are mostly cemented with LMC (L16: Fig. 3.24P & 3.25). The debris deposits grade upward into deposits rich in 0.5-2mm grains that are concentrically laminated with micrite (L15: Fig. 3.24O) resembling 'aggregate grains' (Fig. 3.25).

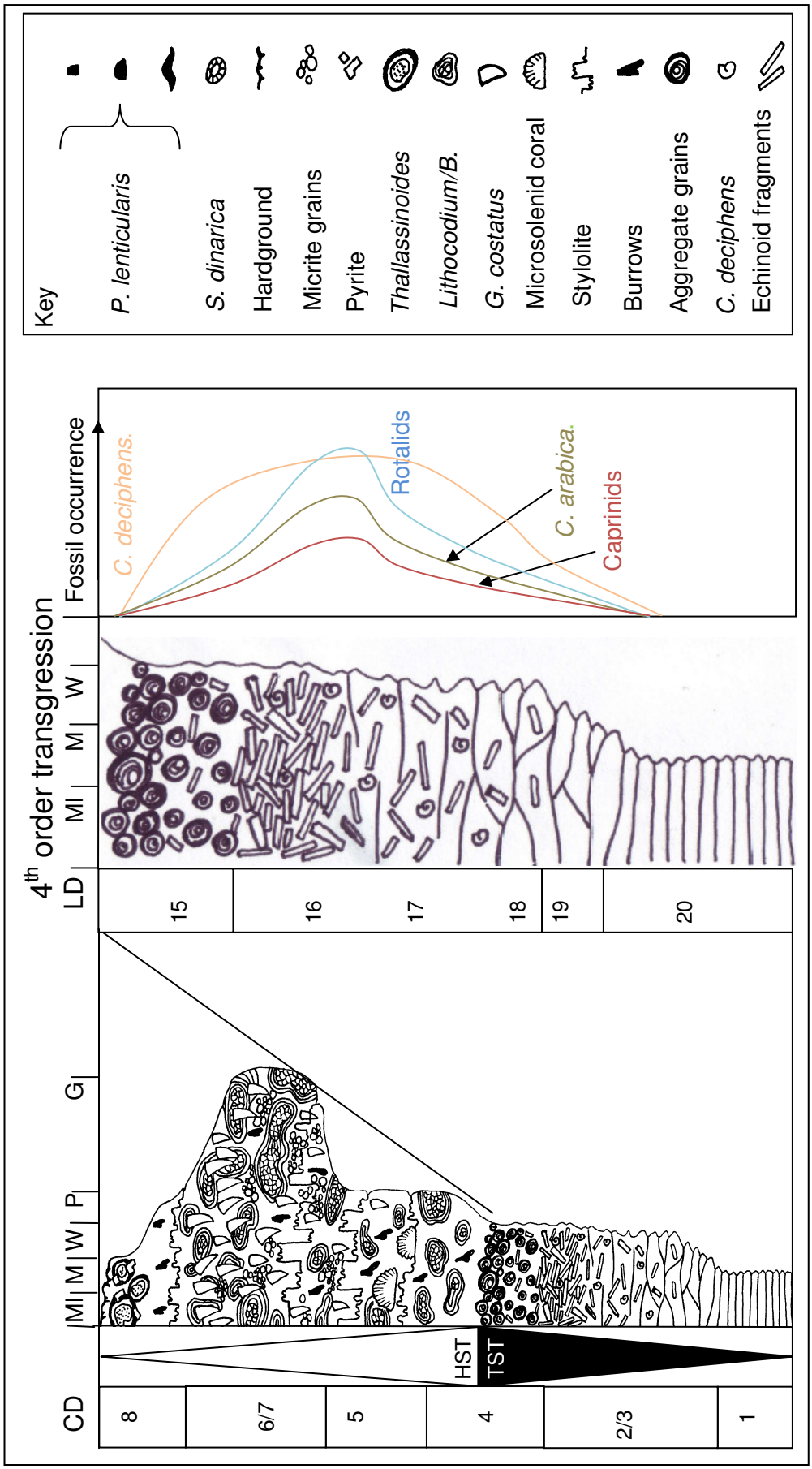

Figure 3.25: Lithofacies associated with the 4th order TST's within each HFC, in the 3rd order HST's of the Lower Lekhwair Formation (plus Cycle 4a in the Upper Lekhwair Formation). CD stands for Core Descriptions whereas LD stands for Lithofacies Descriptions.

The 4th order HST's for Cycles 7a, 7b, 4a and 4b start with bioturbated bioclastic wackestone containing *Lithocodium/B*. (Figs. 3.24C & 3.27). The *Lithocodium/B.* present has two distinct parts; a) an inner 'sponge-like' centre consisting of fine 250-500µm irregular chambers surrounded by b) fine micritic 'algae-like' laminations (Fig. 3.27A). In places the *Lithocodium/B.* shows a vacuolated medulla (Banner et al. 1990) (Fig. 3.27B). The internal chambers represent the descriptions of phrenotheca (Fig 3.27A & 3.2). These deposits directly overlie the aggregate grain beds and represent the first visible reduction of mud within the matrix.

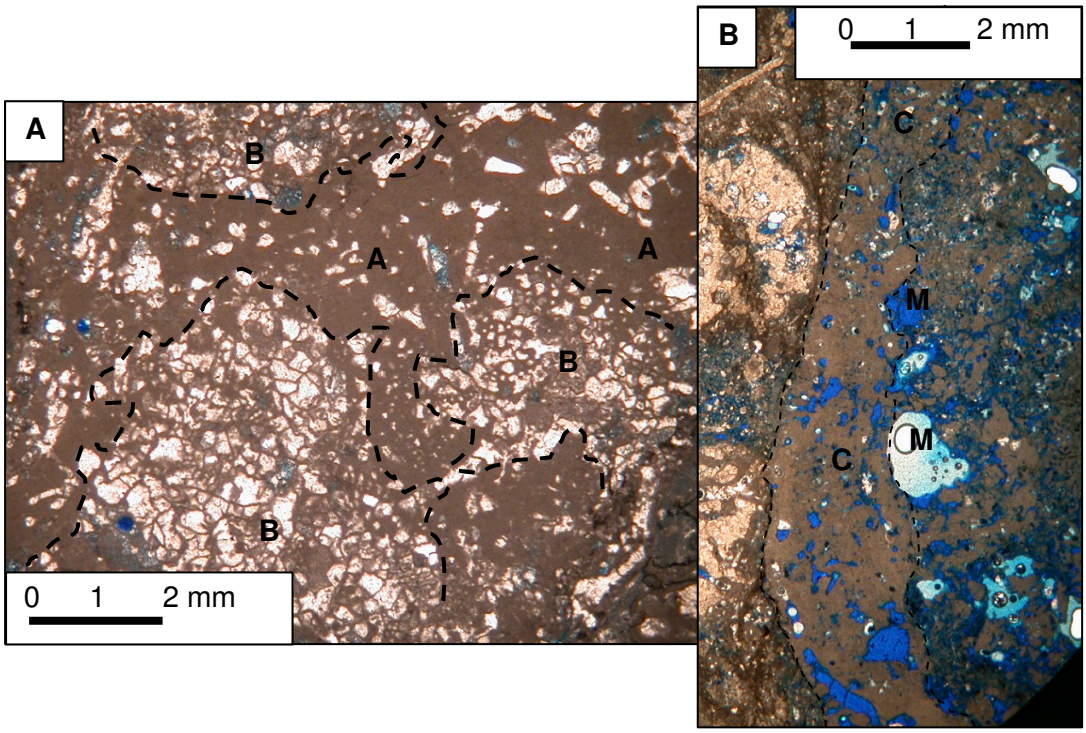

Fig. 3.27: A) Lithocodium/B. *with (A) representing the* Lithocodium *and (B) representing the* Bacinella (as suggested by Leinfelder (1993) and Schmid & Leinfelder (1996). *B) The partially calcified "vacuolated" Medulla (M) surrounded by the thick outer cortical wall (C) (as stated by Banner et al. 1990).*

Overlying the bioturbated *Lithocodium/B.* wackestone is muddy wackestone and packstone (L7 (coarse matrix) & L12 (fine matrix): Figs. 3.24G & 3.24L) containing isolated fragments of microsolenid coral (Fig. 3.17G) and stromatoporoid (Fig. 3.17H) (Figs. 3.19—3.23 & Appendices 1A-1E for biodiversities).

Further up section the lithology becomes less muddy and contains *Cladocoropsis* (Fig. 3.17F) and *G. costatus* (Fig. 3.17A) within packstone and grainstone (L13 (finest), L10, L11 & L5 (coarsest): Figs. 3.24M, 3.24J, 3.24K & 3.24E) (Figs. 3.19-

3.23 & Appendices 1B-1E for biodiversities). The *G. costatus* have thick costae, are on average 1-1.5cm in radius, are isolated within the matrix and, unlike the caprinids (Fig. 3.17B) within the 4th order TST's, are not broken and appear whole suggesting they are relatively in situ.

Many benthic foraminifera become abundant and increase, from 0.5mm to 4mm, in length into the 4th order late HST's (L5: Fig. 3.24E), including *P. infracretacea* (Fig. 3.17I), *R. Lugeoni* (Fig 3.17J), *Textularia sp.* (Fig. 3.17K) *Bigenerina sp.* (Figs. 3.17L & 3.17M), *Reophax sp.* (Fig. 3.17N), *D. hahounerensis* (Fig. 3.17O), *N. brönnimanni* (Fig 3.17H) and *V. arenata* (Fig 3.17D) (Figs. 3.19-3.23 & Appendices 1B-1E for biodiversities).

At the base of the 4th order HST, within the majority of 4th order HFC's, *Lithocodium/B.* is abundant up-section before the appearance of microsolenid coral and *G. Costatus.* However, in some cases, the *Lithocodium/B.* is abundant further up section from the microsolenid corals and *G. Costatus* (Figs. 3.19-3.24 & Appendices 1B-1E for biodiversities). *Lithocodium/B.,* within most 4th order HFC's, has remained present throughout the 4th order HST and in some cases bounds up the entire lithology (L8: Fig. 3.24H). Micrite-filled *Lithophaga* (Fig 3.17D) and clionid sponges have bored through *G. costatus* shells. The *Lithocodium/B.* has exploited these borings and grown upon the shells (Fig. 3.28).

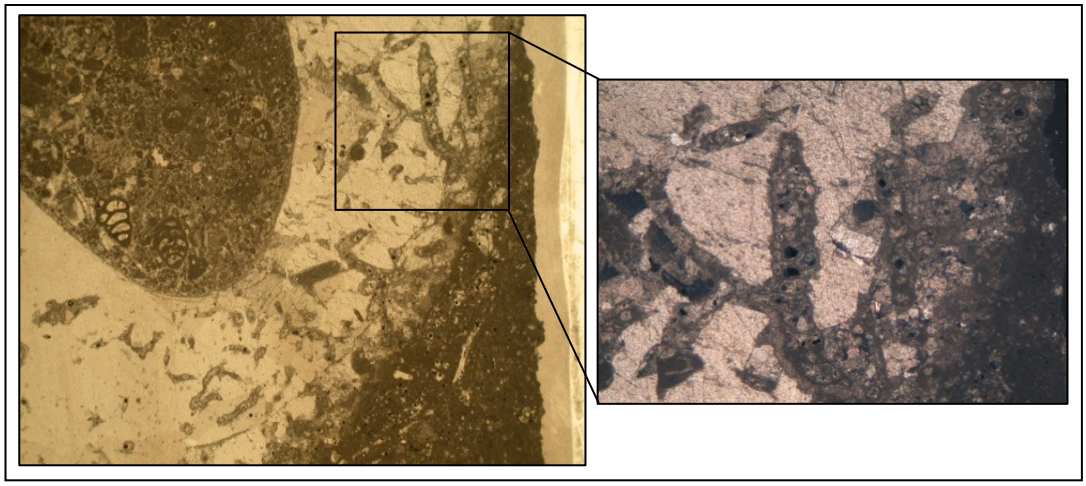

Figure 3.28: The Lithocodium/B. *has exploited the borings within* G. costatus *shells*

Within the final few feet of each 4th order HFC are firmgrounds (L1, L2 & L3: Figs. 3.24A, 3.24B & 3.24C). The firmgrounds constitute a firm substrate that was burrowed by *Thallassinoides* (*Glossifungites*: Section 4.3.1). *Thallassinoides* are filled with dolomite, and sediment, and are haloed by framboidal pyrite.

Hardgrounds cap most firmgrounds, which are immediately overlain by deep water argillaceous micrites/mudstones, and the next 4th order HFC. There is no evidence for meteoric diagenesis as there are no meniscus cements, other vadose cements, and karstic features, within any of the 4th order HFC firmgrounds (Fig. 3.29 & Section 4.3.2).

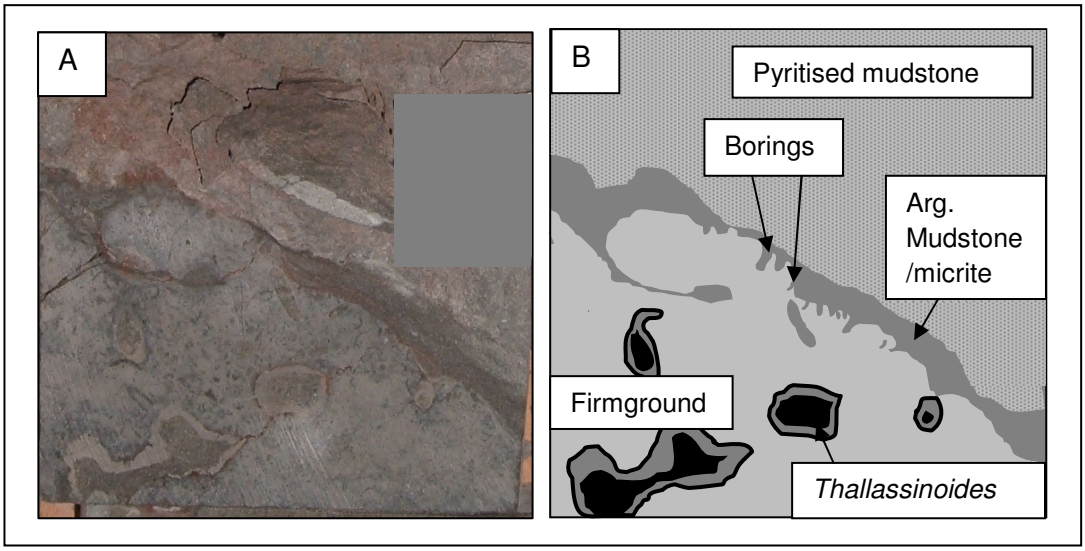

Figure 3.29: hardground capping a firmground assemblage and a 4th order HFC. The presences of borings and an irregular surface indicate a hardground. There is no evidence for meteoric diagenesis, karstic features, mud cracks, or palaeosols, indicating subaerial exposure. A) photograph of a hardground against B) a schematic diagram highlighting the main features (Section 4.3.2).

The entire 4th order HST's, during a 3rd order HST, are summarised in Figure 3.30 for the Lower Lekhwair Formation (plus Cycle 4a).

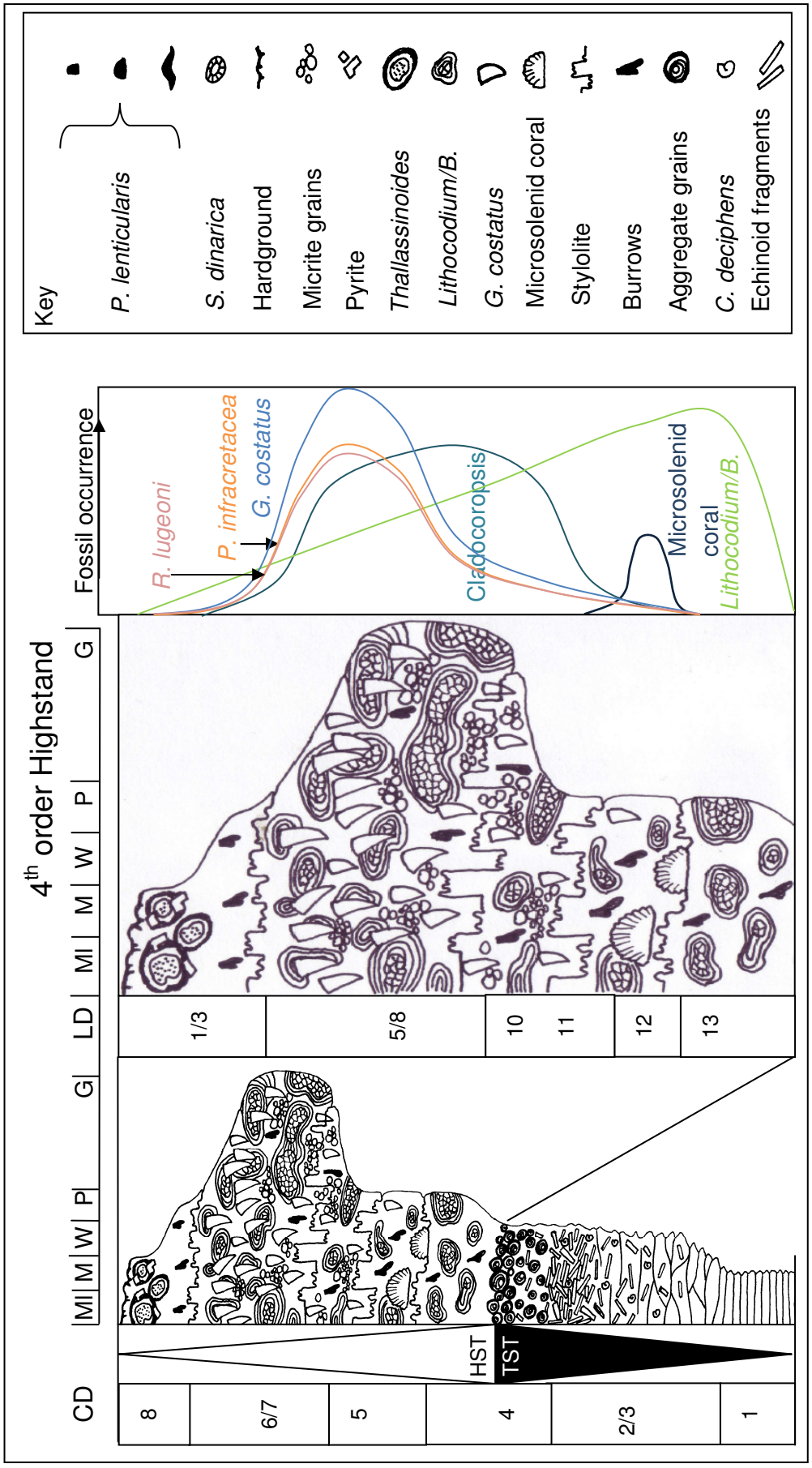

Figure 3.30: Lithofacies associated with the 4th order HST's during a 3rd order HST within the Lower Lekhwair Formation. CD stands for Core Descriptions whereas LD stands for Lithofacies Descriptions.

The Lower Kharaib Formation

The 4th order TST within the Lower Kharaib Formation (Cycle 1) shows a slightly different fossil succession. The base is muddy, dominated by echinoid, *S. dinarica* and *C. lineolatus* (Fig. 3.18E) fragments (L14) (Figs. 3.24N & 3.31), that in places is concentrated in dolomite rhombs (L2) (Figs. 3.24B & 3.31). There are no 'algal-rich' debris deposits present (Figs. 3.19, 3.22 & 3.23: Appendix 1A for biodiversities).

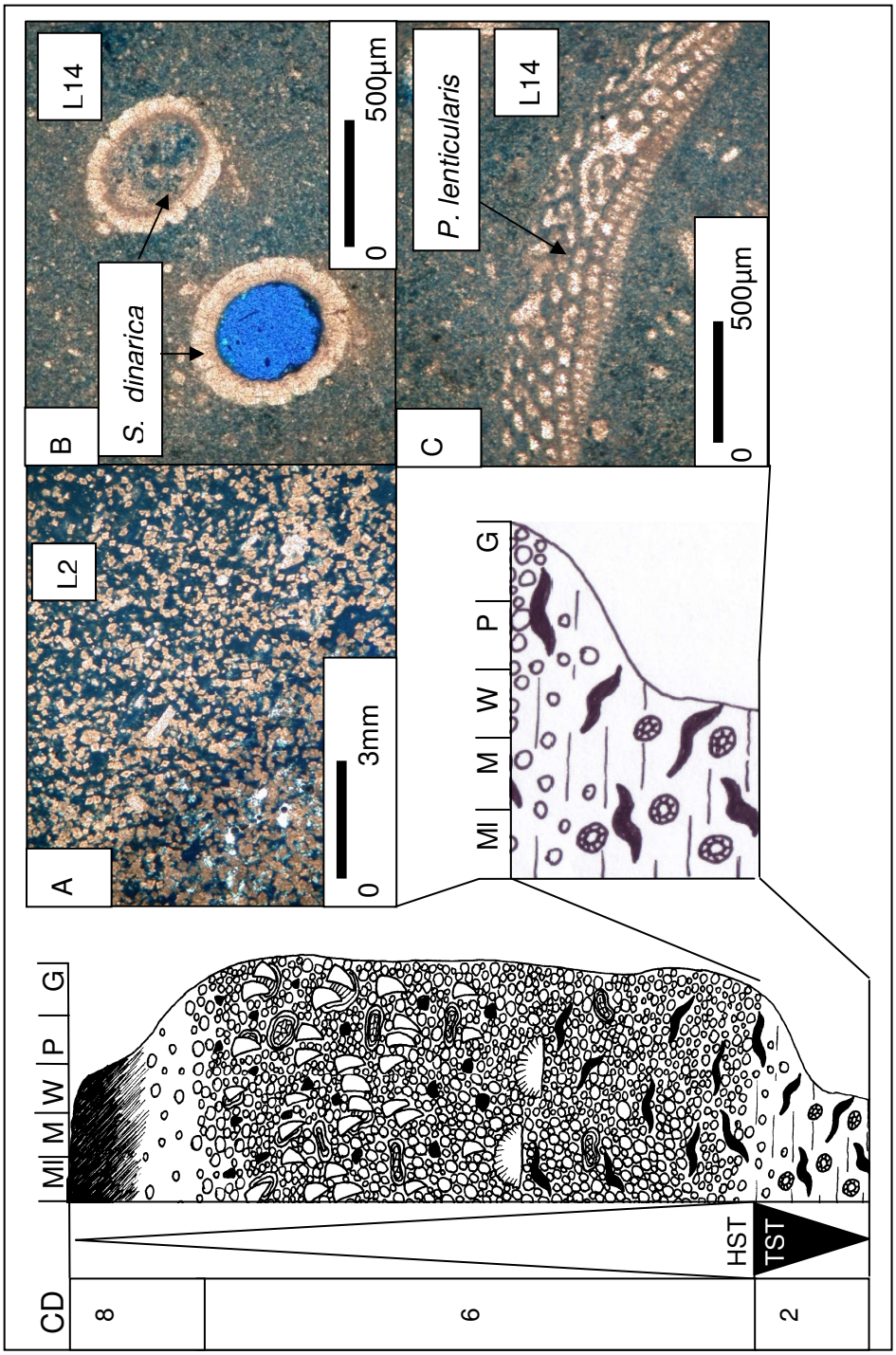

Figure 3.31: The TST sequence for the Lower Kharaib Formation. It is only 10ft thick and is muddy with some dasycladacean algae fragments. The entire TST is a mixture of A & B) L14, and C) L2. CD stands for Core Descriptions whereas LD stands for Lithofacies Descriptions.

P. lenticularis changes from a large 3-4mm flat discoidal morphologies (Fig. 3.18B) within the 4th order late TST/early HST (L14 & L9: Fig. 3.24N & 3.24I) to small 0.5-1mm conical morphologies (Fig. 3.18C) within the 4th order mid-late HST (L6 & L9: Figs. 3.24F & 3.24I). The only area to show a reverse trend is Cycle 1 within Well 4: the final few feet contain an anomalous concentration of large flat *P. lenticularis* within the 4th order late HST and within muddy lithologies (L4: Figs. 3.24D).

The 4th order HST of the Lower Kharaib Formation (Cycle 1), in comparison with Cycles 7a, 7b, 4a and 4b in the Lekhwair Formation below, are far coarser. The lithology is composed of 100-500µm micrite grains with open interparticle porosity. Other than abundance in *P. lenticularis* and the absence of *Thallassinoides*, the 4th order HST's of the Lower Kharaib Formation contains a similar fossil succession compared with 4th order HST's within the Lekhwair Formation. The succession starts with microsolenid coral (Fig. 3.18G) and stromatoporoid fragments (Fig. 3.18H) (L7 & L11: Figs. 3.24G & 3.24K) and grades upward into *G. costatus* (L6 & L9: Figs. 3.24F, 3.24I & 3.32). There is also a higher concentration of *Lithocodium/B.* further up-section from the highest concentration in *G. costatus*. The top of the Lower Kharaib Formation contains an increase in small gastropods (Fig. 2.20E). Figure 3.32 is a summary of the fossil succession, within the Lower Kharaib Formation, representing a 3rd order TST.

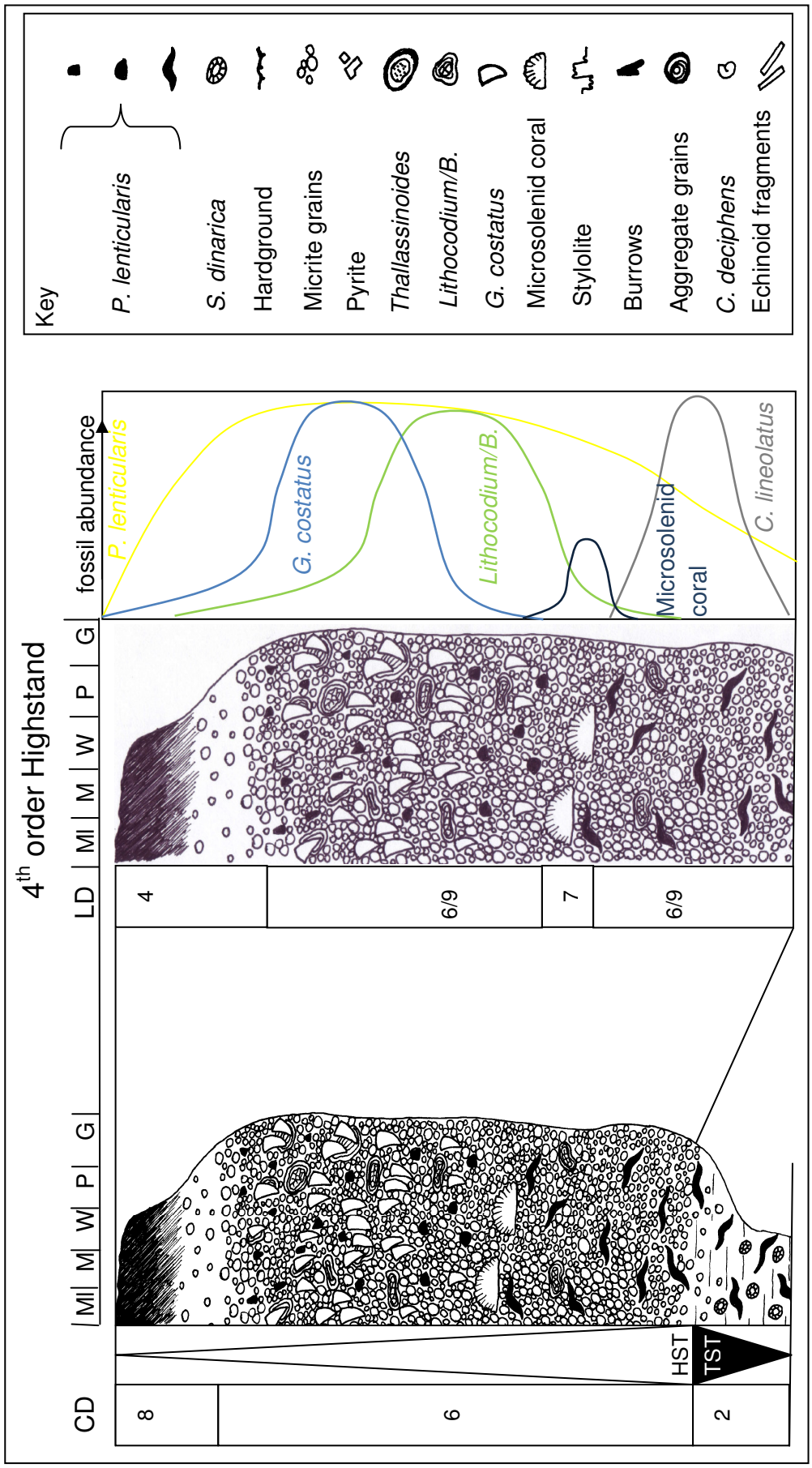

Figure 3.32: lithofacies associated with the 4th order HST's of the Lower Kharaib Formation at the end of a prolonged 3rd order TST. CD stands for Core Descriptions whereas LD stands for Lithofacies Descriptions.

3.5 Interpretations

3.5.1 Deposition during a 4th order TST and a 3rd order HST

The fine nature of the bioclastic micrites/mudstones at the base of each 4th order HFC could either represent a deep basin or a deep lagoon. To solve this dilemma its relationship to the overlying algal-rich debris (L16, L17 & L18) (Figs. 3.24P, 3.24Q & 3.24R) is assessed.

The bioclastic debris is angular and freshly broken, suggesting sudden transport and deposition, reflecting an unstable slope (Alsharhan 1995) and possible debris flows. Another indication of debris flows is the fragmentation of all caprinid shells along with the breakage of small rotalids: both suggest the water column was severely agitated. Another possible creation for this debris could be through sea bed reworking during transgressive flooding events. However the concentration in dasycladacean algae suggests transport from the shallow platform above. The presence of intact *C. deciphens* suggests they are in situ, and therefore prefer deeper water environments in comparison with the caprinids on the platform. This is consistent with studies by Hughes (2000a) and Pittet et al. (2002) who associate *C. deciphens* with deeper water environments, and not consistent with studies from Granier et al. (2003/05) who associates *C. deciphens* with shallow water environments within the Lekhwair Formation.

Within a transgressive lag the deposits should be relatively unsorted with respect to grain size and sorting. This is not the case within the Lekhwair Formation 4th order TST‘s as the algal and echinoid fragments become coarser up section (L18 (finest debris)-L16 (coarsest debris: Fig. 3.24R-3.24P). Coarse grading may reflect the entire debris sequence: as each successive platform built out into the basin, and gradually filled the accommodation space, deposition became proximal to the platform. Therefore a vertical section would gradually provide a snapshot of processes occurring within debris flow further upslope (Figs. 3.24P-3.24R & 3.33). This transition in grain size suggests heavier grains had fallen out of suspension first on the upper slope, leaving finer material being deposited more distally from the platform, to form the bioclastic micrites/muds in the lower slope at the base of each

4th order HFC (L19 & L20: Figs. 3,24S, 3.24T). The coarsest (L16) is similar to the platey limestone in caclirudite facies from studies by Watts (1987), who associates this with the distal component of the carbonate submarine fans Sumeini Group of Oman. Therefore the coarsest (L16) may still be a distal equivalent for more proximal coarser grain flow deposits in the west. These deposits may also signify platform progradation with aggradation (Hillgärtner et al. 2003) as sea level rise forced the platform to shed material and broaden towards the basin. Therefore the environment of deposition for these 'algal-rich' debris deposits is the slope environment, with the bioclastic muds are forming in more distal locations, both in deeper water conditions, possibly in a subtidal environment (Alsharhan 1989, Alsharhan & Kendall 1991) (Fig. 3.33).

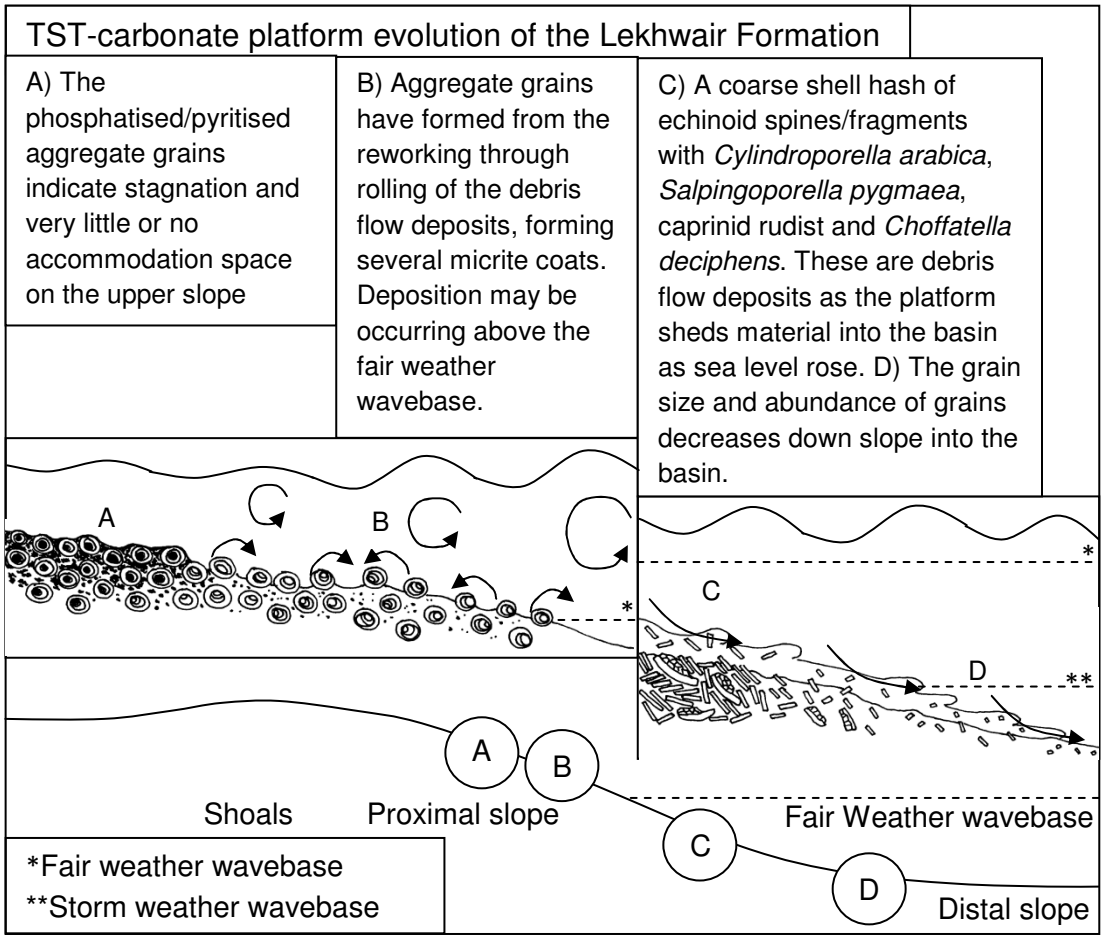

Figure 3.33: processes of formation for the lithologies within the 4th order TST's within the Lower Lekhwair Formation. The aggregate grains may define deposition for the first time above the fair weather wave base, with the top possibly representing the 4th order MFS's. See Fig. 3.24O for photograph of the aggregate grains in L15 and Figures 3.24P-3.24T for photographs of the 'algal-rich' debris in L16-L20.The profile of the slope is exaggerated: the term slope does not mean an increase in slope gradient but represents the areas in front of the prograding

However the possibility of grain flows along the Lekhwair carbonate ramps seems unlikely when calculating the ramps gradient. Only the SB for Cycle 1 is present in all five cores, and to eliminate the structural overprint on the formation due to trap formation, the depth of Cycle 1 SB is compared between Well 1 and Well 5. Both wells are on opposite flanks of the field and therefore have had the least structural overprint. The depth difference is 48m, with the distance between Wells 1-5 being 28.75km. This makes the angle of the slope 0.002°; this seems too shallow a gradient for the propagation of grain flows. This also puts into perspective the slope facies; i.e. it represents a very gentle slope to the east towards the basin. The term slope, for this study, is therefore used to describe the areas in-front of the prograding platform and shoals, and does not represent an increase in slope gradient (Fig. 3.33).

One possibility is that, considering carbonate grain flows are suggested to continue along near horizontal slope for kilometres (+40km: Colacicchi & Baldanza 1986), initiation maybe the key. Considering that these beds were deposited during transgression only, suggest they were deposited by flows triggered by transgression. As stated above, the platforms are broadening and redistributing material into the basin. Short periods of transgression, marked by storm surges would disturb all sediment above the storm weather wave base, proximal to the shoreline, along with any terrigenous sediment within newly flooded areas. The low angle of the slope would mean large proximal areas would be disturbed at once. The higher density, coupled with the large mass of sediment laden water, may have provided enough of an initial force to maintain prolonged grain flows across the low angle slope; however this is all speculation.

However when considering that immediately to the east, in Oman, is shallow carbonate deposits and not deeper water lower slope deposits (Fig. 2.3), the grain flow hypothesis may be invalid. Therefore another possibility is these grain-rich deposits represent meandering sub-marine channel flows across the slope. Studies from Poulsen et al. (1998) have modelled surface current changes in the Mid Cretaceous (~100Ma) and suggested that there may have been several clockwise gyres created in the area by the opening of the Neo-Tethys Ocean, strengthening this possibility. The increase in grain size up-section would therefore relate to a

meandering channel migrating closer to the position of the sampled wells in question. This may well be another plausible explanation and does solve the dilemma of grain flows on a broad stable low angle slope.

The dominant species of dasycladacean algae within the debris of the Lekhwair Formation is *C. arabica* which is defined as a biozone associated with the Mid-Hauterivian by Simmons (1994) (Fig 3.2). This defines the Lekhwair Formation as Mid-Hauterivian in age within the Central Oman Mountains which is slightly different with the age given for the Lekhwair Formation at Abu Dhabi by Sharland et al. (2001), which is Upper Valanginian-Upper Hauterivian. This suggests that the Lekhwair Formation is diachronous across the Arabian plate.

The algal-rich debris may be what Simmons & Hart (1987) and Granier et al. (2003/05) referred to as "algal debris facies". Simmons & Hart (1987) infers the entire Lekhwair Formation to a shallow back shoal environment, which includes the algal debris facies. Within this study the algal debris facies are instead interpreted to represent possible debris flows occurring on the carbonate slope during transgression.

The same algal-rich debris constitutes the nuclei of the aggregate grains within the overlying deposits. The fragments are more rounded suggesting they have undergone more prolonged reworking on the seafloor (Fig. 3.33), which combined with micrite aggradation, possibly indicates tumbling of these aggregate grains and increased water agitation on the sea bed (Fig. 3.24O & 3.33). During the late TST the carbonate ramp may have broadened and expanded towards the basin, placing more distal locations, through aggradation, into shallower conditions above the fair weather wave base. Therefore these tumbled aggregate grains may reflect deposition occurring above the fair weather wavebase for the first time within these 4th order HFC's. This process of environment change is consistent with the transition described by Alsharhan & Kendall (1991) that each HFC within the Lekhwair Formation changes from a deepwater transgressive subtidal environment into an open marine, turbulent and shallow subtidal environment.

Black mineral deposits coating each aggregate grain possibly indicates subsequent periods of stagnation after reworking, when the water column became less turbid (Fig. 3.33). This may reflect complete filling of all accommodation space forming a shallow water ramp. The top of these aggregate grain beds may well represent, and have therefore been attributed with, the 4th order MFS's.

The clasts seen within the talus of the slope are the only indication of the environment upon the platform during the 4th order TST's. The platform may have contained caprinid mounds with microsolenid corals and *Cladocoropsis* forming the main shoals (Fig 3.34B). There may have been a concentration of *C. arabica* and *Trocholina sp.* within a back barrier environment. However the relative succession of biota on the platform is speculative.

Figure 3.34 shows the relationship between the fossils, the environments and relative water depth, during a 4th order TST and a 3rd order HST, for the Lower and Upper Lekhwair Formations.

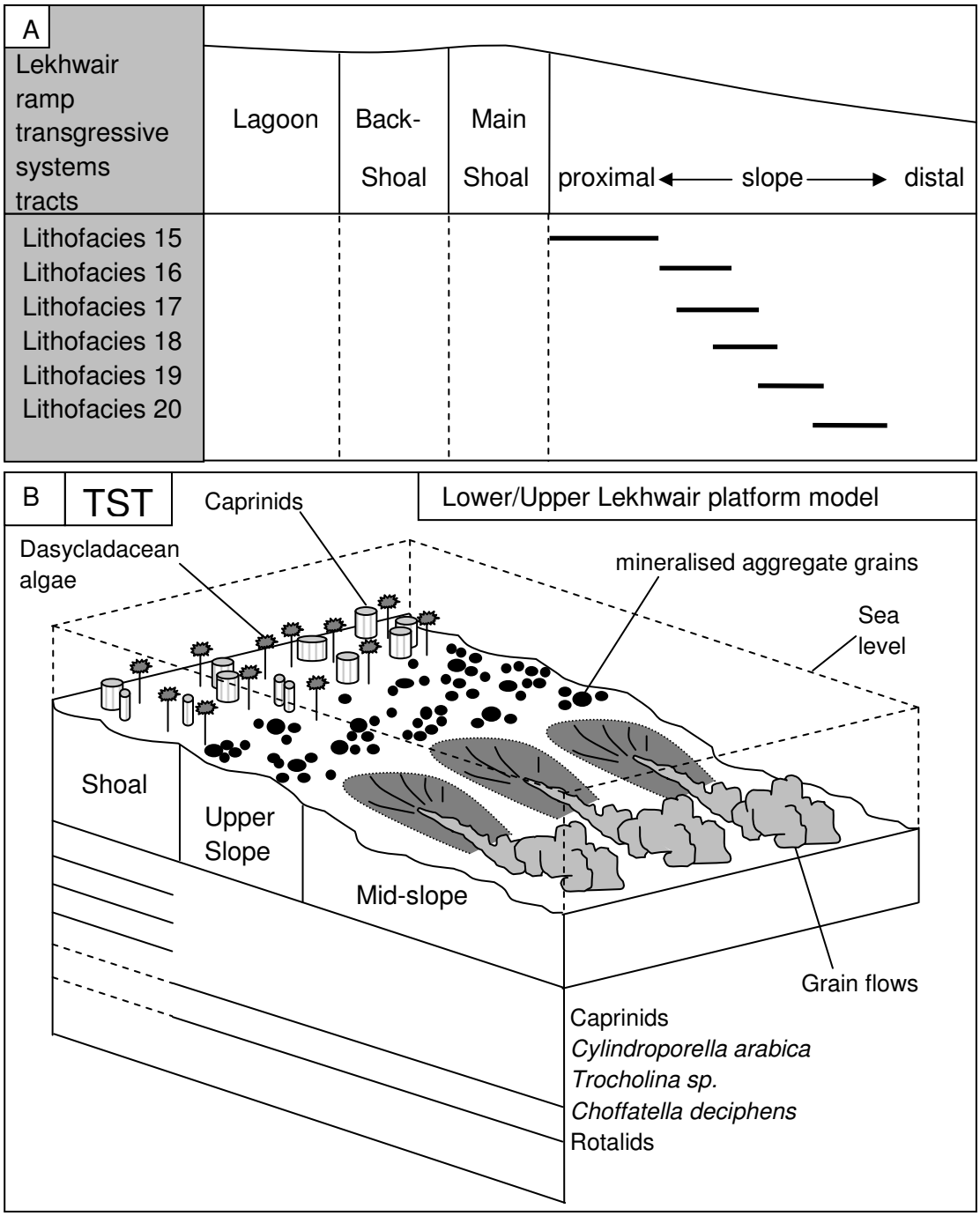

Figure 3.34: Deposition of the Lekhwair Formation during a 4th order TST. A) The lithofacies ordered with respect to their environment of formation. B) Schematic diagram to show the relationships of each environment with respect to relative water depth along the platform of the Lower Lekhwair Formation, during a 4th order TST.

3.5.2 Deposition during a 4th and 3rd order HST

Lithocodium/B. has two distinct parts of *Lithocodium* and *Bacinella* (Leinfelder et al. 1993, Schmid & Leinfelder 1996) (Fig. 3.27A) and in places shows a stepped growth of cortices and medullas, surrounded by a thicker outer wall (Banner et al. 1990) (Fig. 3.27B). The presence of phrenotheca determines the *Lithocodium/B.* assemblage (Schmid & Leinfelder 1996: Fig. 3.2 & 3.27A). The *Lithocodium/B.* in many cases bounds entire lithologies (L8: Fig. 3.24H). *Lithocodium/B.* is abundant within lithologies, capped by corals, sponges and *G. costatus,* which overlay aggregate grain beds. This suggests that *Lithocodium/B.* prefers to colonise an open marine environment (possibly subtidal) upon a barren upper slope, in front of the main shoals, before they prograde out towards the basin. This would also suggest that the *Lithocodium/B.* prefers deeper waters with respect to the *G. costatus*, which is consistent with studies from Pittet et al. (2002). There is no evidence for silliciclastic or clay detritus within the *Lithocodium/B.,* which does not support suggestions from Immenhauser et al. (2005), Pittet et al. (2002) and Schmid & Leinfelder (1996), that *Lithocodium/B.* prefers a mesotrophic environment.

Overlaying the *Lithocodium/B.* burrowed wackestones, within the 4th order early-mid HST are isolated fragments of microsolenid coral and stromatoporoid. This indicates the Lekhwair ramp, unlike the Shu'aiba Formation (Alsharhan 1995), had no significant barrier. Instead the Lekhwair ramp appears to have microsolenid coral and stromatoporoid shoals that may have given some protection for species living behind on the platform.

Further up-section a concentration in fine micrite grains within packstone and grainstone, along with the sudden abundance of *G. costatus,* suggests *G. costatus* prefers a protected environment: this is consistent with studies by Hughes (2000b). Abundance of *G. costatus* in the shoal and back-shoal environments further into the late HST, in comparison with *Lithocodium/B.,* suggests that *G. costatus* prefers shallower environments: this is consistent with studies by Pittet et al. (2002). The concentration in *G. costatus* also suggests that, in comparison with the upper slope, the environment may have become mesotrophic (Strohmenger et al. 2006a). The isolation of the *G. costatus* within the samples suggests they were supported by the

sediment and are most likely in situ (Gili et al. 1995). The presence of *G. costatus* within a protected back shoal environment above, and *Lithocodium/B.* within an open upper slope environment below, constrains microsolenid corals and stromatoporoids as representing the main shoals on the Lekhwair platforms.

Within certain 4th order HFC's *Lithocodium/B.* is abundant with *G. costatus* within the 4th order mid-late HST's, instead of with the microsolenid corals in the 4th order early HST. This indicates *Lithocodium/B.* on certain platforms may have preferred shallow water protected conditions within a back barrier environment: this is consistent with the Shu'aiba Formation (Alsharhan 1995, Hughes 2000b, Masse et al. 1998).

Lithocodium/B. is present in small numbers within back-shoal environments as encrustations on *G. costatus* shells and *Cladocoropsis* fragments. This implies that the *Lithocodium/B.* has formed after the formation of *G. costatus* and *Cladocoropsis* within a back-shoal environment and that it must require a hard substrate to colonise the seabed. This is consistent with Schmid & Leinfelder (1996) suggesting that *L. aggregatum* requires a basal wall to grow. The *Lithocodium/B.* encrustaceans have utilised and grown into *Lithophaga* borings on empty isolated *G. costatus* shells. *Lithocodium/B.* is present throughout the platform environment: generally *Lithocodium/B.* seems to prefer an open marine environment on the upper slope whereas it can survive in smaller numbers within back-shoal environments; this appears consistent with studies for Jones et al. (2004) suggesting a large palaeodepth range for *Lithocodium a.* of 2.5-40m.

The highest abundance and the largest *P. infracretacea* and *R lugeoni* occur with abundant *G. costatus,* abundant micrite grains and therefore back-shoal environments, instead of a deep lagoon (Hughes et al. 2002a). The increasing amount of benthic organisms within the late HST, along with the appearance of borings and suspension feeders may indicate the platform became mesotrophic as it became shallower (Hallock et al.1988, Hallock & Schlager 1986, Mutti & Hallock 2003, Wood 1993).

Firmgrounds capping each 4th order HFC suggest the environment had either become shallower, or carbonate production rates had reduced. The position of the transition proposed by this study differs slightly in comparison with studies by Alsharhan (1989) and Alsharhan & Kendall (1991) as they attribute the coarser porous grainstone at the tops of their HFC's with intertidal platforms and inner shelf lagoons.

Only the firmgrounds display enough evidence to suggest a lagoonal environment. An increase of *Thallassinoides* suggests the environment had become less turbid and more stagnant. The high diversity of broken bioclasts from all environments across the platform suggests storm surges may have transported material from the entire platform towards the coastline, trapping platform sediments into a stagnant, more restricted environment. These heavily burrowed sediments overlying *G. costatus* packstone and grainstone appear to represent the progression from a back-shoal into a muddy restricted lagoon and conditions of non-deposition (Alsharhan 1995) (Section 4.3.1).

A change in lithology occurs above the firmgrounds from highly bioturbated bioclastic rich micrites/mudstones representing a lagoon, to argillaceous bioclastic micrites/mudstones representing the slope toe and basin. This marks a dramatic deepening, the start of the next 4th order HFC and the next 4th order TST. These transitions are represented by hardgrounds that cap the firmgrounds. These surfaces represent the 4th order SB's (Section 4.3.2).

The LST's are absent, probably because sea level fluctuations within the Cretaceous were not significant enough to expose the Lekhwair platform. For example, any dissolution of the aragonitic portions of *G. costatus* shells can be explained by the instability of aragonite and HMC on the seafloor in the presence of Cretaceous calcite seas (Section 2.1). Therefore this study does not support studies by Alsharhan & Kendall (1991) that an increase in depositional porosity within the upper HFC's of the Lekhwair Formation implies freshwater leaching during sea level fall.

Figures 3.35 and 3.36 show the relationship of fossils, the environments and relative water depth during a 4th order HST, and 3rd order HST, in the Lower (Fig. 3.36A) and Upper (Fig. 3.36B) Lekhwair Formations.

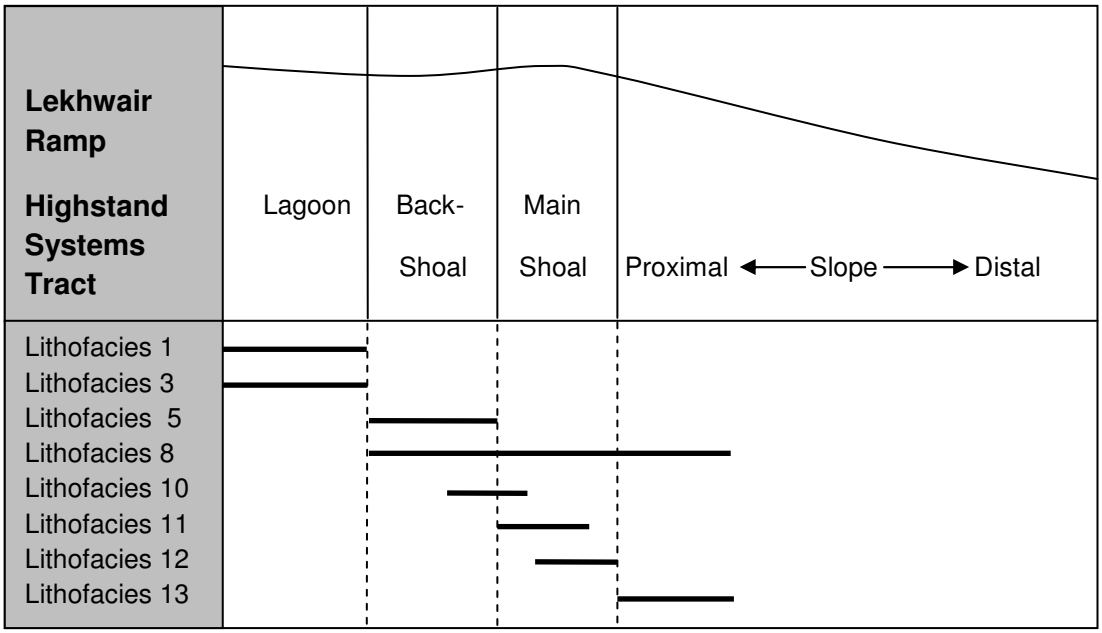

Figure 3.35: The succession of lithofacies for the Lekhwair Formation during a 4th order HST.

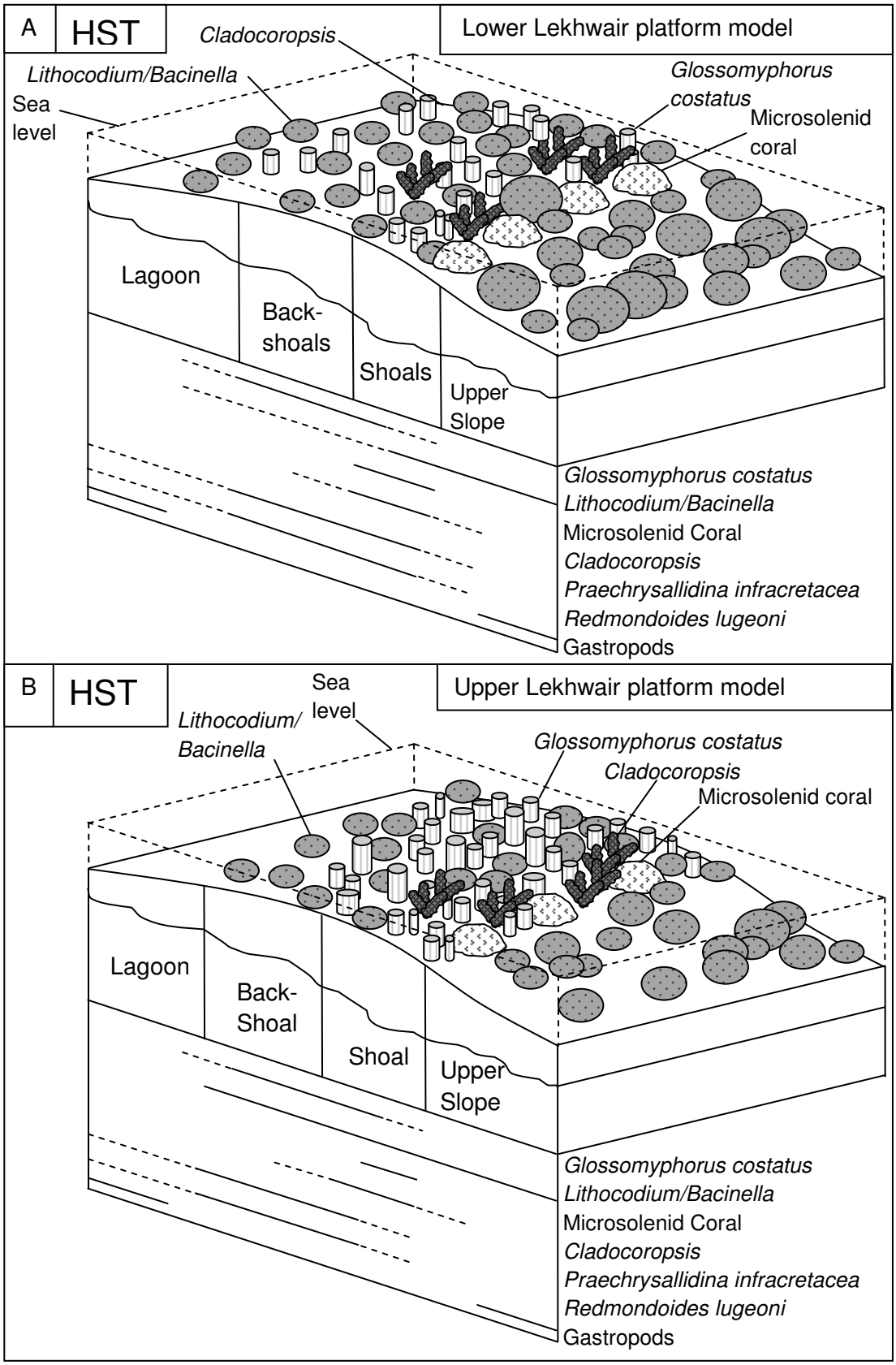

Figure 3.36: Two depositional models showing the biodiversities within their separate environments for A) the Lower Lekhwair Formation and B) the Upper Lekhwair Formation (Cycle 4a).

3.5.3 Deposition during a 4th and 3rd order TST

The 4th order late TST of the Lower Kharaib Formation is very muddy and contains *S. dinarica* and *C. lineolatus* (L14: Figs 3.24N, 3.24K & 3.24E). The first appearance of *S. dinarica* is diachronous across the Arabian plate, as it occurs much later within this study in the Upper Hauterivian (~124Ma), in comparison with Simmons & Hart (1987) in the Mid-Valanginian in the Oman Mountains (~130Ma). The first appearance of *C. lineolatus* is diachronous across the Arabian plate, as within this study it occurs slightly earlier in the Upper Hauterivian (~124Ma), in comparison with Simmons (1994) in the Upper Valanginian (Lower Valanginian: Simmons & Hart 1987) in the Oman Mountains. *C. lineolatus* is associated with a fore bank environment, whereas *S. dinarica* is associated with a lagoonal environment by Hughes (2000b). The muddy lithology, coupled with a low biodiversity may represent a deep lagoon. However there is no evidence for bioturbation such as *Thallassinoides*, which are used in this study within the Lekhwair Formation, and by Hillgärtner et al. (2003) on the Lower Kharaib Formation, to infer a lagoonal environment. Instead the Lower Kharaib Formation environment may be the platform and uppermost slope before the shoals prograde during the subsequent HST towards the basin, which is consistent with Hughes (2000b) for *C. lineolatus*. The overlying microsolenid coral and *G. costatus* pelletal grainstone representing a shoal and back-shoal environment confirms this lithology represents an upper slope environment.

S. dinarica and *C. lineolatus* could have originated from further upslope in a shallower environment, and been transported by a debris flow downslope. However there is no evidence for debris flows during the 4th order TST. There are two possibilities: 1) as this top reservoir was deposited at the end of a 3rd order TST the platform may have been more laterally extensive: all the accommodation space may have been filled. Therefore, either the platform was too broad and shallow to allow for the initiation of debris flows, or more likely 2) these flows were occurring much further east into the Neo Tethys. Consequently this HFC has a very thin 4th order TST that progresses quickly into the 4th order HST.

Figure 3.37 shows the relationship between the fossils, the environments and water depth during a 4th order TST, a 3rd order TST, in the Lower Kharaib Formation.

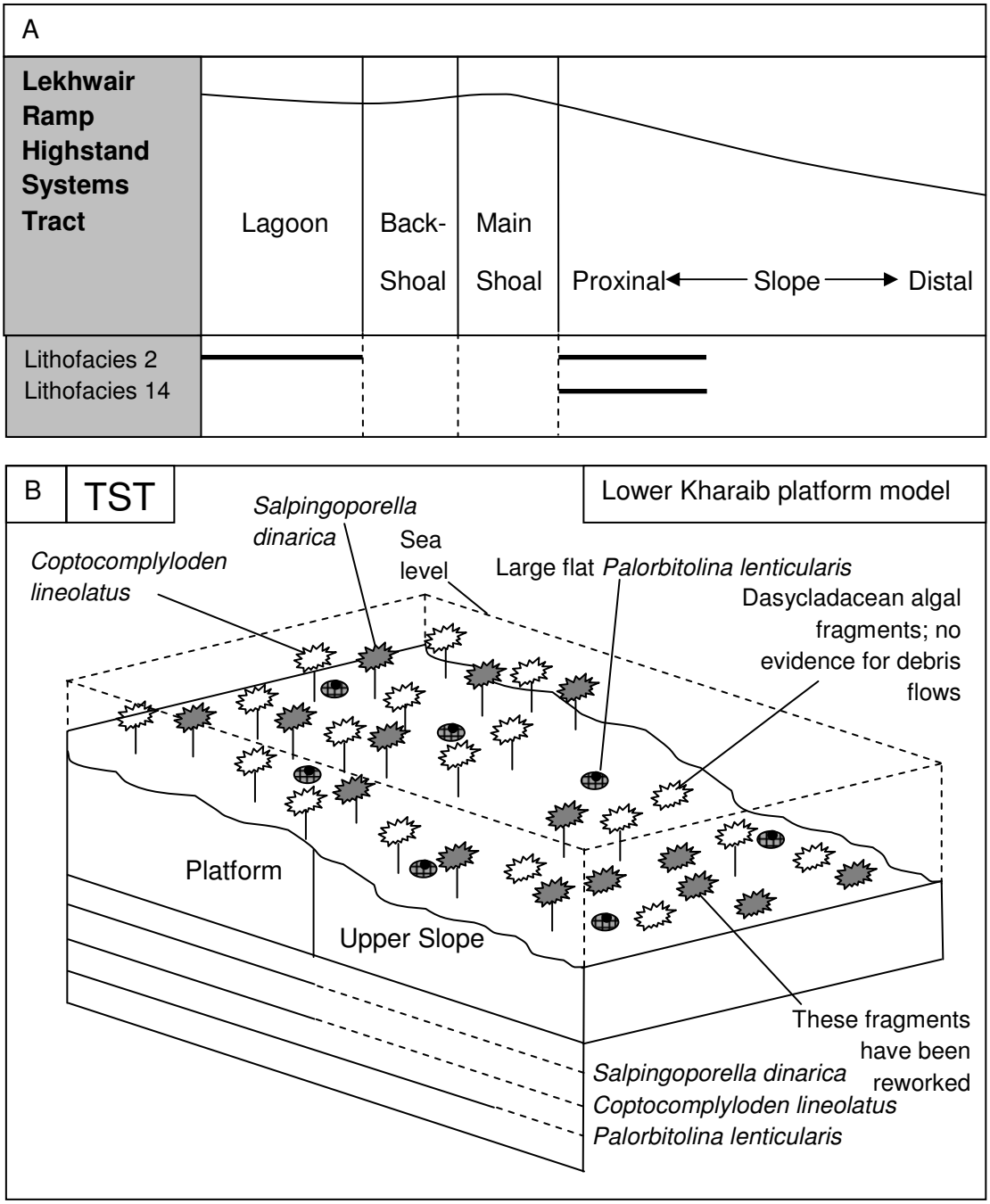

Figure 3.37: Deposition of the Lower Kharaib Formation during a 4th order TST. A) The lithofacies associated with their environments within the Lower Kharaib platform during a 4th order TST. B) The environments of the Lower Kharaib Platform ordered relative to depth.

3.5.4 Deposition during a 4th order HST and a 3rd order TST

Microsolenid coral and stromatoporoid fragments represent the main shoals (L7 & L11: Figs. 3.24G & 3.24K) with *G. costatus* and *Lithocodium/B.* representing more back-shoal environments (L6 & L9: Fig. 3.24F & 3.24I): this is consistent with the Shu'aiba Formation (Alsharhan 1995, Hughes 2000b, Masse et al. 1998). The absence of significant bioturbation within the surrounding grain-rich matrix suggests the entire Lower Kharaib Formation does not represent a lagoon (Hillgärtner 2003) but instead a back-shoal environment (more consistent with Strohmenger et al. 2006a).

The coarser nature of the Lower Kharaib Formation, in comparison with all the 4th order HFC's within the Lekhwair Formation below, indicates more proximal depositional conditions for the platform with respect to the shoreline. *C. deciphens* disappears while *P. lenticularis* appears within the Lower Kharaib Formation. There is also an increase of *G. costatus* and a decrease of *Lithocodium/B.* from the base Lekhwair Formation into the Lower Kharaib Formation (Fig. 3.38). The *G. costatus* prefers shallower back-shoal environments and increases in number up-section into the Kharaib Formation, while *Lithocodium/B.* generally prefers a deeper upper slope environment and decreases in number up-section into the Lower Kharaib Formation. The morphology of the *Lithocodium/B.* also changes up-section, as it bounds the reservoirs of the Lower Lekhwair Formation, whereas within the Lower Kharaib Formation there are only small centimetre sized patches with millimetre thick encrustaceans on *G. Costatus* and *Cladocoropsis* fragments. This suggests the platform environment is becoming shallower through geological time. Therefore deposition within the Kharaib Formation may be occurring at the shallowest point in comparison with the entire Lekhwair Formation.

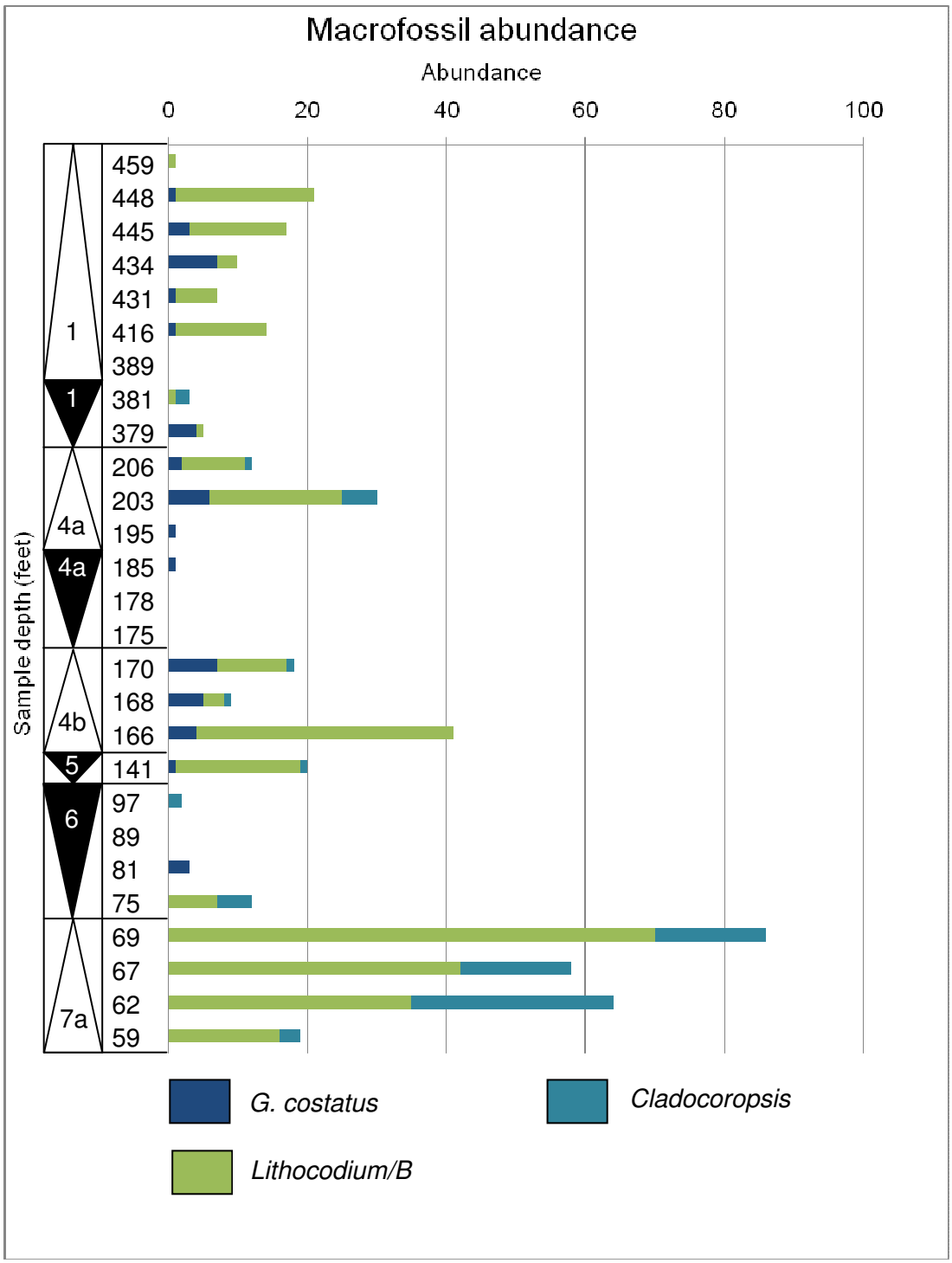

Figure 3.38: abundance of Lithocodium/B. *is high within the Lower Lekhwair Formation while the* G. costatus *is absent. Within the Lower Kharaib Formation the* Lithocodium/B. *has reduced dramatically while the rudists have become more abundant. Each bar represents a single 2" by 3" thin section. The y-axis shows the specific depths for each bar (sample) (Section 1.2 for depth calculations). The black triangles represent 4th order TST's while the white triangles represent 4th order HST's. The succession is from Well 4.*

The inverse relationship between *Lithocodium/B.* and *G. costatus* from the Lekhwair Formation into the Lower Kharaib Formation (Fig. 3.38) may relate to studies by Immenhauser et al. (2005), which show a cyclic shift between *Lithocodium/B.* and rudists within the Shu'aiba Formation of Oman. Abundant *Lithocodium/B.* correlates with O.A.E.'s (Ocean Anoxic Events), with black shale deposition in the basin and platform drowning (Immenhauser et al. 2005). The process of black shale deposition and an O.A.E. is outlined by Jenkyns (1980) and involves a turbulent, shallow water, epeiric sea, with well oxygenated mixed upper layers that promotes much primary productivity by zooplankton and phytoplankton (Fig 3.39). A stable primary nutrient supply will maintain concentration in zooplankton and phytoplankton, uptake in oxygen, maintaining the oxygen-depleted nutrient rich bottom waters. The oxygen depleted waters will sink and slide down the platform due to their higher density (Jenkyns 1980). These bottom waters generate black shale in the deep basin (Jenkyns 1980) (Fig 3.39). The majority of the Lekhwair deposition may have been within oxygen depleted waters. The Lower Kharaib Formation may be the only HFC that was deposited in oxygen rich mixed top waters, promoting more filter feeders such as *G. costatus* (Mutti & Hallock 2003).

However, the position of black shale and O.A.E.'s shows the closest one between the Mid Barremian at 118Ma and the Upper Albian at 100Ma. This time period is later than Lekhwair and Lower Kharaib deposition (129Ma-123Ma: Sharland et al. 2001), suggesting the inverse relationship between *G. costatus* and *Lithocodium/B.* is not linked to an O.A.E. and the processes outlined by Jenkyns (1980).

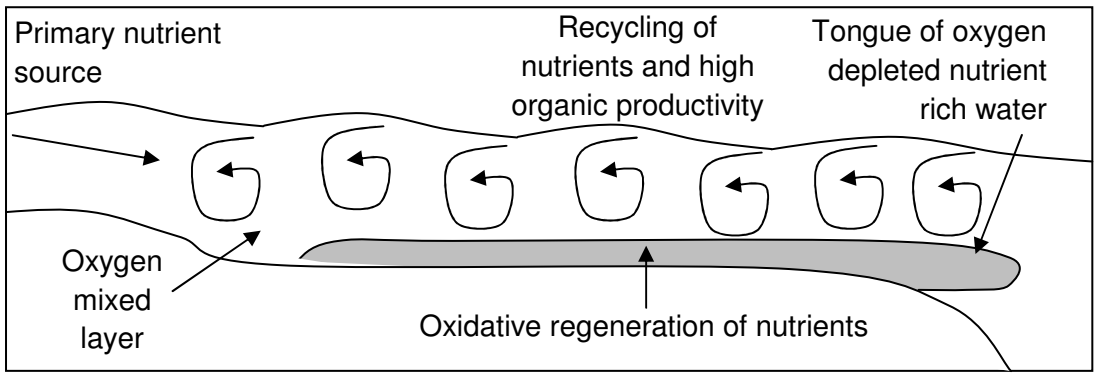

Figure 3.39: The processes behind the formation of oxygen depleted bottom waters during TST of a shallow epeiric sea (redrawn from Jenkyns (1980).

Abundance in rudists is interpreted by Strohmenger et al. (2006a) as representing high nutrient levels. An increasing gradient of nutrients can cause symbiotic animals (*Lithocodium/B.*) to lose competition to faster growing macro algae and sponges and it promotes dense populations of phytoplankton, which is an abundant food resource for filter feeding benthos (*G. costatus*) (Hallock et al. 1988, Mutti & Hallock 2003). The rise in plankton productivity also reduces the light conditions within the water column for corals (Mutti & Hallock 2003). Higher light levels can lead to extension of the photic zone to greater depths allowing for more specialisation, promoting a high biodiversity and spatial diversity (Wood 1993). If the Lower Kharaib Formation represented more mesotrophic conditions and deposition in lower light levels there would be a lower biodiversity with respect to the Lekhwair Formation below. There is a small reduction in biodiversity within three wells with the Lower Kharaib Formation (Figs. 3.19-3.23 & 3.40: Appendix 1A-1E). There are less small gastropods, *Cladocoropsis, P. infracretacea*, *R. lugeoni* and *Bigenerina sp.* with respect to the Lekhwair Formation below, indicating a possible small slowdown of the carbonate factory (Fig. 3.40).

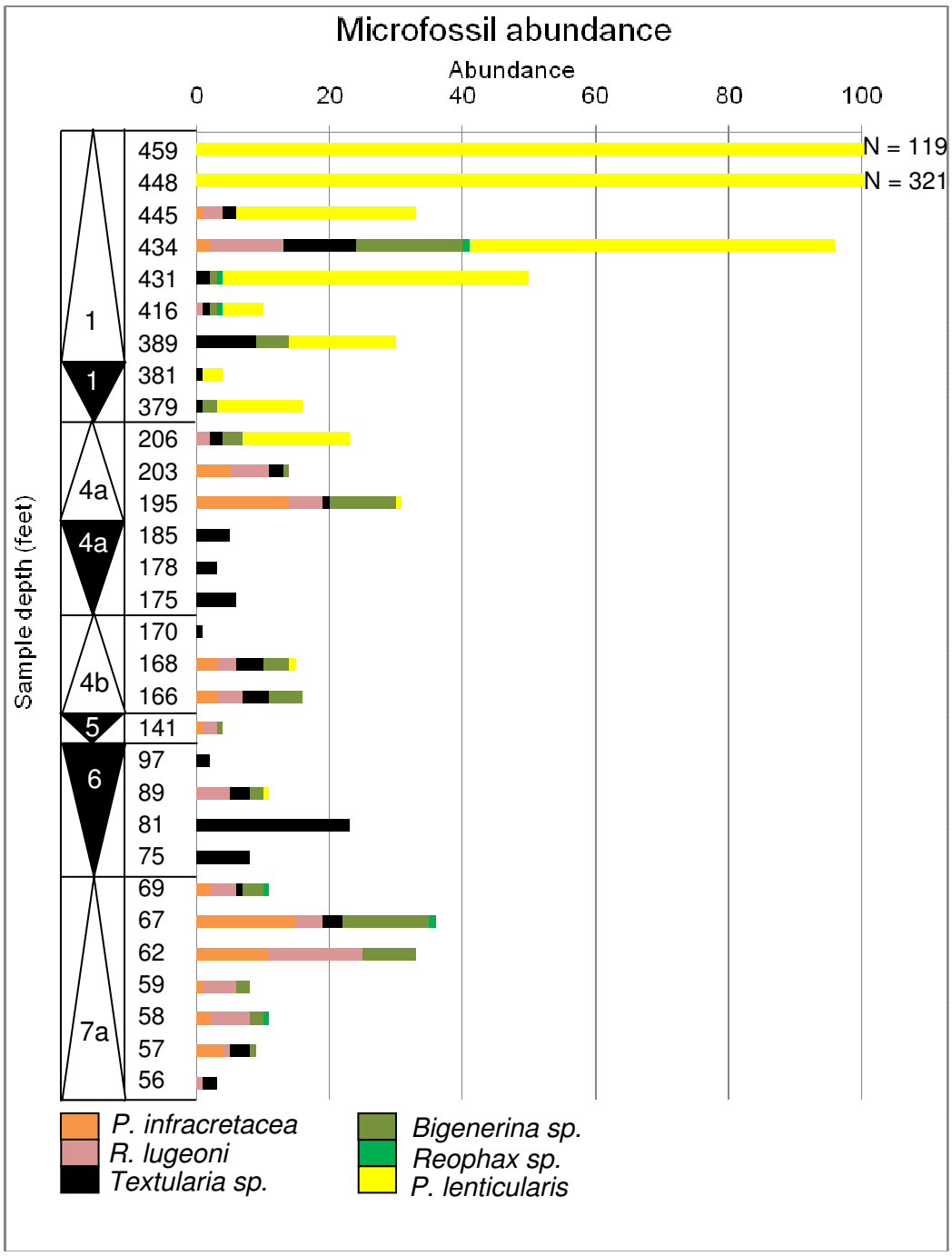

Figure 3.40: benthic abundance decreases into the Lower Kharaib Formation while the amount of P. lenticularis *dramatically increases. Each bar represents a single 2" by 3" thin section. The y-axis shows the specific depths for each bar (sample) (Section 1.2 for depth calculations). The black triangles represent 4th order TST's while the white triangles represent 4th order HST's. The succession is from Well 4.*

The grain rich matrix does not appear to be related to increased bioerosion, as the Lower Kharaib Formation is mostly absent from *Lithophaga* and cleonid sponge borings, suggesting against mesotrophic conditions. Therefore, instead of nutrient availability, the increase in *G. costatus* is suggested to be the cause of a more carbonate sediment dominated environment (Gilli et al. 1995). This is confirmed within this study as *G. costatus* is isolated within the samples, suggesting they require sediment to anchor themselves into the sea bed. In comparison with *Lithocodium/B.* requiring a more solid substrate, this inverse relationship may just be the change from more mud dominated platforms (Lekhwair Formation) into more grain dominated platforms (Lower Kharaib Formation) and has no relation to nutrient fluxes.

Within the Lower Kharaib Formation there is abundance of *P. lenticularis.* A previous study by Simmons et al. (2000) puts the first appearance of *P. lenticularis* within the Upper Barremian in Yemen, constrained between 123-120Ma (Sharland et al. 2001). The base of the Lower Kharaib Formation, where *P. lenticularis* first occurs, is dated at Abu Dhabi to the Upper Hauterivian and ~124Ma (Sharland et al. 2001); the first appearance of *P. lenticularis* is diachronous across the Arabian plate between Yemen and Abu Dhabi. However this comparison may not be valid considering the Orbitolinidae inception and extinction points in Simmons (2000) are considered broadly correct and therefore their chronostratigraphic significance are uncertain pending further research.

Studies from Vilas et al. (1995) suggest that *P. lenticularis* grows large because of high nutrient fluxes. If this were the case, within the Lower Kharaib Formation, a source for nutrients (terrigenous run off) would deposit siliciclasts. There are no siliciclasts within the Lower Kharaib Formation suggesting that nutrient fluxes had not increased. The appearance and abundance of *P. lenticularis* is mirrored by significant reduction in other benthic foraminifera: *P. infracretacea* and *R. lugeoni* (Fig. 3.40). However these reductions are small and probably do not represent a slowdown in the carbonate factory. Therefore abundance of *P. lenticularis* within the shallowest succession (Lower Kharaib Formation), in comparison with Textulariacea, suggests it may require shallower platform conditions and higher light

levels. This supports studies by Hottinger et al. (1997) and Hallock (1985) that *P. lenticularis* utilises sunlight through algal symbiosis within its internal chambers.

The shallowing environment may have caused a morphological change of *P. lenticularis,* with the large flat form dominating the 4th order TST, which change upwards into small and conical forms within the 4th order HST (Fig. 3.41), which is consistent with studies by Granier et al. (2003/05), Pittet et al. (2002) and Simmons et al. (2000).

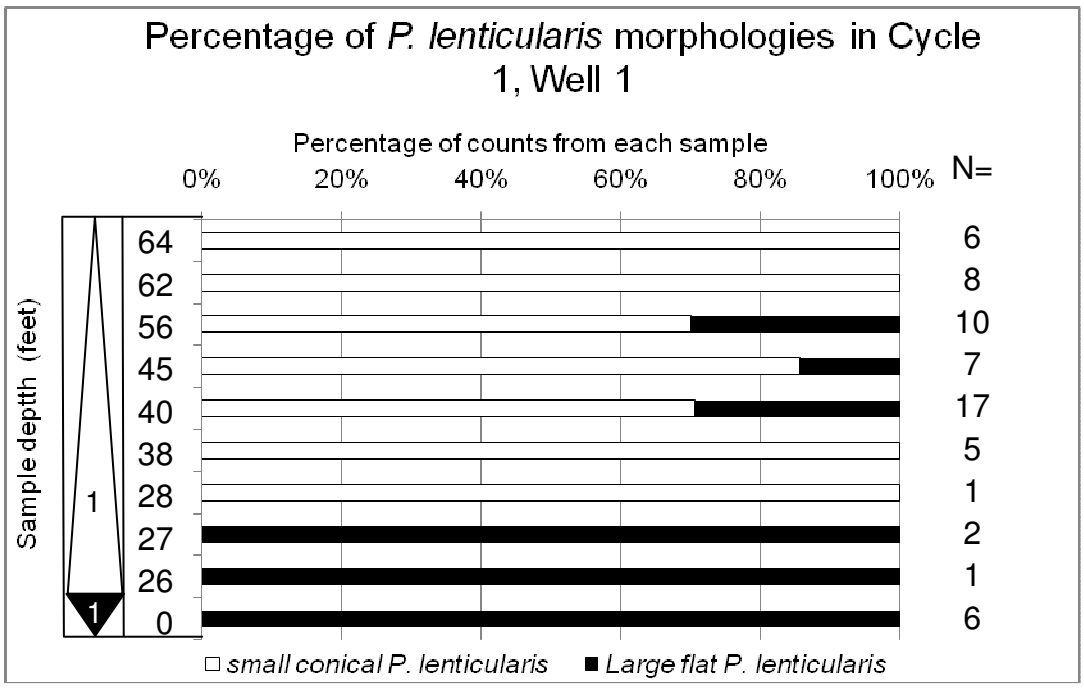

Figure 3.41: There is a change in P. lenticularis *morphology from large flat* P. lenticularis *in the TST to small conical* P. lenticularis *in the HST. Each bar represents a single 2" by 3" thin section. The y-axis shows the specific depths for each bar (sample) (see Section 1.2 for depth calculations).The column on the right of the graph is the total number of counts recorded for both* P. lenticularis *morphological types. The white triangles represent 4th order HST's while the black triangles represent 4th order TST's.*

This morphological change suggests that the thin TST, containing the highest concentration of large flat *P. lenticularis*, had more favourable conditions to enable foraminifera's to grow larger. The TST may have more clay detritus (Pittet et al. 2002, Simmons et al. 2000) and does suggest carbonate growth rates at that particular point may have been low. Studies from Davis et al. (2002) suggest that the TST components represent the distal detritus from pro-deltas in the west, while the HST

represent the retrogradation of these pro-delta complexes along with the retrogradation of the carbonate ramp deposits (Fig. 3.42).

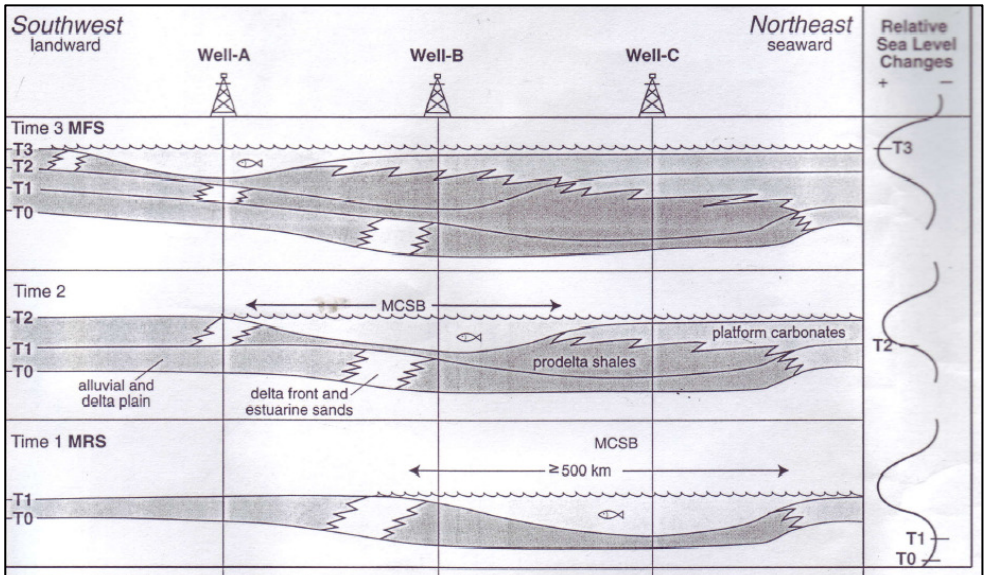

TIME and DATA	WELL-A	WELL-B	WELL-C
T3 Maximum flooding surface (maximum landward retreat of shoreline)	Most proximal deepest water location **TRUE MFS** - maximum onlap - correct age determination	Shallowing water? True **MFS** difficult to identify in limestones without regional perspective	Shallowing water? True **MFS** difficult to dentify in lime-stones without regional perspective
T1 to T3 Retrogradation due to decreasing sediment supply and eustatic rise in sea level	Deepening water? **TRUE TST** Retrogradation recognized	Deepening followed by shallowing water? Apparent but false **MFS** at **T2**	Shallowing water? Apparent but false highstand signature. Retrogradation not recognized
T1 Maximum regression surface. (Maximum seaward advance of shoreline)	Shallowest water? **TRUE MRS** Retrogradation recognized	Shallowing water? True **MRS** difficult to identify in prodelta shales	?Deepest water? Apparent but false **MFS**
T0 to T1 Progradation due to increasing sediment supply and eustatic fall in sea level	Shallowing water **TRUE HST**	Highstand signature difficult to identify in prodelta shales	?Deepest water? Apparent but false **MFS**

Fig. 3.42: The retrogradation of the pro-delta complexes in the west during the HST sequences, along with the carbonate ramp complexes (redrawn from Davis et al. 2002).

Therefore a high light index combined with some terrigenous nutrient fluxes during the TST has favoured the growth of larger *P. lenticularis*. The retrogradation of the carbonate ramps, along with increased carbonate growth rates, and the absence of clays, suggests that terrigenous supply was cut off preventing the *P. lenticularis* from growing to such a large size.

Another possibility for this morphological change is as the water column became shallower into the 4th order late HST, the light intensity would have increased on the sea bed. This may have caused the *P. lenticularis* to remain small, as a similar amount of light could have been captured on a smaller surface area in comparison with larger flatter *P. lenticularis* morphologies under lower light intensities in deeper water.

This study generally agrees with the interpretation of *P. lenticularis* representing shallow platform environments (Alsharhan 1995, Hughes 2000b, Pittet et al. 2002), but *P. lenticularis* is also present within micrites, mudstones and wackestones representing deeper water conditions with potential detritus influx (Alsharhan 1995, Granier et al. 2003/05, Masse et al. 1998; 1997, Pittet et al. 2002, Simmons et al. 2000, Vilas et al. 1995) allowing for the species to grow into its larger flatter morphology: i.e. it can maximise sunlight capture through photosynthesis, and its algal relationship (Hottinger et al. 1997, Hallock 1985), combined with nutrient fluxes to enable it to grow to large sizes (van Buchem et al. 2002, Davis et al. 2002, Vilas et al. 1995).

Figure 3.43 shows the relationship of fossils, the environments and relative sea level during a 4th order HST, a 3rd order TST, within the Lower Kharaib Formation.

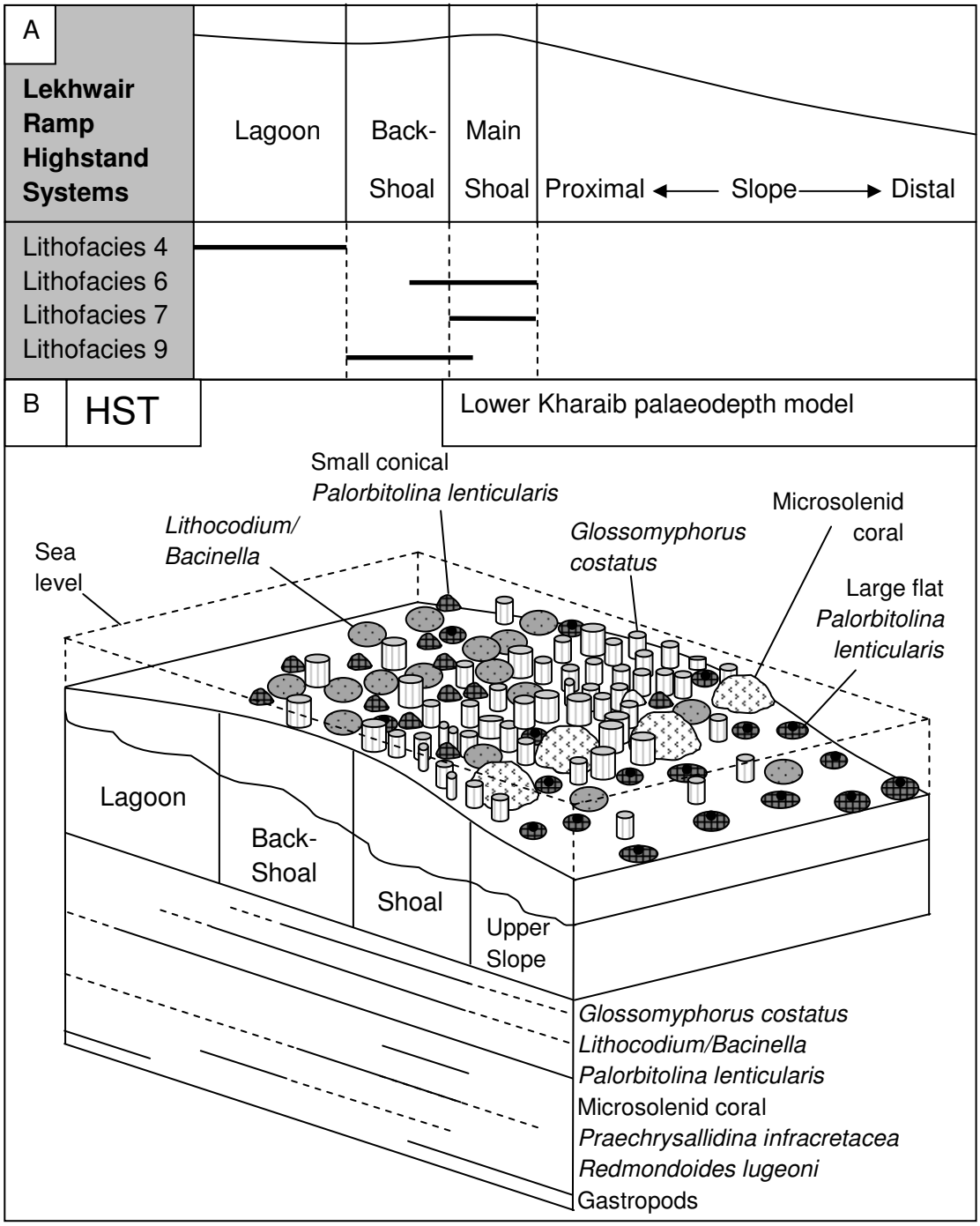

Figure 3.43: Deposition of the Lower Kharaib Formation during a 4th order HST. A) The lithofacies are associated with their environments on the Lower Kharaib Formation during a 4th order HST. B) A schematic representation of the Lower Kharaib Formation showing the relationships of the different environments across the platform.

3.6 Deposition and reservoir heterogeneity

Within each reservoir, the mid-late HST contains the coarsest grain-packstone, and is associated with abundant Textulariacea and *G. costatus*. The concentration of *Lithocodium/B.* only within the reservoir units does exert a control on primary reservoir quality when regarding the amount of porosity, as suggested by Banner et al. (1990). The bounded sections at the base of the Lekhwair Formation have much intra-skeletal porosity (Section 5.3.3) (termed intraparticle by Banner et al. 1990).

Generally these coarser areas correlate across the structure (between the five wells) within most 4th order HFC's conforming to sheet-like, highly porous, layers bounded above and below by denser, less porous units. These non-reservoir areas are associated with the early highstand and transgressive micrites/muds (associated with abundant dasycladacean algae, rotalids, *C. deciphens* and caprinid fragments) and the firmground assemblage. Therefore each reservoir is vertically heterogeneous and compartmentalised, with more pores being open and well connected in the mid-late highstand. These reservoir areas are also cut by impermeable stylolite horizons, which compartmentalise the reservoirs further in two/three separate units within each mid-late HST. With respect to all the reservoirs, the Lower Kharaib Formation (Cycle 1) appears to be the most well connected, porous reservoir, which is relatively homogenous across the structure. Combined with this being the thickest reservoir, with the greatest vertical expanse of pack-grainstone, makes this the best reservoir facies within the entire studied sequence.

3.7 Conclusions

1) Each 4th order HFC shows a shoaling upward trend, with microsolenid corals and stromatoporoids forming the main shoals, *G. costatus*, *Cladocoropsis*, *P. infracretacea* and *R. lugeoni* forming within the back-shoals, and small gastropods alongside *Thallassinoides* burrows forming mainly within muddy restricted shelf lagoons.

2) No 'algal-debris' deposits were found within any reservoir and 4th order HST. Rather, the algal-rich debris deposits comprise the 4th order TST's and could either represent the platform shedding material to the east, through debris

flows initiated by transgression during platform flooding, or by migrating surface palaeo-currents and their associated submarine channels. The presence of intact *C. deciphens* within the debris suggests they are in-situ and prefer deeper waters in comparison with the broken caprinids, which were transported downslope.

3) The aggregate grain beds show evidence for agitation followed by a period of stagnation. These aggregate grains are the first evidence up-section to display constant reworking and therefore may represent deposition occurring above the fair weather wave base. Following stagnation may indicate accommodation space, created from the underlying transgression, is filled and the tops of these aggregate grain beds may also represent 4th order MFS's.

4) Caprinid rudists occur on the platform during 4th order transgressive periods along with high amounts of dasycladacean algae.

5) *Lithocodium* may need a hard substrate to colonise the sea bed before it grows into the adult form that combines with the *Bacinella* component. *Lithocodium/B.* generally prefers deeper water, in comparison with the back-shoal *G. costatus,* within an open marine environment along the upper slope. *G. costatus* seems to require grain rich sediments, in order to anchor itself into the sea bed.

6) The entire sequence from the Lower Lekhwair Formation into the Lower Kharaib Formation is shoaling upwards, as the Lower Kharaib Formation shows a much coarser matrix of 100-500µm micrite grains. Therefore the Lower Khariab Formation is the thickest and contains best, most connected, reservoir facies

7) The inverse relationship of increasing *G. costatus* and decreasing *Lithocodium/B.* from the Lekhwair Formation into the Lower Kharaib Formation may be to do with the environment changing from solid and mud rich sediments in the Lekhwair Formation (which supports *Lithocodium/B.*) to more grain rich sediments in the Lower Kharaib Formation (which

supports *G. costatus*). This relationship probably does not represent changing nutrient levels.

8) *P. lenticularis* morphology changes from large/flat to small/conical morphologies as the Lower Kharaib Formation shoals upwards from the late TST into the late HST. This may either be associated with an increasing light index in the water column, as the platform becomes shallower during the 4th order late HST, or more likely, the absence of terrigenous nutrients in the HST has prevented *P. lenticularis* from growing large, in comparison with the TST (marked by a reduction in argillaceous contents).

9) The first appearance of species *C. lineolatus*, *S. dinarica* and *P. lenticularis* are diachronous across the Arabian plate (although there is some ambiguity with the latter species).

Chapter 4

Sequence stratigraphy framework

Within the last Chapter the sequence stratigraphy and the 4th order SB's/MFS's have been assumed. It is now appropriate to explain the reasons for the 4th order SB/MFS placements and how the 4th order HFC cycle stacking pattern was developed; both aspects are the basis for forming a sequence stratigraphic framework, which is displayed at the end of this Chapter.

It is important to develop a sequence stratigraphic framework for the Lekhwair and Lower Kharaib Formations. A starting point involves identifying the HFC boundaries, which are used to constrain the lithological cyclic natures of each HFC. This study has focused on identifying the 4th order SB's and not the MFS's (Galloway 1989); although the stratigraphy is layer cake and the broad kilometre sized lithological geometries are difficult to establish. The reason is that on this fine scale, each 4th order HFC is capped with a firmground which makes a visual approximation of where the SB should be far easier in comparison with constraining the 4th order MFS positions. Each well, at any specific depth horizon, contains a similar HFC lithological cyclicity in comparison with its neighbours. The similarity probably represents genetically related positions upon one carbonate ramp. It is now clear why a sequence stratigraphic framework (as opposed to lithostratigraphy) is required; these genetically related lithological units can be correlated between the five wells, and across the offshore field, to determine their lateral and vertical extents. This provides a framework to upscale sample support from specific locations within the wells. This also provides an estimation of the extents of the highest porosity/permeability horizons, the extent of the seals, and also the extent of reservoir compartmentalisation. A sequence stratigraphic framework is also important for future work on the distribution of cements, other diagenetic processes.

Sequence stratigraphy associates lithology with relative sea level change to provide an approximation for changing accommodation space for sediment accumulation. Therefore this Chapter associates the most permeable reservoir horizons with sea level change, and changing carbonate growth rates, to see whether these factors have influenced the formation of the best reservoirs.

It is also important to review past literature on where 4th order SB's and MFS's are placed within 4th order HFC's. There are differing reasons for where SB's within the Lekhwair, Kharaib and Shu'aiba Formations are placed. There are also discrepancies with the interpretations for the Lekhwair and Kharaib Formation HFC stacking patterns. It is important to understand why SB positions are debated in the literature, and how to interpret the HFC stacking patterns, in order to make an accurate sequence stratigraphic framework for the Lekhwair and Lower Kharaib Formations.

More specifically, the correct positions of the 4th order SB's are established by core observation (Section 1.2). In combination with petrography of the firmgrounds, including observation on bioclasts, minerals and sedimentary features, any significant deepening is identified. The 4th order HFC thicknesses are used to develop 4th and 3rd order stacking patterns for each well. The 4th order SB's are stacked and correlated across the entire offshore field forming a sequence stratigraphic framework.

Certain guidelines have been followed in order to complete the sequence stratigraphic framework (presented in Section 4.6):

1. The positions and thickness changes of the seven basic lithologies (Section 3.4.1) relate directly to the core observations. Any thickness changes for a single lithology between two wells, the upper and lower limits, are joined with straight lines.

2. Lithological changes between two wells could occur anywhere over a distance of several kilometres. To construct a sequence stratigraphic framework as objectively as possible, and to prevent any artificial lithological

trends being generated, any lateral lithological change is placed halfway between the two respective wells.

3. Each lithological body is drawn to taper downwards towards the basin representing downlap (towards Well 5), and to taper upwards away from the basin representing onlap (towards Well 1). The *Glossomyphorus c.* shoals and the *Lithocodium/B.* biostromes may not have developed onlap and downlap geometries. Petrographic evidence from Section 3.4.4 suggests that no significant barriers had formed, and consequently *G. costatus* and *Lithocodium/B.* shoals may not have had significant topography. Therefore all lithologies have been drawn with onlap and downlap geometries.

4. There is little core recovery, and therefore little observation, between Cycles 2a and 3. Consequently the lithological trends of the Lower Kharaib Formation (Cycle 1) cannot be easily compared with the Lekhwair Formation. Therefore for comparisons see Sections 3.4 and 3.5: this provides detailed petrographic information about both the Lower Kharaib and Upper Lekhwair Formations.

5. Each successive well is placed slightly lower towards the east to signify the slight gradient of the carbonate ramp towards the Rayda Basin.

4.1 Previous work

4.1.1 The sequence stratigraphy of the Lekhwair and Lower Kharaib Formations

A detailed sequence stratigraphic framework for the Lekhwair Formation was completed by Alsharhan & Kendall (1991). The Lekhwair Formation comprises six shoaling and thickening up HFC's implying steady sea level rise (Fig. 4.1C). Each HFC has an argillaceous impermeable mudstone base (transgressive, subtidal open marine setting) that grades upwards into microporous wackestone and finally into porous pack-grainstone (regressive, shallower water, near wavebase) (Alsharhan & Kendall 1991). The transition back into dense mud, capping the reservoir, defines the SB's. The positioning of the SB's by Alsharhan and Kendall (1991) are a

combination of core logging and eustatic sea level cyclicity outlined by Haq et al. (1987) (Fig. 4.1C).

The entire Arabian plate sequence stratigraphy was also outlined by Sharland et al. (2001) and updated by Davies et al. (2002), which defines the major 3rd order MFS horizons throughout the Cretaceous (Fig. 4.1B). Three MFS horizons are associated with the Lekhwair and the Lower Kharaib Formations: K40 (near the Lekhwair Formation base: base of Thamama IV: Zakum Member), K50 (near the base of Thamama III) and K60 (above the top of Thamama IIIA) (Sharland et al. 2001: Davies et al. 2002) (timescale references to Gradstein & Ogg 2004: Section 2.4 & Fig. 4.1B).

Another detailed study of the Lekhwair, Kharaib and Shu'aiba Formations was completed by Strohmenger et al. (2006a; 2007), and Yose et al. (2006), is tied (where possible) on the MFS.SB placements and nomenclature from Sharland et al. (2001) (Fig. 4.1A). However the sequence stratigraphic framework was also based on subdivisions established by ExxonMobil (Micham 1977, Vail et al. 1977: correlating sediment packages and genetically related lithofacies using SB's and not MFS's i.e. GSS: Galloway 1989). Consequently, K50 is at the base of the Lower Kharaib Formation, (instead of the top of the Zakum Member) and K60 is within the Upper Kharaib reservoir horizon, instead of the Upper Kharaib transgressive sequence (Fig. 4.1A). Each MFS has also had the SB below associated with it (Fig. 4.1A).

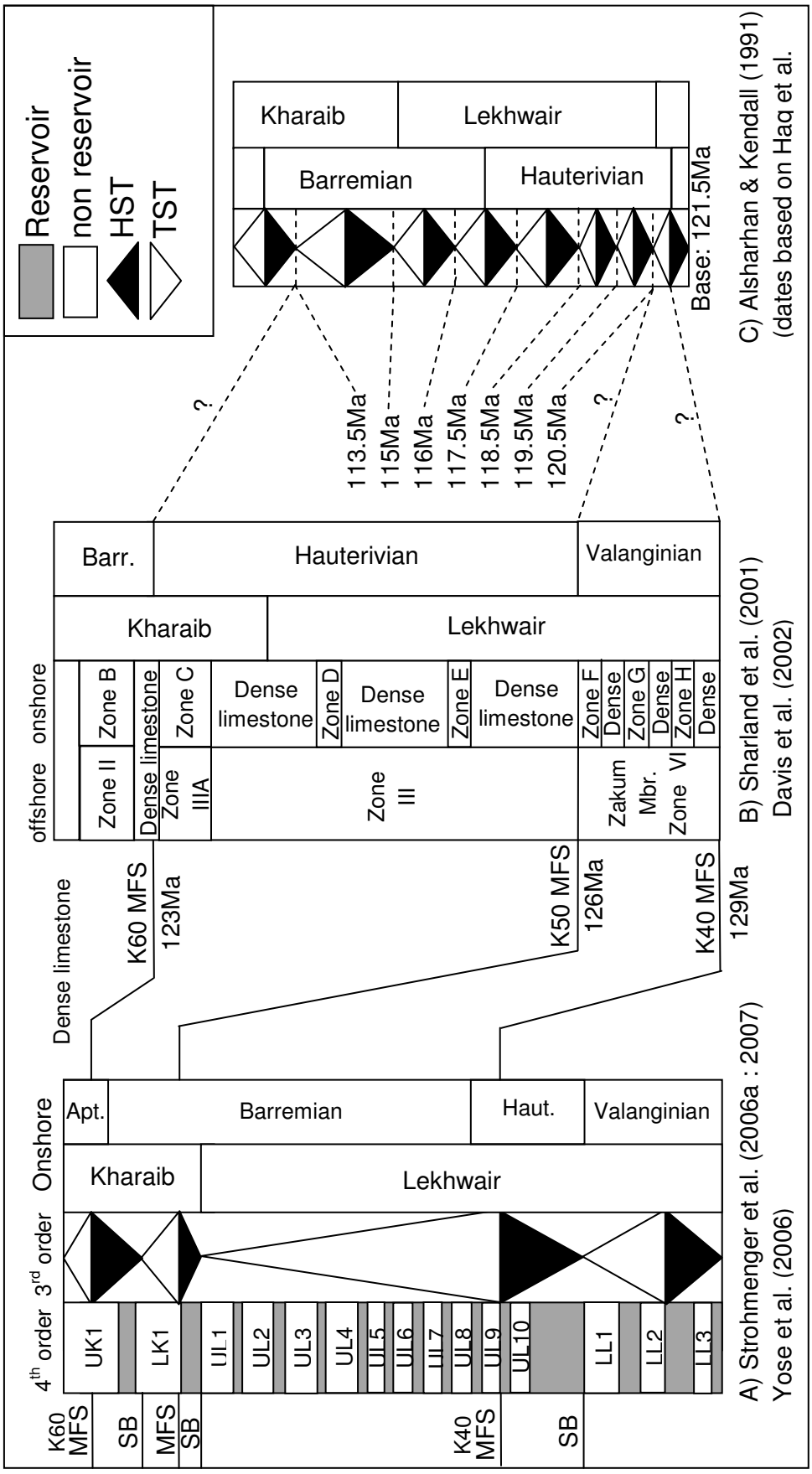

Figure 4.1: HFC's of the Lekhwair and Kharaib Formations proposed by A) Strohmenger et al. (2006a: 2007) and Yose et al. (2006) (the initials for the reservoirs on (A) are: UK: Upper Kharaib, LK: Lower Kharaib, UL: Upper Lekhwair and LL: Lower Lekhwair), B) by Sharland et al. (2001) & Davies et al. (2002) and C) by Alsharhan & Kendall (1991) (based on dates from Haq et al. (1987).

4.1.2 Placing sequence boundaries at hardgrounds

Evidence for sub aerial exposure, which represents sea level fall, is used to define the positions of the 4th order SB's within Early Cretaceous carbonate sequences. For example, the Lekhwair Formation is a shallowing upward succession of 4th order HFC's, with the topmost HFC containing the most depositional porosity: Alsharhan & Kendall (1991) suggest the porosity was enhanced by freshwater leaching during sea level fall. Alsharhan & Kendall (1991) provide no further evidence to support this conclusion. Granier et al. (2003/05) also suggests the leaching of aragonite bioclasts, and their later filling with sediment, within the Upper Lekhwair Formation are evidence for subaerial exposure. Granier et al. (2003/05) provides no further evidence to support this claim.

Within the Barremian-Aptian Lekhwair, Kharaib and Shu'aiba Formations, the large scale depositional cycles show the transition from rudist and miliolid dominated lithologies in the top of each 4th order HFC, to Orbitolinidae and algae dominated lithologies of the next 4th order HFC (Pittet et al. 2002). Both these lithologies are interpreted by Pittet et al. (2002) as shallow water: the transition between these lithologies shows little change in palaeo-bathymetry. However at the base of the Upper Lekhwair Formation are mud cracks, at the base of the Lower Kharaib Formation are truncated coral heads and at the base of the Hawar Member are root traces on the platform top (Pittet et al. 2002). These features are interpreted by Pittet et al. (2002) as evidence of exposure. These features also display a potential degree of relative sea level fall, which is why Pittet et al. (2002) has used these positions to represent SB's between the large scale depositional cycles (Fig. 4.2A).

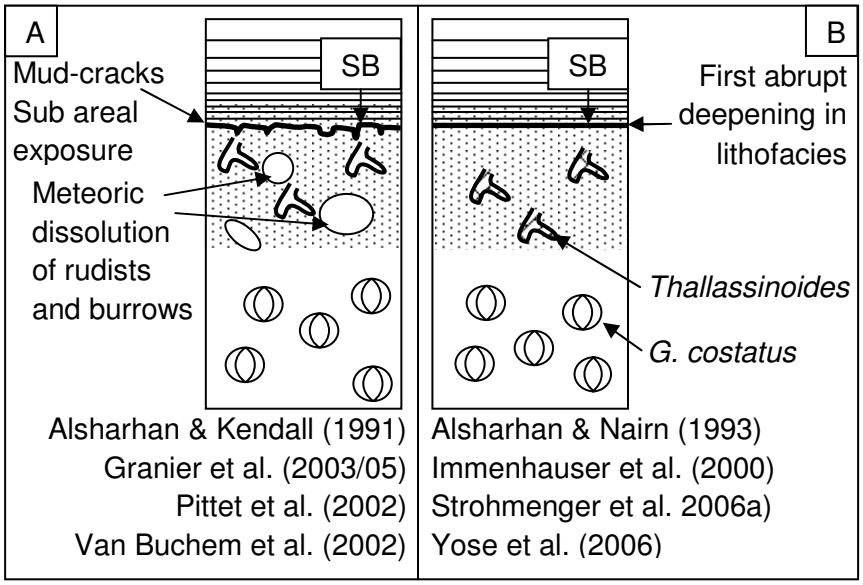

Figure 4.2: two main methods used to determine the position of SB's. A) The presence of meteoric dissolution and subaerial exposure aids in pinpointing the SB's (Granier et al. (2003/05), Pittet et al. (2002), van Buchem et al. (2002)). B) In the absence of meteoric dissolution an abrupt change in lithology, indicating a pronounced deepening can also be used to determine the SB's (Immenhauser et al. (2000), Yose et al. (2006)).

The SB's at Wadi Mu' Ayin within the Lower Kharaib Formation are also placed by van Buchem et al. (2002) between rudist grainstone/rudstone and miliolid wackestone/mudstone, at surfaces lined with mud cracks, displaying evidence for subaerial exposure (Fig. 4.2A). At this transition the Lower Kharaib Formation is capped by firmgrounds containing LMC filled *Thallassinoides*. These burrows have been used to indicate a short period of exposure (van Buchem et al. 2002) (Fig. 4.2A). The exact reasoning for associating exposure within LMC filled *Thallassinoides* is not explained.

The absence of evidence displaying sea level fall and subaerial exposure, any dramatic change in lithology which displays profound deepening of the water column, is used to determine the SB positions. For example, each 4th order HFC's of the Lekhwair Formation consists of deep water lime mudstones and marls overlain by shallow water fossiliferous wackestone and packstone with ooidal and peloidal packstone and grainstone (Alsharhan & Nairn 1993). Alsharhan & Nairn (1993)

suggest the hardgrounds are SB's as they separate sediments defining lithification of the platform slope below and dense accumulations of the TST above (Fig. 4.2B).

Studies by Yose et al. (2006) have also used the rapid change in lithology from peloidal skeletal packstone and grainstone of the HST, to burrowed miliolid rich wackestone of the TST, to locate SB's (Fig. 4.2B). The abrupt transition from shallow high energy shoals, to muddier, deeper water lagoons within the Lower Kharaib Formation indicates flooding: these positions are used to determine SB's (Strohmenger et al. (2006a).

Rapid changes in lithology were also used for identifying the Aptian-Albian boundary at the top of the Shu'aiba Formation (Immenhauser et al. 2000). The discontinuity surface caps peloidal grainstone and skeletal rudstone containing rudist debris, coral fragments, oncoids and reworked intraclasts. Above the surface is the Nahr Umr Formation containing ochre argillaceous packstone rich in Orbitolinidae (Immenhauser et al. 2000). The transition across the discontinuity surface is associated with profound deepening: the SB was placed at the Aptian-Albian boundary.

4.1.3 Placing sequence boundaries at the base of firmgrounds

The Zakum member (basin equivalent of the Lekhwair Formation) of onshore Kuwait, through Qatar, United Arab Emirates and into North Oman, is described as alternating "porous limestones separated by dense argillaceous intervals" (Davis et al. 2002) at the proximal section in Qatar. Each 4th order HFC contains basal shale, representing a regressive event, which cleans upwards into porous limestone. Davis et al. (2002) concludes the cleaning upward trend represents the retreat of 'shoreline attached' argillaceous units (pro-deltas) and the formation of porous shallow water limestone, and therefore associates these sequences with transgression. The top of each HFC indicates deepening and shoreline regression, making the entire HFC a retrogradational package. With this in mind, in Section 3.4.1 and Fig 3.14, the firmgrounds show a mud increase from the underlying mid-HST packstone and grainstone: this may be indicating regression. Deepening may have already occurred, within each 4th order HFC, before the hardground surface is reached.

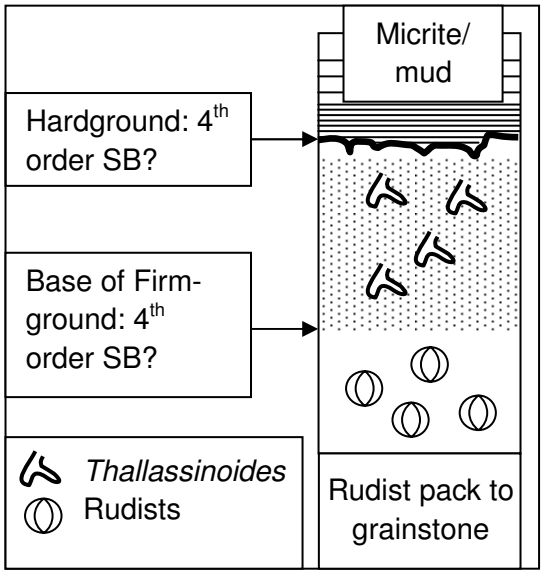

Figure 4.3: There are potentially two positions for the SB's; at the hardgrounds or at the base of the firmgrounds.

A main feature of firmgrounds is the *Thallassinoides*: many authors ascribe *Thallassinoides* with deeper water environments. For example, within the Tertiary slopes of New Jersey, *Thallassinoides* are recorded by Savrda et al. (2001) within lithologies displaying sediment starvation and transgressive ravinement: *Thallassinoides* have formed during sea level rise (Fig. 4.4A).

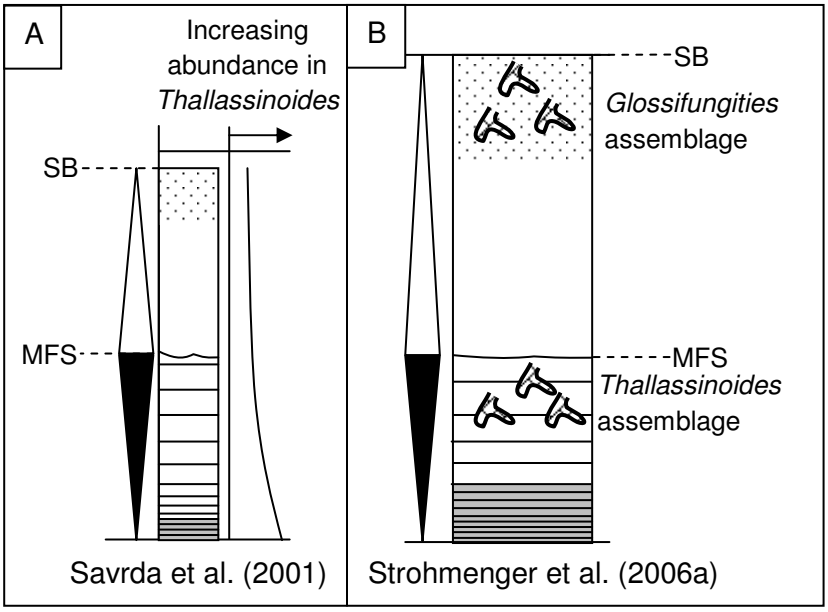

Figure 4.4: A) The amount of Thallassinoides *recorded by Savrda et al. (2001) is greatest just below the MFS, while B)* Thallassinoides *have only been found by Strohmenger et al. (2006a) below the MFS, only* Glossifungites *are found at the SB's (compiled from data by both Savrda et al. (2001) and Strohmenger et al. (2006a) .*

A similar conclusion is reached by Lindsey et al. (2006) within the Jubaila Formation (Kimmeridgian age) of the Ghawar field. *Thallassinoides* are observed within firmgrounds capping each 4th order HFC. Lindsey et al. (2006) has also observed *Thallassinoides* with sponge spicules, *Lenticularis spp.* and calcispheres of the deep basin. *Thallassinoides* also readily occur down slope from the main barrier of stromatoporoids and corals (Lindsey et al. (2006).

The Upper Kharaib Formation depositional cycles are capped by *Glossifungites* burrowed firmgrounds (Strohmenger et al. 2006a). The description of *Glossifungites* given by Strohmenger et al. (2006b) is they are filled with younger sediment, are dolomitised, are commonly associated with exposure, and flooding surfaces. Another definition of *Glossifungites* from Gingrass et al. (1999) is 'burrowing into firm substrates (firmgrounds) which may be exposed when sediment accumulations are exhumed during erosional changes in sea level'. In comparison, *Thallassinoides* burrows are observed by Strohmenger et al. (2006a) mostly within intervals below MFS's and within the late TST's of the Upper Kharaib Formation (Fig. 4.4B).

4.2 Observations

These observations are linked to the core descriptions outlined in Section 3.4.1. The extra information displayed here regards the problems behind positioning the 4th order SB's, including the final few feet of each 4th order HFC and the different types of *Thallassinoides* burrows. The thicknesses of the 4th order HST and TST sequences are also displayed for all five wells to show the 4th order HFC cycle stacking patterns of the Lekhwair and Lower Kharaib Formations across the offshore field.

The firmgrounds and the hardgrounds capping the 4th order HFC's show several signs of deepening. It is not immediately clear where the 4th order SB's should be placed; i.e. at the hardgrounds (B and C on Fig. 4.5) or at the base of the firmgrounds (A on Fig. 4.5).

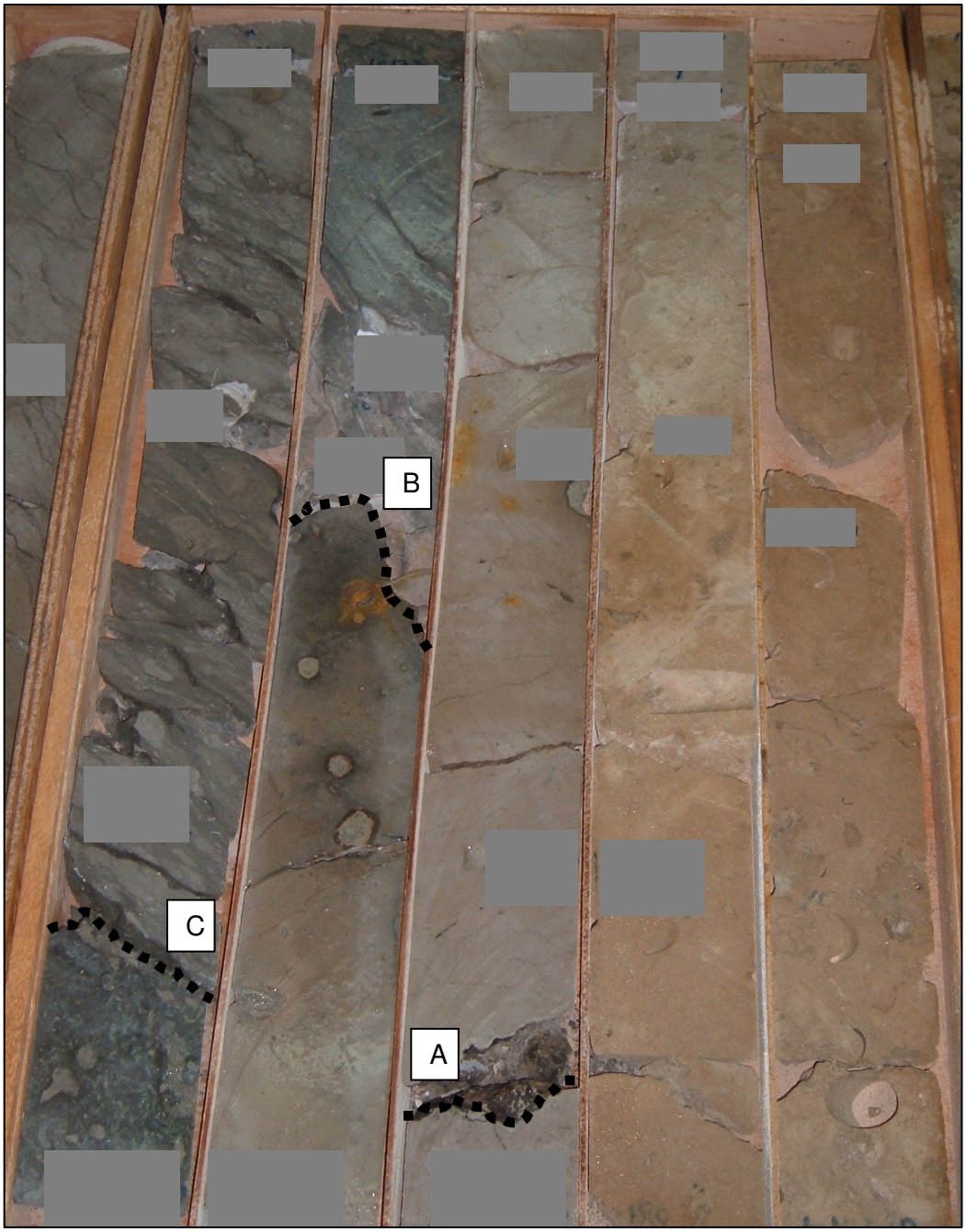

Figure 4.5: core box containing the last 20ft of a 4th order HFC starting from the bottom right hand corner with G. costatus *packstone, progressing into a firmground assemblage, multiple hardground surfaces and micrite/mudstone associated with the TST of the next 4th order HFC. There are several places the 4th order SB's can be placed: A) at the base of the firmground or B & C) at hardgrounds.*

The Lekhwair Formation contains *Thallassinoides* through all 4th order HFC's (Figs. 4.6A-F). The *Thallassinoides* measure 1-2cm in diameter, and are filled with sediment. There are *Thallassinoides* below some 4th order MFS horizons (Fig 4.6E & 4.6F). The *Thallassinoides* within the firmgrounds are haloed with framboidal pyrite, filled with dolomite rhombs and sediment. These *Thallassinoides* represent burrowing into a firm substrate which is consistent with the definition of a *Glossifungites* assemblage (Gingrass et al. 1999) (Fig 4.6D). The lithology associated with *Glossifungites* contains a high biodiversity of broken rotalids and echinoid fragments along with whole Textulariacea, gastropods and many small miliolids (Appendix 1A-1E). The Textulariacea present are *Praechrysallidina infracretacea* and *Redmondoides lugeoni*.

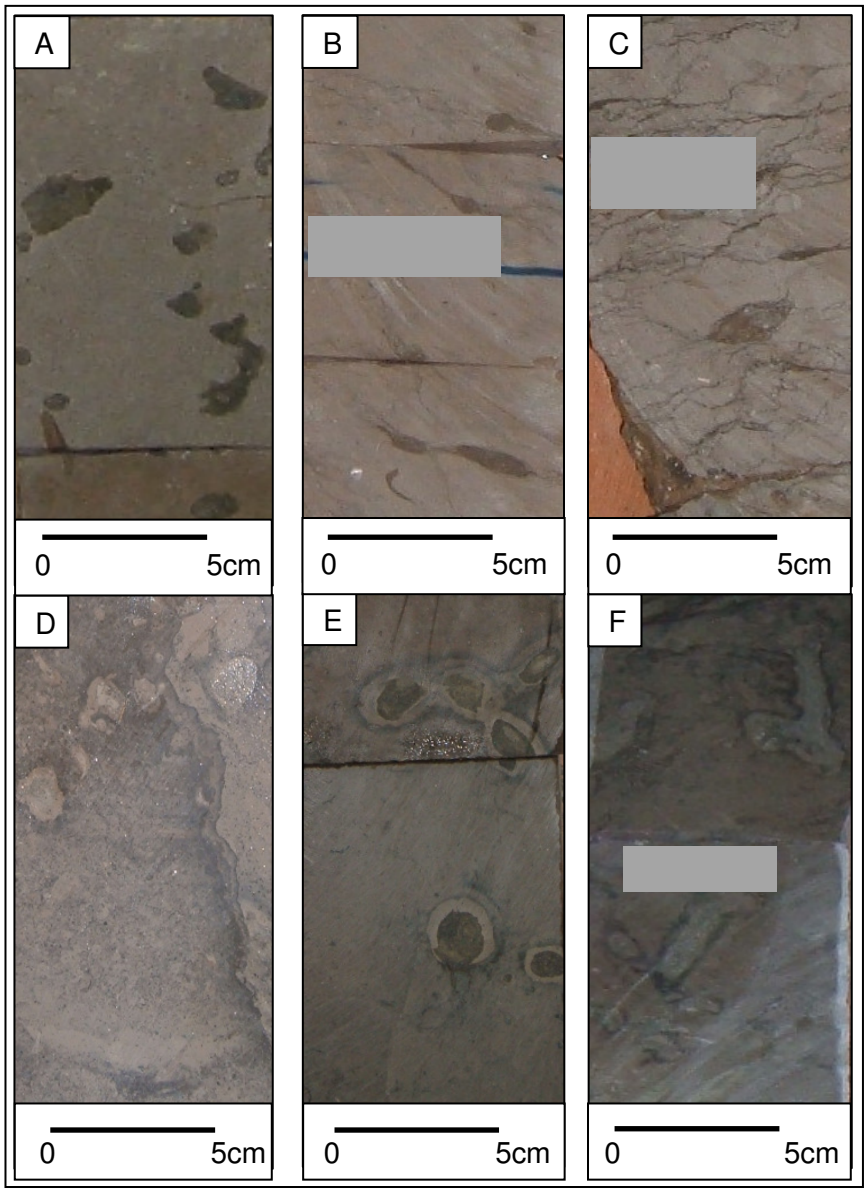

Figure 4.6: The positions of Thallassinoides*: A) mottled burrows within the HST, B & C) compacted burrows from the TST, D) within the firmgrounds capping the 4th order HFC's in the late HST, E) burrows below an MFS and F) burrows within the TST.*

Overall the Lekhwair Formation comprises nine 4th order HFC's while the Lower Kharaib Formation consists of one 4th order HFC and is the thickest out of the entire sequence. The bottom six 4th order HFC's (Cycles 7b to 4b) within the Lower Lekhwair Formation show a thinning up trend. The top four HFC's within the Lekhwair Formation followed by the Lower Kharaib Formation (Cycles 4a-1) display a thickening upward trend (Appendix 2A-2E).

The non-reservoirs thin upwards from the Lower Lekhwair towards the base of the Lower Kharaib Formation (Fig. 4.7-4.11). Many of these Lower Lekhwair Formation non-reservoirs comprise roughly half their 4th order HFC. Within the Upper Lekhwair Formation and especially the Lower Kharaib Formation the non-reservoirs are thin (Figs. 4.7 -411). It would appear that each successive flooding event was smaller than the last (Figs. 4.7-4.11).

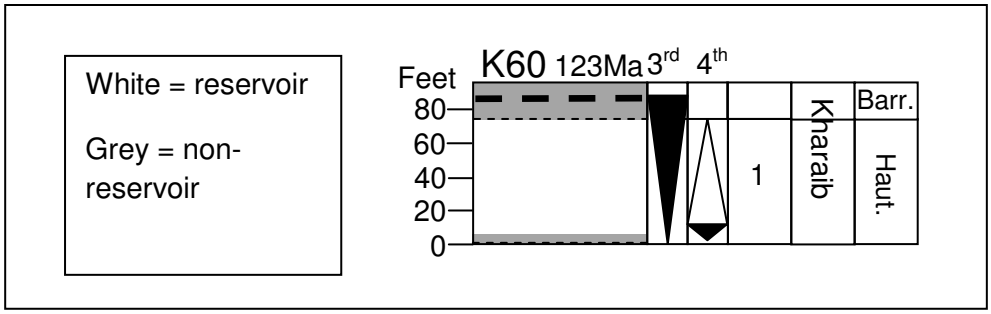

Figure 4.7: The 4th order HFC's of Well 1. The thicknesses of the 4th order HFC, along with the HST's and TST's through the Lower Kharaib Formation, are shown (Appendix 2A & Section 1.2). The open triangles represent the HST's, the black triangles represent the TST's and the black dashed lines represent the 4th order sequence boundaries.

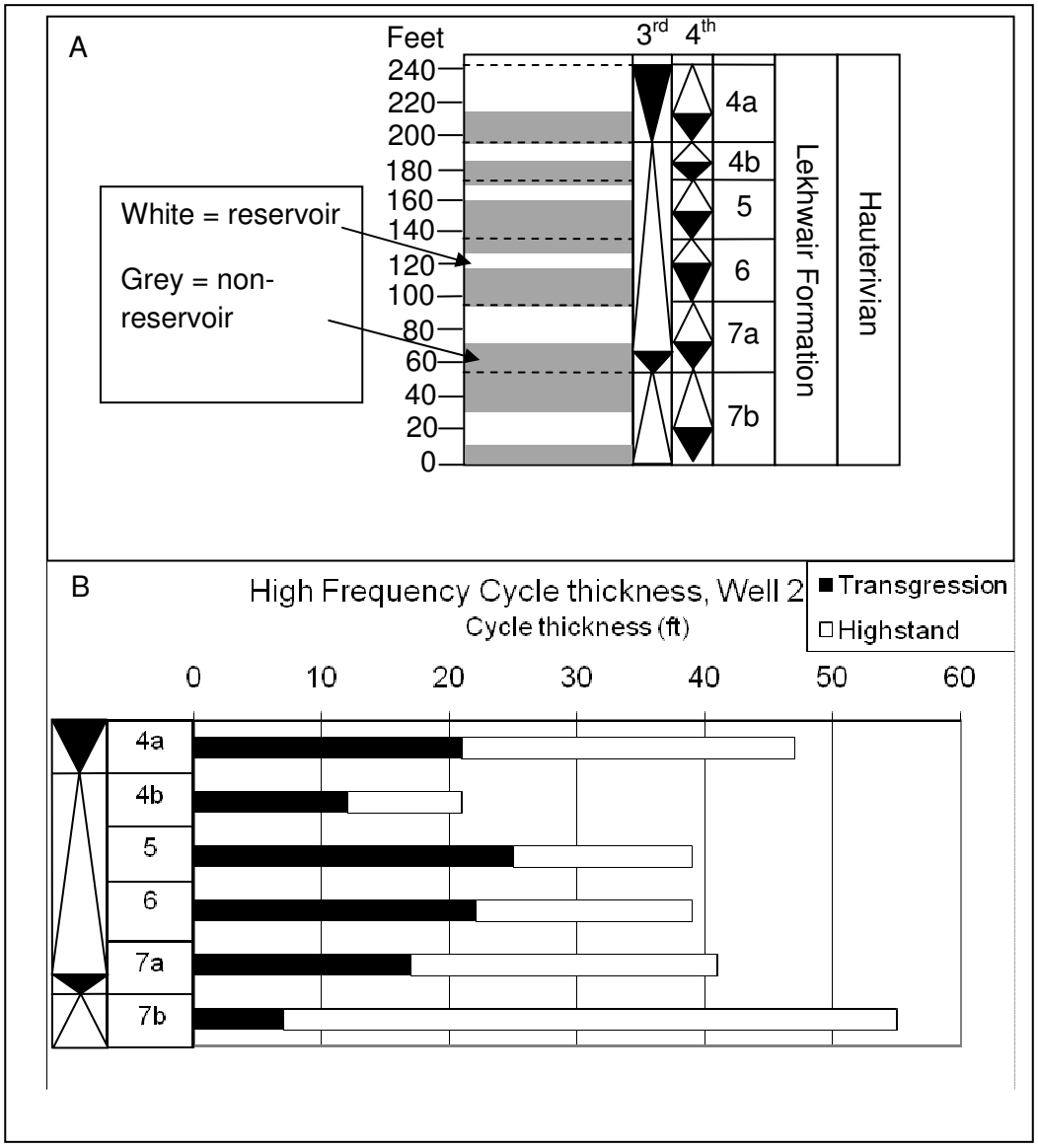

Figure 4.8: The 4th order HFC's of Well 2. A) The thicknesses of the 4th order HFCs along with B) the thicknesses of the HST's and TST's, through the Lekhwair Formation, are shown (Appendix 2B & Section 1.2). The open triangles represent the HST's, the black triangles represent the TST's and the black dashed lines represent the 4th order SB's. On (B) the black bars represent the thicknesses of the TST's while the open bars represent the thicknesses of the HST's.

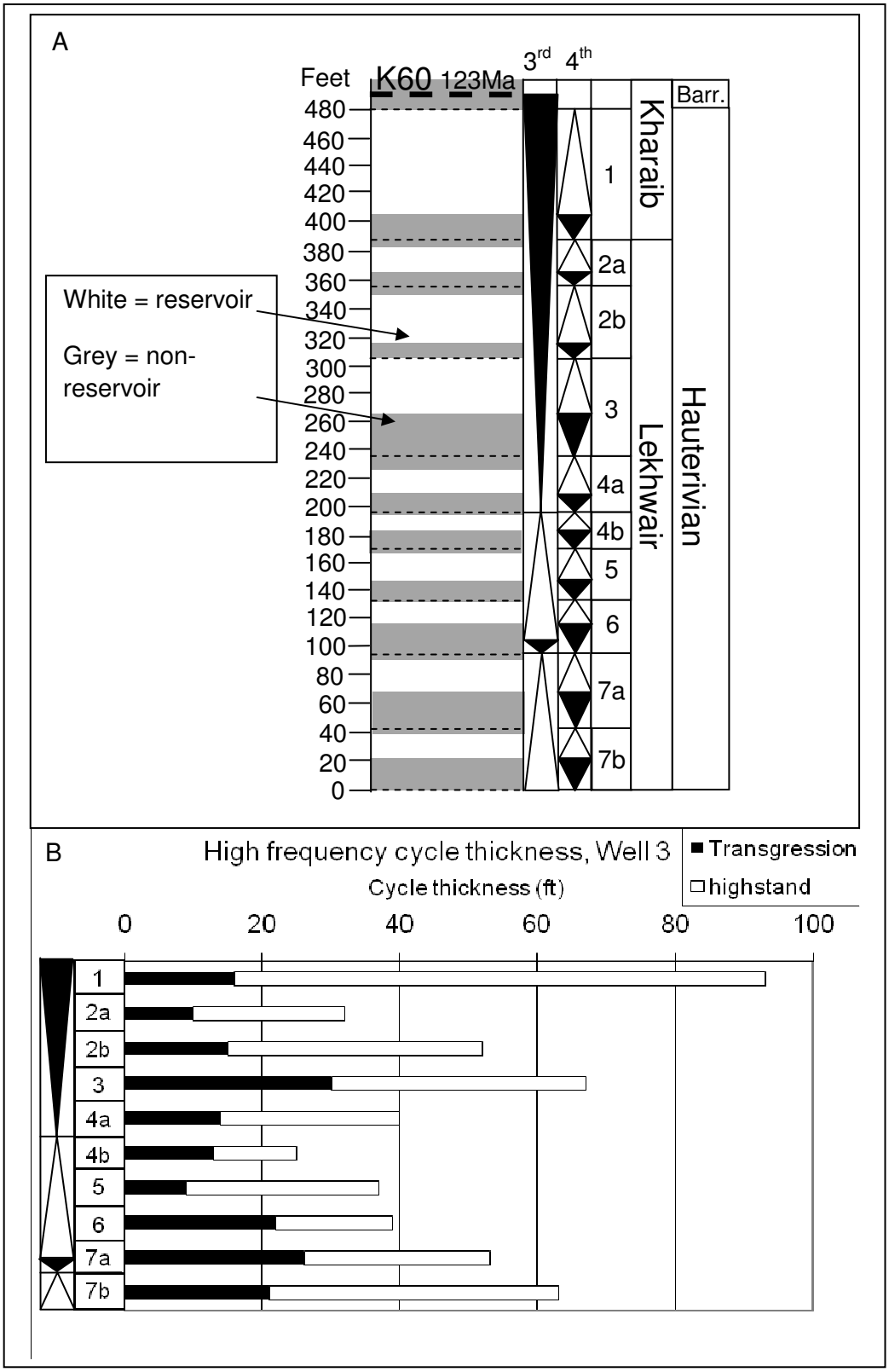

Figure 4.9: The 4th order HFC's of Well 3. A) The thicknesses of the 4th order HFC's along with B) the thicknesses of the HST's and TST's, through the Lekhwair and Kharaib Formations, are shown (Appendix 2C & Section 1.2). The open triangles represent the HST's, the black triangles represent the TST's and the black dashed lines represent the 4th order SB's. On (B) the black bars represent the thicknesses of the TST's while the open bars represent the thicknesses of the HST's.

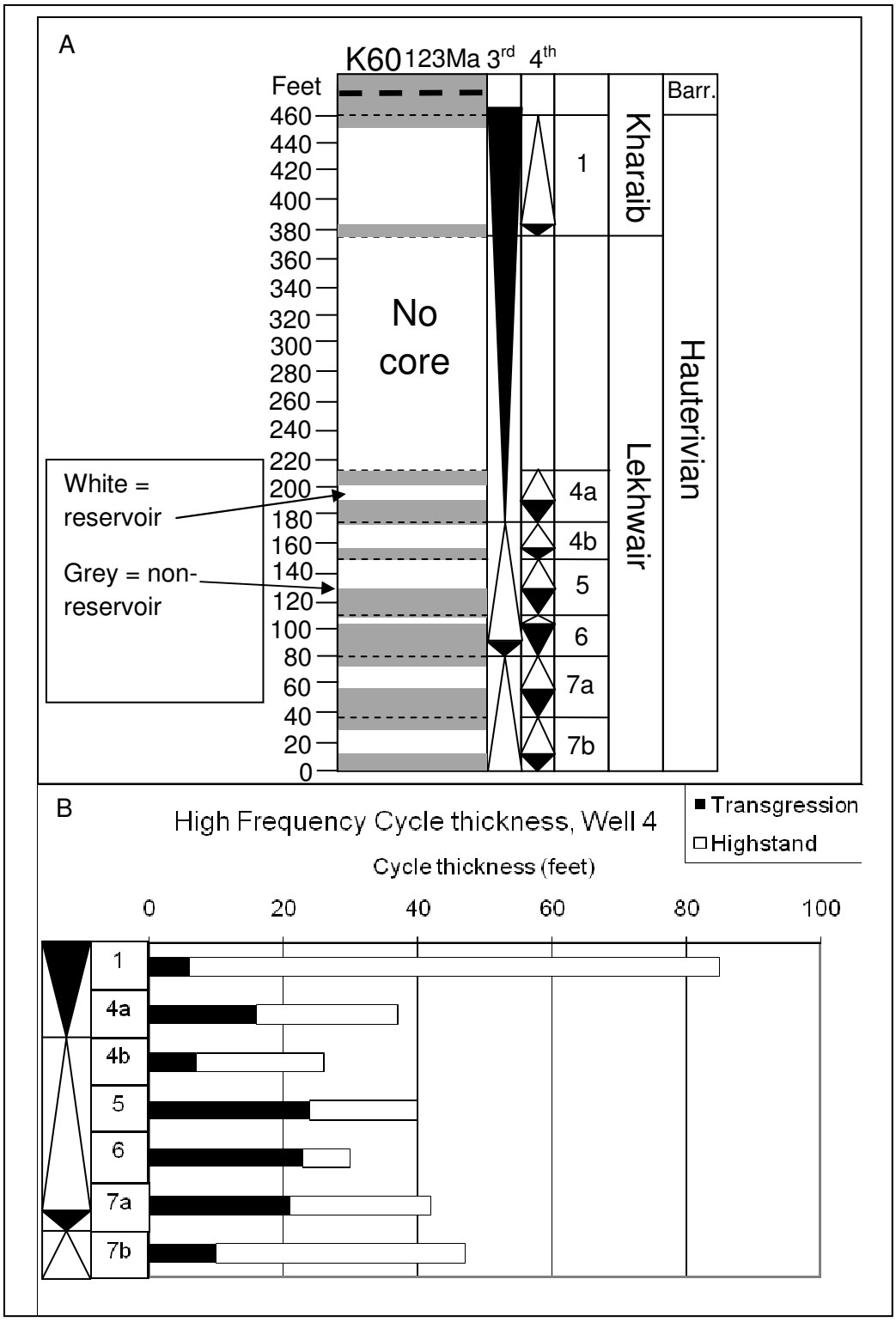

Figure 4.10: The 4th order HFC's of Well 4. A) The thicknesses of the 4th order HFC's along with B) the thicknesses of the HST's and TST's, through the Lekhwair and Kharaib Formations, are shown (Appendix 2D & Section 1.2). The open triangles represent the HST's, the black triangles represent the TST's and the black dashed lines represent the 4th order SB's. On (B) the black bars represent the thicknesses of the TST's while the open bars represent the thicknesses of the HST's.

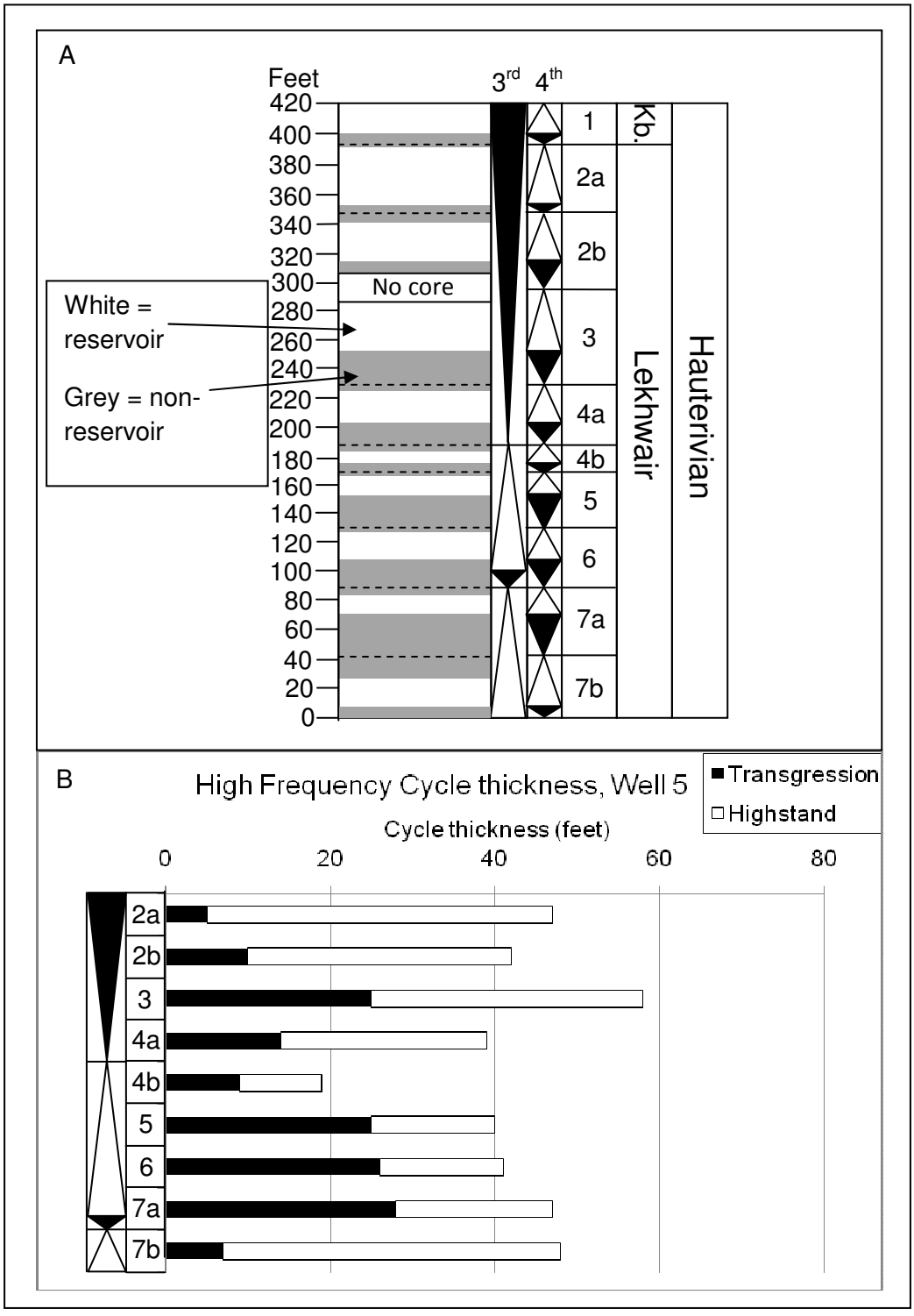

Figure 4.11: The 4th order HFC's of Well 5. A) The thicknesses of the 4th order HFC's along with B) the thicknesses of the HST's and TST's, through the Lekhwair and Kharaib Formations, are shown (Appendix 2E & Section 1.2). The open triangles represent the HST's, the black triangles represent the TST's and the black dashed lines represent the 4th order SB's. On (B) the black bars represent the thicknesses of the TST's while the open bars represent the thicknesses of the HST's.

4.3 Discussion

4.3.1 Firmground formation

Although the absence of the LST sequences within the Lekhwair and Lower Kharaib Formations makes it slightly more difficult to locate the 4th order SB's, there is usually an indication of where the 4th order SB's should be placed by the abrupt change in lithology. *Thallassinoides* burrowed firmgrounds (*Glossifungites* assemblage), capped with hardgrounds, which abruptly changes up into deepwater micrites/mudstones suggests that the hardgrounds signify significant deepening: the 4th order SB's should be associated with these hardgrounds. However there are other factors that make the specific positioning of each 4th order SB difficult:

1) There are no meniscus cements or karst surfaces, and therefore no definite evidence for meteoric processes and subaerial erosion within the Lekhwair and Lower Kharaib Formation firmgrounds and hardgrounds (Section 3.5.2).

2) The lithology of the firmground is usually muddier than the *Glossomyphorus costatus* back-shoals below, suggesting that deepening may have already occurred before the hardground was formed.

3) In most 4th order HFC's several mineralised surfaces exist throughout the firmground before the hardground (Fig. 4.5): which surface should be defined as the SB?

One possible position for 4th order SB's are at the base of the *Thallassinoides* burrowed firmgrounds (*Glossifungites* assemblage). This possibility was considered when reviewing suggestions from Davis et al. (2002) that Zakum Member HFC's are a series of retrogradational and deepening upward cycles. For this to be appropriate for the Lekhwair and Lower Kharaib Formations, siliciclasts and micro-quartz grains need to be present within the carbonates, to validate the proximity of retreating pro-delta deposits, to the west of the present day field position, during the Lower Cretaceous; this inspection was carried out to establish any changing nutrient conditions between the Lekhwair and Lower Kharaib Formations and whether terrestrial nutrient fluxes had increased promoting the abundance of *P. lenticularis* in

the Lower Kharaib Formation over Textulariacea in the Lekhwair Formations (Section 3.5.3). As stated in Section 3.5.4, petrography revealed that no silicilasts are present in any of the HST samples, and further studies on the SEM, using secondary electron images, revealed that within the late HST samples of the Lower Kharaib Formation only a few micro-quartz grains were present. The top of the Lower Kharaib Formation is considered in this study to potentially be the shallowest, most proximal part of the studied sequence and therefore should be the most likely place to find terrigenous siliciclasts from retrograding pro-delta complexes. However, as stated in Section 3.5.4, the base of every 4th order TST sequence appears to have an argillaceous rich unit which may represent distal fluxes from pro-delta complexes in the west, before they retrograded along with the carbonate platforms in the subsequent 4th order HST sequences, representing a cleaning upward signature (Davis et al. (2002).

With respect to *Thallassinoides* being found within deeper water environments, Lindsay et al. (2006) has studied the Upper Jurassic and the organisms that formed the *Thallassinoides* could have lived at completely different palaeodepths in comparison with organisms that lived in the Lower Cretaceous. The *Thallassinoides* on the Tertiary New Jersey slope could have also been burrowed by completely different organisms in comparison with *Thallassinoides* in the Early Cretaceous and may also have preferred deeper water conditions (Savrda et al. 2001).

Comparing studies by Strohmenger et al. (2006a) with this study, the latter has found no *Thallassinoides* burrows within the Lower Kharaib Formation. However, when considering the Lekhwair Formation, this study is consistent with Strohmenger et al. (2006a) as *Glossifungites* assemblages only exist below surfaces that display significant signs of deepening: i.e. firmgrounds capping all the 4th order HFC's (Figs. 4.6D-4.6F). *Thallassinoides* are present throughout the Lekhwair Formation within most lithologies (Fig. 4.6), and therefore may have been produced by a whole range of organisms that prefer many different environments and palaeodepths, including in some cases, the late TST's (Strohmenger et al. (2006a).

The *Glossifungites* assemblages are present with many Textulariacea (*P. infracretacea* and *R. lugeoni*). Lindsay et al. (2006) attribute *R. lugeoni* within

proximal shoal environments above the fair weather wavebase. *P. infracretacea* is associated by Hughes et al. (2000a) within moderately deep lagoons and rudist back barrier environments (Section 3.3.3). Both Textulariacea species within the Lekhwair Formation are whole and appear relatively in situ. This suggests the Lekhwair Formation firmgrounds are products of shallow water environments (possibly lagoonal) and not of the deep basin.

Many authors (Alsharhan 1995, Strohmenger et al. 2006a) use the presence of bioturbated mud to reflect periods of low sedimentation and low water turbidity (Sections 3.3.1-3.3.3). Storm surges can place bioclastic fragments from platforms into near shore environments. Consequently, the combination of muddy sediments, extensive bioturbation, in situ shallow water Textulariacea and, a high diversity of bioclastic fragments, suggest a restricted shallow water environment coupled with low energy and low sedimentation: i.e. a lagoon. The Lekhwair Formation firmgrounds share all these traits and appear more representative of a lagoon than a deep water slope environment.

4.3.2 Hardground formation

Within the Lekhwair Formation hardgrounds only cap the *Thallassinoides* burrowed firmgrounds. Hardgrounds have also not formed on every firmground that caps every 4th order HFC: there must be certain marine conditions that promote early cementation and lithification of the sea bed. Why would hardgrounds form within shallow water, restricted lagoons, instead of within deepwater basins during deposition of the Lekhwair and Lower Kharaib Formations?

At Abu Dhabi, Qatar and Oman Granier et al. (2003/05) suggests the Lekhwair Formation shows evidence for leached aragonite bioclasts along bored hardgrounds: studies of the Lekhwair Formation from Alsharhan & Kendall (1991) also conclude that freshwater leaching has occurred at the top of the Lekhwair Formation (Section 3.3.1). This leaching is used as evidence for sea level fall and subaerial exposure (Alsharhan & Kendall 1991, Granier et al. 2003/05). However, the Lekhwair was deposited within 'calcite producing' seas with an Mg to Ca ratio of 1 to 1 (Hardie 1996: Section 2.1). Therefore aragonite and HMC bioclasts would have dissolved out

in this chemical environment, either leaving open vugs, moulds, or be replaced by LMC. There are no karstic surfaces and meniscus cements present within the Lekhwair and Lower Kharaib Formation late HST's: alone, leaching and dissolution are not good indicators for meteoric processes, subaerial exposure, sea level lowstand and for the placing the 4th order SB's within the Lekhwair and Lower Kharaib Formations.

Another possible way to prove the hardgrounds are forming in shallow water conditions is the heavy pyritisation of *Thallassinoides* firmgrounds below. Studies from Immenhauser et al. (2000) associate heavy minerals, such as goethite, with marine seafloor lithification and sea level fall. While Immenhauser et al. (2000) does not suggest a mechanism for mineralisation and sea level fall, Ku et al. (1999) provides a possible link between hardground formation and the mineralisation of the *Thallassinoides*. Microbial sulphate reduction can readily occur several centimetres below the sediment surface within organic rich lime muds (Ku et al. 1999, Patterson & Walter 1994, Walter et al. 1993). This is confirmed within the Lekhwair Formation by Dickson et al. (2008) as the earliest locus of sulphate reduction occurs 4-5cm below the sediment water interface. Incubation experiments on the South Florida Platform sediments showed a reduction in SO_4^{2-}, but increased bicarbonate ions (Ku et al. 1999). This suggests bacterial sulphate reduction leads to an increase in carbonate alkalinity and to carbonate supersaturation in the water column (Ku et al. 1999). This may explain the proximity of hardgrounds to pyritised *Thallassinoides* burrowed firmgrounds in the Lekhwair Formation. Observations from Dickson et al. (2008) and Immenhauser et al. (1999) show that hardgrounds have selectively formed capping 4th order HFC's with larger negative $\delta^{13}C$ shifts (Fig. 4.12). The pyrite forms when there is a suitable quantity of Fe^{3+} ions that combine with HS (Hydrogen sulphide) ions to form Fe_2S (pyrite) (Dickson et al. 2008). CO_2 depleted in ^{13}C (down to -25‰), produced from sulphate reduction by bacteria on organic matter, would potentially become incorporated into the forming carbonate sediments producing a more negative $\delta^{13}C$ signature within the hardgrounds and the surrounding sediments (Dickson et al. 2008) (Fig. 4.12). This is consistent with studies by Ku et al. (1999) that suggest bacterial sulphate reduction

causes carbonate supersaturation in the water column and the formation of hardgrounds.

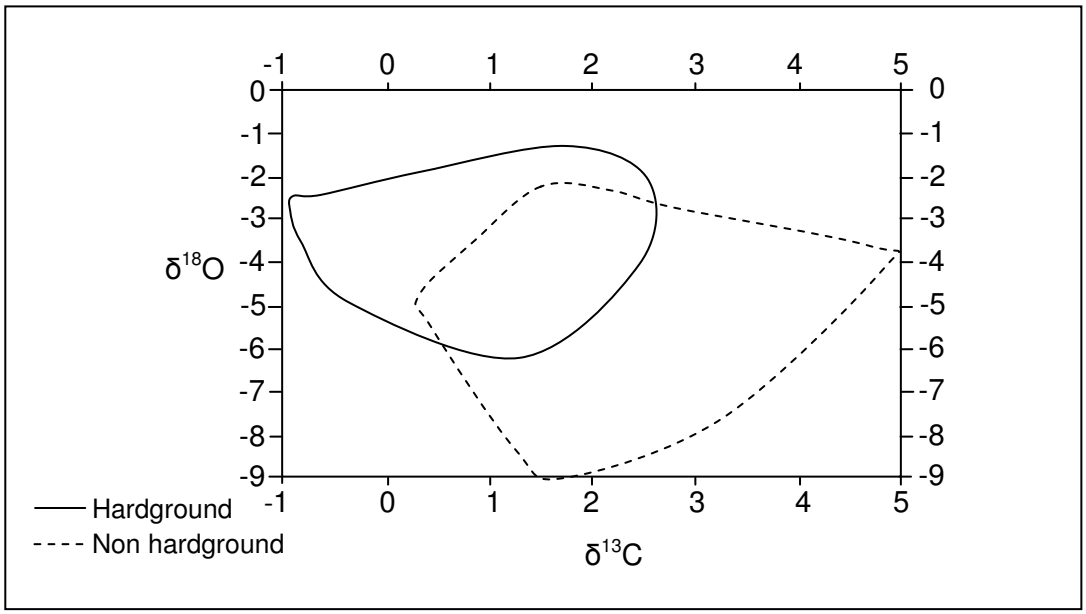

Figure 4.12: The SB's with hardgrounds are associated with bacterial sulphate reduction, which suggests a possible link (Dickson et al. 2008)

The association of the pyritised *Thallassinoides* with shallow water *P. infracretacea* and *R. lugeoni* confirms the firmgrounds below have formed within a lagoonal environment. The supersaturation of carbonate within the water column may have caused the rapid cementation of the seafloor: the hardgrounds could have formed as a consequence of microbial action within a shallow water environment and not during early flooding and transgression. The hardgrounds are therefore not direct products of sea level change however they are placed at the positions between many 4th order HFC's that display a pronounced deepening.

There are no root traces, desiccation cracks, or truncated coral heads, capping the Lekhwair and Lower Kharaib Formation 4th order HFC's, and sea level fall cannot be determined through these means unlike studies from Pittet et al. (2002) and van Buchem et al. (2002). Instead, the dramatic change in lithology, such as the abrupt transition from *Glossomyphorus costatus* and *Lithocodium/B.* packstone and grainstone with *Thallassinoides* burrowed firmgrounds below the hardground, into argillaceous micrites/mudstones above the hardground, does represent the transition across a SB (Immenhauser et al. 2000, Alsharhan & Nairn 1993, Strohmenger et al.

2006a, Yose et al. 2006). This study will therefore use the hardgrounds as 4th order SB's for the Lekhwair and Lower Kharaib Formations. These hardgrounds will be used to correlate the 4th order HFC's across the offshore field, Abu Dhabi, to create a detailed sequence stratigraphic framework on the 4th and 3rd order scales.

4.3.3 4th order MFS placements

The stratigraphic positions of the 4th order MFS are defined by the aggregate grain beds which are outlined previously in Section 3.5.1 (L15: Figs. 3.24O & 3.33). The top of these aggregate grain beds mark the 4th order MFS. The development of the sequence stratigraphic framework will be based on these placements.

4.4 Carbonate Production

The HFC stacking pattern for the Abu Dhabi region is outlined by Alsharhan & Kendall (1991) and based on Haq et al. (1987) (Fig. 4.1C), which shows the HFC's within the Lekhwair Formation were deposited over 1Myr periods (with the exception of one cycle that lasts for 1.5Myr). A slightly longer time period is associated by Alsharhan & Kendall (1991) for deposition of the Lower Kharaib Formation: 1.5Myr.

The Lower Lekhwair HFC's contain relatively thick 4th order TST's indicating a prolonged time period was taken in filling the accommodation space to form the HST's. Carbonate production within the Lower Lekhwair Formation appears to have undergone 'catch up' with sea level; i.e. carbonate growth could not initially keep pace with sea level rise. Whereas the 4th order TST's within the Upper Lekhwair and the Lower Kharaib Formations are very thin. This does not correspond to the overall thickening of the 4th order HFC's, as the overall 3rd order TST associated with the Upper Lekhwair and Lower Kharaib Formations suggests that greater amounts of accommodation space were produced with each successive 4th order HFC (Figs. 4.9A & 4.9B). There should have been enough accommodation space to promote a prolonged deepwater environment and thick 4th order TST's, before highstand conditions were reached. Therefore the rate of sea level change may have slowed allowing for carbonate production to 'catch up' with sea level more quickly in comparison with the Lower Lekhwair below. The time periods suggested by

Alsharhan & Kendall (1991) and Haq et al. (1987) have only associated a slightly longer time period with deposition of the Lower Kharaib Formation. This suggests against the possibility that rate of sea level change had decreased during the formation of the Lower Kharaib Formation, as a significantly longer time period would be required to deposit Cycle 1, which is on average three times thicker than the Lower Lekhwair Formation 4th order HFC's.

Instead, carbonate production rates may have increased from the Lower Lekhwair Formation, into the Upper Lekhwair Formation and the Lower Kharaib Formation. Carbonate production rate may have kept pace, and responded to greater increments in sea level rise, over time. This catch up followed by keep up, suggests that each successive platform, associated with each 4th order HFC was getting shallower, producing the shallowest and coarsest platform environment for the Lower Kharaib Formation (Section 3.5.3).

This is consistent with the rise in abundance of *G. costatus* and the assumption from Gili et al. (1995) that rudists require sediment dominated environments (Section 3.4.5 & 3.5.3). The rise in carbonate production may have caused more erosion and more carbonate sediment for the *G. costatus* to colonise the sea bed. This confirms that an increase in nutrient availability is not the cause for the rise in *G. costatus* in the Lower Kharaib Formation (Section 3.5.3).

4.5 3rd order stacking pattern

The most recent sequence stratigraphic framework that encompasses the Lekhwair and Lower Kharaib Formations was developed by Strohmenger et al. (2006a: 2007) (Fig. 4.13B). This only involves the 3rd order cycles, and is based on dated MFS horizons set out by Sharland et al. (2001) and updated by Davis et al. (2002) (Fig. 4.13C). Two MFS horizons outlined by Sharland et al. (2001) and Davis et al. (2002) agree with observations from this study: K50 (126Ma) near the base of the Lekhwair Formation (within the TST of Cycle 8) and K60 (123Ma) above the top of the Lower Kharaib Formation (above Cycle 1 within the TST of the Upper Kharaib Formation) (Figs. 4.13A & 4.13C).

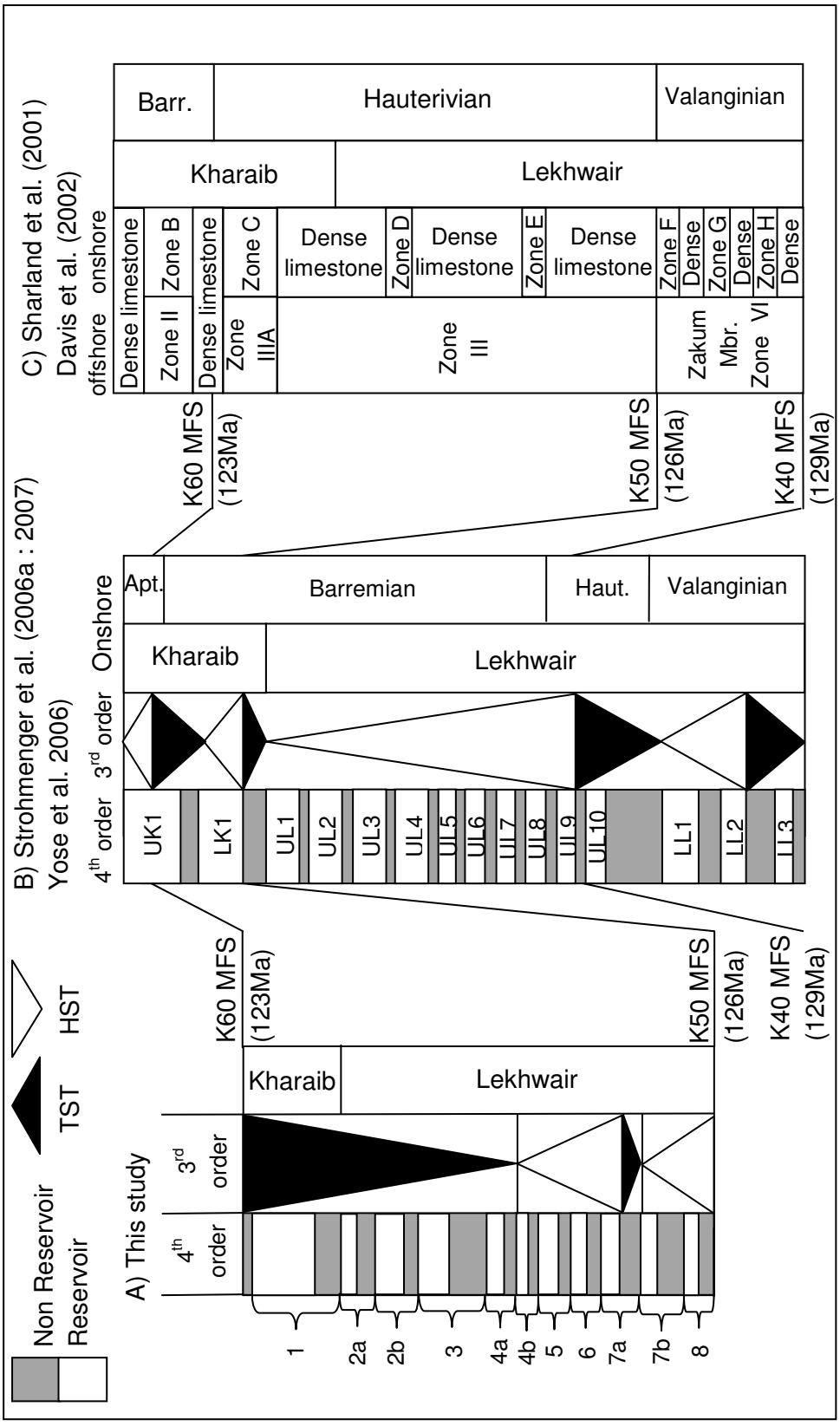

Figure 4.13: sequence stratigraphy of the Lekhwair and Kharaib Formations of A) this study in comparison with B) Strohmenger et al. (2006a: 2007) & Yose et al. (2001) and C) Sharland et al. (2001) & Davis et al. (2002) (Figures 3.7-3.11 for scale). The initials on (B) are UK: Upper Kharaib, LK: Lower Kharaib, UL: Upper Lekhwair and LL: Lower Lekhwair.

The Lower Lekhwair Formation shows an upward thinning 4th order HFC succession, representing the reduction of accommodation space and progradation, which reflects two 3rd order HST's separated by a small 3rd order TST (Fig. 4.13A) (Strasser et al. 1999). Therefore 3rd order SB's are placed with the 4th order SB's of Cycles 7b and 4b (Fig. 4.13A). The 3rd order MFS within the 4th order TST of Cycle 8 is consistent with the placement of K50 BY Sharland et al. (2001) and Davis et al. (2002) (Figs. 4.13A & 4.13C). The next 3rd order MFS is placed within the 4th order TST of Cycle 7a and is not present in studies by Sharland et al. (2001) and Davis et al. (2002). This study has placed an extra MFS within the thickest, most pronounced argillaceous micrites/mudstones within the lower Lekhwair Formation, as this should represent a profound and prolonged deepening, consistent with a longer term 3rd order sea level rise imprinted onto a 4th order TST (Fig. 4.13A).

The Upper Lekhwair and the Lower Kharaib Formations show an upward thickening 4th order HFC succession, representing the increase of accommodation space and retrogradation, reflecting a single 3rd order TST (Fig. 4.13A) (Strasser et al. 1999). The final 3rd order MFS surface is placed above Cycle 1 and the Lower Kharaib Formation: consistent with the placement of K60 by Sharland et al. (2001) and Davis et al. (2002) (Figs. 4.13A & 4.13C).

Strohmenger et al. (2006a: 2007) cycle stacking pattern shows three 3rd order cycles, instead of two, with the systems tracts being the opposite of this study (Fig. 4.13A & 4.13B). For example, Strohmenger et al. (2006a: 2007) associates the final five 4th order HFC's of the Upper Lekhwair Formation with a 3rd order HST while displaying the HFC stacking pattern as thickening upwards (Fig. 4.13B). The accommodation space is therefore increasing during deposition of the Upper Lekhwair Formation, characteristic of a long term sea level TST and not a HST. This study can therefore not agree with the cycle stacking pattern outlined by Strohmenger et al. (2006a: 2007). Instead this study suggests that the Lower Lekhwair Formation represents two 3rd order HST's (separated by a thin TST) with the Upper Lekhwair and the Lower Kharaib Formations representing a prolonged 3rd order TST (Fig. 4.13A).

4.6 Sequence stratigraphic framework for the Lekhwair and Lower Kharaib Formations

The lithologies are general and directly relate to the core observations (Appendix 2A-2E). Only applying 7 broad lithologies (Section 3.4.1) instead of 20 lithofacies, as outlined in Section 3.4.3, reduces the complexity of Figure 4.14, allowing the reader to assess the lithological trends more easily. All the following observations relate to the sequence stratigraphic framework developed for the Lekhwair and Lower Kharaib Formations (Fig. 4.14).

Many authors (Aziz & El-Satter 1997, Al-Silwadi et al. 1996, Davis et al. 2002, van Buchem et al. 2002) associate deepening and the progression into the deep basin with the East. The thickness of basal micrite/mudstone increases towards Well 5 (Cycles 6, 7a and 7b) confirming increasing proximity towards the basin towards the east to northeast (Fig. 4.14).

A thin layer of *G. costatus* and *Lithocodium/B.* packstone and grainstone is within Cycle 7b in Well 2 which progresses into a thick sequence of *G. costatus* and *Lithocodium/B.* wackestone and packstone in Well 3. Cycles 7a and 6, in Wells 3 and 4, instead have thick layers of *G. costatus* and *Lithocodium/B.* packstone and grainstone. This may be indicating the shoals (represented by the coarsest lithology) are prograding towards the basin within each successive ramp of the Lower Lekhwair Formation, which is consistent with a 3rd order HST (Fig. 4.14).

The thickness of pyritised mudstone and argillaceous micrites/mudstones within the base of Cycle 7a continues across the entire field: this is consistent with the extra 3rd order MFS placement and a thin 3rd order TST (Fig. 4.14).

Generally the *G. costatus* and *Lithocodium/B.* wackestone and packstone within the 4th order HST's of Cycles 7b and 7a, changes into *G. costatus* and *Lithocodium/B.* packstone and grainstone within the 4th order HST's of Cycles 6, 5 and 4b, indicating a shallowing up trend. This confirms that the Lower Lekhwair Formation is a shoaling upward succession of 4th order HFC's (Fig. 4.14).

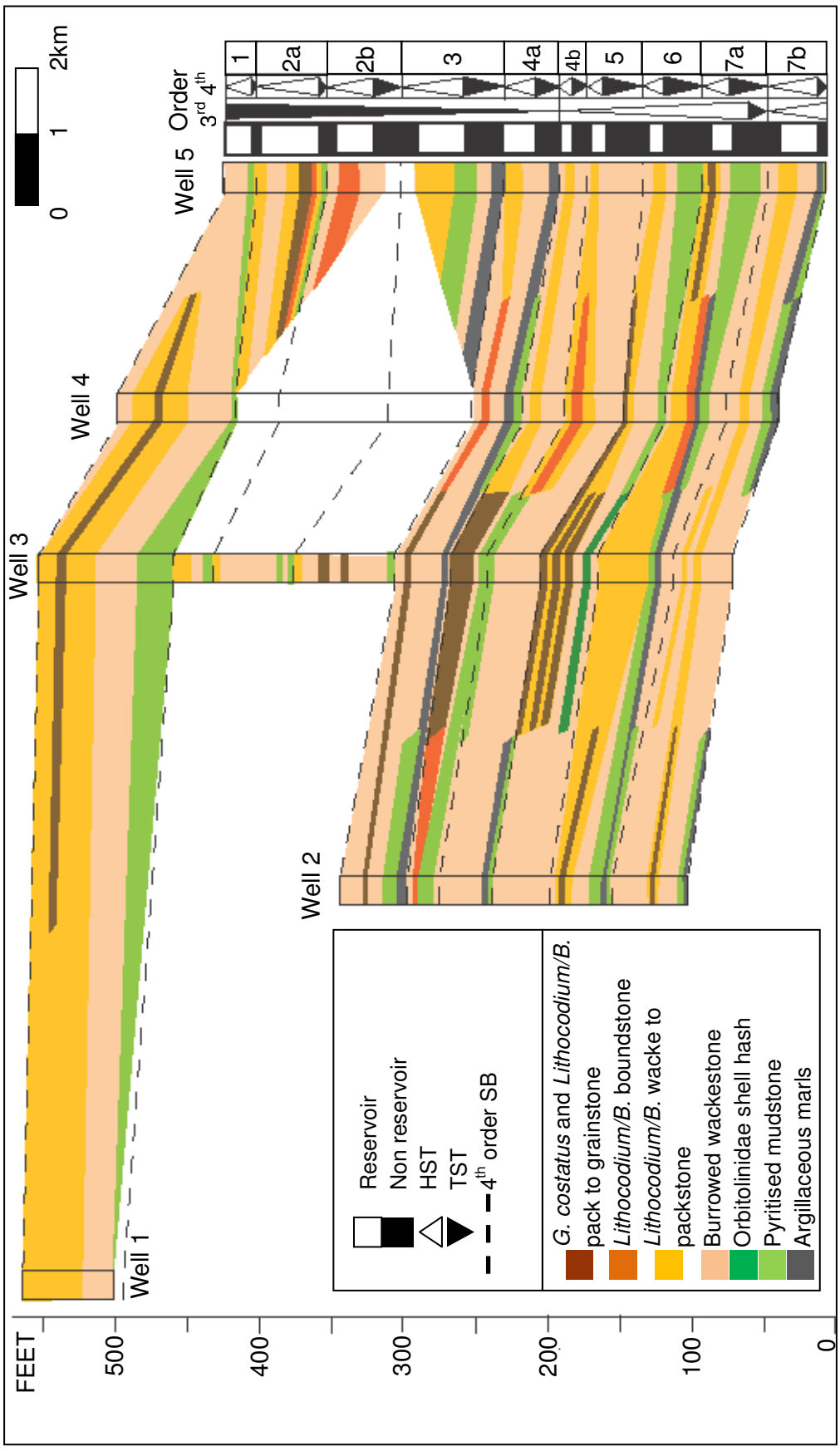

Figure 4.14: sequence stratigraphy of the Lekhwair and Lower Kharaib Formations. The seven broad lithologies (not including firmgrounds because of their small vertical extents) are used to construct a framework (based on core observations) (Appendix 2A-2E (see Section 1.7 for Well positions).

4.7 Reservoir heterogeneities

The coarsest lithologies are the *G. costatus* and *Lithocodium/B*. wacke-packstone, and pack-grainstone. Estimations of their lateral and vertical extents are displayed in Figure 4.14. It shows that the grainstone patches are localised around Well 3, near the top of the second 3rd order cycle within the Lekhwair Formation. Although there is ambiguity in this, the pack-grainstone bodies are roughly 2-3km in length and 250ft thick. The thickest wacke-packstone lithologies are also centred on Well 3 within the base of the Lekhwair Formation, being 400-500ft thick which thins out towards Wells 2 and 4. Therefore this pack-wackestone body shows much more lateral extent in comparison with the pack-grainstone dominated reservoir within overlying HFC's.

All coarser bodies are not that laterally extensive within the Lekhwair Formation in comparison with the Lower Kharaib Formation. The wacke-packstone body not only extends for almost 12km, (from Well 1 to between Wells 4-5) but remains relatively thick over this distance of almost 500ft. Although there is no sample support from Well 2, samples from Well 1 and 3 are petrographically very similar and have very well connected interparticle pore systems. This suggests that the Lower Kharaib Formation is the most extensive and the better connected reservoir within this studied sequence.

All HFC's show compartmentalisation of the coarser grain-pack-wackestone patches; the transgressive wacke-mudstones below, and the firmgrounds above, both seal the reservoirs into layer cake bodies. Therefore the Lekhwair Formation shows consistent vertical compartmentalisation, and heterogeneity every 40ft, along with horizontal heterogeneity every 2-3km. Due to the increased thickness of the Lower Kharaib Formation the vertical heterogeneity is less frequent.

Within each reservoir there is also heterogeneity; each reservoir has large burrowed wackestone sections, usually in the early highstands within the Lekhwair Formation. Petrographically the pore systems are not well connected, but they are oil stained in core section. These areas may represent lower grade reservoir areas, adding to the vertical heterogeneity of the Lekhwair Formation reservoirs. The

Lower Kharaib Formation does have a smaller vertical extent of burrowed wackestone, however petrographically the reservoir, in comparison with the Lekhwair Formation, is better connected and still appears to be the best reservoir horizon.

4.8 Conclusions

1) The presence of shallow water Textulariacea suggests these pyritised *Thallassinoides* firmgrounds (*Glossifungites* assemblage) indicate shallow water lagoons close to the shoreline. Supersaturation of LMC within the water column, caused by bacterial sulphate reduction, has formed hardgrounds within lagoons. The following deposition of deepwater argillaceous micrites/mudstones above places the 4th order SB's at the hardgrounds.

2) The Lekhwair and Lower Kharaib Formations are composed of two 3rd order sequences. The Lower Lekhwair is composed of two 3rd order HST's separated by a thin TST. The Upper Lekhwair and the Lower Kharaib Formations form an extensive 3rd order TST. The thinning of the 4th order TST's up section indicates that carbonate growth rates may have increased from the Lekhwair into the Lower Kharaib Formations. Overall the Lekhwair and the Kharaib Formations reflect a shallowing upward trend. This confirms the shallowest platform environment is associated with the reservoir of the Lower Kharaib Formation; which is also considered the best reservoir facies within this study.

Chapter 5
Dynamics of cementation and oil charge

There is controversy as to how cementation and diagenesis respond to the emplacement of oil. There are two main proposals suggesting the interaction of oil with cementation. One suggests cementation (and stylolitisation) can be inhibited by the presence of oil preserving reservoir quality in field crests (cementation can overlap oil charge) (Neilson et al. 1996; 1998), while another suggests that cementation can continue in the mixed presence of oil and water (Heasley et. al. 2000). While oil emplacement does prevent further cement nucleation, existing cements will continue to grow in the presence of oil (Heasley et al. 2006).

This study aims to achieve a more detailed understanding as to how $\delta^{18}O_{VPDB}$ have evolved through progressive cementation within a giant offshore field, Abu Dhabi. For the first time, each macrocement zone was targeted by Ion Microprobe analysis. Specific 10-15µm diameter spots were analysed for $\delta^{18}O_{VPDB}$, along single transects, from the oldest to the youngest cement zone. Coupled with the position of oil inclusions, changing $\delta^{18}O_{VPDB}$ values are relatively placed within a cementation sequence, with respect to the timing of oil emplacement. LMC macrocements were selected from the water leg, transition zone and the oil leg, so cementation during oil charge could be compared in and around the field crest. For the first time, a detailed assessment of how cementation had evolved during oil emplacement is established. This Chapter has been published as a short paper to Sedimentary Geology (Cox et al. 2010).

5.1 The dynamics of cementation

Rocks that become buried within the substratum become compressed mechanically and chemically which can reduce pore space. The amount of pore space in sedimentary rocks decreases regularly with increasing burial depth. However, subsurface oil reservoirs retain their porosity at greater burial depths (Robinson and Gluyas, 1992; Emery et al., 1993). One reason for this difference is that oil reservoir pore systems contain less cement in comparison with surrounding oil free pore systems. Water is the medium by which solutes are transported from dissolution to reprecipitation sites; the introduction of oil partially displaces the water, causing the inhibition and retardation of growing cements (Burgess & Peter 1985, Heasley et al., 2000, Worden et al., 1998).

It is suggested that cementation and oil migration occur at similar times (Gluyas et al., 1993) however oil charge is a slow process and results in the gradual filling of the field crest pore systems down structure (Marchand et al., 2001). Cementation therefore does not cease immediately at oil charge, instead cement growth will slow in the crest and will continue in the presence of oil until the final oil water contact is reached. Cements within the oil leg in both quartz cemented sandstone reservoirs (Bjørkum et al., 1993; Emery et al., 1993; Walderhaug, 1990) and LMC cemented carbonate reservoirs (Neilson et al., 1996, 1998) contain inclusions of oil indicating that they grew in pores that contained both water and oil. Studies by Walderhaug (1994, 1996) have modeled the retardation of quartz cement growth during oil charge. This model has been applied to North Sea fields and shows that >15 Myr may have been needed to fill the structure crests with oil (Marchand et al. 2001; 2002).

In retrospect, when considering that millions of years are required for oil to completely fill structural crests, the porewater conditions from which the cements have grown would have most likely changed. Porewaters can evolve with increasing temperature, as a result of increasing burial, which will consequently be reflected in the chemistry of the cements. The chemistry of trace elements within LMC can be changed by many processes and can be hard to understand (Richter, 2003), whereas the control of stable isotope composition is better understood (Kim & O'Neil 1997).

Increasing temperature and burial will cause more negative $\delta^{18}O_{VPDB}$ to be incorporated within growing cements. Conversely, porewaters may evolve towards more positive $\delta^{18}O_{VPDB}$ values through several dissolution and reprecipitation reactions (Lawrence 1988). Although both these processes can cancel one another out, LMC's analysed from deeper burial depths show more negative $\delta^{18}O_{VPDB}$ values (Hudson, 1977).

The suggestion of oil emplacement inhibiting cement growth is applied to several Cretaceous reservoirs from Abu Dhabi (Kirkham et al., 1996; Nielson et al., 1998); however rates of cementation have never been compared across structure within the oil and water legs. Therefore, this study aims to explore the relationship between cementation and oil charge, by using $\delta^{18}O$ data derived from in situ Ion Microprobe measurements (for methodology see Section 1.2).

5.2 Oxygen isotopes as temperature/burial depth proxies

$\delta^{18}O$ isotopes values are used for determining proxies for depth of progressive cementation and oil charge. It is therefore important to understand the proxy relationship of $\delta^{18}O$ isotopes values to reservoir temperature and to burial depth.

Experiments were completed by Kim & O' Neil (1997) for understanding the controls upon $\delta^{18}O$ isotope fractionation into carbonates. Synthesizing divalent metal carbonates, by bubbling N_2 through bicarbonate solution over a temperature range of 10-40°C, shows that for an increase in temperature, the fractionation of $\delta^{18}O$ within a carbonate reduces from the formation water i.e. at higher temperatures less $\delta^{18}O$ is fractionated into forming carbonates (Kim & O'Neil 1997). Consequently a direct relationship between $\delta^{18}O$ isotopes values and temperature was proposed by Kim & O' Neil (1997). Increasing reservoir temperature through progressive burial causes the reduction in $\delta^{18}O$ fractionation into any forming carbonate cement, producing lighter $\delta^{18}O$ compositions. Therefore $\delta^{18}O$ becomes more negative with increasing burial. The equation for the conversion to reservoir temperature is:

Equation 5.1: $$1000\ln\alpha_{(calcite\text{-}water)} = 18.56(10^3 T K^{-1}) - 32.54$$

(Kim & O' Neil 1997, Thorrold et al. 1997)

5.3 Results

5.3.1 The Lower Kharaib Formation macropores

This section only considers the manually counted macropore spaces (Section 1.2 for methodology) within Cycle 1 and the Lower Khariab Formation (Fig. 5.1 & Appendix 3A). Cycle 1 is today at 2.4km depth, in the water leg at Well 1, and at 2.2km depth in the oil leg at Well 4.

The main difference between the water leg and the oil leg of the Lower Kharaib Formation is the volume of cements. The water leg has 65-99.5% of its macropores cemented while the oil leg has, in places, only 5.3% cemented (Fig. 5.1).

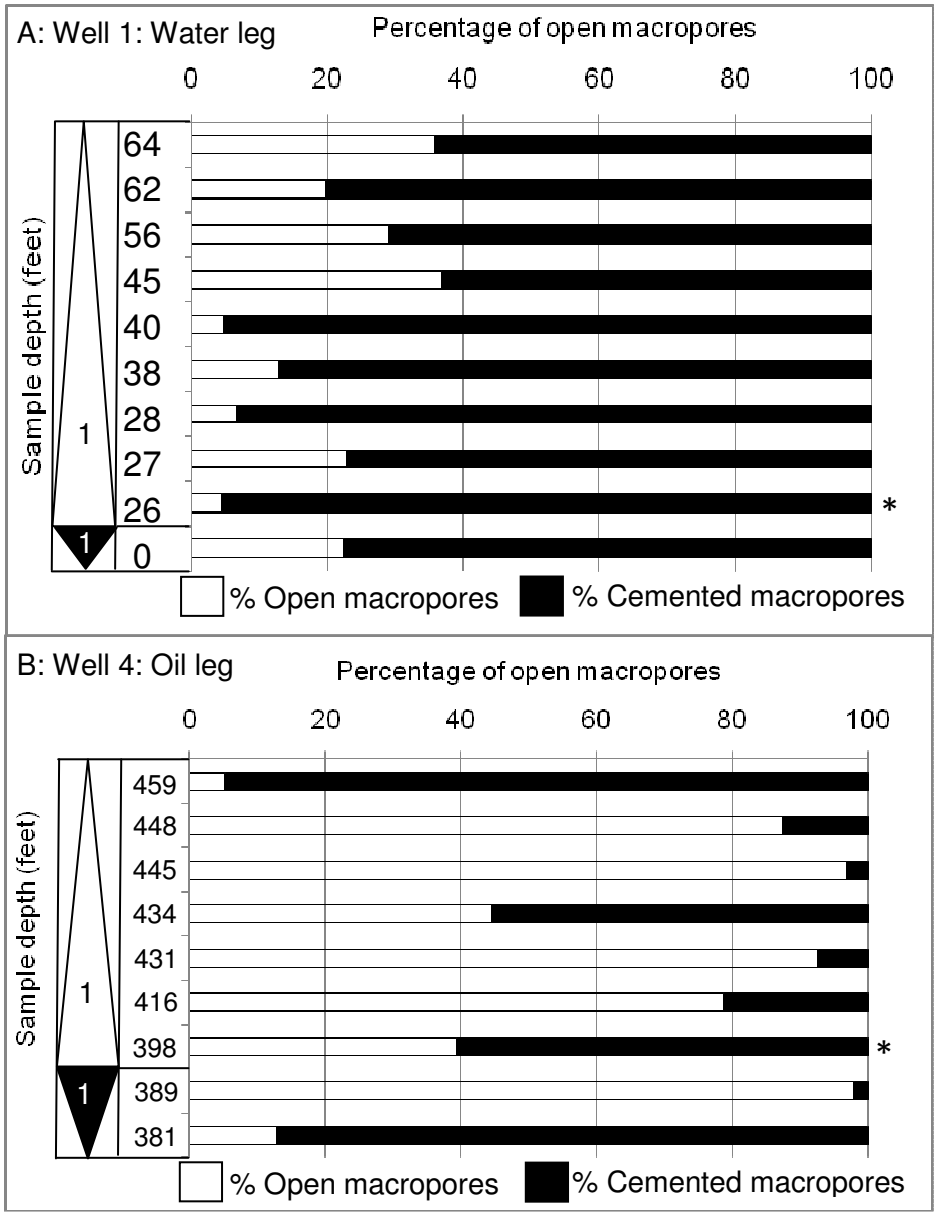

*Figure 5.1: Manually counted macropore data according to depth. These graphs are a combination of pore counts from the reservoirs (Appendix 3A) and samples from the non-reservoirs observed with no open macropores. A) Water leg and B) oil leg in Cycle 1 and the Lower Kharaib Formation. The specific depths for each sample are on the y-axis (Section 1.2 for depth calculations), * represents the samples used for Ion Microprobe analysis. The white triangles represent the HST's, the black triangles represent the TST's and the numbers within the triangles represent the 4th order HFC's. The numbers to the right represent the total amount of pores counted within each sample.*

Commercially measured core plugs (for methodology see Section 1.2) for the oil crest samples have porosities of 0-40%, with permeabilities of 0.1-830mD. By contrast, the water leg samples occupy a distinct field of lower porosity and permeability values of 2-23% and 0.1-9.5mD, respectively (Fig. 5.2)

Cycle 1 in Well 1 is dominated by well connected interparticle macropore space indicating this would have been a good reservoir horizon (Fig. 5.2). In reality, this reservoir, within the water leg occupies a distinct field of lower porosity and permeability values and cements are noted to occlude nearly all macropores with potentially only the micropores remaining open (Section 7.3 & 7.4).

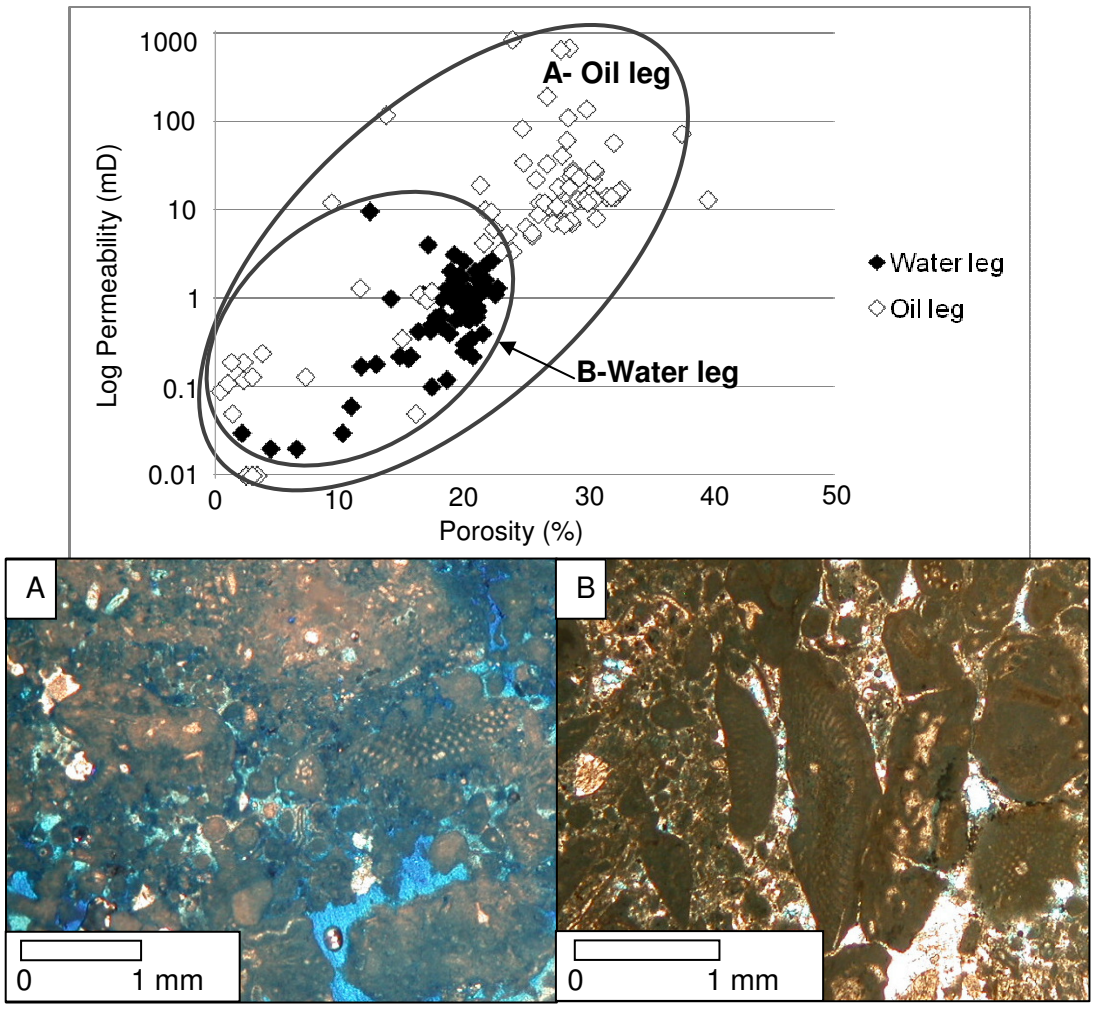

Figure 5.2: Porosity and permeability data for the oil and water legs within the Lower Kharaib Formation reservoir. (A) The oil leg shows relatively high porosity and permeability, and photomicrographs reveal the retention of interconnected macropores, (B) The water leg shows relatively lower porosity and permeability values, which is reflected in the photomicrographs showing near complete macropore occlusion with cement potentially leaving only the microporosity open.

5.3.2 Lekhwair Formation macropores

This Section considers the manually counted macropore spaces within Cycles 4a and 4b of the Lekhwair Formation (Figs. 5.3 & 5.4: Appendix 3A: Section 1.2 for methodology). Cycle 4a is at 2.2km depth in the transition zone at Well 2 and is at 1.9km depth in the oil leg at Well 3.

The main difference is the amount of open and occluded macropore space between the transition zone and the oil leg: on average near 80% of macropores are open in Well 3, on average 50-60% of macropores are open in Well 5 and on average 40% of macropores open in Well 2. The majority of samples from the TST's are 100% cemented.

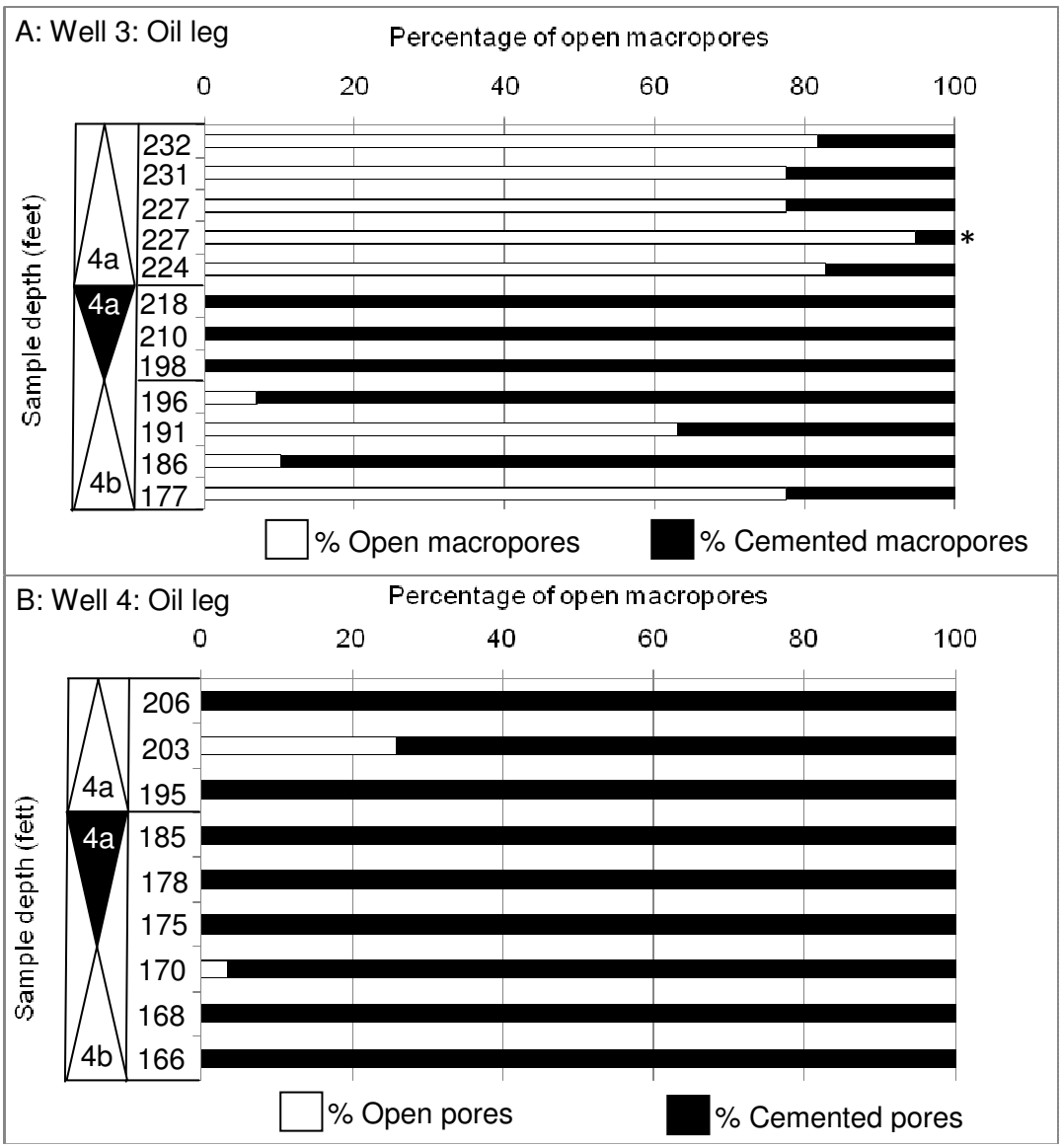

*Figure 5.3: Manually counted macropore data according to depth. These graphs are a combination of pore counts from the reservoirs (Appendix 3A) and samples from the non-reservoirs observed with no open macropores. A) oil leg in Well 3 and B) oil leg in Well 4: both from Cycles 4a and 4b (Lekhwair Formation). The specific depths for each sample are on the y-axis (Section 1.2 for depth calculations), * represents the samples used for Ion Microprobe analysis. The white triangles represent the HST's, the black triangles represent the TST's and the numbers within the triangles represent the 4th order HFC's.*

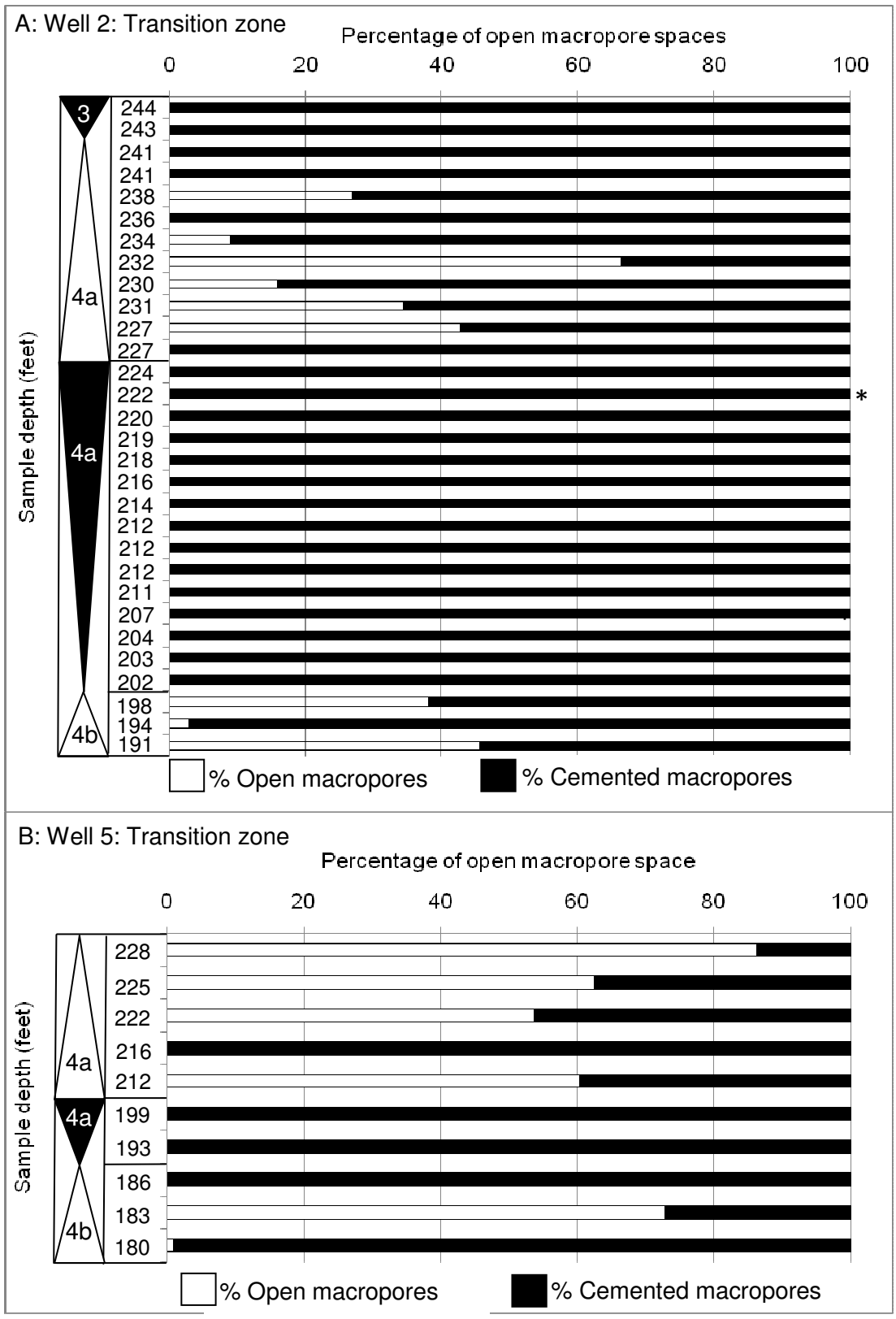

Figure 5.4: Manually counted macropore data according to depth. These graphs are a combination of pore counts from the reservoirs (Appendix 3A) and samples from the non-reservoirs observed with no open macropores. A) Transition zone in Well 2 and B) transition zone in Well 5: both from Cycles 4a and 4b (Lekhwair Formation).

Commercially measured core plugs (for methodology see Section 1.2) for the oil crest sample (Wells 3 and 4) have porosities of 0%-25%, and permeabilities of 0.01-100mD. By contrast, transition zone samples (Wells 2 & 5) occupy a distinct field of lower porosity and permeability values of 0-20% and 0.1-16mD, respectively (Fig. 5.5)

The highest permeability within Well 3, in the oil leg, is 100mD, while the highest within Well 2, in the transition zone, is 16mD. This is reflected in the lithologies: the oil leg has more open interconnected macropores and less cements in comparison with the transition zone.

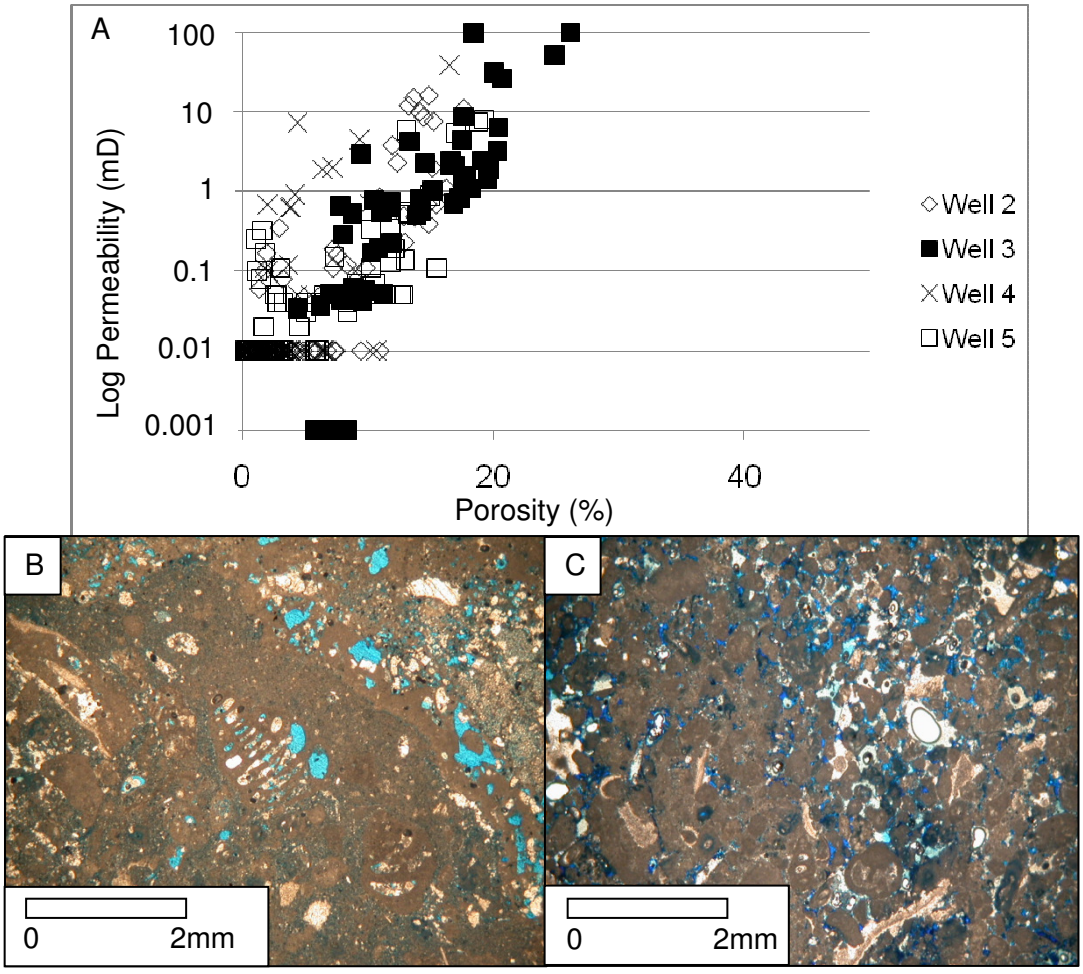

Figure 5.5: Porosity and permeability data for the oil leg and the transition zone within Cycles 4a and 4b of the Lekhwair Formation. (A) Porosity and permeability data measured commercially from core plugs. The transition zone in Well 2 has permeability <16mD, whereas the oil leg in Well 3 has permeability <100mD. (B) Photomicrograph of the transition zone in comparison with C) a photomicrograph of the oil leg: the oil leg shows more open interconnected pores and less cement.

5.3.3 Macropore types

Vugs are defined as open macropore space that bears no relation to depositional fabric: i.e. these pores spaces are diagenetic and have formed from dissolution of the matrix. There are two subcategories: large vugs (>1mm in diameter) (Fig 5.6A) and small vugs (<1mm in diameter) (Fig. 5.6B). Vugs are mostly absent and are never a dominant macropore type throughout the Lower Kharaib and Lekhwair Formations.

The internal chambers within *Lithocodium/Bacinella* (Fig. 5.6C) and large foraminifera (Fig. 5.6D) are termed intra-skeletal pores.

The interparticle pores are the result of close packing of micrite grains. In most cases these macropore are interlinked creating a regular interconnected pore system (Fig. 5.6E).

Moulds are defined as macropore spaces created and/or enhanced, through dissolution, within bioclasts. Small moulds are internal chambers of large foraminifera being <1mm in diameter (Fig. 5.6F). The majority of moulds however, exist within the *G. costatus* shells, these constitute large moulds and are >1mm in diameter (Fig. 5.6G).

Fracture porosity is defined by porosity generated from fractures and faults seen petrographically (Fig 5.6H). Some of these, however, may be the result of coring and are artificial. Therefore fracture porosity is counted but not considered for any further analysis within this study.

There was very little or no intraparticle porosity within all samples (not including microporosity) and therefore these macropores have not been included.

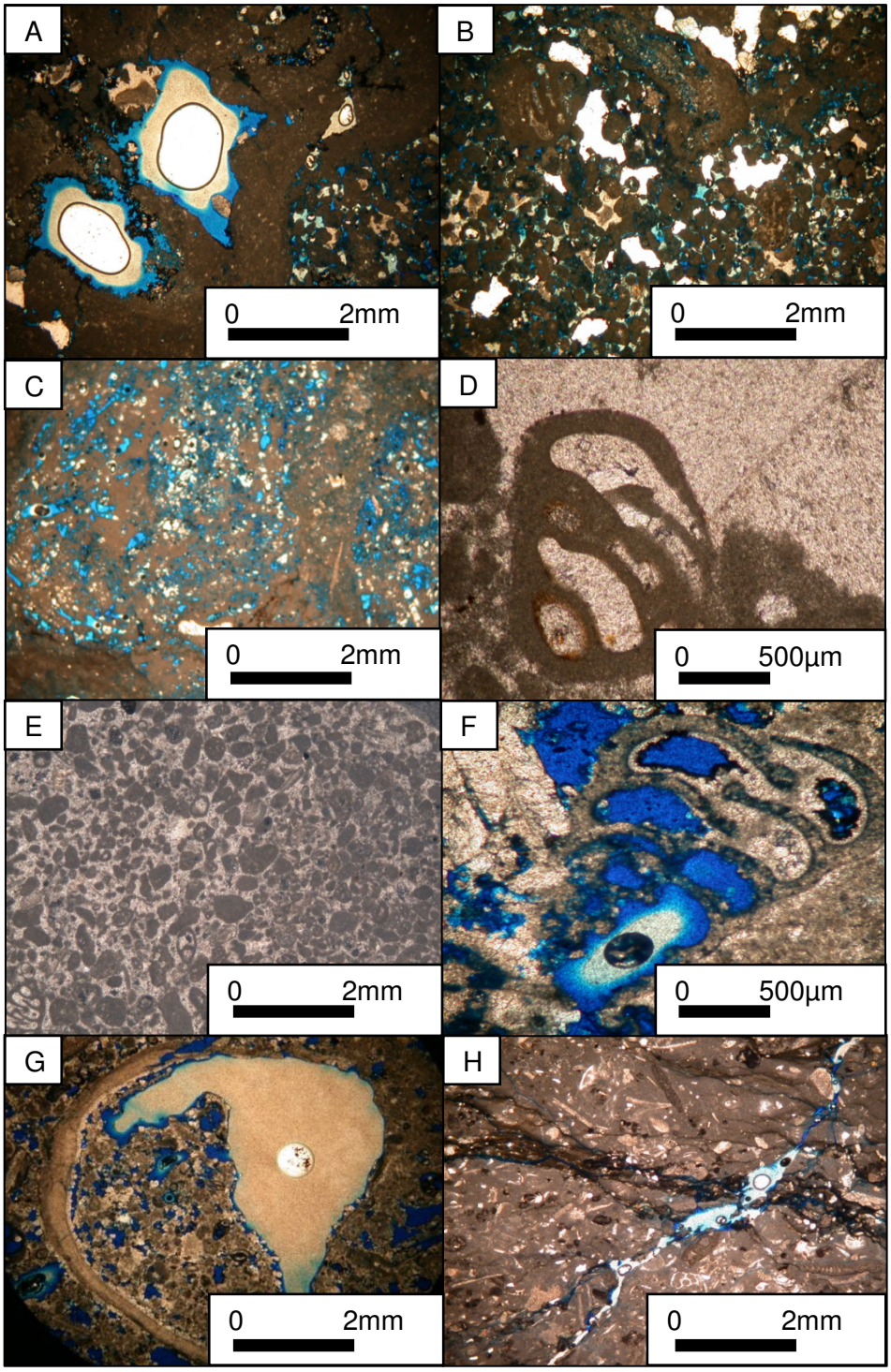

Figure 5.6: types of macropores within the Lekhwair and Lower Kharaib Formations. A) The large vugs, B) the small vugs, C & D) the intra-skeletal pores, E) interparticle pores, F) small moulds, G) the large moulds and H) the fracture porosity.

5.3.4 Macropore types on the 3rd order scale

Macropore types were counted manually (for methodology, see Section 1.2) for all samples within the Lower Kharaib and Lekhwair Formations. Well 4 has the largest sample coverage and is therefore shown in Figure 5.7 (for other Wells see Appendix 3A & 3B). The most dominant macropore types are interparticle pores and intra-skeletal pores. The Lower Lekhwair Formation is dominated by intra-skeletal pores whereas the Lower Kharaib Formation is dominated by 100-250µm interparticle pores (Fig. 5.7). Macropore count increases dramatically from the Lekhwair into the Lower Kharaib Formation, from 800-900, to over 2000 (Fig. 5.7). The large moulds within the *G. costatus* shells (Fig. 5.6G) are not incorporated within this study, as relating their counts to the total proportion of porosity is problematic, considering their enormous size in comparison with most other macropore types. Therefore, the percentage of pore types shown in Figure 5.7 are not accurate and are only indications of which macropore type dominates the macropore systems, and determines the porosity and permeability relationships, for any one specific sample.

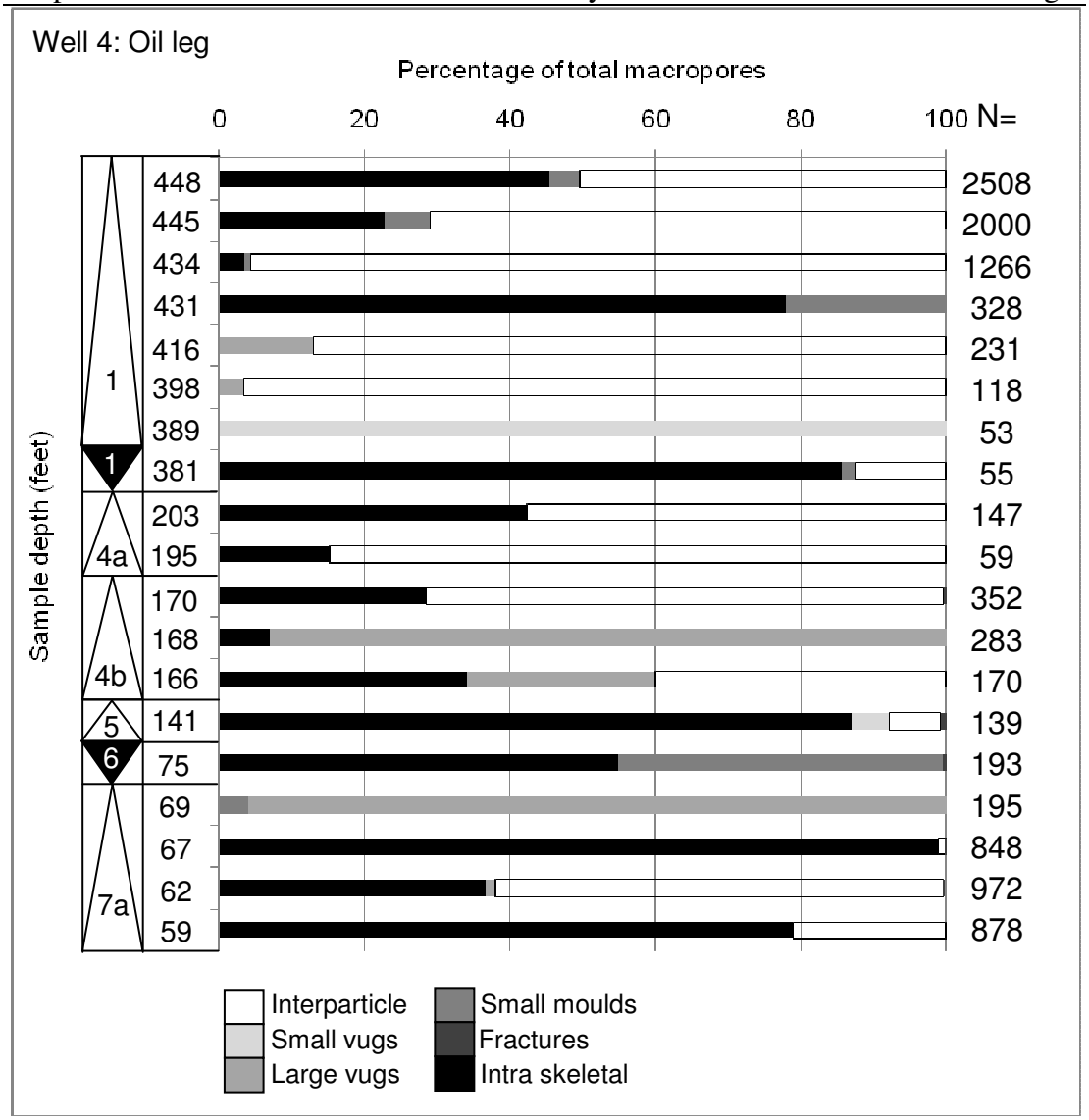

Figure 5.7: macropore types within the Lekhwair and Lower Kharaib Formations from Well 4. The number of intra-skeletal pores generally decreases up into the Lower Kharaib Formation while the number of interparticle pores generally increases from the Lekhwair Formation. The specific depths for each sample are on the y-axis (Section 1.2 for depth calculations). The white triangles represent the HST's, the black triangles represent the TST's and the numbers within the triangles represent the 4th order HFC's. For data on Wells 1, 2, 3 & 4 see Appendix 3A & 3B.

5.3.5 In situ $\delta^{18}O$ data

Ion Microprobe $\delta^{18}O$ data are given in Tables 5.1, 5.2, 5.3 and 5.4 according to CL zone. The mean data for each CL zone, with variance, are given in Figure 5.8. Some zones present a large range in values: others show little variability. The large range in values for some zones may be real, or may indicate that either isotopically

distinct zones have similar colour and luminescence, or that many very thin zones are present which cannot be easily separated. Many zones, particularly in the early stages of the water leg, are thinner than 10µm and cannot be adequately sampled individually with a 10-15µm diameter ion beam.

Four LMC macrocements were selected in the water leg Cycle 1, three in the oil leg Cycle 4a, three in the oil leg Cycle 1 and four in the transition zone Cycle 4a for analysis. Examples of the LMC macrocements are shown in Figure 5.8.

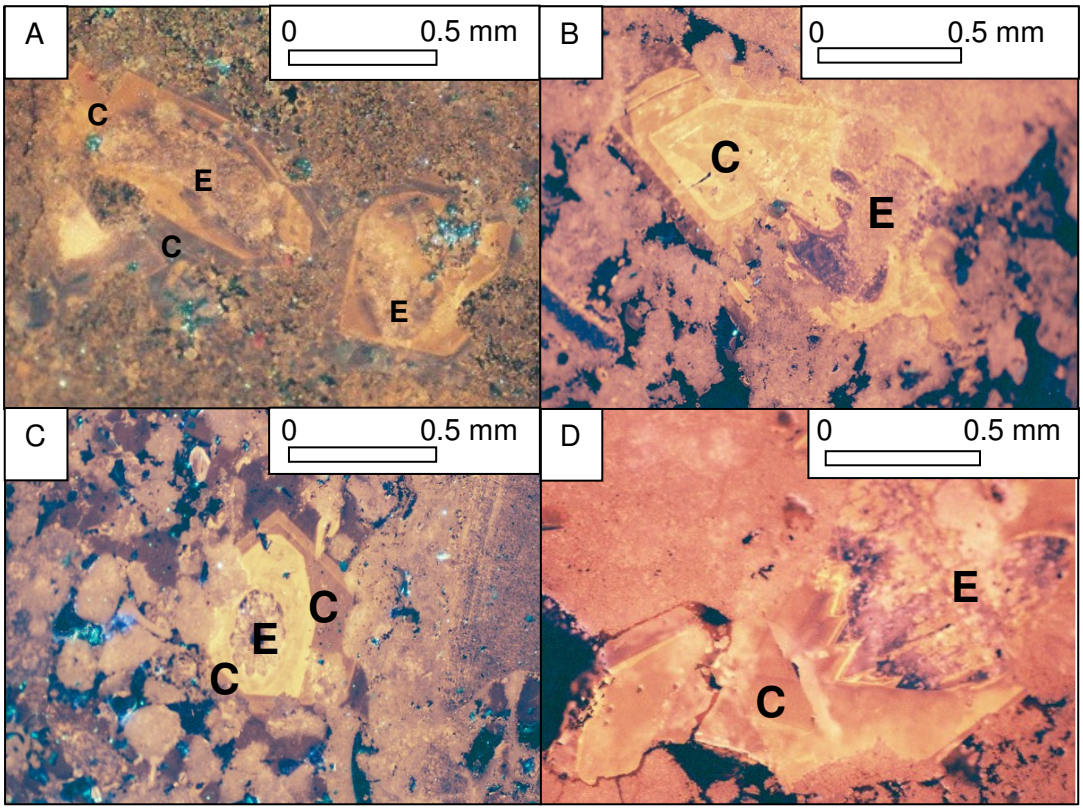

Figure 5.8: Cathodoluminescence images of LMC syntaxial cements (C), nucleating upon echinoderm fragments (E) within A) the water leg: Cycle 1, B) the oil leg: Cycle 4a, C) the transition zone: Cycle 4a and D) the oil leg: Cycle 1. Note the differences in cement zones volumes, and how the final zones in the water leg and the transition zone samples occlude the majority of available pore space. The black and blue areas on both images reflect open pore space.

Zone	Zone Colour	Zone luminescence	Transect 1 ($\delta^{18}O$)	Transect 2 ($\delta^{18}O$)	Transect 3 ($\delta^{18}O$)	Transect 4 ($\delta^{18}O$)	Zone average ($\delta^{18}O$)
1	Black	Dull	-7.8	-7.2 -7.6 -6 -6.5	-7.4	-3.6	-6.6
2	Brown	Moderate	No data	No data	No data	No data	No data
3	Brown	Dull	-8.2	-9.9 -5.1			-7.7
4	Orange	Moderate	-7.3		-9.2 -8.4	-7 -5.6	-7.5
5	Black	Dull		-9.1			-9.1
6	Brown	Dull	-9.3		-9.3	-9.9 -9.9	-9.6
7	Brown	Dull	-9.2			-9.2	-9.2

Table 5.1: In situ $\delta^{18}O$ ion Microprobe data for the water leg, Well 1, Cycle 1.

Zone	Zone Colour	Zone luminescence	Transect 1 ($\delta^{18}O$)	Transect 2 ($\delta^{18}O$)	Transect 3 ($\delta^{18}O$)	Transect 4 ($\delta^{18}O$)	Zone average ($\delta^{18}O$)
1	Black	Dull	-5.4 -4.4	-3.7 -2		-4.2 -3.5 -4.1	-3.9
2	Yellow	Bright	No data	No data	No data	No data	No data
3	Buff	Moderate	-4.5 -5.6	-2.3 -4.5	-6.2	-4.1	-4.5
4	Yellow	Moderate			-6.3	-3.3 -3 -2.9	-3.9
5	Dark orange	Moderate	-9.8		-9.4		-9.6
6	Orange	Moderate		-7.4	-9.1		-8.3
7	Dark orange	Moderate	-8.9		-8.2	-8.4	-8.3
8	Dark purple	Dull	-8.6 -8.3 -8.7	-8.6 -8.6	-8.6	-8.8 -8.7 -8.2 -8.6	-8.6

Table 5.2: In situ $\delta^{18}O$ ion Microprobe data for the transition zone, Well 2, Cycle 4a.

Zone	Zone colour	Zone luminescence	Oil inclusions	Transect 1 ($\delta^{18}O$)	Transect 2 ($\delta^{18}O$)	Transect 3 ($\delta^{18}O$)	Zone average ($\delta^{18}O$)
1	Black	Dull	0	-1.7 -1.7		-1.3	-1.6
2	Red	Moderate	No data	No data	No data	No data	No data
3	Buff	Moderate	0	-5.2	-2.9 -5.3 -2.5 -3.3 -3.6	-0.3 -2.4	-3.2
4	Yellow	Moderate	1	-4.6		-3.4 -4.7 -4.6	-4.3
5	Orange	Dull	2 @ boundary, 1	-8.3 -6.9	-8.5 -7.1	-7	-7.6
6	Dark purple	Dull	7		-6.9 -6.3 -6.5 -5.8 -6.1	-6.3 -5.6 -5.6 -4.9	-6

Table 5.3: In situ $\delta^{18}O$ ion Microprobe data for the Oil leg, Well 3, Cycle 4a.

Zone	Zone Colour	Zone lumine-scence	Oil inclusions	Tran-sect 1 ($\delta^{18}O$)	Tran-sect 2 ($\delta^{18}O$)	Tran-sect 3 ($\delta^{18}O$)	Tran-sect 4 ($\delta^{18}O$)	Zone average ($\delta^{18}O$)
1	Black	Dull	0	-1.2				-1.2
2	Orange	Moderate	0					
3	Yellow	Bright	0				-4.7	-4.7
4	Orange	Moderate	0				-4.1	-4.1
5	Brown	Dull	0				-4.1	-4.1
6	Orange	Moderate	0	-3.8				-3.8
7	Yellow	Moderate	0				-4.4 -4.4	-4.4
8	Red	Moderate	6				-5.5 -4.4	-5
9	Orange	Moderate	4		-6.3 -8.4 -8.7	-6 -6.4 -8.2	-5.9 -6	-7
10	Yellow	Moderate	2		-9.6 -9.1	-8.8		-9.2
11	orange	Moderate	0		-10.3			-10.3
12	Reddy brown	Dull	2	-7.4 -7.5		-7.8	-7.9 -7.8 -7.9	-7.7

Table 5.4: In situ $\delta^{18}O$ ion Microprobe data and position of oil inclusions for the oil leg, Well 4, Cycle 1

5.3.6 Oil inclusions

A total of 27 oil inclusions were found in 4 syntaxial cements within the oil leg samples, in Zones 8, 9, 10 and 12 (Tables 5.3 & 5.4). All the oil inclusions were found in the oil leg and measure between 1-5µm in diameter and fluoresced pale apple green indicating moderate maturity. The amount of oil inclusions decrease towards the youngest cement zone, with 6 in Zone 8, 4 in Zone 9, 2 in Zone 10, and 2 within Zone 12. A further 13 oil inclusions were found in 10 syntaxial macrocements within the oil leg Well 3 samples in Zones 3, 4, 5 and 6. The amount of oil inclusions increases towards the youngest cement zone with 2 at the boundary of Zones 3 and 4, 1 within Zone 4, 3 within Zone 5 and 7 within Zone 6. The oil leg samples from Well 4 and Well 3 show the exact opposite trend in oil inclusion abundance.

5.3.7 SEM Imaging

SEM imaging shows that the micrite contains equant crystals: in the oil leg they are present as either anhedral, or subhedral to euhedral microrhombic fabrics (Section 7.2). Crystal sizes are difficult to determine in the anhedral fabric, but they are 3-10µm in microrhombic fabrics (Sections 7.2 & 7.3). Microrhombic microspars present an open texture with micropores (defined as <10µm, Cantrell & Hagerty 1999). A generation of cement has occluded the majority of microporosity producing an anhedral fabric exclusively within the water leg (Section 7.3.4).

5.3.8 Bulk stable isotopes

Table 5.5 presents $\delta^{13}C$ and $\delta^{18}O$ data from bulk micrite samples, the oil and water legs, and from Cycle 1. The $\delta^{18}O_{VPDB}$ of bulk micrite (Cycle 1) from the water leg shows an average of -7.4‰ (n=10) compared with -6.3‰ (n=11) from the oil leg. The bulk micrite (Cycle 4a) for the transition zone shows an average of -3.8‰ (n=24), compared with -4.2‰ for the oil leg (n=13).

WL Cycle 1		OL cycle 1		OL Cycle 4a		TZ Cycle 4a	
$\delta^{13}C$	$\delta^{18}O$	$\delta^{13}C$	$\delta^{18}O$	$\delta^{13}C$	$\delta^{18}O$	$\delta^{13}C$	$\delta^{18}O$
2.6	-7.3	3.4	-5.5	2	-3.7	1.5	-3.1
2.8	-7.9	2.9	-5.5	2.7	-4.0	2.5	-3.2
3	-7.5	2.9	-5.9	2.4	-4.2	2.7	-3.2
3.2	-7.3	3	-6.9	2.2	-3.7	2.5	-5.0
3.1	-7.7	3.2	-6.6	2.3	-3.8	2.7	-3.5
3.3	-7.5	2.9	-7.0	2.6	-4.6	2.8	-3.7
4.3	-7.5	3.1	-6.7	2.9	-5.0	2.7	-4.0
2.8	-7.4	3.2	-6.7	2.2	-5.0	2.5	-3.3
3.2	-7.4	3.3	-6.4	1.3	-3.3	2.5	-4.4
3.3	-6.1	3.4	-4.7	2.3	-5.5	2.2	-4.6
		2.1	-7.1	2.1	-4.7	2.3	-3.9
				1.5	-3.2	2.3	-5.2
				1.4	-3.4	1.9	-4.4
						2.3	-4.0
						2.3	-4.6
						2.1	-3.9
						1.9	-4.0
						2.2	-3.4
						1.5	-4.2
						1.1	-4.3
						1.4	-3.5
						0.6	-3.6
						0.7	-2.4
						1	-2.7
3.2	-7.4	3.0	-6.3	2.1	-4.2	2.0	-3.8

Table 5.5: The $\delta^{13}C$ and $\delta^{18}O$ data from bulk micrite samples, the bottom row is the average for each column.

5.4 Cement stratigraphy

5.4.1 The water leg

Cathodoluminescence revealed 7 cement zones in the water leg within Well 1 (Fig. 5.13A, Table 5.1). The oldest cement zone in the water leg shows highly variable range in $\delta^{18}O$ data, from -3.6‰ to -7.8‰ (n=7) (Fig. 5.9). Subsequent zones show consistently negative values decreasing to a value of -9.2‰ (zone average for the youngest zone: Figs. 5.9 & 5.13A). The most negative $\delta^{18}O$ value exists within Zone 6 of -9.9‰. The earliest water leg zone is very thin (<10µm), with later zones

showing a general increase in thickness from 100->200µm towards the youngest pore filling cement. Consequently the final brown zone is volumetrically larger and is almost pore filling, only leaving 1.9% of pores open (Fig. 5.1A). Many smaller cement nucleation's of this final brown zone are observed in surrounding smaller pore spaces.

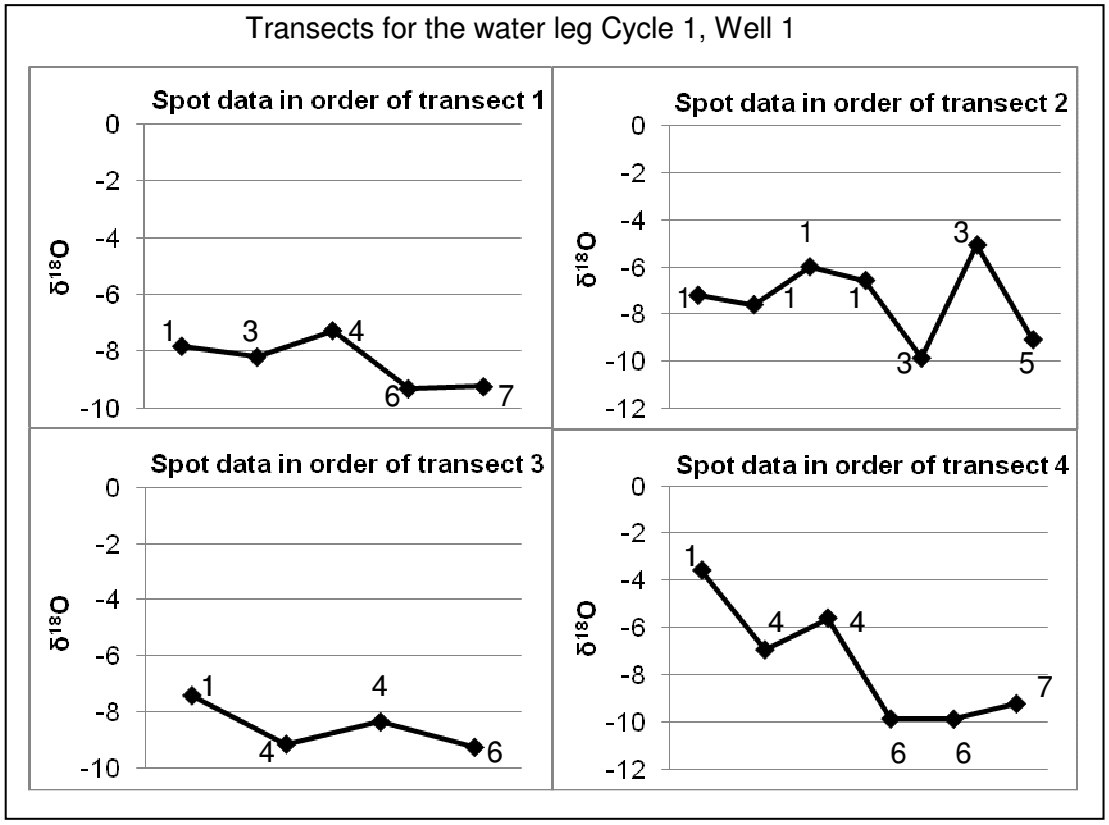

Figure 5.9: four individual transects of the water leg. Each show either very negative $\delta^{18}O$ values or show a steady progression to -9‰. The numbers correspond to the zones associated with the data points (Fig. 5.13A). See Table 5.1 for data.

5.4.2 Transition zone

Within the transition zone from Well 2, Cathodoluminescence revealed 8 cement zones (Fig. 5.13B, Table 5.2). The oldest cement zone within the transition zone has an average $\delta^{18}O$ value of -3.9‰, with the subsequent three zones showing a decrease in negativity to -9.6‰ (average for Zone 5: Figs. 5.10 & 5.13B). This zone has the most negative $\delta^{18}O$ value of -9.8‰. The final three cement zones show a slight return to less negative $\delta^{18}O$ values, back to -8.6‰ (average for Zone 8: Figs. 5.10 &

5.13B). The youngest dark purple cement is volumetrically the largest in the sequence occluding most pore space, leaving only 31-84% of open pore space (Fig 5.4A).

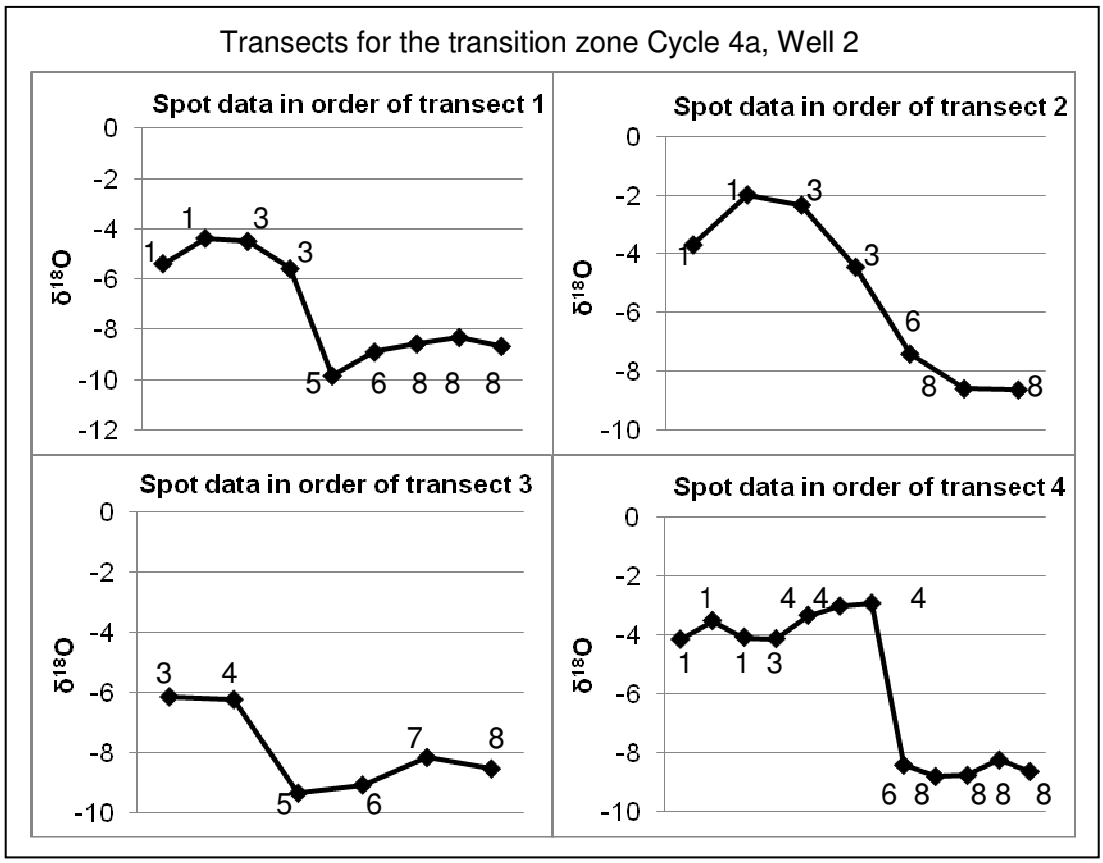

Figure 5.10: four individual transects of the transition zone. Two of these transects show a slight decrease in $\delta^{18}O$ negativity within the oldest zones followed by a steady progression to -9‰. The final few data points show a slight return to less negative $\delta^{18}O$ values. The numbers are the zones associated with the data points (Fig. 5.13B). See table 5.2 for data.

5.4.3 The oil leg

For the oil leg in Well 3 (Cycle 4a) Cathodoluminescence revealed 6 zones (Fig. 5.13C, Table 5.3). The earliest cement zone has an average $\delta^{18}O$ value of -1.6‰ (Fig. 5.11). The subsequent four zones show an increase in $\delta^{18}O$ negativity to -7.6‰ (average for Zone 5: Figs. 5.11 & 5.13C). The most negative value present is in Zone 5, which is -8.5‰. The final Zone 6 shows a decrease in negativity with an average of -6‰, with a single least negative value of -4.9‰ (Fig. 5.11).

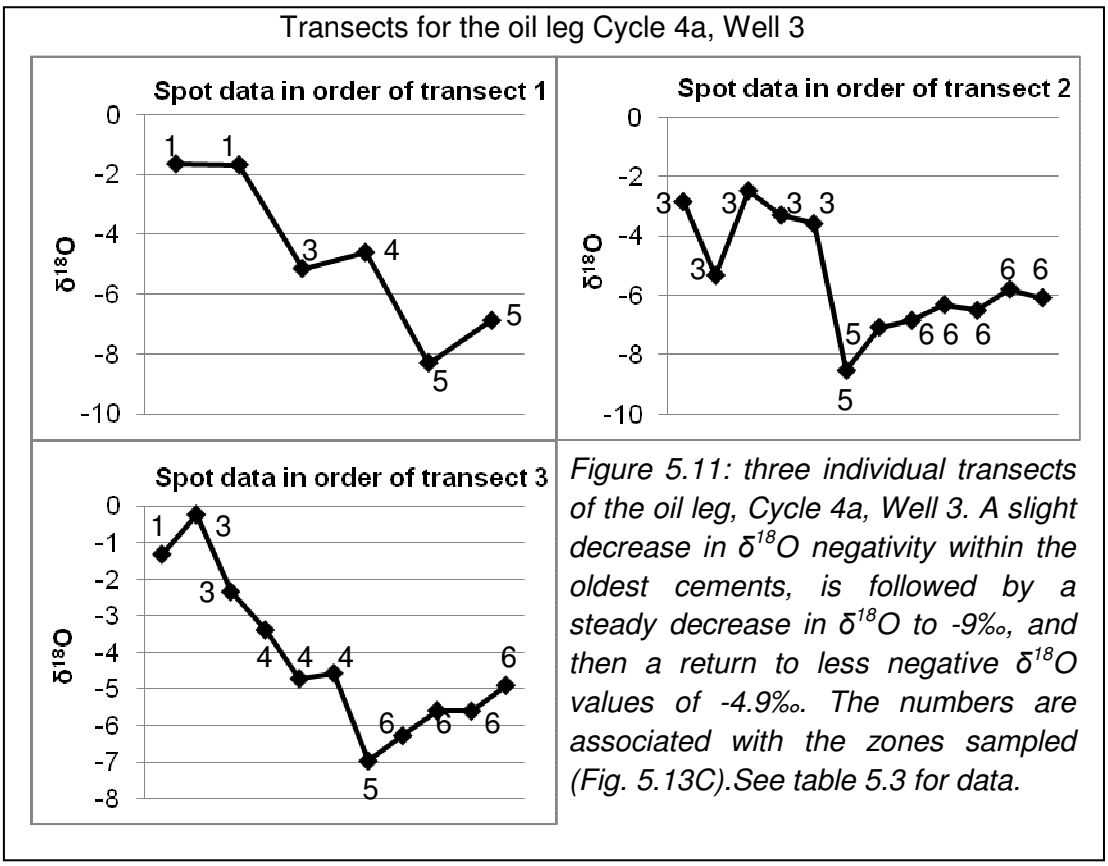

Figure 5.11: three individual transects of the oil leg, Cycle 4a, Well 3. A slight decrease in $\delta^{18}O$ negativity within the oldest cements, is followed by a steady decrease in $\delta^{18}O$ to -9‰, and then a return to less negative $\delta^{18}O$ values of -4.9‰. The numbers are associated with the zones sampled (Fig. 5.13C).See table 5.3 for data.

In the oil leg in Well 4 (Cycle 1), Cathodoluminescence revealed 12 zones (Fig. 5.13D, Table 5.4). The earliest cement zone shows a value of -1.2‰, with subsequent zones showing a steady progression, in negativity, to -10.3‰ in Zone 11 (Fig. 5.12). The final cement zone shows a return to a less negative $\delta^{18}O$ value to -7.7‰ (Fig. 5.12). Within both oil leg samples the eight earliest cements are very thin measuring 10-50µm in thickness. Zones 9 and 10 are 200µm thick with the youngest 11th and 12th Zones measuring 100µm in thickness. The youngest cement zones for both oil leg samples are not pore filling and appear volumetrically smaller compared with the youngest cement zones within the water leg and the transition zone.

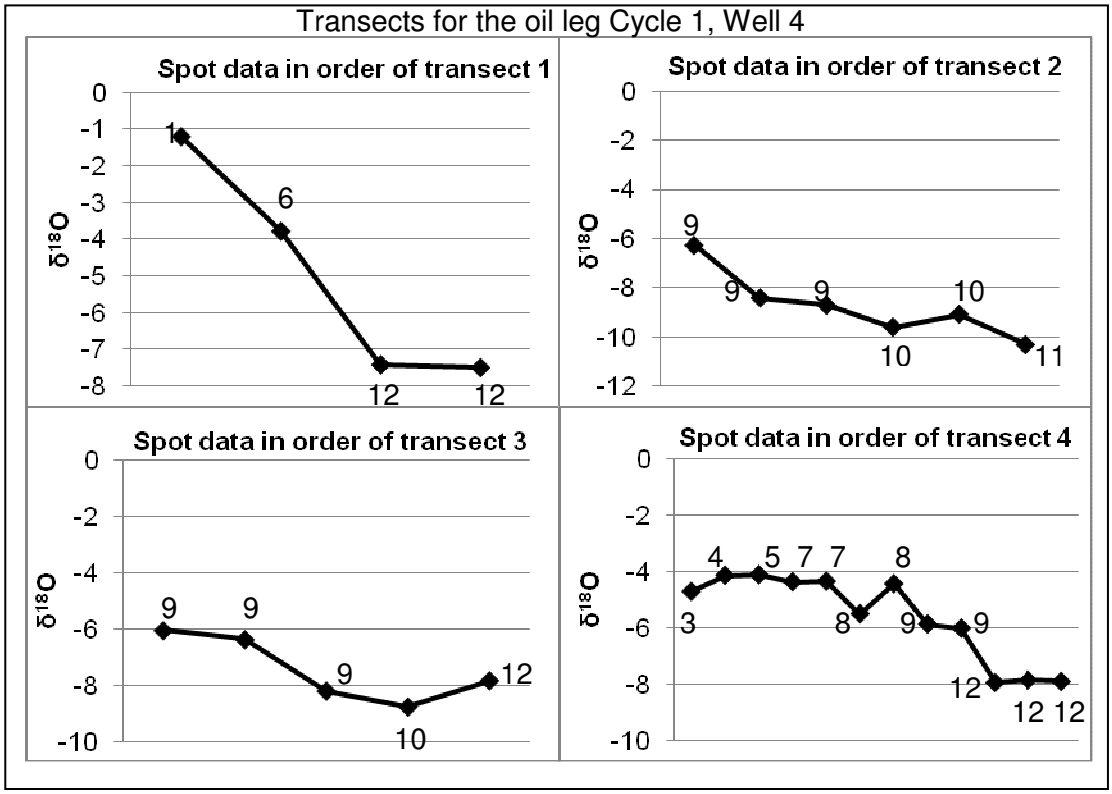

Figure 5.12: four individual transects of the oil leg, Cycle 1, Well 4. The data shows a steady decrease in $\delta^{18}O$ values to -10‰.The numbers correspond to the zones associated with the data points (Fig. 5.13D). See Table 5.4 for data.

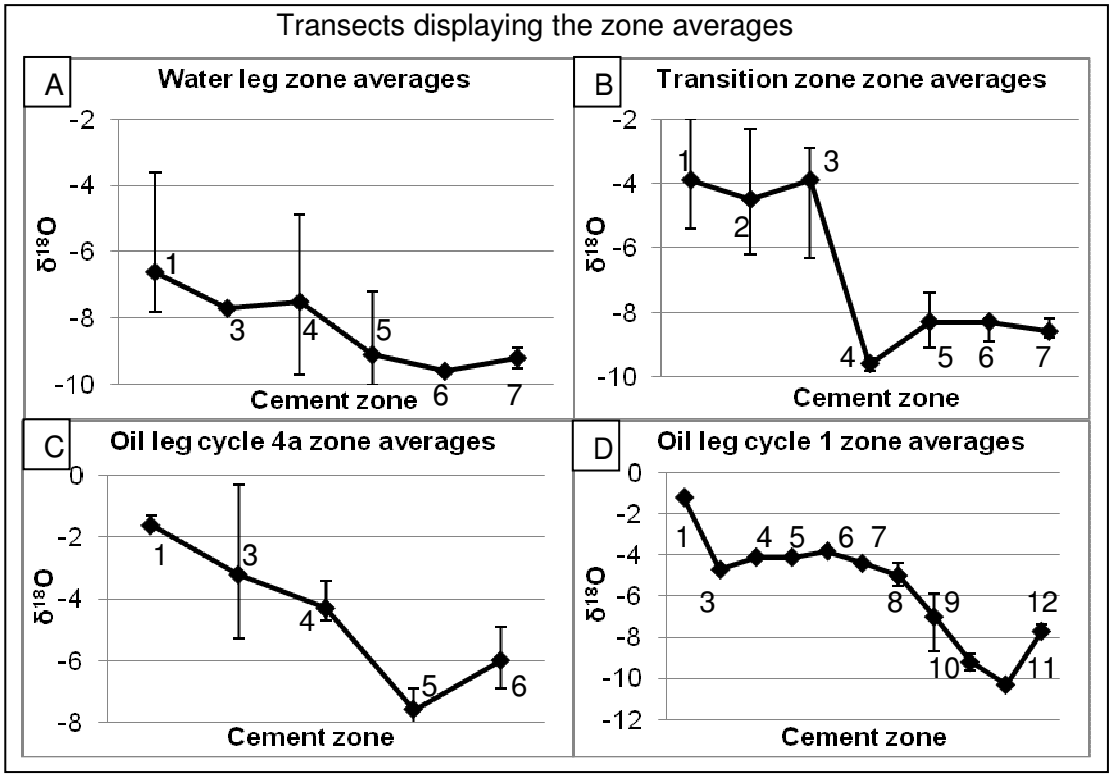

Figure 5.13: A) averages for each zone in the water leg, Cycle 1 B) in the transition zone, Cycle 4a C) in the oil leg Cycle 4a and D) in the oil leg for Cycle 1. This data show reductions in negativity in the last zone only for the oil leg, to -7‰ in Cycle 1, and to -4.9‰ in Cycle 4a. The zone number is placed next to each data point. Each data point has error bars that display the positive and negative ranges.

5.5 Macropore types and cements across the field

In the Lower Kharaib Formation, the oil leg has a maximum permeability of 830mD, while the water leg has a maximum permeability of 9.5mD (Fig. 5.2). The lithology is very similar across the entire field and therefore this dramatic reduction in permeability towards the water leg, and the flanks, must be due to the oil leg being less cemented (20-60% cemented pores) in comparison with the water leg having 60-90% of its pore cemented (Fig. 5.1 & 5.3).

The Lower Kharaib Formation, within the oil leg, has the highest permeability of 830mD, in comparison with Cycle 4a in the Lekhwair Formation, which has a maximum permeability of 100mD (Figs. 5.2 & 5.5). This may be partly due to the difference in macropore types that dominate both the Lekhwair and Lower Kharaib Formations (Fig 5.7). The Lekhwair Formation, as discussed in Sections 3.4.4 & 3.5.1 is far muddier than the Lower Kharaib Formation (Sections 3.4.5 & 3.5.3), and this may have allowed *Lithocodium/B.* to colonise the Lekhwair platforms more readily in comparison with the Lower Kharaib Formation, due to it appearing preference for firmer substrates (Section 3.4.5 & 3.5.3). *Lithocodium/B*. is the main reason for abundance in intra-skeletal pores which constitute a large fraction of the total porosity (Fig. 5.7). However the lower permeability's of the Lekhwair Formation suggest that the intra-skeletal pores are either cemented or disconnected meaning that sample concentrated in *Lithocodium/B.* does not necessarily mean enhanced primary reservoir quality, unlike suggestions from Banner et al. (1990).

In comparison, the Lower Kharaib Formation has abundant interparticle pores due to the reservoir being concentrated in micrite grains (Section 5.3.5: Fig. 5.7). A possibility is an increase in carbonate production caused carbonate erosion to increase, producing increasing volumes of carbonate sediment (Section 4.4). Therefore, both the deposition environment and the volume of cements appear to be controlling factors in the distribution of the highest porosity and permeability relationships within this offshore field, Abu Dhabi.

5.6 Conversion to temperature and burial depth

The $\delta^{18}O$ and the temperature are unknown for formation waters within the Lower Kharaib and Lekhwair Formations. $\delta^{18}O$ data collected from LMC brachiopod shells, conodonts and belemnites from several sedimentary basins across the globe during the Cretaceous (Veizer et al. 1999) are used to determined an estimate. LMC shells, unlike HMC and aragonite shells have not been diagenetically altered on the seafloor and should therefore reflect $\delta^{18}O$ of the surrounding seawater. The collective data reflect an average of -1‰ for the Lower Cretaceous (Podlaha et al. 1998, Veizer et al. 1999) (Section 6.2.1).

If this study assumes there has been no porewater evolution during burial, the calculations yield a temperature of 96.3°C for the position of the earliest oil inclusion found, which was within Zone 8 of the oil leg and Well 4 (Cycle 1). Assuming a constant geothermal gradient of 36°C/km (Gumati 1993) this indicates the earliest depth of oil emplacement with 2.67km.

For the water leg the most negative $\delta^{18}O$ value of -9.9‰ is within the youngest cement zone, which yields a temperature of 128.8°C, indicating a burial depth of 3.6km. This could potentially be the deepest point of cementation recorded within the water leg, when the majority of the macroporosity had fully occluded.

For the transition zone the most negative $\delta^{18}O$ value is within Zone 5 of -9.8‰, which relates to a temperature of 128.5°C, and to a burial depth of 3.6km. The youngest cement zone has a $\delta^{18}O$ average value of -8.6‰, reflecting a temperature of 121°C, and a burial depth of 3.36km. The formation of the final 3 cement zones is occurring as the surrounding porewaters are changing back to heavier ^{18}O compositions.

For the oil leg in Well 3 (Cycle 4a), Zone 5 has the most negative $\delta^{18}O$ value of -8.5‰, representing a temperature of 120.7°C and a burial depth of 3.35km. This potentially represents cementation occurring within the oil leg (Cycle 4) at the deepest point of burial. The value of -4.9‰ within the youngest cement zone, indicates a temperature of 89.9°C, and a burial depth of 2.49km.

For the oil leg within Well 4 (Cycle 1) the penultimate cement zone (Zone 11) has the most negative $\delta^{18}O$ value of -10.3‰, indicating a temperature of 131.3°C, and a burial depth of 3.64km. This potentially indicates the deepest point of cementation within the oil leg (Cycle 1), as the next, and youngest, cement zone with a $\delta^{18}O$ value of -7.4‰, yields a temperature of 112.8°C, indicating a burial depth of 3.13km. This is consistent with the calculations on the oil leg in Cycle 4a: the final cement zones for both samples in the oil leg are forming from porewaters equilibrating back to heavier ^{18}O compositions.

All the data within the water leg, the oil leg and the transition zone proceed to a very narrow range of $\delta^{18}O$ data between -8.5‰ to -10.3‰. The water leg average has a variance of -0.4‰, for the transition zone it is -0.9‰, for the oil leg in Cycle 1 it is -0.8‰ for Zone 10 and -0.5‰ for Zone 12, suggesting that little pore fluid evolution had occurred during burial. However, there are large variances in $\delta^{18}O$ within the oldest cements suggesting that porewaters had significantly evolving during initial and shallow burial of the Lekhwair and Lower Kharaib Formations.

Using the equation from Kim & O'Neil (1997) and assuming a $\delta^{18}O$ of -1‰ for LMC at 10°C and -10‰ for LMC at 100°C, the $\delta^{18}O$ values for the porewaters are calculated to be -0.3‰, and -2.6‰, respectively. This implies porewater evolution, through water-rock interaction, had occurred when producing LMC cements with incorporated values of -9‰ to -10‰, from -1‰ (Cretaceous seawater). It also shows the starting $\delta^{18}O$ porewater composition, during initial burial, may not have been -1‰: possible reason for this is through mixing from meteoric waters or Lower Cretaceous seawater was less negative from the global average (Veizer et al. 1999). Therefore this study cannot assume that porewaters had not evolved during the progressive burial of the Lekhwair and Lower Kharaib Formations.

5.7 Cementation and oil charge

It has been proposed that oil may progressively displace porewater so slowing cementation (Heasley et al. 2004). Oil will continue to flood, replacing the water, until all macropores are oil wet with only micropore systems remaining water wet.

This indicates that at a critical oil saturation, all cementation will cease (Heasley et al. 2004). The data presented here supports this relationship.

The number of oil inclusions is highest in Zone 8 (corresponding to -5.5‰) but then decreases towards the youngest cement phase. This indicates that oil emplacement occurred during burial and was followed by further cement growth.

The penultimate cement zone in the oil leg reaches similar values of -9‰ to -10‰ which is consistent with the final pore filling cements in the water leg. Therefore both the oil and water legs appear to have cemented to similar burial depths. Further cementation in the crest, producing the final cement zone indicates that cements had grown for longest within the oil leg, confirming that diagenesis was not immediately halted by the onset of oil, and much cement had formed within the partially oil-wet pore systems (Heasley et al. 2000).

5.7.1 Cement volumes

There are major differences in cement volume across the structure, but accurate quantification of these differences, is problematic. The majority of cements are present in the water leg, where up to 99.5% of interparticle pore space is occluded, while in the field crest interparticle pore space remains ~95% open (Fig. 5.1).

Due to the vagaries of thin section orientation oblique to cement growth direction, measured zone width may not reflect true cement thickness. However these thicknesses can be considered to be an approximate measure of relative growth rates, so enabling comparison of cement zone volumes between the two legs. Within the oil leg, cement zones are frequent prior to oil charge (Zone 8), but subsequent zones decrease from 200µm to 100µm in thickness towards the youngest cement phase. By contrast, the water leg cements zones increase in thickness to >200µm, after inferred oil emplacement, with the final zone often occluding all remaining pore space.

More in situ $\delta^{18}O$ analyses were possible in thicker zones. The frequency of $\delta^{18}O$ data arranged in 1‰ bins can therefore serve to reveal the relative dynamics of cement growth rates in the two legs (Fig. 5.14). In the oil leg, more positive $\delta^{18}O$ values show increasing frequency of occurrence until initial oil emplacement (at -5‰), elevating slightly from -6‰ to -9‰, but after that frequency decreases. By

contrast in the water leg, $\delta^{18}O$ values below -5‰ are uncommon, but more negative values increase progressively in frequency after initial oil emplacement.

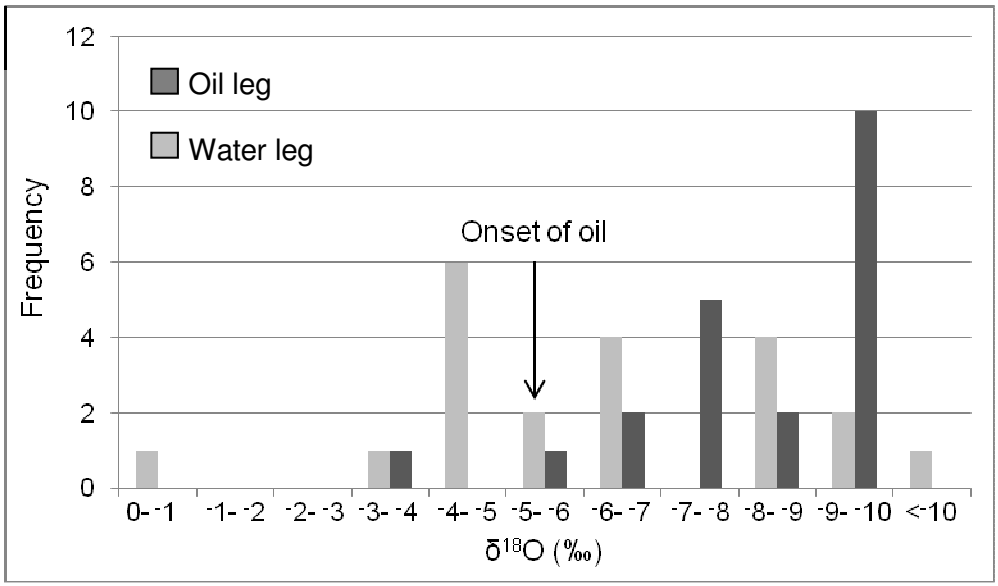

Figure 5.14: Frequency distribution of Ion Microprobe $\delta^{18}O$ data in 1‰ classes for the oil and water legs. Initial oil emplacement is highlighted with respect to the first oil inclusion occurrence at -5.5‰. The majority of $\delta^{18}O$ data within the water leg is more negative than -5‰, suggesting the majority of cementation had occurred after oil charge. Within the oil leg there is much $\delta^{18}O$ data between -1.2‰ and -5‰, with less data beyond -5‰, indicating the majority of cementation in the oil leg had occurred before oil charge.

The final cement zone, post dating initial oil emplacement, within the water leg is far more volumetrically extensive and shows new cement nucleation's corresponding to the youngest cement phase. This is not the case in the oil leg where the final cement zones, post dating the onset of oil, are thinner, are not fully pore occluding and no new cement nucleation's exist. This suggests that a much higher flux of solutes was available during burial, after the onset of oil, solely in the water leg (Figs. 5.8 & 5.15).

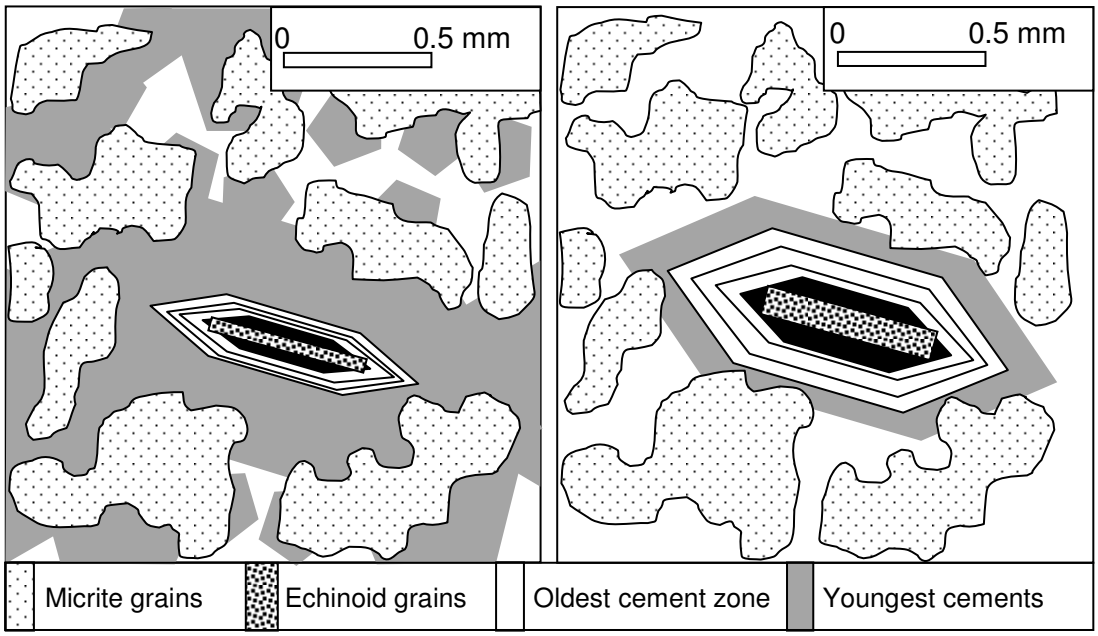

Figure 5.15: A) Water leg: The final cement phase is pore filling. There are several new nucleation sites of the youngest LMC cement phase. There may have been a sudden influx of solutes during burial to allow for widespread nucleation and cementation of ~98% of interparticle pore space within the water leg. B) Oil leg: The cement phases are generally much thicker forming much larger macrocements in comparison with the water leg. The youngest cement phase is not pore filling and is relatively thin compared with the water leg. The macrocements are therefore isolated leaving up to 90% of interparticle pore space open (Fig. 5.7 for related images).

As shown on the SEM images (Fig. 5.16) the oil leg contains the most interconnected micropore networks. In contrast, the water leg micropores are heavily occluded to form in places a more anhedral micropore fabric (Fig. 5.16). The incorporation of smaller cement crystals within larger ones, along with macrospars incorporated into anhedral fabrics suggests that the water leg had another generation of cement occlusion. This also suggests that the microporosity within the water leg was reduced by a phase of micropore-fill cementation, as opposed to enhanced crystal growth, as suggested by Moshier (1989a).

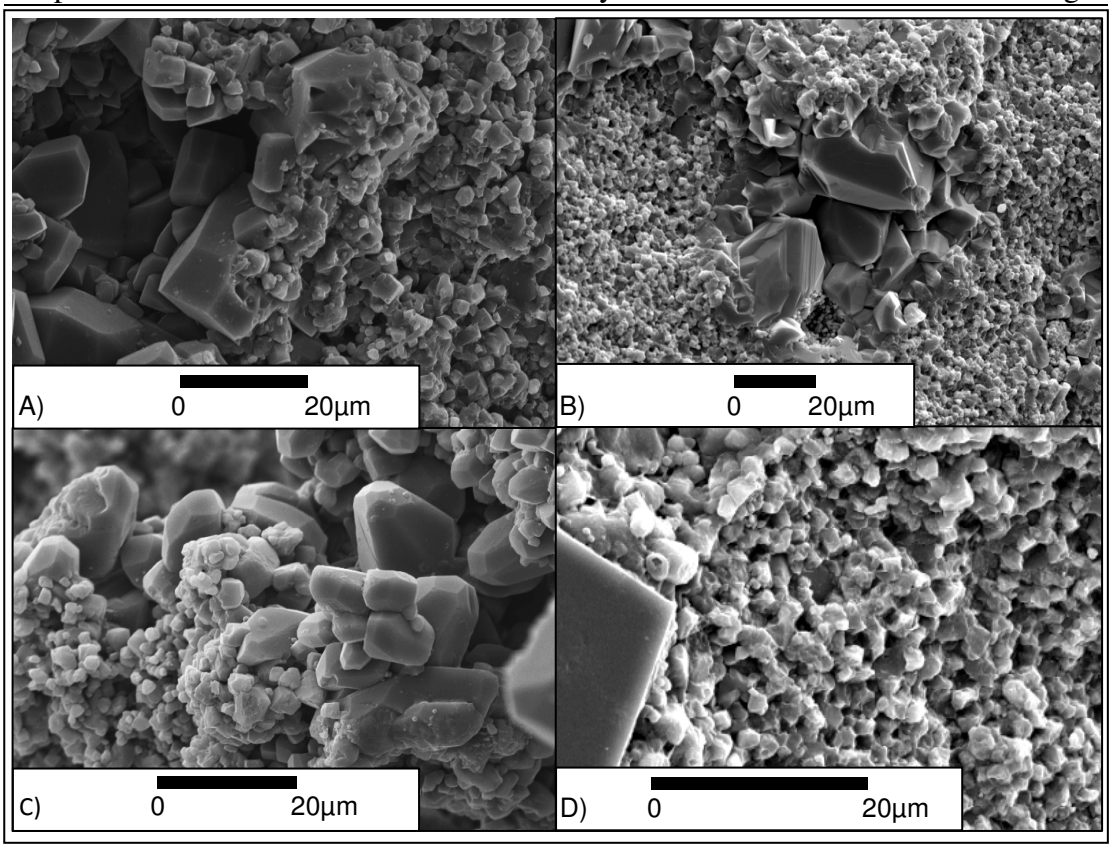

Figure 5.16: SEM images of the micropore fabrics. A & C) The open subhedral-euhedral fabrics of the oil leg in Cycle 1. There is much open microporosity. B & D) The water leg micropores were selectively occluded by a generation of micropore fill cement producing a more anhedral micropore fabric.

The main source for these cements could have been through dissolution, due to stylolites, which is observed within both the Lekhwair and Lower Kharaib Formations, within the oil and water legs (this study), by Burgess & Peter (1985) (for the Lower Kharaib Formation) and Oswold et al. (1995) (for the Kharaib Formation). This suggests that the final water leg cements, and $\delta^{18}O$ values of -8‰ to -10‰, are products of the deep burial realm. Paths for solutes must have remained open within the water leg, while the introduction of oil in the oil leg (pre-dates cements with $\delta^{18}O$ values of -8‰ to -10‰) can be inferred to have caused the shutdown of its macropores.

Within carbonates, the positively charged calcite surfaces in contact with the negative dipoles of organics in oil, causes attraction (Heasley et al. 2000: Hirasaki & Zhang 2004). More specifically, the oil-water interface is negatively charged because of the disassociation of the carboxylic acids within the oil (Zhang & Austad 2006).

When the brine at the rock-water is more concentrated in Ca^{2+} over CO^{3-} these areas are positively charged (Zhang & Austad 2006). The concentration of bicarbonate ions near the calcite surfaces determines oil wettability: a high concentration promotes a negative charge on calcite surfaces and a water-wet system whereas a low concentration promotes a positive surface charge and an oil-wet system (Hirasaki & Zhang 2004). The brines present within the Lekhwair and Lower Kharaib Formations would need to have been Ca+ rich to promote an early oil-wet system. Consequently a thin film of oil forms around the macropore interiors. The inside of the macropores can remain water-filled allowing for solutes to be transported. These oil films therefore do inhibit any further cement nucleation, but does not stop any future increments in macrocement growth. It appears that as cementation was slowing within the oil leg with its pores systems becoming oil-wet, the water leg had a volumetric increase in cement growth cementing all its pores in the deep burial realm.

This is confirmed by $\delta^{18}O$ isotope analysis of the bulk micrite within the water leg. The water leg shows slightly more negative values in comparison with the oil leg (Fig. 5.17 & Table 5.5). The entire water leg system was altered diagenetically in the deep burial realm by a sudden surge in solutes, which was most likely sourced from stylolites. In the oil leg, instead of stylolitisation being inhibited by oil emplacement (Neilson et al. 1998), stylolitisation had occurred in oil leg within both the Lekhwair and Lower Kharaib Formations, and solutes paths were shut down by oil, reducing the amount of solutes being able to reach the precipitation sites (Burgess & Peter 1985, Oswold et al. 1995).

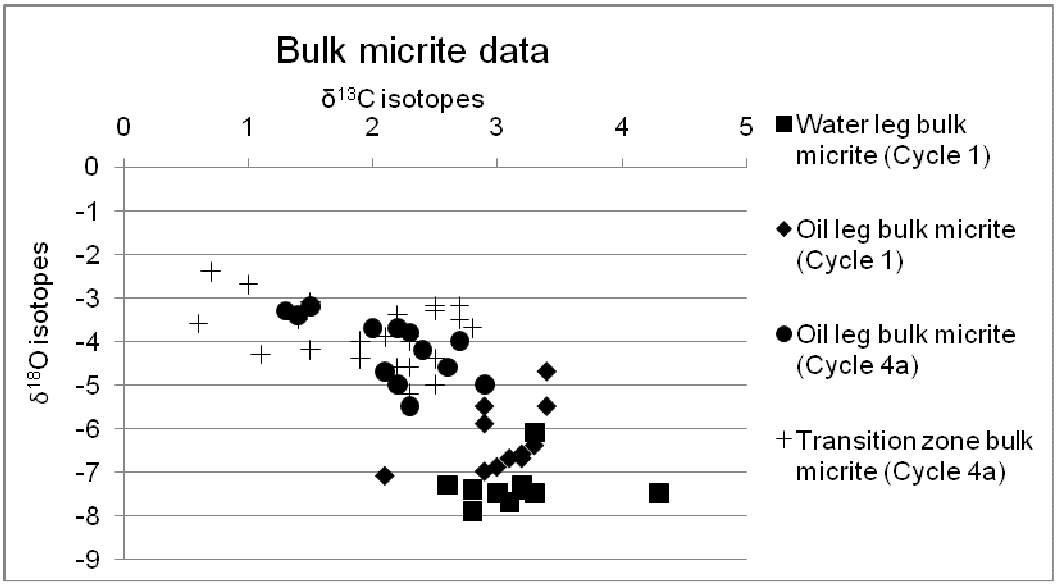

Figure 5.17: The bulk micrite data for the water leg shows more negative $\delta^{18}O$ values of -9‰. This indicates the water leg may have been altered at deeper depths, in comparison with the oil leg, when a sudden surge in solutes flooded the pore systems, possibly sourced from stylolites (Table 5.5, Appendix 4 for data).

Oil would have successively shut down oil leg macropores as it slowly percolated through the system, leaving only the micropores open (Sections 7.3.4).
A shift from a macropore-dominated to a micropore-dominated pore system would have increased the tortuosity for fluid flow. Consequently the permeability of the pore system decreases and solutes would therefore take longer to reach the precipitation sites. Cementation would have then slowed preferentially in the oil leg as the water leg became fully occluded.

The lithology is the same within the water and oil legs within the Lower Kharaib Formation (Cycle 1). Therefore the lower porosity and permeability relationships of the water leg are mostly the result of diagenesis through this late pore occluding cementation episode, late in Lekhwair and Lower Kharaib Formation burial. This is indicating that lithology and pore type are not the only factors controlling the distribution of the highest porosity and permeability relationships.

5.8 Porewater changes

Using the well depths for the SB's of Cycle 2a, and the distances between the five wells, a cross-section profile of the offshore field is generated (Section 1.2). Using the conversion to reservoir temperature and burial depth (Section 4.3), the values for the deepest and youngest cements for the water leg, the transition zone and the oil leg are calculated, along with the depth of the earliest recorded oil inclusions (Table 5.6). The geothermal gradient of 36°C/km from Gumati (1993) is assumed for these calculations (Section 2.3).

The depth difference between the youngest cements in the water leg and the crest (oil leg) provides an estimate of the amount of uplift, of the stratigraphy, due to trap formation (Tables 5.6, 5.7 & Fig. 5.18). To assess the validity of this method, this data is compared with the actual depths of Cycle 1 SB within the water leg and the oil leg (Tables 5.6 & 5.7). The depth difference between the youngest LMC cements of the Lower Kharaib Formation in the water leg and the present day depths of the Lower Kharaib Formation, also in the water leg, provides a measure for entire uplift of the stratigraphy (Tables 5.6 & 5.7). The water leg was chosen for this as it appears to have undergone the least amount of uplift due to trap formation.

Well number	Well 1	Well 2	Well 3	Well 4	Well 5
Cumulative distance (miles)	0	5.44	9	10.25	16
Deepest cements					
$\delta^{18}O$	-9.9	-9.8	-8.5	-10.3	No data
T (°C)	128.8	128.8	120.8	131.3	No data
Depth (ft)	11745	11713	10991	11975	No data
Depth (m)	3580	3570	3350	3650	No data
Depth (km)	3.58	3.57	3.35	3.65	No data
Youngest cements					
$\delta^{18}O$	-9.9	-8.2	-4.9	-7.4	No data
T (°C)	128.8	118.3	89.9	112.9	No data
Depth (ft)	11745	10761	8202	10302	No data
Depth (m)	3580	3280	2500	3140	No data
Depth (km)	3.58	3.28	2.5	3.14	No data
Depth difference					
Difference (ft)	0	952	2789	1673	No data
Difference (m)	0	290	850	510	No data
Earliest oil inclusion					
$\delta^{18}O$	-5.5				
T (°C)	96.3				
Depth (km)	1.67				

Table 5.6: The conversion of the deepest and youngest cement $\delta^{18}O$ values to reservoir temperature and burial depth.

Using the youngest cement	Feet	Metres	Kilometres
Uplift from trap formation	3543	1080	1.08
Using the sample depths	Feet	Metres	Kilometres
Uplift from trap formation	2039	621.5	0.62
Formation Uplift	3860	1176.5	1.18

Table 5.7: The uplift due to trap formation and to Formation uplift.

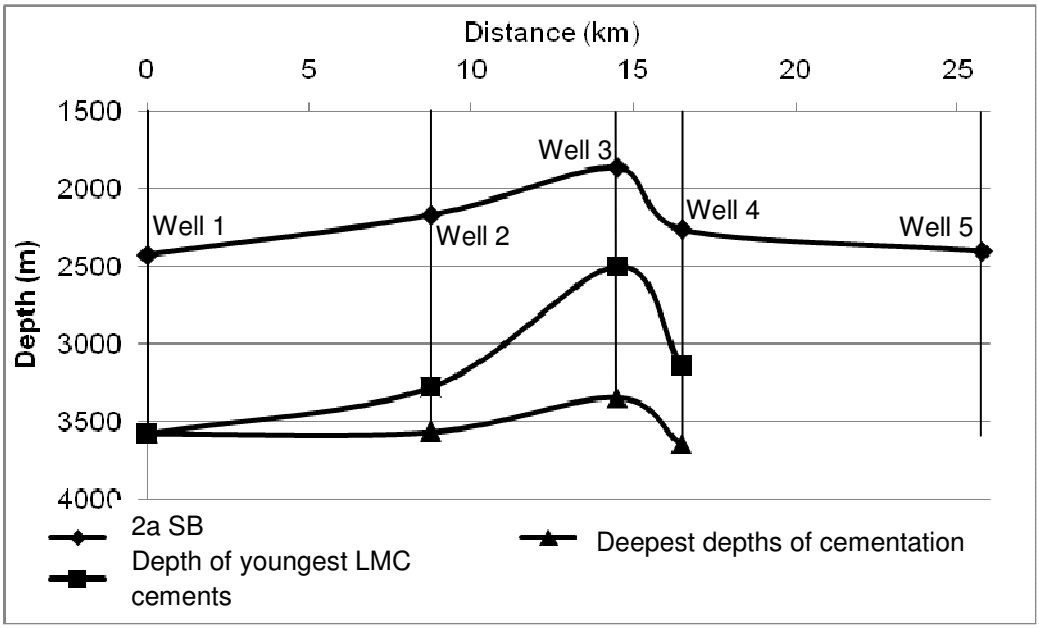

Figure 5.18: Depth profile of the offshore field. The amount of uplift associated with the $\delta^{18}O$ data from the youngest cement zones shows the majority of uplift had occurred at Well 3, which is consistent with the present day field structure.

The generated SB profile shows that Well 3 is at the highest point in the crest, confirming Well 3 has undergone the most uplift (Fig 5.18). This is consistent with the $\delta^{18}O$ profile from the youngest cements, which also shows Well 3 at the highest point in the crest, suggesting the possibility that the trend towards less negative $\delta^{18}O$ values may represent uplift due to the Semail Ophiolite obduction (Fig. 5.18) (Section 1.2 for Well positions).

For the water and oil legs, within the Lower Kharaib Formation (Cycle 1), the present day depth difference is 621.5m whereas for the youngest cement depths the calculated difference is 1080m (Table 5.7). The depths calculated from the $\delta^{18}O$ values of the youngest cements show a profile with much greater amplitude in comparison with the actual field (Fig. 5.18), suggesting pore fluid evolution.

The amount of formation uplift calculated between the deepest cements and the present day depths indicates 1176m of uplift (Tables 5.6 & 5.7; Fig 5.18), which may be due to the Zagros Orogen. This value is quite large suggesting that other factors may have influenced the $\delta^{18}O$ values incorporated within these cements: i.e. such as pore-rock interaction.

This study cannot rule out other external factors that may have contributed to the reduction in $\delta^{18}O$ negativity. For instance, the introduction of oil may have introduced O^{18} into the porewaters decreasing the $\delta^{18}O$ negativity. However, the relative timing of the return to less negative $\delta^{18}O$ values, suggests the processes behind this trend post dates the deepest point of burial. The onset of oil occurred much earlier and therefore may not be the cause for the reduction in $\delta^{18}O$ negativity.

Another possibility for the reduction in $\delta^{18}O$ negativity is from external porewaters entering the Lower Kharaib and Lekhwair Formations through faults or fractures. At the base of Well 4 many faults and fractures are present that are joined to a nearby fault that cross cuts all the sealed reservoirs. Fluxing of porewater through the rising salt diapirs could have proceeded up fault detachments from the diapir crests and into the Cretaceous sediments (Al-Barwani & McClay 2008). Salt brines could have mixed with the porewaters during the formation of the final cements lowering the $\delta^{18}O$ negativity. $\delta^{18}O$ studies upon the cements within these faults provide $\delta^{18}O$ values of -8‰ to -9.8‰ (Section 6.2.2), that suggests complete fault occlusion occurred during the formation of the youngest cements in the water leg, which may relate to the relative formation of the penultimate cement zones in the oil leg. These particular faults had cemented before uplift and trap formation, and also halokinesis. It is unlikely that if salt brines had circulated into the Lower Kharaib and Lekhwair Formations, they had flux through these faults. However the entire offshore field is overprinted with a rhombohedral fault system, that according to Edwards (2006) and Edwards et al. (2006), formed post-Fiqa times (Section 2.2). One of these faults may have aided the transport of salt brines into the Lower Cretaceous sediments.

It is difficult to determine the exact cause for the return to less negative values selectively within the oil leg. The fact that uplift had occurred makes it plausible that

the Semail Ophiolite obduction had caused porewaters to evolve back to -4.9‰ in the crest, in shallower, cooler conditions. In reality all three: i.e. the introduction of oil, salt brines combined with uplift all probably had some effect towards the return to less negative $\delta^{18}O$ values in the final cements of the oil leg.

Therefore, in retrospect, it would be inconsistent to assume that porewaters have not evolved prior to the deepest point of burial from -1‰ (Cretaceous seawater). The fluctuations of $\delta^{18}O$ data along both oil and water leg transects suggest that porewaters were continuously evolving during burial (Figs. 5.9-5.13), probably through porewater-rock interactions (Lawrence 1988). This indicates the values calculated for reservoir temperature and burial depth, for the deepest and youngest cements had not precipitated from porewaters with $\delta^{18}O$ values of -1‰ (i.e. Cretaceous seawater). This is consistent with the estimates for $\delta^{18}O$ values for the porewater with calcites of -9‰ and -10‰ (Section 4.6). The exact depths produced, for example of 3.6km for the deepest point of burial, are therefore not considered accurate and are only considered rough indications for the Lekhwair and Lower Kharaib burial histories. The calculated amounts for uplift due to trap formation and overall Formation uplift (Tables 5.6 & 5.7), are also indications, and do not represent accurate values.

Further work is clearly required to fully define the exact depths of burial for both the Lekhwair and Lower Kharaib Formations. Information on bottom hole temperatures for Wells 1 to 5, present day temperatures of Cycles 1 and 4a and present day pore fluid chemistries in Cycles 1 and 4a, would all be required for future studies.

5.9 Timing of oil charge and trap formation

The first oil inclusion appears before the deepest point of burial and therefore before 92Ma in the Late Cretaceous: initial oil emplacement appears to pre-date trap formation and the Eocene (when oil migration and charging is suggested to have occurred: Gumati 1993, Taher 1997). The amount of oil inclusions within the Lower Kharaib Formation is greatest early in its burial history (-5.5‰: Tables 5.3 & 5.4), before the majority of cement formation (Zones 8 to 12: Table 5.4) and is therefore

consistent with Neilson et al. (1996) that initial oil charge had occurred earlier, possibly within the Upper Cretaceous. Considering that the Bab Member did not reach maturity until the Eocene, this cannot have been the source for these earliest oil inclusions (Section 2.3). This does not rule out migration from the Jurassic Hanifa Formation at 90Ma, and does seem the most likely source for the oil within the Lekhwair and Lower Kharaib Formations (Section 2.3). The third alternative which considers a local oil source (Wilson 2005) is also possible (Section 2.3). This would suggest that trap formation had not necessarily determined the presence of the offshore field, but the presence of small localised oil sources may instead have been the main determining factor, in terms of changing pore system wetability (Section 5.7.1).

Many of the reservoirs within the Lower Kharaib and the Upper Lekhwair Formations are separated into compartments, by impermeable stylolite horizons (Appendix 2A-2E). These stylolite horizons are regularly spaced at 10-15ft and contain black insoluble layers. These layers may represent higher order (5^{th} order) cyclicity and could have produced CO_2 from the degradation of the organic matter, dissolving the surrounding carbonate, and starting stylolitisation (Dunham & Larter 1981). This is consistent with the relationship found by Burgess & Peter (1985), where higher amounts of stylolitisation occur with an increase in the presence of argillaceous units. The presence of clay particles prevents grain-grain cementation, causing small anastomising pressure dissolution seams to form, as a consequence of the friable nature of the sediment (Burgess & Peter 1985, Wanless 1979). The presence of Fe-dolomite in the stylolites (Section 6.1.3) indicates a nearby source of iron, which also suggests that insoluble clay-rich layers were present prior to stylolitisation (Dunham & Larter 1981). These insoluble's may have also been a small source for oil for the 'Thamama Group' during the late Cretaceous. Therefore a large early oil source from the Jurassic Haifa (most plausible) or a small internal source of oil had occurred within the Lekhwair and Lower Kharaib Formations. Either situation may have provided oil coating of key positions within the carbonate pore systems to allow for main oil charge to repel the remaining water from the pore system more easily in the late Eocene.

Within the Upper Lekhwair Formation the number of oil inclusions increases toward the youngest cement phase, which opposes the trend seen in the younger Lower Kharaib Formation above (Tables 5.3 & 5.4). This would suggest that oil had progressively flooded the reservoirs from the top down, further supporting studies by Taher (1997) that the Lower Kharaib Formation was a good carrier bed for oil. These trends in oil inclusion abundance occur before signs of uplift and the Semail Ophiolite obduction in the Lower Cretaceous. If this does indicate a flooding history from the Lower Kharaib Formation, downwards into the Lekhwair Formation, the oil cannot be sourced from the Bab basin in the East, as oil migration from there cannot have occurred before the late Eocene (Taher 1997). This also suggests against vertical migration from the Jurassic Hanifa Formation below. This flooding history may be sourced from the Kharaib beds, or from other formations above (Hawar Member). However the oil inclusion dataset is small and the volumetric amount of oil observed within all the oil inclusions is also very small. There is not enough data here to represent a certain flooding history: therefore, this is not a definite conclusion for this study.

This study has also not undertaken any chemical analysis of the oil inclusions to ascertain where they are all from the same source rock: i.e. are the inclusions the same as the current pore filling oil?

In response from Wilson (2005) reporting that traps are impermeable from flank cementation and trap formation, many faults had developed post deposition of the Fiqa Formation (Edwards 2006, Edwards et al. 2006: Section 2.2) which may have provided conduits for oil to migrate into the field after trap formation. There are oil inclusions within the youngest cement phases during uplift that may relate to a second phase of oil charge during the Late Eocene. A proportion of oil that is present within the structure today may have migrated from the East, and its emplacement was determined by the present position of the trap. This study can therefore suggest that the Lekhwair and Lower Kharaib Formations were subject to at least two phases of oil emplacement.

5.10 Conclusions

1. In a giant Cretaceous carbonate field from U.A.E., the crest within the oil leg is relatively free of cements, with only 5.3% of primary interparticle pores being fully cemented, compared with 65-99.5% pores from the water leg. The porosity and permeability relationships are highest within the oil leg of the Lower Kharaib Formation. This is most likely to do with the abundance of interparticle pores, instead of abundances in intra-skeletal pores within the Lekhwair Formation, and the crest being relatively free of cements.

2. Oil leg LMC macrocements show 12 zones with oil inclusions (n= 27) occurring in four of the final five cement zones. In situ $\delta^{18}O$ data reveals that LMC macrocements within the water leg and oil leg may have both grown to similar burial depths, with complete pore occlusion of the water leg within the deep burial realm. Cementation had continued beyond this point within the oil leg, possibly during uplift and obduction of the Semail Ophiolite. Cementation had continued for longest within the oil leg and the crest. These data confirm that cement growth was not terminated early in the oil leg and that cementation continued in the presence of oil.

3. The onset of oil occurs early in the Lekhwair and Lower Kharaib Formation burial histories. The slow introduction of oil into the crest would have displaced the porewater, creating an oil wet system. The growing LMC macrocements became separated from their source of solutes: with only the micropore systems remaining water wet, transportation of solutes to the precipitation sites would have become increasingly tortuous. Cementation effectively slowed within the oil leg with respect to the water leg until a critical oil saturation was reached, preventing all cementation.

4. The return to less negative values within the youngest cements may be due to uplift associated with the Semail Ophiolite obduction. However the actions of oil emplacement, or external porewaters mixed with brines, both bringing in ^{18}O, cannot be ruled out as causal factors.

5. The presence of the first oil inclusions suggests oil was present within the Lekhwair and Lower Kharaib Formations before trap formation. While there are oil inclusions within the youngest cement zones, which may have been derived from the Bab Basin in the east (in the Late Eocene), either vertical oil migration from the Jurassic Hanifa Formation or a small local internal source must have sourced the earlier oil inclusions. Therefore at least two phases of oil emplacement occurred during the burial history of the Lekhwair and Lower Kharaib Formations.

6. The values for reservoir temperature and burial depth are not considered as accurate values for the Lekhwair and Lower Kharaib Formations. Instead they are only considered as estimates and indications for burial depth. Further work is required to determine more accurate burial depths for the Lekhwair and Lower Kharaib Formations.

Chapter 6

Stable isotope analysis

It is important to understand which diagenetic processes have had the most profound effect upon the Lekhwair and Lower Kharaib Formation pore systems. Previously, within Cycles 1 and 4a, the proportion of cements and their distribution from the oil leg to the water leg is established (Sections 5.3.5 to 5.7.1). However, many other diagenetic processes, in addition to cementation, need to be taken into account. For example, the formation of cements within Cycle 7a at the base of the Lekhwair Formation, the alteration of bulk micrite within the water leg, transition zone and oil leg, the formation of stylolites, and the formation of cements within fractures and faults. Combining this information with the volumes of cements, enables a more detailed understanding of the diagenetic evolution of the Lekhwair and Lower Kharaib Formations. This Chapter aims to:

1) Establish a sequence of main diagenetic events using the cross-cutting relationships observed via petrography. The main diagenetic processes within the Lekhwair and Lower Kharaib Formations are then divided into three main settings in order of occurrence: 1) syn-depositional, 2) shallow-intermediate burial and 3) deep burial, creating a paragenetic sequence and a diagenetic timeline. There are no specific burial depths attributed to these zones: any process that subsequently occurs after borings (i.e. syn-deposition) are attributed to initial burial. The start of shallow burial is associated with mechanical compaction (few 10's metre burial: Mazzullo & Harris 1992), whereas diagenetic processes that occur prior to stylolites (i.e. deep burial) are attributed to intermediate burial. The distinction between shallow and intermediate burial is difficult to define: therefore both these realms are added together.

2) Separated component analysis using $\delta^{13}C$ and $\delta^{18}O$ stable isotopes, in order to constrain the sequence of diagenetic events. Sample coverage includes: the bulk micrite, dolomite cements and LMC cements (extracted from the outermost areas abutting into open pore spaces) from the water leg, transition zone and the oil leg. The same samples used for petrography in Chapter 2 are analysed for $\delta^{13}C_{VPDB}$ and $\delta^{18}O_{VPDB}$.

3) $\delta^{13}C_{VPDB}$ trends from the Lekhwair Formation into the Lower Kharaib Formation are compared with recorded $\delta^{13}C$ shifts from the Early Cretaceous. This provides a chronostratigraphy for deposition of the Lekhwair and the Lower Kharaib Formations. Any $\delta^{13}C$ shifts are compared with biodiversity changes in order to test previous studies that suggest $\delta^{13}C$ isotope shifts are associated with high nutrient levels and biocalcification crises. $\delta^{13}C$ data is also compared with the 4th order HFC stacking patterns of the Lekhwair and Lower Kharaib Formations, to determine the environment and sea level conditions that are associated with $\delta^{13}C$ shifts.

4) $\delta^{18}O_{VPDB}$ data is plotted against stratigraphy, separated with respect to the different wells and the different 4th order HFC's, in order to determine any $\delta^{18}O$ shifts laterally and vertically across the structure.

5) Finally, $\delta^{13}C_{VPDB}$ and $\delta^{18}O_{VPDB}$ stable isotope data are summarised, alongside the data ranges and averages for the different types of cement and bulk micrite from the water leg, transition zone and the oil leg. The validity of assuming that more negative $\delta^{18}O$ values means increasing relative burial depth (Kim & O'Neil 1999: Section 4.3), for the Lekhwair and Lower Kharaib Formations, is then determined.

6.1 Cross-cutting relationships

6.1.1 Syn-deposition

1) The *Glossomyphorus costatus* shells have two components: 1) an inner layer, composed of an individual crystal which displays no growth fabrics, and 2) an outer orange layer which does display growth fabrics (Fig. 6.1).

2) The thin inner LMC shell is discontinuous in Figure 6.1, possibly displaying differential dissolution after the inner shell was stabilised to LMC (Fig. 6.1).

3) Several millimetre LMC cements have formed where the inner stabilised LMC shell remains and where it is largely absent due to dissolution (Fig 6.1).

4) The small cements are overgrown by larger pore filling LMC cements (Fig 6.1).

5) Borings cross-cut the stabilised inner LMC shell, the phase of dissolution and both cement phases (Fig 6.1).

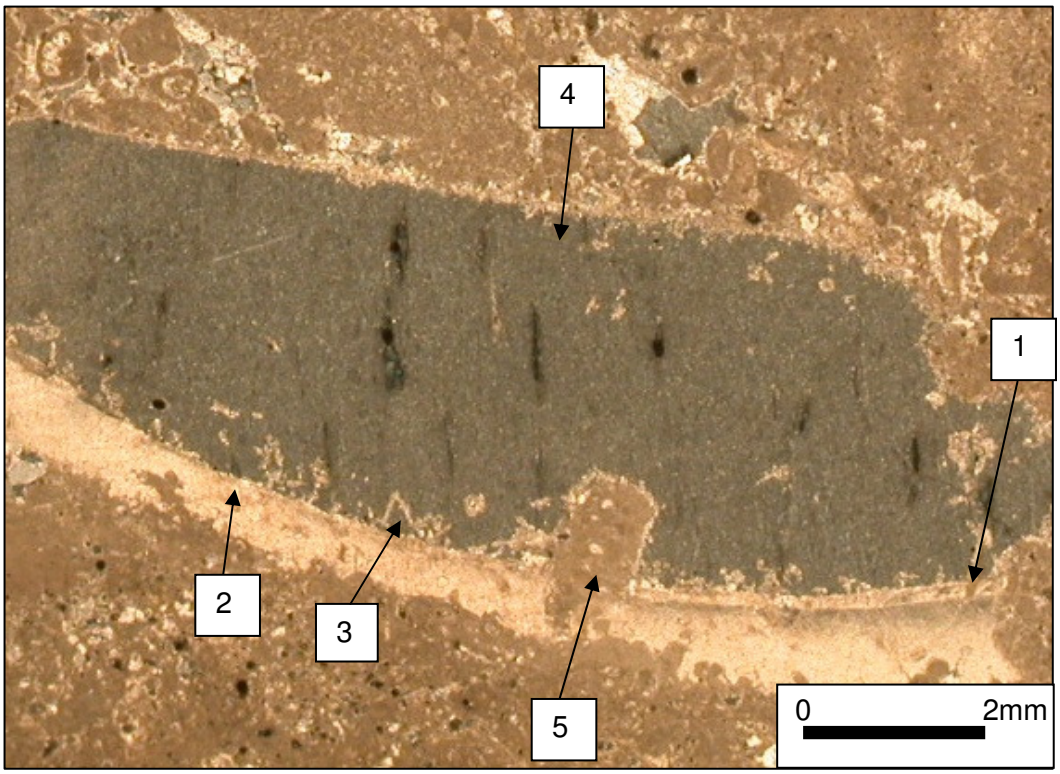

Figure 6.1: Syn-depositional diagenetic phases. 1) The stabilisation of the inner aragonite shell of the G. costatus *to LMC, 2) the differential dissolution of the inner stabilised LMC shell, 3) the formation of smaller LMC cements upon the stabilised inner shell, 4) a pore filling LMC phase that engulfs the smaller LMC cements and 5) a micrite filled boring that cross-cuts the* G. costatus *shell, the stabilised inner shell and the pore filling LMC cements. This suggests that at least two phase of cementation occurred before boring action.*

6) Dolomite rhombs are mostly present within the firmground assemblages, seen as 40-50µm dolomite crystals observed under the SEM with larger dolomite rhombs of up to 250µm observed petrographically (Fig. 6.2A). Dolomite is present in two places: 1) within *Thallassinoides* burrows, found within the firmgrounds at the top of each 4th order HFC, and 2) within the matrix. Both forms of dolomite show in places

close juxtaposition to echinoid fragments (Fig 6.2B). They block early diagenetic syntaxial LMC overgrowths.

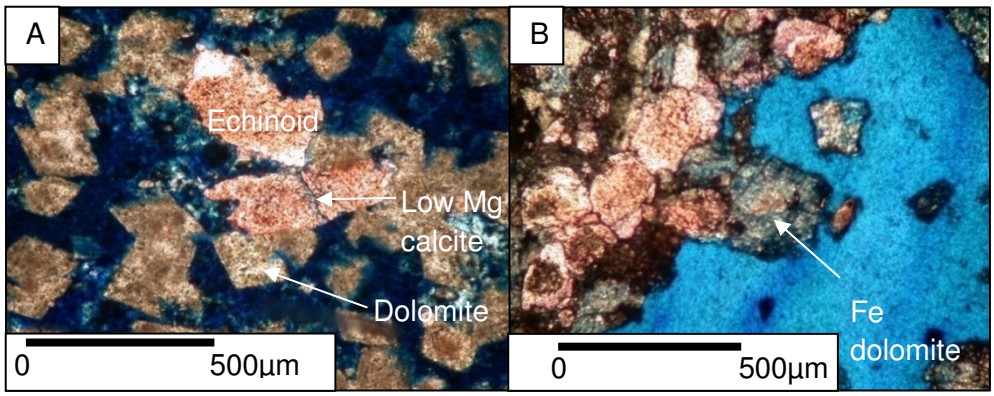

Figure 6.2: dolomite rhombs within the Thallassinoides *burrows and within the matrix. A) Dolomite rhombs are juxtaposed to echinoid fragments and appear to have blocked syntaxial cement growth. B) The exteriors of many dolomite rhombs have been altered to Fe-dolomite.*

7) Framboidal pyrite surrounds the *Thallassinoides* burrows (Fig 6.3A & 6.3B).

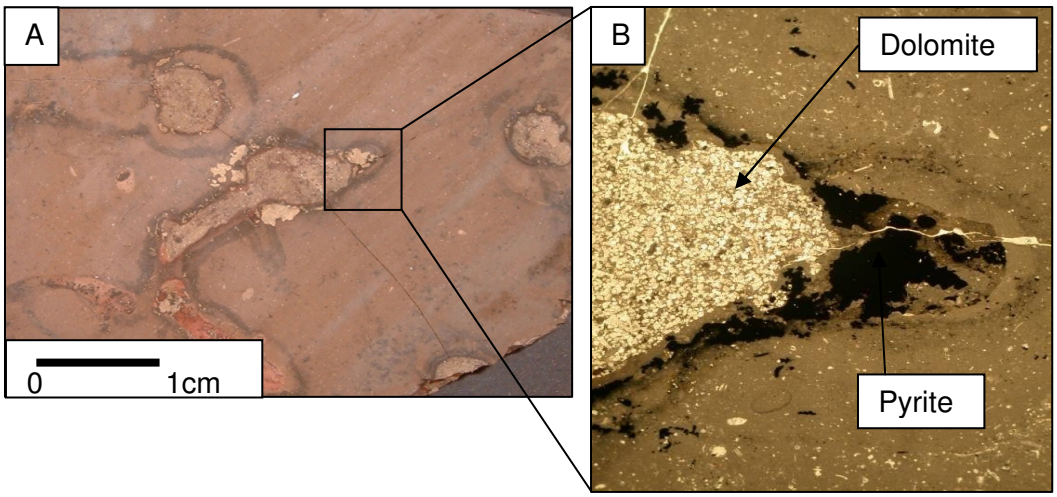

Figure 6.3: pyrite haloes around the Thallassinoides *burrows. A)* Thallassinoides *in core specimen. B) Burrow in thin section: both images show the significant framboides of pyrite surrounding the burrows. The* Thallassinoides *are filled with dolomite rhombs.*

6.1.2 initial-intermediate burial

8) Mechanical compaction of the micrite and mud horizons is observed within the base TST of each 4th order HFC. Many compaction seams run horizontally across the

micrites and muds of the TST's and the base of each 4th order HFC (L19 & L20: Figs. 3.24S, 3.24T & 6.4).

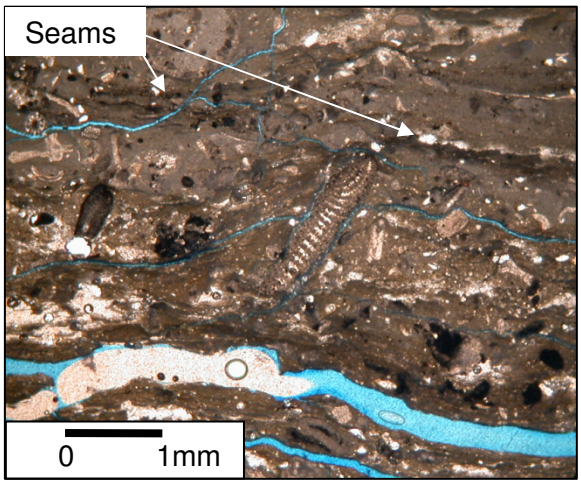

Figure 6.4: The micrites and muds at the base of the TST's in each 4th order HFC show extensive compaction. There are many darkened seams that extend across entire core specimens showing compaction of the matrix and many bioclasts. The arrows point to the compaction seams.

9) Staining reveals further cement growth after the syntaxial overgrowths: these cements grade from light peach, to pink, and then to purple (Fig. 6.5A). The purple colour is usually constrained to the outermost edges of the burial spars (Fig 6.5A & 6.5B).

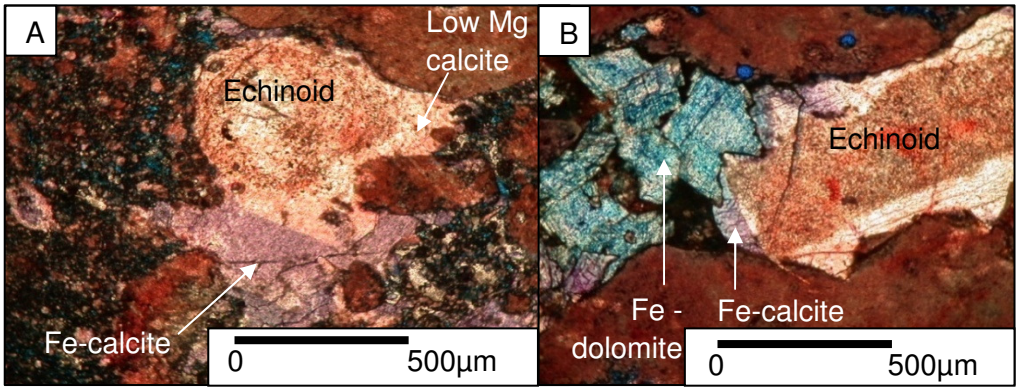

Figure 6.5: The syntaxial cement overgrowths. A & B) Several cement phases grow from the echinoid fragments. Staining highlights the increase in the concentration of Fe through progressive burial.

10) In many cases entire *G. costatus* shells and microsolenid coral fragments are replaced with saddle dolomite. The reservoirs are the only areas to show the formation of Fe-saddle dolomite (Fig. 6.6).

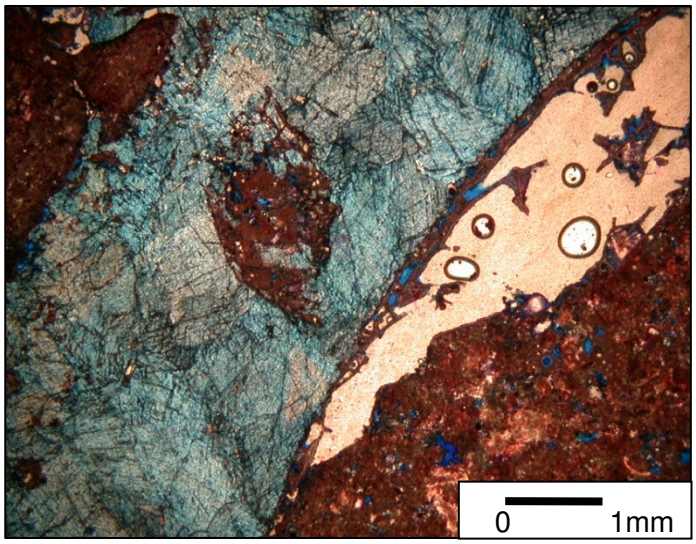

Figure 6.6: G. costatus *shells are replaced with Fe-saddle dolomite. This dolomite usually overgrows syntaxial LMC and Fe-calcite on echinoid fragments (Fig. 5.6).*

11) Many *G. costatus* shells and large vugs, within the water leg and the transition zone, are completely occluded with LMC (Fig 6.7). Under Cathodoluminescence this represents the purple or dark red zone: the youngest cement phase within the water leg and one of the youngest cements within the transition zone (Sections 5.3.5 & 5.4).

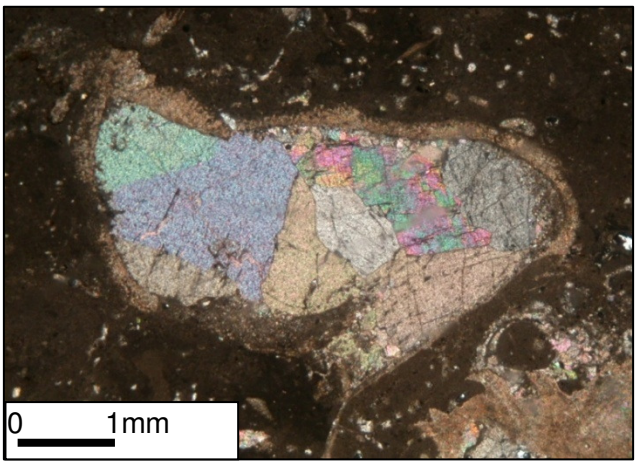

Figure 6.7: G. costatus shells and many other large vugs are fully occluded with LMC. This pore filling cement phase corresponds with the youngest cement zones seen under Cathodoluminescence in the water leg and the transition zone (Section 5.4 & 5.3.5).

6.1.3 Deep burial

12) Stylolites have black residues within their seams (Fig. 6.8B). They cross-cut the youngest pore filling cements (within transition zone & oil leg) (Figs. 6.8A & 6.8B).

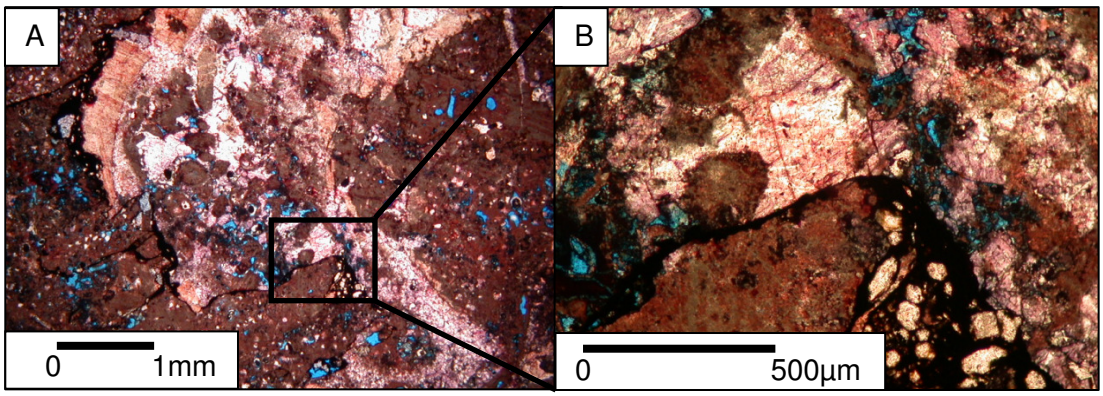

Figure 6.8: The stylolites within the Lekhwair Formation. A & B) The stylolites cross-cut deep burial LMC cements.

13) Extra porosity is present along the stylolites

14) Within many stylolite seams, Fe-dolomite (Fig. 5.9B) has formed alongside another highly birefringent mineral. This mineral has two distinct cleavages; the two cleavages form rectangular box shapes (Fig 6.9A).

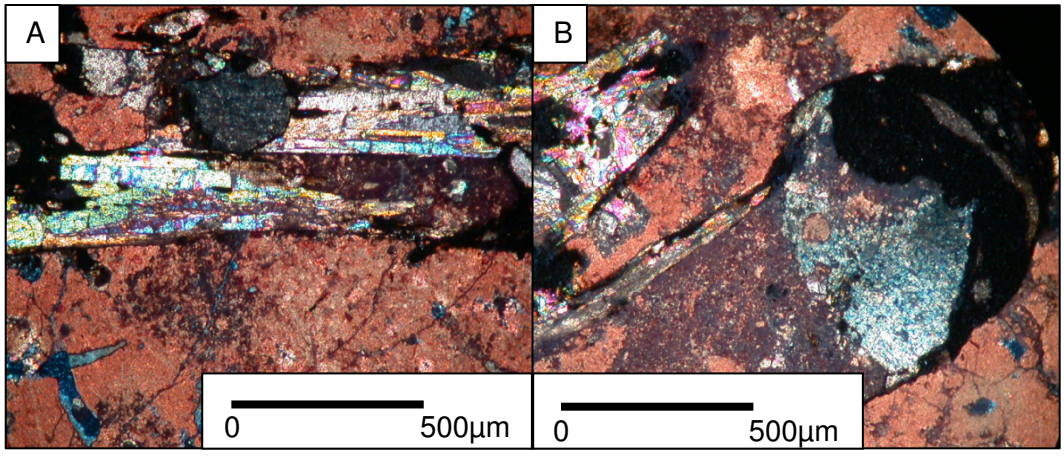

Figure 6.9: Minerals within the stylolite seams: A) A highly birefringent mineral and B) Fe-dolomite.

6.1.4 Interpretation of cross-cutting relationships

1) With respect to *G. costatus*, the growth lines within the orange exterior shell suggest this component was always composed of LMC and was minimally diagenetically altered. No growth fabrics within the inner shell suggest this was aragonite and has undergone stabilisation to LMC.

2) Micrite-filled borings appear to cross-cut cements within *G. costatus* shells, suggesting mineral stabilisation, dissolution, and two phases of cementation may have occurred before boring action (Fig. 6.1). All these stages could therefore be syn-depositional, with an added possibility of these cements being meteoric. Another possibility is these cements could have formed after the formation of the boring. The cements could have stabilised from a precursor around the boring. The boring cast is micrite and therefore would not have been affected during any episode of mineral stabilisation.

3) The dolomite rhombs have formed before the formation of the syntaxial overgrowths around the echinoid fragments. The dolomites may have formed at syn-deposition (Fig 6.2). Whether these dolomites and the syntaxial overgrowths have formed during or after the borings is uncertain. Most dolomites also show an outer skin alteration to blue Fe-dolomite (Fig.6.2B). However the contact between the non Fe- and Fe-dolomites is regular suggesting that the Fe-dolomite may be another phase of cementation, and not replacement.

4) Burrows are below the sediment water interface as a network of bifurcating horizontal and vertical tubes forming the *Thallassinoides*. The pyrite has formed around the *Thallassinoides* suggesting it had formed after burrow formation (Section 4.2). Therefore pyrites had formed around the burrows within the sediment and not at the sediment water interface (Fig. 6.3). This is consistent with the locus of the earliest pyrite formation, being placed at 4-5cm below the sediment water interface by Dickson et al. (2008), during initial burial.

5) Studies from Mazzullo & Harris (1992) suggest that micrite/mud compaction occurs after only a few 10's metre burial (rough transition from initial-shallow burial). This indicates that formation of these seams may have occurred after the formation of the cement phases, borings and pyrite formation, during syn-deposition,

and may have formed in the shallow burial realm: When mechanical compaction stopped is unknown.

6) The sequence of cement zones within the macrocements is similar to syntaxial overgrowths selected for the Ion Microprobe analysis (Section 5.3.5 & 5.4). These cements may have successively formed during progressive burial: probably through shallow-intermediate burial (Fig 6.5). The surrounding matrix is muddy and only shows fine pore spaces, much smaller than the area covered by the cement overgrowths. This suggests that the cements may have displaced the surrounding mud matrix progressively as they grew (Fig 6.5).

7) The large Fe-saddle dolomites have overgrown the LMC cements (Fig. 6.6) suggesting the Fe-saddle dolomite phase is one of the last cementation episodes, possibly during intermediate-deep burial. Their formation also suggests an increase in Fe^{2+} within the formation waters. This could have been derived from the onset of acidic porewater before oil charge. It could have also been caused from the dewatering of the micrites/muds (4^{th} order TST bases). However the Fe-saddle dolomites are only constrained to the reservoirs and the mid-late HST's within every 4^{th} order HFC. A concentration in micrites/muds only occurs at the base of the TST (Section 3.4.1). In Section 5.9, it has been suggested that formation of stylolites within the HST's, and the reservoirs, could have been focused on compactable insoluble layers. These layers contain Fe-dolomite, suggesting they may have been sources for Fe^{2+} for Fe-saddle dolomite formation (Fig. 6.9B).

8) Large pore filling burial cements have formed after the majority of cementation and represent the last LMC cement fills within the water leg and the transition zone, and the penultimate cement zones within the oil leg ($\delta^{18}O$ values of -8‰ to -10‰: Section 5.3.5 & 5.4: Fig. 6.7).

9) Stylolite formation represents the deep burial realm. Stylolites cross-cut the burial spars (within the transition zone and oil leg), suggesting the burial spars ($\delta^{18}O$ values of -8‰ to -10‰: Section 5.4) represent intermediate and possibly deep burial (Fig 6.8). This also constrains the earlier LMC syntaxial cement growths to the shallow and intermediate burial.

10) The black residue within the stylolites could either be residue from compacted insoluble horizons, or could be residue from oil migrating along the stylolite (Fig.

6.8). The oil may have been corrosive generating secondary porosity within the stylolites (Fig. 6.10A & 6.10B). Therefore a phase of dissolution may have formed at deep burial after the formation of the stylolites. However there is another possibility: surrounding these stylolites are similar sized pores. Continued stylolitisation would have brought pores on either side of the stylolite closer together through pressure dissolution and chemical compaction (Fig. 6.10A & 6.10C). Pores once isolated from the stylolites would be placed next to the stylolites.

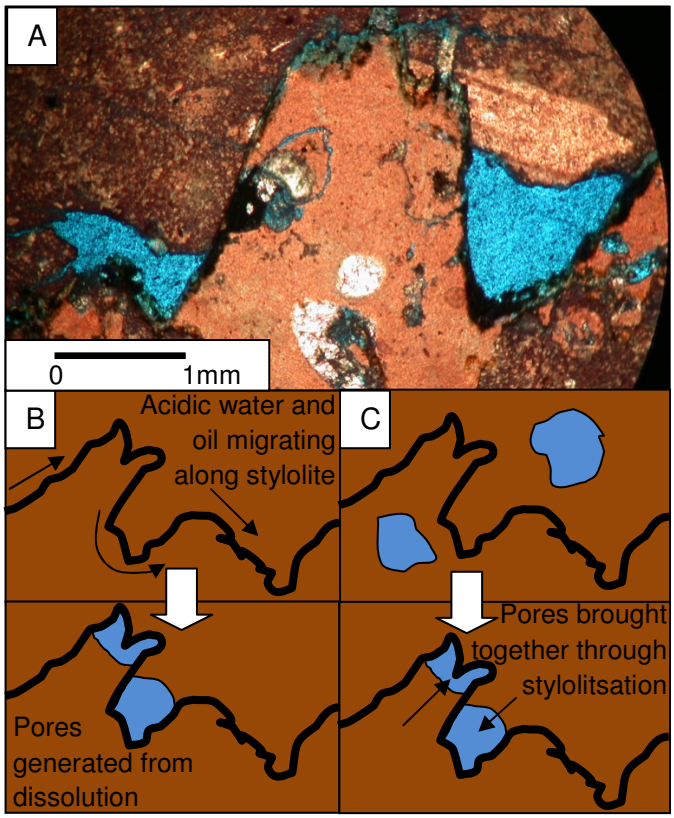

Figure 6.10: Two possible formation processes for pores along the stylolites: A) A photomicrograph of the macropores on the stylolites under plane polarised light: B) these may have formed from another phase of dissolution due to acidic porewater before oil flux along the stylolites or C) continued stylolitisation would have brought distant pores together until juxtaposition on the stylolite.

11) The formation of these highly birefringent minerals (possibly anhydrite) may have occurred after stylolitisation and a second phase of dissolution in the deep burial realm (Fig. 6.9A).

6.1.5 Summary of cross-cutting relationships

The relative sequence of events constrained petrographically by their cross-cutting relationships, including the formation of burrows, pyrite, dolomite and LMC, stylolites along with mechanical compaction (Fig. 6.11).

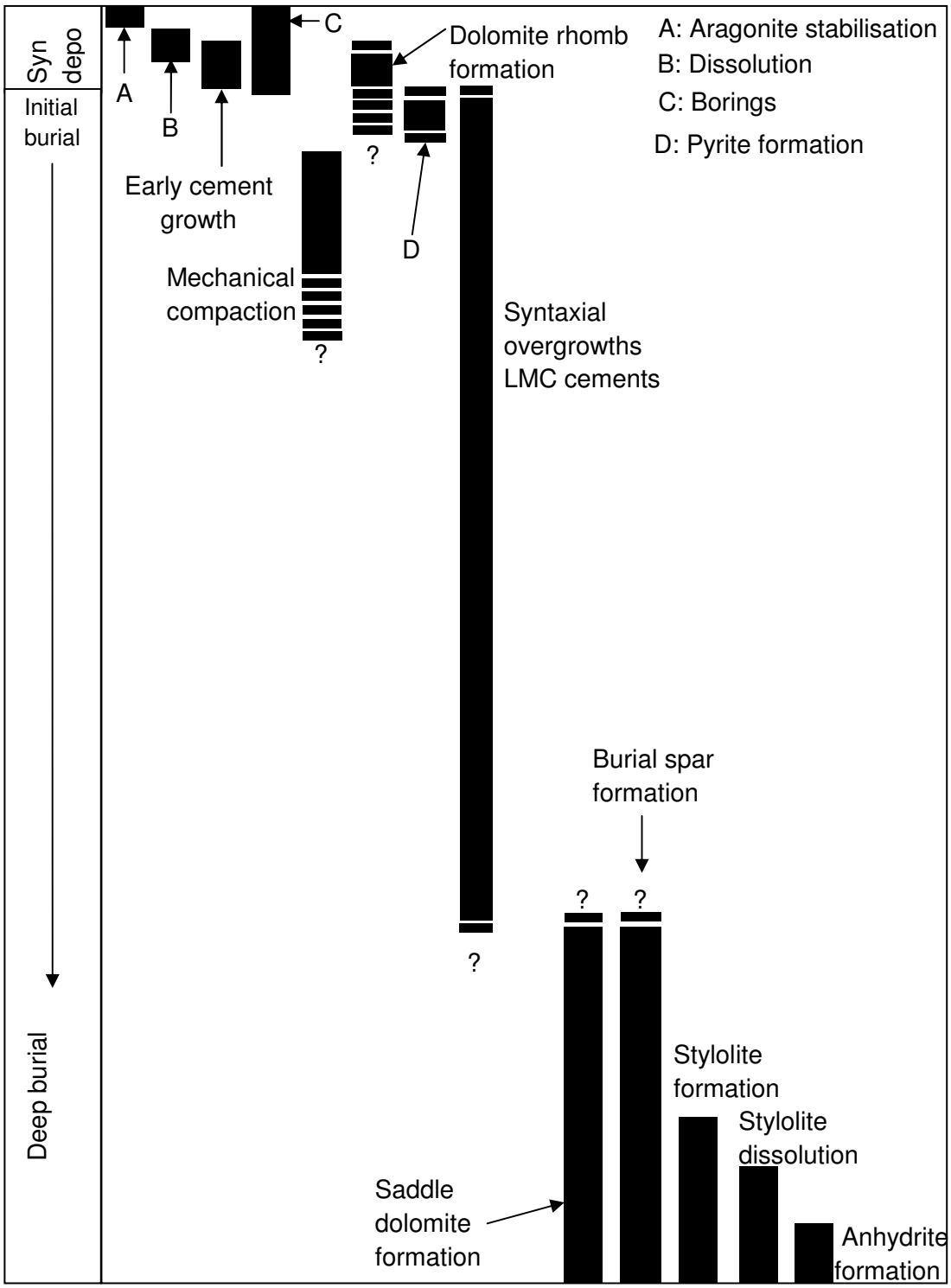

Figure 6.11: Paragenetic sequence for the Lekhwair and Lower Kharaib Formations as suggested by their cross-cutting relationships.

6.2 Stable isotope data

The next section displays all the plots of the stable isotope $\delta^{18}O$ and $\delta^{13}C$ data for the five wells across the offshore field (Section 1.2).

Data from all five wells are plotted up together on the $\delta^{13}C$ and $\delta^{18}O$ isotope verses depth (ft) plots. The depth of the 4th order SB's varies between the five wells and therefore putting them at specific places on each plot is problematic. To solve this issue a table of the depth ranges for Cycles 1, 4a, 4b and 7a for the five Wells is presented here (Table 6.1). The depths for each HFC can then be compared to the data plotted on the $\delta^{13}C$ and $\delta^{18}O$ isotope verses depth (ft) plots. The depths provided in Table 5.1 are calculated using Cycle 8 SB near the bottom of the Lekhwair Formation, as the base of the scale. These depths relate directly to the stratigraphic scale on the $\delta^{13}C$ and $\delta^{18}O$ isotope verses depth (ft) plots.

HFC	Minimum depth (ft)	Maximum depth (ft)
1	403	480
4a	212	242
4b	175	196
7a	79	96

Table 6.1: depth ranges for Cycles 1 (Lower Kharaib Formation), 4a, 4b and 7a (Lekhwair Formation) across the five wells. The depths relate directly to the depth scale on the $\delta^{13}C$ and $\delta^{18}O$ isotope verses depth (ft) plots.

6.2.1 $\delta^{13}C$ data

A positive $\delta^{13}C$ excursion is recorded during the Late Valanginian in the Southern Alps, the Gulf of Mexico, the North Atlantic and the Central Pacific (Lini et al. 1992) (Fig. 6.12). The amount of nutrients within the oceans had increased during the Lower Cretaceous as sea levels rose, due to increased flood basalt volcanism (Section 2.1), which caused the erosion of newly flooded continental masses, which mobilised more C^{12} into the water column (Föllmi 1993, Föllmi et al. 1994). Both the rise in ocean water temperature and the availability of nutrients caused a surge in

plankton (primary) productivity (Deuser et al. 1968) through photosynthesis and the uptake in C^{12} (Föllmi 1993, Lini et al. 1992). The organic carbon (C^{12}) burial rate increased due to the acceleration of the carbon cycle (Föllmi 1993). The effect upon the $\delta^{13}C$ ratio incorporated within forming sediments and shells of organisms is a positive $\delta^{13}C$ signature (Fig 6.12). Therefore readers have argued that a positive $\delta^{13}C$ shift is due to rising sea level, increasing organic productivity rates, increasing organic carbon burial and a draw down in C^{12} (Föllmi 1993, Lini et al. 1992).

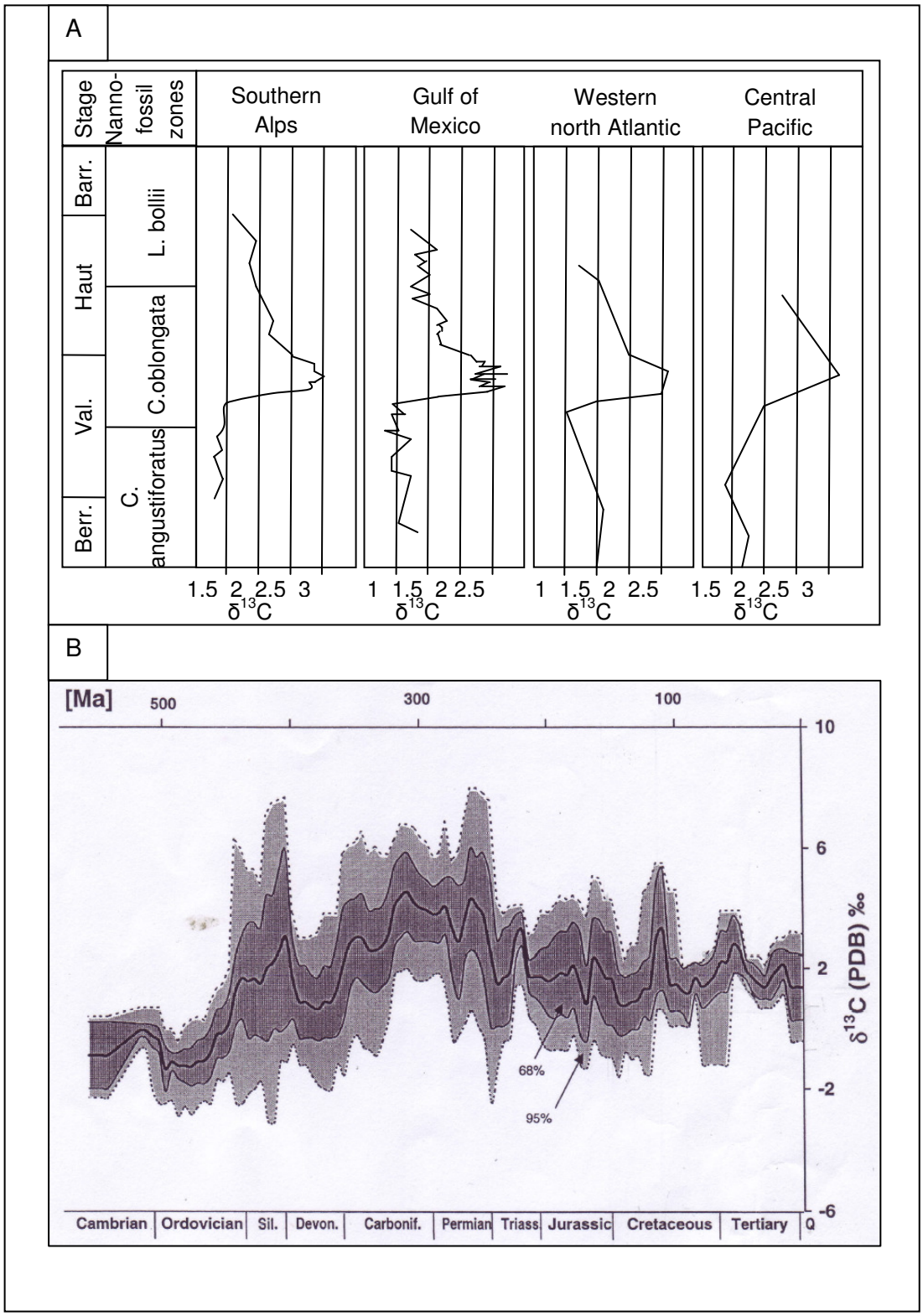

Figure 6.12: A) In many places across the globe, the Early Cretaceous (Upper Valanginian) is linked with a positive $\delta^{13}C$ excursion to +3‰. The abbreviations mean: Berr: Berrisian, Val: Valanginian, Haut: Hauterivian and Barr: Barremian (redrawn from Lini et al. 1992). B). Global Data from LMC and phosphatic shells concurs showing a positive $\delta^{13}C$ to +4‰ in the Lower Cretaceous (Veizer et al. 1999).

Stable $\delta^{13}C$ isotopes data with respect to the stratigraphy

Figure 6.13 shows the $\delta^{13}C$ stable isotope data for the bulk micrite against stratigraphic depth. With respect to the bulk micrite, Cycles 7a and 7b at the base of the Lekhwair Formation show a $\delta^{13}C$ range from -0.1‰ to +2.2‰, Cycles 4a and 4b shows a $\delta^{18}O$ range from -0.1‰ to +2.9‰ and Cycle 1 shows a $\delta^{18}O$ range from +2.6‰ to +4.3‰. There is a positive trend in the $\delta^{13}C$ isotope ratio from the base towards the top of the Lekhwair Formation, and into the Lower Kharaib Formation (Fig. 6.13). The $\delta^{13}C$ data range also decreases towards Cycle 1.

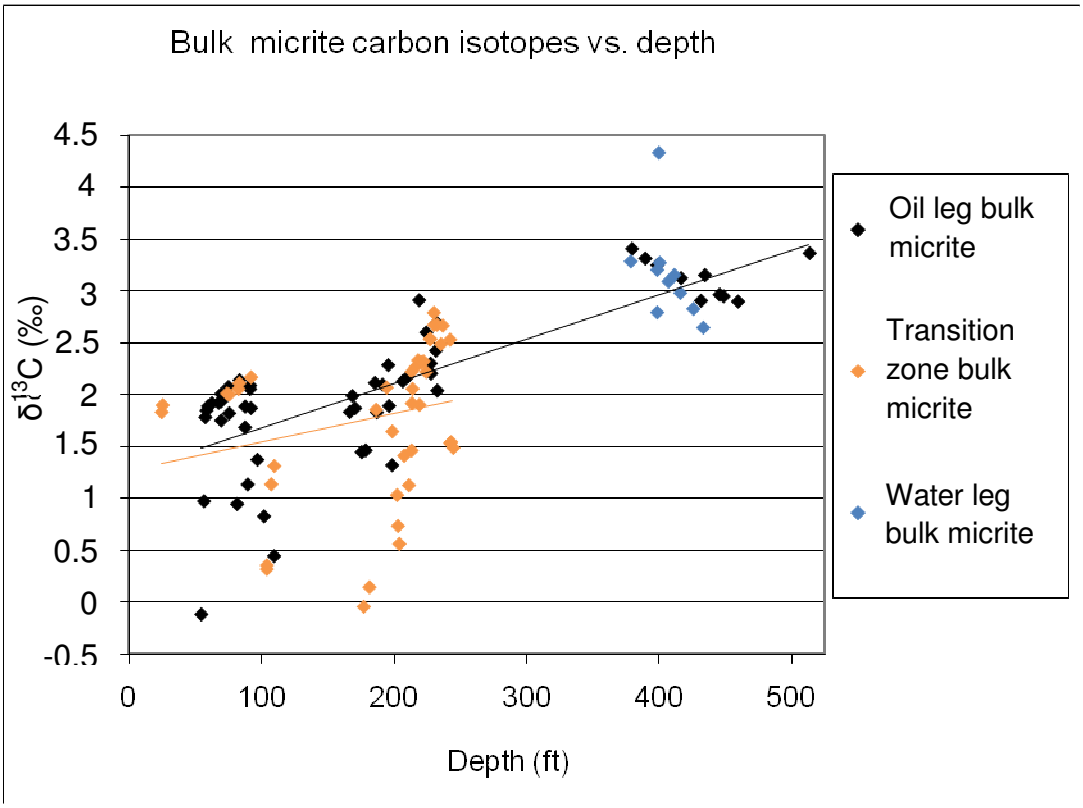

Figure 6.13: The $\delta^{13}C$ composition of the bulk micrite shows a positive trend from -1‰ to +4‰ from the Lower Lekhwair into the Lower Kharaib Formation (Appendix 4 for data tables). The R^2 for the oil leg bulk micrite data is 0.0555 (black line). The R^2 for the transition zone bulk micrite is 0.5937 (orange line).

Figure 6.14A shows $\delta^{13}C$ stable isotope data for the youngest LMC cements against stratigraphic depth. The $\delta^{13}C$ isotopes within the youngest LMC cements with respect to the 4th order HFC's show a similar positive carbon trend from the base of the Lekhwair Formation up into the Lower Kharaib Formation. Cycle 7a shows a $\delta^{13}C$ range from +0.7‰ to +1.5‰, Cycles 4a and 4b shows a $\delta^{13}C$ range

from +1‰ to +2.4‰ and Cycle 1 shows a $\delta^{13}C$ range from +2‰ to +3.3‰ (Fig. 6.14A).

Figure 6.14B shows $\delta^{13}C$ stable isotope data for the dolomite rhombs and saddle dolomites against stratigraphic depth. The burrow dolomite has a $\delta^{13}C$ range from +1.6‰ to +4.1‰ while the saddle dolomites show a $\delta^{13}C$ range from +1.5‰ to +2.5‰. The burrow and saddle dolomite cements also show a positive $\delta^{13}C$ trend from +1.5‰ to +2.5‰, in Cycle 7a in the Lower Lekhwair Formation, to +3‰ to +4.1‰, in Cycle 1 in the Lower Kharaib Formation (Fig. 6.14B). The LMC youngest cements show similar regressions with the bulk micrite $\delta^{13}C$ data trend from the base to the top of the Lekhwair Formation, and into the Lower Kharaib Formation. The dolomite cements also appears consistent with the bulk micrite $\delta^{13}C$ data shift: however there is not enough data to be certain.

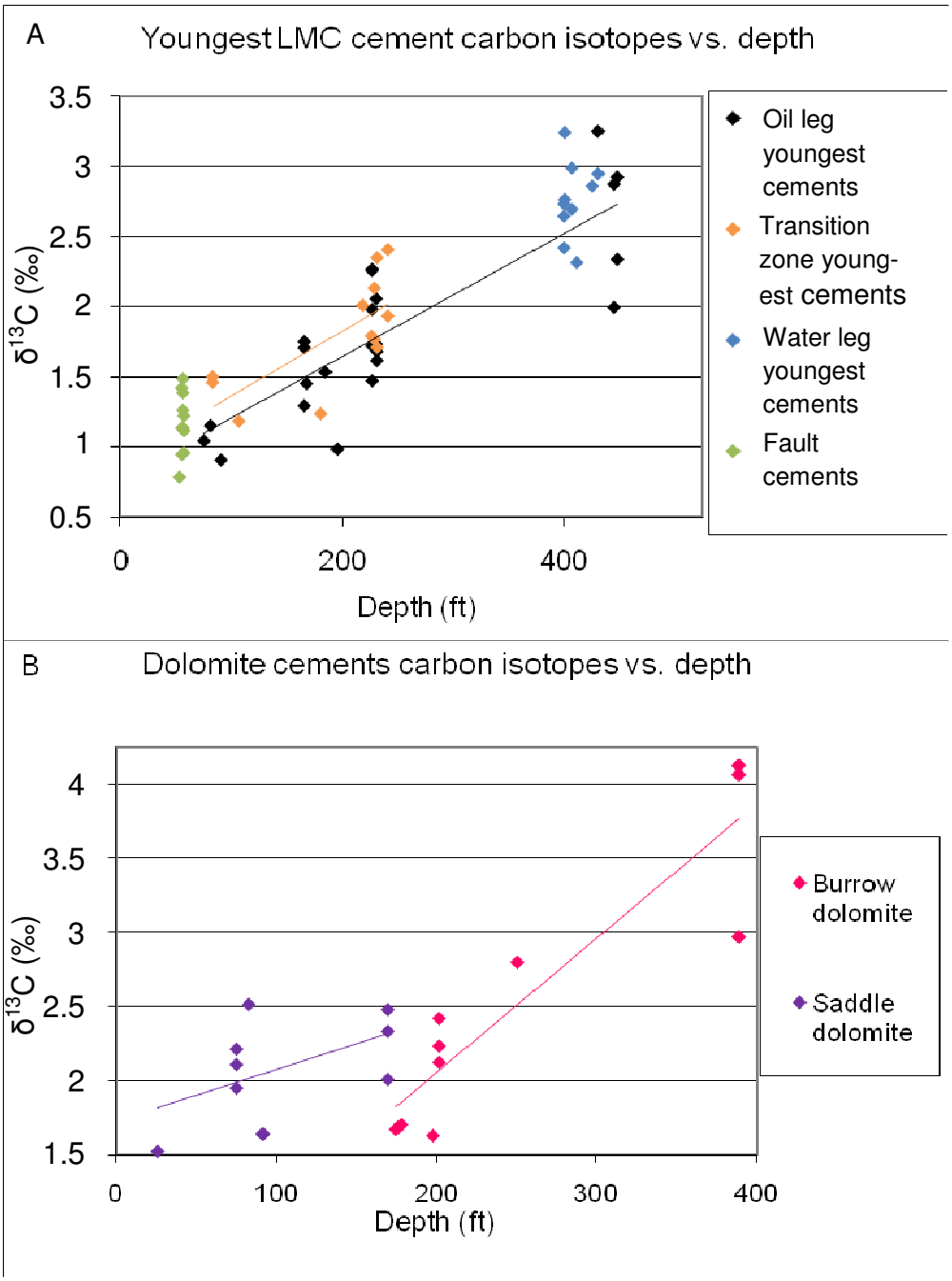

Figure 6.14: $\delta^{13}C$ data from the youngest LMC cements and dolomites. A) Youngest LMC cement $\delta^{13}C$ isotope data against the stratigraphic depth (Appendix 4 for data tables). The R^2 for the oil leg is 0.7064 (black line). The R^2 for the transition zone is 0.5184 (orange line). B) Dolomite cement $\delta^{13}C$ isotope data against the stratigraphic depth (see Appendix 4 for data tables). The R^2 for the burrow dolomites is 0.8307 (pink line). The R^2 for the saddle dolomites is 0.2814 (purple line).

Timing of the positive $\delta^{13}C$ trend

Within the southern Alps of North Italy (Northern Tethys Ocean) below the Valanginian-Hauterivian boundary, a similar positive $\delta^{13}C$ shift is noted to +3‰ (Weissert et al. 1998, Weissert & Erba 2004). For the entire Cretaceous, composite bulk sediments were collected by Katz et al. (2005) along with previous data collected by Shackleton & Hall (1984) from the open Ocean Atlantic Drilling Project. A similar positive carbon shift of +2.5‰ at the Valanginian-Hauterivian boundary occurs, which increases to +3‰ up-section into the mid-Aptian (Katz et al. 2005).

More global studies by Veizer et al. (1999) also display a positive $\delta^{13}C$ shift in the Lower Cretaceous. Data was collected from phosphatic and calcitic shells, including mainly brachiopod shells, conodonts, and belemnites, covering a timescale from the Cambrian-Cretaceous. The $\delta^{13}C$ shift is more variable (being from such a large data set) showing a mean of +1‰, with 68% of all data weighted around this mean displaying a range of 0‰ to +2‰ (Veizer et al. 1999).

Considering the change in $\delta^{13}C$ values from the Lekhwair into the Lower Kharaib Formation occurs over a 6Myr period, it cannot be labelled as a shift. Therefore, although the $\delta^{13}C$ positive trend appears to peak within the Lower Kharaib Formation, without any specific localised shift it is difficult to use the $\delta^{13}C$ trend for chronostratigraphic purposes. However, with respect to studies from Weissert (1998), Weissert & Erba (2004) and Lini et al. (1992), the nearest shift is located at the Valanginian-Hauterivian boundary, which is considered to be 3Myr earlier (126Ma) by Sharland et al. (2001) than the deposition of the Lower Kharaib Formation (123Ma) (where the $\delta^{13}C$ shift peaks in this study). This discrepancy may indicate that more than one positive $\delta^{13}C$ shift within the Early Cretaceous is present, which seems plausible considering that studies from Katz et al. (2005) (shift only to +3‰: whole of Aptian) and Vahrenkamp (1996), Weissert (1998) and Weissert & Erba (2004), have located another positive $\delta^{13}C$ shift of up to 4‰ 3Myr later in the early mid Aptian (120-113Ma: Vahrenkamp 1996). However as stated before,

without being able to used the $\delta^{13}C$ trend for chronostratigraphic purposes there is too much uncertainty and therefore this is not a definite conclusion for this study.

The $\delta^{13}C$ shift toward the base of the Kharaib Formation for Katz et al. (2005), Weissert et al. (1998) and Weissert & Erba (2004) is given as +2‰; 2‰ less positive than recorded within this study. The positive $\delta^{13}C$ shift is most likely caused by high seafloor basaltic volcanism, which produced more CO_2, intensified the greenhouse conditions, caused increased plankton productivity, and increased organic carbon burial (Section 2.1). Other local processes within the carbonate ramps of the Lekhwair and Lower Kharaib Formations may have caused the stronger positive shift of +1‰ to +3.5‰. For instance, the concentration of biological activity could have been greater in the Lekhwair and Lower Kharaib Formation carbonate ramps in comparison with carbonate platforms now present in the southern Alps of Northern Italy, allowing for a more positive $\delta^{13}C$ signature to become incorporated into the sediments.

Relationship of $\delta^{13}C$ shifts with sequence stratigraphy

A similar positive $\delta^{13}C$ trend from +1‰ to +4‰ is recorded within the 'Thamama Group' by Vahrenkamp (1996) in the Aptian and the Shu'aiba Formation during the production of the thickest HFC's and a 3rd order TST (Fig 6.15).

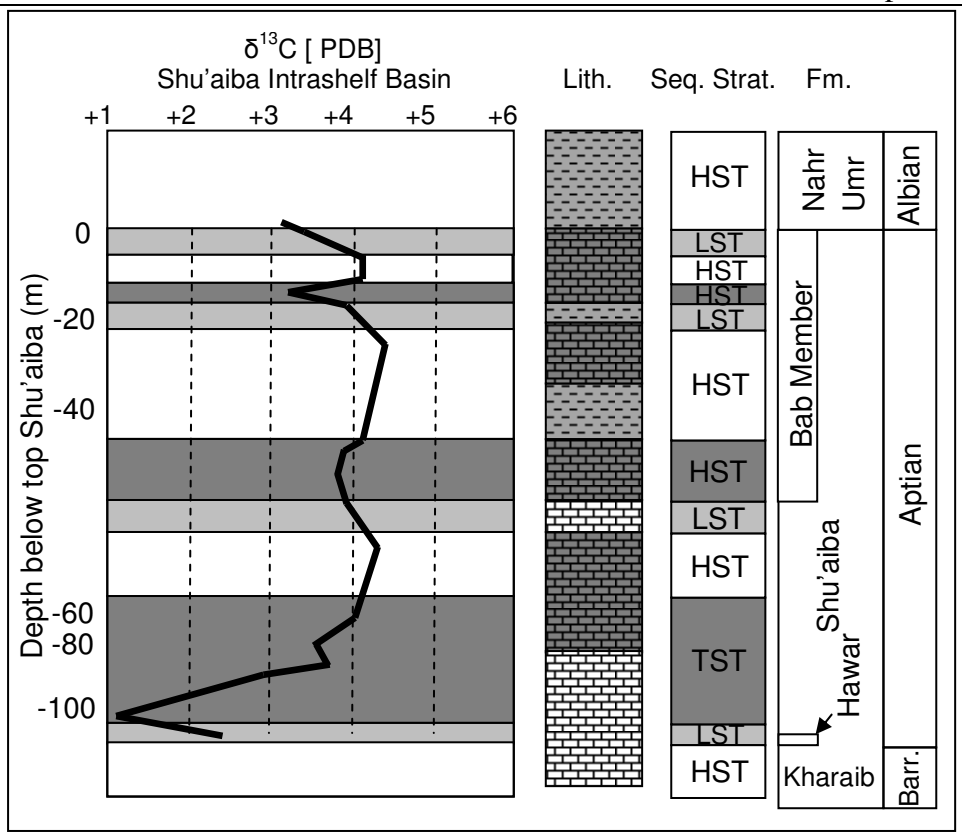

Figure 6.15: A shift to +3‰ to +4‰ is recorded in the Aptian and the Shu'aiba Formation during the thickening of HFC's and a 3rd order TST. The abbreviations on the right hand column are: Barr: Barremian, Lith: Lithology, Seq. Strat.: Sequence Stratigraphy and Fm: Formation (redrawn from Vahrenkamp 1996).

This trend is also noted by Grötsch et al. (1998) in the Upper Aptian in the Shu'aiba Formation; a positive $\delta^{13}C$ excursion and black shale deposition are the result of sea level rise (Fig. 6.16). This positive $\delta^{13}C$ shift within the Shu'aiba Formation is correlated with time equivalent formations at Mt. Kanala and at Italy, indicating that as $\delta^{13}C$ excursion are independent of biozonation: they can be used to correlate time equivalent shallow water carbonate formations (Grötsch et al. 1998).

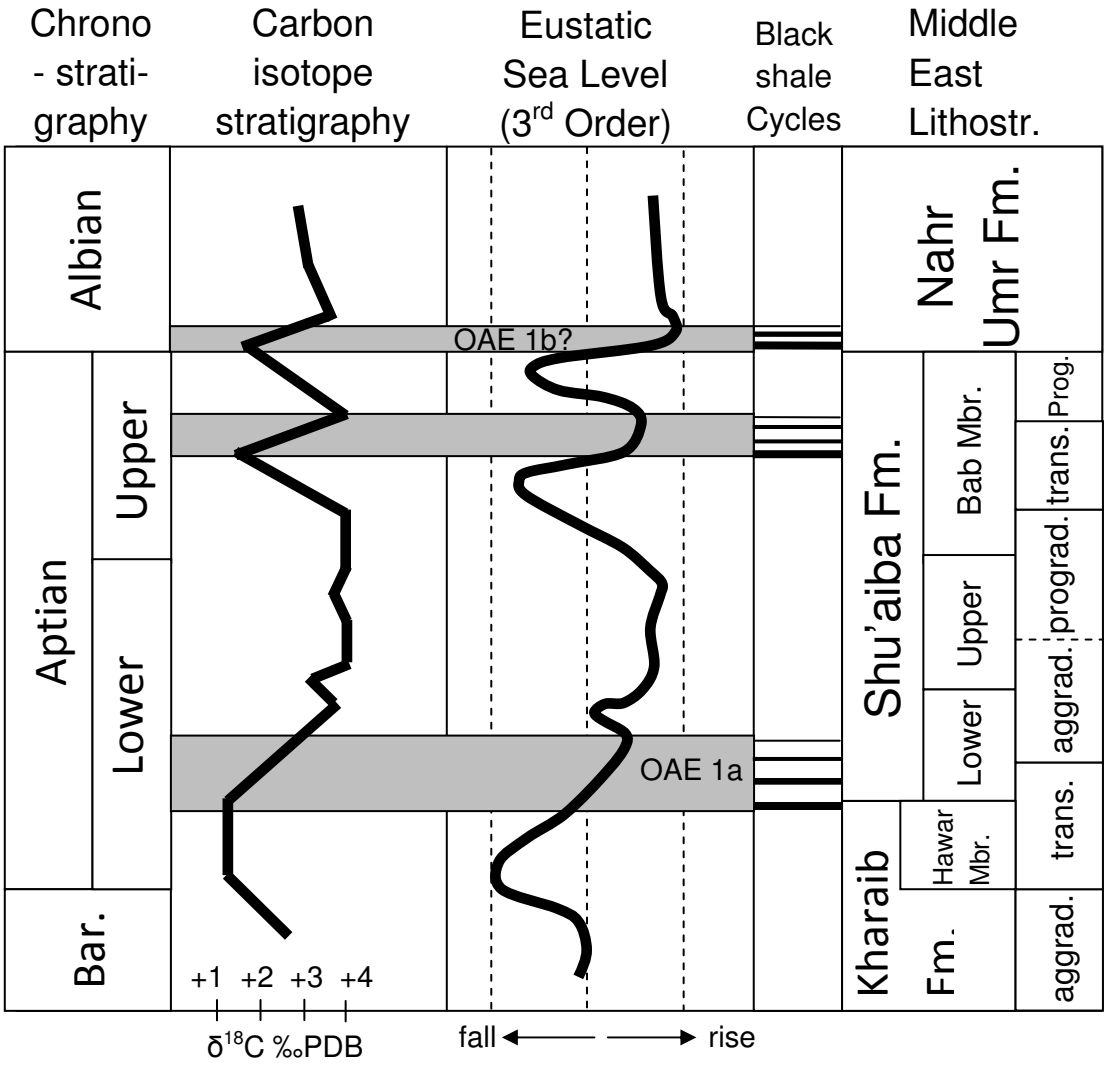

Figure 6.16: positive $\delta^{13}C$ shift to +3.5‰ is associated with a prolonged 3rd order TST and black shale deposition in the Upper Aptian in the Shu'aiba Formation. The abbreviations mean: Bar: Barremian, aggrade: aggradation, trans: transgression, Prograd: progradation, Mbr: Member, Fm: Formation and Lithostr: Lithostratigraphy (redrawn from Grötsch et al. 1998).

This study has a positive $\delta^{13}C$ trend recorded during a thickening upward trend of the 4th order HFC's defining a long term 3rd order TST (consistent with Grötsch et al. (1998) and Vahrenkamp (1996)) (Fig. 6.16 & 6.17). Whether this positive trend can be used to correlate the base of the Lower Kharaib Formation across the offshore field is uncertain, considering there is no abrupt shift at the base of the lower Kharaib Formation or within the Lekhwair Formation. Therefore this study cannot emulate the study by Grötsch et al. (1998) that $\delta^{13}C$ shifts are used to correlate time equivalent shallow water carbonate formations. There are also no black shales

present within the Lekhwair of Lower Kharaib Formations to correlate with this positive $\delta^{13}C$ shift (Section 3.5.3), unlike Grötsch et al. (1998).

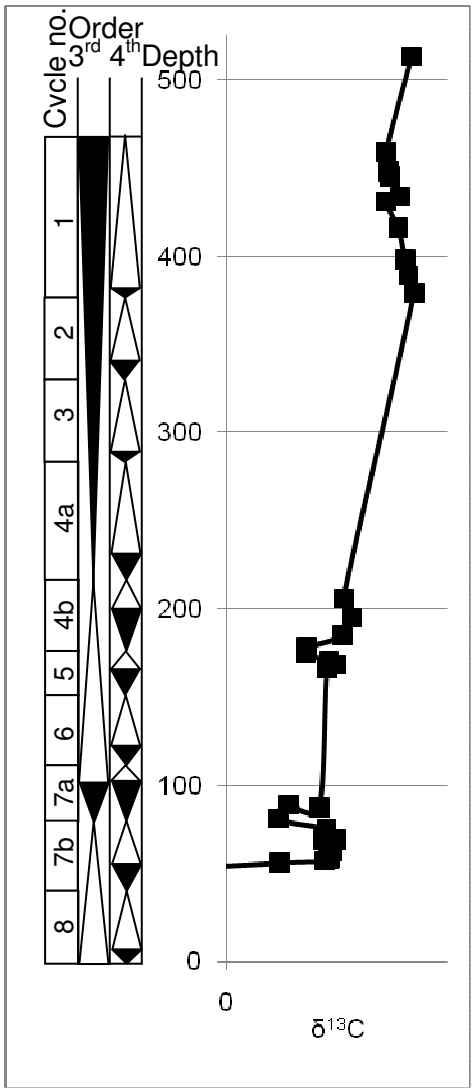

Figure 6.17: the $\delta^{13}C$ isotope signature becomes more positive from +1‰ in the Lower Lekhwair Formation to +3.5‰ in the Lower Kharaib Formation. This is associated with the thickening of the 4th order HFC's and a 3rd order TST.

These trends are consistent with studies by Föllmi (1993) and Föllmi et al. (1994) that sea level rise had caused increased continental erosion, the mobilisation of C^{12} into the oceans, causing an increase in global carbon cycling and organic carbon burial rates, producing a positive $\delta^{13}C$ trend (Lini et al. 1992).

Links with $\delta^{13}C$ trends and changes in organic productivity

A positive $\delta^{13}C$ shift is recorded from the Tithonian-Albian on the north Tethyan Margin with a change from oolites and corals, to crinoids and bryozoans, rich in siliciclasts, with condensed phosphate beds capped with erosional surfaces (Föllmi et al. 1994). This transition reflects platform drowning: orthophosphates poison calcite growth by inhibiting the external shell production of organisms (Hallock & Schlager 1986, Simkiss 1964). Terrigenous run-off from lowland river plains partially flooded due to sea level transgression could have been the source of phosphates (Föllmi et al. 1994). Therefore, Föllmi (1993) and Föllmi et al. (1994) have noted a link between positive $\delta^{13}C$ shifts with phosphate rich sediments, sea level transgression and platform drowning.

River influenced coastlines on the Tethyan Ocean have positive $\delta^{13}C$ shifts associated with black shale horizons (OAE's: Section 3.5.3), suggesting platform drowning (Weissert et al. 1998). Rudist and nannoconid (most robust and heavily calcified nannoconids) abundance decreases as an increase in organisms with smaller with thinner mineralised parts occurs during the positive $\delta^{13}C$ excursion. This suggests that nannoconids and other organisms with large mineralised parts are having difficulty in secreting carbonate skeletons (Weissert & Erba 2004). Therefore Weissert & Erba (2004) has concluded that major shifts in the $\delta^{13}C$ record are consistent with 'bio-calcification crisis' in the Valanginian (~132Ma), early Aptian (~118Ma) and late Aptian (~113Ma).

A small decrease in biodiversity from the Lekhwair into the Kharaib Formation is recorded (Section 3.5.3), but not enough to support a 'bio-calcification crisis' (Weissert & Erba 2004). There is an increasing dominance of smaller organisms with thinner mineralised parts, such as *Palorbitolina lenticularis,* up into the Lower Kharaib Formation. However, this is coupled with an increase in *G. costatus* which in not consistent with Weissert & Erba (2004) (Fig. 6.18A, 6.18B & 6.18D). There are no crinoids, bryozoans, orthophosphates and siliciclastic grains in the Lower Kharaib Formation. Carbonate production has also possibly increased towards the Lower Kharaib Formation (Section 4.4 & Figs. 6.10-6.14). Although this study has

only recorded a longer term (over 6myr) positive $\delta^{13}C$ trend from the Lekhwair into the Lower Kharaib Formation, in comparison with the more abrupt shifts recorded by Föllmi (1993) and Weissert & Erba (2004), this study cannot associate the conclusions by Föllmi (1993), Föllmi et al. (1994) and Weissert & Erba (2004) with the positive $\delta^{13}C$ trend from the Lekhwair Formation up into the Lower Kharaib Formation.

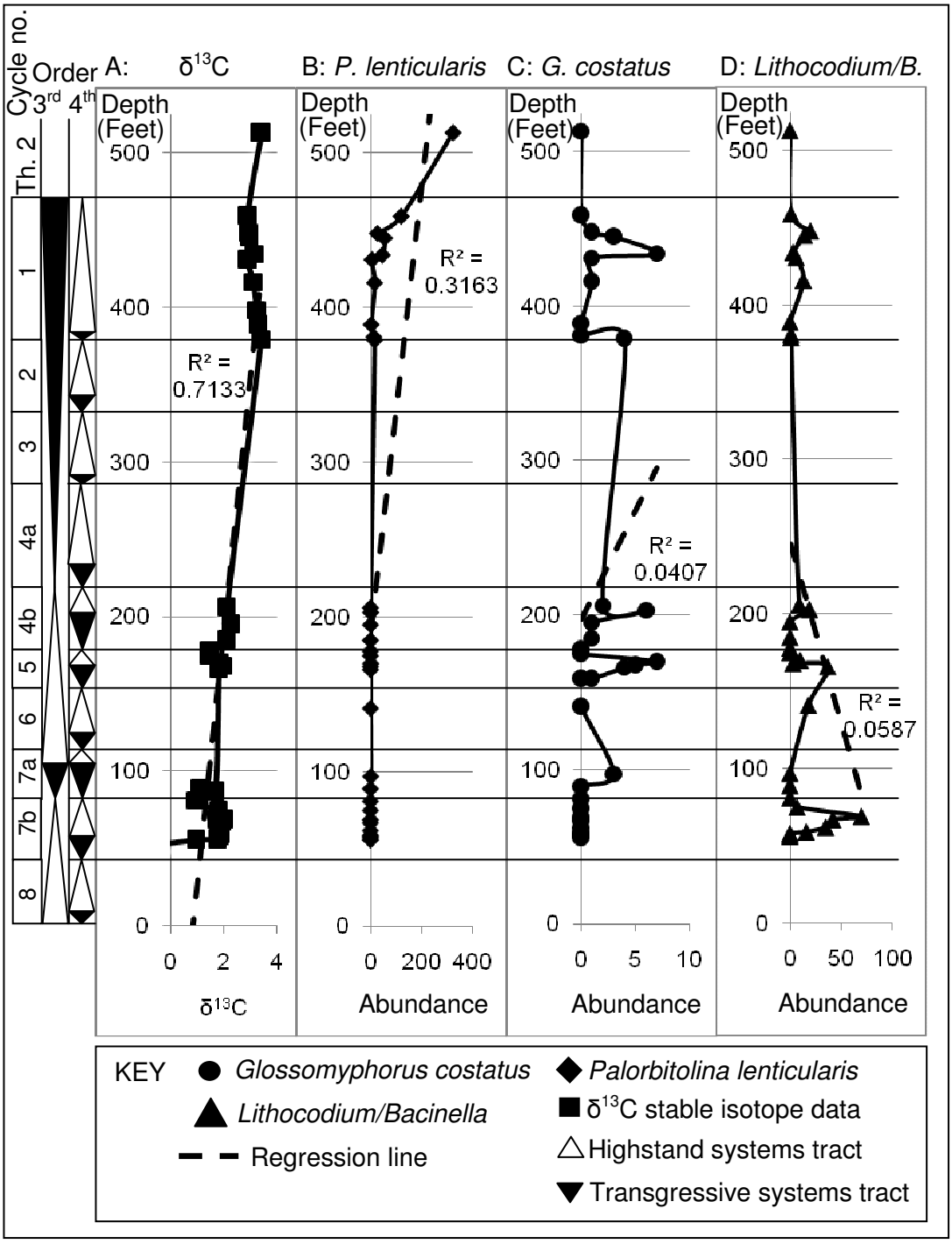

Figure 6.18: trends between the fossil counts and the $\delta^{13}C$ isotopes. A) The $\delta^{13}C$ positive trend into the Lower Kharaib Formation (Cycle 1), B) the abundance of P. lenticularis *increases, C) the abundance of* G. costatus *increases, and D) the abundance in* Lithocodium/B. *decreases towards the Lower Kharaib Formation (Appendix 1A-1E for fossil abundance data). This indicates that with a positive $\delta^{13}C$ trend there is also an increase in* P. lenticularis *and* G. costatus. *The abbreviation Th. 2: Thamama 2.*

$\delta^{13}C$ isotope data from dolomites

Early dolomite formation is associated with circulating marine porewaters, when dolomite has similar $\delta^{13}C$ values with the surrounding LMC micrite (Török 2000). It would be difficult to attribute the Lekhwair Formation dolomites to this process as circulating Cretaceous seawater contains lower Mg^{2+} and higher Ca^{2+} in comparison with modern day aragonite seas (Section 2.1). The dolomite cannot have formed from pure chemical and mechanical compaction of the matrix (Dix 1993) as the dolomites contain more positive $\delta^{13}C$ values of +2‰ to 2.4‰ (Fig 6.14B) compared with the surrounding micrite of +1.8‰.

Sulphate reduction is linked to the production of pyrite (Dickson et al. 2008) which is seen surrounding dolomitised *Thallassinoides* burrows (Fig. 6.3). Only negative $\delta^{13}C$ values represent dolomite forming within the sulphate reducing zone (Baker & Burns 1985). The majority of dolomites cannot have formed from bacterial sulphate reduction as most have positive $\delta^{13}C$ values ranging from +1.5‰ to +4‰ (Fig 6.14B). Positive $\delta^{13}C$ isotope values represent conditions of methanogenesis at shallow-intermediate burial depths (Baker & Burns 1985). However, $\delta^{13}C$ values of +9.1‰ are associated with strong methanogenesis by Raven & Dickson (2007), indicating that if methanogenesis is influencing dolomite formation within the Lekhwair Formation, its processes have had little influence on the $\delta^{13}C$ partitioning. In conclusion, the interpretations for $\delta^{13}C$ isotopes from dolomites are uncertain.

6.2.2 $\delta^{18}O$ data

Stable $\delta^{18}O$ isotope data with respect to the stratigraphy

In Figure 6.18 the $\delta^{18}O$ stable isotope data for the bulk micrite is plotted against stratigraphic depth. The $\delta^{18}O$ isotopes within the base Cycles 7a and 7b show a range of -3.2‰ to -7‰, Cycles 4a and 4b show a range from -2.5‰ to -6.9‰ and the top Cycle 1 shows a range between -4.7‰ and -7.9‰ (Fig. 6.19). The $\delta^{18}O$ values show a slight negative trend from the base of the Lekhwair Formation and into the Lower Kharaib Formation (Fig. 6.1). The spread in $\delta^{18}O$ data is also becoming less clustered

from the Lower Lekhwair Formation into the Lower Kharaib Formation from -3‰ to -7‰, and -5‰ to -8‰, respectively.

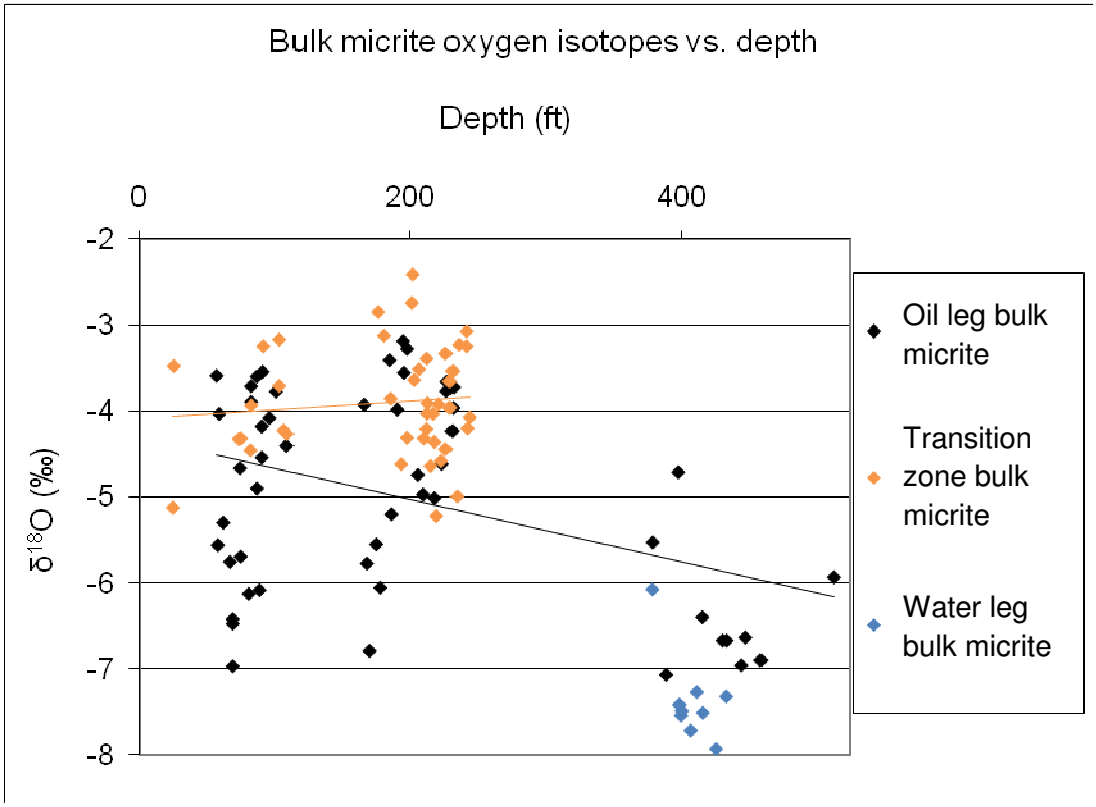

Figure 6.19: *$\delta^{18}O$ isotope data for the bulk micrite. There is a slight negative trend towards the Lower Kharaib Formation. The spread of data also becomes more restricted towards the Lower Kharaib Formation (Appendix 4 for data tables). The R^2 for the oil leg bulk micrite data is 0.1069 (black line). The R^2 for the transition zone bulk micrite data is 0.0644 (orange line).*

Figure 6.20A shows the $\delta^{18}O$ stable isotope data for youngest LMC cements against stratigraphic depth. $\delta^{18}O$ for the youngest LMC cements exists within a narrow range from -7.5‰ to -10‰ with the exception of four data points with $\delta^{18}O$ values of -6‰ (Fig. 6.20A).

Figure 6.20B shows the $\delta^{18}O$ stable isotope data for burrow and saddle dolomites against stratigraphic depth. Burrow dolomites have a $\delta^{18}O$ range from -2.5‰ to -6.4‰, while saddle dolomites have a $\delta^{18}O$ isotope range from -5.3‰ to -8.4‰ (Fig 6.20B). There is no significant $\delta^{18}O$ trend within the saddle dolomites whereas for the dolomite rhombs there is a slight negative trend towards the Lower Kharaib Formation from -2.5‰ to -5.3‰ in Cycles 7a, 4b and 4a, towards -5.4‰ and -6.4‰

in Cycle 1 (Fig 6.20B). However there is not enough data to be certain of these trends (Fig. 6.20B).

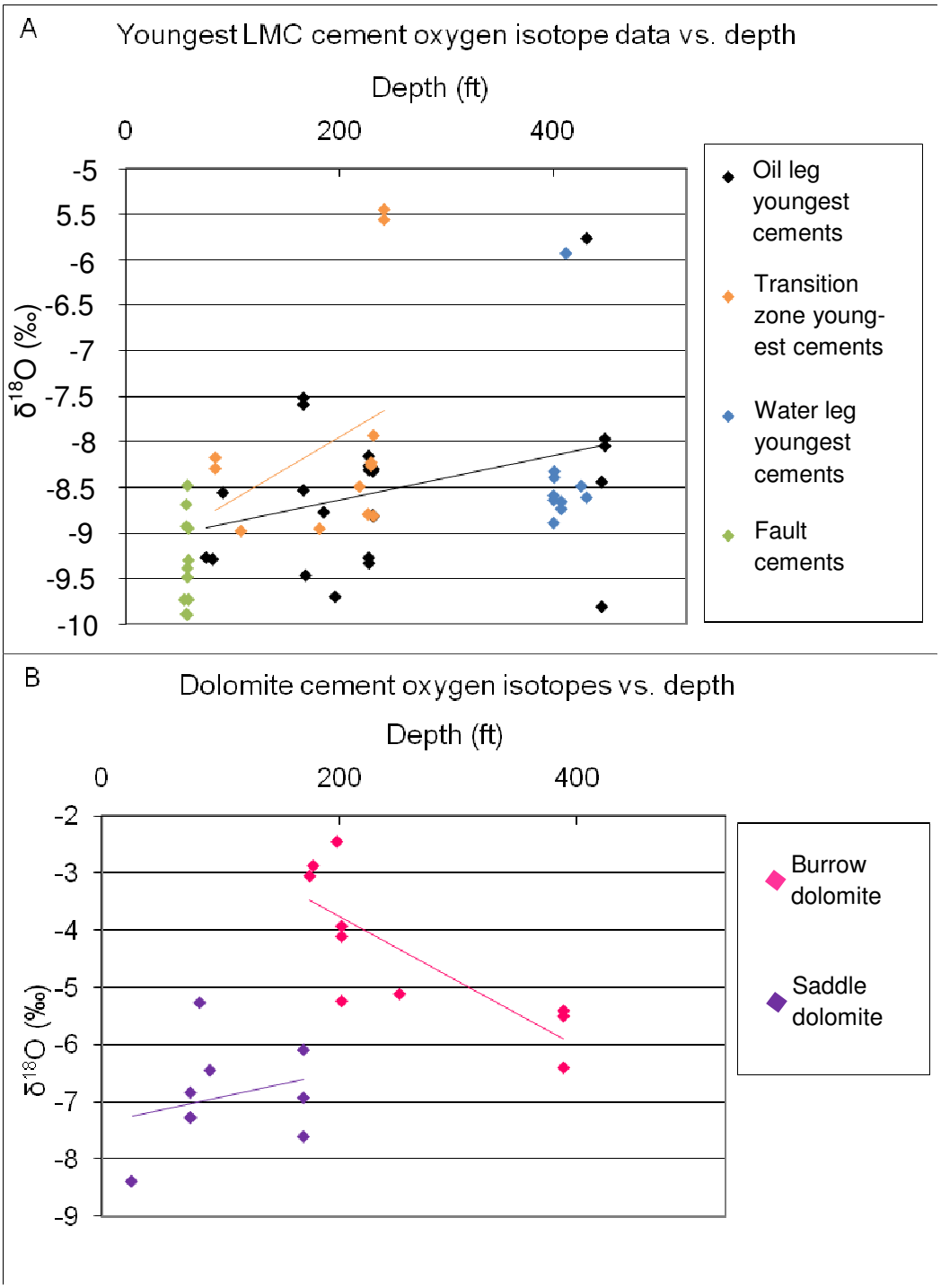

Figure 6.20: The $\delta^{18}O$ data for youngest LMC cements and dolomite cements. A) $\delta^{18}O$ data for the youngest LMC cements shows majority values of -8‰ and -9‰ (Appendix 4 for data tables). The R^2 for the oil leg is 0.1069 (black line). The R^2 for the transition zone is 0.1307 (orange line). B) $\delta^{18}O$ values for dolomite cements (Appendix 4 for data tables). The R^2 for burrow dolomites is 0.6334 (pink line). The R^2 for saddle dolomites is 0.0704 (purple line).

Stable $\delta^{13}C$ and $\delta^{83}O$ isotope data with respect to the 4th order HFC's and the wells

With respect to the 4th order HFC's the most positive $\delta^{13}C$ bulk micrite data are within Cycle 1 (Fig. 5.20A). The most negative $\delta^{18}O$ values are also in Cycle 1 (Fig 6.21A). This is the case for each well that covers Cycle 1 (Fig. 6.21B). For Cycles 7a, 4b, and 4a, and both the transition zone and the oil leg bulk micrites, $\delta^{18}O$ values only reach -5‰ in Wells 2 and 3; but $\delta^{18}O$ values reaching -7‰ are restricted to Well 4 (Fig. 6.21B). This also shows the bulk micrite data clusters with respect to the separate 4th order HFC's and not the wells. Similar values are recorded from separate wells that are kilometres apart. For example, data from Cycle 1 in Wells 1 and 4, which are over 10 kilometres apart, cluster at +3‰ for $\delta^{13}C$ and between -5‰ and -8‰ for $\delta^{18}O$, away from the main dataset (Figs. 6.21A & 6.21B).

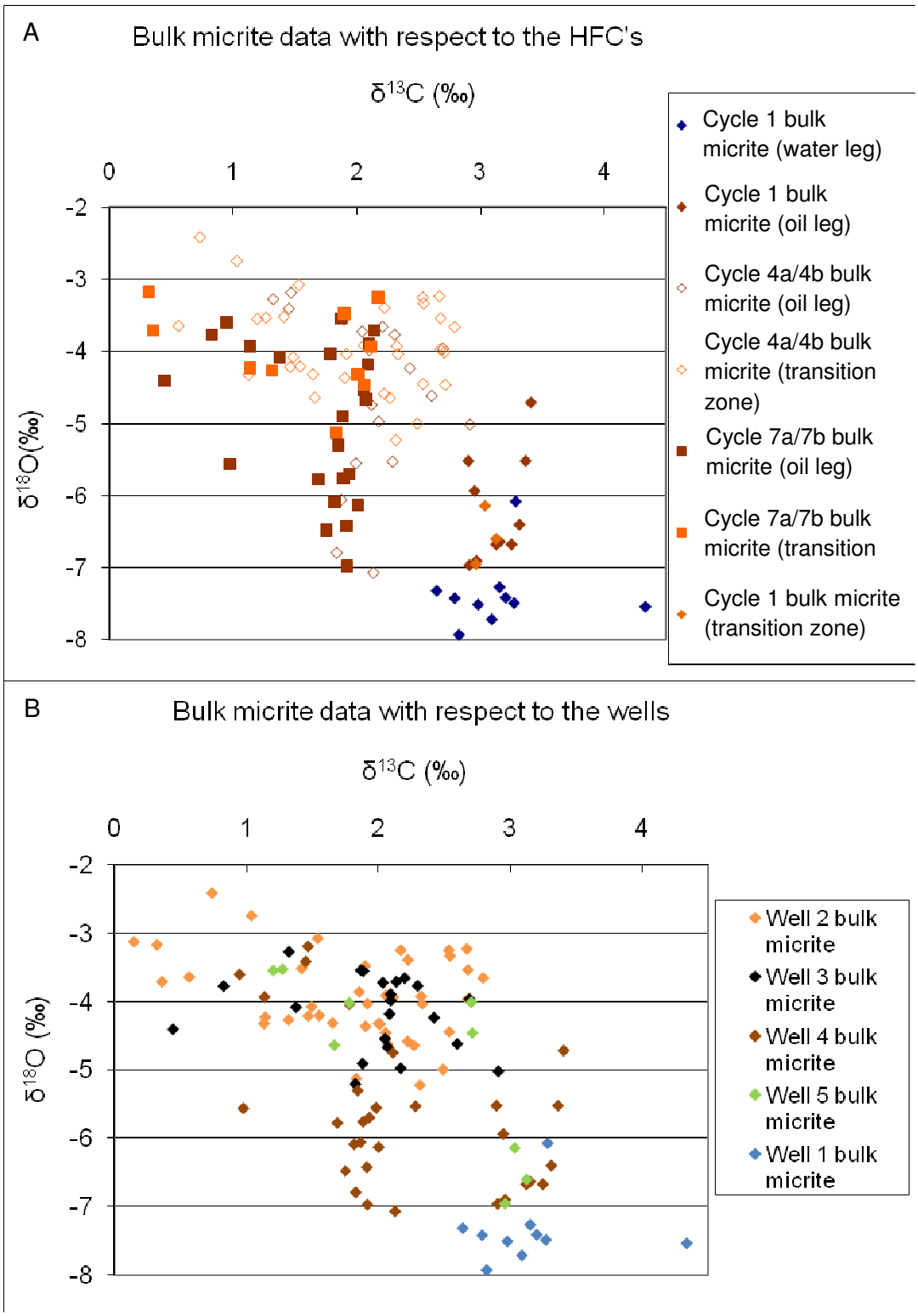

Figure 6.21: Two graphs showing the bulk micrite $\delta^{13}C$ isotopes plotted against the $\delta^{18}O$ isotope data with A) respect to the 4th order HFC's and B) respect to the wells (Appendix 4 for data tables).

$\delta^{18}O$ isotope data for the bulk micrite

The spread of data reduces into the Lower Kharaib Formation, and for the water leg of Cycle 1: a final cementation phase was clearly accompanied by alteration of the micrite within the deep burial realm (Fig. 6.19, Section 5.7.1). However $\delta^{18}O$ data for the oil leg for Cycle 1 in Well 4 also shows a very confined set of values, although the values are not as negative (-5‰ to -7‰) in comparison with Cycle 1 in the water leg (-7‰ to -10‰) (Fig. 6.19, Section 5.7.1). This suggests that Cycle 1 in the oil leg was also altered, but slightly earlier during progressive burial in comparison with the water leg. Cycle 1 $\delta^{18}O$ data is generally more negative than Cycles 4a, 4b and 7a, showing a slight negative shift in the $\delta^{18}O$ data into the Lower Kharaib Formation (Cycle 1). This indicates that each 4th order HFC has probably followed a distinctive diagenetic pathway. Already shown in Sections 3.4.1 & 4.6 is the compartmentalisation of the entire field, with every reservoir being bounded by non-reservoirs above and below, which makes vertical fluid flow difficult (Section 3.4.2, Fig. 3.14): this $\delta^{18}O$ data confirms reservoir compartmentalisation.

The vast spread of $\delta^{18}O$ data with respect to the bulk micrite of the transition zone and the oil leg suggests that the micrite was progressively diagenetically altering, possibly through rock-water interactions, during increasing burial. There is a more confined spread of $\delta^{18}O$ bulk micrite data of the transition zone in comparison with the oil leg (Fig. 6.21). The majority of transition zone bulk micrite data only shows a spread with values no more negative than -5‰, whereas the oil leg bulk micrite has a significant spread of data including values of -7‰ (Fig. 6.21). This suggests that within the oil leg, the bulk micrite may have been selectively diagenetically altered at deeper depths associated with $\delta^{18}O$ values of -7‰. This may have been caused by the presence of acidic porewater and oil. However the initial oil charge is associated with cements with $\delta^{18}O$ values of -5.5‰ (Sections 5.3.6 & 5.7) which suggests a much shallower depth of emplacement.

A closer inspection of the oil leg data in Figure 6.21 highlights that the majority of $\delta^{18}O$ data with values more negative than -5‰ in the oil leg exist within Cycle 7a, 7b and Cycle 1 of Well 4. The base of Well 4 is highly fractured, as a fault swarm is

present near Well 4 at these depths. The opening and activation of faults could have brought in fluids altering the micrite selectively within Cycles 7a and 7b in Well 4 of the crest (oil leg). Whether the alteration of Cycle 1 in the oil leg is also a cause of fluid migration at deep burial depths along newly open faults and fractures is unclear. The fault would have opened at depths associated with $\delta^{18}O$ values of >-5‰, possibly during intermediate-deep burial for the Lekhwair and Lower Kharaib Formations. Fault cements have similar $\delta^{18}O$ values between –8‰ and -10‰ in comparison with the youngest cements, suggesting fault occlusion occurred with the last burial spar formation within intermediate-deep burial depths (Fig 6.20A).

$\delta^{18}O$ isotopes for the LMC youngest cements

The youngest LMC cement growths between the water leg, transition zone and the oil leg have $\delta^{18}O$ values of -8‰ to -10‰ reflecting final cementation possibly in the intermediate-deep burial realm. However, four data points have values of -6‰ which are consistent with the Ion Microprobe data from the LMC macrocements within the transition zone and the oil leg (Sections 5.4 & 5.7). This confirms $\delta^{18}O$ values within the youngest zones of the LMC cements are returning to less negative values of -6‰. This is also consistent with the suggestion that porewaters have evolved at shallower depths as the entire Lekhwair Formation became uplifted by the Semail ophiolite obduction at 92Ma.

$\delta^{18}O$ isotope for dolomites

The conversion for temperatures from the dolomites will use an equation from Vasconcelos et al. (2005): established for dolomites precipitating out from water at lower temperatures.

Equation 6.1: $$1000\ln\alpha_{(\text{dolomite-water})} = 2.73 \times 10^6 T^{-2} + 0.26$$

This relationship was determined by the synthesis of dolomite from using sulphate reducing bacteria. This method allows for dolomite to become precipitated at low temperatures (between 25-45°C).

Using the equation for the partitioning of $\delta^{18}O$ from porewater into dolomite (Vasconcelos et al. 2005), the values for reservoir temperature are too high, with values ranging from 300-500°C. This is not consistent with $\delta^{18}O$ partitioning from porewater into LMC, as the most negative $\delta^{18}O$ value for -10.3‰ provides a temperature of 131°C (Section 5.6). Separated component analysis on the dolomite cements, in this study does not constrain their relative depth of formation. The only outcome that can be gathered from the equation by Vasconcelos et al. (2005) is estimating the $\delta^{18}O$ composition of the formation waters. Assuming the temperature of dolomite formation, the values for the $\delta^{18}O$ of the porewater are +1.1‰ for precipitation at 10°C and +1.5‰ for precipitation at 100°C. This is quite different to the average of -1‰ for Cretaceous seawater used for the calculations of reservoir temperatures from the LMC cements (Section 5.6). This suggests that the formation waters must have evolved, through water-rock interaction, during progressive burial to form the dolomites within the Lekhwair and Lower Kharaib Formations.

6.3 $\delta^{18}O$ and $\delta^{13}C$ data summary

Figure 6.22 summary considers all datasets. With respect to the $\delta^{18}O$ data this plot shows the data ranges of micrite alteration, dolomite formation, fault cement formation and youngest LMC cement formation (Fig. 6.22). The $\delta^{13}C$ and $\delta^{18}O$ averages for all datasets are shown in Table 6.2.

	N=	$\delta^{13}C$ range	$\delta^{13}C$ averages	$\delta^{18}O$ range	$\delta^{18}O$ averages
A	54	-0.1 to 3.4	2.1	-3.2 to -7.1	-5
B	61	0 to 3.1	1.8	-2.4 to -7	-3.9
C	10	2.6 to 4.3	3.2	-6.1 to -7.9	-7.4
D	9	1.5 to 2.5	2.1	-5.3 to -8.4	-6.9
E	6	2.1 to 4.1	3	-3.9 to -6.4	-5.1
F	4	1.6 to 2.8	2	-2.5 to -5.1	-3.4
G	26	0.9 to 3.3	1.8	-5.8 to -9.8	-8.5
H	12	1.2 to 2.4	1.8	-5.5 to -9	-8
I	10	2.3 to 3.2	2.8	-5.9 to -8.9	-8.3
J	12	0.8 to 1.5	1.2	-8.5 to -9.9	-9.3

Table 6.2: $\delta^{13}C$ and $\delta^{18}O$ data ranges and averages for the main data groups (also shown below on the summary diagram; Figure 6.22). A: oil leg bulk micrite, B: transition zone bulk micrite, C: water leg bulk micrite, D: saddle dolomites, E: dolomites rhombs in Thallassinoides, *F: dolomite rhombs in matrix, G: oil leg youngest LMC cements, H: transition zone youngest LMC cements, I: water leg youngest LMC cements and J: fault LMC cements.*

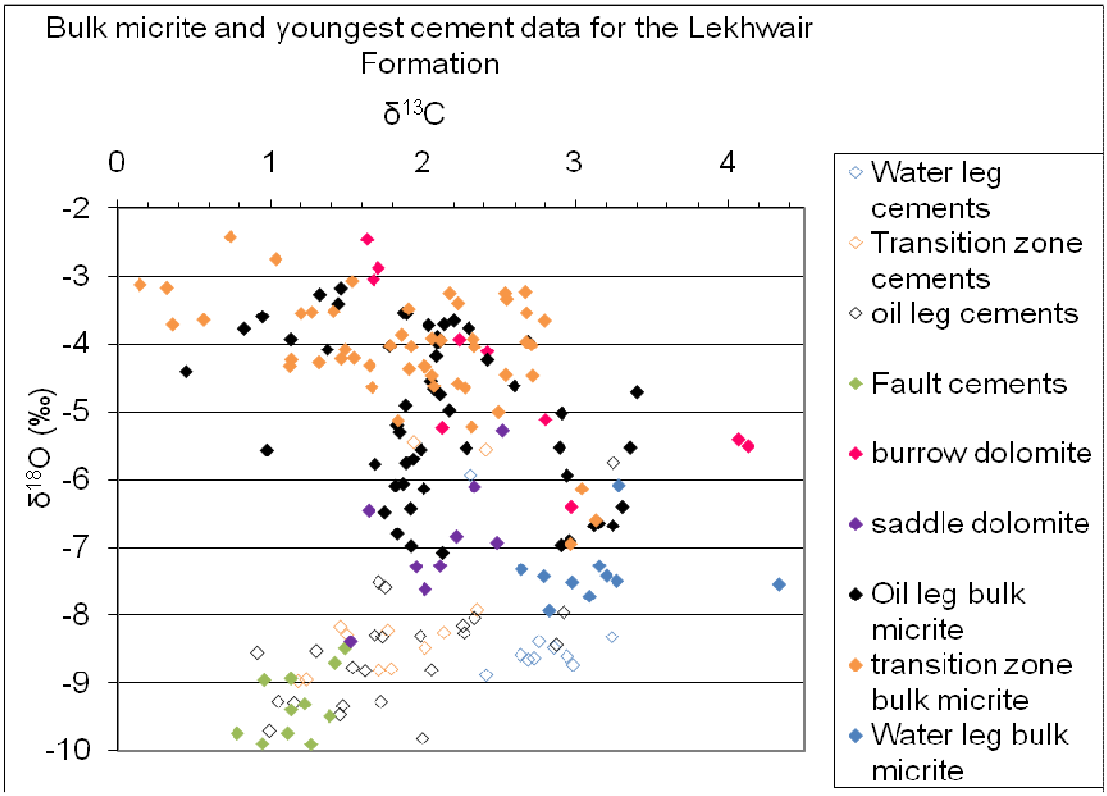

Figure 6.22: $\delta^{13}C$ isotopes verses the $\delta^{18}O$ isotopes for the bulk micrite, youngest LMC cements, saddle dolomites and dolomite rhombs (see Appendix 4 for data tables).

In summarising all the data there is a clear progression, through the alteration of the $\delta^{18}O$ values, from the oil leg and transition zone bulk micrites, towards the most negative $\delta^{18}O$ values within the youngest LMC cements. This does suggest a relative sequence of diagenetic events, however there are several lines of evidence that point towards formation water evolution during progressive burial of the Lekhwair and Lower Kharaib Formations, which goes against using the $\delta^{18}O$ data as proxies for reservoir temperature. 1) The vast spread in $\delta^{18}O$ data for most categories suggests there has been possible evolution of the formation waters, 2) the difference in $\delta^{18}O$ values between Cycle 1 and Cycles 4a, 4b and 7a suggests that the micrite and possibly the LMC cements within each reservoir have evolved in different ways and therefore cannot be specifically correlated, 3) the porewaters that precipitated the burrow and saddle dolomites were potentially enriched in $\delta^{18}O$ by 2.5‰ in comparison with Cretaceous seawater and 4) the return to less negative $\delta^{18}O$ values selectively within the oil leg youngest cement zones suggests many possibilities

including the evolution of the formation waters towards an enrichment in ^{18}O. Therefore the same conclusion in Section 4.9 is reached for the $\delta^{18}O$ data within this Chapter: porewater evolution must have occurred during progressive burial. $\delta^{18}O$ data are therefore not used to calculate reservoir temperatures and specific burial depths.

Only two definitive conclusions are suggested: 1) the borings determine that several phases of cementation, along with a phase of dissolution, may have occurred in syn-deposition and 2) the presence of stylolites cross-cutting the burial spars (oil leg & transition zone), suggests that the Lekhwair and Lower Kharaib Formations macrocements had formed during intermediate-deep burial depths. This constrains the deep burial cements with $\delta^{18}O$ values of -8‰ to -10‰, between intermediate and deep burial depths. However, as these burial cements are volumetrically larger in comparison with early syntaxial overgrowths (i.e. they needed a larger source of solutes), they may be products of stylolitisation (Section 5.7), suggesting that burial spar formation continued into the deep burial realm. In the oil leg subsequent cements show a return to less negative values (Section 5.4 & 5.3.5), which has been previously partly attributed to uplift in Section 5.8: LMC burial spars and $\delta^{18}O$ values of -8‰ and -10‰ must represent some of the deepest cement fills that formed into the deep burial realm, before uplift.

Everything that had occurred between syn-deposition and deep burial cannot be relatively constrained, and therefore the paragenetic sequence in Fig. 6.11 may not be accurate and should only be used a guide for the diagenetic processes that have occurred during burial of the Lekhwair and Lower Kharaib Formations.

6.4 Conclusions

1. Within the bulk micrite and the LMC cements, a positive $\delta^{13}C$ trend occurs at the transition from the Lekhwair Formation into the Lower Kharaib Formation. The trend may be linked to the end of a prolonged 3rd order TST of the Lower Kharaib Formation. This positive $\delta^{13}C$ trend has no abrupt shifts for use in chronostratigraphic correlation and therefore this study does not associate any relative age estimates with this positive $\delta^{13}C$ trend.

2. The $\delta^{18}O$ data for the bulk micrite shows that Cycle 1 has possibly undergone a different diagenetic evolution in comparison with Cycles 4a, 4b and 7a. This confirms the compartmentalisation of all the reservoir horizons across the field. It also shows that the porewaters have possibly evolved differently within the separate reservoirs.

3. The dolomites have positive $\delta^{13}C$ values implying formation under slight methanogenesis and not at near surface conditions associated with microbial sulphate reduction: however this is not a definite conclusion for this study.

4. The dolomite rhombs may have formed relatively early, possibly during syn deposition, however this is uncertain.

5. The Fe-saddle dolomite requires a supersaturation of Fe^{2+} in the water column. The introduction of acidic porewaters and oil within the reservoir horizons, the mechanical compaction causing basal TST micrite/mud dewatering, and/or compaction of thin insoluble layers within the reservoir could have provided Fe^{2+} in solution to form the first Fe-saddle dolomites.

6. The $\delta^{18}O$ data of the youngest LMC cements is consistent with a separate Ion Microprobe study where the most negative $\delta^{18}O$ values are -8‰ to -10‰.

7. Stylolites have formed in the deep burial realm after LMC burial spar formation. This constrains burial spar formation and $\delta^{18}O$ values of -8‰ and -10‰ with intermediate-deep burial depths. These stylolites possibly have anhydrite within them.

8. The faults may have opened within the deep burial realm and altered the micrite selectively within Cycles 7a and 7b (and possibly Cycle 1) within Well 4. The faults have then been cemented during burial spar formation within the intermediate-deep burial realms.

9. Porewater must have evolved during the progressive burial of the Lekhwair and Lower Kharaib Formations, and therefore the $\delta^{18}O$ data cannot be used to calculate proxies for reservoir temperature and specific burial depths. Instead a paragenetic sequence is compiled with only cross-cutting relationships

(determined petrographically). Future work is needed regarding the collection of bottom hole temperatures and porewater compositions for the five wells across the offshore field, Abu Dhabi, to resolve this issue.

Chapter 7

Origins of microporosity

Microporosity is described by Moshier (1989b) as a 'chalky texture' as it exists as intercrystalline micropores between euhedral to subhedral rhombs that reflects the regular pore space seen between coccoliths in chalk. The micropore size is differently defined: Choquette & Prey (1970) define pores less than 62.5µm to microporosity; Pittman (1971) defines pores less than 1µm to microporosity and Cantrell & Hagerty (1999) defines pores less than 10µm to microporosity. The latter system is based upon the lower detection limits of a standard petrographic microscope. This definition will be used here to define micropores within the Lekhwair and Kharaib Formations. Any pores larger than 10µm in diameter are considered as macropores, a separate distinction for mesopores is not considered for this study.

Microporosity can be a large contributor to the total porosity of a rock and can therefore be very important when considering the porosity and permeability relationships of a carbonate. Cantrell & Hagerty (1999) has devised a method for quantifying the amount of microporosity within a sample (Section 1.2). For grainstone and mud-lean packstone, the average micropore fraction is small: 19.8% and 37.6%, respectively. For packstone the average micropore fraction is 53.8%, whereas for wackestone and mudstone almost the entire rock is micropores (~100%) (Fig. 7.1).

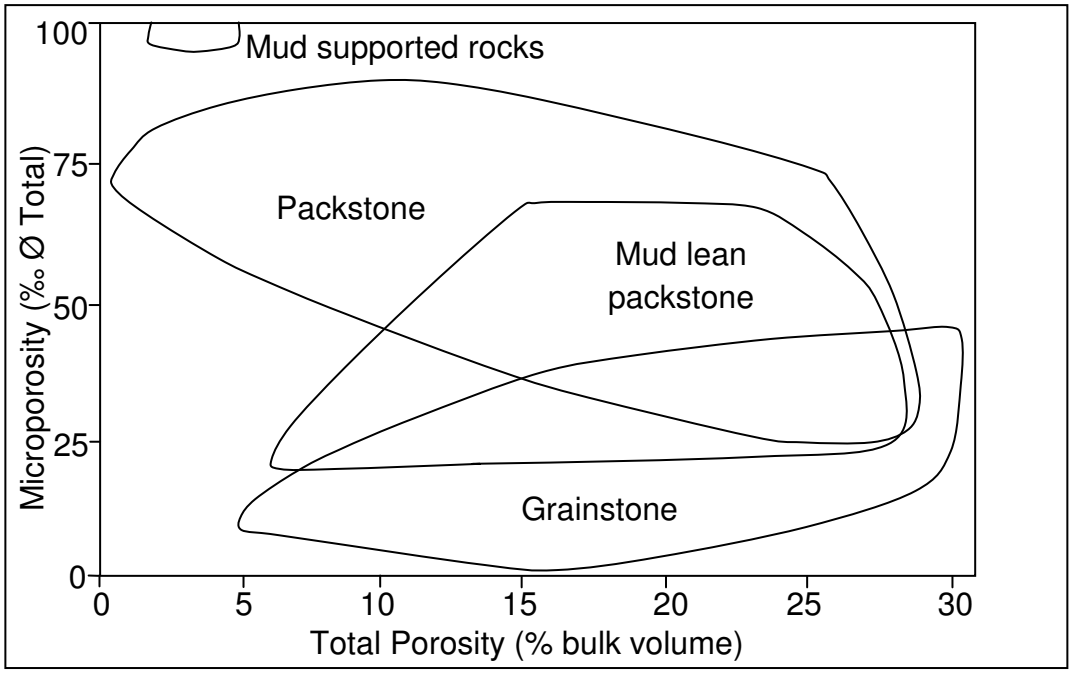

Figure 7.1: More microporosity is associated with increasing mud contents within the lithofacies. Therefore mudstone contains the highest proportion of microporosity with respect to the total porosity of the rock (Cantrell & Hagerty 1999).

The percentage of permeability that is associated with the microporous fractions of a carbonate is also highlighted by Lønøy (2006) (Section 8.1.2). For 1mD permeability within a Cretaceous chalk sample, 25.8% of microporosity of the total pore volume is required, whereas for a Tertiary chalk sample, 31.3% of the total pore volume is required (Lønøy 2006). With respect to studies by Cantrell & Hagerty (1999) where many of their mud-dominated facies have a microporous fraction close to 100%, the regression calculated by Lønøy (2006) suggests that mudstones and packstones could have 3-4mD of permeability totally attributed to the microporous fraction of the rock. However, comparing the studies by Cantrell & Hagerty (1999) and Lønøy (2006) is problematic, as the same samples are not used: but they do indicate that a micropore-dominated reservoir horizon could be exploited and treated as a lower grade reservoir.

The presence of micropores is clearly important when considering the porosity and permeability relationships of a carbonate. It is therefore necessary to gain a good understanding of the types of micropores, a classification of micropore fabrics and the environments and diagenetic processes attributed with the formation of

microporosity. This information can then be applied to the micropore fabrics of the Lekhwair and Lower Kharaib Formations in order to understand their formation.

The proportion of microporosity within most of the studied samples from the Lower Kharaib and Lekhwair Formations is calculated using the technique employed by Cantrell & Hagerty (1999) (Section 1.2). This provides a quantitative assessment of the dominance of microporosity within the Lekhwair and Lower Kharaib Formation pore systems.

In conjunction, for each sample, secondary electron images are used separately to visually compare the proportion of microporosity along with the micropore fabrics. Porosity and permeability data measured commercially (Section 1.2) is plotted for the specific sample depths, used under the SEM and for the Cantrell & Hagerty (1999) method. The sample ranges cover both the HST's and TST's of selected 4th order HFC's along with the oil leg, transition zone and the water leg.

Comparing the visual assessments with the Cantrell & Hagerty (1999) method, the proportion of microporosity with respect to the total amount of porosity for each sample is established. The changing porosity and permeability values are related to the proportion of microporosity, which provides an understanding of how the microporosity contributes to the porosity and permeability relationships for each sample. The stratigraphic positions of the most interconnected micropore fabrics are identified, and the processes behind their formation are established.

7.1 Previous work

7.1.1 Micropore fabrics

For the Arab carbonates of Saudi Arabia four micropore fabrics are described: 1) microporous grains (Fig. 7.2A), 2) microporous matrix (Fig. 7.2B), 3) microporous fibrous and bladed cements (Fig. 7.2C) and 4) microporous equant cements (Fig. 7.2D) (Cantrell & Hagerty 1999). The first microporous fabric consists of uniform sized subhedral crystals, ranging from 1-4µm (Cantrell & Hagerty 1999) (Fig 7.2A). This micropore fabric is present within many skeletal and non-skeletal grains: at high magnification under SEM both the skeletal and non-skeletal grains share similar

microporous fabrics which suggests that the controlling factor for the formation of microporous grain fabrics is original mineralogy and not grain type (Cantrell & Hagerty 1999). The second micropore fabric consists of 1-10µm subhedral crystals that are not uniformly distributed forming a continuous pore network connected by 1µm pore throats (Cantrell & Hagerty 1999) (Fig. 7.2B). The third fabric consists of bladed crystals 30-40µm long, and 5-10µm wide, and represents isopachous early marine cements (Fig 7.2C). This forms tubular shaped micropores measuring 0.1-1µm in diameter that exist in-between the blades of calcite. The fourth micropore fabric is composed of 30-40µm subhedral to anhedral cements (Fig 7.2D). The micropores exists between the crystals, they are flat and laminar in shape being 3µm thick (Cantrell & Hagerty 1999).

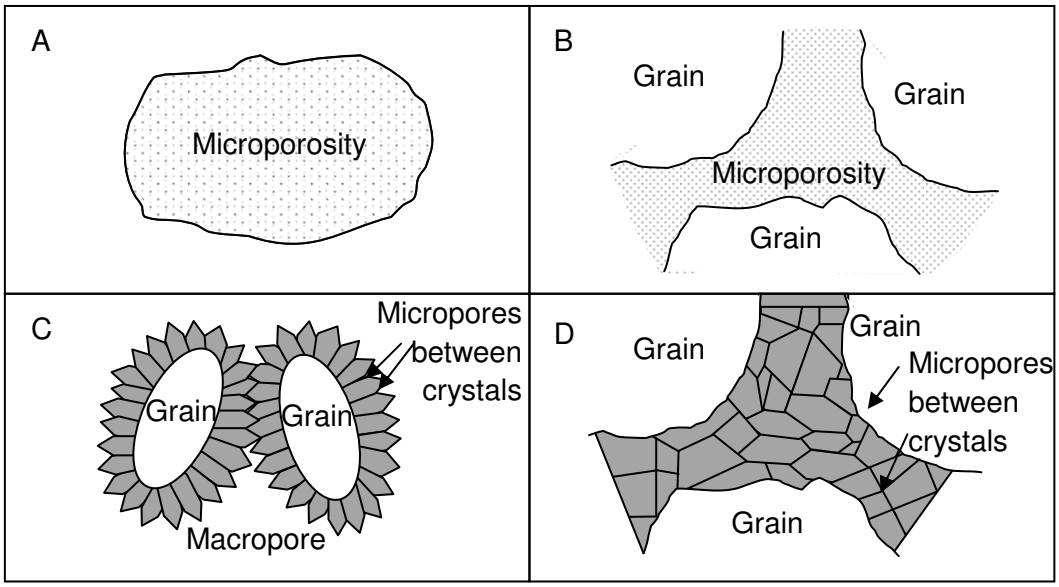

Figure 7.2: types of microporosity within the Arab Carbonates in Saudi Arabia. A) Intraparticle microporosity within micrite grains, B) intraparticle porosity within the matrix, C) intercrystalline microporosity between isopachous meteoric cements and D) intercrystalline microporosity within pore filling calcite burial spars (redrawn from Cantrell & Hagerty 1999).

Three main micropore fabrics are described for the Shu'aiba Formation of the Sajaa Field Eastern U.A.E (Moshier 1989a) (Fig. 7.3). The term idiotopic represents microporous fabrics that are highly porous and are composed of micro rhombic calcites (Moshier 1989a). The term hypidiotopic represents subhedral to euhedral

textures and the term xenotopic represents low porosity (<5% open porosity) coupled with interlocking subhedral to anhedral calcite microspars (Moshier 1989a). The micropore fabrics are: 1) Blocky crystal framework texture (idiotopic): composed of 0.1-68µm euhedral microspar surrounded by well connected, 2-4µm sized, tabular, polygonal, and equant micropores. This fabric is the only one to display microspar rounding (Fig 7.3A) (Moshier 1989a). 2) Porous crystal mosaic (hypidiotopic): composed of 0.5-18µm, subhedral microspar with surrounding tabular and wedge shaped micropores (Fig 7.3B) (Moshier 1989a). 3) Non porous crystal mosaic (xenotopic): composed of 1-30µm anhedral-subhedral moderately sorted interlocking microspar surrounded by 2-3µm polygonal and tabular micropores. (Fig. 7.3C) (Moshier 1989a).

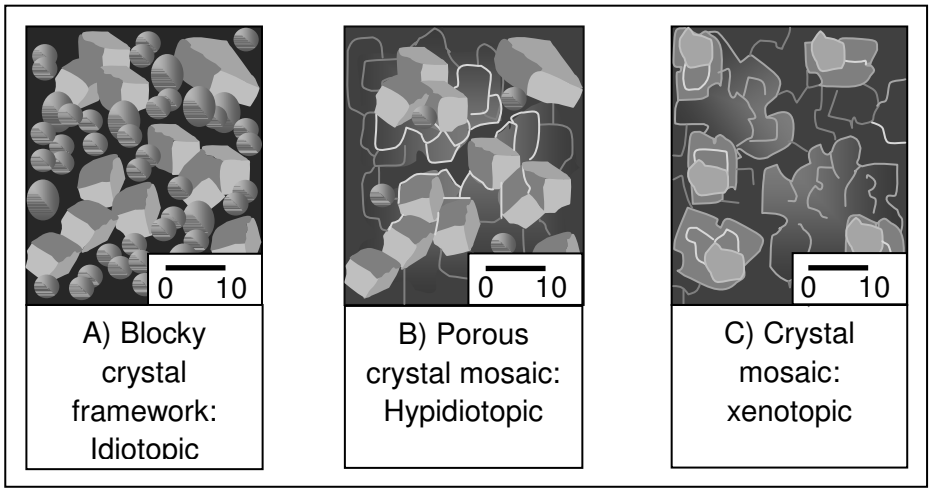

Figure 7.3: microspar fabrics within the Shu'aiba Formation of the Sajaa Field. A) The most porous fabric, B) a halfway house between the blocky crystal fabric and the crystal mosaic and C) the most impermeable fabric which is associated with highly stylolitised horizons. The cubes represent 4-5µm microspars, whereas the spheres represent 1-2µm rounded microspars. The scale bar is in microns (Redrawn from Moshier 1989a).

Lambert et al. (2006) has identified three fabrics from Jurassic and Cretaceous carbonate reservoirs of the Middle East. They are: 1) rounded micrite (Fig. 7.4A), micro-rhombic micrite (Fig. 7.4B) and compacted anhedral micrite (Fig. 7.4C) (Lambert et al. 2006). The rounded micrites contain rounded microspars and are found at the top of microporous oil-filled reservoirs. The micro-rhombic micrites are observed in the middle-base of the reservoir horizons which are oil or water filled. The microspars within this fabric are euhedral-subhedral and have punctic

(infrequent points and irregularities on crystal surface) to serrate (regular points on crystal surface) crystal contacts. The compact anhedral micrites are found near stylolite horizons, within the reservoir bases and flanks. The microspars within the fabric are subhedral-anhedral with serrate to coalescent contacts. Within the lower porosity fractions (mid-lower reservoir) the microspars are >4.5µm whereas within highly porous sections (upper reservoir) the microspars are <3.5-4µm (Lambert et al. 2006). Rounding of the microspars within the upper reservoir has reduced their sizes by 30% in comparison with euhedral microspars within the mid-lower reservoir (Lambert et al. 2006).

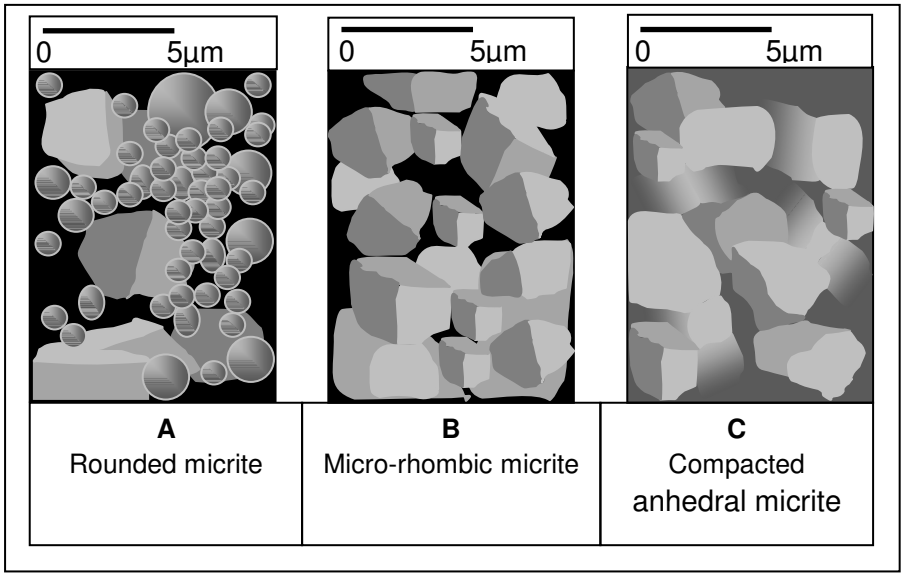

Figure 7.4: micropore fabrics of Jurassic and Cretaceous carbonates of the Middle East. A) The most porous fabric which is associated with the upper components of reservoirs, B) this fabric is associated with the middle and lower portions of reservoir horizons and C) the most impermeable fabric which is associated with stylolite horizons. The cubes represent 3-4µm microspars whereas the spheres represent 1-2µm rounded microspars (redrawn from Lambert et al. 2006).

The descriptions of the cement fabrics from Cantrell & Hagerty (1999) provide two different categories for the micropores between meteoric cements and within pore-filling burial calcites, which in reality are the same (Figs.7.2C and 7.2D). The description does not provide any information about the textures of the microporosity within the matrix and the grains (Cantrell & Hagerty 1999) (Figs. 7.2A and 7.2B). The description of the micropore fabrics from Moshier (1989a) do not mention the smaller rounded micrites within the idiotopic texture which are unique to this fabric and are therefore important (Fig. 7.3A). The descriptions from Lambert et al. (2006)

provide information about both the shapes of the microspars and the overall fabrics, including the rounded microspar. However Lambert et al. (2006) used 'micrites' to describe a fabric composed of microspars. Both these terms have different definitions and therefore the term micrite for describing micropore fabrics will not be used within this study. In general, the descriptions of the micropore fabrics within this study are based on the terms used by Lambert et al. (2006).

7.1.2 Origins of microporosity

There are many hypotheses as to how micropore fabrics have developed. The formation of microporosity is variously attributed to processes that have occurred during syn-deposition, shallow burial, through meteoric processes, intermediate burial and deep burial.

Micropore formation at syn-deposition

Studies by Kaldi (1989) suggest that micropore formation within the Kee Scarp reef complex of Northwest Territories, Canada had occurred very early, prior to the deposition of the overlying Canol shales. The process of micropore formation within bioclasts is outlined by Kaldi (1989). The first phase is labelled as incipient microporosity and is the product of neomorphic replacement of stromatoporoid components into optically continuous LMC. The cleavage planes (incipient microporosity) within LMC would have allowed for the circulation of mixed marine and meteoric fluids undersaturated in LMC to percolate through the crystal causing dissolution (through solution-reprecipitation reactions) (Fig. 7.5). Further dissolution led to larger micropores being developed, allowing for larger volumes of corrosive fluids to enter. This mechanism led to the collapse of some spar crystals, to the rounding of some spar crystals and the development of an enhanced micropore network which Kaldi (1989) has labelled as mature microporosity (Fig. 7.5).

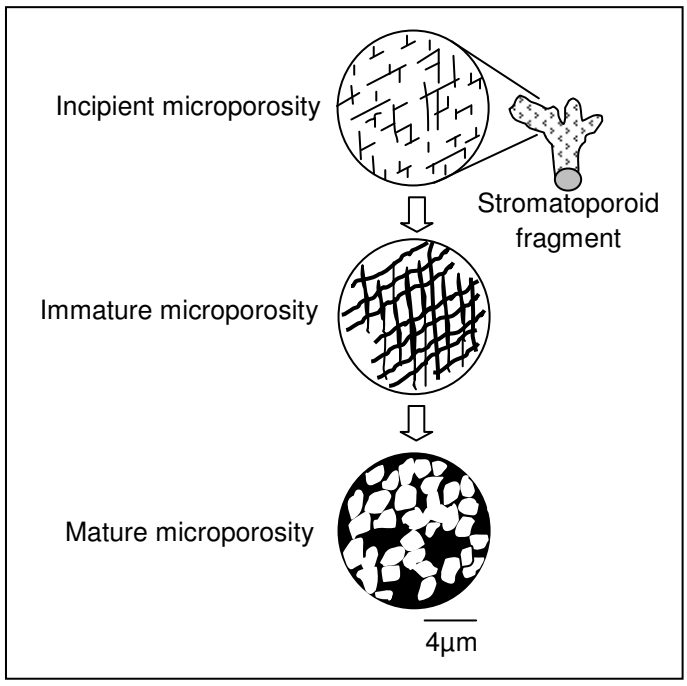

Figure 7.5: Microporosity is present within bioclasts by the enhancement of micro fractures (redrawn from Kaldi 1989).

Micropore formation during mineral stabilisation

On the West Andros Island in the Bahamas, the Holocene aragonite muds are stabilised to LMC (Steinen 1982). In places, there are LMC microspars that have precipitated into the aragonite moulds implying the process of neomorphism. The original aragonite needles are seen under SEM protruding out from LMC microspars suggesting that LMC in some places had precipitated directly onto precursor minerals, engulfing and enlarging them to form microspar (Steinen 1982). The process of aragonite mud stabilisation involves the precipitation of LMC onto the aragonite needles along with aragonite dissolution and the neomorphism of LMC microspar (Steinen 1982).

The Pliocene and Pleistocene micrites from South Florida and the Great Bahama Bank are compared with modern Holocene equivalents (Lasemi & Sandberg 1984). The amount of aragonite within Holocene micrite from the Great Bahama Bank is 68-99%. The high amount aragonite in the modern equivalents, coupled with abundant aragonite relics within the LMC microspars within the Pliocene and Pleistocene micrites, suggests the Pliocene and Pleistocene micrites had an aragonite

precursor (Lasemi & Sandberg 1984). An observed difference under SEM between Aragonite Dominated Precursor (ADP) micrites in comparison with (low Mg) Calcite Dominated Precursor (CDP) micrites is only the ADP micrites contain pits and aragonite relics within the LMC microspars (Lasemi & Sandberg 1984). The ADP micrites do not appear to have formed from aggrading neomorphism as this process would have completely removed all the aragonite (Lasemi & Sandberg 1984).

Similar void fill cements are observed within microspars from the Bahamas by Lasemi & Sandberg (1984), in comparison with studies from Steinen (1984). There may have been an early cementation episode within the South Florida Pliocene and Pleistocene sediments during mineral stabilisation engulfing the precursor aragonite and HMC (Lasemi & Sandberg 1984). This possibility may explain the porosity contrast between the Holocene and the Pliocene and Pleistocene sediments. The original porosity of the modern sediments is 50-70% whereas within the ADP sediments (Pleistocene and Pliocene sediments) it is commonly <5% (Lasemi & Sandberg 1984). The sediments were not significantly buried to account for the porosity loss from mechanical compaction (Lasemi & Sandberg 1984). There has clearly been a phase of cementation reducing the amount of porosity during the transformation from aragonite to LMC. The presence of an aragonite precursor instead of a LMC one may have controlled the amount of micropore retention during mineral stabilisation.

Within the Shu'aiba Formation and the Sajaa Field, eastern U.A.E., Moshier (1989a) has determined that the most important diagenetic event for redistributing carbonate and forming the micropore systems was mineral stabilisation and the precipitation of microspars. Several lines of evidence suggest that the microspars have formed early during the Shu'aiba burial history: 1) microspars within the Shu'aiba matrix have a $\delta^{87}Sr/\delta^{86}Sr$ similar to the range presumed for Cretaceous seawater, 2) a range in $\delta^{18}O$ values close to -4‰ and 3) a narrow range in $\delta^{13}C$ values for the microspars. While the narrow range in $\delta^{13}C$ values discounts microspar formation through meteoric diagenesis, the depleted $\delta^{18}O$ values of -4‰ suggests formation is due to the circulation of more depleted $\delta^{18}O$ fluids during

progressive burial (Moshier 1989a). By using the equation provided by O'Neil et al. (1969), along with assuming SMOW (0‰) for the interstitial porewaters and a geothermal gradient of 28.8°C/km, Moshier (1989a) has calculated the depths of formation of the Shu'aiba Formation matrix. The temperature of formation for the microspars is 36-41°C and 380-550m burial depth.

The original precursor is determined by Moshier (1989a) by extrapolating the Sr and Mg contents of the microspars to higher concentrations: the precursor was dominantly LMC and HMC. The formation of the porous crystal frameworks (hypidiotopic fabric: Fig. 7.3B) is associated with the growth of microspars calcite and the reduction of pore space during mineral stabilisation.

Cathodoluminescence images of the blocky calcite cements (within the idiotopic fabric: Fig. 7.3A) show the transition from non-CL cements to CL cements (Moshier 1989a). Trace element analysis across this transition show an increase Mn and Sr but a decrease in Mg (Moshier 1989a). The non-CL cements are therefore assumed to have precipitated as LMC directly from marine pore waters (Moshier 1989a). The CL luminescence and chemistry of the microspar suggests microspar formation was complete after the formation of the non-CL cements but contemporaneous with the start of the large mould and vug occlusion with equant CL cements. The formation of the CL cements is suggested to have occurred at deeper burial depths with respect to mineral stabilisation, within the intermediate burial realm, as these LMC spars have more negative $\delta^{18}O$ values than the surrounding microspars (Moshier 1989a).

Chemical compaction and the formation of stylolites are constrained by Moshier (1989a), from 600-900m burial depth (Dunnington 1967), forming the non-porous crystal mosaics (xenotopic fabric: Fig. 7.3C). The effect has reduced the micropore space but increased the size of individual microspars. The precipitation of an extensive micropore-fill cementation episode is attributed with these effects as opposed to enhanced crystal growth (Moshier 1989a) (Section 5.7.1).

Only the later introduction of corrosive fluids along wispy stylolites is interpreted to have caused dissolution and microporosity enhancement in the deep burial realm (Moshier 1989a). Carbon dioxide driven off by the transformation of oil to methane

would form acidic porewaters, which is measured at 1560ppm (Moshier 1989a). This concentration level is deemed as insufficient for widespread porosity enhancement by Kharaka et al. (1983). This, combined with the low organic content within the Shu'aiba Formation, has lead Moshier (1989a) to conclude that the onset of acidic porewaters and oil are derived from another source, perhaps delivered by a phase of basinal fluid expulsion during deep burial.

Therefore mineral stabilisation was the dominant process on forming the microspars. The formation of macrospars during intermediate burial only caused pore occlusion and no new micropore formation. Only the actions of late dissolution from the circulation of externally sourced fluids further enhanced the micropore fabrics (Moshier 1989a).

Micropore formation by meteoric diagenesis

Budd (1989) suggests that microspars are products of mineral stabilisation due to meteoric circulation within the Kharaib and Shu'aiba Formations (Budd 1989). Selective reduction of Mg and Sr along with lower $\delta^{18}O$ values (-4.5‰ to -6‰: in comparison with -2.5‰: estimated value for Cretaceous biogenic sediment by Moldovanyi & Lohmann 1984) indicate meteoric water circulation which caused mineral stabilisation, flushing of Mg and Sr, and the depletion in $\delta^{18}O$ to form the microspars within unconfined and confined aquifers (Budd 1989). However Budd (1989) does not fully explain why more negative $\delta^{18}O$ values reflect meteoric diagenesis, over pore-water interaction through increasing temperature and burial.

The LMC microspars within the West Stuart City rocks of Texas contain elevated levels of Mg, indicating a HMC precursor (Perkins 1989). The slightly depleted $\delta^{18}O$ values (-3.9‰ to -4.7‰) of the microspars imply either mineral stabilisation due to restricted flow meteoric (phreatic) water fluxes or marine water fluxes at higher temperatures during to burial (Perkins 1989).

Within the Pleistocene and Oligocene Enewetak Atoll sediments, the concentration of aragonite and HMC in the presence of undersaturated freshwater has caused widespread dissolution. Both aragonite and HMC are far less stable than LMC, and dolomite, at near surface and the burial realm (Saller & Moore 1989).

Dissolution has therefore left a 'meshwork' of aragonite needles creating microporous aragonite 5-10m below palaeofreshwater lenses (Saller & Moore 1989). Aragonitic microporosity is described as a halfway house, through dissolution, towards complete recrystallisation to a 'calcitised aragonite' fabric occluding all the depositional microporosity (Saller & Moore 1989).

The dominant porosity types in the Cotton Valley Limestone in East Texas, from the Indian Rock Gilmer, Teague Townsite and Overten fields was determined to be intragranular with intracrystalline microporosity within calc arenite facies (Ahr 1989). This microporosity is cross-cut by stylolitisation, compaction fracturing, fracture filling of calcite, and rhombic dolomite and quartz replacement (Ahr 1989). This suggests that microporosity formation was formed by an early diagenetic process.

The microporous ooids within the Overton Field have heavier $\delta^{18}O$ values (-4.2‰ to -5.7‰) than the surrounding spar cements (-6.7‰ to -9.1‰) (Ahr 1989). Therefore the microporosity is suggested to have formed from the recrystallisation of the ooids in the presence of freshwater followed by spar growth in warmer, deeper sub surface waters (Ahr 1989). Therefore micropore formation within the Cotton Valley Limestones occurred in a near surface environment from the possible introduction and circulation of freshwater.

Micropore formation by shallow burial dissolution

There are two phases of micropore formation within the Kee Scarp carbonates in Northwest Territories (Al-Aasm & Amzy (1996). The initial formation of microporosity is associated by Al-Aasm & Amzy (1996) with the stabilisation of reef components by circulation of marine derived porewaters slightly enriched in $\delta^{18}O$ at 40-50°C. The second generation of microporosity has formed during shallow-intermediate burial (Al-Aasm & Azmy 1996). There are three main lines of evidence: 1) Micro cracks have formed from mechanical compaction within the stromatoporoid fragments which are surrounded by microporosity (microporosity has formed after mechanical compaction and the formation of the micro-cracks), 2) the micropores are not compacted meaning they have formed within the burial realm after the majority

of mechanical compaction and 3) the leaching of echinoid ossicles that still contain micropore fabrics (the micropores must have occurred in the burial realm, as echinoid fragments are rarely dissolved out in freshwaters systems) (Al-Aasm & Azmy 1996).

Micropore formation by deep burial dissolution

Comparing fluid inclusion microthermometry with $\delta^{18}O$ isotopes, within single LMC spars, is used by Esteban & Taberner (2003) to determine the causes of carbonate dissolution at depth. The decrease in $\delta^{18}O$ negativity within successive cement zones after a dissolution event suggests "mixing corrosion by formation fluids and an externally sourced fluid at high temperature" (Esteban & Taberner 2003). Therefore the onset of acidic porewaters, hydrothermal fluids and salt brines could all act to dissolve microspars and enhance micropore systems.

The onset of hydrocarbons combined with carbonic acids and carbon dioxide are also interpreted as causes of dissolution of LMC microspar in the Barremian Kharaib Formation by Lambert et al. (2006). The timing of dissolution is constrained by Lambert et al. (2006) to the deep burial realm. The rounded microspars were euhedral-subhedral during microspar formation which is indicated by euhedral pits on burial macrospar surfaces. The burial macrospar has clearly engulfed the surrounding microspars when they were euhedral, before dissolution, constraining dissolution after burial spar formation in the deep burial realm (Lambert et al. 2006). This makes rounding and the generation of the micropore networks secondary (Lambert et al. 2006). The microspars cannot have formed by mineral stabilisation, but instead by dissolution during burial (Lambert et al. 2006).

The retention of the micropore fabrics, coupled with little dissolution before oil charge requires limited porewater movements: this situation would occur at an oil-water front (Lambert et al. 2006). The preservation of microporosity after dissolution suggests that oil flooded the Kharaib reservoirs immediately after dissolution, preventing further cementation of the micropores during increased burial (Lambert et al. 2006).

The amount of microspar dissolution is gauged through size reduction and rounding of the microspar (Lambert et al. 2006) (Fig. 7.6). The more dissolution, rounding and size reduction had produced the best reservoirs with the highest porosity and permeability relationships (rounded microspars: Fig. 7.4A) (Lambert et al. 2006). The size reduction of the microspars equates to 30%, consequently enhancing the surrounding microporosity. Dissolution is very important when regarding the development of the most interconnected micropore networks within the Kharaib Formation (Lambert et al. 2006) (Fig. 7.6).

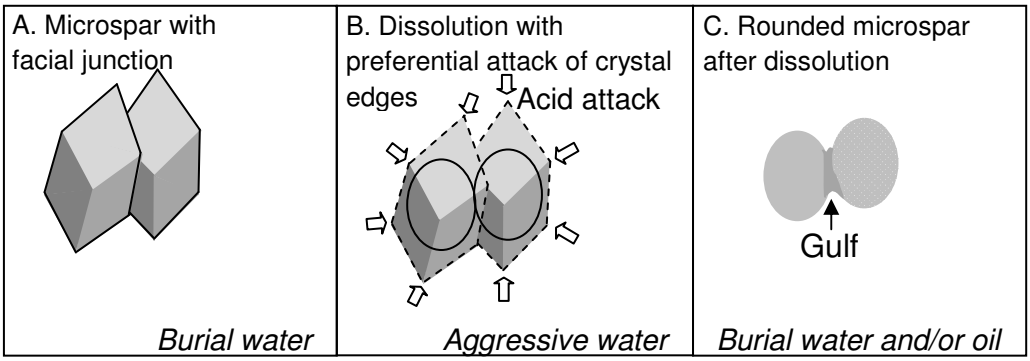

Figure 7.6: process of microspar dissolution within the Kharaib Formation. A & B) Oil charge introduces corrosive fluids that round the microspar, (C) the carbonate is then redistributed to occlude the gulfs separating the microspars to form impermeable barriers (redrawn from Lambert et al. 2006).

The Upper Jurassic Haynesville oolitic grainstones in East Texas contain considerable micromouldic porosity within ooids (Dravis 1989). Only the base and the top of these grainstone units are cemented, which is due to the expulsion of solutes from extensive pressure solution and compaction of the bounding micritic facies (Dravis 1989). These grainstones have undergone much chemical compaction and are heavily stylolitized. There is an equal amount of micromoulds distributed between the ooids and the stylolite horizons. The stylolites appear to 'float' within the microporous regions while the microporous ooids show no signs of compaction: compaction would have reduced the microporosity if it had formed before burial. All this evidence suggests that micromouldic formation had not occurred until deep burial, during or after the formation of stylolites (Dravis 1989). Many ooids are coated with a layer of bitumen which appears to have protected the ooid from micropore formation, suggesting that micropore formation had occurred after

bitumen emplacement in the deep burial realm (Dravis 1989). Oyster shells have developed similar micromoulds in comparison with ooids. The oyster shells are composed of LMC, and would not have been subject to dissolution and the development of a micropore fabric during mineral stabilisation. Therefore these micromoulds are products of dissolution caused from the upward migration and circulation of aggressive fluids at deep burial (Dravis 1989).

7.2 Lekhwair and Lower Kharaib Formations: this study

7.2.1 The proportion of microporosity

The amount of microporosity is calculated for the majority of the samples (Figs. 7.9, 7.12, 7.15, 7.18 and 7.21: Appendix 5) within the Lekhwair and Lower Kharaib Formations using the method from Cantrell & Hagerty (1999) (Section 1.2). This section is split into 5 sub sections (for the five wells): each has three Secondary Electron images of the micropore fabrics from three separate intervals within selected 4th order HFC's. The same positions are then labelled on porosity and permeability plots, and to bar charts showing the proportion of microporosity in comparison with the total pore volume. These comparisons enabled the micropore fabrics to be directly linked to the amount of porosity, permeability and to the amount of open micropores.

Well 1 (water leg)

Figure 7.7 shows three locations within Cycle 1, Well 1, and the water leg, where A) represents the cycle top, B) represents the reservoirs and the HST and C) represents the base TST micrite/mudstone (Table 7.1 for micropore fabric descriptions).

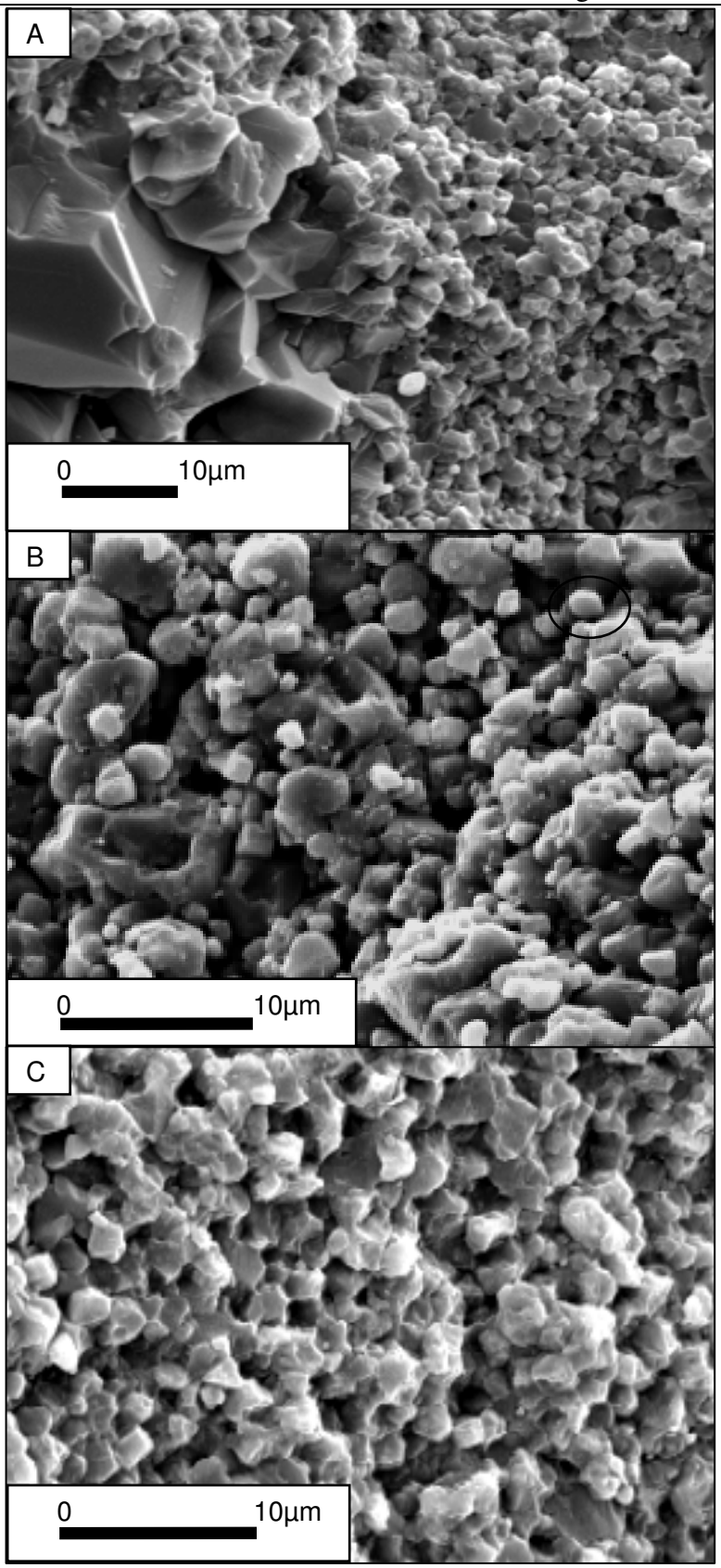

Figure 7.7: micropore fabrics of Cycle 1 in the water leg: A) the cycle top, B) the mid-late HST and C) the TST micrite/mudstone at the base of Cycle 1. There is local cementation occluding the majority of the micropore system, leaving a small portion of microporosity open throughout the entire HFC. Some of the smaller 1-2µm microspars show some rounding (see circle on B).

All three images in Figure 7.7 show a degree of cementation and micropore occlusion: there are still some micropores open at all three positions within Cycle 1 within the water leg. The positions are placed on Figure 7.8 in relation with the stratigraphy and porosity and permeability data. Locations A and B show a porosity of ~20% with location C showing a porosity of ~10% (Fig. 7.8A). The permeability ranges from 2mD at B down to <1mD at A and C (Fig. 7.8B).

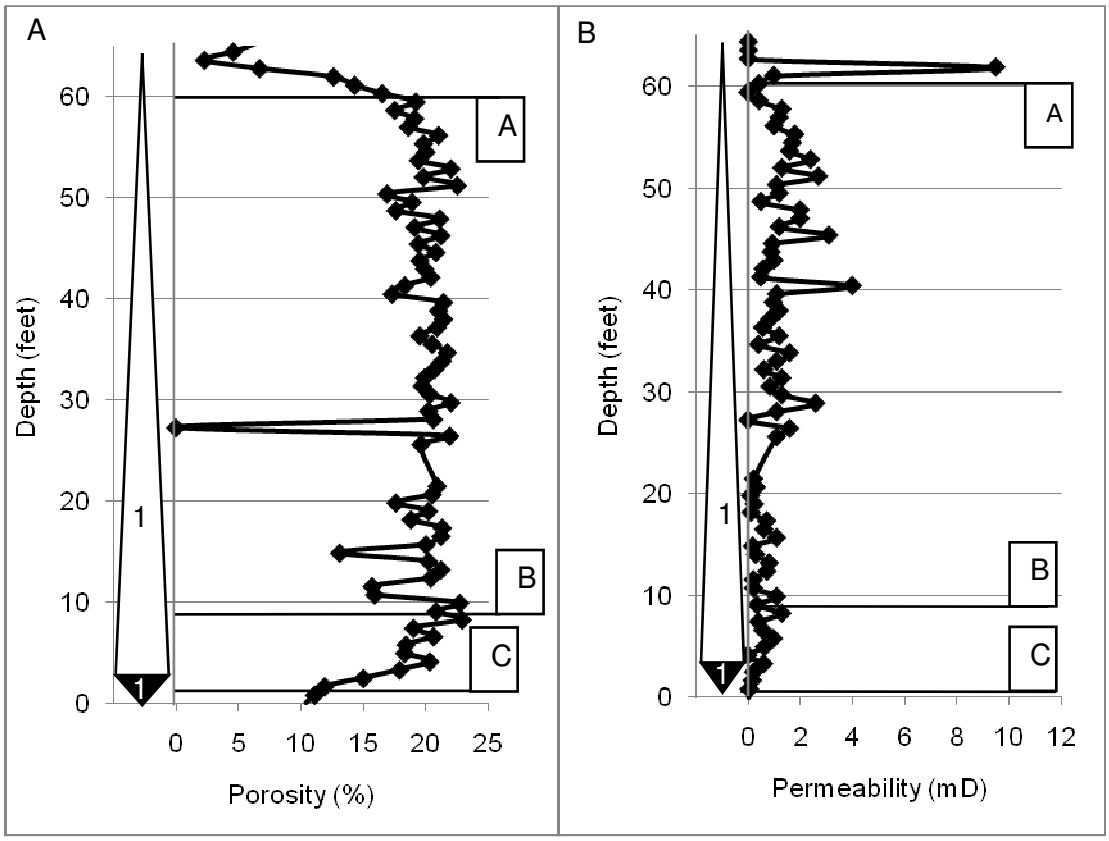

Figure 7.8: porosity and permeability data for Cycle 1 in the water leg: A) porosity data B) permeability data. Positions A, B and C directly relate to the Secondary Electron images in Figure 7.7. The black triangles represent the TST while the white triangles represent the HST of Cycle 1.

The proportion of micropores within the water leg samples and Well 1 almost equals the total proportion of open porosity with respect to the rock volume at location A, B and C (Fig 7.9). The proportion of microporosity is near 100% of the total open pore volume of the samples (Fig. 7.9).

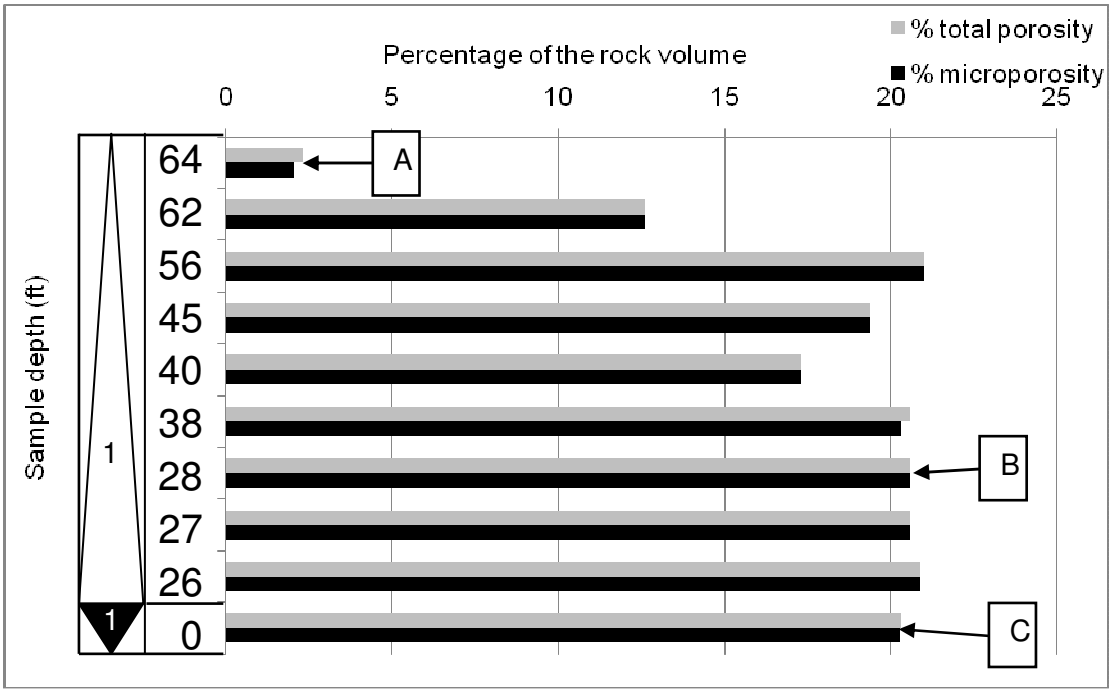

Figure 7.9: percentage of total porosity and micropores within Well 1 with respect to the total rock volume. The letters A, B and C directly relate to the micropore fabrics in Fig. 7.7. The depths for the specific samples are on the y-axis (Section 1.2 for depth calculations). The black triangles represent the TST's while the white triangles represent the HST's.

Well 2 (transition zone)

Figure 7.10 shows three locations within Cycle 4a, Well 2, and the transition zone, where A) represents the cycle top, B) represents the mid-late HST and C) represents the TST micrite/mudstone at the base of Cycle 4a (Table 7.1 for micropore fabric descriptions).

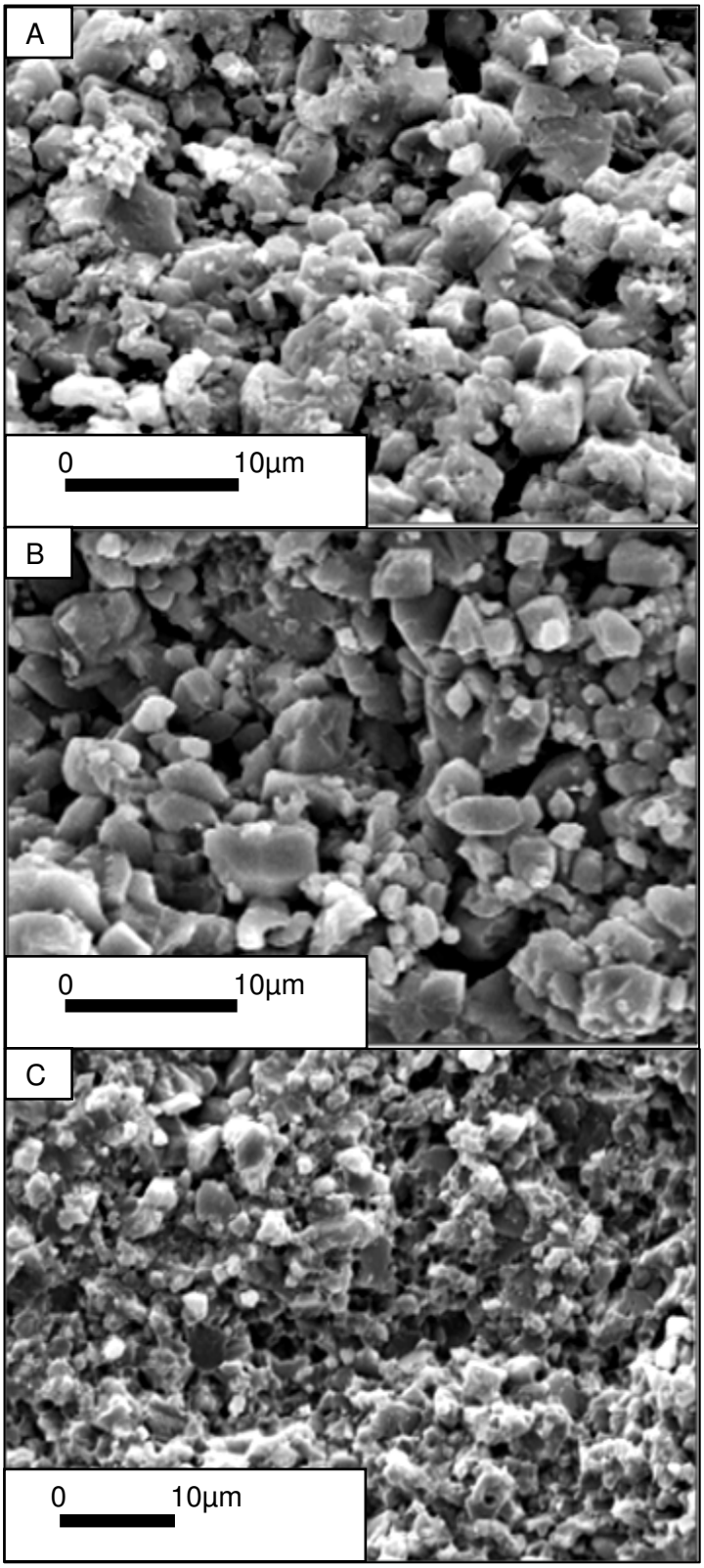

Figure 7.10: micropore fabrics of Cycle 4a in the transition zone: A) at the cycle top, B) the mid-late HST and C) the TST micrite/mudstone at the base of Cycle 4a. Although there is local cementation occluding a minority of the micropore system, a significant portion of microporosity is still open throughout most of the entire HFC.

The most interconnected micropore fabrics appear to be within the mid-late HST of Cycle 4a (Fig. 7.10). Position A has ~10%, position B has ~15% and position C has 1.2% porosity (Fig. 7.11A) The amount of permeability at positions A and C is <1mD, while at position B it is ~10mD (Fig 7.11B).

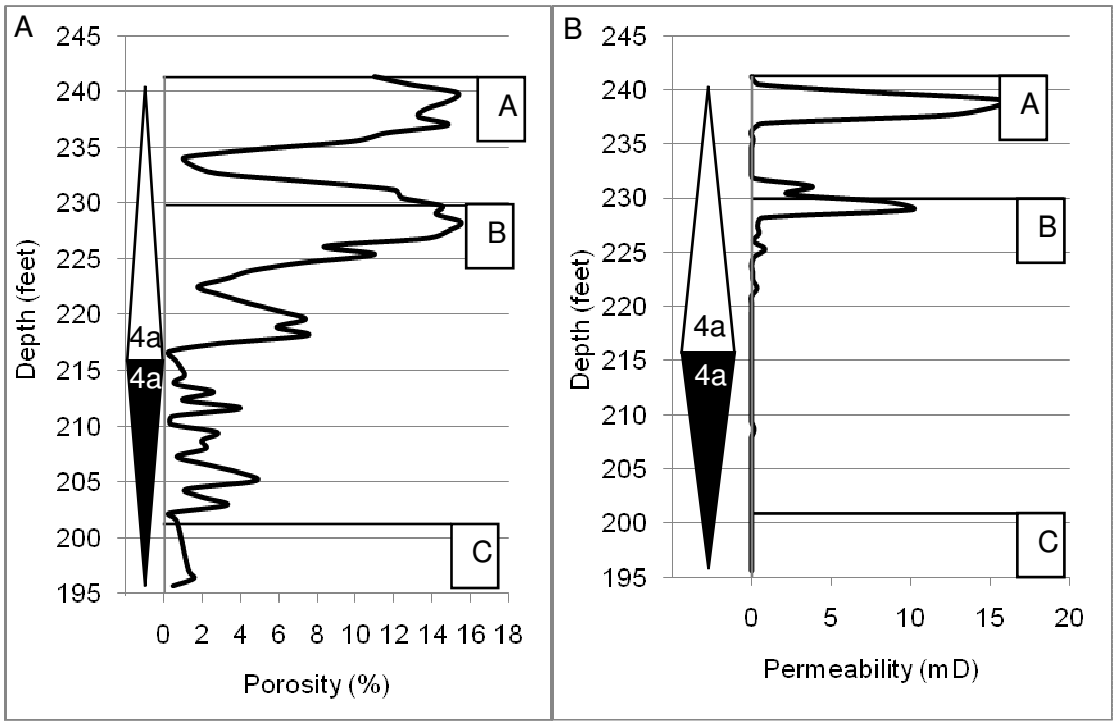

Figure 7.11: porosity and permeability data for Cycle 4a in the transition zone: A) porosity data B) permeability data. Positions A, B and C directly relate to the Secondary Electron images in Figure 7.10. The black triangles are the TST's and the white triangles are the HST's within Cycle 4a.

The proportion of microporosity in most samples is near 90% of the total open pore volume, which increases to near 100% in the base of most HFC's (Fig. 7.12). Apart from Cycle 7a where there are no samples from the TST, the base of the TST for Cycles 4a, 4b, and 6 have samples where almost all the pore volume is microporosity. In both Cycles 4a and 4b, where there are samples for the HST's and TST's, the proportion of microporosity generally increases into the TST and the base of each HFC from the HST (Fig. 7.12). However there is one anomaly where only 40% of the total open pore volume is microporosity near the base of the TST of Cycle 4b.

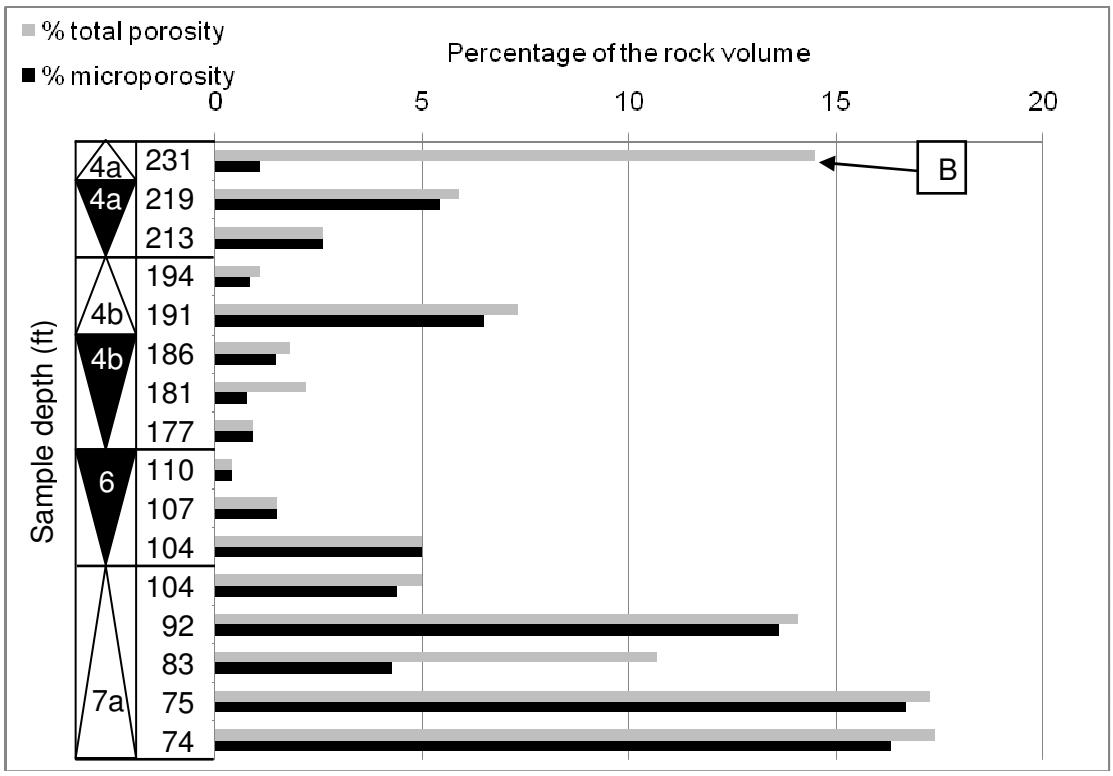

Figure 7.12: percentage of total porosity and micropores within Well 2 with respect to the total rock volume. B directly relates to the micropore fabric in Fig. 7.10B. The depths for the specific samples are on the y-axis (Section 1.2 for depth calculations). The black triangles represent the TST's while the white triangles represent the HST's.

Well 3 (oil leg)

Figure 7.13 shows three locations within Cycle 4a, Well 3, and the oil leg, where A) represents the reservoir and the mid-late HST, B) represents the late TST and C) represents the basal TST micrite/mudstone of Cycle 4a (Table 7.1 for micropore fabric descriptions).

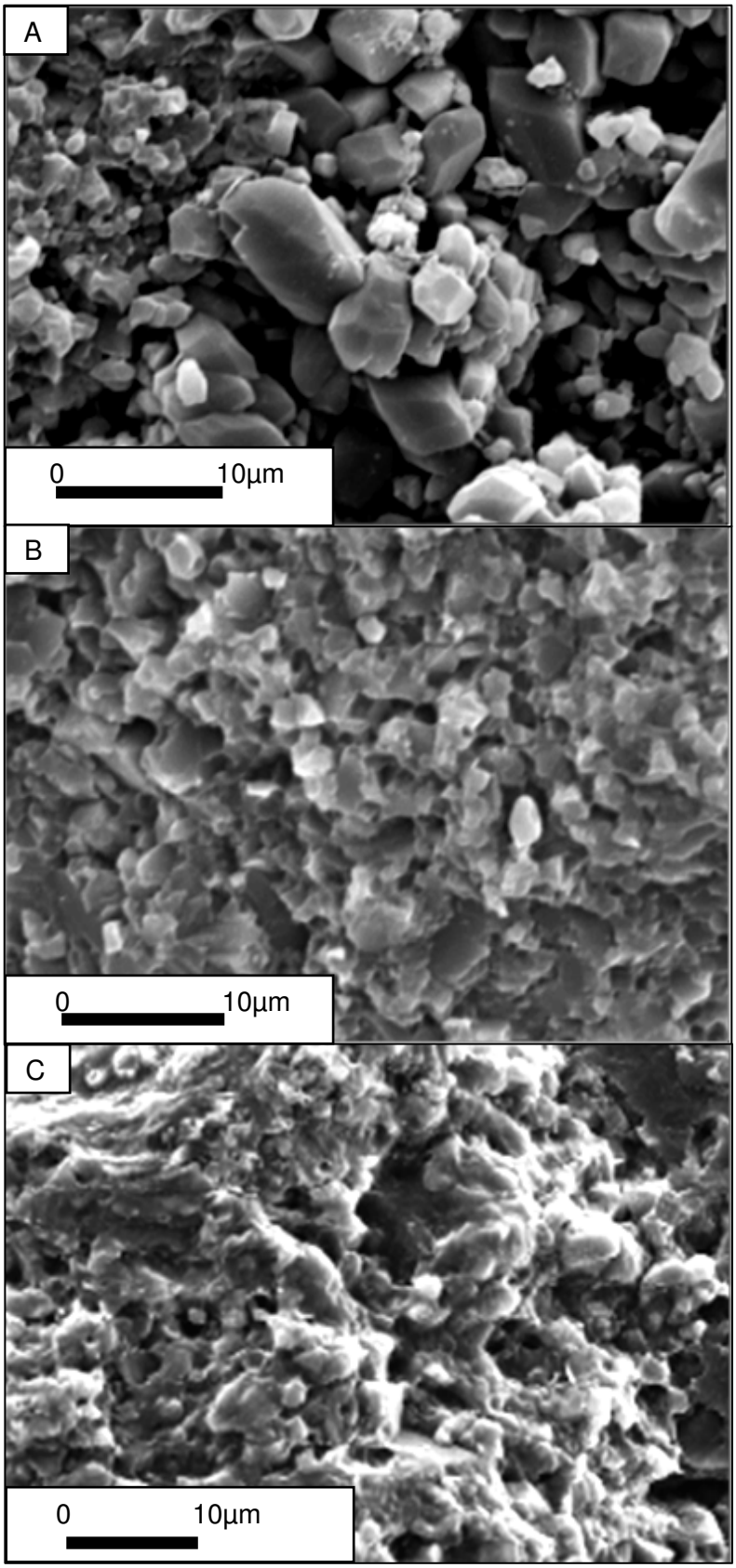

Figure 7.13: micropore fabrics in Cycle 4a and the oil leg: A) the mid-late HST, B) the late TST and C) the TST micrite/mudstone at the base of Cycle 4a. There is local cementation occluding the majority of the micropore system, a portion of microporosity is still open throughout the entire HFC.

On Figure 7.13, position A shows a slightly larger proportion of open micropores with position B and C showing more progressive micropore occlusion towards the base of Cycle 4a. The porosity reduces dramatically from position A with values of 17-18% to <1% at both B and C (Fig. 7.14A). The permeability shows the same trend with A having values of 100mD, while positions B and C have values of <1mD (Fig. 7.14B).

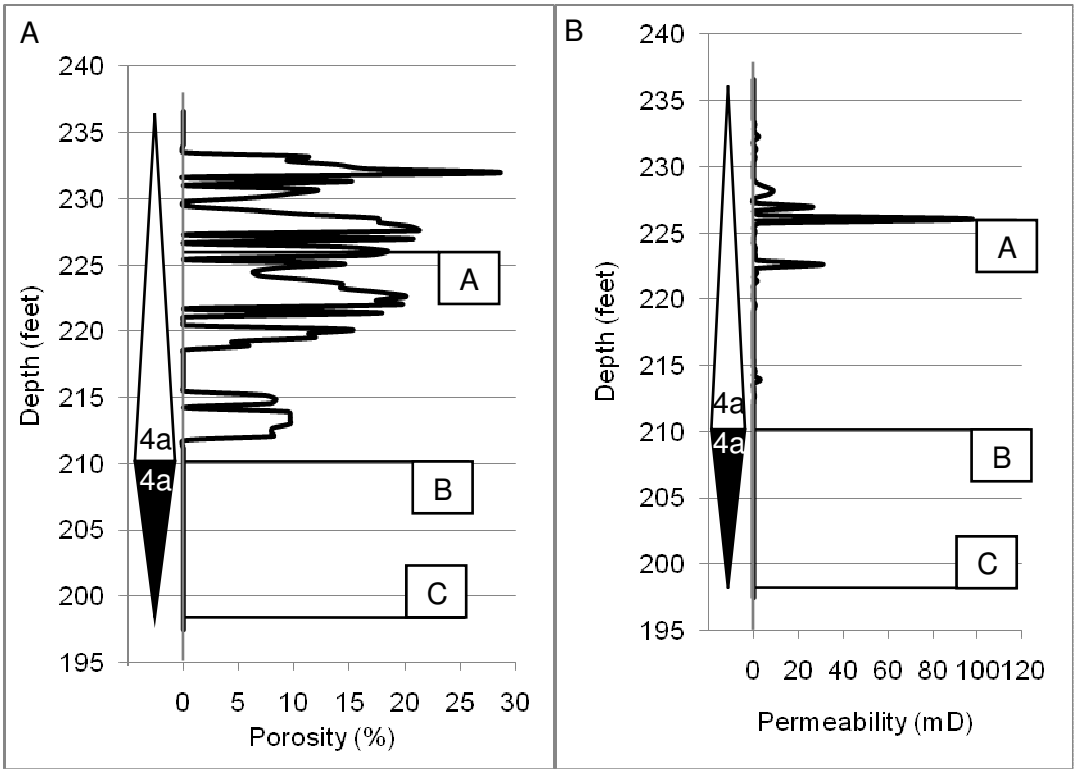

Figure 7.14: porosity and permeability data for Cycle 4a in the oil leg: A) porosity data B) permeability data. Positions A, B and C directly relate to the Secondary Electron images in Figure 7.13. The black triangles represent the TST's, while the white triangles represent the HST's of Cycle 4a.

The proportion of total open porosity in comparison with the total rock volume within the oil leg, the crest and Well 3 is greatest in Cycle 7a at the base of the Lekhwair Formation (Fig. 7.15). All the samples within Cycle 7a have 85-95% of the total open pore volume attributed to microporosity (Fig 7.15). The exception to this is a sample at the base of the HST in Cycle 7a, where only 40% of the total open pore volume comprises microporosity. However there are no samples within the TST for comparison of the microporosity proportion with the HST samples. Within Cycle 4a, where there are samples from both the HST's and TST's, the proportion of

microporosity in comparison with the total open pore volume is 30-40% in the late HST, is 75% in the mid HST, 95% in the early TST and at the base of the HFC it is almost 100% (Fig. 7.15). However the opposite trend is seen within Cycle 4b, where the proportion of microporosity in comparison with the open pore volume is smallest within the early TST at the base of the HFC of 50-60% and increases towards 90% within the overlying HST (Fig. 7.15).

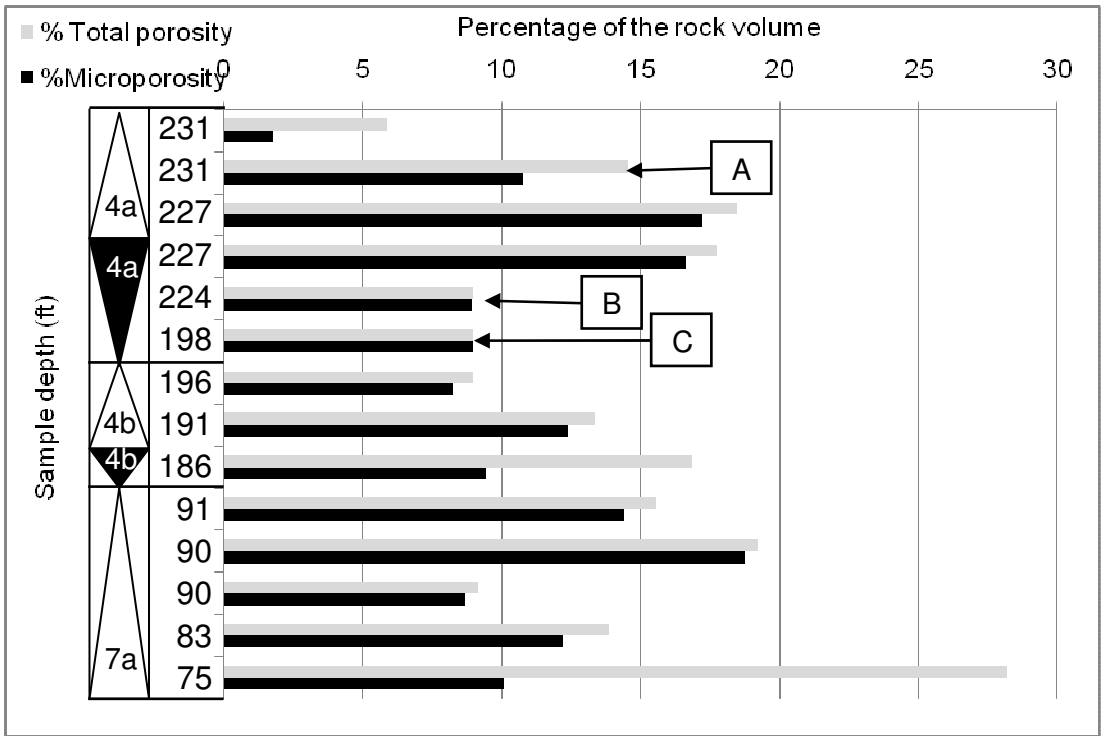

Figure 7.15: percentage of total porosity and micropores within Well 3 with respect to the total rock volume. A, B and C directly relate to the micropore fabrics in Fig. 7.13. The depths for the specific samples are on the y-axis (Section 1.2 for depth calculations). The black triangles represent the TST's while the white triangles represent the HST's.

Well 4 (oil leg)

Figure 7.16 shows three locations within Cycle 1, Well 4 and the Oil leg, where A) represents above Cycle 1 SB B) represents the reservoir and the late HST and C) represents the base TST micrite/mudstone of Cycle 1 (Table 7.1 for micropore fabric descriptions).

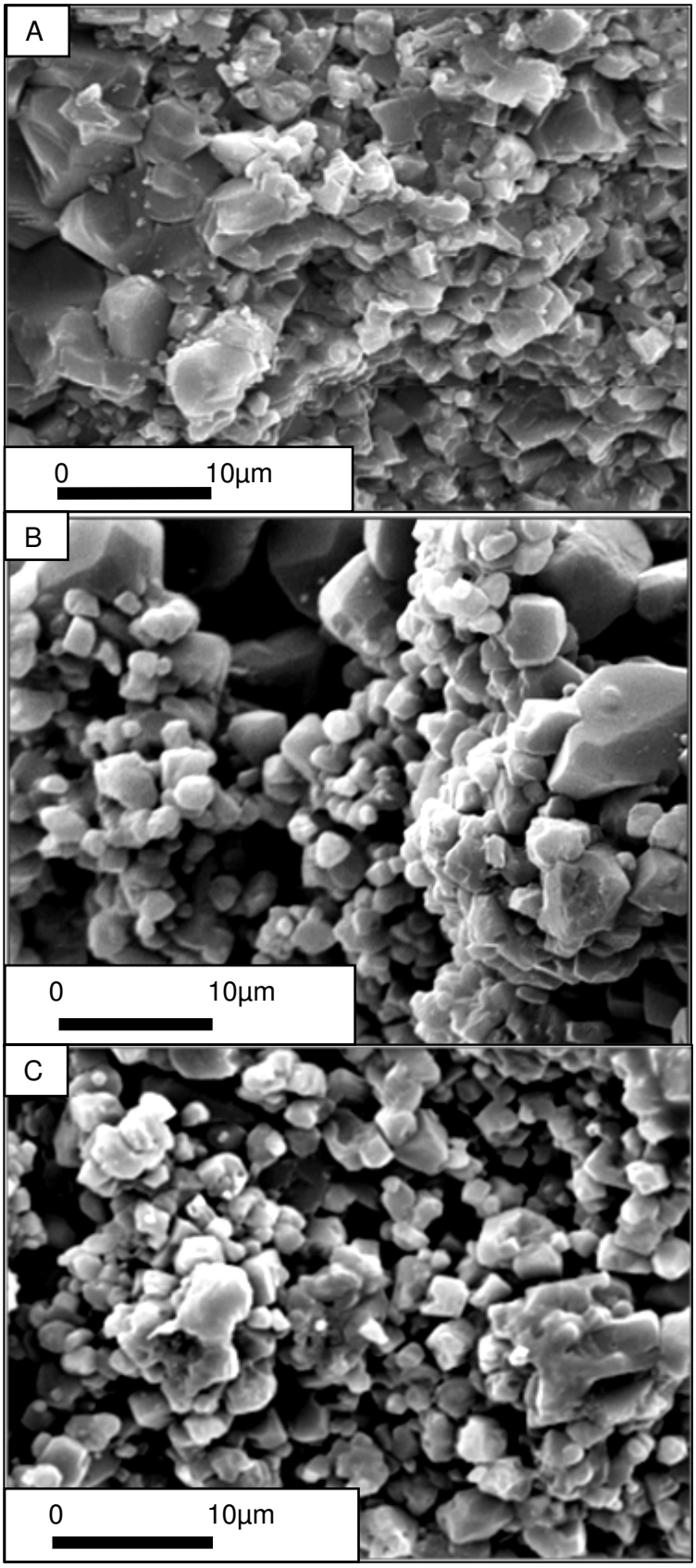

Figure 7.16: micropore fabrics within Cycle 1 and the oil leg: A) above Cycle 1 SB, B) the late HST and C) the TST micrite/mudstone at the base of Cycle 1. Although there is another pore occluding phase within Cycle 1, a significant portion of microporosity is still open throughout most of the entire HFC.

Image B on Figure 7.16, within the late HST and the reservoir, displays the most open micropore fabric in comparison with images A and C. With respect to the stratigraphy this shows that the majority of micropores are open within the reservoirs and the late HST's. The amount of porosity is drastically reduced from positions B to C, from 28% to ~2% (Fig. 7.17A), while the permeability is low for both B and C, between 1mD to 10mD (Fig. 7.17B).

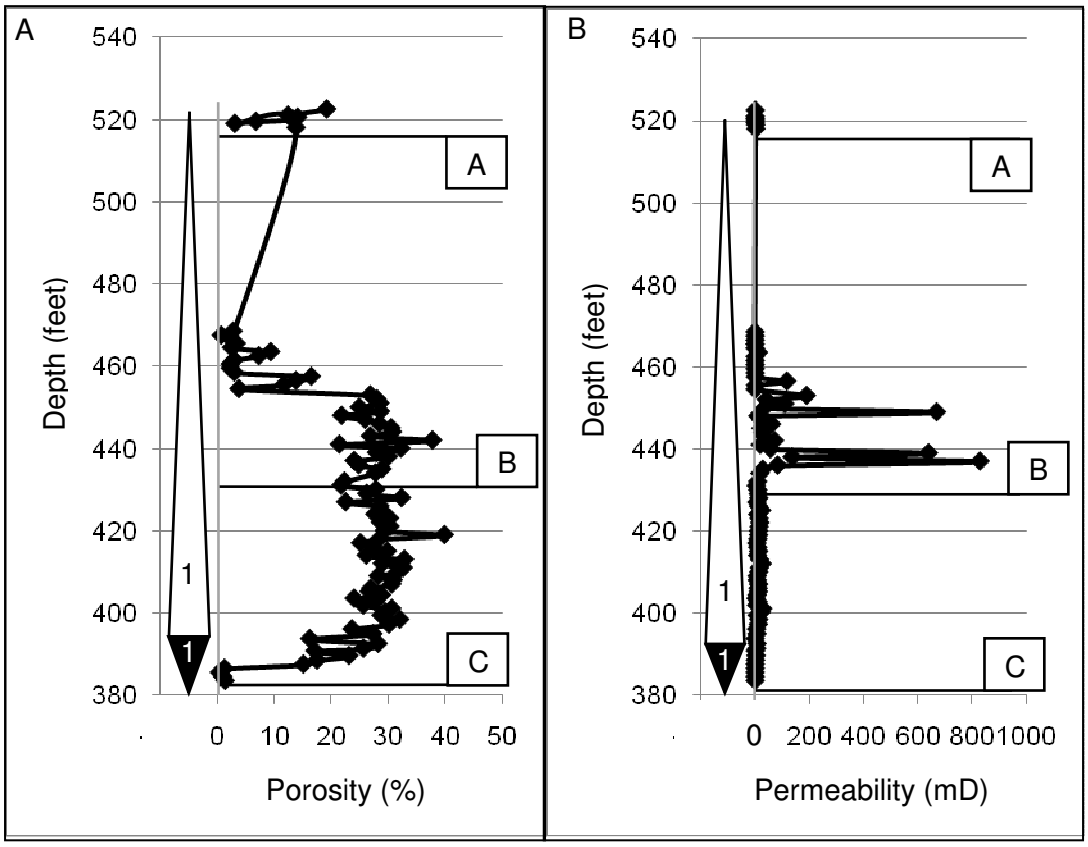

Figure 7.17: porosity and permeability data for Cycle 1 in the oil leg: A) porosity data B) permeability data. Positions A, B and C directly relate to the Secondary Electron images in Figure 7.16. The black triangles represent the TST while the white triangles represent the HST within Cycle 1.

The proportion of total open porosity in comparison with the total rock volume within the oil leg, the crest and Well 4 is greatest within the HST of Cycle 1 (Fig. 7.18). Cycle 1 has also a variable proportion of microporosity ranging from 5-90% (Fig 7.18). The average proportion of microporosity for Cycle 1 HST is 60%. The only sample within Cycle 1 that has almost all of its total open pore volume attributed to microporosity is within the TST. The proportion of open porosity in comparison with the total rock volume is very low within the TST of Cycle 6 and it

is difficult to interpret the microporosity trends (Fig. 7.18). For Cycle 4a the amount of porosity in comparison with the total rock volume is greatest within the TST, with 70-100% being microporosity, while in Cycle 4b the highest proportion of porosity is at the base of the HST of 60-70% being microporosity (Fig. 7.18). There is, however, poor sample coverage throughout Cycles 4a and 4b, and the proportion of micropores cannot be compared between the HST's and TST's.

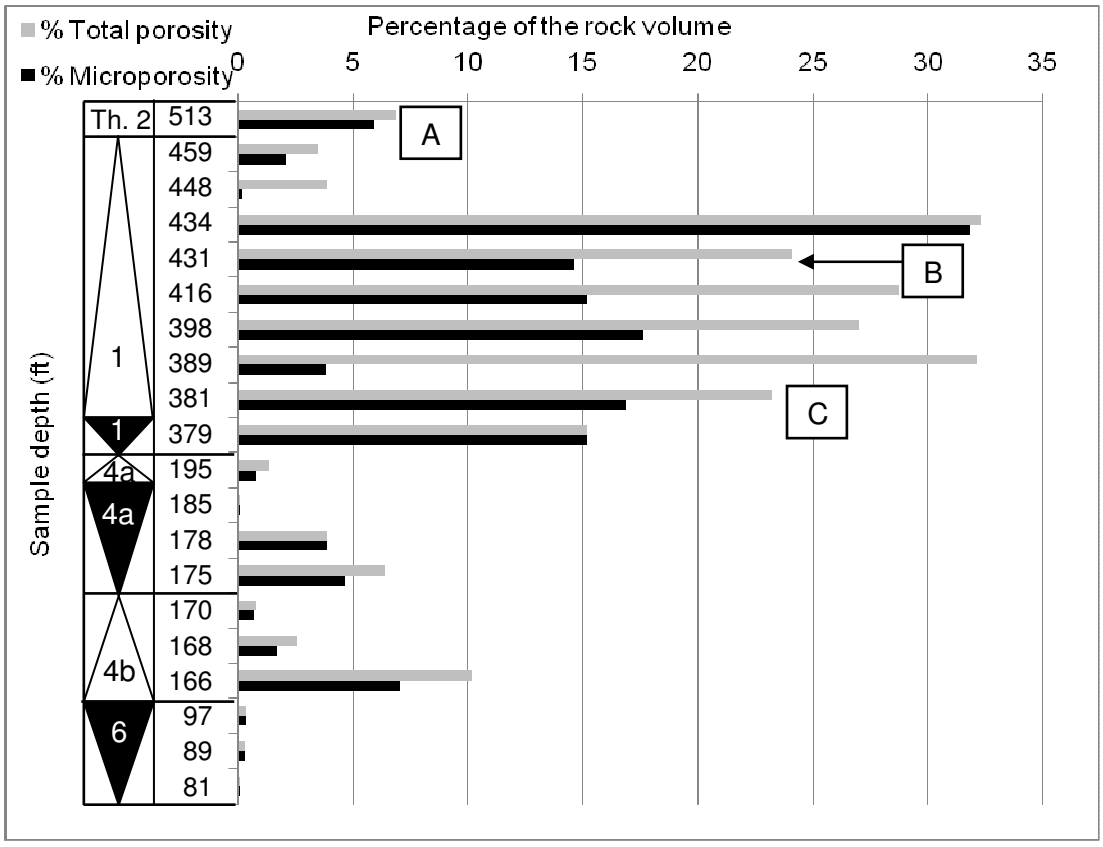

Figure 7.18: percentage of total porosity and micropores within Well 4 with respect to the total rock volume. A, B and C directly relate to micropore fabrics displayed in Figure 7.16. The depths for the specific samples are on the y-axis (Section 1.2 for depth calculations). The black triangles represent the TST's while the white triangles represent the HST's.

Well 5 (transition zone)

Figure 7.19 shows two locations within Cycles 6 and 7a, Well 5 and the transition zone, where A) represents the basal TST micrite/mudstone of Cycle 6 and B) represents the mid-late HST of Cycle 7a (Table 7.1 for micropore fabric descriptions).

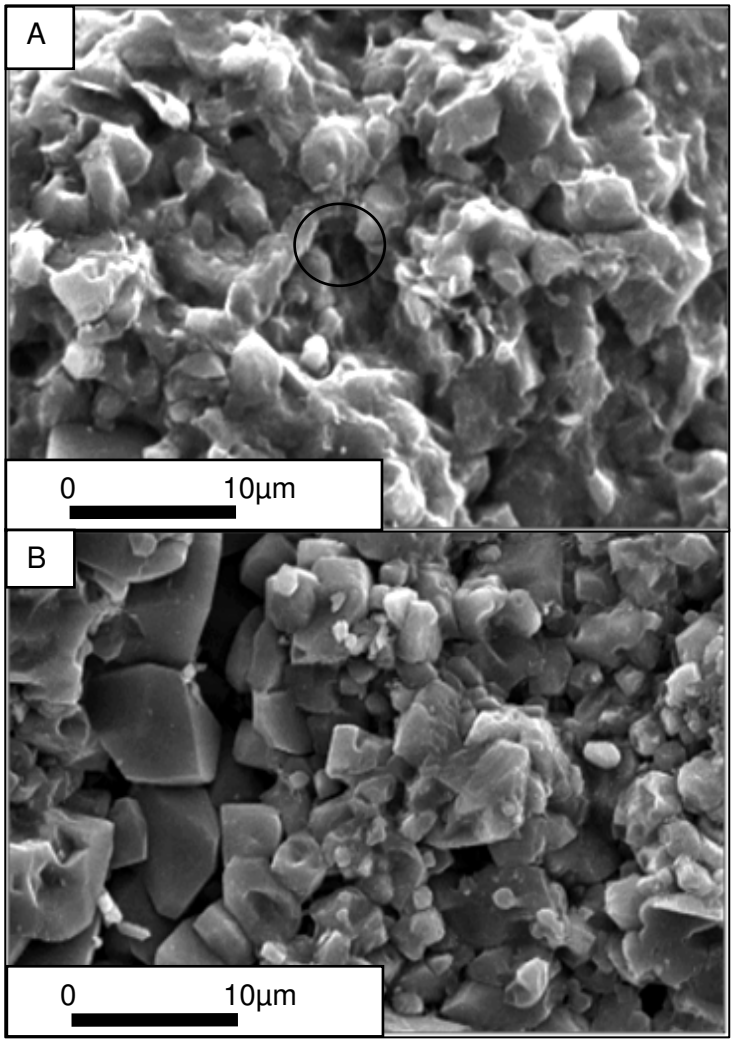

Figure 7.19: micropore fabrics of the transition zone in A) in the basal TST micrite/mudstone of Cycle 6 and B) the mid-late HST of Cycle 7a. Although there is much micropore occlusion, a small portion of microporosity is still open throughout most of the entire HFC (see circle on A).

The best interconnected micropore systems appear to be within the mid HST of Cycle 7a (Fig. 7.19). The amount of porosity is less within the TST at the base of Cycle 6 from 5% at position A to 10% at position B (Fig. 7.20A) within the HST of Cycle 7a. The permeability also decreases from 0.12mD at position B to 0.01mD at position A. (Fig. 7.20B).

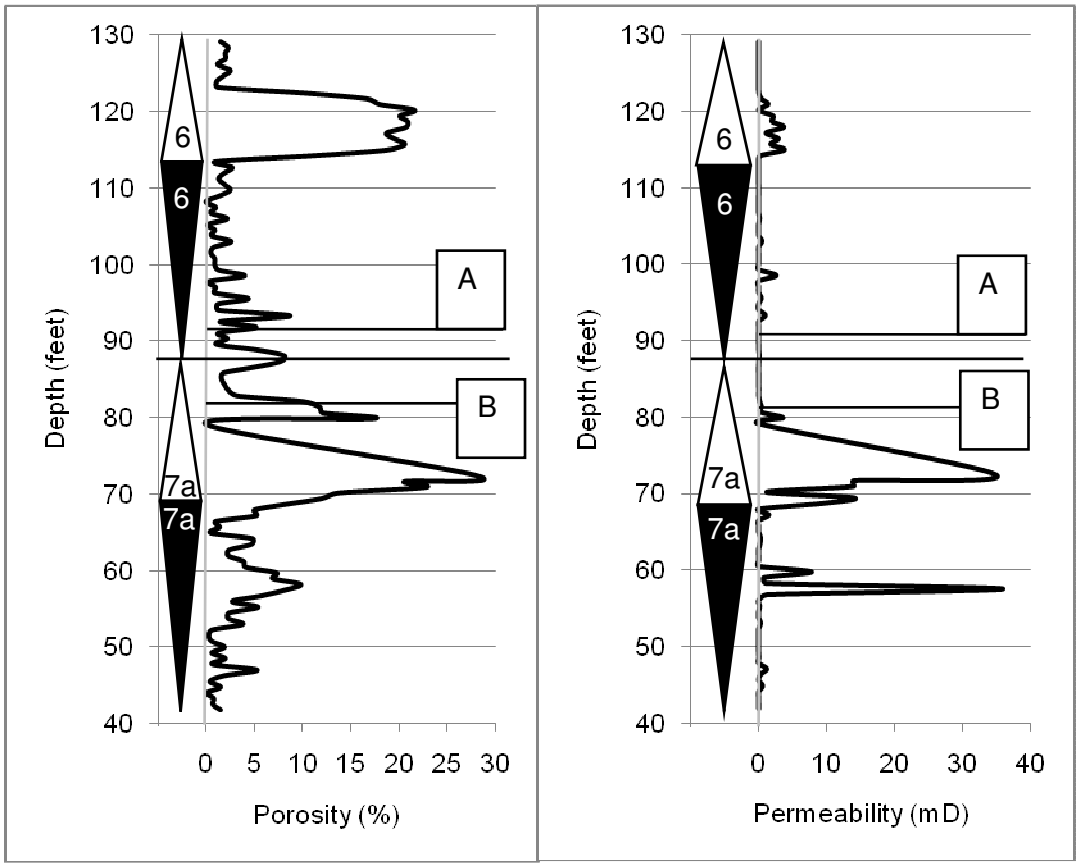

Figure 7.20: porosity and permeability data for Cycles 6 and 7a in the transition zone: A) porosity data B) permeability data. Positions A and B directly relate to the Secondary Electron images in Figure 7.19. The black triangles represent the TST's while the white triangles represent the HST's.

The proportion of total open pore volume with respect to the total rock volume within the transition zone and Well 5 is greatest within Cycle 7a and the base of the Lekhwair Formation (Fig 7.21). Within Cycle 7a the proportion of microporosity with respect to the total open pore volume is 10-20% within the late HST, with the proportion increasing to 60% in the early HST and increasing further to 90% within the TST (Fig 7.21). The proportion of microporosity in comparison with the total open pore volume in Cycle 4a is similar within the HST and the TST of 70-90% with the sample at the base of the HFC having near 100% microporosity (Fig 7.21). Cycles 3, 5 and 6 only have samples within either the HST's or the TST's and therefore a comparison throughout these HFC's is not possible, however the amount of microporosity appears to be highly variable throughout these HFC's.

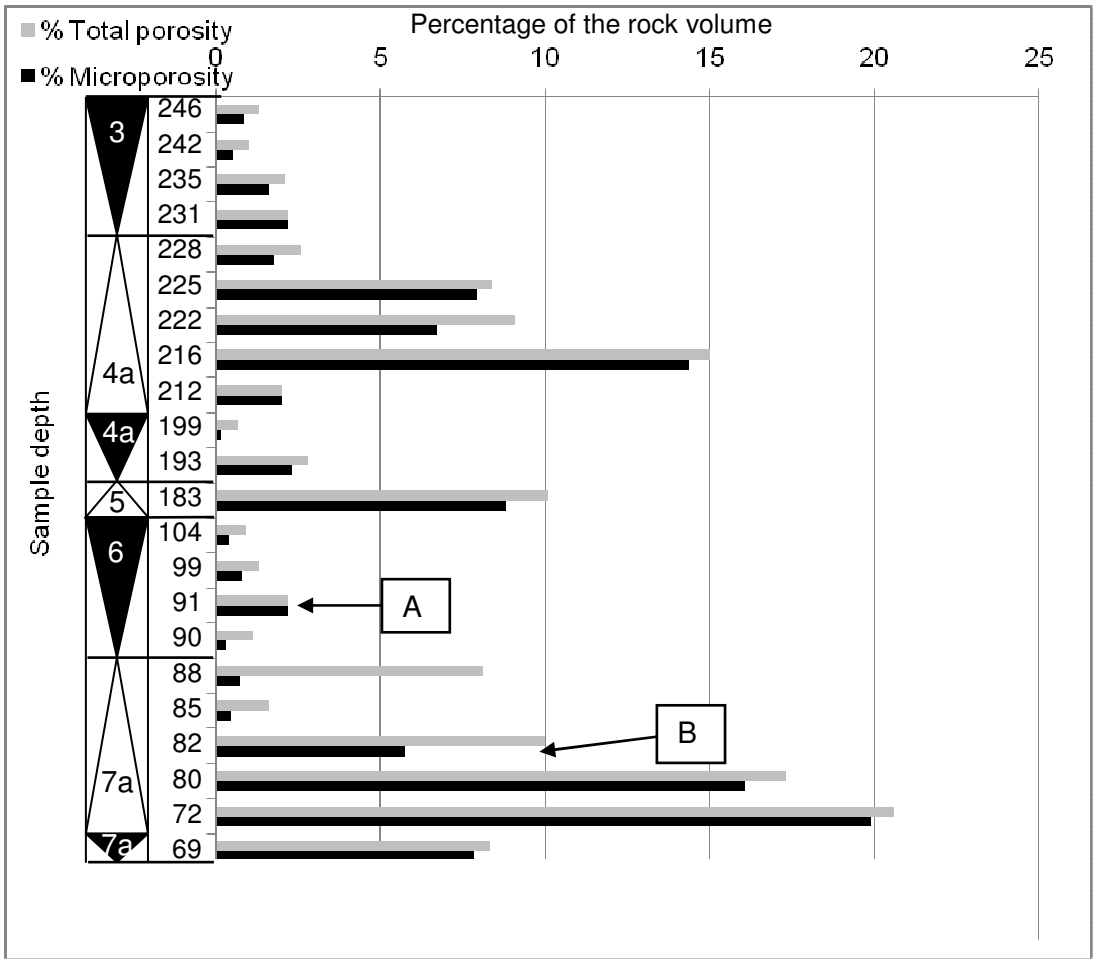

Figure 7.21: percentage of total open porosity and micropores within Well 5 with respect to the total rock volume. A and B directly relate to the micropore fabrics displayed in Figure 7.19. The depths for the specific samples are on the y-axis (Section 1.2 for depth calculations). The black triangles represent the TST's while the white triangles represent the HST's.

Sample depth (ft)	Open Micropores		Microspars		Micropore fabric	Micropore connectivity
	Size (µm)	Shape	Size (µm)	Shape		
64	Isolated 1 to 5		1 to 4	Subhedral to euhedral	Interlocking, blocky microspars	Appears Impermeable
28	1 to 7		3 to 4 (blocky), 1 to 2 (rounded)	Anhedral to subhedral	Mostly blocky, some enhanced pores	Some interconnectivity
0	Isolated 1 to 5		1 to 4	Subhedral to euhedral	Interlocking, blocky microspars	Appears impermeable
242	1 to 5		1 to 5	Anhedral to subhedral	Rounded spars occluded with	Appears mostly impermeable
231	1 to 8		3 to 6 (blocky), 1 to 2 (rounded)	Euhedral to subhedral (blocky), anhedral (rounded)	Slightly blocky microspars with smaller rounder microspars	Well to moderately connected
202	1 to 5		1 to 5	Anhedral	Coalesced layer of LMC	Appears impermeable
231	1 to 10		4 to 10 (blocky), 1 to 3 (rounded)	Euhedral to subhedral (blocky), Anhedral (rounded)	Blocky microspars with smaller rounder microspars	Well connected
224	Isolated 1 to 5		<4	Anhedral	Coalesced layer of LMC	Appears impermeable
198	Isolated 1 to 10		<4	Anhedral	Coalesced layer of LMC	Appears impermeable
513	Isolated 1 to 10		1 to 5	Subhedral to anhedral	Coalesced layer of LMC	Appears impermeable
431	1 to 8		3 to 5 (blocky), 1 to 2 (rounded)	Euhedral to subhedral (blocky), anhedral (rounded)	Slightly blocky microspars with smaller rounder microspars	Well connected
381	1 to 10		3 to 5 (blocky), 1 to 2 (rounded)	Euhedral to subhedral (blocky), anhedral (rounded)	Slightly blocky microspars with smaller rounder microspars, patches of anhedral LMC	Moderately connected
91	1 to 5		3 to 5	Anhedral	Coalesced layer of LMC	Appears impermeable
82	1 to 5		3 to 4 (blocky), 1 to 2 (rounded)	Euhedral to subhedral (blocky), anhedral (rounded)	Slightly blocky microspars with smaller rounder microspars, patches of anhedral LMC	Moderately connected

Table 7.1: microspar, micropore and micropore fabric descriptions for Well 1 (first 3 grey rows), Well 2 (next 3 white rows), Well 3 (next 3 grey rows), Well 4 (next 3 white rows) and Well 5 (last two grey rows). The descriptions of the macrospars are not included in this table.

7.2.2 Micropore fabrics (this study)

In relation to the micropore assessments of the five wells (Figs. 7.7 to 7.21: Table 7.1), many similarities exist. This next section provides four general micropore fabrics based on the previous assessments, and some of the descriptive nomenclature form Lambert et al. (2006) (Section 7.1.1), and places them in stratigraphic order in relation to a typical 4th order HFC (Fig. 7.22 & 7.23):

1. Open euhedral-subhedral blocky and rounded microspars (middle reservoir horizon) (Fig 7.22A & 7.23).

2. Partially open subhedral-anhedral rounded microspars (top and base reservoir horizon) (Fig. 7.22B & 7.23).

3. Cemented blocky euhedral-subhedral microspars (top and base reservoir horizon and mostly represents the water leg) (Fig 7.22C & 7.23)

4. Interlocking anhedral microspars (non-reservoir and firmground horizons) (Fig 7.22D & 7.23).

Figure 7.22: micropore fabrics of the Lekhwair and Lower Kharaib Formations. A) Open euhedral-subhedral blocky and rounded microspars, B) partially open subhedral-anhedral rounded microspars, C) cemented blocky euhedral-subhedral microspars and D) interlocking anhedral microspars.

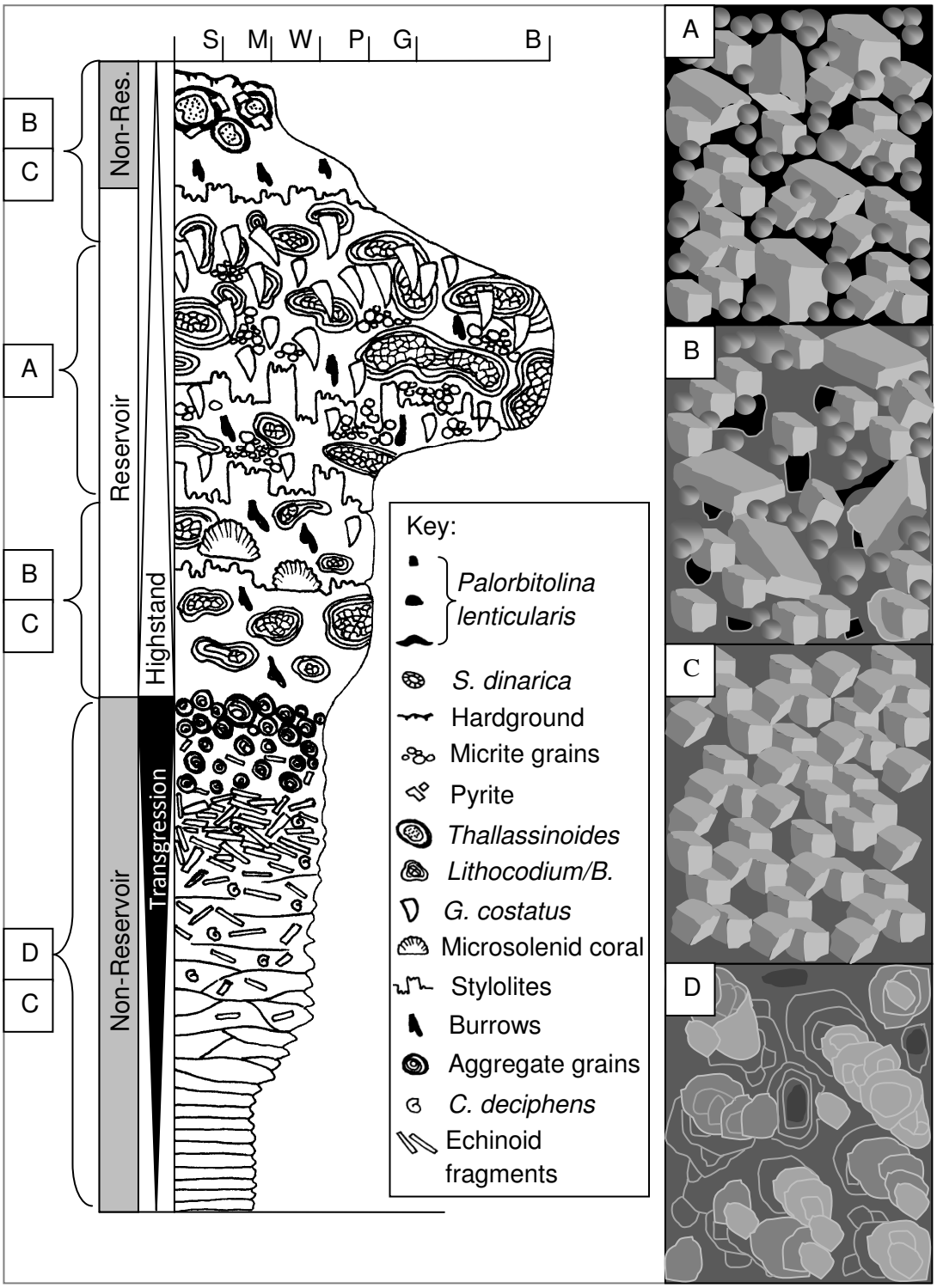

Figure 7.23: micropore fabrics placed relative to a typical 4th order HFC. A-D on the schematic diagrams of the micropore fabrics relate to the previous Secondary Electron images in 7.22A-7.22D. A-D relate directly to the adjacent schematic drawings. On the schematic diagrams the small cubes represent 3-5µm microspars, the large cubes represent 15-40µm microspars, the small spheres represent 1-2µm rounded microspars and the flat round objects on schematic drawing (D) are anhedral microspars.

The reservoirs within the Lower Khariab and Lekhwair Formations are very similar; they are a mixture of euhedral and subhedral slightly blocky 5-10µm microspars, with 10-40µm euhedral blocky LMC spars that fill pre-existing 100-200µm pore spaces (Fig. 7.22A & 7.23). There are many smaller euhedral and subhedral 3-5µm microspars alongside 1-2µm rounded anhedral microspars that can be perfectly spherical (Fig 7.22A & 7.23).

Towards the non-reservoirs, the microspars of the reservoirs become smaller, more rounded, and coalesce (Fig. 7.22B & 7.23). The micropore fabric is a transition between the open euhedral blocky fabric of the reservoirs and the anhedral cemented fabric of the non-reservoirs. Therefore the micropore fabric appears to become coarser and blockier towards the middle of reservoirs. The middle reservoirs contain the best interconnected micropores.

The micropore fabrics of the non-reservoirs, associated with the basal TST micrite/mudstone, are fully occluded. The majority of microporosity has completely disappeared: the matrix is completely altered to form an anhedral barrier of LMC (Fig. 7.22D & 7.23). The 'layer cake' nature of the Lower Khariab and Lekhwair Formations means these impermeable non-reservoirs (belonging to 4th order TST's and late HST firmgrounds) can be predicted across the entire oil field. Therefore without faults breaking the non-reservoirs vertical fluid flow between the stacked reservoirs appears unlikely.

A fourth micropore fabric, resembling micropore Fabric 2 outlined previously (Fig. 7.22C & 7.23), mostly comprises 1-4µm microspar that have coalesced to form a partial barrier leaving reasonably connected regular 1-5µm open micropores. However, all the microspar is blocky and shows no rounding. This fabric is primarily in the water leg reservoir and in some lower grade reservoirs within the oil leg and transition zone in the early HST's.

7.2.3 Cementation sequence (this study)

Two main cementation phases are recognised within the Lower Khariab and the Lekhwair Formations that have precipitated after 1) the formation of the 1-10µm microspar that relate to the stabilisation of aragonite and HMC components to LMC

and to the stabilisation of LMC muds to micrite (Fig. 7.24): 2) 10-40µm spar cements that have initially formed within large 100-200µm moulds, vugs and interparticle porespaces (Fig. 7.24) and 3) 40-200µm LMC burial cements that have formed within 1-2cm moulds associated with *G. costatus* shells and other large macropores (Fig. 7.24).

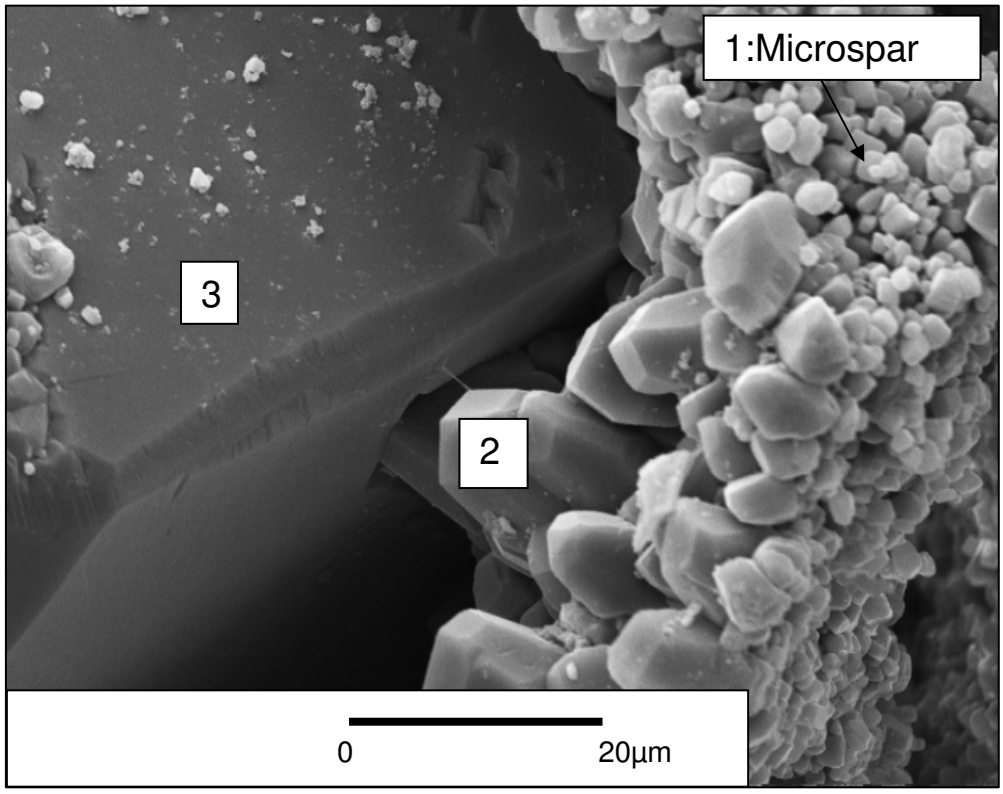

Figure 7.24: formation of microspar followed by two generations of LMC spar cements. 1) These are the earlier cements along with 2) the burial spars.

7.3 Interpretations

7.3.1 General micropore relationships

Most samples from the Lekhwair and Lower Kharaib Formations have some microporosity open. With respect to the percentage of total open pore space, all samples within the water leg have near 100% microporosity for both the TST and HST (Fig. 7.7 to 7.9). The percentage of microporosity within the transition zone for the majority of the samples is roughly 40-90% for the HST's and roughly 80-100% for the TST's, with respect to the percentage of total open pore space (Figs. 7.10-

7.12 & 7.19-7.21). For the oil leg the proportion of microporosity is roughly 60-90% in the HST's and roughly 80-100% in the TST's with respect to the percentage of total open pore space (Figs. 7.13-7.18). Proportions of microporosity become greater towards the water leg, the flanks of the field and towards the TST's within most 4th order HFC's. The water leg reservoirs appear to be micropore-dominated. An amount of microporosity remains open with most samples, while the amount of open macropores reduces towards the water leg and the field flanks (Section 4.8.1). The water leg has much more primary macroporosity occluded with cements. This probably relates to the final pore occluding cement phase recognised within the water leg with $\delta^{18}O$ values of -9‰ to -10‰ (Section 4.8.1). The majority of water leg macropores are occluded suggesting that the porosity and permeability values are more a consequence of the remaining open microporosity in comparison with the highest porosity and permeability relationships of the oil leg. Therefore open microporosity is important within the Lower Kharaib Formation reservoir, and also possibly for the Lekhwair Formation reservoirs.

With respect to the four general micropore fabrics, the open euhedral-subhedral blocky and rounded microspars represents the best interconnected micropore fabric seen within the entire Lekhwair and Lower Kharaib Formations (Figs. 7.22 & 7.23). The open euhedral-subhedral blocky and rounded microspars are found within the upper HST's, abundant *Glossomyphorus costatus*, with *Lithocodium/Bacinella* and the coarsest lithofacies (L4, 5, 6, 8 & 9: Section 3.4.3). However the decrease in the amount of open micropores towards the basal TST micrite/mudstone and the firmgrounds at the top of each 4th order HFC are not necessarily constrained to any specific lithofacies. This suggests that micropore formation was a result of a diagenetic process and was not controlled from processes associated with deposition.

With respect to the oil and water legs reservoirs, within the Lower Kharaib Formation (Cycle 1), they both show the same bimodal distribution of larger 3-5µm microspars with smaller 1-2µm microspars (Figs. 7.7, 7.13 & 7.16). These smaller microspars may have always been small from their inception, and have not been the products of significant dissolution selectively within the oil leg (Lambert et al. 2006).

There are two main differences within the water and oil leg micropore fabrics. 1) The water leg HST shows a phase of microspar formation that resembles a cementation episode, which occludes a significant proportion of micropores. The oil leg is devoid of this pore occluding phase and consequently has a well connected micropore fabric (Figs. 7.7, 7.13 & 7.16). 2) The majority of rounding occurs within the HST's of the reservoirs within the oil leg as 1-2µm microspars that are rounded and completely spherical (Figs. 7.13 & 7.16). There is a small proportion of the 1-2µm microspars within the water leg that are rounded, however some still shows a blocky appearance (Fig. 7.7). Consequently there are more connections and more open pore throats between the rounded microspars in the oil leg in comparison with the water leg (Figs. 7.7, 7.13 & 7.16). There may have been a very small amount of size reduction during the rounding of the smaller 1-2µm microspar enlarging the surrounding pore throats (Lambert et al. 2006) (Fig. 7.25), however this is not a definite conclusion for this study. A possible reason behind why the smaller microspars appear more rounded may be because the smaller size makes them more susceptible to corrosion and dissolution from aggressive pore fluids.

7.3.2 Processes of micropore formation and occlusion

Mineral stabilisation of aragonite and HMC during syn-deposition had occurred within the Lower Kharaib and Lekhwair Formations. The aragonite portions of *G. costatus* shells are replaced by LMC (Section 6.1.1: Fig. 6.1). The microporosity within the Lekhwair and Lower Kharaib Formations may have developed early from mineral stabilisation, which is consistent with studies of Moshier (1989a). The stabilisation would have mobilised calcium carbonate into solution for redistribution and the formation of the microspars. The absence of aragonite needles in the micropore fabrics suggest that microspar formation was caused by aggrading neomorphism (Lasemi & Sandberg 1984) and not from the direct cementation of LMC onto the aragonite needle precursors (Lasemi & Sandberg 1984, Steinen 1982). There are no heavier $\delta^{18}O$ values with respect to Cretaceous seawater (-1‰) for the bulk micrite (assumed to represent the LMC microspars) (Section 6.2.2) or the LMC cements (Section 5.3.5 & 5.4), or any petrographic evidence (Section 3.4) that supports the micropore fabrics within the Lekhwair and Lower Kharaib Formations

formed as a consequence of meteoric fluxes as described by Ahr (1989), Budd (1989), Perkins (1989) and Saller & Moore (1989) or from fracturing and enhancement from meteoric marine mixed porewaters (Kaldi 1989).

Within the basal TST micrites/mudstone (non-reservoirs) and the firmgrounds capping each 4th order HFC, the micropores are almost absent in the interlocking anhedral microspars (Figs. 7.22D & 7.23). A comparison between the micropore fabrics within the HST and TST of both the oil and water legs indicates that a phase of microspar formation has occluded the micropore fabrics of the TST's. The transformation of smectite to 50% smectite and 50% illite produces 290mg of water for 1g of clay (Mazzullo & Harris 1992). An assumption is that micrite and mud compaction and dewatering has flooded these areas, providing a source of solutes for extensive cementation, as suggested by Dravis (1989) for the grainstones in the Upper Jurassic Haynesville oolites. Instead of another microspar phase forming, dewatering caused widespread cementation occluding the pore throats: i.e. an extensive micropore fill cementation episode has occurred as opposed to a phase of enhanced crystal growth (Moshier 1989a).

In the oil leg enough microporosity was open to allow for dissolution of the microspar within the TST, whereas in the water leg TST all the microspars are blocky and display no evidence for dissolution. The HST in the water leg also shows slightly less dissolution and is occluded by another cement phase in comparison with the oil leg HST. The water leg shows greater cementation within both its HST and TST, suggesting that another cement phase may have occurred within the water leg along with cementation from basal TST micrite/mud compaction and dewatering. The basal TST micrites/mudstone are very thin, and measure similar thicknesses between the water and oil legs of the Lower Kharaib Formation (Cycle 1) (Figs. 4.7-4.11). A much thicker expanse of basal TST micrite/mud would be required to cause the increase in micropore occlusion seen within the water leg. Therefore pore occlusion must relate to the final cement phase in the water leg with $\delta^{18}O$ values of -9‰ to -10‰ (micropore fill cementation: Moshier (1989a): Section 5.7.1). It appears that the final cementation phase exclusively within the water leg has prevented the majority of dissolution and therefore only the oil leg micropore throats

were significantly enhanced by dissolution. The dissolution had not caused a dramatic increase in porosity but does show a marked increase in the interconnectivity of the pore throats, the permeability, and the oil leg micropore system, in the HST (Fig. 7.25). This is consistent with the amount of rounded microspars being greatest in the mid-late HST where there is usually a permeability spike of up to 100mD (800mD for Cycle 1 in Well 1) (Figs. 7.8 & 7.17: Appendix 6).

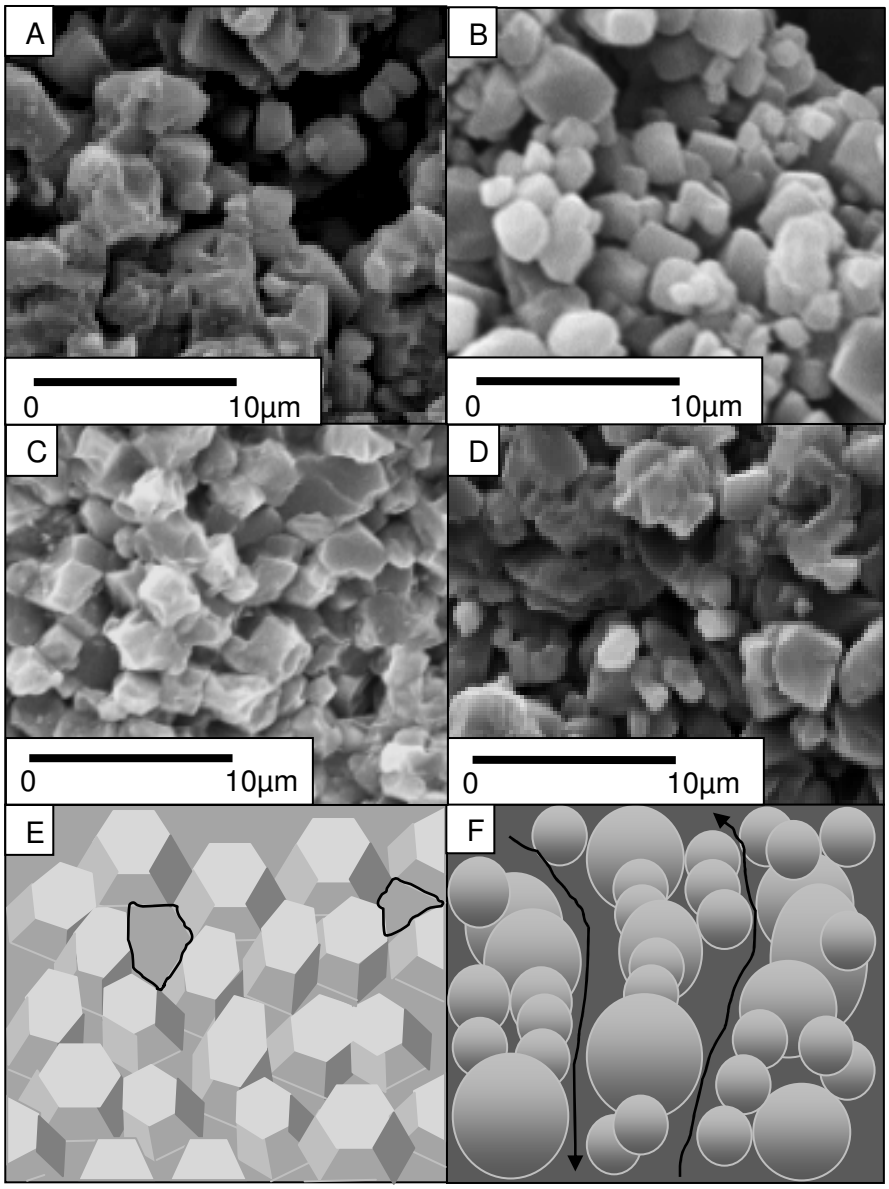

Figure 7.25: comparison of open micropore fabrics in the HST and occluded micropores within the TST. (A) The occluded micropores in the TST of the oil leg, (B) the open micropore fabric within the HST of the oil leg, C) the occluded micropores of the TST in the water leg and D) the open micropores in the HST of the water leg. E & F) Rounding and dissolution has not enhanced porosity by much, but has enhanced the interconnectivity of the micropores and the permeability within the HST's of the oil leg (highlighted by the irregular black boxes in (A) and the irregular black arrows in (B).

7.3.3 Timing of micropore enhancement

The intermediate-deep burial spar cements (3 on Fig. 7.24) within the *G. costatus* shells have grown and engulfed the smaller spars (2 on Fig. 7.24) indicating they are late cement fills. This has not had a dramatic effect on the interconnectivity of the micropore networks in comparison with mineral stabilisation. The overall appearance indicates that several generations of spars have formed from the outside of the macropores (appears consistent with Fig. 6.5), into the centre, forming the burial spars (3 on Fig. 7.24) last. Both the Ion Microprobe data and the stable isotope data, collected from similar burial spars within *G. costatus* shells, show these burial spars (3 on Fig. 7.24) have the most negative $\delta^{18}O$ values (-8‰ to -10‰: Section 5.7.1), suggesting that these are the late cement growths which post date the smaller spars (2 on Fig. 7.24) lining the interiors of macropores (Fig 7.24).

Further evidence which supports this sequence, is the burial spars (3 on Fig. 7.24) display euhedral pits on their surfaces (Fig. 7.26) indicating they had once grown into the smaller spars (2 on Fig. 7.34), and the euhedral microspars (1 on Fig. 7.24) that are now subsequently rounded (consistent with studies from Lambert et al. 2006). This confirms that the microporosity had not formed during intermediate-deep burial cementation (Al-Aasm & Amzy 1996, Dravis 1989) but it had formed earlier before the formation of the smaller spars (2 on Fig. 7.24) and the burial spar (3 on Fig. 7.24) cements. This study therefore confirms the observations of Moshier (1989a) that early formation of microporosity was followed by several generations of cement. These burial spar cements must have grown before dissolution and microporosity enhancement. These burial spars are also cross-cut by stylolites (products of the deep burial realm: Section 6.1.3): the dissolution event cannot have occurred earlier than the deep burial realm. The rounded microspars are preserved and not cemented further which is consistent with studies from Lambert et al. (2006) suggesting that oil had entered immediately after dissolution. However, initial oil had entered the reservoir much earlier, before the majority of burial spar cements had formed (-5.5‰: Sections 5.3.6 & 5.9): this confirms that at least two phases of oil emplacement had occurred within the Lekhwair and Lower Kharaib Formations (Section 5.9) and that a second phase of oil emplacement was required to stop all

cementation (critical oil saturation: Heasley et al. 2004: Section 5.7) in the deep burial realm and during subsequent uplift.

Comparison of the euhedral pits and similar sized rounded microspar indicates that microspar was once euhedral and blocky as the large burial spar grew and engulfed them. Burial spar growth had occurred prior to dissolution and rounding of the surrounding microspars.

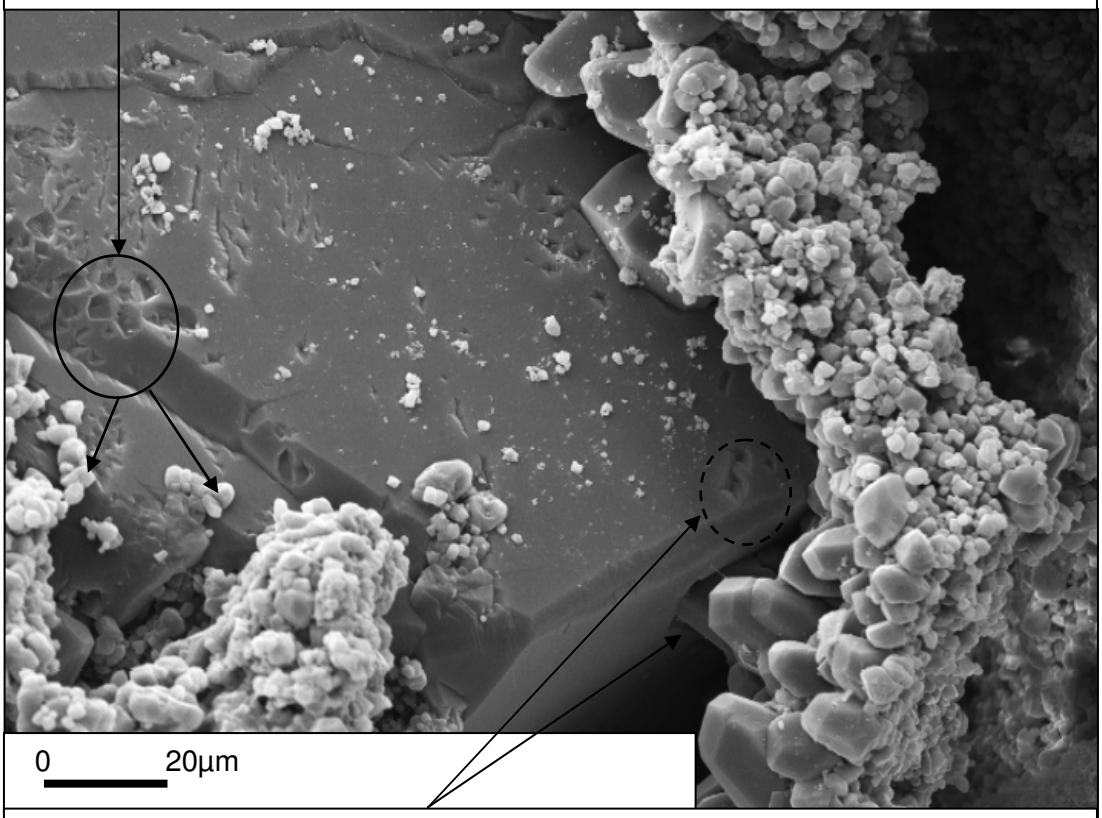

The burial spar cement has definitely formed after the smaller 15-40µm smaller spars, as it has smaller euhedral pits on its surface that correspond to the smaller spars, and the smaller spars have been engulfed by the large burial spar.

Figure 7.26: formation of microspar followed by cementation: followed by the 15-40µm smaller spars (labelled as 2 on Fig. 7.24) and then 40-200µm burial spars (labelled as 3 on Fig. 7.24). The burial spar shows euhedral embayments from the surrounding smaller spars and the microspars. The microspars are now rounded constraining dissolution after the formation of the majority of burial spar cement in the deep burial realm.

The degree of dissolution seen under SEM would require fluid quantities similar to main oil charge. The production of CO_2 from the decomposition of organic matter, and its dissolution into the pore fluids creates carbonic acids (Giles & Marshall 1986). One mole of CO_2 dissolved into solution (carbonic acid) is enough to dissolve

one mole of LMC, and half a mole of dolomite (congruent dissolution: one mole of dolomite for incongruent dissolution) (Giles & Marshall 1986). However CO_2 usually becomes incorporated into LMC precipitates within the source rock (Giles & Marshall 1986) causing a 'buffering effect' (Mazzullo & Harris 1992) and may not have allowed for the formation of acidic porewaters.

The generation of carboxylic acids from organics can also cause dissolution. With increasing temperature and depth, the equilibrium in the reaction between LMC and carboxylic acid shifts towards LMC (Giles & Marshall 1986). Larger amounts of carboxylic acid (acetic acid) are required to dissolve the same amount of LMC at increasing burial depths (Giles and Marshall 1986). Therefore the decomposition of organic matter and the onset of oil may not be enough to promote the widespread dissolution seen within the Lower Kharaib and Lekhwair Formations.

Another possibility is the fluxing of brines up into the crest from the Precambrian Ara salt layer beneath the offshore field, through detachments from the diapir crests (Al-Barwani & McClay 2008, Alsharhan & Kendall 1991), causing dissolution and decreasing the negativity of $\delta^{18}O$ values towards an enrichment in ^{18}O (Duane et al. 2004, Esteban & Taberner 2003) (Section 5.8). The compaction of evaporites and the transformation of gypsum to anhydrite (both possibly caused by salt diapirism) could have produced formation fluids undersaturated in LMC (Cantrell & Hagerty 1999, Shearman 1978). Upon migration and cooling, up through the fault detachments, the fluids became more corrosive and aggressive towards the surrounding carbonates. Once these LMC undersaturated fluids had migrated up into the cooler Lower Kharaib and Lekhwair reservoirs above, LMC became progressively dissolved enhancing the micropore networks, due to a significant temperature drop in the pore fluids (Giles & de Boer 1989). This is consistent with studies from a separate field from Dravis (1989) which suggests that late dissolution and micropore formation during deep burial was caused by upward migration and circulation of aggressive fluids.

Micrite/mudstone compaction and dewatering, along with progressive macrospar cementation, have reduced the amount of micro- and macroporosity within the Lower Kharaib and Lekhwair Formations. Only the introduction of corrosive fluids,

after burial spar formation, had enhanced the microporosity: this conclusion is consistent with studies from Moshier (1989a) on the Shu'aiba Formation. Both early mineral stabilisation and late dissolution during deep burial/uplift appear to be controlling factors in the formation of the best (most permeable) micropore fabrics.

7.3.4 Controlling factors on micropore formation

This section addresses the micropore systems of the Lower Kharaib Formation and Cycle 1, as samples are only available for both the oil and water legs in Cycle 1. This section is also a summary of the processes attributed with micropore fabric formation and the cementation sequence (Section 7.3.1-7.3.3). The micropore fabrics within both the water and oil legs have undergone similar processes until the deep burial realm. The sequence involves the formation of microspar through mineral stabilisation, which is followed by two main cement generations. Although two main cement generations are clearly visible on the Secondary Electron images, these cements may have several stages within them (Sections 5.3.5 & 5.4). The defining event is widespread dissolution within the oil leg (Fig. 7.25) which is constrained to after the formation of burial spars in the deep burial realm (burial spars with $\delta^{18}O$ values of -8‰ and -10‰: Section 5.7.1 & Fig. 7.27). Dissolution could have continued during uplift of the stratigraphy from the Semail Opniolite obduction, as the $\delta^{18}O$ values within the cements returned to -6‰ and -4‰. Consequently the oil leg micropore fabrics were enhanced the most, by the enlargement of its pore throats (Figs. 7.15, 7.16, 7.25 & 7.27). In comparison, the final cement phase within the water leg (with $\delta^{18}O$ values of -9‰ to -10‰: Section 5.7.1) occluded the majority of macro- and micropore space (Section 5.7.1 & Figs. 7.7, 7.25 & 7.27), increasing the tortuosity of the pore system. Consequently, corrosive fluids could not penetrate the water leg micropore fabrics as easily, in comparison with the oil leg, reducing the effects of dissolution (Fig 7.27).

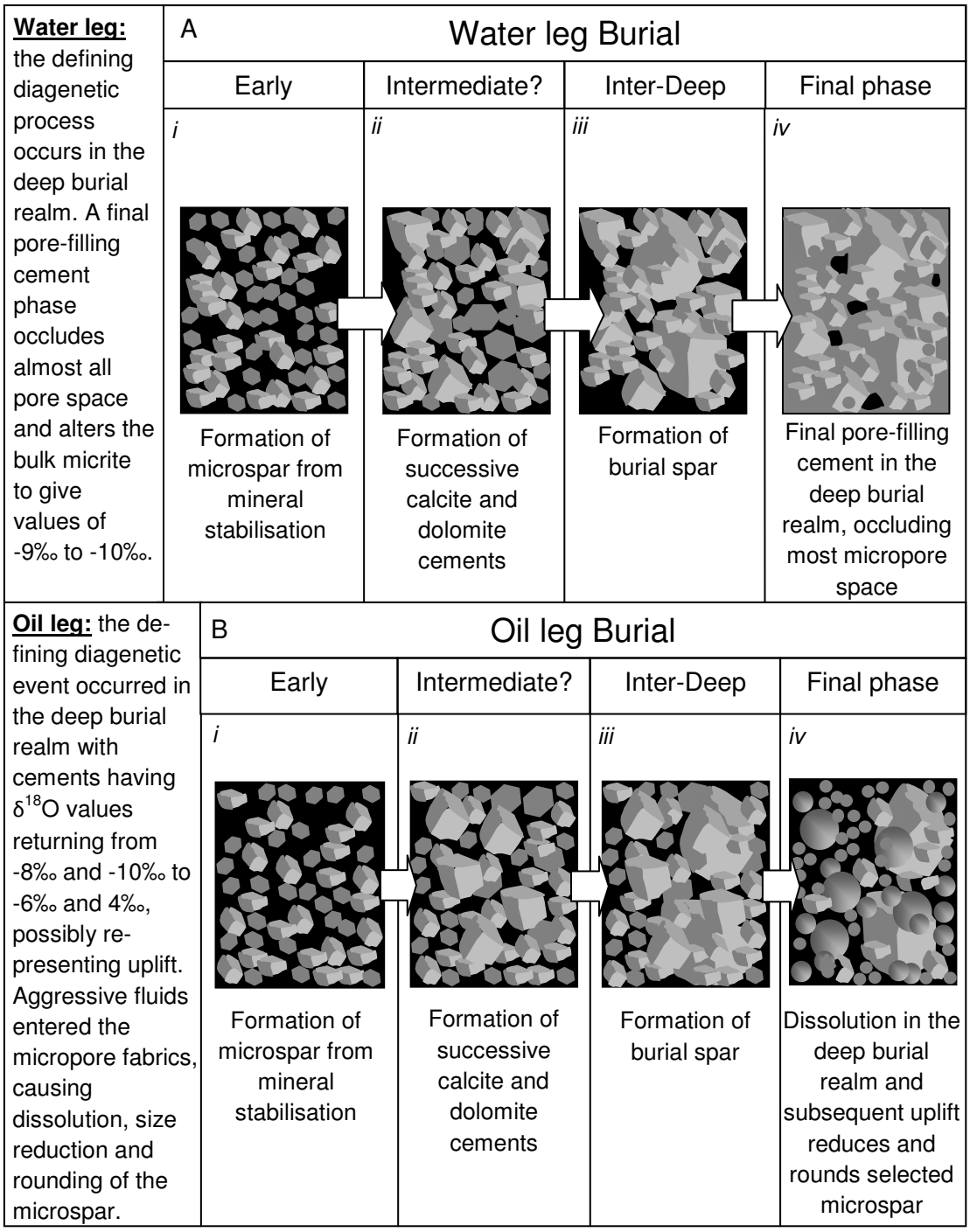

Figure 7.27: evolution of the micropore fabrics within the reservoirs of the Lower Kharaib Formation. Ai-iv) the evolution of the water leg micropore fabrics and Bi-iv) the evolution of the oil leg micropore fabrics. Only the final phase determines the difference between the water and oil leg pore systems. The small cubes represent 3-5µm microspars (1 on Fig. 7.24), the medium sized cubes represent 15-40µm smaller spars (2 on Fig. 7.24), the large cubes represent 40-200µm burial spars (3 on Fig. 7.24) and the spheres represent 1-2µm rounded microspars.

This is consistent with the deepest alteration of the water leg micrite in comparison with all other samples, indicating that a sudden surge in solutes had entered, altered and cemented up the majority of the water leg in the deep burial realm (Section 5.7.1). This all relates back to oil charge, which had occurred even earlier in the crest, which progressively shut down the macropores of the present day oil leg (Section 5.7). This prevented solute transfer within the oil leg and any new cement nucleation, consequently leaving the micropores open to allow for aggressive pore fluids to enter and selectively enhance the oil leg micropore fabric. Oil charge has not only determined the distribution of cements and the best macropores networks, but has also indirectly determined the distribution of the best micropore networks.

The widespread areas of open microporosity within the Lekhwair and Lower Kharaib Formations suggest that much oil may be within these systems and extraction from these areas may be inevitable to recover a significant amount of oil from these reservoirs. In relation to Section 1.1.2, targeting these micropore areas first and pushing the oil from the macropores, using the micropores, is now a possibility when considering these reservoirs. It now becomes clear that, for a good oil recovery, a method is required to differentiate these micropore and macropore sections within each reservoir of the Lekhwair and Lower Kharaib Formations.

7.4 Conclusions

1. There are three main micropore fabrics: 1) Open euhedral-subhedral blocky and rounded microspars (mid-late HST and middle reservoirs), 2) partially open subhedral-anhedral rounded microspars (upper and lower reservoirs) and 3) interlocking anhedral microspars (firmgrounds and non-reservoirs). The transition from micropore Fabric 1-3 occurs from the centre of the reservoir horizons towards the non-reservoirs above and below. Micrite/mud compaction and dewatering had caused the occlusion of the micropores, within the uppermost and lowermost portion of each 4^{th} order HFC, through an extensive phase of micropore-fill cementation.

2. A fourth micropore fabric is identified within the cemented portions at the base of certain reservoirs of the oil leg and the majority of the reservoir within the water leg. The texture resembles micropore Fabric 2 without the effects of dissolution.

3. Two main LMC cement phases have occurred after the initial formation of the microspars: 1) the mineral stabilisation of the 1-5µm microspar, 2) the growth of 5-15µm spar within the macromoulds and 3) large 15-200µm burial spar that, in some cases, have completely occluded the macropores.

4. The formation of late burial spar cements shows that microspar dissolution must have occurred late in the Lower Kharaib and Lekhwair Formation burial history, after burial spar formation. This is probably due to both oil charge and the influx of salt brines from the Precambrian Ara salts below. Dissolution was greatest within the oil leg while the effects were reduced within the water leg. The water leg received a final cement phase which occluded the majority of micro- and macropores: consistent with isotope studies of the bulk micrite and the final pore filling cement in the water leg, with values of $\delta^{18}O$ -9‰ to -10‰. Therefore a final cementation phase had occurred only within the water leg in the deep burial realm which must have prevented the majority of aggressive fluids from entering and causing widespread dissolution.

5. Mineral stabilisation was the main event at redistributing carbonate, forming the LMC microspars and forming the micropore fabrics during early burial. Only the actions of dissolution during deep burial, and uplift, had enhanced the micropore throats through microspar rounding: increasing rock permeability. Not much extra porosity was generated through dissolution.

6. In Chapter 4, early oil charge is given as the main reason for the distribution of cements across the offshore field, as oil prevented extensive cementation within the oil leg. Therefore aggressive fluids could penetrate the oil leg more easily during deep burial and subsequent uplift, causing widespread dissolution and micropore/pore throat enhancement. Oil charge has therefore

indirectly determined the distribution of the best micropore networks within this offshore field, Abu Dhabi.

7. The Lekhwair and Lower Kharaib Formations have a significant amount of open microporosity. When considering oil extraction methods, the microporosity should be used to recover oil from the macropores, to ensure a good oil recovery. Therefore a new method is required to constrain where these micropores region are within each reservoir within the Lekhwair and Lower Kharaib Formations.

Chapter 8

Rock type analysis for micropore-dominated pore systems

The depositional architecture of the Lower Kharaib Formation shows the shallowest and coarsest reservoirs (Sections 3.4.5 & 4.4) potentially contain the highest porosity and permeability relationships. The Lower Kharaib Formation lithological distribution is consistent across the structure (Section 4.6). However, there are significant decreases in porosity and permeability from the oil leg towards the water leg (Sections 5.3.1, 5.3.2 & 5.7.1). Towards the flanks, and the water leg, macropore and micropore occlusion increases: the distribution of cements is therefore controlling the distribution of the highest porosity and permeability relationships (Sections 5.3.1, 5.7.1, 7.2.1 & 7.2.2). Proportions of open microporosity within both the Lower Kharaib and Lekhwair Formation reservoirs increase towards the flanks and the water leg. The reservoirs surrounding the crest are more micropore dominated (Section 7.2.1). Therefore any rock typing method needs to account for both the effects of diagenesis (the distribution of cements) and the distribution of microporosity.

The porosity and permeability relationships of the Lekhwair and Lower Kharaib Formations are assessed by plotting porosity and permeability data (within each 4^{th} order HFC) against stratigraphy (HST & TST), the reservoirs, the non-reservoirs and the broad lithological units (Section 3.4.1).

The 20 lithofacies generated, in Section 3.4.3, cannot be applied to every porosity and permeability data point (measured commercially) for every foot of the core as only 110 samples were taken from the five Wells. To use the petrographic classifications, the lithofacies for large sections of each Well would have to be

assumed. Only the lithologies generated from core logging encompass the depths covered by the commercially measured porosity and permeability data. The origin of the porosity and permeability data within this Chapter are explained in Section 1.2.

The highest porosity and permeability relationships are shown with respect to 3rd and 4th order scales. For the 3rd order scale, summary diagrams are produced for each Well. This enables comparison of porosity and permeability relationships across the entire stratigraphy within the Lekhwair and Lower Kharaib Formations. For each 4th order HFC, porosity and permeability data is compared with the lithological successions, the reservoirs and non-reservoirs (Appendix 6).

Diagenesis, through the amount of cementation and increasing burial, is already associated with the porosity and permeability relationships in Sections 5.3.1 and 5.3.2: these trends are referred to in this Chapter.

The Lucia (1999), Lønøy (2006) and Petrotype atlas methods (Corbett & Potter 2004), for determining the highest porosity and permeability relationships within carbonates, are compared for the Lower Kharaib Formation. The Lower Kharaib Formation is the only 4th order HFC sampled within the oil and water legs, and is therefore the best HFC to test these petrotyping methods.

Finally a new method is proposed from the porosity and permeability relationships of the Lower Kharaib Formation. This is designed to show not only the best reservoirs, but also the lower grade, but potentially oil-producing reservoirs. This shows the importance of distinguishing macropore- and micropore-dominated reservoirs. To validate this new method, it is tested on two 4th order HFC's of the Lekhwair Formation.

8.1 Rock typing in carbonates

8.1.1 Lucia Method

The method outlined by Lucia (1999) is based upon the grain size, the grain sorting and the amount of interparticle pore space in the absence of vugs. Instead of mud-supported and grain-supported as suggested by Dunham's classification, the terms mud-dominated and grain-dominated are used by Lucia (1999) (Fig. 8.1).

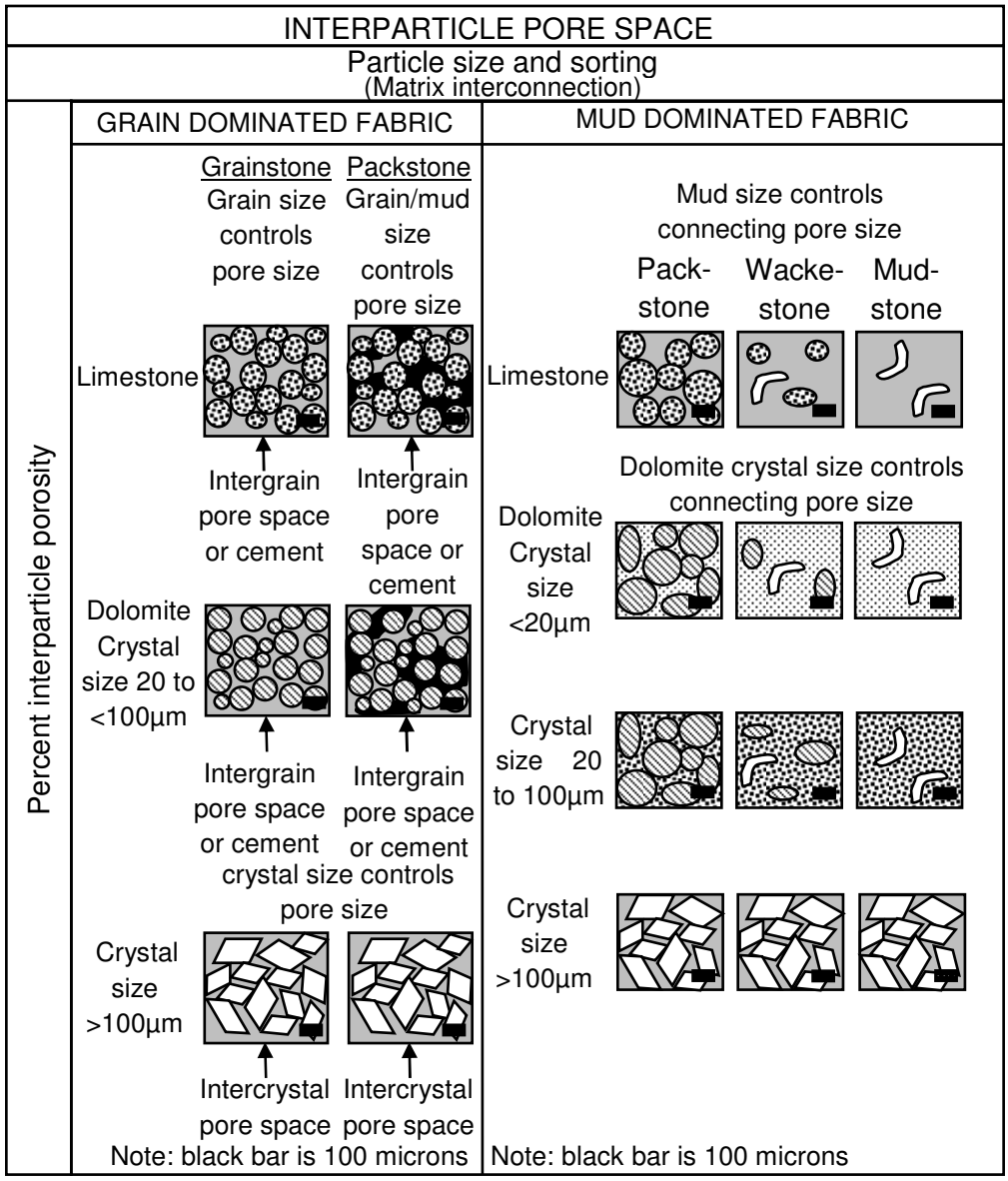

Figure 8.1: petrophysical classification scheme by Lucia (1995). It is based on grain/crystal size, sorting and distribution. The larger grains and crystals are associated with the larger interparticle pore spaces (redrawn from Lucia 1995).

Three pore classes are based on: the amount of grains verses mud, and the grain size, which ultimately defines the size and the amount of surrounding interparticle pore space (Fig. 8.2). Much data was collated and plotted on porosity air permeability plots which showed separation between ooid grainstone, grain-dominated packstone and mud-dominated wackestone and mudstone. Grain size and sorting define the permeability fields (three classes) whereas the amount of interparticle porosity defines the pore size distribution.

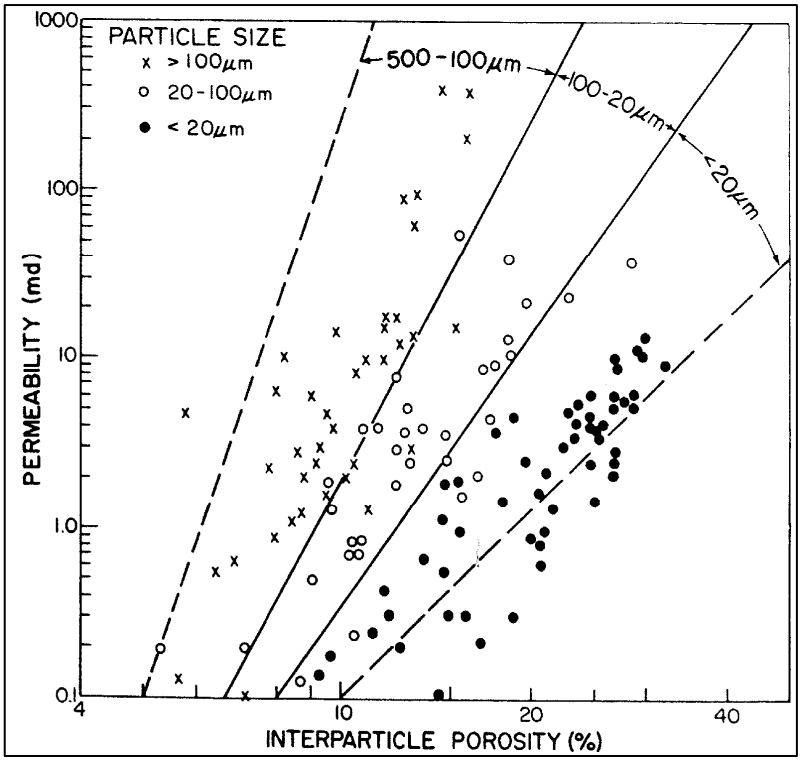

Figure 8.2: The three classes outlined by Lucia (1999). The data is separated according to grain size, which determines the size and the amount of surrounding interconnected interparticle pore space.

The limitation of this model is that classing is determined by grain size, which defines the interparticle pore size, but not other significant pore sizes, such as macro moulds and macro vugs >500μm. There is also no specific classification for microspars, which would produce <10μm micropores, which is the cut off and definition used by Cantrell & Hagerty (1999), and similarly this study, for microporosity. Considering the heterogeneity of a typical carbonate, a classification system concentrated on one pore type (interparticle pores) would probably not provide enough information for reservoir characterisation, and may not maximise oil recovery.

8.1.2 Lønøy Method

The Lønøy (2006) method employs a new pore classification system based upon the proportion of a single dominant pore type, its size and distribution, within a single rock type or lithofacies. Lønøy (2006) recognises the amount of cements

within a pore system will reduce the pore size/throats but not the grains size/sorting within a lithology. Therefore Lønøy (2006) has based his classification on pore size and not grain size (Lucia 1999).

This method incorporates the subdivision of interparticle porosity laid out by Lucia (1999). The three interparticle pore types from Lucia (1999), and the interparticle and intercrystalline pore types from Choquette & Prey (1970), are subdivided into 12 new categories (6 interparticle pore types and 6 intercrystalline pore types) (Table 8.1). The Lønøy (2006) method also provides three new pore types: micromouldic, macromouldic, and mudstone microporosity (Table 8.1). Chalky micropores are associated with micropores developed from diagenesis, whereas the micropores within Cretaceous and Tertiary chalks are primary in origin. Lønøy (2006) does not provide any further information about the origin of these chalks.

The data used to determine these new pore types was gathered from 3000 core plugs that were all determined to be dominated by one pore type. The dominance of a specific pore type, and whether this pore type was distributed uniformly or sparsely, was determined petrographically. Helium porosity and air permeability was measured from mostly horizontal plugs. Thin sections were impregnated with blue epoxy resin, the amount, the size, and distribution of the pore types was assessed visually (Lønøy 2006).

Pore type	Pore size	Pore distribution	Pore fabric	R^2
Interparticle	Micropores (10-50µm)	Uniform	Interparticle, uniform micropores	0.88
		Patchy	Interparticle patchy micropores	0.79
	Mesopores (50-100µm)	Uniform	Interparticle uniform mesopores	0.86
		Patchy	Interparticle patchy mesopores	0.85
	Macropores (>100µm)	Uniform	Interparticle uniform macropores	0.88
		Patchy	Interparticle patchy macropores	0.87
Intercrystalline	Micropores (10-20µm)	Uniform	Intercrystalline uniform micropores	0.92
		Patchy	Intercrystalline patchy micropores	0.79
	Mesopores (20-60µm)	Uniform	Interchrystalline uniform mesopores	0.94
		Patchy	Intercrystalline patchy mesopores	0.92
	Macropores (>60µm)	Uniform	Intercrystalline uniform macropores	0.8
		Patchy	Intercrystalline patchy macropores	
Intraparticle			Intraparticle	0.86
Moldic	Micropores (<10-20µm)		Mouldic micropores	0.86
	Macropores (>20-30µm)		Mouldic macropores	0.9
Vuggy			Vuggy	0.5
Mudstone microporosity	Micropores (<10µm)		Tertiary chalk	0.8
			Cretaceous chalk	0.81
		Uniform	Chalky micropores, uniform	0.96
		Patchy	Chalky micropores, patchy	

Table 8.1: pore types outlined by Lønøy (2006). The R^2 category within the last column is the regression line or 'line of best fit' calculated for each pore type distribution (redrawn from Lønøy 2006).

The interparticle class sizes set out by Lønøy (2006) differ from the class sizes set out by Lucia (1999). The smallest size is defined by Lucia (1999) as <20µm (Fig. 8.2), in comparison with 10-50µm for Lønøy (2006) (Table 8.1). The intermediate

size for Lønøy (2006) is 50-100µm (Table 8.1) which is larger than the parameters set by Lucia (1999) of 20-100µm (Fig. 8.2). The largest size of interparticle pore is defined as >100µm by both Lønøy (2006) and Lucia (1999) (Table 8.1 & Fig. 8.2, respectively). Unlike the pore classification scheme by Lucia (1999), Lønøy (2006) defines a separate category for microporous mudstones. The definition for micropores of (<10µm) is the same to this study and Cantrell & Hagerty (1999).

The porosity and permeability for a reservoir unit is sorted into 12 categories by determining the dominant pore type distribution for each sample petrographically. The groups of data are plotted and the line of best fit (R^2) is then calculated (Table 8.1). Rocks dominated by interparticle pores show that when pore size increases, or when the pore distribution becomes patchier, the k/Ø increases.

For each distribution, the percentage of the specific pore type required to maintain 1mD (represented by 0 on the y axis) of flow through its pore system is interpolated from the R^2 line (line of best fit) (Table 8.2). Depending upon the uniformity of macro interparticle pores defines the cut-off with respect to 1mD of fluid flow. For uniform macro interparticle porosity the cut-off is 8.2%, while for patchy distribution it is 5.5%, of the total porosity (Fig. 8.3). This cut-off becomes very important when comparing macropore- and micropore-dominated rocks. For instance, for Tertiary chalk the cut-off is 31.3%, while for Cretaceous chalk it is 25.8%, and for chalky micropores it is 27% (Table 8.2). A reservoir rock dominated by micropores is only reservoir quality at much higher porosity fractions, in comparison with an interparticle-dominated rock (Table 8.2). This also points out that micropore-dominated rocks can be important and can serve as lower grade reservoirs.

Pore size	Pore type	Cut-off (%)
Micro	Uniform interparticle	15.3
	Patchy interparticle	8.1
Meso	Uniform interparticle	11.1
	Patchy interparticle	5.8
Macro	Uniform interparticle	8.2
	Patchy interparticle	5.5
Micro	Uniform intercrystalline	22.4
	Patchy intercrystalline	18.6
Meso	Uniform interparticle	16.9
	Patchy interparticle	9.1
Macro	Uniform interparticle	5.4
	Patchy interparticle	n/a
Micro	Tertiary chalk	31.3
Micro	Cretaceous chalk	25.8
Micro	Chalky micropores	27
Macro	Mouldic pores	13.1
Micro	Mouldic pores	16.2
	Intraparticle pores	14.1
	Vuggy pores	6.2

Table 8.2: percentages required to maintain 1mD of fluid flow with respect to the different pore type systems: these values are interpolated using the R^2 lines (data collated from Lønøy 2006).

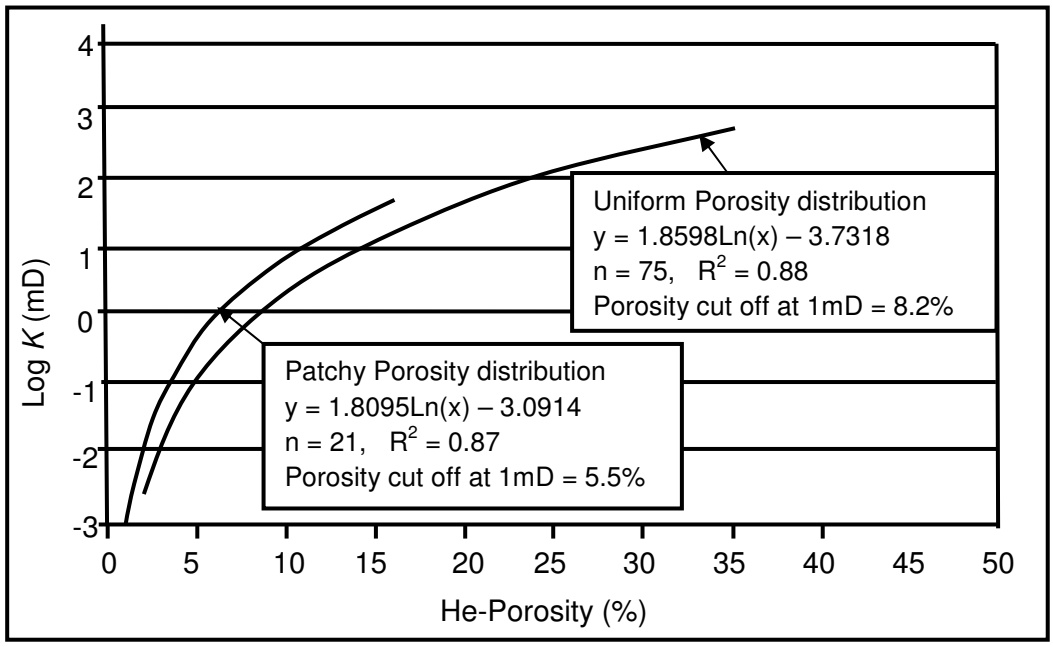

Figure 8.3: Two logarithms for patchy and uniform macro interparticle pore-dominated reservoirs. The 1mD threshold is much lower for patchy interparticle pores over a uniform distribution, highlighting the importance of pore types in the formation of the highest porosity and permeability relationships (redrawn from Lønøy 2006).

The main benefit compared with the Lucia (1999) method, is the Lønøy (2006) method incorporates a category for microporosity. The main issue with the Lønøy (2006) method is the division between uniform and non-uniform (patchy) pore type distributions. Where exactly is the boundary between the two and how subjectively were these different categories initially determined. Individuals using this scheme may make different decisions upon what constitutes a uniform distribution of moulds verses a non-uniform distribution. The degree of pore type dominance within each sample is also unclear. Which pore type class should individuals put a carbonate rock sample if it is equally dominated by two different pore types?

8.1.3 Petrotyping methods

The Winland-Pittman plot is an example where porosity and permeability data is plotted up on a semi log scale with R_{35} divisions (Gunter et al. 1997, Jennings & Lucia 2001, Shenawi et al. 2009). Power law models were devised by Winland-Pitman, associating porosity and permeability with pore throat sizes:

Equation 8.1 : $$k = \alpha_{wp} \emptyset^{b_{wp}} r_{35}^{c_{wp}}$$

(Jennings & Lucia 2001)

Alternatively, this can be expressed as:

Equation 8.2: $$\ln(k) = \ln(\alpha_{wp}) + (b_{wp}) \ln(\emptyset) + c_{wp} \ln(r_{35})$$

(Jennings & Lucia 2001)

This equation can be rewritten to find the R_{35} values. These divisions directly relate to different pore throat sizes (Fig. 8.4) and can be calculated using this equation:

Equation 8.3: $$\text{Log}(r_{35}) = 0.732 + 0.588 \text{ Log}(k) - 0.864 \text{ Log}(\emptyset)$$

(Gunter et al. 1997, Shenawi et al. 2009)

Where k is the uncorrected permeability, $\emptyset$ is the porosity, r_{35} is the pore throat radius measured with mercury-injection cappillary-pressure experiments, with a mercury saturation of 35% and α_{wp}, b_{wp} and c_{wp} are constants.

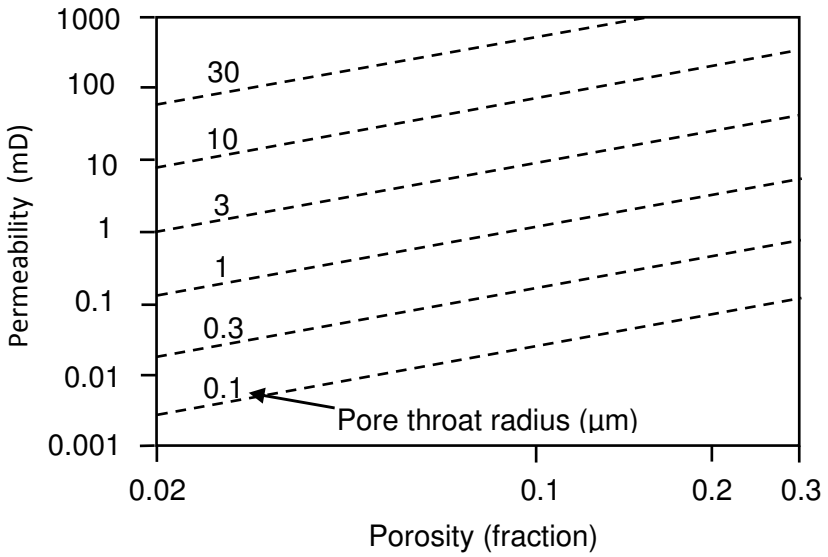

Figure 8.4: pore throat sizes on the Winland-Pittman model. Each dotted line represents a R_{35}. The pore throat size is displayed above each dotted line (redrawn from Jennings and Lucia 2001).

By combining the Winland-Pittman model, with Stratigraphic Flow Profiles (plotting the vertical and horizontal stratigraphic extent of high flow units) and Modified Lorenz Plots (plotting the % flow capacity against the % storage capacity), Gunter et al. (1997) has integrated information on flow potential, flow capacity and storage capacity. Information on rock types and the geological framework for specific reservoirs within the Platten dolomite of the Zechstein Group were also considered. This provides information on the number, the extent, and the future performance, of flow units within specific reservoir horizons (Gunter et al. 1997).

The Carmen-Kozeny models are used to separate out porosity and permeability data into classes determined by Flow Zone Indicator (FZI) (Jennings & Lucia 2001). Where α_{ck} is a constant (=1014), K, ø and f are in Md: the equation to derive the FZI for the Carmen-Kozeny models are:

Equation 8.4: $$Ln(k) = \ln(\alpha_{ck}) + \ln(ø^3/(1-ø)^2) + 2\ln(f)$$

(Jenning & Lucia 2001)

Where f is the FZI which is a value derived from the pore geometry (F_s), the flow path tortuosity (τ) and the particle surface area per unit of particle volume (S_{gv}). The FZI can be calculated by:

Equation 8.5: $f = 1/\sqrt{F_s \tau S_{gv}}$

(Jennings & Lucia 2001)

The Carmen-Kozeny model also plots FZI as straight lines, on double logarithmic plots (both axis), with similar divisions to the Winland-Pittman model (Fig 8.5). With decreasing porosity of a specific f, the radius of the pore throats decreases (Fig. 8.5), which is highlighted by the steepness of the lines in comparison with the Winland-Pittman model (Jennings & Lucia 2001).

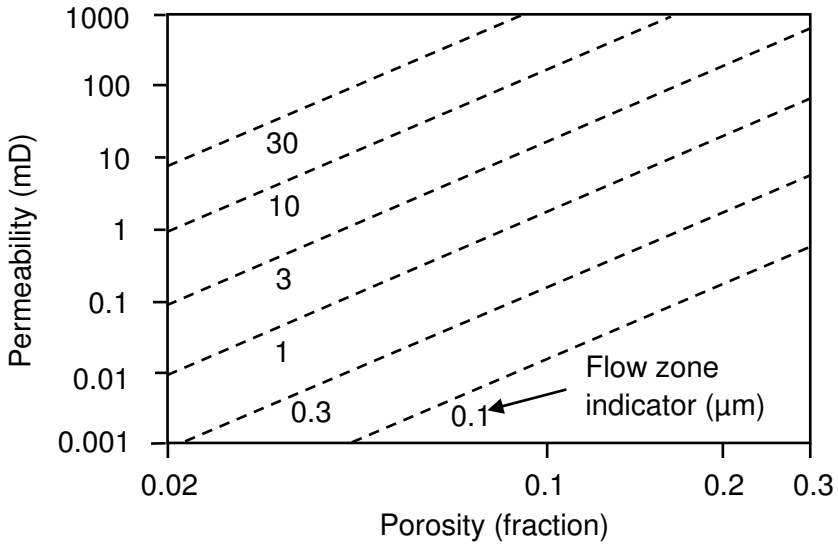

Figure 8.5: Carmen-Kozeny plot showing the FZI's (f) as sloped dotted lines (redrawn from Jennings and Lucia 2001).

Another slightly different method exists which involves attributing data within separate Hydraulic Flow Units (HFU's) which are defined by FZI's (Amaefule et al. 1993). A flow unit differs from a petrophysical group: petrophysical groups are single or groups of lithofacies with similar porosity and permeability relationships whereas flow units are "petrophysical groups with spatial continuity", defining zones with similar flow properties within the reservoir units that should be preserved during up scaling (Gomes et al. 2008). That is, flow units are areas with spatially continuous flow properties that are not defined by specific lithofacies, pore types, and pore distributions, within single reservoir units, that should be preserved during up scaling. The porosity and permeability data can be plotted on a base map of different flow units (Corbett & Potter 2004), defined by FZI's:

Equation 8.6: $FZI = RQI/\Phi z = (0.0314(\sqrt{k}/\phi))/(\phi/1-\phi)$

(Amerfule et al. 1993, Corbett 2009, Shenawi et al. 2009)

Where RQI is the Reservoir Quality Index, which is based on the proportion of permeability to the amount of porosity, and the Φ_Z is the pore volume to grain volume ratio. On a log-log plot of RQI data plotted against Φ_Z, all samples with similar FZI values will align along a sloped line (Amaefule et al. 1993). Samples that lie on the same line have the same pore throat attributes and constitute a single HFU (Shenawi et al. 2009).

Studies from Corbett & Potter (2009) have also used FZI to constitute different flow units, however instead of associating data along single sloped lines (HFU's) the data is placed within bands (Global Hydraulic Element: GHE's). By rearranging the previous equation, lines for constant FZI are determined (Corbett & Potter 2009):

Equation 8.7: $$K = \emptyset \left[(FZI)(\emptyset/1-\emptyset) / 0.0314 \right] 2$$

For each FZI a GHE has been assigned to it (Table 8.3 & Fig. 8.6). Ten separate GHE's are established (Corbett 2009). The placement of lines separating the GHE bands is arbitrary and is only designed to cover the largest possible range of porosity and permeability relationships (Corbett & Potter 2009).

FZI	GHE
48	10
24	9
12	8
6	7
3	6
1.5	5
0.75	4
0.375	3
0.1875	2
0.0938	1

Table 8.3: The FZI values converted the GHE values (redrawn from Corbett 2009).

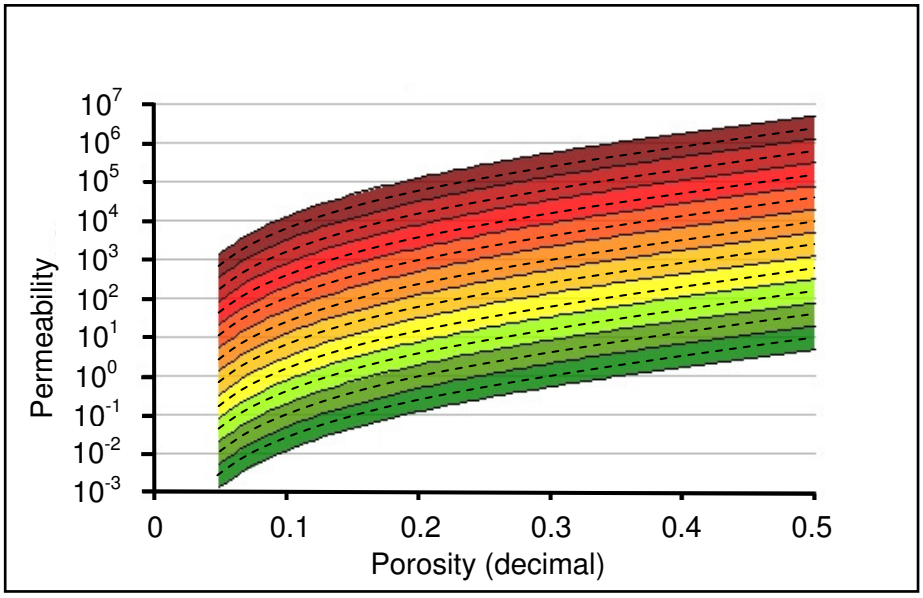

Figure 8.6: The Petrotype atlas method: each coloured band represents a GHE, which is centred on FZI's (dotted lines). To see values for FZI bands see Table 8.3) (redrawn from Corbett & Potter 2004).

The Lucia (1999) method only considers the amount of grains, their size and distribution, which defines the size and distribution of interparticle pores: this would suit characterising the reservoirs of the Lower Kharaib Formation, as it contains the highest proportion of interparticle pore spaces (Sections 3.5.3 & 5.3.4). However not involving the other pore types, and more importantly the microporosity, will not provide the best overview for the Lekhwair formation reservoirs, and will ultimately not maximise its oil producing potential.

With the Petrotype atlas method, instead of relating the highest porosity and permeability data to only interparticle pore systems, data from the entire succession is plotted and grouped according to their flow properties. These individual flow units are then tied to separate lithological units defined by petrographic analysis (Gomes et al. 2008). The most likely result is several reservoirs, containing many different internal flow units, being recognised as good oil producing units, which may overcomplicate the situation. However this will provide a better overview for a carbonate pore system. For instance, lower grade flow units (i.e. GHE 1 to 3: Fig. 8.6) can also be attributed to lower grade reservoir horizons, which may be dominated by less well connected pore types, or by microporosity. A more detailed understanding of where the best and the lower grade reservoirs exist within a specific carbonate succession can potentially be achieved.

8.2 Results

8.2.1-General lithological classifications

The abbreviations for the seven general lithologies that are used within this Chapter, based on Section 3.4.1, are as follows (Table 8.4):

Lithology	Abbreviations
Argillaceous Micrite/mudstone	AM
Pyritised Micrite/mudstone	PM
Orbitolinidae Shell Hash	*o*SH
Burrowed Wackestone	BW
G. costatus and *Lithocodium/B.* wackestone and packstone	*g*WP
G. costatus and *Lithocodium/B*. packstone and grainstone	*gl*PG
Lithocodium/B. boundstone	*l*B

Table 8.4: abbreviations used for the general lithologies within this Chapter.

8.2.2 Summary diagrams for Wells 1-5.

Well 1 (water leg)

Well 1 only covers the Lower Kharaib Formation, in the water leg (Cycle 1), and mainly comprises BW with *gl*WP: both lithologies are concentrated in micrite grains. Consequently there is abundance in interparticle porosity (Section 5.3.4 & 5.5), producing a well connected interparticle pore system, which is reflected in the porosity and permeability data. The porosity on average is 20% while the permeability is 0.1-9.5mD (Fig. 8.7).

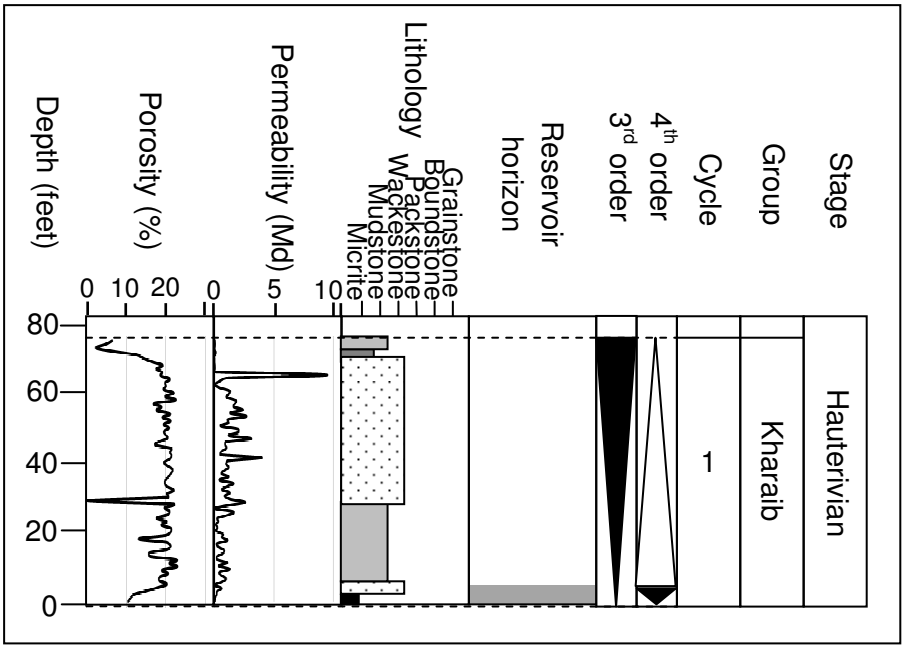

Figure 8.7: porosity and permeability data against the stratigraphy for Well 1. The white triangles represent the HST's while the black triangles represent the TST's. The dotted black lines represent 4th order SB's. Black represents AM, dark grey represents PM, light grey represents BW, sparse dots represents gl*WP, black with white dots represent* l*B and concentrated dots represents* gl*PG. In the reservoir column white represents reservoir and light grey represents non-reservoir.*

Well 2 (transition zone)

The highest porosity values exist within Cycle 7a of 25%: all the other 4th order HFC's have porosity spikes ranging between 20-25% (Fig. 8.8). The permeability is highest in Cycle 6 of 25mD, and in Cycle 7a of 20mD (Fig. 8.8). The high porosity and permeability mostly coincides with the 4th order HST's, reservoirs, BW, *gl*WP, *l*B and g*l*PG (Fig. 8.8).

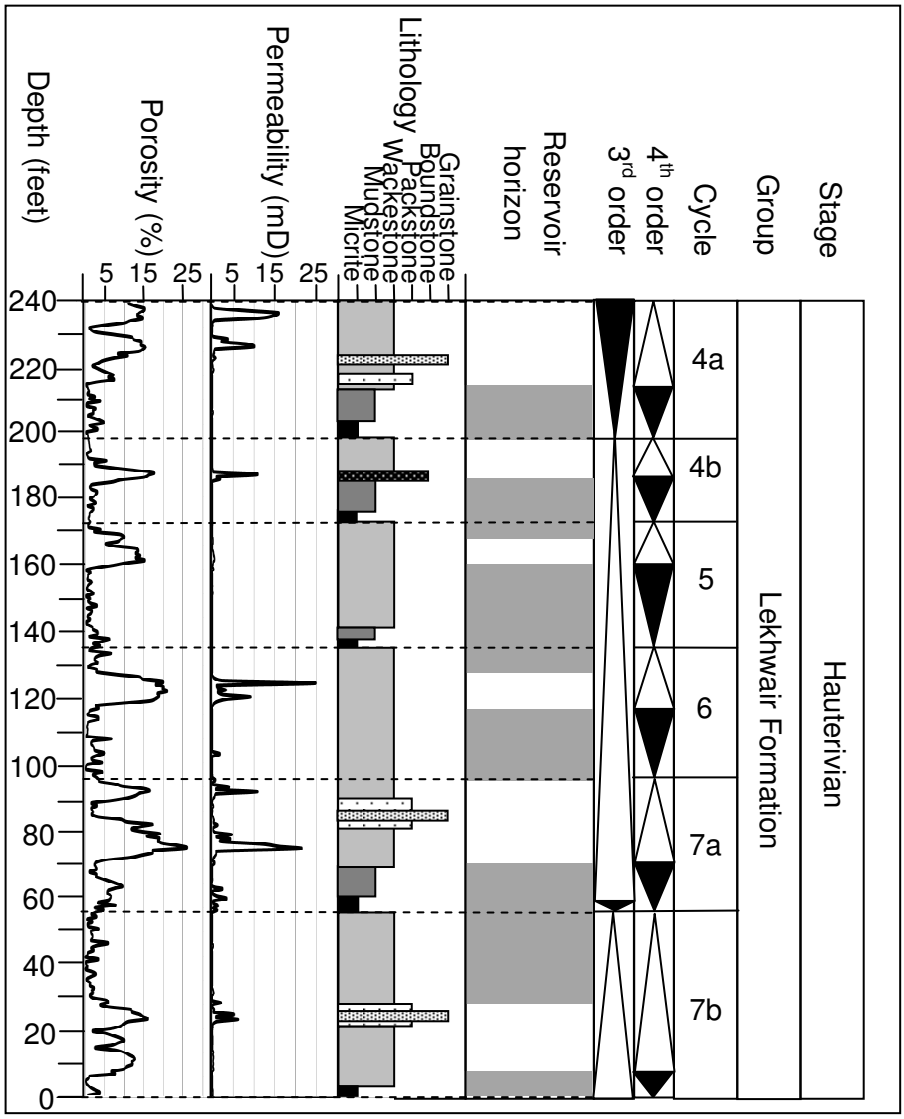

Figure 8.8: porosity and permeability data against the stratigraphy for Well 2. The white triangles represent the HST's while the black triangles represent the TST's. The dotted black lines represent 4th order SB's. Black represents AM, dark grey represents PM, light grey represents BW, sparse dots represents g*lWP, black with white dots represent* l*B and concentrated dots represents* g*lPG. In the reservoir column white represents reservoir and light grey represents non reservoir.*

Well 3 (oil leg)

The highest porosity values are present within Cycles 1, 3, 6 and 7a of 30% (Fig. 8.9). The porosity generally decreases within the reservoirs toward the base of the Lekhwair Formation and Cycle 7b: with porosity values of 10-15% (Fig. 8.9). The highest permeability exist within Cycle 3 of near 350mD, with Cycle 7a having near 150mD and the majority of all the other 4th order HFC's have permeability near 50mD (Fig. 8.9). The highest porosity and permeability spikes mostly coincide with one another with HST's, reservoirs, BW, *gl*WP and *gl*PG within each 4th order HFC.

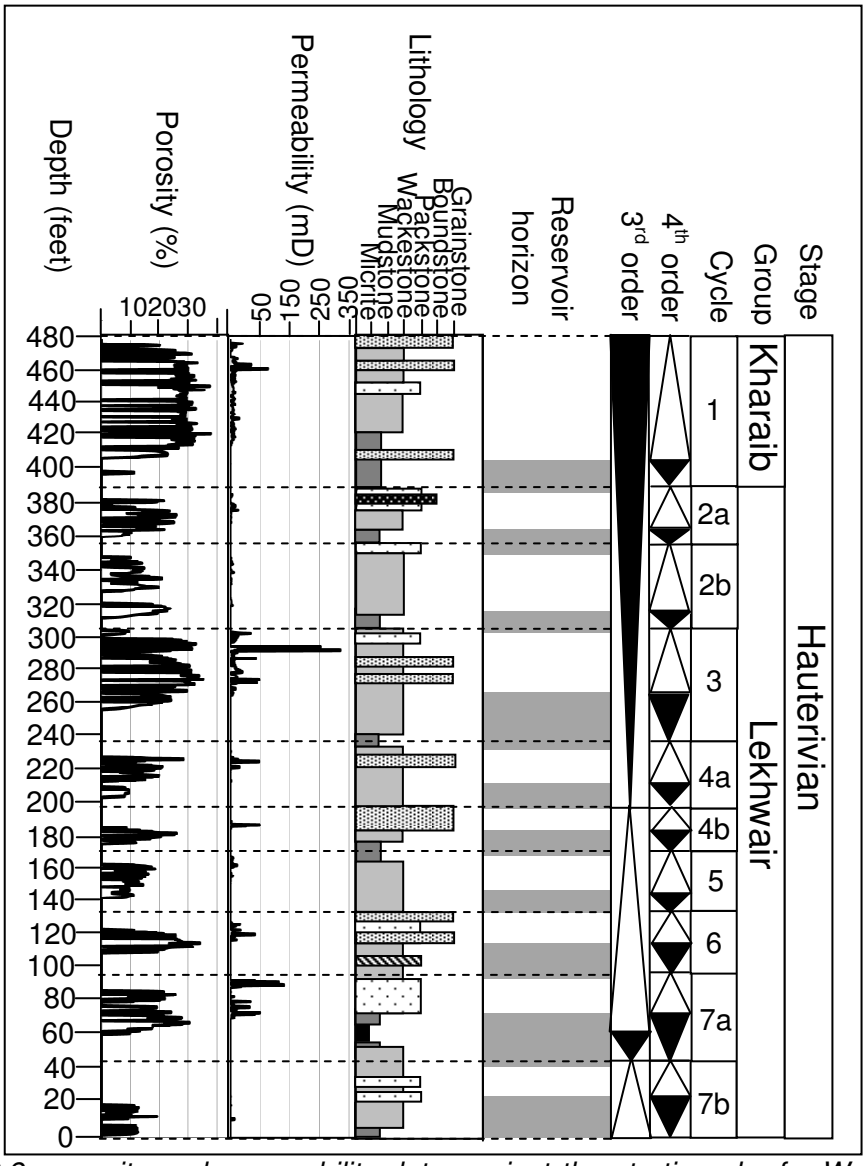

Figure 8.9: porosity and permeability data against the stratigraphy for Well 3. The white triangles represent the HST's while the black triangles represent the TST's. The dotted black lines represent 4th order SB's. Black represents AM, dark grey represents PM, light grey represents BW, sparse dots represents gl*WP, black with white dots represent* l*B and concentrated dots represents* gl*PG. In the reservoir column white represents reservoir and light grey represents non reservoir.*

Well 4 (oil leg)

The highest porosity and permeability values exist within Cycle 1 (Lower Kharaib Formation) with average values of 25-30% and 800-900mD, respectively (Fig. 8.10). These data mark the highest permeability values recorded within the study. The highest porosity and permeability data mostly coincides with HST's, reservoirs, BW, *gl*WP and *gl*PG (Fig. 8.10). All the other 4th order HFC's have ~10% porosity and 10-30mD permeability (Fig. 8.10).

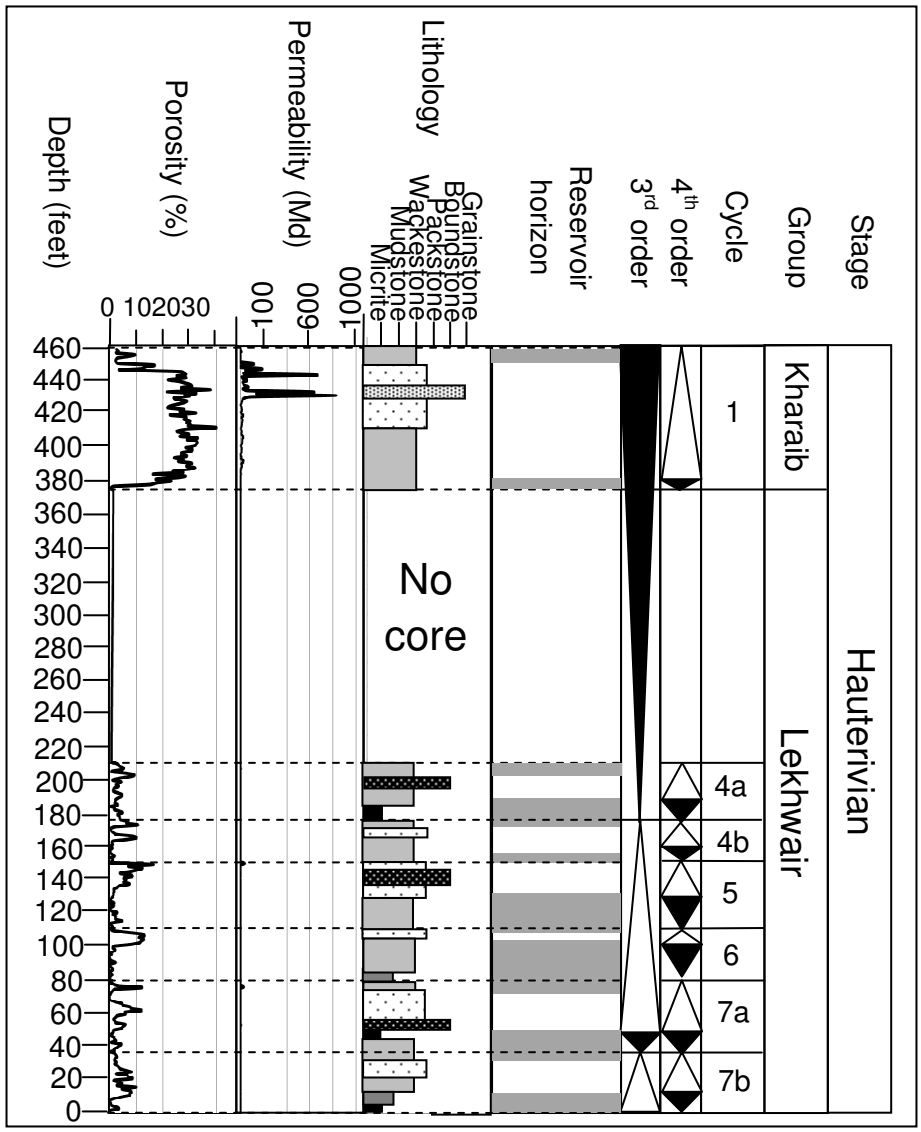

Figure 8.10: porosity and permeability data against the stratigraphy for Well 4. The white triangles represent the HST's while the black triangles represent the TST's. The dotted black lines represent 4th order SB's. Black represents AM, dark grey represents PM, light grey represents BW, sparse dots represents gl*WP, black with white dots represent* l*B and concentrated dots represents* gl*PG. In the reservoir column white represents reservoir and light grey represents non reservoir.*

Well 5 (transition zone)

The highest porosity values are within Cycles 3 and 7b with values of 25% (Fig. 8.11). All the other 4th order HFC's have porosity values of 10-20% (Fig. 8.11). The highest permeability values are 20-35mD and coincide with the highest porosity values in Cycles 3 and 7b (Fig. 8.11). These highest porosity and permeability values also coincide with HST's, reservoirs, BW, *gl*WP (Fig. 8.11).

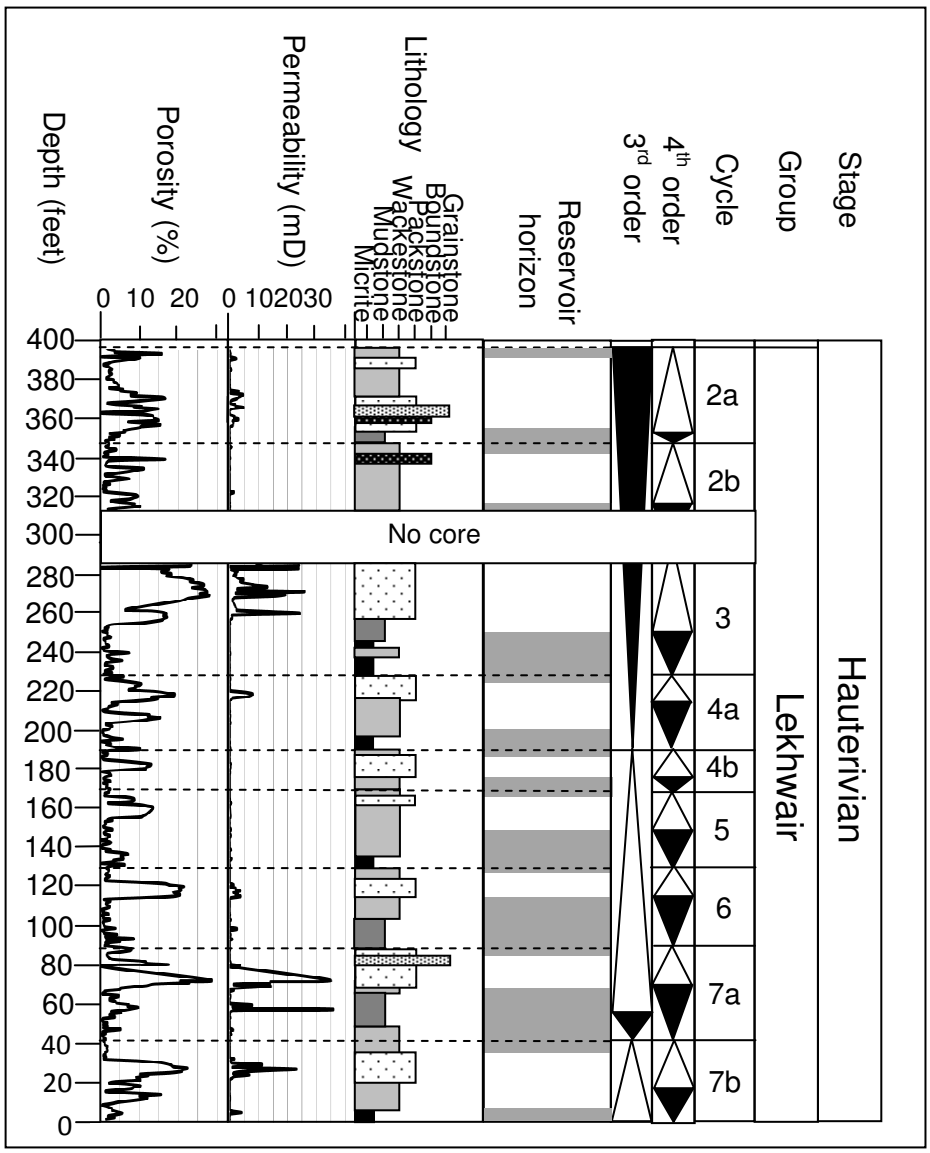

Figure 8.11: porosity and permeability data against the stratigraphy for Well 5. The white triangles represent the HST's while the black triangles represent the TST's. The dotted black lines represent 4th order SB's. Black represents AM, dark grey represents PM, light grey represents BW, sparse dots represents gl*WP, black with white dots represent* l*B and concentrated dots represents* gl*PG. In the reservoir column white represents reservoir and light grey represents non reservoir.*

8.2.3 Reservoir permeability

On the porosity and permeability plots in Appendix 6, the permeability spikes only for a small proportion within most reservoirs. In core, the lowermost and topmost feet of every reservoir horizon are oil free despite no change in lithology (Section 3.4.1 & Fig. 3.14). Lønøy (2006) implies that rocks with <1mD are not considered as reservoirs. However, each reservoir contains an extensive area of low permeability (<1mD), which in core, are oil stained. Table 8.5, shows the percentage of permeability data, from within each oil stained reservoir, with values >1mD and <1mD.

	Permeability (mD)	Well 1	Well 2	Well 3	Well 4	Well 5
Cycle 1	>1	42.5	n/a	82.9	94.8	n/a
Cycle 1	<1	57.5	n/a	17.1	3.2	n/a
Cycle 2a	>1	n/a	n/a	45.1	n/a	29.6
Cycle 2a	<1	n/a	n/a	54.9	n/a	70.4
Cycle 2b	>1	n/a	n/a	29.6	n/a	3.1
Cycle 2b	<1	n/a	n/a	70.4	n/a	96.9
Cycle 3	>1	n/a	n/a	62.5	n/a	68.4
Cycle 3	<1	n/a	n/a	37.5	n/a	31.6
Cycle 4a	>1	n/a	23.5	17.7	0	14.3
Cycle 4a	<1	n/a	76.5	82.3	100	85.7
Cycle 4b	>1	n/a	25	38.7	0	0
Cycle 4b	<1	n/a	75	61.3	100	100
Cycle 5	>1	n/a	0	28.4	37.5	0
Cycle 5	<1	n/a	100	71.6	62.5	100
Cycle 6	>1	n/a	76.9	55.3	0	50
Cycle 6	<1	n/a	23.1	44.7	100	50
Cycle 7a	>1	n/a	34.4	22.4	7.7	55.6
Cycle 7a	<1	n/a	65.6	77.6	92.3	44.4
Cycle 7b	>1	n/a	13.8	2.7	12.5	75.3
Cycle 7b	<1	n/a	86.2	97.6	83.5	24.7

Table 8.5: percentage of each reservoir containing permeability >1mD, and <1mD.

8.2.4 4th order porosity and permeability trends with the lithologies

The lithological trends, shown here, relate to the porosity and permeability relationships displayed in Appendix 6. The AM has porosity of 0-11% and permeability of 0.01-10mD (Fig. 8.12A). The PM has porosity of 0-26% and permeability of 0.01-10mD (Fig. 8.12B) (2 outliers exist with permeability ranging

up to 50mD). The *o*SH has too few data to remark on its porosity and permeability relationships. The BW has porosity and permeability distributions covering six orders of magnitude from 0%-37% and from 0.001-370mD, respectively (Fig. 8.13A). The *gl*WP has high porosity and permeability (which spans 5 orders of magnitude), ranging from 0- 40%, and from 0.01-670mD, respectively (one outlier with 0.001mD) (Fig. 8.13B). The *l*B has lower porosity and permeability, ranging from 0-20% and from 0.01-100mD, respectively (Fig. 8.14A). The *gl*PG has porosity of 5-32% and permeability (6 order magnitude range) of 0.001-830mD (Fig. 8.14B): the *gl*PG has the highest porosity and permeability relationships.

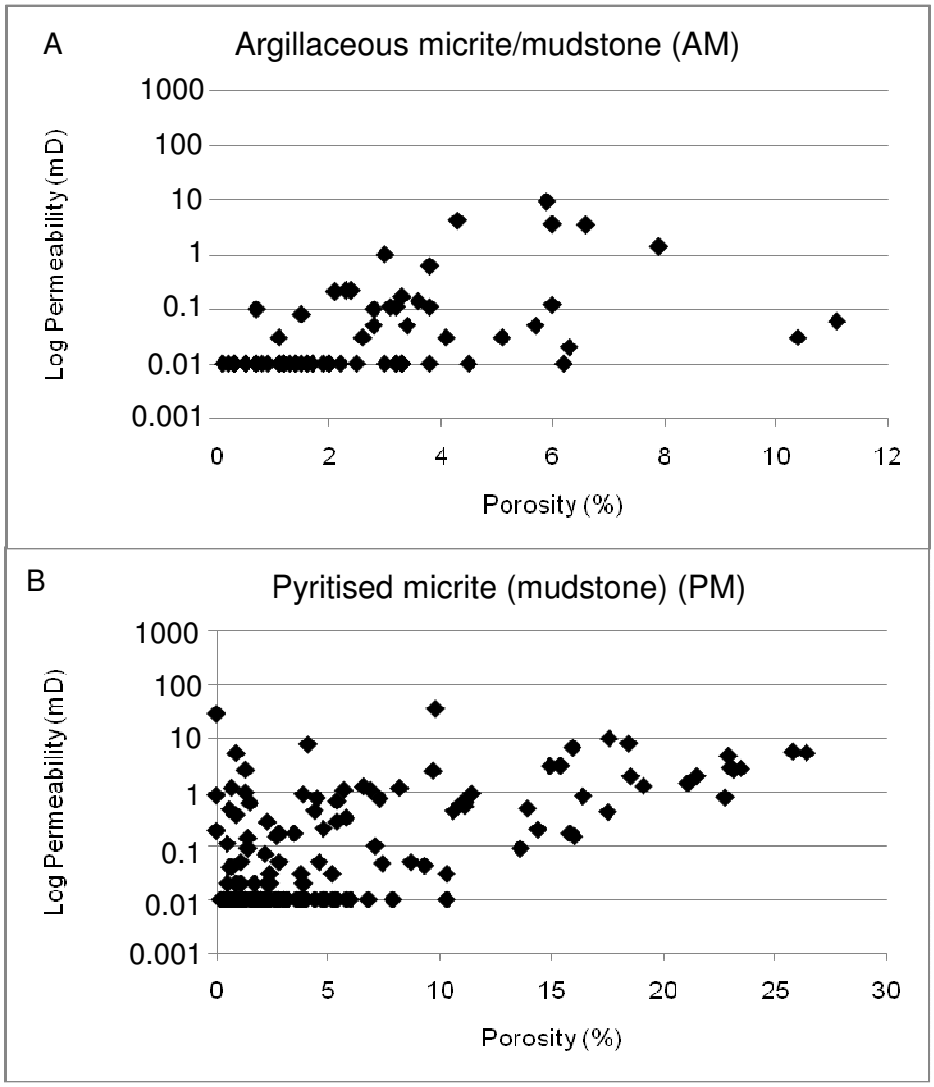

Figure 8.12: data for the Lekhwair and Lower Kharaib Formations is classed into six broad lithologies on Log permeability against porosity plots: A) AM, and B) PM, are plotted.

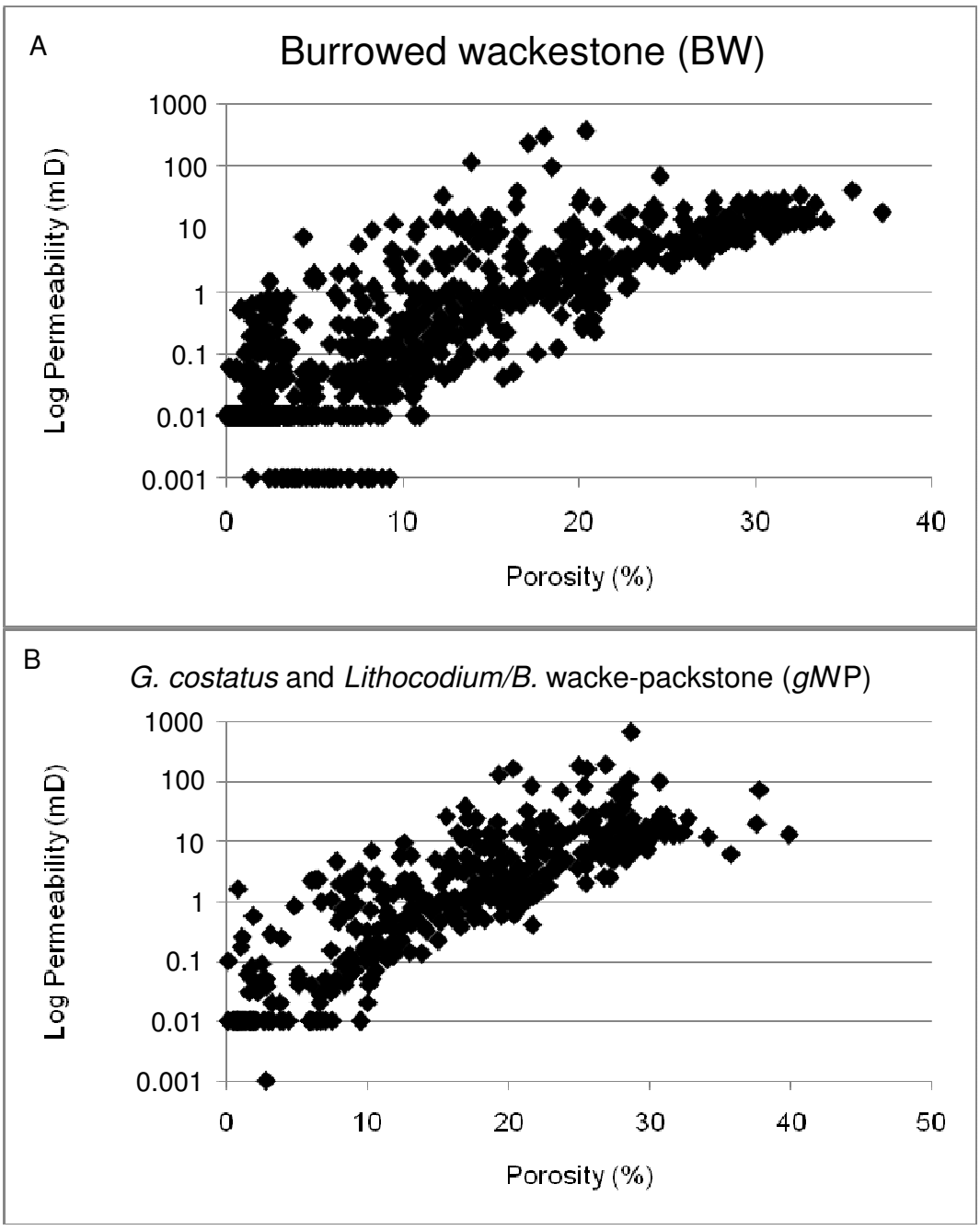

Figure 8.13: data for the Lekhwair and Lower Kharaib Formations is classed into six broad lithologies on Log permeability against porosity plots: A) BW, and B) gl*WP*, *are plotted.*

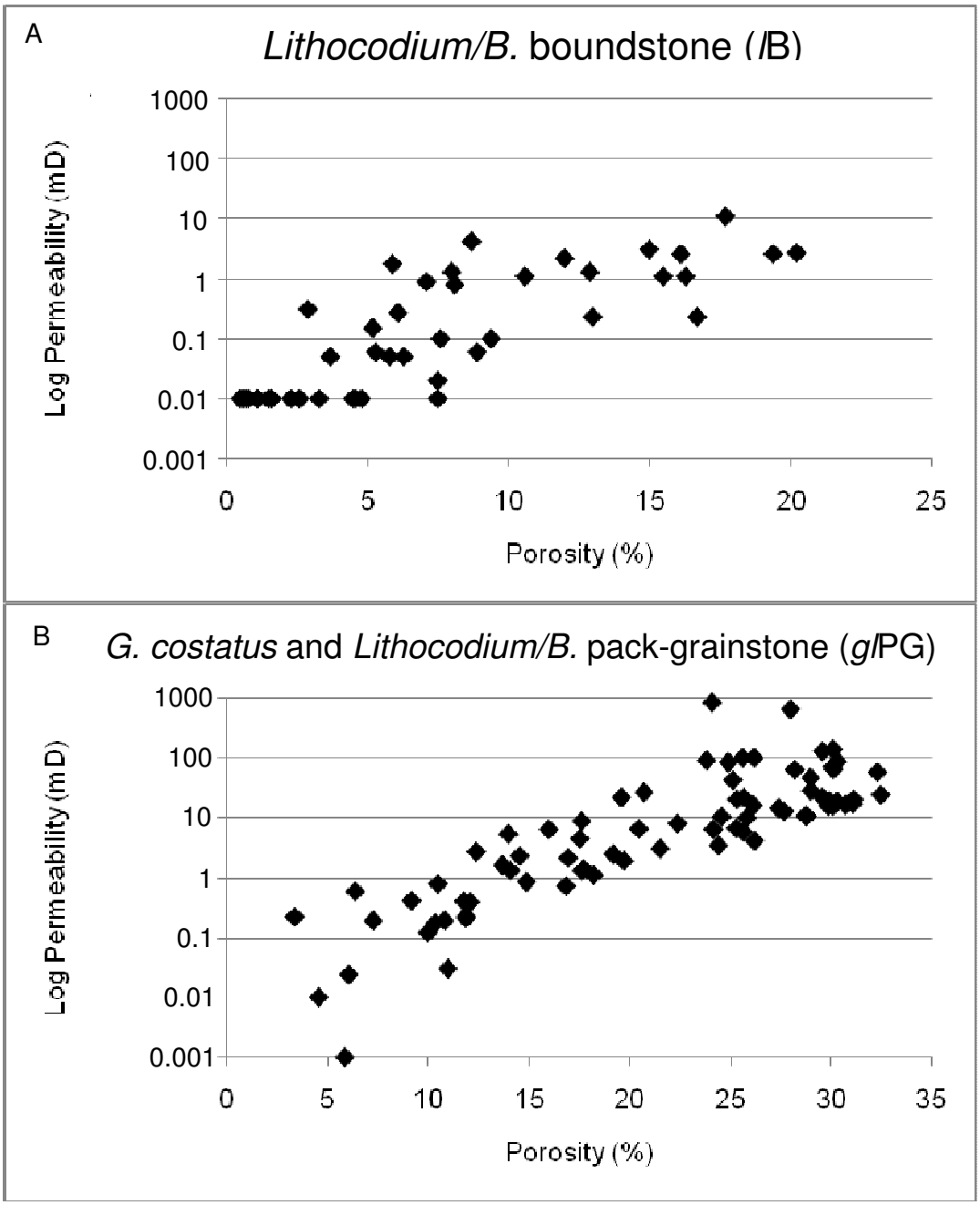

*Figure 8.14: data for the Lekhwair and Lower Kharaib Formations is classed into six broad lithologies on Log permeability against porosity plots: A) l*B*, and B) gl*PG*, are plotted.*

8.3 Interpretations

8.3.1 Lithological trends

The AM and the PM have low porosity and permeability relationships (Fig. 8.12A & 8.12B): this is expected considering that they comprise the majority of the basal TST muds/micrites within every 4th order HFC.

The highest porosity and permeability relationships are within the BW, the *gl*WP and *gl*PG fractions (Figs. 8.13A, 8.13B & 8.14B). However, all three lithologies show large ranges in porosity and permeability. The data distribution representing 10-37% porosity and 10-370mD permeability for BW (up to 40% porosity and 670mD permeability for *gl*WP; up to 32% porosity and 830mD permeability for *gl*PG) must relate to the porosity and permeability spikes that are associated with the mid-late HST's (Figs. 8.7-8.11: Appendix 6). The data distributions for BW, the *gl*WP, and the *gl*PG, representing porosity values of 0%-10% and permeability of 0-10mD must represent the lower grade reservoirs associated with the early and late HST's (Figs. 8.7-8.11: Appendix 6).

The *l*B shows relatively high porosity of up to 20% but low permeability of up to 10mD (Fig 8.14B). This may be related to the abundance of *Lithocodium/B.* within this lithology, which contains many intra-skeletal pores representing its internal chambers, which are mostly isolated and disconnected (Sections 5.3.4 & 5.5).

The Lower Kharaib Formation and Cycle 1 (oil leg) (Figs. 8.7-8.11) shows the highest porosity and permeability relationships, as its reservoirs are dominated by more interconnected interparticle pore spaces (Sections, 3.5.3, 5.3.4 & 5.5), in comparison with the intra-skeletal pore-dominated Lekhwair Formation (Sections 5.3.4 & 5.5).

The Lekhwair Formation shows high permeability spikes that correspond with the highest porosity values within the BW, *gl*WP and *gl*PG within the mid-late HST of each 4th order HFC (Figs 8.7-8.11: Appendix 6). These spikes are also associated with small grainstone patches (open interparticle pore spaces) (Section 3.5.2), with larger proportions of open macropores (Sections 5.3.1 & 5.3.2), with the greatest abundance of rounded 1-2µm microspars and micropore Fabric 1 (Section 7.2 &

Appendix 5). The porosity and permeability decreases away from the mid-late HST's, towards the TST bases and towards the capping firmgrounds within most 4th order HFC's. This mimics the trends in cementation and pore occlusion from micropore Fabrics 1, towards 2, and then 3, (Section 7.2.2), suggesting that the 4th order porosity and permeability trends within the Lekhwair Formation are a direct result of cementation and micro/macropore occlusion, due to basal TST micrite/muds dewatering, from mechanical compaction, during progressive burial (Section 7.3.2).

8.4 Rock typing methods

In this section, data for the Lower Kharaib Formation are plotted using the Lucia (1999), Lønøy (2006) and the Petrotype atlas method. The Lower Kharaib Formation was selected because it's the only 4th order HFC, within this study, which traverses the entire field from the water leg in the flanks, to the oil leg in the crest.

8.4.1 Lucia method

The Lucia (1999) method clearly shows the oil leg containing the highest porosity and permeability relationships (Fig. 8.15). Data from both the oil leg and water leg plots mostly within Class 2: considered by Lucia (1999) to represent grain-dominated packstone comprised of 100-20µm grains (Fig. 8.15). This method confirms an important finding: the water leg and the oil leg are dominated by similar sized grains, which is consistent with petrographic observations. However the grains observed throughout the Lower Kharaib Formation, form grainstone, and are 100-500µm in size producing many 100-250µm interparticle pores (Sections 3.4.5, 3.5.3 & 5.3.1.). Therefore, the majority of data for both the oil and water legs should have plotted within Class 1: i.e. grainstone (Fig. 8.15).

There is a marked difference in the porosity and permeability relationships between the water leg and the oil leg that cannot be revealed with this method (Fig. 8.15). The water leg data plots in completely different space in comparison with the oil leg (Fig. 8.15): this method does not highlight the reduction in open macropores. The main difference, is the water leg has up to 98% of its macropores cemented resulting in a maximum of 9.5mD permeability, in comparison with the oil leg where over 90% of its pores are open resulting in 830mD of permeability (Sections 5.3.1 &

5.3.2). The water leg has very little open interparticle pore space, but is instead dominated by interconnected microporosity (Section 7.2.1 & Figs. 7.7-7.9). The water leg is a micropore-dominated reservoir, as opposed to the oil leg which is more macropore-dominated. This study agrees with Lønøy (2006), who concludes that the Lucia (1999) method of classing porosity and permeability by particle size, instead of pore size, does not provide an understanding of diagenesis and the volume of cements within a reservoir.

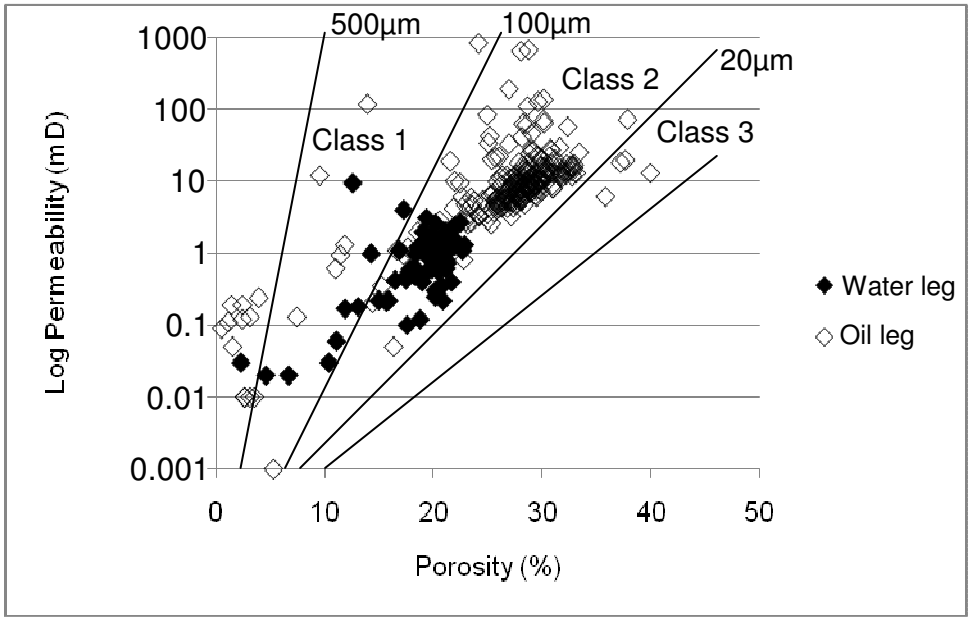

Figure 8.15: porosity and permeability data from the Lower Kharaib Formation plotted using the Lucia (1999) method: Class 1 represents grainstone, Class 2 represents grain-dominated packstone and Class 3 represents mud-dominated fabrics. The class divisions do not separate out the water leg which is micropore-dominated and the oil leg which is macropore-dominated. The oil leg data cluster with permeability of <1mD mostly represents the non-reservoir horizons.

8.4.2 Lønøy method

The method from Lønøy (2006) would class the water leg data, due to macropore cementation, as being micropore-dominated. The water leg data would therefore be plotted as a separate dataset in comparison with the oil leg. This is done in Figure 8.16, with R^2 and regression lines added. The result is expected: although both the water leg and oil leg lithologies share very a similar primary interparticle pore system, both data sets plot different regression lines. This confirms that the amount and distribution of pore types are not the sole contributors to porosity and permeability relationships within Lower Kharaib Formation (Fig. 8.16). This

dramatic difference in porosity and permeability is due to the final pore-occluding cement phase with $\delta^{18}O$ values of -9‰ and -10‰, selectively within the water leg (Section 5.7.1), leaving only the micropores open (Section 7.3.4). Oil emplacement has therefore not only controlled the amount of open macropores, but also indirectly controlled the distribution of open micropores, which are both determining the porosity and permeability relationships of the oil and water legs (Sections 5.7.1 & 7.3.4), within the Lower Kharaib Formation.

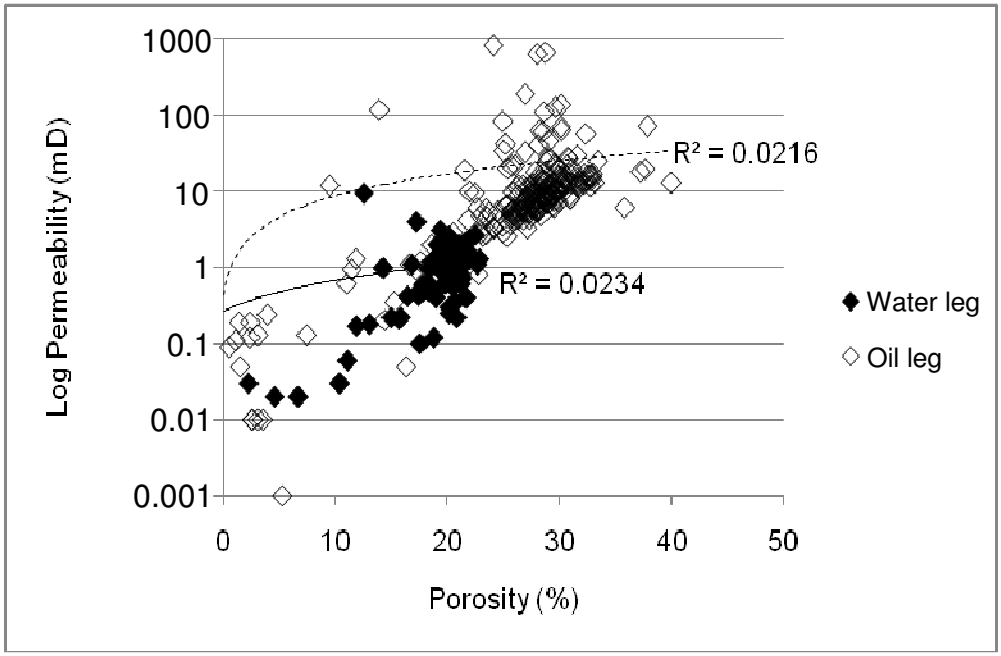

Figure 8.16: porosity and permeability data from the Lower Kharaib Formation plotted using the Lønøy's (2006) method. Despite the water leg and the oil leg sharing similar pore systems, both have very different regression lines. This is most likely due to the final cementation phase with $\delta^{18}O$ values of -9‰ and -10‰, selectively within the water leg, leaving only the micropores open. The oil leg data cluster with permeability of <1mD mostly represents the non-reservoir horizons.

8.4.3 Petrotype atlas method

Comparison of the water leg, transition zone and the oil leg within Cycle 1 (Lower Kharaib Formation), shows that most of the water leg data plots within GHE 1 and 2 (Fig. 8.17A) while the transition zone only plots within GHE 2 and 3 (Fig 8.17B). The oil leg only has data that plots above GHE 3, within GHE 4 and 5 (Figs. 8.18A & 8.18B).

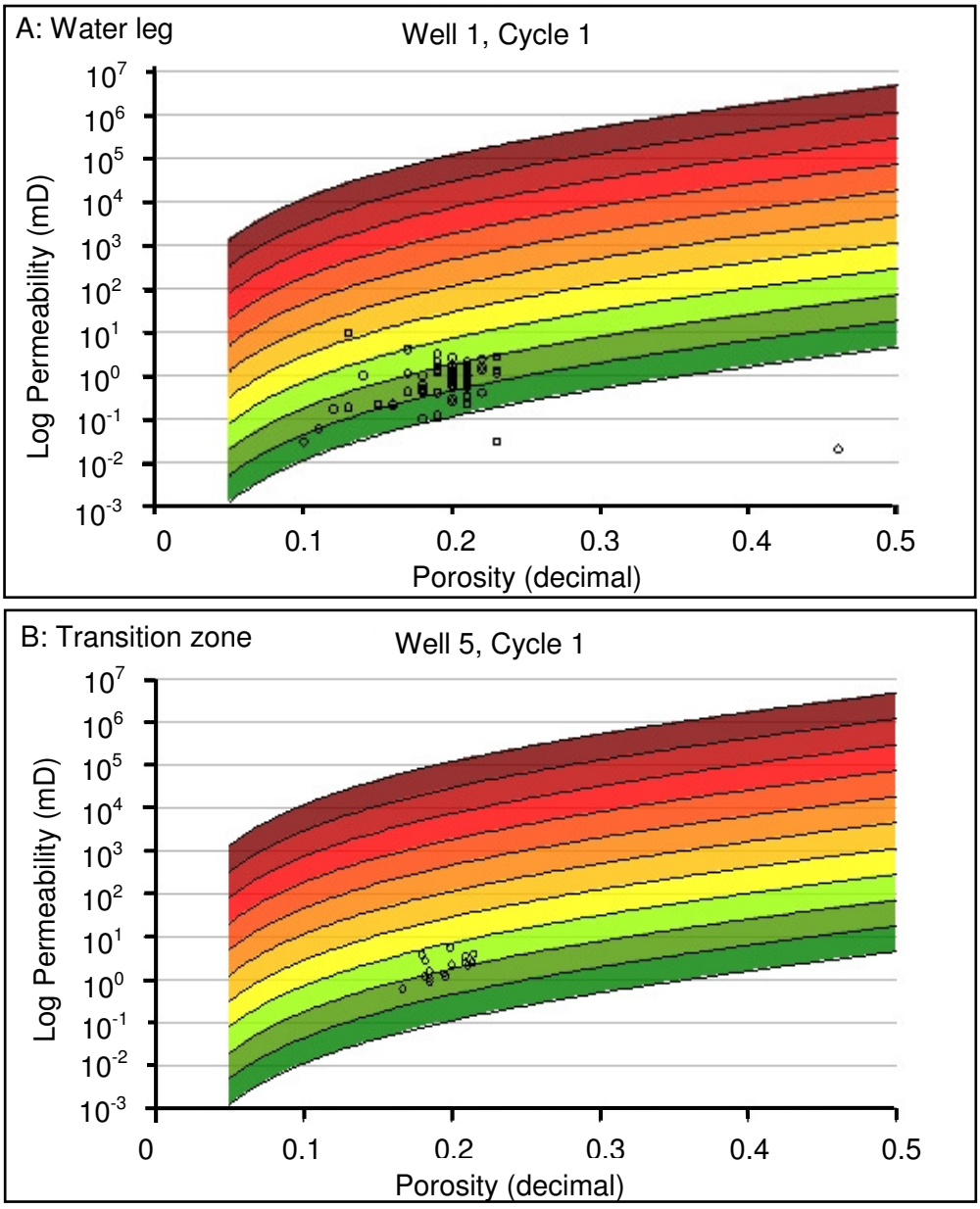

Figure 8.17: porosity and permeability data from the Lower Kharaib Formation plotted using the Petrotype atlas method, with data from A) the water leg, B) the transition zone. The class divisions separate out the water leg (i.e. GHE 1, 2 and 3), which is micropore-dominated.

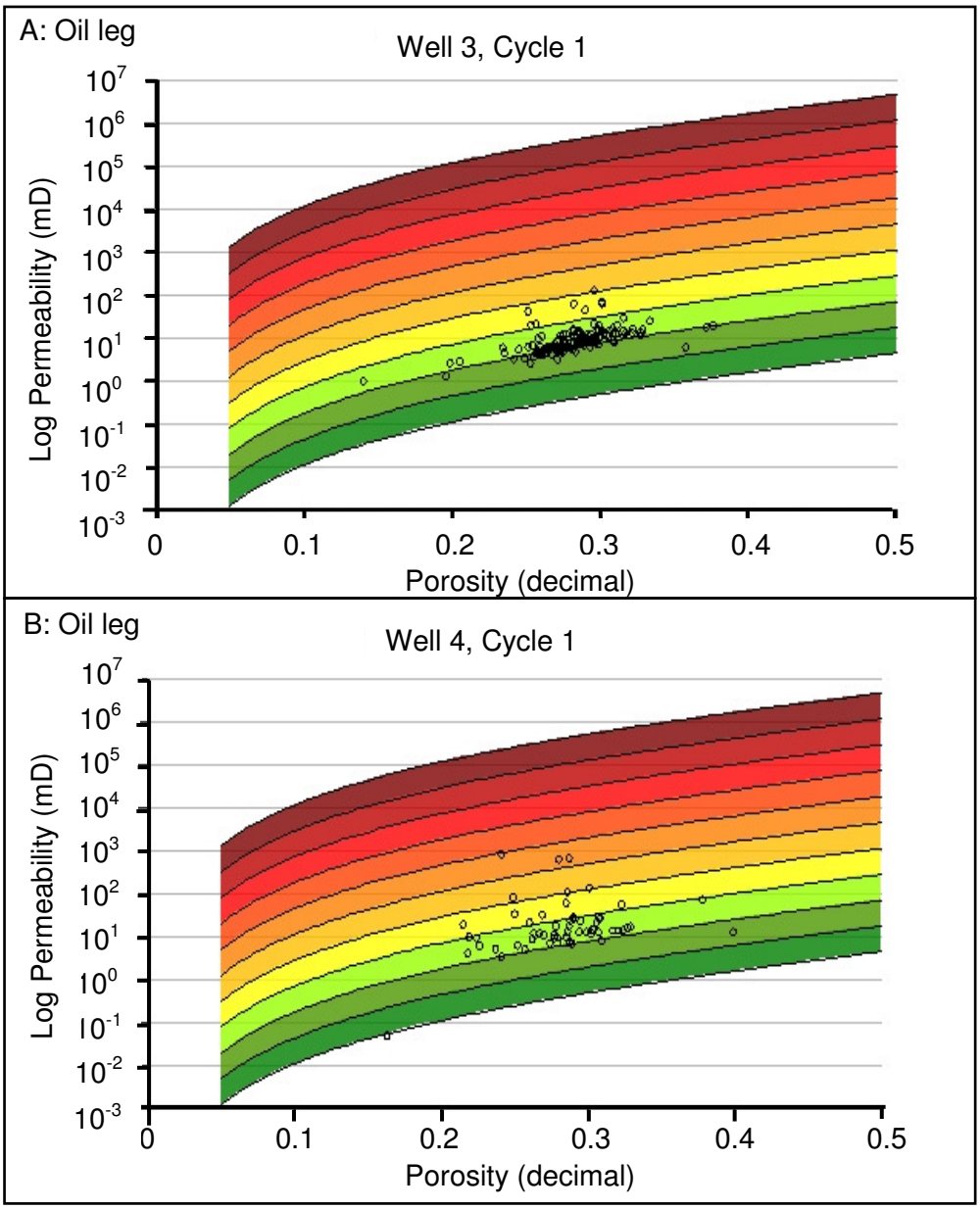

Figure 8.18: porosity and permeability data from the Lower Kharaib Formation plotted using the Petrotype atlas method, with data from A) the oil leg in Well 3 and B) the oil leg in Well 4). The class divisions separate out the oil leg, which is macropore-dominated (i.e. GHE 3+).

The depositional fabric for the Lower Kharaib Formation, as described before, is similar between the oil leg and water leg, as it is composed of grainstone with similar amounts of interparticle porosity, across the structure. The reduction in permeability and porosity towards the water leg indicates that data plotting in GHE 1-2, as opposed to 4-5, are a result of diagenesis and increasing cementation (Section 5.7.1).

Microporosity has remained open in most reservoirs across the structure (Sections 7.2.1 & 7.2.2). The major difference is that the oil leg is dominated by interparticle macropores, whereas the water leg is more dominated by micropores (Section 7.2.1 & 7.2.2). GHE's 1-3 therefore represent micropore-dominated reservoirs while GHE >3 represent macropore-dominated reservoirs. Data distributions relating to greater volumes of cementation are closer, along the same GHE zones, to the y-axis (Figs. 8.17 & 8.18). This method does highlight the impact of diagenesis, and the different flow parameters that exist within the water leg and the oil leg, despite the lithology being the same.

The Petrotype atlas method clearly highlights the importance of microporosity within these carbonates. It therefore seems appropriate to construct another method that accounts for micropore-dominated reservoirs, based on the data from this section on the Lower Kharaib Formation, which can then be subsequently tested on reservoirs within the Lekhwair Formation.

8.5 'Micropore model'

Several Lekhwair Formation reservoirs, within the 4th order HFC's, have 60-80% (with some reservoirs having 100%) of permeability data of <1mD (Table 8.5). These areas are oil stained and can therefore be classed as lower grade reservoirs. The porosity and permeability relationships for these areas lie within the same plotting space as porosity and permeability data from the water leg (Figs. 8.15-8.18). From Sections 5.3.1, 5.3.2 and 7.2, the transition through these lower grade reservoirs, from the porosity and permeability highs in the mid-late HST's into the impermeable basal TST micrite/mudstones, involves the reduction of open macropores leaving only micropores open. Therefore these lower grade reservoirs are most likely micropore-dominated. All theses reservoirs are laterally continuous for many tens of kilometres across this offshore field (the field is roughly 500sq kilometres (extent of Zone IV): Hassan & Wada, 1979). The potential volumetric amount of oil within these micropore-dominated reservoirs is therefore very high.

Being able to determine the stratigraphic positions and the extents of these micropore-dominated reservoirs, as stated in Section 7.3.4, will influence the method

of oil extraction; i.e. a more prolonged sustained oil recovery can be achieved if oil is extracted via the micropores and not the macropores (Section 1.1.2) although much higher entry pressures would be required when exploiting micropore-dominated reservoirs. The micropore-dominated reservoirs can also be distinguished from non-reservoir horizons.

This study proposes a new method which combines components from Petrotype atlas, which conform to the porosity/permeability data distribution of the Lower Kharaib Formation, with other aspects from this study: i.e. the intra-skeletal pore bracket. This 'combination method' defines a new division highlighting data potentially representing micropore-dominated reservoir sections (Fig. 8.19), hence this new model is termed 'Micropore model'. Data distributions representing micropore-dominated reservoirs can be highlighted and separated out from reservoir datasets, and from data associated with the non-reservoir horizons (Fig. 8.19). The main distinction on the Petrotype atlas plots for macropore- and micropore-dominated systems is GHE 3, which is defined as 0.1mD at 5% porosity, and 100mD at 50% porosity. A line is drawn at this point separating out data that represents micro- and macropore-dominated systems. The gradient of the line is:

Equation 8.8: $$y = 0.0974e^{0.1378x}$$

Data that plots within the micropore-dominated bracket and on the line defined in Equation 8.8 is classed as representing micropore-dominated reservoirs. Therefore only data that plots above the line defined in Equation 8.8 are classed as representing macropore-dominated reservoirs.

A second line is drawn separating out the non-reservoir data, at 0.1mD, at all porosities, which seems appropriate for the Lekhwair and Lower Kharaib Formations. However, other carbonate reservoirs may require this line to be placed slightly higher or lower, i.e. this line is not definitely defined, and should probably vary depending on the carbonate. Data that plots on or below this line is classed as representing non-reservoirs.

Therefore, unlike the Petrotype atlas method, which has ten arbitrary bands (GHE's: Fig. 8.6), the new 'Micropore model' only focuses on defining two lines as a starting point. New categories could be added through further testing in the future.

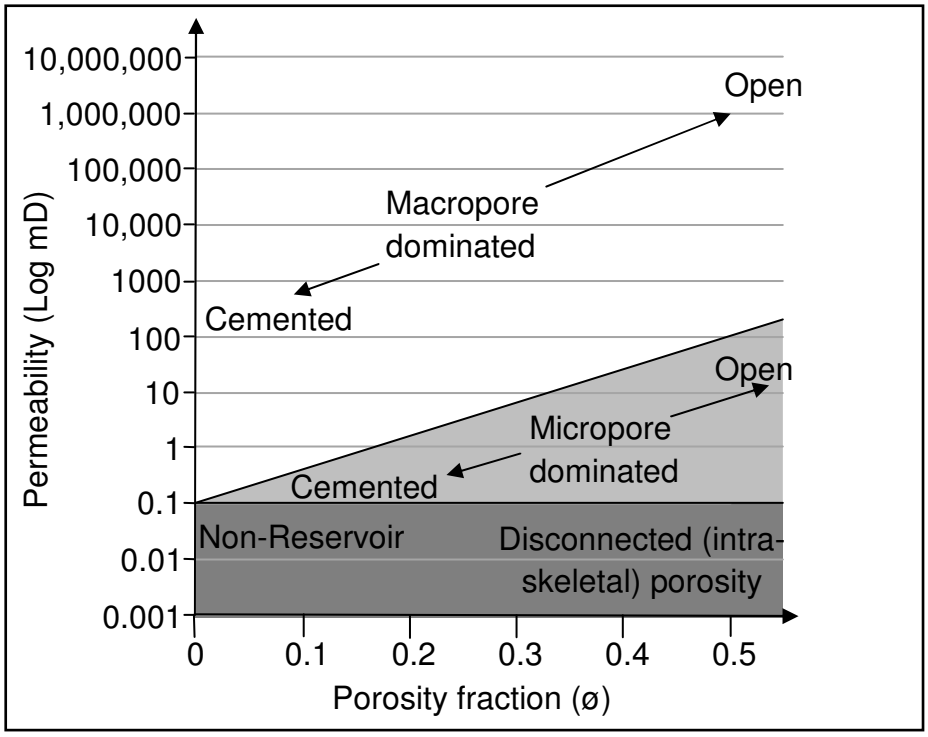

Figure 8.19: A new 'Micropore model' incorporating an area for data representing micropore-dominated reservoirs (light grey area), from the macropore-dominated reservoirs (white area) and the non-reservoir areas (dark grey area). Lower permeable areas can be separated from the main dataset and from data representing the non-reservoirs.

8.6 Application of 'Micropore model'

The porosity and permeability data are plotted for Cycle 4a in Well 2 (Fig. 8.20) and Cycle 4a in Well 3 (Fig 8.21) from the Lekhwair Formation (Figs. 8.20 & 8.21). The same boundaries outlined in Figure 8.19 are applied to each dataset to determine whether all data with permeability <1mD fits within the micropore-dominated reservoir bracket (GHE 1, 2 and 3).

Data are already separated for these HFC's according to reservoir and non-reservoir sections (Appendix 6). A small proportion of the reservoir data plots within the micropore-dominated bracket (Figs. 8.20 & 8.21). A small proportion plots within the non-reservoir bracket, and the rest plots within the macropore-dominated

bracket (Figs. 8.20 & 8.21). This provides a better characterisation of Cycle 4a Reservoir. This shows that micropore-dominated sections can be separated from non-reservoir sections within specific reservoir horizons (Figs. 8.20 & 8.21). This should enable any future oil prospector, when analysing the Lekhwair Formation, to define a larger area for oil extraction.

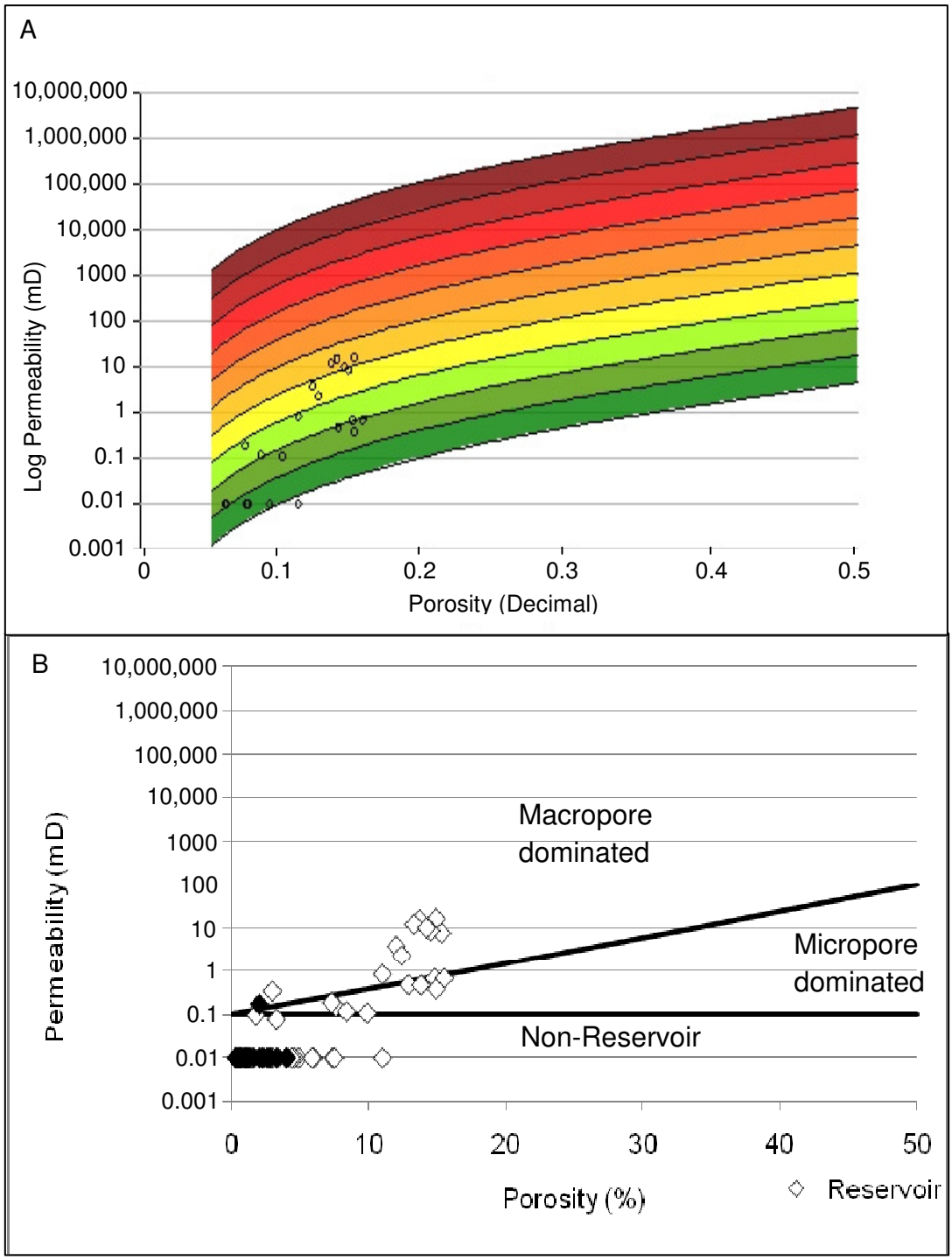

Figure 8.20: porosity and permeability data for Well 2, Cycle 4a: A) the Petrotype atlas method and B) the new 'Micropore model': the two lines define the micropore-dominated reservoir bracket.

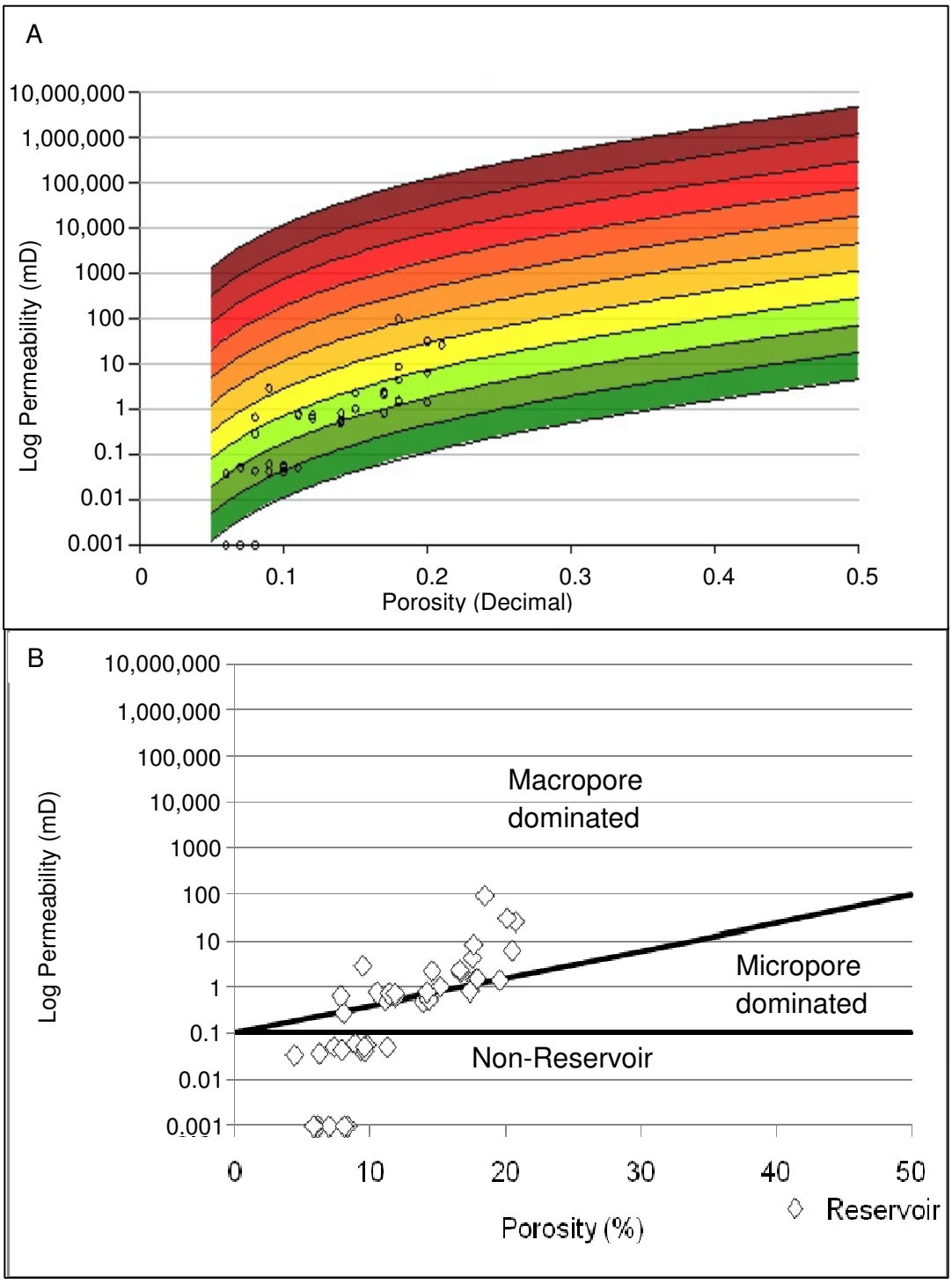

Figure 8.21: porosity and permeability data for Well 3, Cycle 4a: A) the Petrotype atlas method and B) the 'Micropore model': the two lines define the micropore-dominated reservoir bracket.

8.7 Macropore-dominated verses micropore-dominated sections

All the porosity and permeability data of the Lekhwair Formation needs to be plotted using the 'Micropore model'. The amount of porosity and permeability data that may plot within the micropore-dominated bracket can be established. Therefore all the data is plotted using the 'Micropore model' within respect to the six general lithologies. All lithologies show data plotting within the micropore-dominated brackets. However as the AM, PM and *o*SH are rarely oil stained (and rarely reservoirs): these lithologies are not considered a key part in understanding the porosity and permeability relationships. The interest lies within BW, *gl*WP, *l*B and *gl*PG. Not all data could be plotted on the LOG permeability plots, especially for the non-reservoirs, because the porosity and permeability values are zero, and therefore do not plot. This is the reason for percentage values within Table 8.6 for the non-reservoirs being larger in comparison with Figs. 8.22-8.27.

8.7.1 Argillaceous micrite/mudstone (AM)

As expected a large share of the data plots within the non-reservoirs bracket with a small majority within the micropore-dominated reservoirs bracket. However, the AM (comprises 4% of the dataset), is rarely oil stained and is therefore not important (Fig. 8.22).

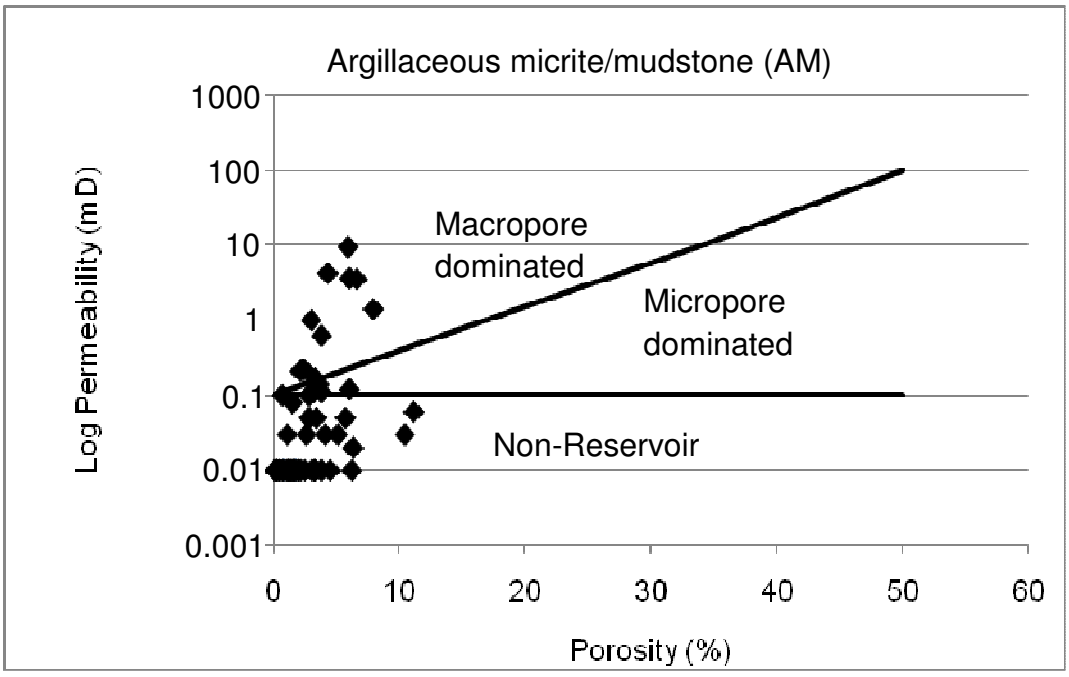

Figure 8.22: porosity and permeability data for AM. The two lines define the micropore-dominated reservoir bracket. Black diamonds represent the non-reservoir sections within each 4th order HFC.

8.7.2 Pyritised micrite (mudstone) (PM)

The PM, which comprises 13% of the dataset, does have a sizable amount of data plotting within the micropore-dominated bracket, with the majority of data plotting within the non-reservoir and especially the macropore-dominated bracket. However, this lithology is rarely oil stained and is therefore not important (Fig. 8.23).

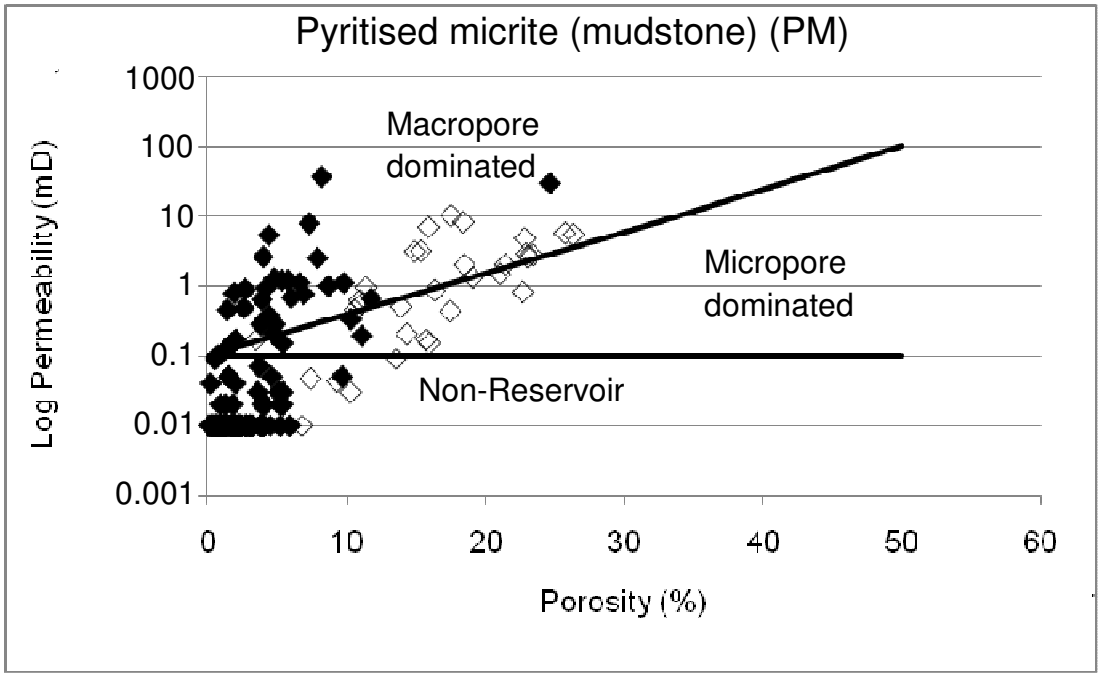

Figure 8.23: porosity and permeability data for PM. The two lines define the micropore-dominated reservoir bracket. Black diamonds represent the non-reservoir sections, and the white diamonds represent the reservoir sections, within each 4th order HFC.

8.7.3 Burrowed wackestone (BW)

The BW, comprising 53% of the entire dataset, has a small fraction of reservoir data plotting within the micropore-dominated and almost half the data plotting within the non-reservoir brackets (Fig. 8.24 & Table 8.6). Some non-reservoir data also plots within the micropore-dominated bracket (Fig. 8.24).

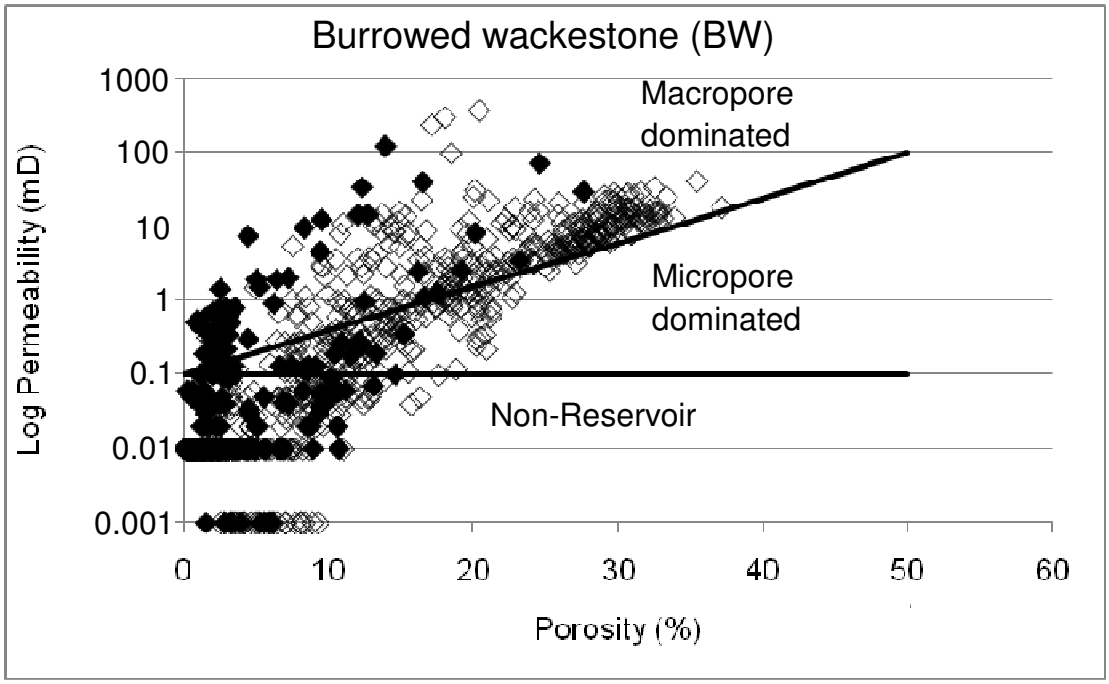

Figure 8.24: porosity and permeability data for BW. The two lines define the micropore-dominated reservoir bracket. Black diamonds represent the non-reservoir sections, and the white diamonds represent the reservoir sections, within each 4th order HFC.

8.7.4 G. costatus and Lithocodium/B. wacke-packstone (glWP)

The *gl*WP, comprising 21.5% of the total dataset, has almost a fifth of the reservoir data plotting within the micropore-dominated bracket and a quarter plotting in the non-reservoir bracket (Fig. 8.25 & Table 8.6). There are some non-reservoir data that plots within the micropore-dominated bracket (Fig. 8.25).

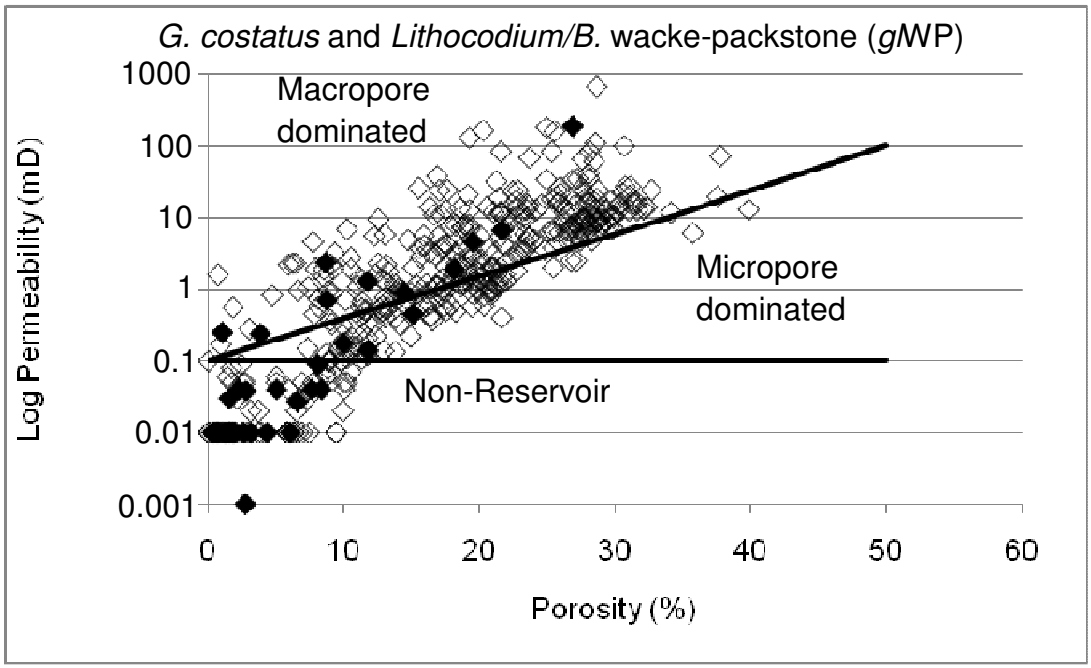

Figure 8.25: porosity and permeability data for gl*WP. The two lines define the micropore-dominated reservoir bracket. Black diamonds represent the non-reservoir sections, and the white diamonds represent the reservoir sections, within each 4th order HFC.*

8.7.5 G. costatus and Lithocodium/B. pack to grainstone (glPG)

The *gl*PG, has 6% of the total dataset, with only a small fraction of reservoir data plotting within the micropore-dominated bracket, but almost half plotting within the non-reservoir bracket (Fig. 8.26 & Table 8.6). It is expected that micropore-dominated reservoirs are limited within *gl*PG, due to it containing the highest porosity/permeability values and therefore the most interconnected macropores.

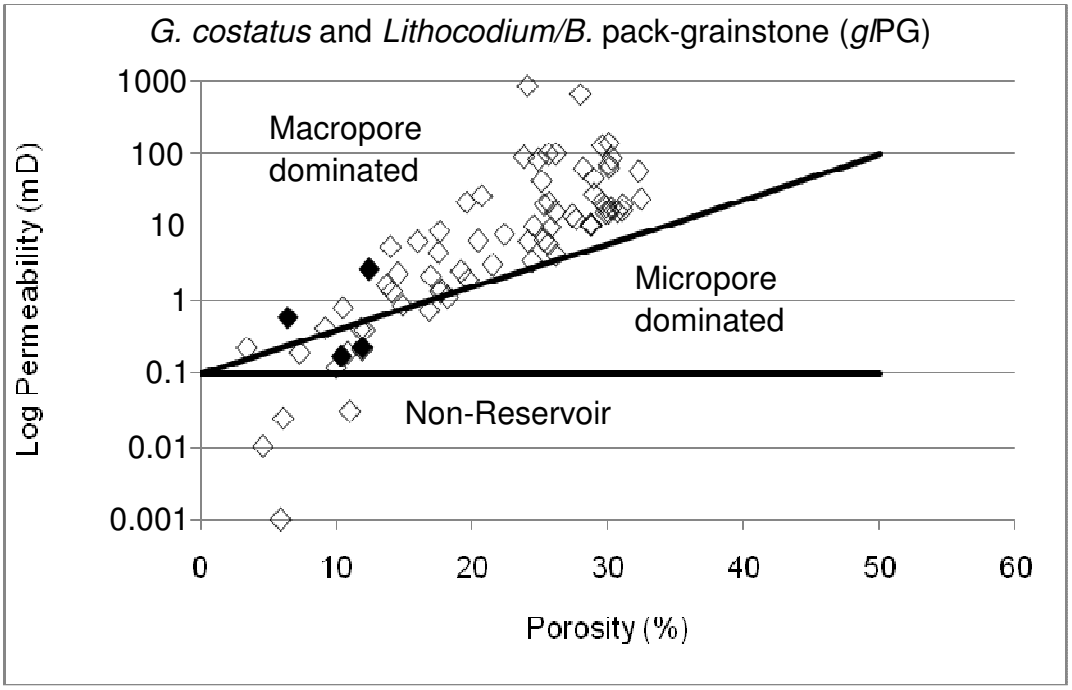

Figure 8.26: porosity and permeability data for gl*PG. The two lines define the micropore-dominated reservoir bracket. Black diamonds represent the non-reservoir sections, and the white diamonds represent the reservoir sections, within each 4th order HFC.*

8.7.6 Lithocodium/B. boundstone (lB)

The *l*B, comprising 2% of the total dataset, has only a small fraction of reservoir data plotting within the micropore-dominated bracket, with over half plotting within the non-reservoir bracket (Fig. 8.27 & Table 8.6).

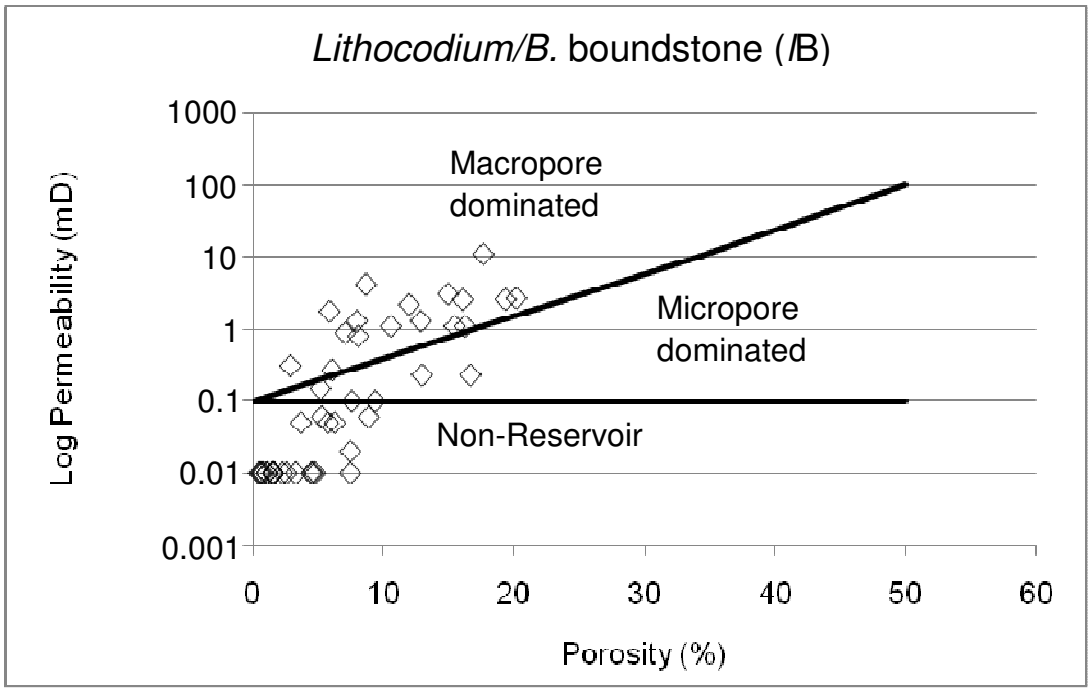

Figure 8.27: porosity and permeability data for lB. The two lines define the micropore-dominated reservoir bracket. Black diamonds represent the non-reservoir sections, and the white diamonds represent the reservoir sections, within each 4th order HFC.

Lithology	Reservoir				Non-reservoir	Total dataset
	% macropore	% micropore	% non-reservoir	% total		
AM	0	0	100	2.2	97.8	3.9
PM	33.4	16.6	50	17.6	82.4	13.1
BW	38.2	17.2	44.6	58.2	41.8	53.2
*g*WP	55.3	19	25.7	88.9	11.1	21.5
*gl*PG	48.4	6.4	45.2	97	3	5.6
*l*B	37	6.5	56.5	100	0	2

Table 8.6: percentages of porosity and permeability data that plot within the macropore-dominated, the micropore-dominated, and the non-reservoir brackets: within the 'micropore model'. This table only considers the reservoir data (white diamonds on Figs.8.22-8.27

8.7.7 'Micropore model' summary

These plots (Figs. 8.22-8.27) are showing that each lithology is composed of at least three major components: 1) macropore-dominated reservoirs, 2) micropore-dominated reservoirs and 3) non-reservoirs. The 'Micropore model' in Figure 8.28B shows that data points, for the same lithology, with very low porosity and permeability (A on Fig. 8.28) reflect completely different open pore systems, in comparison with data of 3 orders of magnitude higher porosity and permeability (B on Fig 8.28). This confirms that calculating a line of correlation through all data points for a single lithology, or lithofacies, (i.e. Lucia (1999) method, Lønøy (2006) method, Winland-Pittman Model, Carmen-Kozey Model) may be incorrect, in comparison with grouping porosity and permeability data into defined and tested categories.

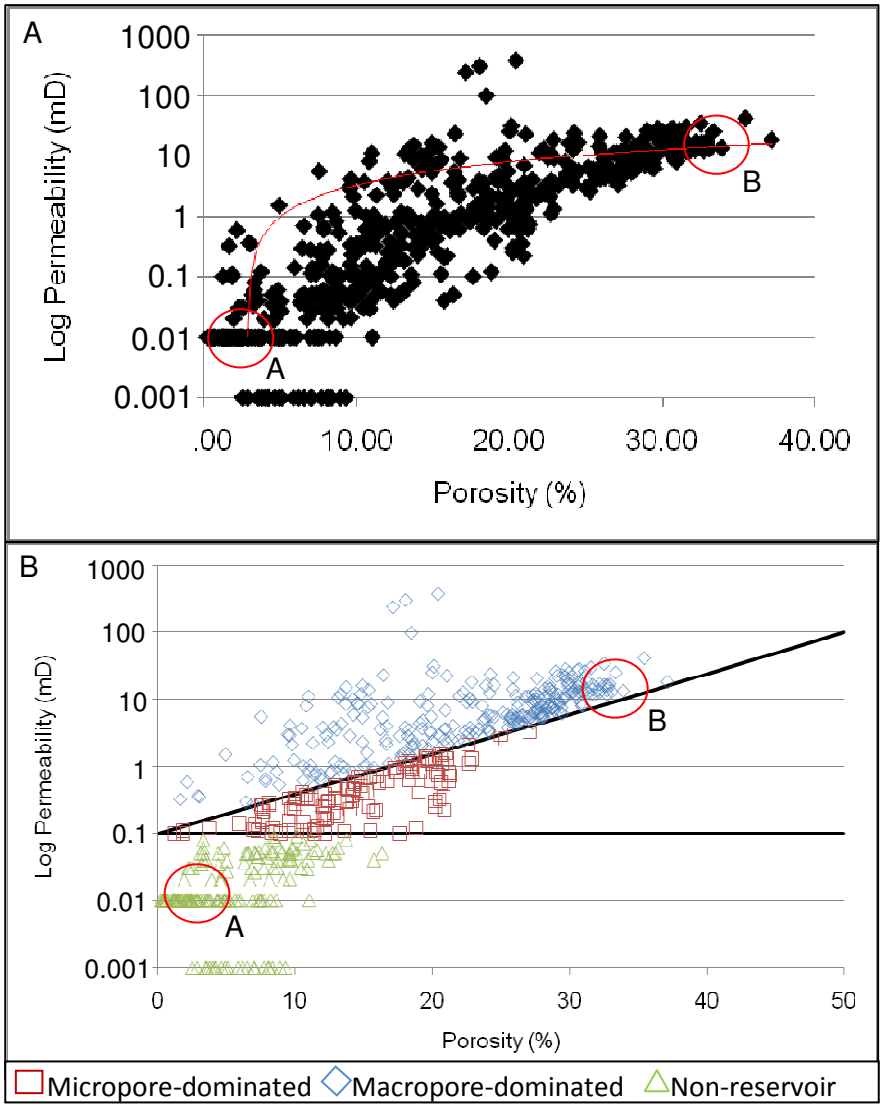

Figure 8.28: porosity and permeability relationships of BW: this lithology was chosen for this figure because it is the largest dataset. A) The data plotted for the whole lithology, with a regression line. B) This lithology has at least three separate internal components: calculating a line of best fit, and therefore correlating the data between positions A and B is incorrect considering these positions reflect very different pore systems, despite the lithology being similar.

8.8 Conclusions

1. The highest porosity and permeability relationships throughout this study exist within the Lower Kharaib Formation and Cycle 1. This is due to the lithology being coarser and more concentrated in packed micrite grains, which supports a well connected open interparticle pore system.

2. Within the Lekhwair Formation, the highest porosity and permeability relationships exist within the reservoirs, within the mid-late HST of each 4th order HFC. These relationships are also associated with grainstone patches, the highest amount of open interparticle pore space, highest amounts of rounded 1-2µm microspars, to micropore Fabric 1, to *gl*WP and to *gl*PG.

3. The oil staining of the reservoirs does not fully correspond to the high permeability values. Many reservoir horizons have areas with slightly lower porosity values of 0-5% and permeability of <1mD that are oil stained in core. These areas appear micropore-dominated. Diagenesis has progressively occluded the macropores of the uppermost and lowermost portions of each reservoir horizon (early and late HST, respectively) leaving only a portion of the micropores open. The macropore-dominated reservoir section appears restricted in most 4th order HFC's to the mid-late HST. The reduction in the amount of macropores was possibly caused by macropore cementation, due to the compaction and dewatering of the micrites/muds, at the TST bases of every 4th order HFC.

4. Analysis of the Lower Kharaib Formation, using the Lucia (1999) method, shows all the Lower Kharaib Formation data plots within two classes, confirming the lithological similarity between the water leg and the oil leg. However, it also shows that forming classes, using grain size rather than pore size, does not account for cementation which reduces the sizes of pores and pore throats. Further analysis, using the Lønøy (2006) method, shows that from the oil leg towards the water leg, the reduction in porosity and permeability is not solely determined by the amount and distribution of pore types. It is also determined by diagenesis through the volume of cements. A new method of pore classification is required that includes the effects of diagenesis.

5. Many Lekhwair Formation reservoirs have sections that plot within the same space as the micropore-dominated water leg of the Lower Kharaib Formation. These sections can encompass up to 80-100% of the reservoir horizons: this proportion indicates the amount of micropore-dominated reservoir within the

Lekhwair Formation. These reservoirs are laterally continuous across the entire field. A significant quantity of oil within this offshore field is housed within micropore-dominated reservoirs. It therefore seems important to be able to distinguish the porosity and permeability relationships of micropore-dominated systems from data representing non-reservoirs. The new 'Micropore model' is able to separate out these relationships: the positions of the micropore-dominated reservoirs can then be used to extract oil from surrounding macropores to provide a more prolonged sustained oil recovery.

6. The 'Micropore model' also provides better characterisation of the Lekhwair and Lower Kharaib Formation reservoirs: it highlights three distinct components within most lithologies: 1) micropore-dominated, 2) macropore-dominated and 3) non-reservoirs. This indicates that, for each lithology within the Lekhwair and Lower Khariab Formations, calculating a line of correlation through all data points may be incorrect. Instead associating all the data into definable and tested categories provides a more detailed understanding for reservoir performance for specific lithologies or lithofacies. All the components can then be included when up-scaling reservoirs, throughout the entire structure, which should maximise oil potential from the Lower Kharaib and Lekhwair Formations.

Chapter 9

Conclusions

9.1 Deposition of the Lekhwair Formation

Each 4th order HFC shoals upwards within the Lekhwair Formation. Algal-rich debris deposits only comprise the 4th order TST's and possibly represent the platform shedding material to the east, through grain flows initiated by transgression, or by the migration of surface palaeo-currents and their associated submarine channels. Caprinid rudists occur on the platform during 4th order TST's along with high amounts of dasycladacean algae, mainly *Cylindroporella arabica* and *Salpingoporella pygmaea* (Fig. 9.1C).

Aggregate grains may indicate deposition, for the first time within each 4th order HFC, above the fair weather wave base. The tops of these aggregate grain beds represent the 4th order MFS's (Fig. 9.1C).

Microsolenid coral and stromatoporoid fragments appear to represent the main shoals. *G. costatus* is associated with back-shoal environments, along with *Cladocoropsis*, *Praechrysallidina infracretacea*, *Redmondoides Lugeoni, Textularia sp., Bigenerina sp., Reophax sp.* and *Debarina hahounerensis* (Fig 9.1B*).* Both *P. infracretacea* and *R. lugeoni* become larger up-section into the late HST within most 4th order HFC's. The appearance of *Lithophaga* and cleonid sponge borings occurs within the *G. costatus* shells within back-shoal environments.

Lithocodium/Bacinella may require a hard substrate to colonise the sea bed before it grows into the *Lithocodium aggregatum* adult form that combines with the

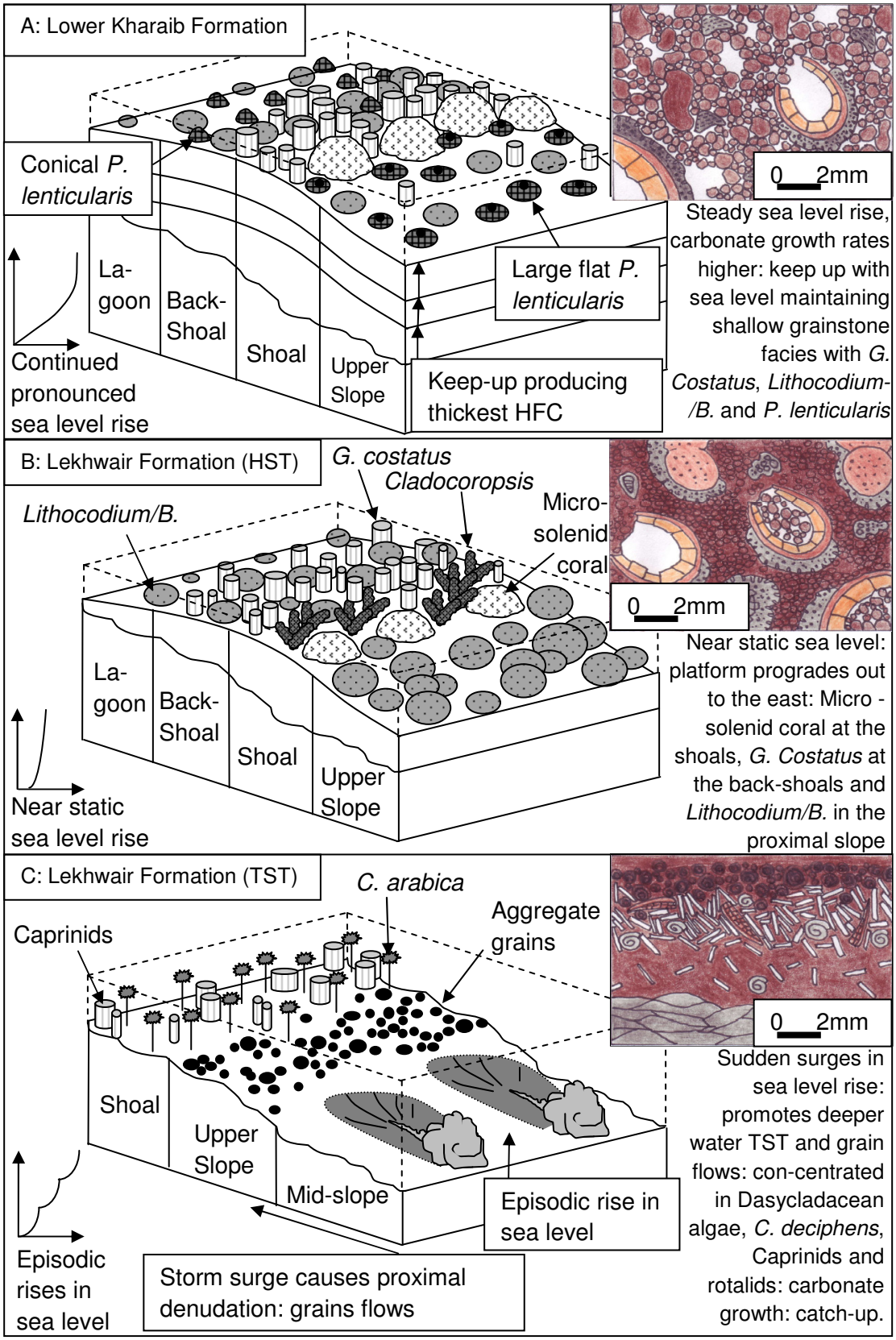

Figure 9.1: Deposition of the Lekhwair Formation during C) a 4th order TST. B) a 4th order HST and A) the Lower Kharaib Formation deposited during a prolonged 3rd order TST. The reservoir of the Lower Kharaib Formation has more interconnected interparticle pores due to carbonate growth 'keeping up' with sea level, maintaining shallow water conditions.

Bacinella irregularis. *Lithocodium/B.* generally prefers deeper water in comparison with the back shoal *G. costatus* within an open marine environment along the proximal slope (Fig. 9.1B). *Lithocodium/B.*'s presence behind the main shoals with bioerosion may indicate that the *Lithocodium/B.* is very adaptable to the changing environment and can also survive in smaller numbers in restricted mesotrophic conditions.

A firmground caps every 4th order HFC within the Lower Kharaib Formation. These contain *Trocholina alpina*, a high diversity of bioclasts, shallow water Textulariacea and pyritised *Thallassinoides* (*Glossifungites* assemblage) indicating shallow water lagoons. Supersaturation of LMC within the water column, brought on by bacterial sulphate reduction, may have formed hardgrounds within the lagoons. The following deposition of deepwater argillaceous micrites above the hardgrounds places the SB's at the hardgrounds.

9.2 Deposition of the Lower Kharaib Formation

The TST of the Lower Kharaib Formation is very thin containing *Coptocomplyloden lineolatus, Salpingoporella dinarica* and *P. lenticularis*. The first appearances of *S. dinarica*, *C. lineolatus* and *P. lenticularis* are diachronous across the Arabian plate (although there is some ambiguity with the latter species).

The Lower Kharaib Formation HST is much thicker and coarser than the Lekhwair formation HST below, indicating that deposition may have occurred within a much shallower environment.

Within the Lower Kharaib Formation *P. lenticularis* appears and becomes very abundant in comparison with *P. infracretacea* and *R. lugeoni* (Fig. 9.1A). This suggests that *P. lenticularis* may require shallower platform conditions and possibly a higher light index in comparison with Textulariacea. Very little siliciclastic detritus is present within the 4th order HST. However the argillaceous nature of the TST suggests some influx: combination of nutrient fluxes and reasonable light levels has possibly allowed the *P. lenticularis* to grow to large sizes and the flat discoidal shapes in the TST sequence, in comparison with the smaller conical *P. lenticularis* in the HST sequence.

A positive $\delta^{13}C$ trend occurs within the Lower Kharaib Formation near the Valanginian-Hauterivian boundary, possibly signifying another trend in relation to previous work in the literature. This positive $\delta^{13}C$ shift may also be linked to the end of a prolonged 3rd order TST. This trend, however, has no significant shifts and therefore is not used for chronostratigraphic correlation between the five wells and with other studies.

The grain-dominated Lower Kharaib platform may have been more suited for *G. costatus* colonisation whereas the muddier, firmer substrates of the Lower Lekhwair platforms may have been more suitable for *Lithocodium/B*. colonisation (Fig. 9.1A): therefore this inverse relationship may not relate to changing nutrient conditions within the water column.

9.3 3rd order scale: 4th order HFC stacking patterns

The Lekhwair and Lower Kharaib Formations are composed of two 3rd order sequences. The Lower Lekhwair is composed of two 3rd order HST's separated by a thin TST. The Upper Lekhwair and Lower Kharaib Formations form an extensive 3rd order TST. The thinning of non-reservoirs up-section suggests that carbonate growth rates may have increased from the Lekhwair into the Lower Kharaib Formation (Fig. 9.1). Overall the Lekhwair and the Kharaib Formations reflect a shallowing upward trend confirming the Lower Kharaib formation had the shallowest platform (Fig. 9.1A).

9.4 Progressive cementation

Diagenesis within the Lekhwair and Lower Kharaib Formations has undergone similar trends through progressive burial, starting with syn-depositional LMC formation, pyrite growth, LMC syntaxial formation, Fe dolomite and burial spar formation, followed by stylolitisation and anhydrite formation (Figs. 9.2 & 9.3). With respect to cementation, LMC cements within the water and oil legs appear to have grown to similar burial depths, with complete pore occlusion of the water leg within the deep burial realm; which has possibly been sourced from solutes liberated

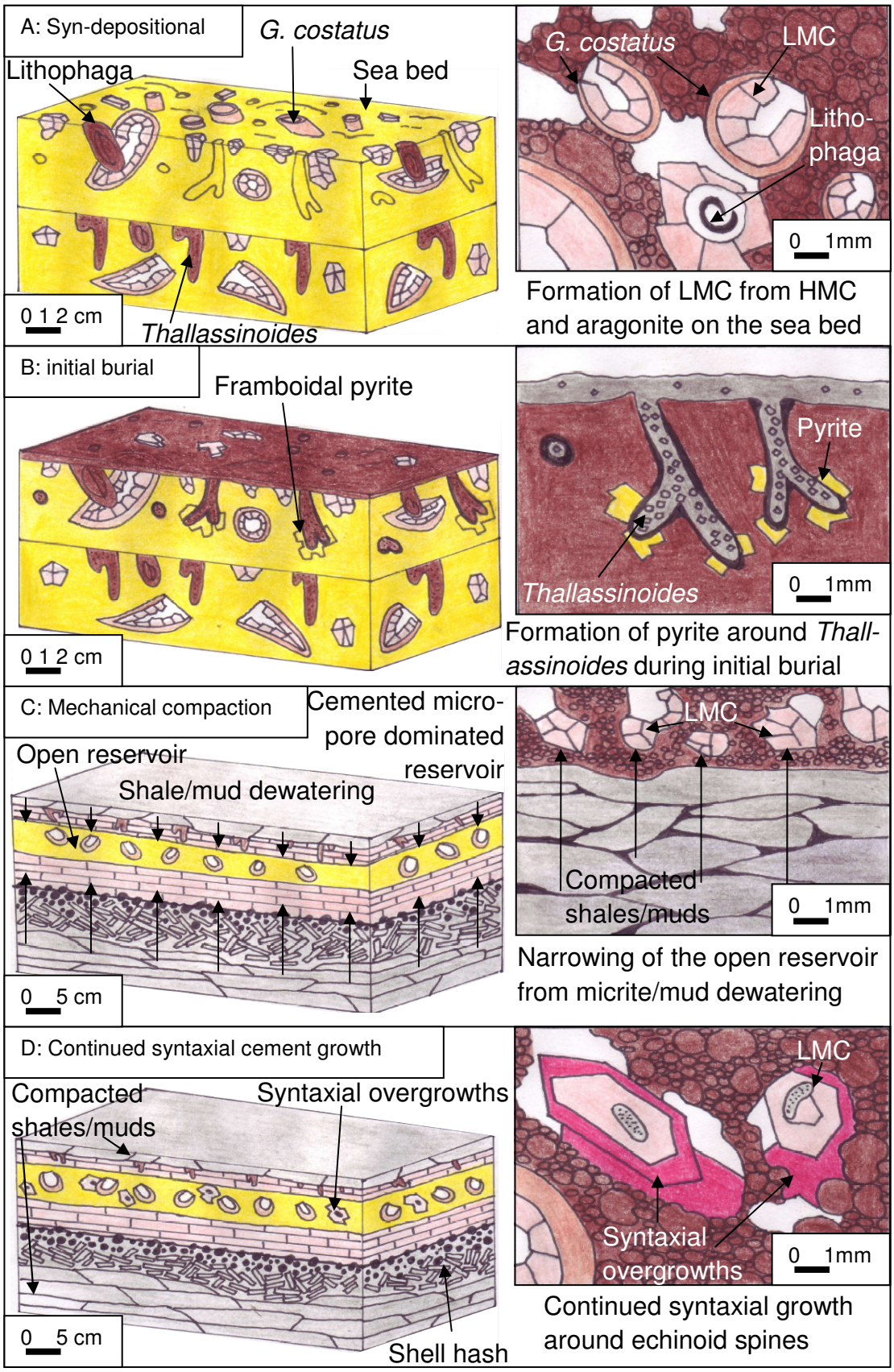

Fig. 9.2: The syn-depositional and shallow burial diagenetic episodes of the Lekhwair Formation crest. The reservoir conduit has narrowed producing lower grade micropore dominated reservoirs.

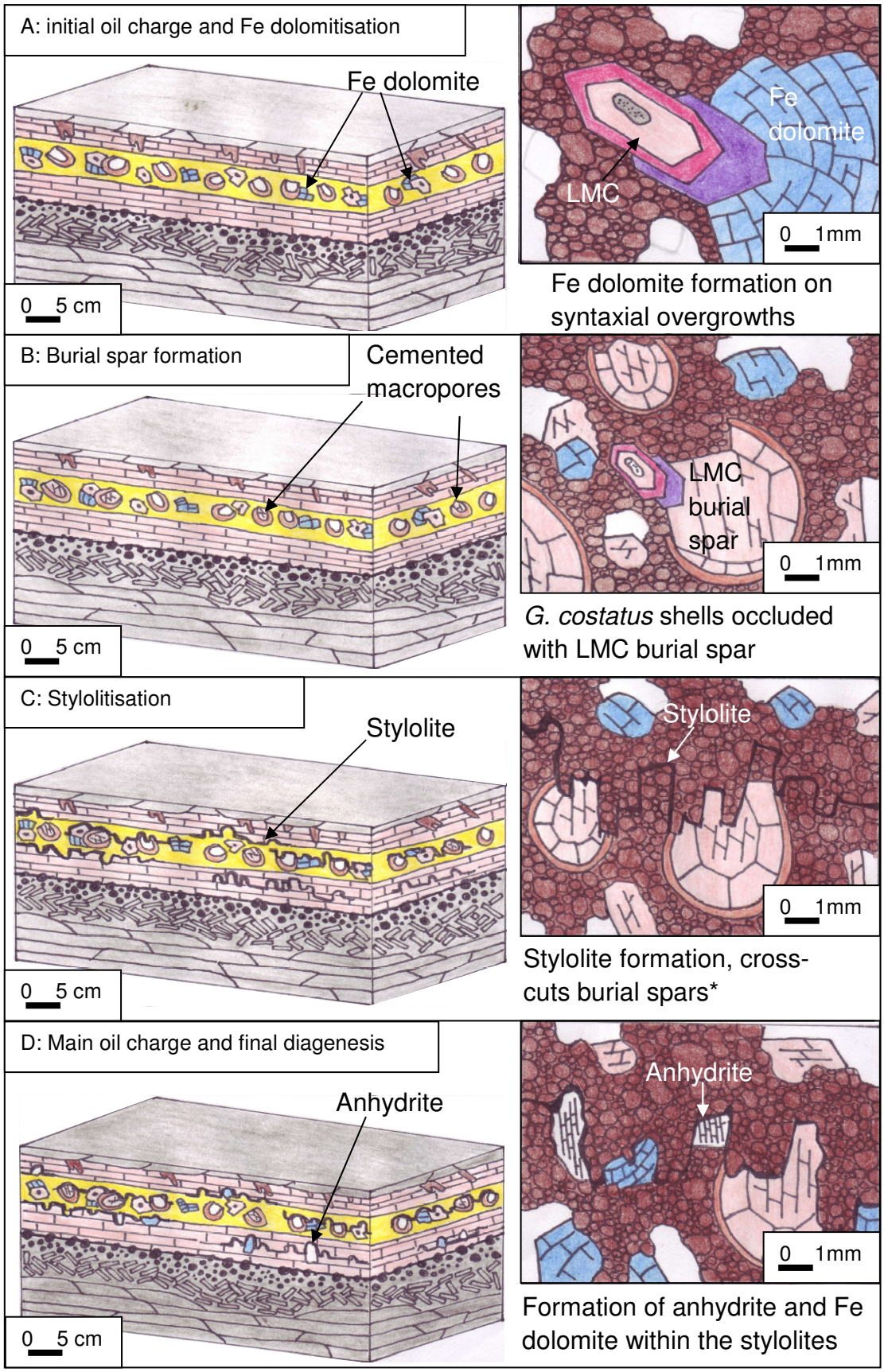

Fig. 9.3: The intermediate and deep burial diagenetic episodes of the Lekhwair Formation crest. Continued cementation of the macropores occurs with full water leg occlusion during stylolitisation.*

at stylolite horizons (Fig. 9.3C). Cementation had continued beyond this point within the oil leg, possibly during uplift and obduction of the Semail Ophiolite. Cementation had continued for longest within the oil leg and the crest confirming that cementation continued in the presence of oil.

The slow introduction of oil into the crest would have displaced porewater by creating an oil-wet system. The growing macrocements became separated from their source of solutes. With only the micropore systems remaining water wet, transportation of solutes to the precipitation sites would have become increasingly tortuous. Cementation effectively slowed within the oil leg with respect to the water leg until a critical oil saturation was reached, preventing all cementation. In comparison, the water leg became occluded in the deep burial realm producing a cemented micropore fabric. Consequently, within the Lower Kharaib Formation (Cycle 1), the crest and the oil leg are relatively free of cements, with only 5.26% of primary interparticle pores being fully cemented, compared with 99.5% pores from the field flanks and the water leg.

Opening faults may have altered the micrite selectively within Cycles 7a and 7b (and possibly Cycle 1) within Well 4. The faults were then cemented in the intermediate-deep burial realm.

The $\delta^{18}O_{VPDB}$ and $\delta^{13}C_{VPDB}$ data show a clustered trend for only the Lower Kharaib Formation (Cycle 1), in comparison with the Lekhwair Formation (Cycles 4a & 7a). This highlights that specific reservoir horizons have undergone separate diagenetic pathways, with porewaters evolving independently within the separate reservoirs, confirming the near compartmentalisation of all reservoirs.

Dolomite cements had formed from very different porewaters with respect to Cretaceous seawater. The relative timing of dolomite formation in comparison with LMC formation cannot be determined. The dolomites have positive $\delta^{13}C$ values implying formation under slight methanogenesis and not at near surface conditions associated with microbial sulphate reduction. The Fe-dolomites appear to overgrow LMC syntaxial growths. They also seem to be replacement of some LMC burial

cements within *G. costatus* shells. Therefore Fe-dolomite may have formed within the intermediate-deep burial realm during LMC burial spar formation.

9.5 Progressive porewater change and trap formation

The profile of the trap generated from the depths of the youngest cements (on the basis of using $\delta^{18}O_{VPDB}$ values as proxies for temperature) matches the actual field profile with Well 3 being at the highest point within the crest. The return to less negative values within the youngest cements may be due to uplift associated with the Semail Ophiolite obduction. However, the profile of the youngest cements has much greater amplitude suggesting that porewaters had significantly evolved from Cretaceous seawater during progressive burial. The actions of oil charge, rock-water interaction, and/or external porewater mixed with brines, all bringing in ^{18}O, cannot be ruled out as causal factors towards this trend. The specific reservoir temperatures and burial depths from the LMC cements therefore cannot be used to determine the Lekhwair and Lower Kharaib Formation burial histories.

The presence of the first oil inclusions with respect to the timing of trap formations, suggests oil was present within the Lekhwair and Lower Kharaib Formations before trap formation. While there are oil inclusions within the youngest cement zones that could correspond to oil that had migrated from the Bab Basin in the east (in the Late Eocene), vertical migration from the Jurassic Hanifa Formation source or a small local source must have formed the earlier oil inclusions. At least two phases of oil emplacement have therefore occurred during burial of the Lekhwair and Lower Kharaib Formations.

9.6 The micropore- and macropore-dominated reservoirs

Within the 4th order HFC's of the Lekhwair Formation there are three main micropore fabrics: 1) Open euhedral-subhedral blocky and rounded microspars (middle reservoirs), 2) partially open subhedral-anhedral rounded microspars (outer reservoirs) and 3) impermeable anhedral microspars (non-reservoirs). The transition from micropore Fabrics 1-3 occurs from the centre of the reservoirs towards, the non-reservoir assemblages below, and towards the firmgrounds above (Fig. 9.4B).

The highest porosity and permeability values within the Lekhwair Formation coincide within most mid-late HST's of every 4th order HFC, with the most rounded microspars, the most open and interconnected micropore fabric (Fabric 1), with grainstone patches and the most open interparticle pore space, within BW, *gl*WP, and *gl*PG (Fig. 9.4D)

Within the Lekhwair Formation, oil staining of the reservoirs covers the highest permeability values within the mid-late HST's and lower porosity/permeability areas of 20-25%, and <1mD, which are associated with the early and late HST's. The latter areas are micropore-dominated, whilst the former areas are macropore-dominated.

Diagenesis, through cementation, had progressively occluded the majority of macropores of the uppermost and lowermost portions of each reservoir (early and late HST, respectively) (Fig. 9.2 & 9.3) leaving micropores open: micropore-dominated. Macropore-dominated reservoir sections are therefore restricted in most 4th order HFC's to the mid-late HST (Figs.9.2 & 9.3). A possible process behind pore occlusion is therefore basal TST micrite/mud dewatering by mechanical compaction (Fig. 9.2C).

The highest porosity and permeability relationships, throughout this study, exist within the Lower Kharaib Formation and Cycle 1. This is due to the lithology being coarser and more concentred in packed micrite grains, which support a well connected open interparticle pore system (Fig. 9.1A). The reservoirs of the Lekhwair formation only have patchy interparticle-dominated pore areas (Fig. 9.1B); in general these reservoirs are muddier and dominated by intra-skeletal pores.

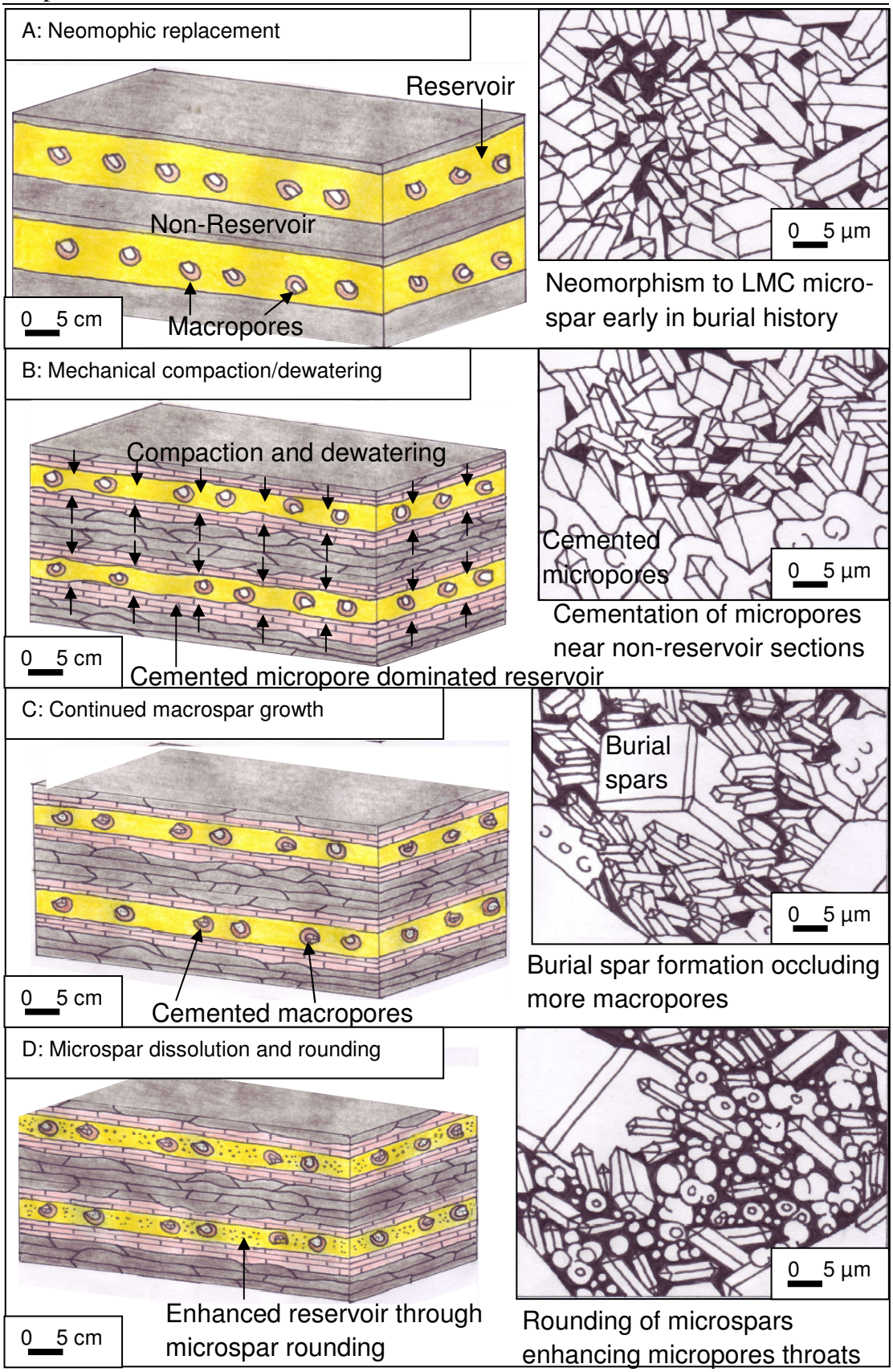

Fig. 9.4: Micropore formation and evolution within the Lekhwair Formation crest. The reservoir conduit is narrowed producing lower grade micropore dominated reservoir; only late microspar rounding has enhanced the reservoirs.

9.7 Reviewing the petrotyping methods

The Lucia (1999) method highlights the highest porosity and permeability relationships but not the micropore-dominated reservoirs, within the Lower Kharaib Formation. Therefore a new method employs an additional category, defined by GHE 3 on the Petrotype atlas method: 'Micropore model'. The new category defines micropore-dominated reservoir sections of the Lekhwair and Lower Kharaib Formations. This is of particular importance in the Lekhwair Formation as many oil stained reservoirs are 80-100% micropore-dominated. A significant quantity of oil within this offshore field may be housed within micropore-dominated reservoirs. It therefore seems important to be able to distinguish the porosity and permeability relationships of micropore-dominated areas from macropore-dominated areas within specific reservoir horizons. Higher entry pressures would be required to recover oil from micropore-dominated areas: being able to separate out these relationships would be useful so that micropore-dominated reservoirs can be approached differently in terms of oil extraction by future oil prospectors. For example, extracting oil from the macropores, via the micropore regions, will provide a more prolonged and stable recovery over the long term, as opposed in trying to extract oil from the micropore regions via the macropores. Therefore combining oil extraction from the macropore- and micropore-dominated areas may increase oil recovery from both the Lekhwair and Lower Kharaib Formations.

The 'Micropore model' also highlights that calculating lines of correlation through datasets defining a specific lithology, or lithofacies, may be incorrect, as lithologies within the Lekhwair and Lower Kharaib Formations have three separate internal components: macropore-dominated, micropore-dominated and non-reservoir. Therefore porosity and permeability data points within 3 orders of magnitude difference may not reflect similar pore systems, and a line of correlation should not be drawn through them, despite the lithology, or lithofacies, being similar.

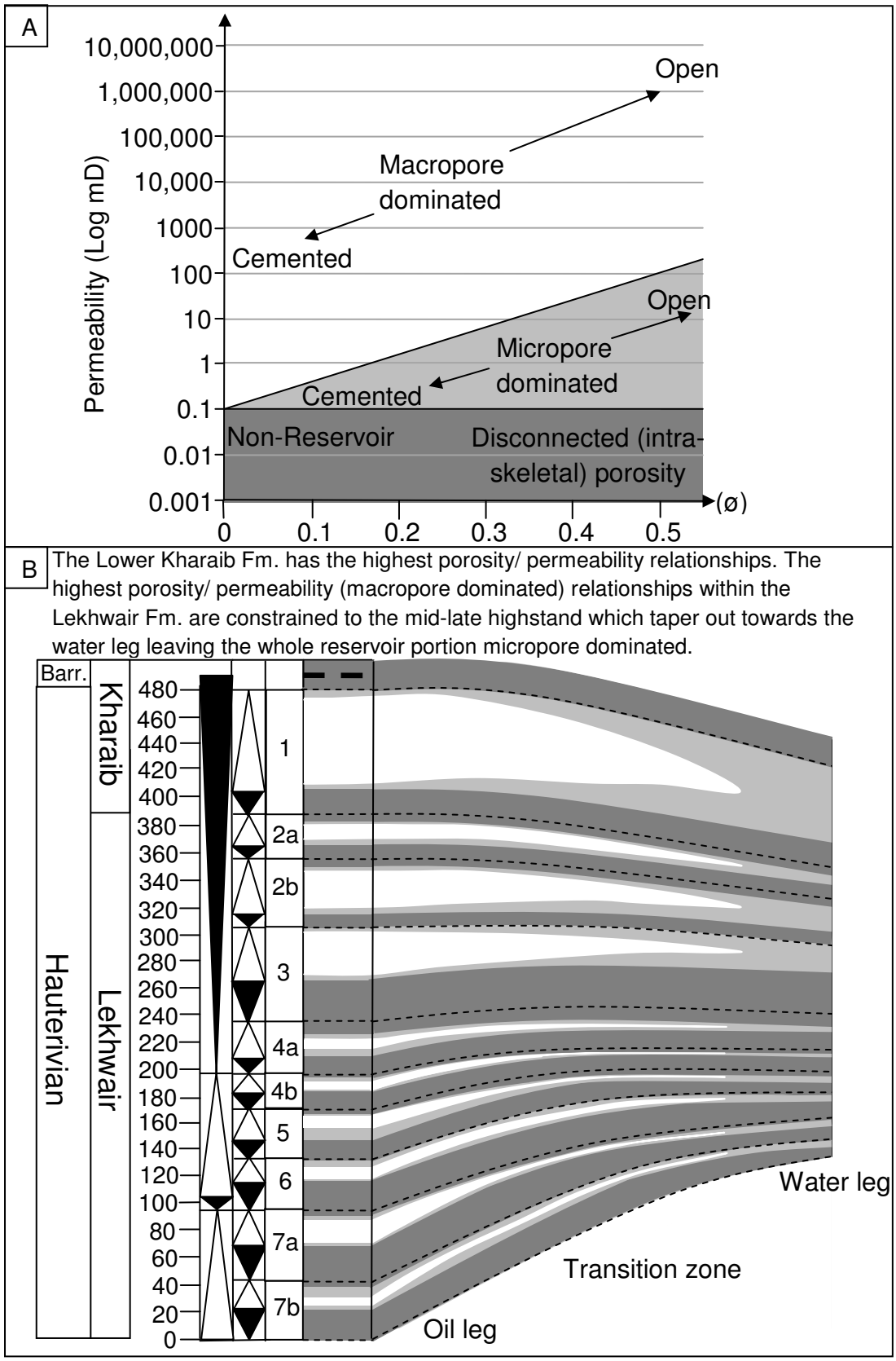

Fig. 9.5: The distribution of macropore dominated reservoirs, micropore dominated reservoirs and non-reservoirs within the Lekhwair and Lower Kharaib Formations. There is a significant amount of micropore dominated reservoir; exploiting this should determine a better oil recovery.

9.8 Porosity and permeability relationships

In terms of the vertical extent, the highest porosity and permeability relationships are the result of deposition at the end of a prolonged 3rd order TST, coupled with increasing carbonate production which had produced the thickest and coarsest reservoir of the Lower Kharaib Formation (Figs. 9.1A & 9.5)

In terms of lateral extent across the fields between the water and oil legs, the distribution of LMC cements clearly determines reservoir quality (Fig. 9.5). A small early source of oil had influenced the distribution of LMC cements by exclusively shutting down the crest macropores, preventing any new cement nucleation. Although stylolitisation was forming within the oil leg, the liberated solutes could not be transported effectively within the partially oil-wet pore systems of the crest. In comparison, the water leg, stylolitisation in the deep burial realm provided solutes for near complete macropore occlusion, with new cement nucleation. This is especially apparent within the Lower Kharaib Formation.

The thicker expanses of basal TST micrites/muds within the Lekhwair Formation caused much cementation of the uppermost and lowermost portions of the reservoirs and the HST's within each 4th order HFC, through the expulsion of solutes due to mechanical compaction and dewatering of the basal TST micrites/muds (Fig. 9.2C and 9.4B).

The micropore fabrics within both the Lekhwair and Lower Kharaib Formations are also a result of oil charge. Rounding and dissolution of the microspars, which involved the enhancement of the micropore throats, increased interconnectivity of the micropores, and increased permeability, had occurred after the majority of LMC burial spar formation. Dissolution may have been caused by the circulation of brines and LMC undersaturated fluids (from the PreCambrian Ara Salts) during deep burial and subsequent uplift, caused by the Semail Ophiolite obduction. Oil charge had caused the oil leg macropores to remain open beyond the deep burial realm. Therefore these aggressive fluids could penetrate the crest more effectively, causing more widespread dissolution and rounding in comparison with the water leg. Oil

charge has also indirectly determined the distribution of the best micropore networks within the Lekhwair and Lower Kharaib Formations.

9.9 Future work

1. A new cross-section could be completed perpendicular to this study orientated north-south, which should cover the water leg, transition zone and the oil leg, to determine the 3D architecture of the Lekhwair and Lower Kharaib Formation carbonate ramps.

2. Sample reservoirs 2a, 2b, 3, 5 and 6 within the five wells to provide a more complete understanding of the fossil successions through the Lekhwair and Lower Kharaib Formations.

3. Sample a separate onshore carbonate field near Abu Dhabi, to determine whether the same factors have controlled the distribution of the highest porosity and permeability relationships.

4. Complete chemical analysis and temperature-salinity experiments on the oil inclusions to determine their provenance. This will confirm whether there has been at least two phases of oil emplacement from separate sources.

5. Obtain bottom-hole temperatures for Wells 1-5 (present day reservoir temperatures across the offshore field).

6. Obtain the present day porewater $\delta^{18}O_{VPDB}$ compositions for the reservoirs within Wells 1-5. This information combined with the bottom-hole temperatures will allow for more accurate temperature and depth proxies, for the cements within the Lekhwair and Lower Kharaib Formations, to be calculated.

7. Analyse more samples under SEM, using Secondary Electron images, for other wells within the offshore field: preferably from another transect perpendicular to this study that traverses the water leg, transition zone and the oil leg. The amount of open microporosity and the micropore fabrics can be compared with this study.

8. Test the ‘Micropore model’ further with porosity and permeability data from other wells within the offshore field, and for wells from a separate onshore field. This will determine the viability of the new ‘Micropore model’.

Bibliography

Ahr, W. M.: (1989): Early diagenetic microporosity in the Cotton Valley Limestone of East Texas. Sedimentary Geology: 63: p275-292.

Al-Aasm, I. S. & Amzy, K. K.: (1996): Diagenesis and evolution of Microporosity of Middle-Upper Devonian Kee Scarp Reefs, Norman Wells, Northwestern Territories, Canada: Petrographic and Chemical evidence. AAPG Bulletin: 80: p82-100.

Al-Barwani, B. & McClay, K.: (2008): Salt tectonics in the Thumrait area, in the southern part of the South Oman Salt Basin: Implications for mini-basin evolution. Geo*Arabia*: 13: no. 4: p77-108.

Al-Hadhrami, H. S., Blunt, M. J.: (2001): Thermally Induced Wettability Alteration To Improve Oil Recovery in Fractured Reservoirs. SPE Reservoir Evaluation & Engineering: 4, No. 3, p179-186.

Al-Naqib, K. M.: (1967): Geology of the Arabian peninsula-Southwestern Iraq-U. S. Geological Survey Professional Paper. Washington: 560-G: p1-54.

Alsharhan, A. S.: (1985): Depositional Environment, Reservoir Units Evolution, and Hydrocarbon Habitat of Shu'aiba Formation. Lower Cretaceous, Abu Dhabi, United Arab Emirates. AAPG Bulletin: 69: p889-912.

Alsharhan, A. S.: (1987): Geology and Reservoir Characteristics of Carbonate Build up in Giant Bu Hasa Oil Field, Abu Dhabi. AAPG Bulletin: 71: p1304-1318.

Alsharhan, A. S.: (1989): Petroleum Geology of the United Arab Emirates. Journal of Petroleum Geology: 12-13: p253-288.

Alsharhan, A. S.: (1995): Facies variation, Diagenesis and Exploration potential of the Cretaceous Rudist-Bearing Carbonates of the Arabian Gulf. AAPG Bulletin: 79: no. 4: p 531-550.

Alsharhan, A. S. & Kendall, C. G. St. C: (1991): Cretaceous chronostratigraphy, unconformities and eustatic sea-level changes in the sediments of Abu Dhabi, United Arab Emirates. Cretaceous Research: 12: p379-401.

Alsharhan, A. S. & Nairn, A. E. M.: (1986): A review of the Cretaceous Formations in the Arabian Peninsula and Gulf: Part 1. Lower Cretaceous (Thamama Group) stratigraphy and Palaeogeography. Journal of Petroleum Geology: 9: p365-392.

Alsharhan, A. S. & Nairn, A. E. M.: (1993): Carbonate platform models of Arabian Cretaceous reservoirs: *in*, Simo, M., Scott, R. & Masse, J. P. (Eds.): Cretaceous carbonate platforms. American Association of Petroleum Geologists: Memoir 56: p173-184.

Al-Silwadi, M. S., Kirkham, A., Simmons, M. D. & Twombley, B. N.: (1996): New Insights into Regional Correlation and Sedimentology, Arab Formation (Upper Jurassic), Offshore Abu Dhabi. Geo*Arabia*: 1: p6-27.

Amaefule, J. O., Altunbay, M., Tiab, D., Kersey, D. G. & Keelan, D. K.: (1993): Enhanced Reservoir Description: Using Core and Log Data to Identify (Flow) Units and Predict Permeability in Uncored Intervals/Wells. SPE: 26436.

Aziz, S. K. & El-Sattar, M. A. A.: (1997): Sequence Stratigraphic modelling of the Lower Thamama Group, East onshore Abu Dhabi, United Arab Emirates. Geo*Arabia*: 2: p179-202.

Baker, P. A. & Burns, S. J.: (1985): Occurrence and Formation of Dolomite in Organic-rich continental margin sediments. AAPG Bulletin: 69: no. 11: p1917-1930.

Banner F. T., Finch E. M. & Simmons M. D.: (1990): On *Lithocodium* Elliott (Calcareous algae); its paleobiological and stratigraphical significance. Journal of Micropalaeontology, 9, p21-35.

Banner, F. T. & Simmons, M. D.: (1994): Calcareous Algae and Foraminifera as Water-Depth Indicators: An Example from the Early Cretaceous of North-Eastern Arabia: *In*, Simmons, M. D. (Ed.): Micropalaeontology and Hydro-carbon Exploration in the Middle East. Chapman & Hall: London: p243-252.

Banner, F. T., Simmons, M. D. & Whittaker, J. E.: (1991): The Mesozoic Chrysalidinidae (Foraminifera, Textulariacea) of the Middle East: the Redmond (Aramco) taxa and their relatives. Bull. Br. Mus. Nat. Hist. (Geol): 47: no. 2: p101-152.

Bathurst, R. G. C.: (1975): Developments in Sedimentology (12). Carbonate sediments and their diagenesis (2^{nd} edition): Elsevier

Beiranvand, B.: (2003): Quantitative Characterization of Carbonate Pore Systems by Mercury- Injection Method and Image Analysis in a Homogeneous Reservoir. Middle East Oil Show, Bahrain, Society of Petroleum Engineers.

Berner, R. A. & Kothavala, Z.: (2001): Geocarb III: A Revised Model of Atmospheric CO_2 over Phanerozoic Time. American Journal of Science: 301: p182-204.

Bjørkum, P. A., Walderhaug, Q., & Aase, N. E.: (1993): A model for the effects of Illitization on porosity and quartz cementation of sandstones: Journal of Sedimentary Petrology: 63: p1089-1091.

Bourbie, T. & Zinszer, B.: (1985): "Hydraulic and Acoustic Properties as a Function of Porosity in Fontainbleau Sandstone". Journal of Geophysical Research: 90: p11524-11532.

Braithwaite, C. J. R.: (1993): Cement sequence stratigraphy in carbonates. Journal of Sedimentary Petrology: 63: no. 2: p295-303.

van Buchem, F. S. B., Pittet, B., Hillgärtner, Grötsch, J.H., Al-Mansouri, A. I., Billing, I. M, Droste, H. H. J., & Oterdoom, W. H.: (2002): High-resolution Sequence Stratigraphic Architecture of Barremian/Aptian Carbonate Systems in Northern Oman and the United Arab Emirates (Kharaib and Shu'aiba Formations). Geo*Arabia*: 7: no. 3: p461-498.

Budd, D. A.: (1989): Micro-rhombic calcite and microporosity in limestones: a geochemical study of the Lower Cretaceous Thamama Group, U.A.E. Sedimentary Geology: 63: p293-311.

Burchette, T. P. & Wright, V. P.: (1992): Carbonate ramp depositional systems. Sedimentary Geology: 79: p3-57.

Burgess, C. J. & Peter, C. K.: (1985): Formation, Distribution, and Prediction of Stylolites as Permeability Barriers in the Thamama Group, Abu Dhabi. SPE: 13698.

Burruss, R. C., Cercone, K. R. & Harris, P. M.: (1983): Fluid inclusion petrography and tectonic-burial history of the Al Ali No. 2 well: Evidence for the timing of diagenesis and oil migration, northern Oman Foredeep. Geology: 11: p567-570.

Cantrell, D. L. & Hagerty, R. M.: (1999): Microporosity in Arab Formation Carbonates, Saudi Arabia. GeoArabia: 4: p129-154.

Choquette, P. W. & Prey, L. C.: (1970): Geological nomenclature and classification of porosity in sedimentary carbonates. AAPG: 54: p207-250.

Christian, L.: (1997): Cretaceous Subsurface Geology of the Middle East region. GeoArabia: 2, p239-256.

Colacicchi, R & Baldanza, A.: (1986): Carbonate turbidites in a Mesozoic pelagic basin: Scaglia formation, apennines—comparison with siliciclastic depositional models Sedimentary Geology: 48, p81-105.

Corbett, P. W. M.: (2009): Petroleum Geoengineering: Integration of Static and Dynamic Models. 2009 Distinguished Instructor Short Coarse: Distinguished instructor series: no. 12.

Corbett, P. W. M. & Potter, D. K.: (2004): Petrotyping: A Base Map and Atlas for Navigating through Permeability and Porosity data for reservoir comparison and permeability prediction. Society of Core Analysts: 30: p1-12.

Cox, P. A., Wood, R. A., Dickson, J. A. D., Al-Rougha, H. B., Shebl, H. & Corbett, P. W. M.: (2010): Dynamics of cementation in response to oil charge: Evidence from a Cretaceous carbonate field, U.A.E. Sedimentary Geology: 228: p246-254.

Davis, R. B., Casey, D. M., Horbury, A. D., Sharland, P. R. & Simmons, M. D.: (2002): Early to mid-Cretaceous mixed carbonate-clastic shelfal systems: examples, issues and models from the Arabian Plate. Geo*Arabia*: 7: p541-597.

Deuser, W. G., Degens, E. T., & Guillard R. L.: (1968): Carbon isotope relationships between plankton and sea water. Geochimica et Cosmochimica acta: 32, p657-660.

Dickson, J. A. D.: (1965): A modified staining technique for carbonates in thin section. Nature: 203: p587.

Dickson, J. A. D., Wood, R. A., Al Rougha, H. Bu. & Shebl, H.: (2008): Sulphate reduction at hardgrounds: Lithification afterburn! Sedimentary Geology: 205: p34-39.

Dix, G. R.: (1993): Patterns of Burial and tectonically controlled dolomatization in an upper Devonian fringing-Reef complex: Leduc Formation, Peace River Arch Area, Alberta, Canada. Journal of Sedimentary Petrology: 63: no. 4: p628-640.

Dravis, J. J.: (1989): Deep-Burial microporosity in Upper Jurassic Haynesville oolitic grainstones, East Texas. Sedimentary Geology: 69: p325-341.

Duane, M. J., Al-Zamel, A., Eastoe, C. J.: (2004): Stable isotope (chlorine, hydrogen and oxygen), geochemical and field evidence for continental fluid flow vectors in the Al-Khiran sabkhas (Kuwait).

Dunham, R. J.: (1962): Classification of carbonate rocks according to their depositional texture: *in*, Ham, W. E. (Ed.): Classification of carbonate rocks, Tulsa, OK. AAPG Memoir: 1: p108-121.

Dunham, J. B., Larter, S.: (1981): Association of stylolitic carbonates and organic matter: Implications for Temperature control on stylolite Formation. AAPG annual convention with divisions: SEPM/EMD/DPA: AAPG Bulletin: 65: no. 5: p922.

Dunne, L. A., Manoogian, P. R. & Pierini, D. F.: (1990): Structural style and domains in the Northern Oman Mountains (Oman and United Arab Emirates): *in*, Robertson, A. H. F., Searle, M. P. & Ries A. C. (Eds.), The Geology and tectonics of the Oman Region. Geological Society, London, Special Publication: 49, p375-386.

Dunnington, H. V.: (1967): Aspects of diagenesis and shape change in stylolitic limestone reservoirs. Proc. 7th World Petroleum Congress: Mexico: p339-352.

Dupraz, C. & Strasser, A.: (1999): Microbialites and Micro-encrusters in shallow coral bioherms (Middle to Late Oxfordian, Swiss Jura Mountains). Facies: 40: p101-129.

Edwards, E.: (2006): Static and Dynamic Characterization of a Major Transtentional Fault Zone: Its Effects on Reservoir Quality and Deliverability from an Offshore Thamama Oil-Field in Abu Dhabi. SPE: 101418.

Edwards, E., Sit H., Al-Rougha, H. Bu., Sultan, A. & Khouri, N.: (2006): Tectonic History and Basement Fault Control on Structural Development of an Offshore Field, Abu Dhabi. SPE: 101416.

Ellison, R. L. & Ahumada, R.: (1995): Sound Reservoir and Production Managment will Enable Fifty-Eight Percent Oil Recovery in Colombia's Cano Limon Field. SPE Asia Pacific Oil and Gas Conference, 20-22 March 1995, Kuala Lumpur, Malaysia.

Emery, D., Smalley, P. C., & Oxtoby, N. H.: (1993): Synchronous oil migration and cementation in sandstone Reservoirs Demonstrated by Quantitative Description of Diagenesis. Philosophical Transactions of the Royal Society of London: 344: p115-125.

Esteban, M., & Taberner, C.: (2003): Secondary porosity development during late burial in carbonate reservoirs as a result of mixing and/or cooling of brines. Journal of Geochemical exploration: 78-79: p335-359.

Folk, R. L.: (1959): Practical petrographic classification of limestones. AAPG Bulletin: 43: p1-38.

Föllmi, K. B.: (1993): Phosphorus and phosphate-rich sediments, an environmental approach. Chemical Geology: 107: p375-378.

Föllmi, K. B., Weissert, H., Bisping, M., Funk, H.: (1994): Phosphogenesis, carbon-isotope stratigraphy, and carbonate-platform evolution along the Lower Cretaceous northern Tethyan margin. Geological Society of American Bulletin: 106: p729-746.

Galloway, W. E.: (1989): Genetic Stratigraphic Sequences in Basin Analysis I: Architecture and Genesis of Flooding-Surface Bounded Depositional Units. AAPG Bulletin: 73: p125-142.

Giles, M. R. & de Boer, R. B.: (1989): Secondary porosity: Creation of enhanced porosities in the subsurface from the dissolution of carbonate cements as a result of cooling formation waters. Marine and Petroleum Geology: 6: p261-269.

Giles, M. R. & Marshall, J. D.: (1986): Constraints on the development of secondary porosity in the subsurface: re-evaluation of processes. Marine and Petroleum Geology: 3: p243-255.

Gilli, E., Masse J. P. & Skelton P. W.: (1995): Rudists as gregarious sediment-dwellers, not reef-builders, on Cretaceous carbonate platforms. Palaeogeography, Palaeoclimatology, Palaeoecology: 118: p245-267.

Gingrass, M. K., Pemberton, S. G., Mendoza, C. A. & Henk, F.: (1999): Assessing the anisotropic permeability of *Glossifungites* surface. Petroleum Geoscience: 5: p349-357.

Glennie K. W., Boeuf, M. G. A., Hughes Clarke, M. W., Moody Stuart, M., Pilaar, W. F. H., & Reinhardt, B. W.: (1974): Geology of the Oman Mountains. Verhandelingen van het Koninklijk Nederlands geologisch minjbouw-kundig Genootschap.

Gluyas, J. G., Robinson, A.G., Emery, D., Grant, S.M., & Oxtoby, N. H.: (1993): The link between petroleum emplacement and sandstone cementation. Petroleum Geology of Northwest Europe: Proceedings of the 4th Conference, Geological Society, London: p1395-1402.

Gomes, J. S., Strohmenger, C. J., Negahban, S. & Kalam, M. Z.: (2008): Carbonate Reservoir Rock Typing-The Link between Geology and SCAL. SPE: 118284.

Gradstein, F. M. & Ogg, J. G.: (1994): A Mesozoic time scale. Journal of Geophysical Research: 99: p24,051-24,074.

Gradstein, F. M. & Ogg, J. G.: (2004): Geologic Time Scale 2004-why, how, and where next! Lethaia: 37: p175-181.

Granier, B.: (2000): Lower Cretaceous stratigraphy of Abu Dhabi and the United Arab Emirates-A reappraisal. The 9th Abu Dhabi International Petroleum Exhibition & Conference, Conference Proceedings, Abu Dhabi: ADIPEC 0918: p526-535.

Granier, B., Al-Suwaidi, A. S., Busnardo, R., Aziz, S. K. & Schroeder, R.: (2003/05): New insight on the stratigraphy of the “Upper Thamama” in offshore Abu Dhabi (U.A.E.). Notebooks on Geology: Article 2003/05: p1-17.

Grötsch, J., Billing, I. & Vahrenkamp, V.: (1998): Carbon- isotope stratigraphy in shallow-water carbonates: implications for Cretaceous black-shale deposition. Sedimentology: 45: p623-634.

Gumati, Y. D.: (1993): Kinetic modelling, thermal maturation and hydrocarbon generation in the United Arab Emirates. Marine and Petroleum Geology: 10: p.153-161.

Gunter, G. W., Finneran, J. M., Hartmann, D. J. & Miller, J. D.: (1997): Early Determination of Reservoir Flow Units using an intergrated Petrophysical Method. SPE: 38679.

Habermann, D., Neuser, R. D. & Richter, D. K.: (1996): REE-activated Catholuminescence of calcite and dolomite: high-resolution spectrometric analysis of CL emission (HRS-CL). Sedimentary Geology: 101: p1-7.

Habermann, D., Neuser, R. D. & Richer, D. K.: (1998): Low limit of Mn^{2+}-activated Catholuminescence of calcite: state of the art. Sedimentary Geology: 116**:** p13-24.

Halbouty, M. T., Meyerhoff, A. A., King, R. E., Dott, R. H. Sr. & Klemme H. D.: (1970): World's giant oil and gas fields, geologic factors affecting their formation, and basin classification. Pt. 1. giant oil and gas fields. AAPG: 14: p502-528.

Hallam, A.: (1985): A review of Mesozoic Climates. J. Geol. Soc. London: 142: p433-445.

Hallock, P.: (1985): Why are larger Foraminifera large? Palaeontology: 11: no. 2: p195-208.

Hallock, P., Hine, A. C., Vargo, G. A., Elrod, J. A. & Jaap, W. C.: (1988): Platforms of the Nicaraguan Rise: Examples of the sensitivity of carbonate sedimentation to excess trophic resources. Geology: 16: p1104-1107.

Hallock, P. & Schlager, W.: (1986): Nutrient excess and the demise of coral reefs and carbonate platforms. Palaios: 1: p389-398.

Haq, B. U., Hardenbol, J. & Vail, P. R.: (1987): Chronology of Fluctuating Sea levels since the Triassic. Science: 235: p1156-1167.

Hardie, L. A.: (1996): Secular variation in seawater chemistry: An explanation for the coupled secular variation in the mineralogies of marine limestones and potash evaporites over the past 600 m.y. Geology: 24: p279-283.

Harland, W. B., Armstrong, R. L., Cox, A.V., Craig, L. E, Smith A. G., Smith D. G.: (1990): A geological time scale 1989: Cambridge University Press, p263.

Hassan, T. H. & Wada, Y.: (1981): Geology and Development of Thamama Zone 4, Zakum Field. Journal of Petroleum Technology: 33: no. 7: p1327-1337.

Hassan, T. H., Mudd, G. C. & Twombley, B. N.: (1975): The stratigraphy and sedimentation of the Thamama Group (Lower Cretaceous) of Abu Dhabi. Ninth Arab Petroleum Congress, Dubai: 107: p11.

Hassan, T. H., & Wada, Y.: (1979): The Geology and Development of the Thamama Zone IV of the Zakum Field, Abu Dhabi. SPE: 7779.

Heasley, E.C., Worden, R. H. & Hendry, J. P.: (2000): Cement distribution in a carbonate reservoir: recognition of a palaeo oil-water contact and its relationship to reservoir quality in the Humbley Grove field, onshore, UK. Marine and Petroleum Geology: 17: p639-654.ws

Hillgärtner, H., van Buchem. F. S. B., Gaumet, F., Razin, P., Pittet, B., Grotsch, J. & Droste H.: (2003): The Barremian-Aptian evolution of the eastern Arabian carbonate platform margin (Northern Oman). Journal of Sedimentary Research: 73: p756-773.

Hirasaki, G. & Zhang D. L.: (2004): Surface Chemistry of Oil Recovery from Fractured, Oil-wet, Carbonate Formations. Society of Petroleum Engineers: 80988.

Hirsch, R. L.: (2006): Peaking of World oil production, an overview. Atlantic Council Workshop on Transatlantic Energy Issues: SAIC, U.S. DOE National Energy Technology Laboratory.

Hottinger, L.: (1997): Shallow benthic foraminiferal assemblages as signals for depth of their deposition and their limitations. Bulletin De La Societe Geologique De France: 168: p491-505.

Hudson, J. D.: (1977): Stable isotopes and limestone lithification. Journal of the Geological Society of London: 133: p637-660.

Hughes, G. W.: (2000a): Saudi Arabian Late Jurassic and Early Cretaceous agglutinated foraminiferal associations and their application for age, palaeoenvironmental interpretation, sequence stratigraphy, and carbonate reservoir architecture. Proceedings of the Fifth International Workshop on Agglutinated Foraminifera: Grzybowski Special Publication: 7: p149-165.

Hughes, G. W.: (2000b): Bioecostratigraphy of the Shu'aiba Formation Shaybah field, Saudi Arabia. Geo*Arabia*: 5: no. 4: p545-578.

Hughes, G. W.: (2004): Palaeoenvironments of Early Aptian agglutinated formainifera of Saudi Arabia. Proceedings of the Sixth International Workshop on Agglutinated Foraminifera: Grzybowski Foundation Special Publication: 8: p195-207.

Immenhauser, A., Creusen, A., Esteben, M. & Vonhof, H. B.: (2000): Recognition and Interpretation of Polygenic Discontinuity surfaces in the Middle Cretaceous Shu'aiba, Nahr Umr, and Natih Formations of Northern Oman. Geo*Arabia*: 5: p299-322.

Immenhauser, A., Hillgärtner, H. & Van Bentum, E.: (2005): Microbial-foraminiferal episodes in the Early Aptian of the Southern Tethyan margin: ecological significance and possible relation to oceanic anoxic event 1a. Sedimentology: 52: p77-99.

Immenhauser, A., Schlager, W., Burns, S. J., Scott, R. W., Geel, T., Lehmann, J., van der Gaast, S. & Bolder-Schruwer, L. J. A.: (1999): Late Aptian to late Barremian sea level fluctuations constrained by geochemical and biological evidence (Nahr Umr Formation, Oman). Journal of Sedimentary Research: 69: no. 2: p434-446.

Jenkyns, H. C.: (1980): Cretaceous anoxic events: from continents to oceans. Journal Geological Society London: 137: p171-188.

Jennings Jr, J. W. & Lucia, F. J.: (2001): Predicting Permeability from Well Logs in Carbonates With a link to Geology for Interwell Permeability Mapping. SPE: 71336.

Johnson, C. C., Sanders, D., Kaufman, E. G. & Hay, W. W.: (2001): Patterns and processes influencing Upper Cretaceous reefs: in, Kiesling, W., Flügel, E. & Golonka, J. (Eds.): Phanerozoic Reef Patterns. SEPM Spec Publ: 72: p549-585.

Jones, R. W., Simmons, M. D. & Whittaker, J. E.: (2004): Chronostratgraphic and Palaeoenvironmental significance of Agglutinated and Associated larger Benthonic Foraminifera from the Lower to "Middle" Cretaceous of the Middle East. Proceedings of the Sixth International Workshop on Agglutinated Formainifera: Grzybowski Foundation Special Publication: 8: p229-235.

Kaldi, J.: (1989): Diagenetic microporosity (chalky porosity), Middle Devonian Kee Scarp reef complex, Norman Wells, Northwest Territories, Canada. Sedimentary Geology: 63: p241-252.

Katz, M. E., Wright, J. D., Miller, K. G., Cramer, B. S., Fennel, K. & Falkowski, P. G.: (2005): Biological overprint of the geological carbon cycle. Marine Geology: 217: p323-338.

Kharaka, Y. K., Carothers, W. W. & Rosenbauer, R. J.: (1983): Thermal decarboxylation of acetic acid: implications for origin of natural gas. Geochimica Cosmochimica Acta: 47: p397-402.

Kim, S-T., & O'Neil, J. R.: (1997): Equilibrium and none-equilibrium oxygen isotope effects in synthetic carbonates. Geochimica et Cosmochimica Acta: 61: p3461-3475.

Kirkham, A., Bin Juma, M., Mckean, T. A. M., Palmer, A. F., Smith, M. J., Thomas, A. H., & Twombley, B. N.: (1996): Fluid Saturation Prediction in a "Transition Zone" Carbonate Reservoir, Abu Dhabi. Geo*Arabia*: 1: p551-565.

Koop, W. J. & Stoneley, R: (1982): Subsidence history of the Middle East Zagros Basin, Permian to Recent. Phil. Trans. R. Soc. London: 305, p149-168.

Ku, T. C. W., Walter, L. M., Coleman, M. L., Blake, R. E. & Martini, A. M.: (1999): Coupling between sulphur recycling and syn-depositional carbonate dissolution: Evidence from oxygen and sulphur isotope composition of pore water sulphate, South Florida Platform, U.S.A. Geochimica et Cosmochimica Acta: 63: no. 17: p2529-2546.

Kuypers, M. M. M., Pancost, R. D. & Sinninghe Damsté, J. S.: (1999): A large and abrupt fall in atmospheric CO_2 concentrations during Cretaceous times. Nature: 399: p342-345.

Lambert, L., Durlet, C., Loreau, J. P. & Marnier, G.: (2006): Burial dissolution of micrite in Middle East carbonate reservoirs (Jurassic-Cretaceous): keys for recognition and timing. Marine and Petroleum Geology: 23: p79-92.

Larson, R. L.: (1991): Latest pulse of the Earth: Evidence for a mid Cretaceous superplume. Geology: 19: p547-550.

Lasemi, Z. & Sandberg, P. A.: (1984): Transformations of aragonite-dominated lime muds to microcrystalline limestones. Geology: 12: p420-423.

Lawrence, J. R.: (1988): The stable isotope geochemistry of Deep-Sea porewaters: *in*, Fritz, P., Fontes, J. Ch. (Eds.): Handbook of Environmental Isotopes. Chapter 9: 3: The Marine Environment, Elsevier, Amsterdam.

Leinfelder, R. R., Nose, M., Schmid, D. U., & Werner, W.: (1993): Microbial crusts of the Late Jurassic: composition, palaeoecological significance and importance in reef construction. Facies: 29, p195-230.

Li, L. & Keller, G.: (1999): Variability in Late Cretaceous climate and deep waters: evidence from stable isotopes. Marine Geology, v. 161, p171-190

Lindsay, R. F., Cantrell, D. L., Hughes, G. W., Keith, T. H., Mueller III, H. W. & Russell, S. D.: (2006): Ghawar Arab-D Reservoir: Widespread porosity in Shoaling-upward carbonate cycles, Saudi Arabia: *in*, Harris, P. M. & Weber, L. J. (Eds.): Giant hydrocarbon reservoirs of the world: From rocks to reservoir characterization and modelling: AAPG memoir 88/SEPM special publications: p97-137.

Lini, A., Weissert, H. & Erba, E.: (1992): The Valanginian carbon isotope event: a first episode of greenhouse climate conditions during the Cretaceous. Tera Nova: 4: p374-384.

Lippard, S. J.: (1983): Cretaceous high pressure metamorphism in NE Oman and its relationship to subduction and ophiolite nappe emplacement. Journal of the Geological Society, London: 140, p97-104.

Lønøy, A.: (2006): Making sense of carbonate pore systems. AAPG Bulletin: 90: p1381-1405.

Lucia, F. J.: (1995): Rock-fabric/Petrophysical Classification of carbonate pore space for reservoir characterization. AAPG Bulletin: 79: p1275-1300.

Lucia, F. J.: (1999): Carbonate Reservoir Characterization. Springer.

Lutfi, A. Salameh, (Abu Dhabi Natl. Oil Co. (ADNOC) Source (2001)). Improved Oil Recovery by New Horizontalization Strategy in Giant Carbonate Reservoir. SPE Middle East Oil Show, 68075.

Marchand, A.M.E., Haszeldine, R.S., Smalley, C.P., Macaulay, C.I., & Fallick A. E.: (2001): Evidence for reduced quartz-cementation rates in oil-filled sandstones. Geological Society of America: 29: p915-918.

Marchand, A. M. E., Smalley, C. P., Haszeldine & Fallick A. E.: (2002): Note on the importance of hydrocarbon fill for reservoir quality prediction in sandstones: AAPG Bulletin: 86: p1561-1571.

Mason, R. A.: (1987): Ion Microprobe analysis of trace elements in calcite with an application to the Cathodoluminescence zonation of limestone cements from the Lower Carboniferous of South Wales, U.K. Chemical Geology: 64: p209-224.

Mason, R. A. & Mariano, A. N.: (1990): Cathodoluminescence activation in manganese-bearing and rare earth-bearing synthetic calcites. Chemical Geology: 88**:** p191-206.

Masse, J. P., Borgomano, J. & Al-Maskiry, S.: (1997): Stratigraphy and tectonosedimentary evolution of a late Aptian-Albian carbonate margin: the northeastern Jebel Akhdar (Sultanate of Oman). Sedimentary Geology: 113: p269-280.

Masse, J. P., Borgomano, J. & Al-Maskiry, S.: (1998): A platform-to-basin transition for lower Aptian carbonates (Shu'aiba Formation) of the northeastern Jebel Akhdar (Sultanate of Oman). Sedimentary Geology: 119: p297-309.

Matthews, R. K. & Frolich, C.: (2002): Maximum flooding surfaces and sequence boundaries: comparisons between observations and orbital forcing in the Cretaceous and Jurassic (65-190Ma). Geo*Arabia:* 7: p503-535.

Mazzullo, S. J. & Harris, P. M.: (1992): Mesogenetic dissolution: Its role in Porosity Development in Carbonate Reservoirs. AAPG Bulletin: 76: p607-620.

Melinte M., & Mutterlose, J.: (2001): A Valanginian (Early Cretaceous) Boreal nannoplankton excursion' in sections from Romania. Marina Micropaleontology: 43, p1-25.

Miller, K. G., Kominz, M. A., Browning, J. V., Wright, J. D., Mountain, G. S., Katz, M. E., Sugarman, P. J., Cramer, B. S. Christie-Blick, N. & Pekar, S. F.: (2005): The Phanerozoic Record of Global Sea-Level Change. Science: 310: p1293-1298.

Milner, P.A.: (1998): Source Rock Distribution and Thermal Maturity in the Southern Arabian Peninsula. Geo*Arabia*: 3: no. 3 p339-356.

Mitchum Jr., R. M.: (1977): Seismic Stratigraphy and Global changes in sea level: Part II-Glossary of terms used in Seismic Stratigraphy: *in*, Payton, C. E. (Ed.): Seismic stratigraphy-Applications to Hydrocarbon exploration. AAPG Memoir: 26: p205-212.

Moore, C. H.: (2001): Carbonate reservoirs, Porosity Evolution and Diagenesis in a Sequence Stratigraphic Framework. Developments in Sedimentology: 55. Elsevier.

Moshier, S. O.: (1989a): Development of microporosity in a micritic limestone reservoir, Lower Cretaceous, Middle East. Sedimentary Geology: 63: p217-240.

Moshier, S. O.: (1989b): Microporosity in micritic limestones: a review. Sedimentary Geology: 63: p191-213.

Murris, R. J.: (1980): Middle East: Stratigraphic Evolution and oil habitat. AAPG Bulletin: 64: no. 5: p597-618.

Mutti, M. & Hallock, P.: (2003): Carbonate systems along nutrient and temperature gradients: some sedimentological and geochemical constraints. International Journal of Earth Science: 92: p465-475.

Neilson, J. E., Oxtoby, N. H. & Simmons, M. D.: (1996): Effect of Petroleum Emplacement on Reservoir Quality in the Thamama Reservoirs of Abu Dhabi. SPE: 36241.

Neilson, J. E., Oxtoby, N. H., Simmons, M. D., Simpson, I. R., & Fortunatova, N. K.: (1998): The relationship between petroleum emplacement and carbonate reservoir quality: examples from Abu Dhabi and the Amu Darya Basin. Marine and Petroleum Geology: 15: p57-72

Nolan, S. C., Skelton, P. W., Clissold, B. P. & Smewing, J. D.: (1990): Maastrichtian to early Tertiary stratigraphy and paleogeography of the Central and Northern Oman Mountains: *in*, A. H. F. Robertson, M. P. Searle and A.C. Reis (Eds.), The Geology and tectonics of the Oman Region. Geological Society, London, Special Publications, 49, p495-519.

O' Neil, J. R., Clayton, R. N. & Mayeda, T. K.: (1969): Oxygen isotope fractionation in divalent metal carbonates. Journal of Chemical Physics: 51: p5547-5548

Oswold, E. J., Mueller III, H. W. & Goff, D. F.: (1995): Controls on Porosity Evolution in Thamama Group Carbonate Reservoirs in Abu Dhabi, U.A.E. SPE: 029797.

Owen, R. M. S. & Nasr, S. N.: (1958): Stratigraphy of the Kuwait-Basra area: *in*: Weeks, L. G. (Ed.): Habitat of Oil. AAPG: Tulsa, p1252-1278.

Patterson, W. P. & Walter, L. M.: (1994): Depletion of ^{13}C in seawater δCO_2 on modern carbonate platforms: significance for the carbon isotope records of carbonates. Geology: 22: p885-888.

Pittet, B., van Buchem, F. S. P., Hillgärtner, H., Razin, P., Grötsch, J. & Droste, H: (2002): Ecological succession, palaeoenvironmental change, and depositional sequences of Barremian-Aptian shallow-water carbonates in northern Oman. Sedimentology: 49: p555-581.

Pittman, E. D.: (1971): Microporosity in carbonate rocks. AAPG Bulletin: 55: p1873-1881.

Perkins, R. D.: (1989): Origin of micro-rhombic calcite matrix within Cretaceous reservoir rock, West Stuart City Trend, Texas. Sedimentary Geology: 63: p313-321.

Podlaha, O. G., Mutterlose, J. & Veizer, J.: (1998): Preservation of $\delta^{18}O$ and $\delta^{13}C$ in Belemnite Rostra from the Jurassic/Early Cretaceous. American Journal of Science: 298: p324-347.

Poulsen, C. J., Seidov, Dan, Barron, E. J. & Peterson. W. H.: (1998): The impact of paleogeographic evolution on the surface oceanic circulation and the marine environment within the Mid-Cretaceous Tethys. Palaeoceanography: 13, No. 5, p546-559.

Price, G.D., Ruffell, A. H., Jones, C. E., Kalin, R. N., & Mutterlose, J.: (2000): Isotopic evidence for temperature variation during the early Cretaceous (late Ryazanian–mid-Hauterivian). Journal of the Geological Society: 157, no. 2, p335-343.

Ramakrishnan, T. S., Ramamoorthy, R, Fordham, E., Schwartz, L., Herron, H., Saito, N., & Rabaute, A.: (2001): A Model-Based Interpretation Methodology for Evaluating Carbonate Reservoirs. SPE: 71704.

Raven, M. J. & Dickson, J. A. D.: (2007): Methanogenesis during Shu'aiba diagenesis: examples from Al-Shaheen Field, Block 5, offshore Qatar. Geo*Arabia*: 12: no. 1: p37-58.

Richter, D. K, Gotte, Th., Gotze, J. & Neuser, R. D.: (2003): Progress in application of Cathodoluminescence (CL) in sedimentary petrology. Mineralogy & Petrology: 79: p127-166.

Ries, J. B.: (2003): Modern High-Magnesium Calcite organisms produce Low-Magnesium Calcite in experimental Mid-Cretaceous seawater. 2003 Seattle Annual Meeting (Nov 2-5): Paper no. 70-13.

Robertson, A. H. F. & Searle, M. P.: (1990): The northern Tethyan continental margin: stratigraphy, structure, concepts and controversies: *in*, Robertson, A. H. F., Searle, M. P. & Ries, A. C. (Eds.): The geology and tectonics of Oman Region. Geological Society Special Publication: 49, p3-25.

Robinson, A., & Gluyas, J.: (1992): Model calculations of loss of porosity in sandstones as a result of compaction and quartz cementation. Marine and Petroleum Geology: 9: p319-323

Saller, A. H. & Moore Jr., C. H.: (1989): Meteoric diagenesis, marine diagenesis, and microporosity in Pleistocene and Oligocene limestones, Enewetak Atoll, Marshall Islands. Sedimentary Geology: 63: p253-272.

Salvador, A.: (1987): Unconformity-bounded stratigraphic units. Geological Society of America, Boulder: 98: p232-237.

Savrda, C. E., Browning, J. V., Krawinkel, H. & Hesselbo, S. P.: (2001): Firmground Ichnofabrics in Deep-water Sequence Stratigraphy, Tertiary Clinoform-Toe Deposits, New Jersey Slope. PALAIOS: 16: p294-305.

Sayers, C. M.: (2008): The elastic properties of carbonates. Society of Exploration Geophysicists: 27: no. 8: p1020-1024

Schmid, D. U.: (1996): Marine Mikrobolithe und Mikroinkrustierer aus dem Oberjura. Profil: 9, p101-251.

Schmid, D. U. & Leinfelder, R. R.: (1996): The Jurassic *Lithocodium Aggregatum-Troglotella incrustans* foraminiferal consortiums. Palaeontology: 39: p21-52.

Scott, R. W.: (1990): Chronostratigraphy of the Cretaceous carbonate shelf, southeastern Arabia: *in*, Robertson, A. H. F., Searle, M. P. & Ries, A. C. (Eds.): The geology and tectonics of Oman Region. Geological Society Special Publication: 49, p89-108.

Searle M. P.: (1988): Thrust tectonics of the Dibba Zone and nental margin along the Musandam Mountains (Oman and United Arab Emirates). Journal of the Geological Society, London: 145, p43-53.

Shackleton, N. J. & Hall, M. A.: (1984): Carbon isotope data from Leg 74 sediments: *in*, Moore, T. C., Rabinowitz, P. D, *et al.* (Eds.): Init. Repts. DSDP, U. S. Government Printing Office, Washington, D. C: p613-619.

Sharland, P. R., Archer, R., Casey, D. M., Davies, R. B., Hall, S. H., Heward, A. P., Horbury, A. D. & Simmons, M. D.: (2001): Arabian Plate Sequence Stratigraphy. Geo*Arabia*: Special Publication 2: Gulf Petrolink, Oriental Press Manama, Bahrain.

Sharland, P. R., Casey, D. M., Davies, R. B., Simmons, M. D. & Sutcliffe, O .E.: (2004): Arabian Plate Sequence Stratigraphy-Revisions to SP2. GeoArabia: 9, no. 1, p199-214.

Shaw, A. B.: (1964): Time in Stratigraphy. McGraw-Hill: p365.

Shearman, D. J.: (1978): Evaporites of coastal sabkhas: *in*. Dean, W. E. & Schreiber, B. C. (Eds.): Marine evaporates. SEPM: short course: no. 4: p6-42.

Shebl, H. T. & Alsharhan, A. S.: (2000): Microfacies analysis of Berriasian-Hauterivian carbonates, Central Saudi Arabia. SEPM Special Publication: 69: p115-127.

Shenawi, S., Al-Mohammadi, H. & Faqehy, M.: (2009): Development of Generalised Porosity-Permeability Transforms by Hydraulic Units for Carbonate Oil Reservoirs in Saudi Arabia. SPE: 126073.

Simkiss, K.: (1964): Phosphates as crystals poisons of calcification: Biological Review: 39: p487-505.

Simmons, M. D.: (1994): Micropalaeontological biozonation of the Kahmah Group (Early Cretaceous), Central Oman Mountains: *in*, Simmons, M. D. (Ed.): Micropalaeontology and Hydrocarbon Exploration in the Middle East. Published by Chapman & Hall, London.

Simmons, M. D., Emery, D., & Pickard, N. A. H.: (1991): *Hensonella Dinarica*, an originally Calcitic Early Cretaceous Dasycladacean Alga. Palaeontology: 34: p955-961.

Simmons, M. D. & Hart, M. B.: (1987): The biostratigraphy and microfacies of the Early to mid-Cretaceous carbonates of Wadi Mi'aidin Central Oman Mountains: *in*, Hart, M. B. (Ed.): Micropalaeontology of Carbonate Environments. Ellis Horwood Ltd, Chichester

Simmons M. D., Sharland P. R. & Casey D. M.: (2007): Arabian Plate sequence stratigraphy: Potential implication for global chronostratigraphy. GeoArabia: 12, no. 4, p101-130.

Simmons, M. D., Whittaker, J. E. & Jones, R. W.: (2000): Orbitolinids from Cretaceous sediments of the Middle East-a revision of the F. R. S. Henson and Associates Collection. Proceedings of the Fifth International Workshop on Agglutinated Foraminifera: Grzybowski Foundation Special Publication: 7: p411-437.

Skelton P. W., Hughes G. W. & Aktas G. (1997): Rudists of the Shu'aiba Formation in the Shaybah Field, eastern Saudi Arabia. Abstract for SEPM Jurassic and Cretaceous carbonate platform conference: December 1997, Al Ain.

Stampfli, G. M. & Borel, G. D.: (2002): A plate tectonic model for the Paleozoic and Mesozoic constrained by dynamic plate boundaries and restored synthetic oceanic isochrones. Earth and Planetary Science Letters: 196, p17-33.

Steinen, R. P.: (1982): SEM observations on the replacement of Bahaman aragonitic mud by calcite. Geology: 10: p471-475.

Steuber, T., Rauch, M., Masse, J. P., Graaf, J. & Malko, M.: (2005): Low-latitude seasonality of Cretaceous temperatures in warm and cold episodes. Nature: 437, p1341-1344.

Strasser, A., Pittet, B., Hillgärtner, H. & Pasquier, J. B.: (1999): Depositional sequences in shallow carbonate-dominated sedimentary systems: concepts for a high-resolution analysis. Sedimentary Geology: 128: p201-221.

Strohmenger, C. J., Weber, L. J., Ghani, A., Al-Mehsin, K., Al-Jeelani, O., Al-Mansoori, A., Al-Dayyani, T., Vaughan, L., Khan, S. A. & Mitchell, J. C.: (2006a): High resolution Sequence Stratigraphy and Reservoir Characterization of Upper Thamama (Lower Cretaceous) Reservoirs of a Giant Abu Dhabi Oil field, United Arab Emirates: *in*, Harris, P. M. & Weber, L. J. (Eds.): Giant hydrocarbon reservoirs of the world: From rocks to reservoir characterization and modelling. AAPG memoir 88/SEPM special publication: p139-171.

Strohmenger, C. J., Patterson, P. E., Al-Sahlan, G., Demko, T. M., Wellner, R. W., McCrimmon, G. G. & Al-Ajmi, N.: (2006b): Sequence Stratigraphy and Reservoir Architecture of the Burgan and Mauddud Formations (Lower Cretaceous), Kuwait: *in*, Harris, P. M. & Weber, L. J. (Eds.): Giant Hydrocarbon Reservoirs of the World: From rocks to Reservoir Characterization and Modelling. AAPG Memoir 88/SEPM Special Publication: p213-245.

Strohmenger C. J., Al-Dayyani T., Clark A. B. S., Ghani, A. & Hafez, H. H.: (2007): Sequence Stratigraphy-Based Geological Modelling of the Thamama (Lower Cretceous) Reservoirs of a Giant Abu Dhabi Oil Field, United Arab Emirates. SPE 111401.

Sugden, W., & Standring, A. J.: (1975): Qater peninsula-Lexique stratigraphique International-Asie, Paris: 3: p7-88.

Svirsky, D., Ryazanov, A., Pankov, M., Yukos, E. P., Corbett, P. W. M. & Posysoev, A.: (2004): Hydraulic Flow Units Resolve Reservoir Description challenges in a Siberian Oil Field. SPE: 87056.

Taher, A. A.: (1997): Delineation of Organic Richness and Thermal History of the Lower Cretaceous Thamama Group, East Abu Dhabi: A modelling Approach for Oil Exploration. Geo*Arabia*: 2: p65-88.

Tilton, G. R., Hopson, C. A. & Wright, J. E.: (1981): Uranium-lead isotope ages of the Semail Ophiolite, Oman, with application to Tethyan ocean ridge tectonics. Journal of Geophysical Research, 86, p2763-2775.

Thorrold, S. R., Campana, S. E., Jones, C. M. & Swart, P. K.: (1997): Factors determining $\delta^{13}C$ and $\delta^{18}O$ fractionation in aragonitic otoliths of marine fish. Geochimica et Cosmochimica Acta: 61: no. 14: p2909-2919.

Toledo, P. G., Scriven, L. E. & Davis, H. T.: (1994): Pore-Space Statistics and Capillary Pressure Curves From Volume-Controlled Porosimetry. SPE Formation Evaluation: 9, No. 1, p46-54.

Török, A.: (2000): Formation of dolomite mottling in Middle Triassic ramp carbonate (Southern Hungary). Sedimentary Geology: 131: p131-145.

Vail, P. R., MitchuM Jr., R. M, Todd, R G., Widmier, J. M., Thompson III, S., Sangee, S. B., Bubb, J. N. & Hatlelid W. G.: (1977): Seismic stratigraphy and global changes of sea level: *in*, C. E. Payton (Ed.), Seismic Stratigraphy-Applications to Hydrocarbon Exploration. AAPG, Memoir 26, p49-212.

Vahidy, H. & Fesharaki, S.: (2003): Middle East Crude oil Production and Exports. Middle East Crude: Production Profile, Export Markets, Pricing Issues and Output Capacity (Report). Middle East Economic Survey: 60: no. 40.

Vahrenkamp, V. C.: (1996): Carbon isotope stratigraphy of the Upper Kharaib and Shu'aiba Formations: Implications for the Early Cretaceous evolution of the Arabian Gulf region. AAPG Bulletin: 80: p647-662.

Vasconcelos, C., Mackenzie, J. A., & Warthmann, R.: (2005): Calibration of the $\delta^{18}O$ paleothermometer for dolomite precipitated in microbial cultures and natural environments. Geology: 33: p317-320.

Veizer, J., Ala, D., Amzy, K., Bruckschen, P., Buhl, D., Bruhn, F., Carden, G. A. F., Diener, A., Ebneth, S., Godderis, Y., Jasper, T., Korte, C., Pawellek, F., Podlaha, O. G. & Strauss, H.: (1999): $^{87}Sr/^{86}Sr$, $\delta^{13}C$ and $\delta^{18}O$ evolution of Phanerozoic seawater. Chemical Geology: 161: p59-88.

Vilas, L., Masse, J. P. & Arias, C.: (1995): *Orbitolina* episodes in carbonate platform evolution: the early Aptian model from SE Spain. Palaeogeography, Palaeoclimatology, Palaeoecology: 119: p35-45.

Walderhaug, O.: (1990): A Fluid Inclusion Study of Quartz-Cemented Sandstones from Offshore Mid-Norway-Possible Evidence for Continued Quartz Cementation During Oil Emplacement: Journal of Sedimentary Petrology: 60: p203-210.

Walderhaug, O.: (1994): Precipitation Rates for Quartz Cement in Sandstones Determined by Fluid-Inclusion Microthermometry and Temperature-History Modelling. Journal of Sedimentary Research: 64: p324-333.

Walderhaug, O.: (1996): Kinetic Modelling of Quartz Cementation and Porosity Loss in Deeply Buried Sandstone Reservoirs: AAPG Bulletin: 80: p731-745.

Walker, J. D. & Geissman, J. W.: (2009): 2009 Geological Timescale: Geological Society of America.

Walley C. D.: (1998): Some outstanding issues in the geology of Lebanon and their importance in the tectonic evolution of the Levantine region. Tectonophysics: 298, no. 1-3, p37-62.

Walter, L. M., Bishof, S. A., Patterson, W. P. & Lyons, T. W.: (1993): Dissolution and recrystallisation in modern shelf carbonates: Evidence from pore water and solid phase chemistry. Phil. Trans. Royal Soc. London: 344: p7-36.

Wanless, H. R.: (1979): Limestone response to stress: pressure solution and dolomitisation. Journal of Sedimentary Petrology: 49: p437-462.

Watts, K. F.: (1988): Triassic carbonate submarine fans along the Arabian platform margin, Sumeini Group, Oman. Sedimentology: 35, p43–71.

Weissert, H., Lini, A., Follmi, K. B. & Kuhn, O.: (1998): Correlation of Early Cretaceous carbon isotope stratigraphy and platform drowning events: a possible link? Palaeogeography, Palaeoclimatology, Palaeoecology: 137: p189-203.

Weissert, H. & Erba, E.: (2004): Volcanism, CO_2 and palaeoclimate: a late Jurassic-Early Cretaceous carbon and oxygen isotope record. Journal of the Geological Society: 161: p695-702.

Wilson, H. H.: (2005): A Review of Geological Data that Conflict with the Paradigm of Catagenic Generation and Migration of Oil. Journal of Petroleum Geology: 28: p287-300.

Worden, R. H., Oxtoby, N. H., & Smalley, P. C.: (1998): Can oil emplacement prevent quartz cementation in sandstones? Petroleum Geoscience: 4: p129-137.

Wood, R.: (1993): Nutrients, Predation and the History of Reef-Building. Palaios: 8, p526-543.

Xie, X, Weiss, W. W., Tong, Z., & Morrow, N. R.: (2004): Improved Oil Recovery from Carbonate Reservoirs by Chemical Stimulation. SPE Symposium on Improved Oil Recovery.

Yose, L. A., Ruf, A. S., Strohmenger, C. J. Schuelke, J. S., Gombos, A., Al-Hosani, I., Al-Maskary, S., Bloch, G., Al-Mehairi, Y. & Johnson, I. G.: (2006): Three-dimensional Characterization of a Heterogeneous Carbonate Reservoir, Lower Cretaceous, Abu Dhabi (United Arab Emirates): *in*, Harris, P. M. & Weber, L. J. (Eds.): Giant hydrocarbon reservoirs of the world: From rocks to reservoir characterization and modelling: AAPG memoir 88/SEPM special publication: p173-212.

Ziegler, M. A.: (2002): Late Permian to Holocene Paleofacies Evolution of the Arabian Plate and its Hydrocarbon Occurrences. G*eoArabia*: 6, p445-504.

Zhang, P. & Austad T.: (2006): Wettability and oil recovery from carbonates: Effects of temperature and potential determining ions. Colloids & Surfaces A: Physiochemical Engineering Aspects: 279, p179-187.

Glossary

$\delta^{13}C$: the ratio of $\delta^{13}C/\delta^{12}C$.

$\delta^{18}O$: the ratio of $\delta^{18}O/\delta^{16}O$.

Accommodation space: the space available between the sea bed and eustatic sea level for potential sediment accumulation (Sharland et al. 2001).

Acidic porewaters: waters that head main oil charge/emplacement. The water mixture can include carbonic and carboxylic acids.

Aggradation: vertical build up of a sedimentary sequence. Usually occurs when there is a relative rise in sea level produced by subsidence and/or eustatic sea-level, and the rate of sediment influx is sufficient to maintain the depositional surface at or near sea level.

Aggrading Neomorphism: the in-situ replacement of HMC and aragonite components to coarse LMC (Bathurst 1975), which can occur as early as syn-deposition and initial burial.

Aggregate grains: grains that are composed of two or more components: each component has formed through separate processes on the sea bed.

Alizarin Red Solution ($C_{14}H_8O_4$): a solution used to stain calcite red.

Anhedral: mineral crystals that display no recognisable shape: the crystal boundaries, surfaces and edges are absent.

Barrier: a significant mound on the sea bed (coral/sponge reefs) that form on the platform providing protection to organisms living behind from wave action.

Basin/Basinal: deeper areas of a sedimentary basin, either in terms of water depth, or sediment thickness (Sharland et al. 2001).

Biocalcification crisis: marine conditions that give organisms great difficulty in secreting and forming mineralised hard parts (HMC, LMC, aragonite). This is observed when there is abundance and dominance of organisms with smaller and thinner mineralised parts (Weissert & Erba 2004).

Bioclasts: fragments from organisms that lived on the sea bed that are either in situ or have been reworked.

Biodiversity: the range of in-situ and fragmented fossils observed within specific lithologies or lithofacies.

Bioerosion: describes the grazing of organisms that causes disintegration of mineralised hard parts of other larger organisms.

Biostratigraphy: correlating depositional units across terranes by using the relative timing of taxa inceptions and extinctions within the lithologies.

Biostromes: organisms that grow to form flat tabular-shaped bodies on the sea bed.

Bioturbation: this generally describes the disturbance of sediment from grazing and/or burrowing organisms.

Biozone: subdivision of a sedimentary succession based on one or more characteristic fossils and/or bioevents. Used for correlation, usually with chronostratigraphic significance (Sharland et al. 2001).

Borings: casts, or voids, left by organisms that hollowed out hard parts (shells) of other larger organisms, LMC, HMC and dolomite cements. Borings indicate the sea bed had lithified during syn-deposition (hardground formation): boring can also be used to constrain other diagenetic processes during syn-deposition.

Birefringence: is the separation of a single ray of light, into two light rays (the ordinary ray and the extraordinary ray) when it passes through minerals, such as calcite crystals, under cross-polarised light, and a polarising light microscope.

Burrows: traces left by organisms that hollowed out sediment on the sea bed to form tubules for habitation. Burrows are used to signify low water energy and periods of non-deposition.

Carbonate ramp: a uniform, gently sloping carbonate depositional system, that passes from very shallow or emergent conditions to deep water conditions over a distance of 10's to 100's of kilometres with no distinct break in slope (after Burchette & Wright 1992).

Cathodoluminescence: a tool that passes a current through a highly polished thin section, causing luminescence of LMC, HMC, dolomite and other minerals. This tool can be used to determine a relative sequence of differing luminescent cement zones, which cannot otherwise be gathered from a polarising light microscope.

Cement: a mineral that precipitates from interstitial porewaters, which nucleates on grains and continues to grow and occlude all available surrounding pore space.

Cement stratigraphy: a relative sequence of oldest to youngest cement zones within syntaxial overgrowths (from the echinoid fragment (oldest) to the last cement abutting into open pore space (youngest)), based on petrographic and Cathodoluminescence observations.

Cleavage plane: a plane of weakness within minerals, due to their crystalline structure, that can be observed under a polarising light microscope.

Congruent dissolution: transition from a solid substance to a liquid of the same composition.

Crest: the structural high point at or near the centre of an oil field within the substratum.

Critical oil saturation: this represents the gradual displacement of water by oil, until enough oil has entered and displaced the water to prevent any further solutes from reaching these sites, inhibiting all cementation.

Debris flows: these are generated on unstable slopes, which readily slip underwater. The density difference between the sediment laden water, and the surrounding seawater, causes grains and finer sediment to rapidly precede downslope into the basin for several kilometres.

Deep burial: deep burial, for this study, is indicated by the presence of stylolites.

Diachronous: a term applied to laterally continuous lithological units, taxa inceptions, and extinctions, which represent the development of the same depositional facies, or the appearance/disappearance of the same species, in different places at different times. Thus, either or both the top and lower bounding surfaces cross time lines (Sharland et al. 2001).

Diagenesis: diagenesis is any chemical, physical, or biological change undergone by sediment after its initial deposition, and during, and after its lithification.

Downlap: the inflextion point on seismic reflectors that typically corresponds to the base-of-slope of a prodelta, shelf or ramp margin. It is present at the meeting point between the down-dip portion of clinoforms and near-horizontal planer reflectors representing basinal settings (Sharland et al. 2001).

Enhanced crystal growth: this defines episodic crystal growth, through additional layers to the exterior crystal surface, which in section would represent several growth bands, or zones.

Euhedral: describes crystals with identifiable shape, bounded by crystal faces, clear and sharp crystal points, and definable crystal boundaries that separate individual crystals from one another.

External precision: the measurement of variability of $\delta^{18}O$ values between spot analysis, for a single sample under the Ion Microprobe, which is determined by consecutive analysis of the UWC (University of Wisconsin Calcite) standard which is determined to be homogenous.

Facies/Lithofacies: the characteristics that define a particular sedimentary rock. These characteristics may be the products of depositional processes, post-depositional modification, palaeontological content or chemical composition (Sharland et al. 2001).

Fair weather wavebase: the maximum depth where reworking of sediment by wave action takes place during fair-weather conditions (Sharland et al. 2001).

Firmground: sediment that has been compacted (firm) but not cemented. These usually indicate periods of low water energy and non-deposition.

Fourth (4^{th}) order: a relatively short term sea level cycle which can last for 0.1-1Myr.

Framboides/Framboidal: term given for "mineralised bacteria" where most, or all, organic matter has been recrystallised to pyrite, forming irregular masses that display little crystal shape.

FZI: Flow Zone Indicator: these are gradients, which plot as straight lines on Log permeability-Log porosity plots, calculated by dividing the Reservoir Quality Index (RQI: dividing the amount of porosity by the amount of permeability) by Φz (pore volume to grain volume ratio).

Geothermal gradient: the relationship between increasing temperature for a degree of burial, for specific points within the substratum.

Glossifungites: *Glossifungites* are an assemblage of burrows (vertical, U-shaped, or sparsely branched) that occur in firm, but not lithified siliciclastic and/or carbonate muds and silts, of intertidal and shallow marine environments, where scouring has often removed the unconsolidated layers of the sediment surface. The surfaces where *Glossifungites* often occur are associated with regression and sea level fall.

GSS: Genetic Stratigraphic Sequence: a package of sediments bounded top and bottom by Maximum Flooding Surfaces (MFS). Each GSS consists of a vertical succession of progradational, aggradational and retrogradational transgressive facies (after Galloway 1989).

GHE: Global Hydraulic Element: these are bands that form a base map for plotting porosity and permeability data. Each GHE covers a finite space, centred on an FZI.

Hardground: an area of the seafloor that has cemented in the marine environment. Hardgrounds imply a pause in sedimentation (Sharland et al. 2001).

HFC: High Frequency Cycle: these are frequently repeated cycles that all share similar internal lithological components that can be easily correlated. This term is also applied to a 4^{th} (or higher) order cycle.

HFU: Hydraulic Flow Unit: areas with spatially continuous flow properties that are not defined by specific lithofacies, pore types, and pore distributions, within single reservoir units, that should be preserved during up scaling (HFU's are defined by FZI's).

HMC: High Magnesium Calcite: the classification given to calcite with Mg/Ca mole ratios of 1.2–5.0 (> 4 mole % Mg^{2+} substituting for Ca^{2+}) (Ries 2003).

HST: Highstand Systems Tract: those linked depositional systems deposited during a highstand, bounded at the top by a Sequence Boundary (SB) and at the base by a Maximum Flooding Surface (MFS) (Sharland et al. 2001).

Hypidiotopic: this term describes a rock texture characterized by the presence of some minerals showing their crystal form (i.e. some euhedral habits).

Idiotopic: this term describes a fabric developed in a crystalline sedimentary rock in which most of the crystals are euhedral.

Incongruent dissolution: dissolution of a mineral, with decomposition, or reaction in the presence of a liquid, converting one solid phase into another: i.e. a solid and a liquid phase are formed.

Initial burial: this involves the first 10 metres of burial, before significant mechanical compaction begins (few 10's metres burial: Mazzullo & Harris 1992).

Internal precision: the measure of variability within each spot analysis under the Ion Microprobe (% Standard Error).

Interparticle: the open pore spaces in-between tightly packed grains (ooids/micrite grains).

Intertidal: the intertidal zone (also known as the foreshore, seashore and the littoral zone) is the area that is exposed to the air at low tide and underwater at high tide (the area between tide marks).

Intraclasts: clasts of sediment, or lithified sediments from other parts of the carbonate ramp: i.e. these have not been transported from outside the ramp environment.

Intraparticle: open pore spaces that exist within grains and clasts.

Intra-skeletal: open pore spaces that exist within bioclasts that can conform to internal chambers of the organism.

Karst/Karstic/Palaeokarst: surface of subaerial exposure developed upon carbonate sediments typically characterised by widespread dissolution and distinctive diagenetic fabrics. The surface may be a short-lived (10,000 years) disconformity on parasequence tops, or a long-lived unconformity (10's of million years) (Sharland et al. 2001).

Lagoon: a restricted near shore environment, behind the main shoals, barriers or coral reefs. The environment is characterised by low water energy with little sedimentation. This environment can be subtidal (deep lagoon) or intertidal.

Lithology: a general term given to a rock containing a specific set of defining depositional and/or diagenetic features.

LMC: Low Magnesium Calcite: this is the classification given to calcite with Mg/Ca mole ratios of < 1.2 (< 4 mole % Mg^{2+} substituting for Ca^{2+}) (Ries 2003).

LST: Lowstand Systems Tract: those linked depositional systems deposited during a lowstand. The basal bounding surface is a Sequence Boundary (SB) or its correlative conformity (Sharland et al. 2001).

Macropore-dominated: this refers to a pore system that is comprised of >50% >10µm diameter sized pore spaces.

Macroporosity: this is defined as open pore space that is >10µm in diameter.

Macrospar: these are LMC crystals >10µm in size.

Meniscus cements: these cements are visible as coats on grains that form pendant shapes, reflecting water dripping through the open pore spaces, and the vadose zone.

Mesotrophic: refers to a water column having a moderate amount of dissolved nutrients resulting in high competition for substrate among organisms (Mutti & Hallock 2003).

Meteoric diagenesis: the chemical and physical alteration of a lithology by the interaction of it with freshwater from terrigenous sources.

Methanogenesis: methanogenesis is the production of CH_4 and CO_2 by biological processes carried out by methanogens.

MFS: Maximum Flooding Surface: an imaginary, isochronous surface within a packet of sediment that corresponds to the most landward flooding surface within a cycle of transgression and regression. It commonly represents the time of deepest water deposition within a basin (Sharland et al. 2001).

Micrite: an abbreviation of "microcrystalline ooze". One of the essentially normal precipitates, formed within the basin of deposition, and showing little or no evidence of significant transport: forms crystals 1-4µm in diameter (Folk 1959).

Micropore-dominated: this refers to a pore system that is comprised of >50% <10µm diameter sized pore spaces.

Micropore fabric: this is an assemblage of microspars (dominant), cements and micropores forming a distinctive texture.

Micro/macropore-fill cement: this refers to a single cementation episode that is volumetrically large enough to completely occlude a micro- or macropore pore systems.

Microporosity: this is defined as open pore space that is <10µm in diameter (Cantrell & Hagerty 1999).

Microspar: these are LMC crystals <10µm in size.

Mineral stabilisation: the transformation of a mineral into a more stable form with respect to the surrounding chemical conditions. In terms of Cretaceous calcite seas, this refers to HMC and aragonite components of organisms being replaced by LMC, either at syn-deposition, or during initial burial.

Moulds: these are pore spaces that have either been created or enhanced, through dissolution, within bioclasts. Moulds can usually form due to the dissolution of HMC and aragonite bioclastic components.

Non-reservoir: these constitute the extent of lithologies and/or lithofacies within every HFC that are oil free.

Oil Charge/Emplacement: this refers to the initial maturation of oil within a reservoir/pore system (with respect to a local source) or the initial slow percolation of oil into a reservoir/pore system from another distant location (oil migration).

Oil kitchen: this refers to areas with abundant oil source rocks that have been buried and subjected to elevated temperature and pressure, causing significant oil maturation.

Oil leg: these are areas of an oil field where all open macropores are oil filled. These areas have displaced the original water the pre-existed within the open pores, therefore oil-filled pore systems sit above water-filled pore systems within an oil field.

Oil-Water contact: the transition within an oil field between the oil-wet pore systems above and the water-wet pore systems below.

Oil-wet: refers to open pores that are oil filled.

Oligotrophic: refers to a water column being deficient in dissolved nutrients, restricting the competition of organisms on the sea bed (Mutti & Hallock 2003).

Onlap: characterised by regular and progressive upward pinching out of the strata toward the proximal margins of a depositional basin.

Open marine: Normal salinity conditions with connections to the open ocean, There are no strict implications for water depth.

Orbitolinidae: this is the Family name for Orbitolinid foraminifera.

Palaeosol: fossil soil; often developed at a Sequence Boundary (SB) or above a palaeokarst (Sharland et al. 2001).

Petrotype atlas: this term refers to the name given to the program used to plot porosity and permeability data upon graphs segregated into ten GHE bands. For the purposes on this study the term 'Petrotype atlas' is also given to the general method of plotting porosity and permeability into GHE's.

Platform: areas of shallow-water carbonate production. May be organised as either a carbonate shelf or a carbonate ramp dependant on the profile of the system at it passes from shallow into deep water (Sharland et al. 2001).

Potassium Ferricyanide ($K_3[Fe(CN)_6]$): a compound used to stain Fe-dolomite blue, and Fe-Calcite, in combination with Alizarin red solution, purple.

Pressure solution: this describes the process of the mobilisation of ions or molecules due to extreme pressure between grain-grain contacts. This usually occurs within stylolite seams at deep burial.

Progradation: generally basinward migration of either clastic or carbonate facies belts within a depositional system characterised by clinoforms. This is the process by which sediment is moved from shallow to deeper water area and infills accommodation space. Progradation can occur within falling, static or rising relative sea level, depending on the available sediment supply (Sharland et al. 2001).

Recrystallisation: the forming of new mineral crystals, from a precursor, either through several dissolution and reprecipitation reactions, or through solid solution.

Reservoir: these constitute the extent of oil stained lithologies and/or lithofacies within every HFC.

Retrogradation: the landward migration of facies belts. This often forms a backstepping (landward stepping) geometry revealed by parasequence or sequence stacking boundaries. It is typical of times when relative sea-level rise is rapid (transgression) (Sharland et al. 2001).

Rock typing: this term describes methods that associate porosity and permeability data into classes or categories, defined either by grain size, pore size or by flow property (pore throat radii).

Saddle dolomite: dolomite crystals that display a 'saddle-shape' habit. Under the polarising microscope the cleavage planes are curved and the crystals have sweeping extinction (another name for saddle dolomite is Baroque dolomite).

SB: Sequence Boundary: an unconformity or its correlative conformity (after Mitchum 1977). Typically an unconformity is identified in proximal settings and the correlative conformity is preserved in distal, deeper water, basinal settings (Sharland et al. 2001).

Second (2^{nd}) order: refers to a long term sea level cycle that can last for 10-100Myr and can relate to the open and closure of rift/sedimentary basins.

Sequence stratigraphic framework: this is a construct of depositional units, bounded by surfaces representing significant shifts in sea level, that are correlated across several 10's kilometres, to form a lithological cross-section of the substratum.

Shell hash: a lithology composed of poorly sorted bioclastic fragments, dominantly shell and echinoid fragments, measuring >1mm in size.

Shoal: a shoal is a long and narrow linear feature, typically composed of sand, silt, small pebbles or carbonate sediment. Shoals develop where an ocean current promotes deposition of granular material, resulting in localised shallowing (shoaling) of the water column, where small isolated moulds can form which may provide a small amount of protection for environments behind.

Spar: a mosaic of crystals larger than those of micrite, formed either as cement or as neomorphic spar (Folk 1959).

Solutes: molecules/ions liberated from dissolution and transported within interstitial porewaters to re-precipitation sites on growing macro- and microspars.

Storm weather wavebase: the maximum depth where the reworking of sediment, by wave action, takes place during storm conditions. Storm wave base is deeper than normal wave base (Sharland et al. 2001).

Stylolites: these are irregular pressure solution seams associated with chemical compaction and the dissolution of carbonate. Stylolites define the deep burial realm.

Subhedral: this describes mineral crystals that display a shape that resembles a half-way point between anhedral and subhedral geometries i.e. crystal faces are partially developed and crystals are partially bounded by crystal faces (Bathurst 1975).

Subtidal: depositional setting below low tide which is constantly submerged (Sharland et al. 2001).

Supersaturation: this refers to a fluid's capacity for solutes: if the fluid's capacity is exceeded under certain temperature and pressure conditions, the solutes will readily fall out of solution causing much re-precipitation.

Sulphate reduction: the reduction of SO_2^{-4}, through bacterial processes to form pyrite (Fe_2S).

Syn-depositional: diagenetic processes occurring in-synch with sedimentation.

Syntaxial: refers to crystal overgrowths where the original crystal and the overgrowth form a single larger crystal, sharing the same crystallographic axes (Bathurst 1975).

Terrigenous: term used to describe material/detritus that has originated from non-marine settings (i.e. from a land mass).

Textulariacea: the superfamily name for Textularia foraminifera.

***Thallassinoides*:** a term given to an assemblage of bifurcating horizontal and vertical tubes, forming an interconnected network.

Third (3rd order): relates to a long term sea level cycle that can last for 0.1-1Myr.

Transition zone: the zone within an oil field where pore systems are oil- and water-wet. These areas are between the oil leg and the water leg, and at the oil-water contact.

TST: Transgressive Systems Tract: those linked depositional systems deposited during a transgression. The upper and lower bounding surfaces are Maximum Flooding Surfaces (MFS's) and Sequence Boundary (SB's), respectively (Sharland et al. 2001).

VPDB: Vienna Pee Dee Belemnite: a standard used as a scale reference for all other $\delta^{13}C$ and $\delta^{18}O$ work: this was based on a Cretaceous marine fossil, *Belemnitella americana*, which was from the Pee Dee Formation in South Carolina.

Vugs: these are pores that have developed from dissolution of the carbonate matrix, and show no relation to the original depositional fabric: i.e. non-fabric selective (Choquette & Prey 1970).

Water leg: area of an oil field where its entire open pore system has remained water filled. These areas are below oil-wet pore systems and oil-water contacts.

Water-wet: refers to open pores that are water filled.

Xenotopic: describes fabrics of a crystalline carbonate rock where most crystals are anhedral.

Appendix 1A

Fossil data graphs, Well 1

There are two graphs; the first outlines all the manual counts for the different types of fossils, whereas the second outlines the biodiversity, from Well 1. Each bar defines a single 2" by 3" thin section. The depths are calculated using the base of Well 1, which is close to Cycle 2a hardground (SB), as the base of the scale. This data is shown in Section 3.4.2. The key for the graphs is shown below:

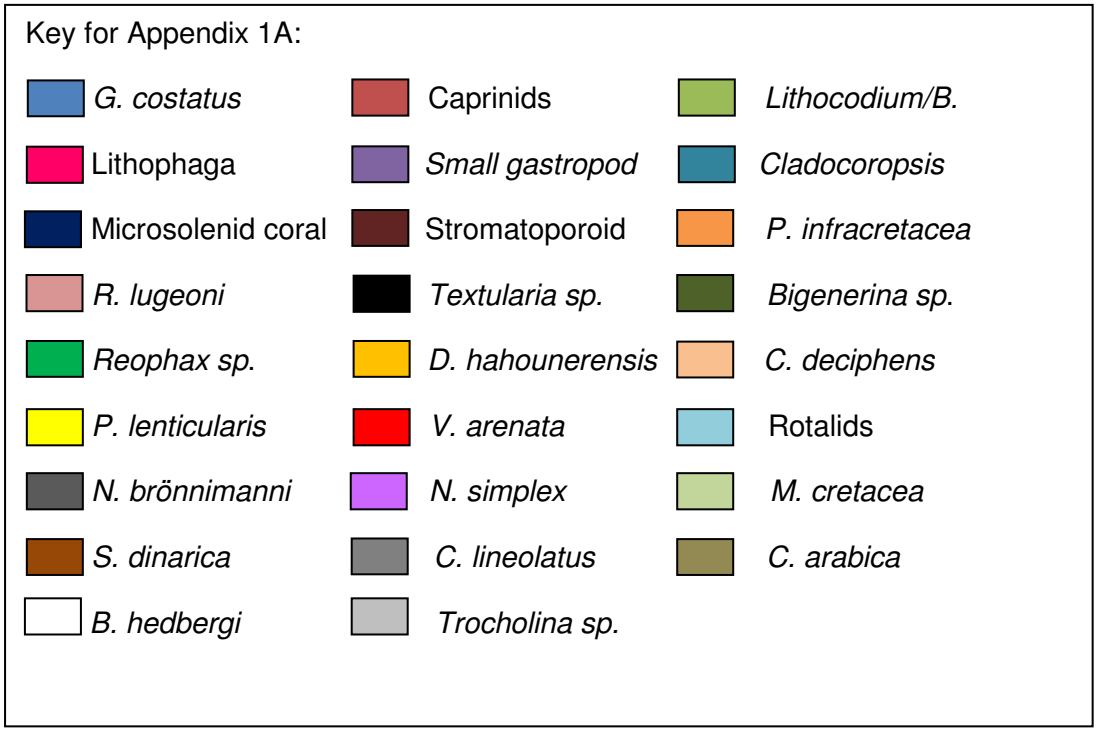

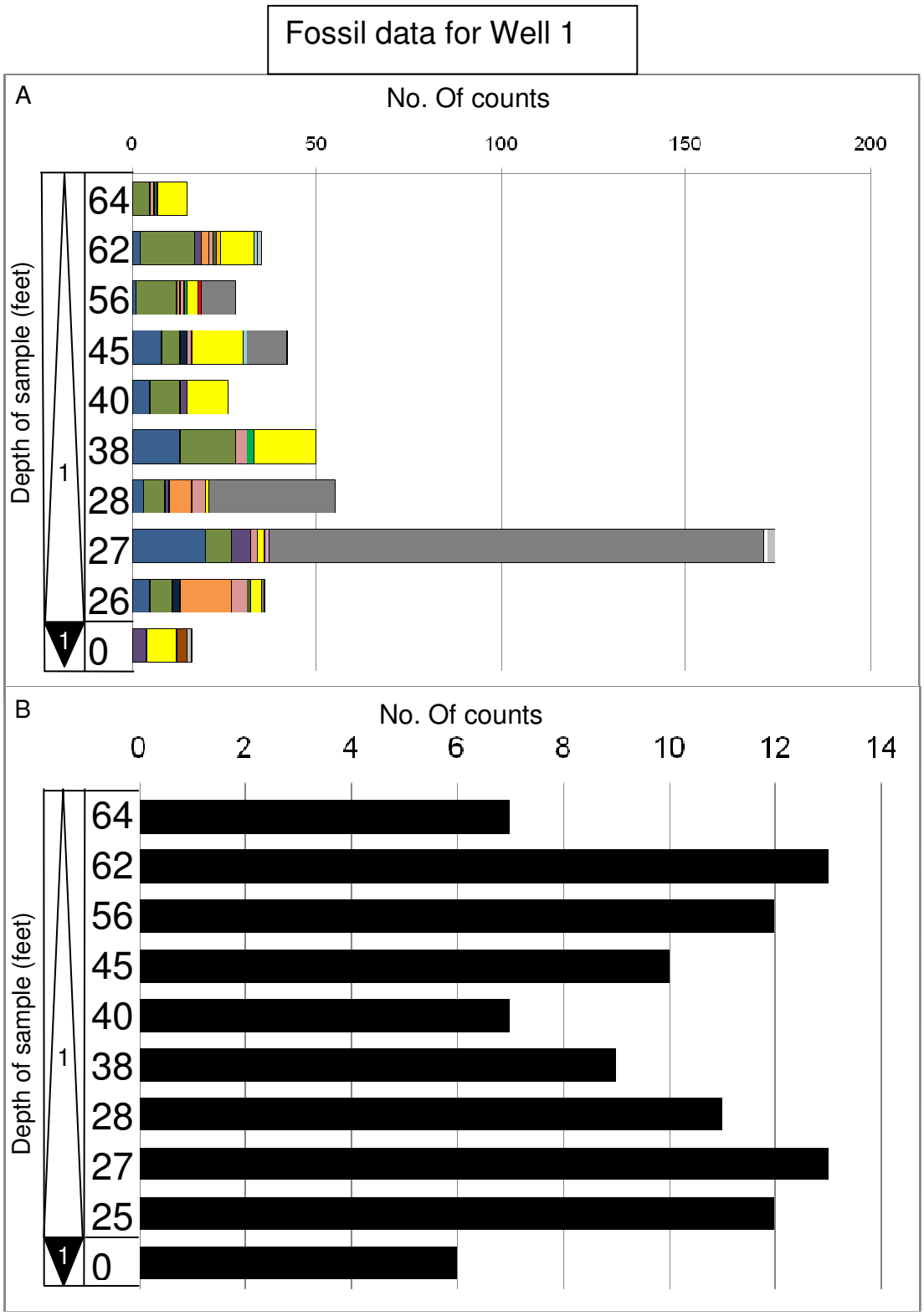

Figure 1.1: biodiversity data from Well 1: A) the manual counts for each species within each thin section. B) The number of different species for each thin section. The y-axis refers to the individual 4th order HFC's. On both graphs each bar represents a single 2" by 3" thin section. The y-axis shows the specific depths for each bar (sample). White triangles represent 4th order HST's while black triangles represent 4th order TST's.

Appendix 1B

Fossil data graphs, Well 2

There are two graphs; the first outlines all the manual counts for the different types of fossils, whereas the second outlines the biodiversity, from Well 2. Each bar defines a single 2" by 3" thin section. The depths are calculated using Cycle 8 SB, as the base of the scale, near the base of Well 2. This data is shown in Section 3.4.2. The key for the graphs is shown below:

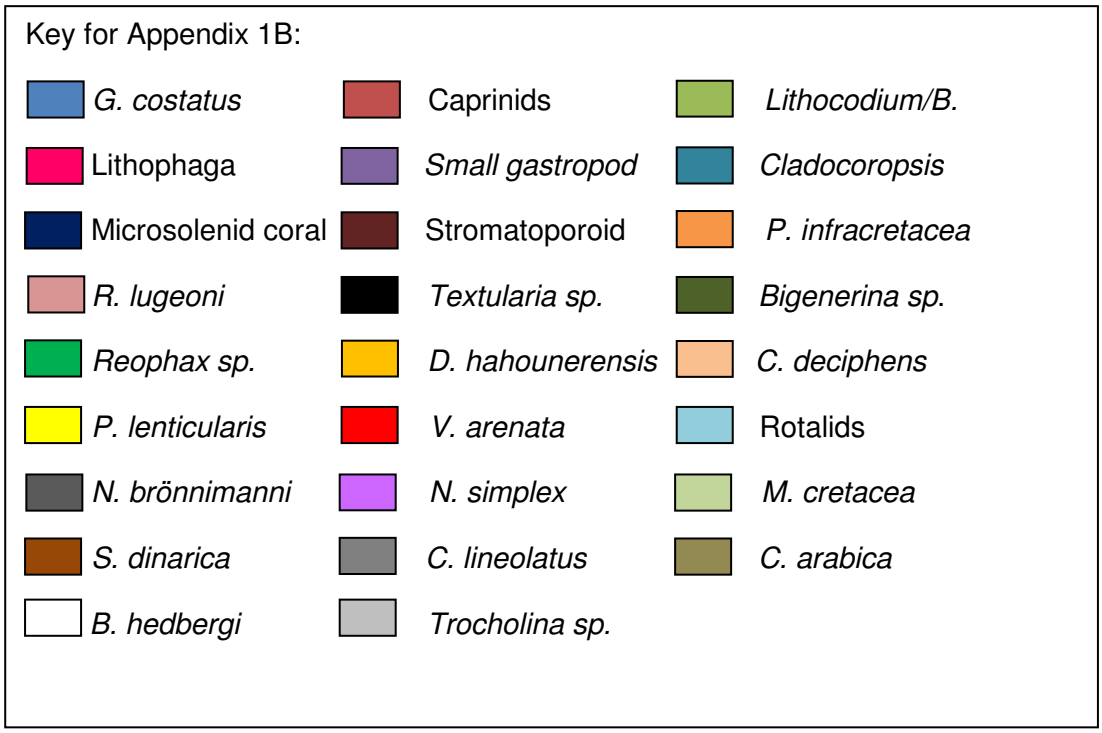

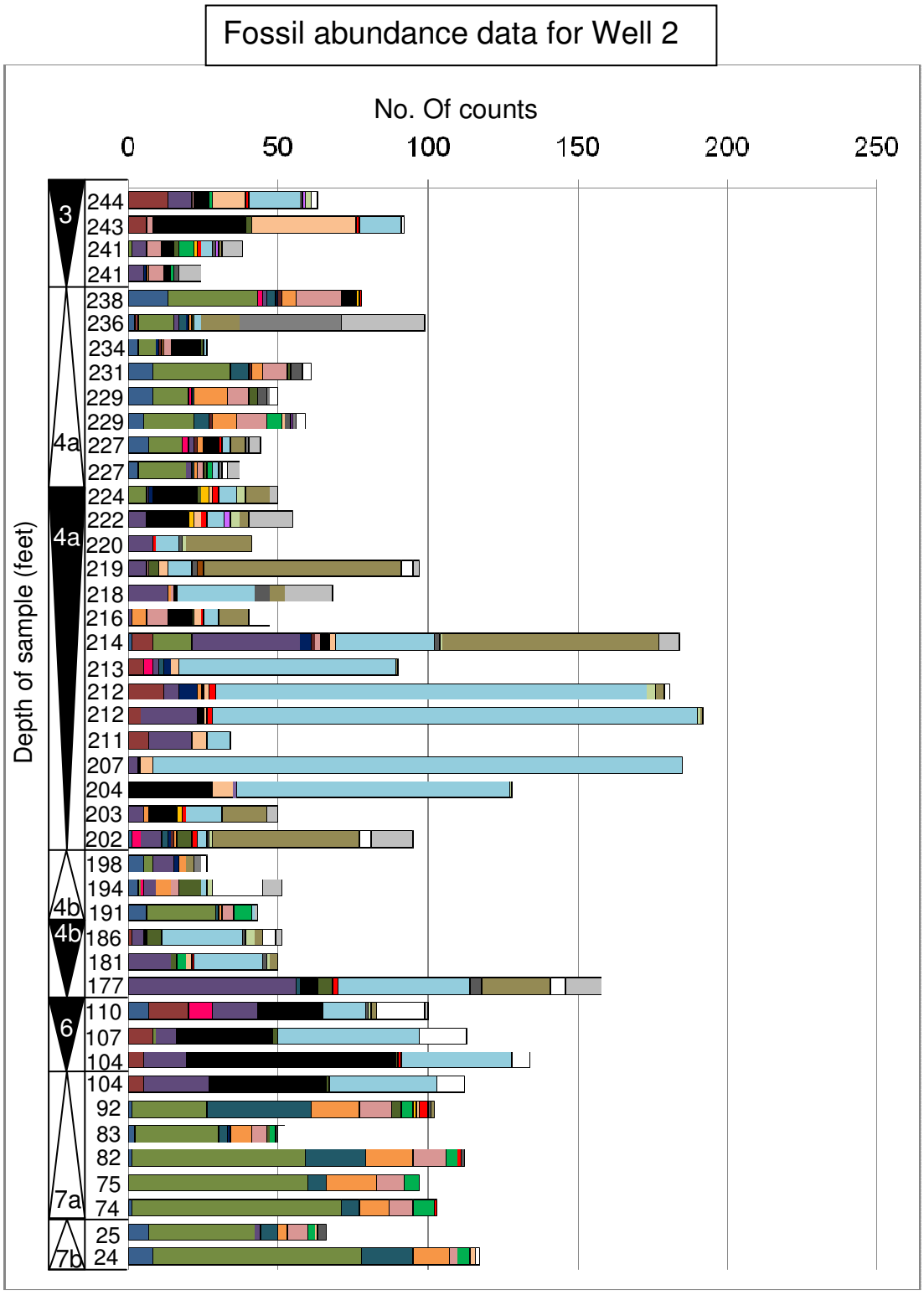

Figure 2.15: *biodiversity data from Well 2: A) the manual counts for each species within each thin section. The y-axis refers to the individual 4th order HFC's. On both graphs each bar represents a single 2" by 3" thin section. The y-axis shows the specific depths for each bar (sample). White triangles represent 4th order HST's while black triangles represent 4th order TST's.*

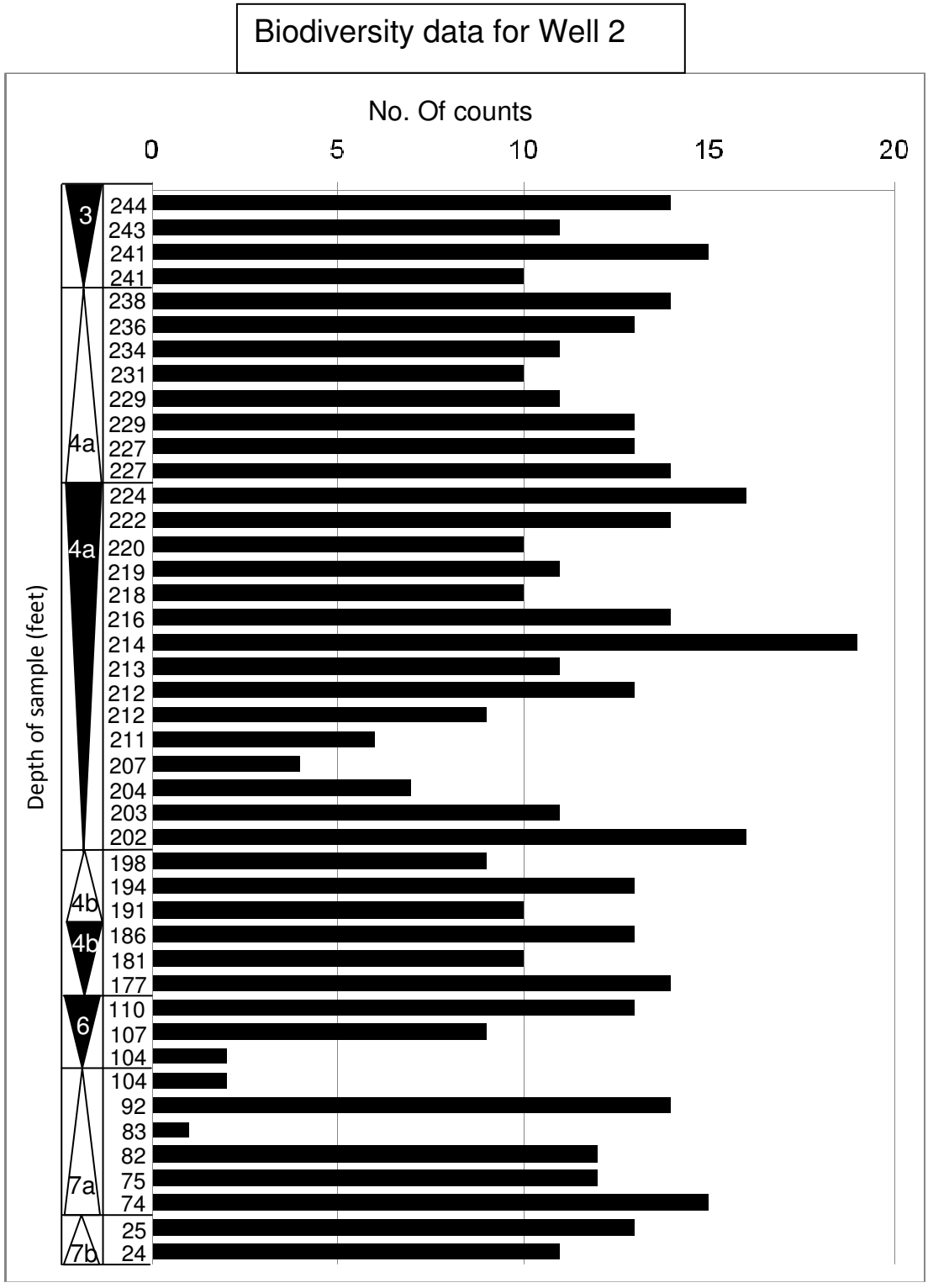

Figure 2.15: *biodiversity data from Well 2: the number of different species for each thin section. The y-axis refers to the individual 4th order HFC's. On both graphs each bar represents a single 2" by 3" thin section. The y-axis shows the specific depths for each bar (sample). White triangles represent 4th order HST's while black triangles represent 4th order TST's.*

Appendix 1C

Fossil data graphs, Well 3

There are two graphs; the first outlines all the manual counts for the different types of fossils, whereas the second outlines the biodiversity, from Well 3. Each bar defines a single 2" by 3" thin section. The depths are calculated using Cycle 8 SB, as the base of the scale, near the base of Well 3. This data is shown in Section 3.4.2. The key for the graphs is shown below:

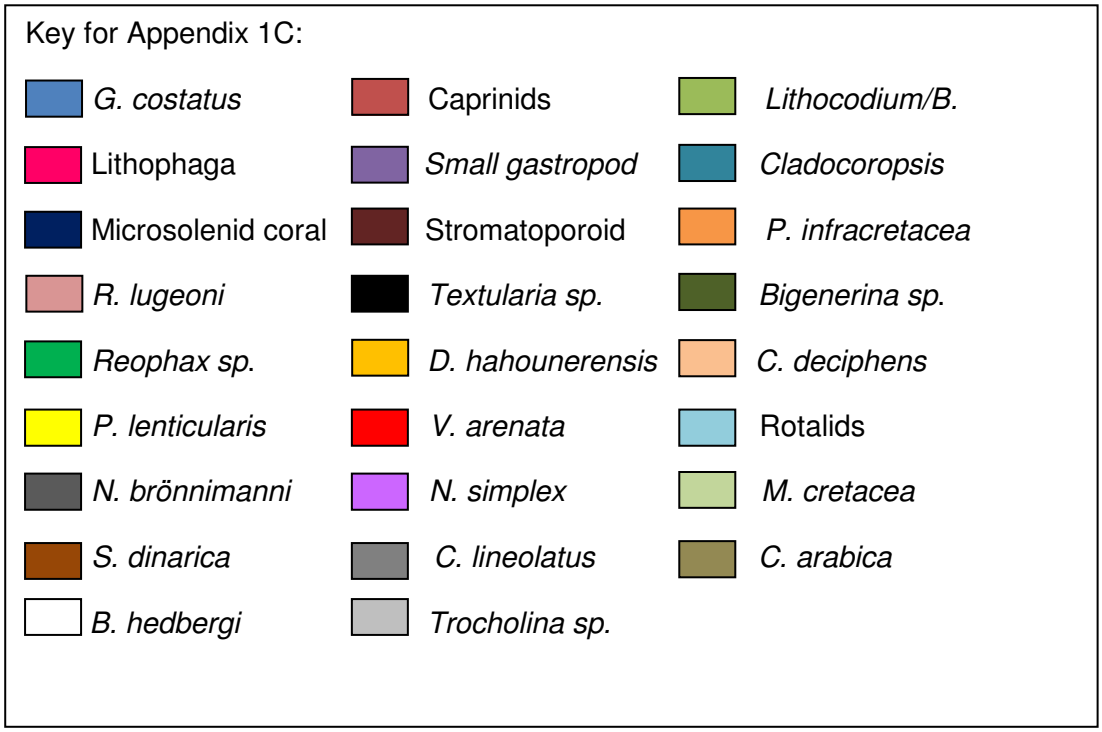

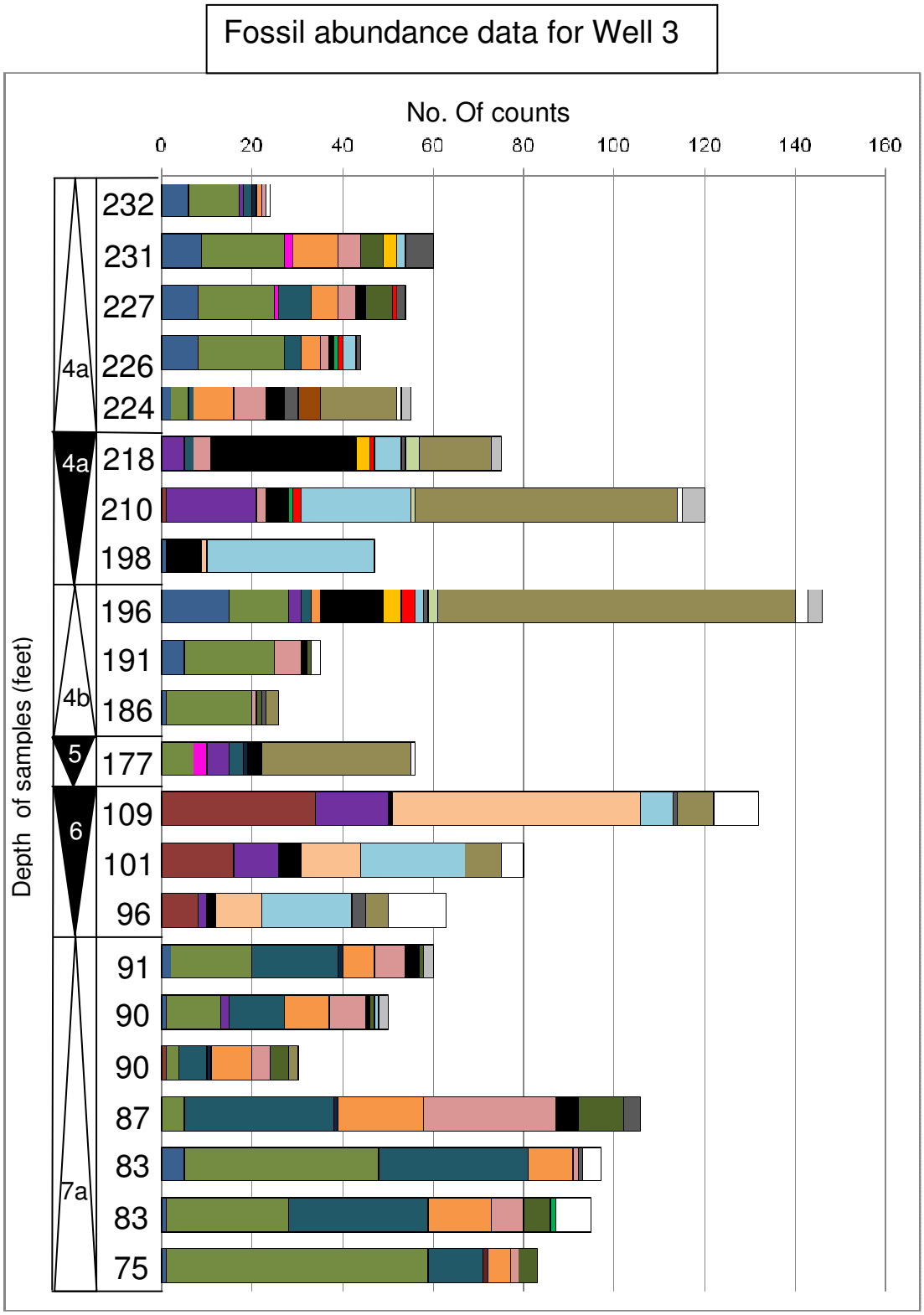

Figure 2.16: *biodiversity data from Well 3: the manual counts for each species within each thin section. The y-axis refers to the individual 4th order HFC's. On both graphs each bar represents a single 2" by 3" thin section. The y-axis shows the specific depths for each bar (sample). White triangles represent 4th order HST's while black triangles represent 4th order TST's.*

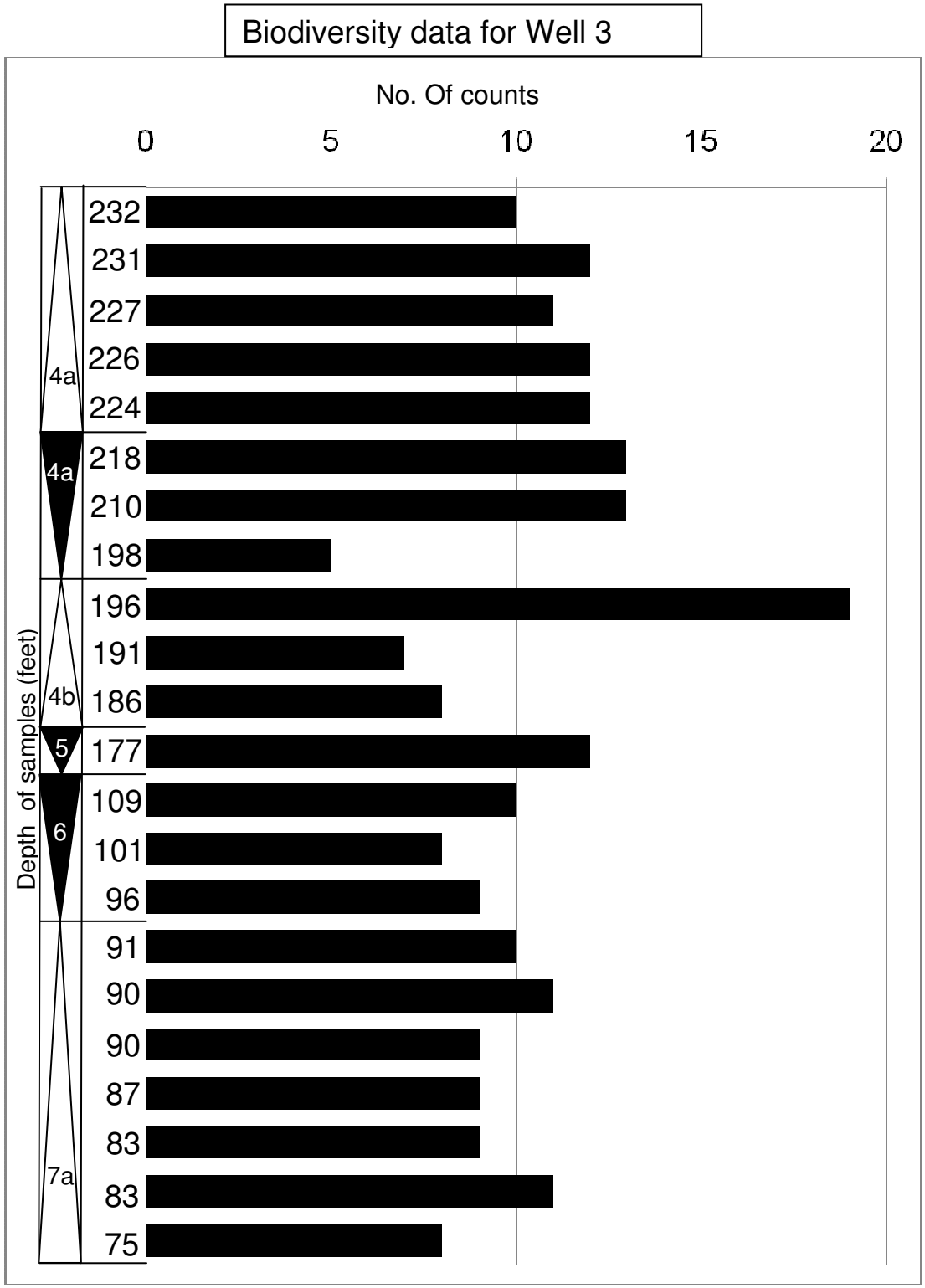

Figure 2.16: *biodiversity data from Well 3: A) the number of different species for each thin section. The y-axis refers to the individual 4th order HFC's. On both graphs each bar represents a single 2" by 3" thin section. The y-axis shows the specific depths for each bar (sample). White triangles represent 4th order HST's while black triangles represent 4th order TST's.*

Appendix 1D

Fossil data graphs, Well 4

There are two graphs; the first outlines all the manual counts for the different types of fossils, whereas the second outlines the biodiversity, from Well 4. Each bar defines a single 2" by 3" thin section. The depths are calculated using Cycle 8 SB, as the base of the scale, near the base of Well 4. This data is shown in Section 3.4.2. The key for the graphs is shown below:

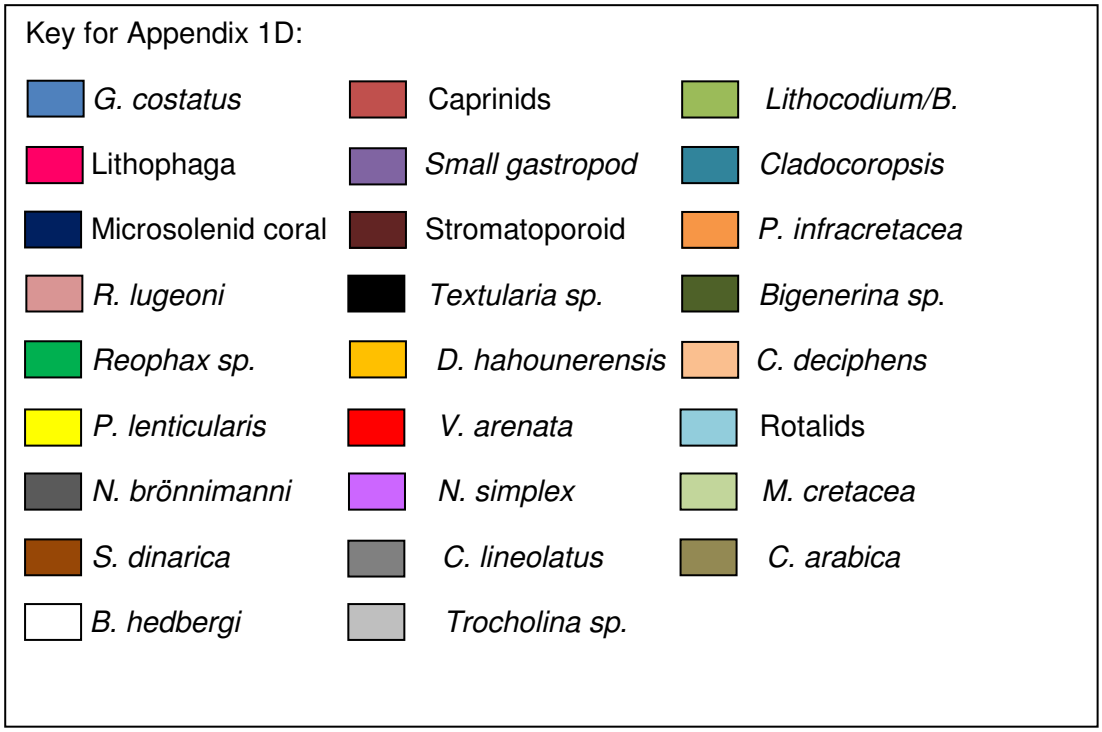

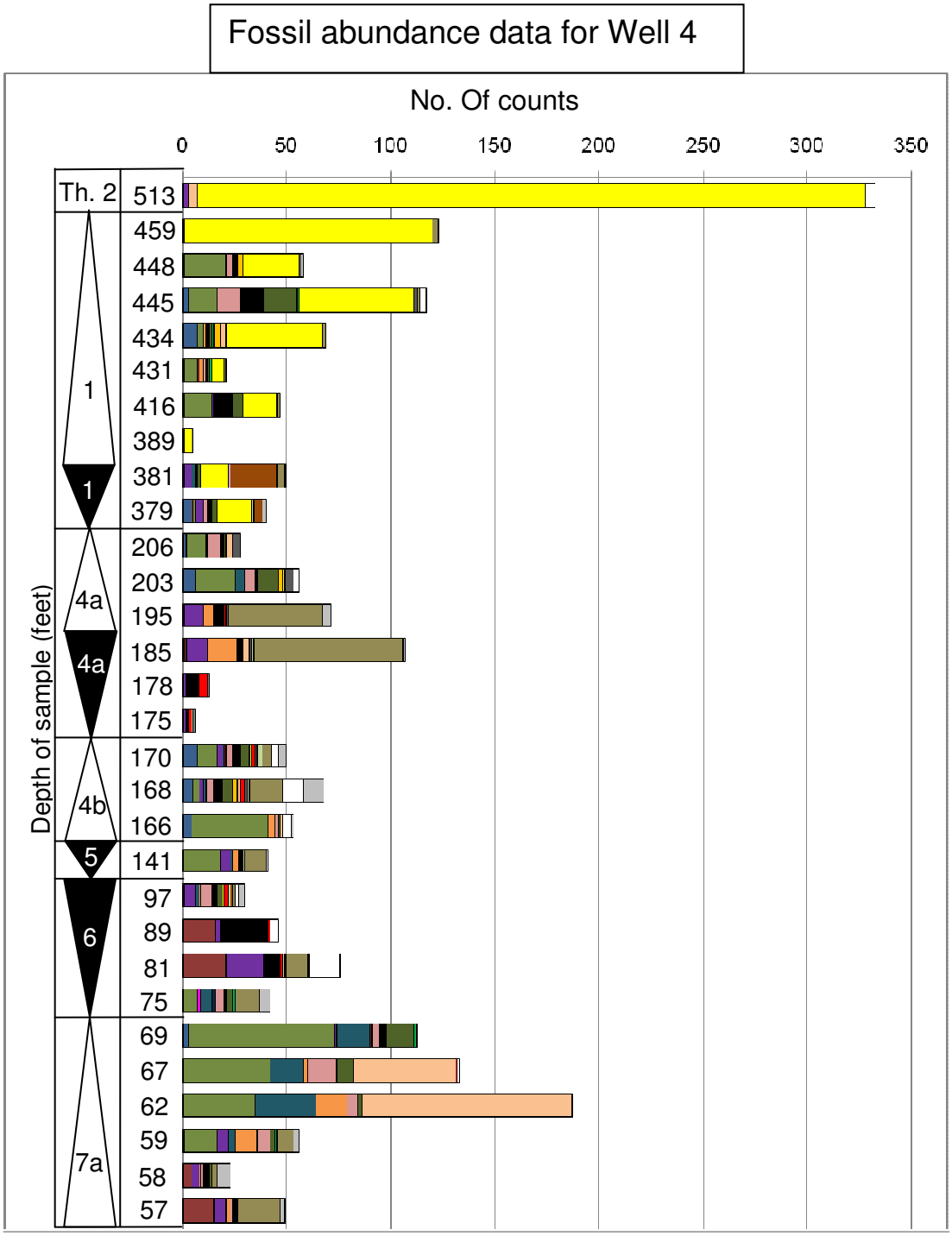

Figure 2.17: *biodiversity data from Well 4: A) the manual counts for each species within each thin section. The y-axis refers to the individual 4th order HFC's. On both graphs each bar represents a single 2" by 3" thin section. The y-axis shows the specific depths for each bar (sample). White triangles represent 4th order HST's while black triangles represent 4th order TST's.*

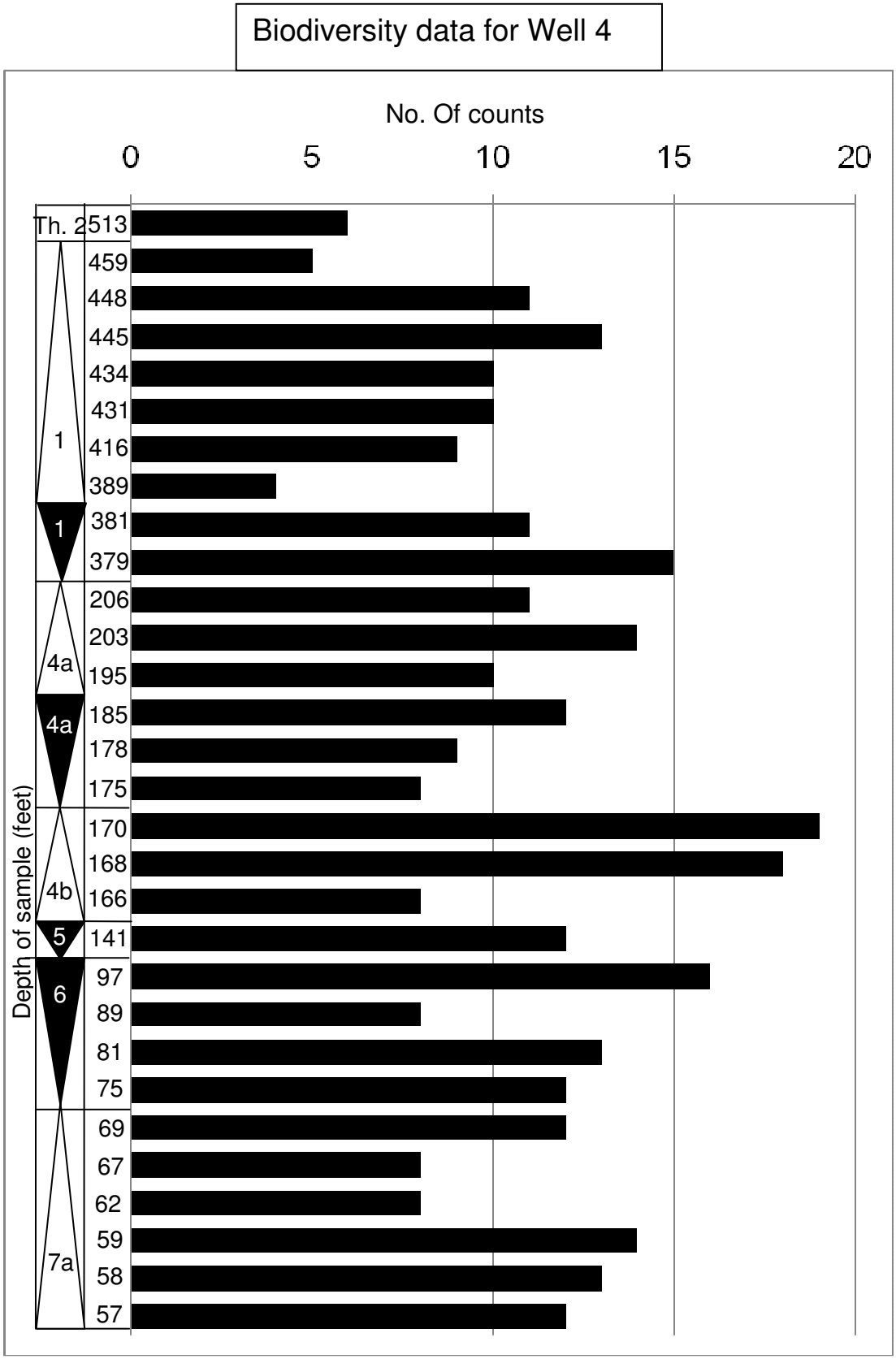

Figure 2.17: *biodiversity data from Well 4: the number of different species for each thin section. The y-axis refers to the individual 4th order HFC's. On both graphs each bar represents a single 2" by 3" thin section. The y-axis shows the specific depths for each bar (sample). White triangles represent 4th order HST's while black triangles represent 4th order TST's.*

Appendix 1E

Fossil data graphs, Well 5

There are two graphs; the first outlines all the manual counts for the different types of fossils, whereas the second outlines the biodiversity, from Well 5. Each bar defines a single 2" by 3" thin section. The depths are calculated using Cycle 8 SB, as the base of the scale, near the base of Well 5. This data is shown in Section 3.4.2. The key for the graphs is shown below:

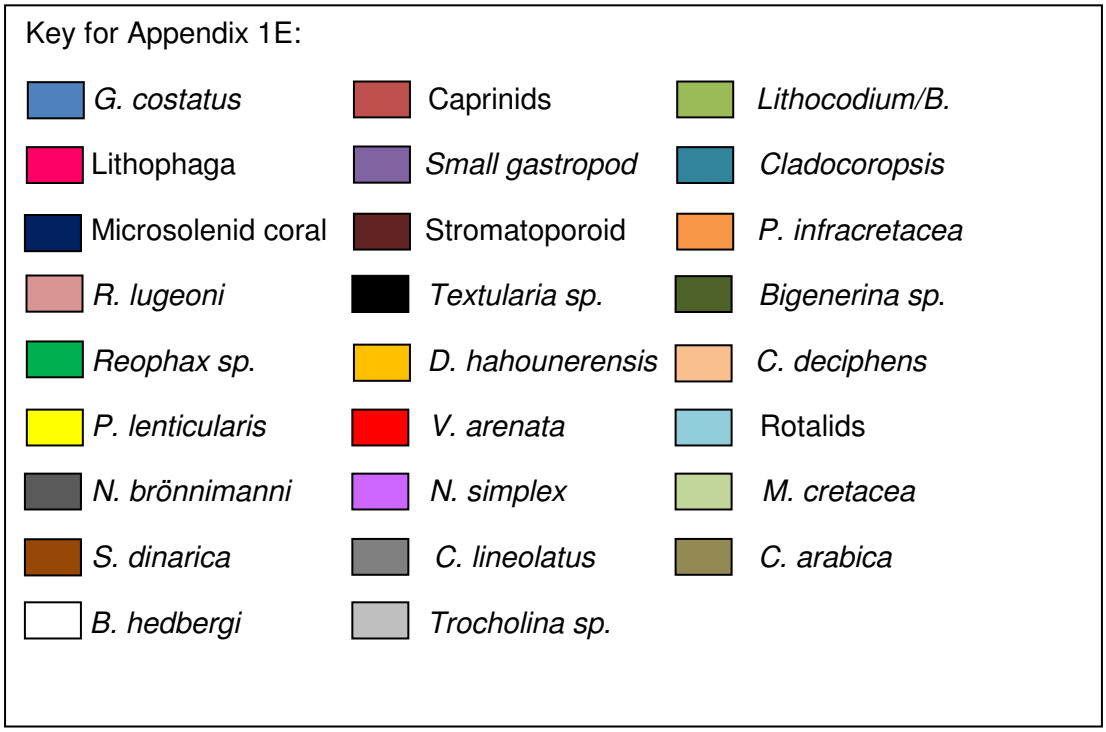

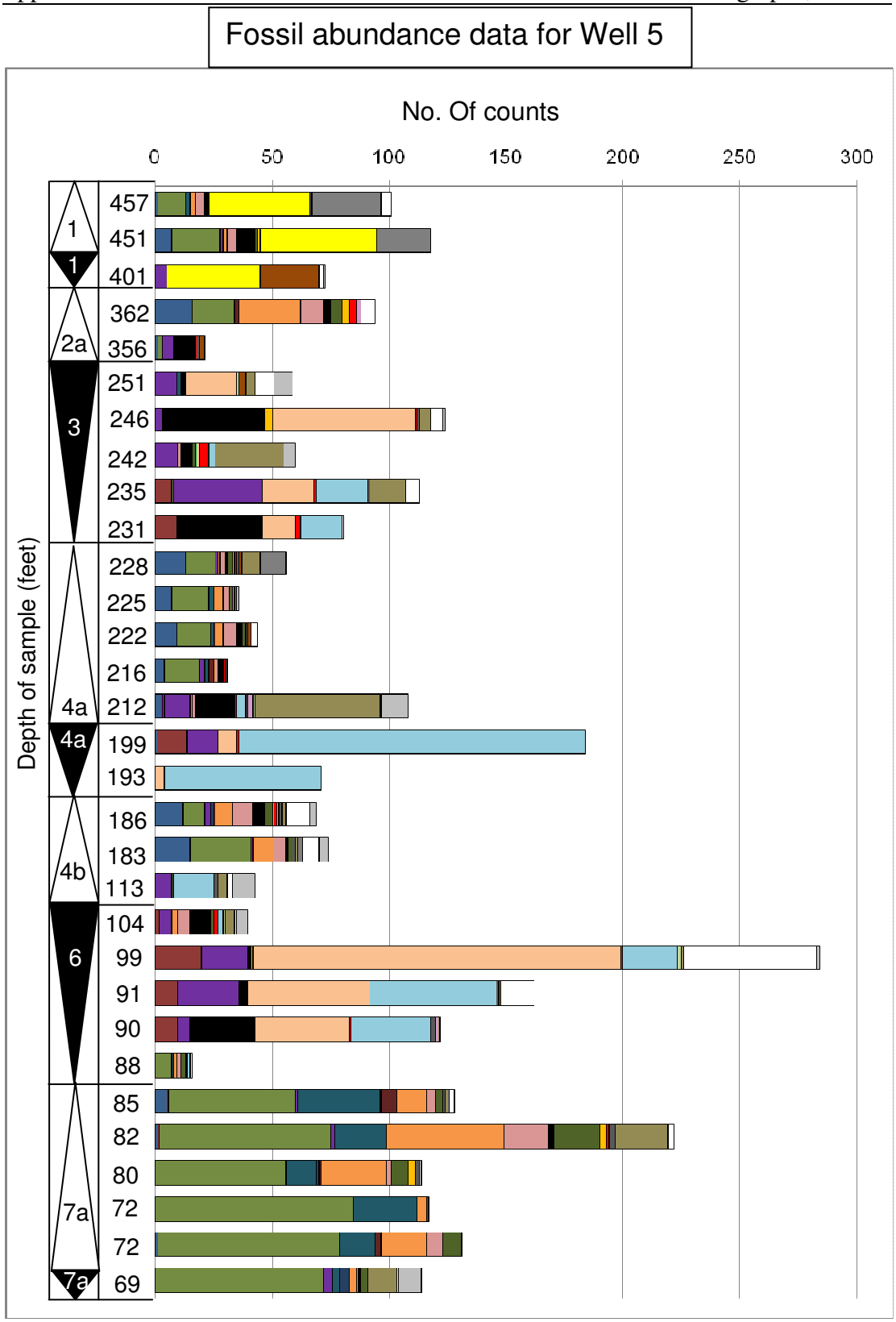

Figure 2.18: *biodiversity data from Well 5: A) the manual counts for each species within each thin section. The y-axis refers to the individual 4th order HFC's. On both graphs each bar represents a single 2" by 3" thin section. The y-axis shows the specific depths for each bar (sample). White triangles represent 4th order HST's while black triangles represent 4th order TST's.*

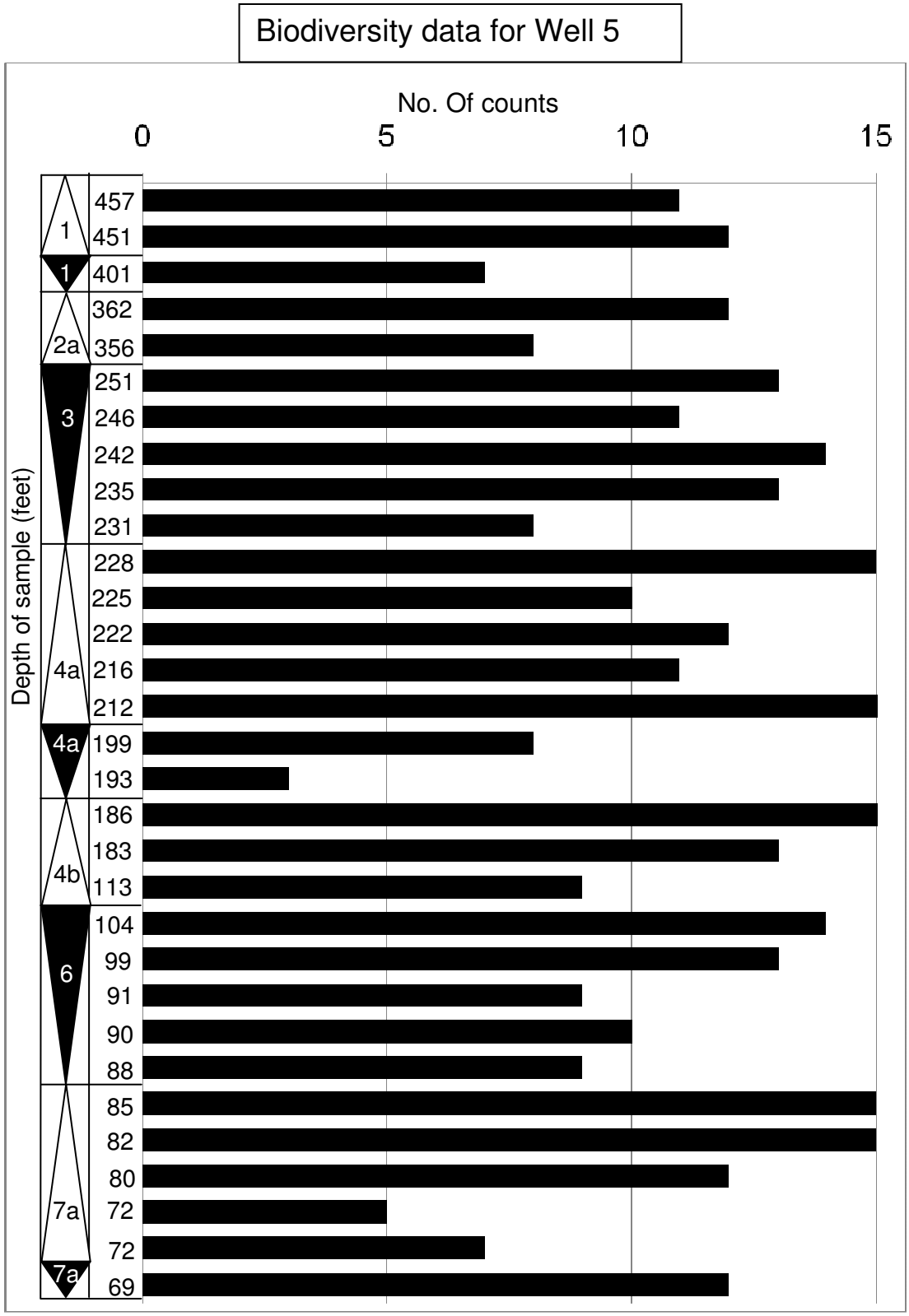

Figure 2.18: *biodiversity data from Well 5: the number of different species for each thin section. The y-axis refers to the individual 4th order HFC's. On both graphs each bar represents a single 2" by 3" thin section. The y-axis shows the specific depths for each bar (sample). White triangles represent 4th order HST's while black triangles represent 4th order TST's.*

Appendix 2A

Well 1, core log

These are the core logs from Well 1. The scale is based on Dunham's classification scheme with Mr meaning Micrite, M meaning Mudstone, W meaning Wackestone, P meaning Packstone, B meaning boundstone and G meaning grainstone. The depths shown on these logs are the deviated core depths (angles of deviation can be seen in Section 1.2: Table 1.1). Each page shows 50ft of core with the first page showing the top 50ft which leads progressively towards the bottom 50ft in the last page. Each page has a key that describes the symbols used within the logs. The logs are accompanied by the reservoir and non-reservoir sections, which are coloured white and grey, respectively. The black triangles represent the TST's and the white triangles represent the HST's. The 4^{th} order SB's and MFS's are also shown. This data relates to Sections 3.4.1 and 4.6.

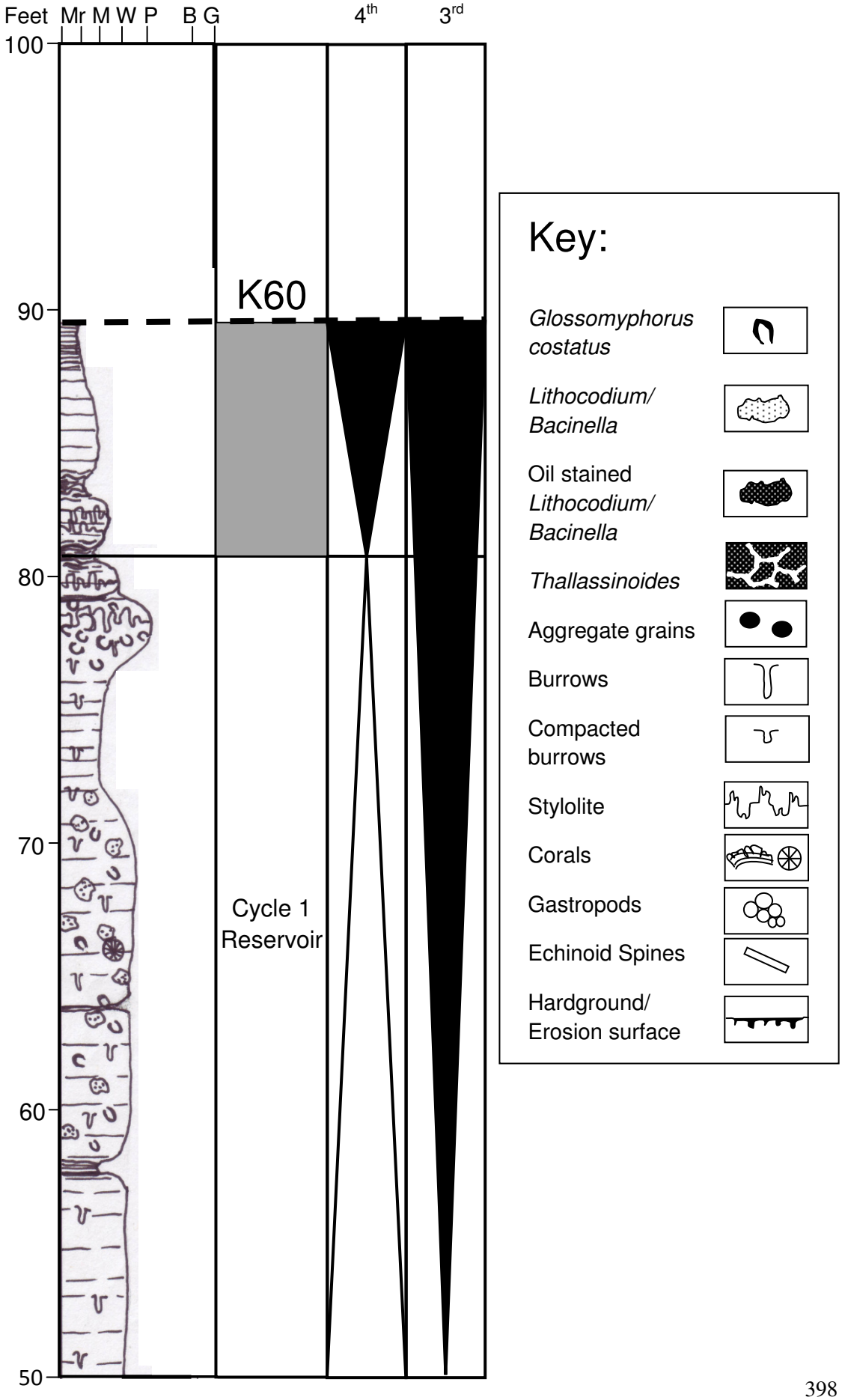
Feet
Mr
M
W
P
B
G
4th
3rd
100
90
80
70
60
50
K60
Cycle 1
Reservoir
Key:
Glossomyphorus costatus
Lithocodium/ Bacinella
Oil stained Lithocodium/ Bacinella
Thallassinoides
Aggregate grains
Burrows
Compacted burrows
Stylolite
Corals
Gastropods
Echinoid Spines
Hardground/ Erosion surface

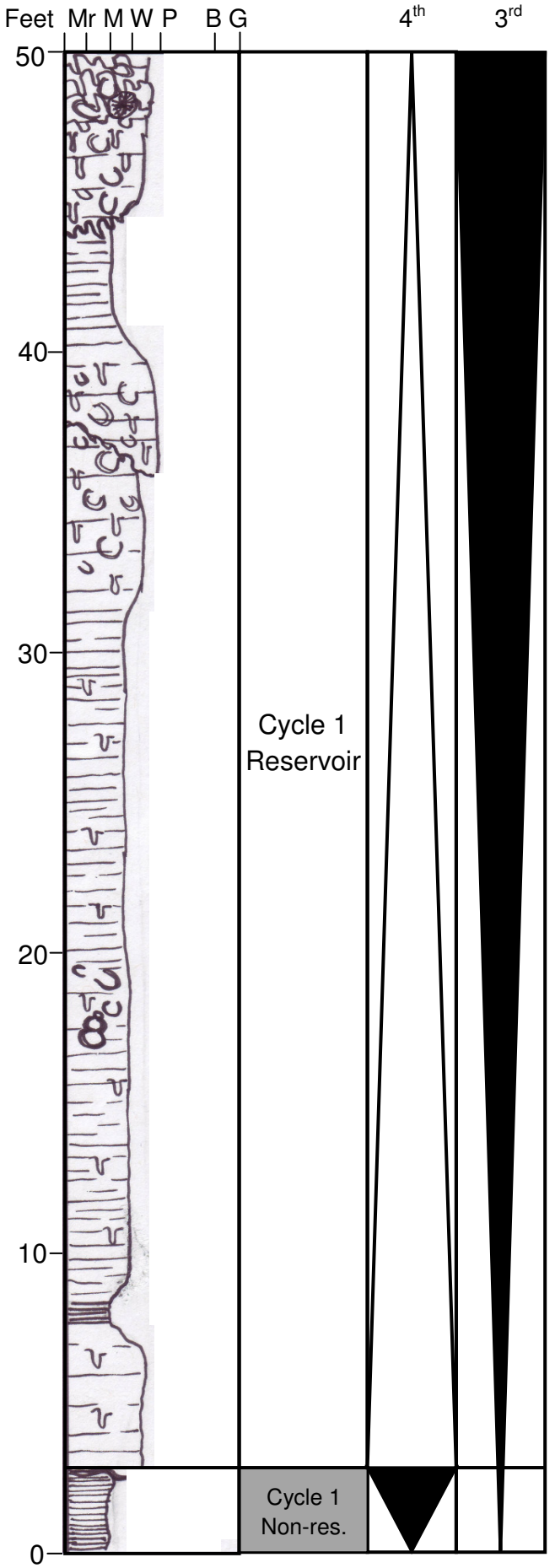
Feet
Mr
M
W
P
B
G
4th
3rd
50
40
30
20
10
0
Cycle 1
Reservoir
Cycle 1
Non-res.

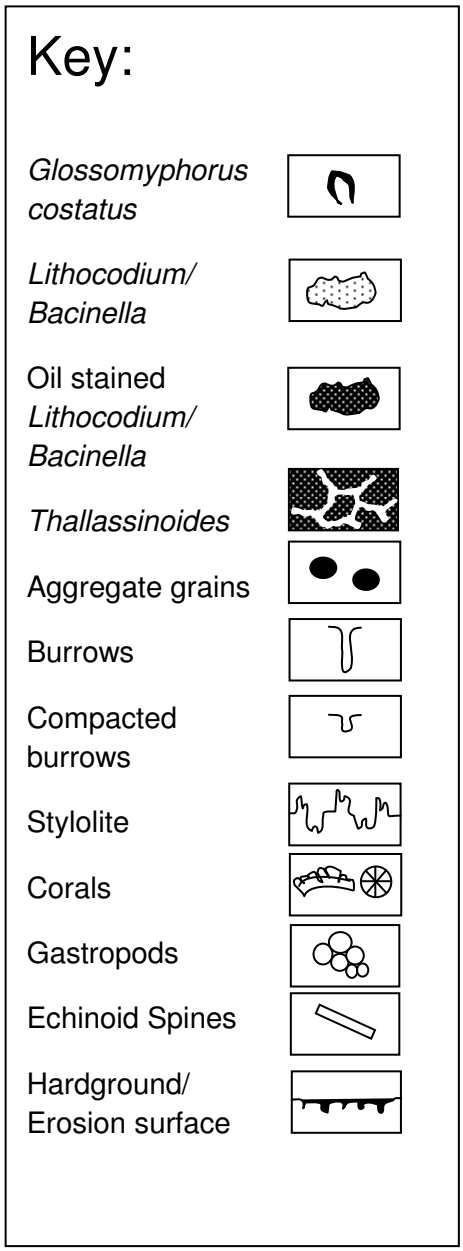
Key:
Glossomyphorus costatus
Lithocodium/ Bacinella
Oil stained Lithocodium/ Bacinella
Thallassinoides
Aggregate grains
Burrows
Compacted burrows
Stylolite
Corals
Gastropods
Echinoid Spines
Hardground/ Erosion surface

Appendix 2B

Well 2, core log

These are the core logs from Well 2. The scale is based on Dunham's classification scheme with Mr meaning Micrite, M meaning Mudstone, W meaning Wackestone, P meaning Packstone, B meaning boundstone and G meaning grainstone. The depths shown on these logs are the deviated core depths (angles of deviation can be seen in Section 1.2: Table 1.1). Each page shows 50ft of core with the first page showing the top 50ft which leads progressively towards the bottom 50ft in the last page. Each page has a key that describes the symbols used within the logs. The logs are accompanied by the reservoir and non-reservoir sections, which are coloured white and grey, respectively. The black triangles represent the TST's and the white triangles represent the HST's. The 4^{th} order SB's and MFS's are also shown. This data relates to Sections 3.4.1 and 4.6.

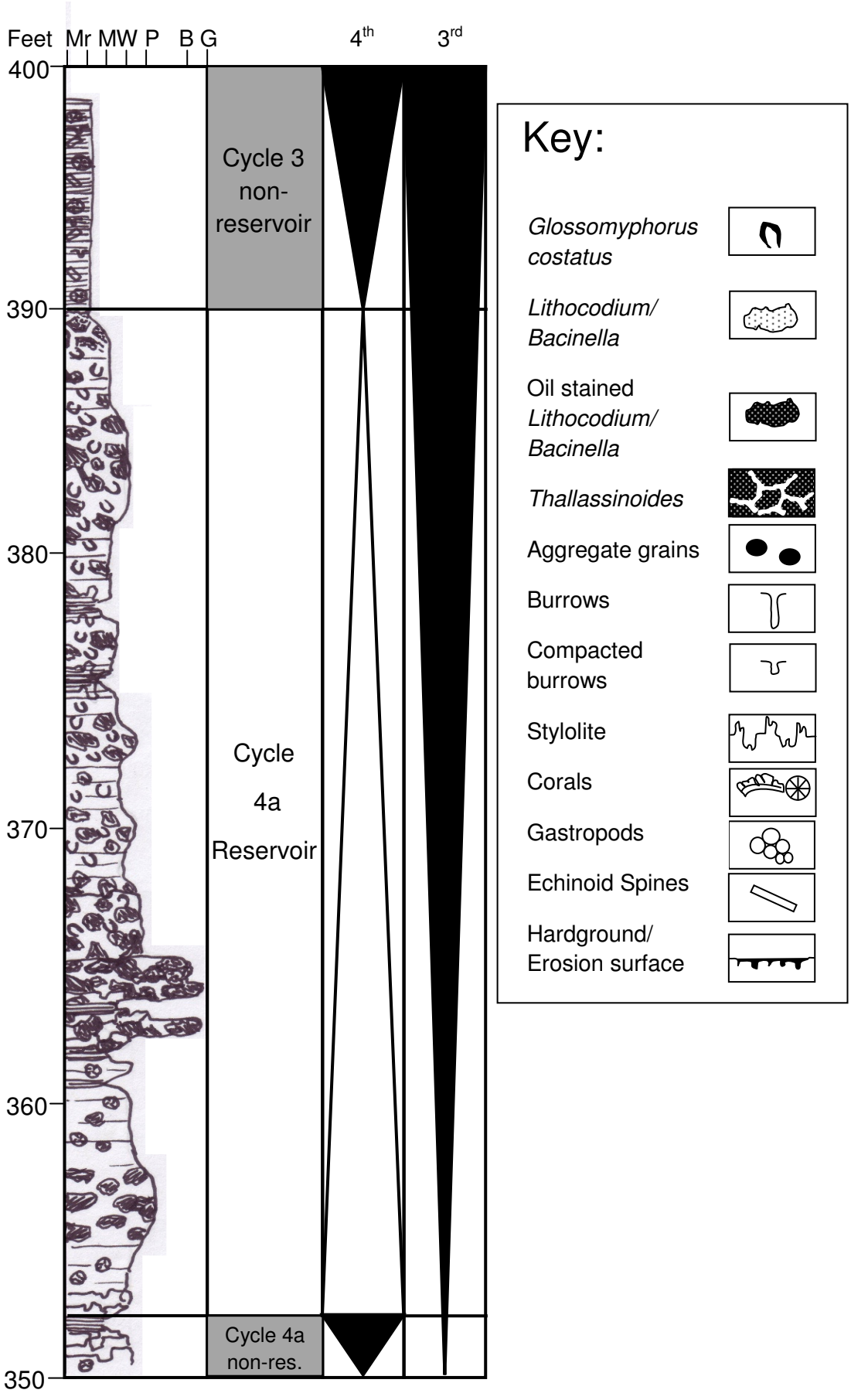
Feet
Mr
MW
P
B
G
4th
3rd
400
390
380
370
360
350
Cycle 3 non-reservoir
Cycle 4a Reservoir
Cycle 4a non-res.
Key:
Glossomyphorus costatus
Lithocodium/ Bacinella
Oil stained Lithocodium/ Bacinella
Thallassinoides
Aggregate grains
Burrows
Compacted burrows
Stylolite
Corals
Gastropods
Echinoid Spines
Hardground/ Erosion surface

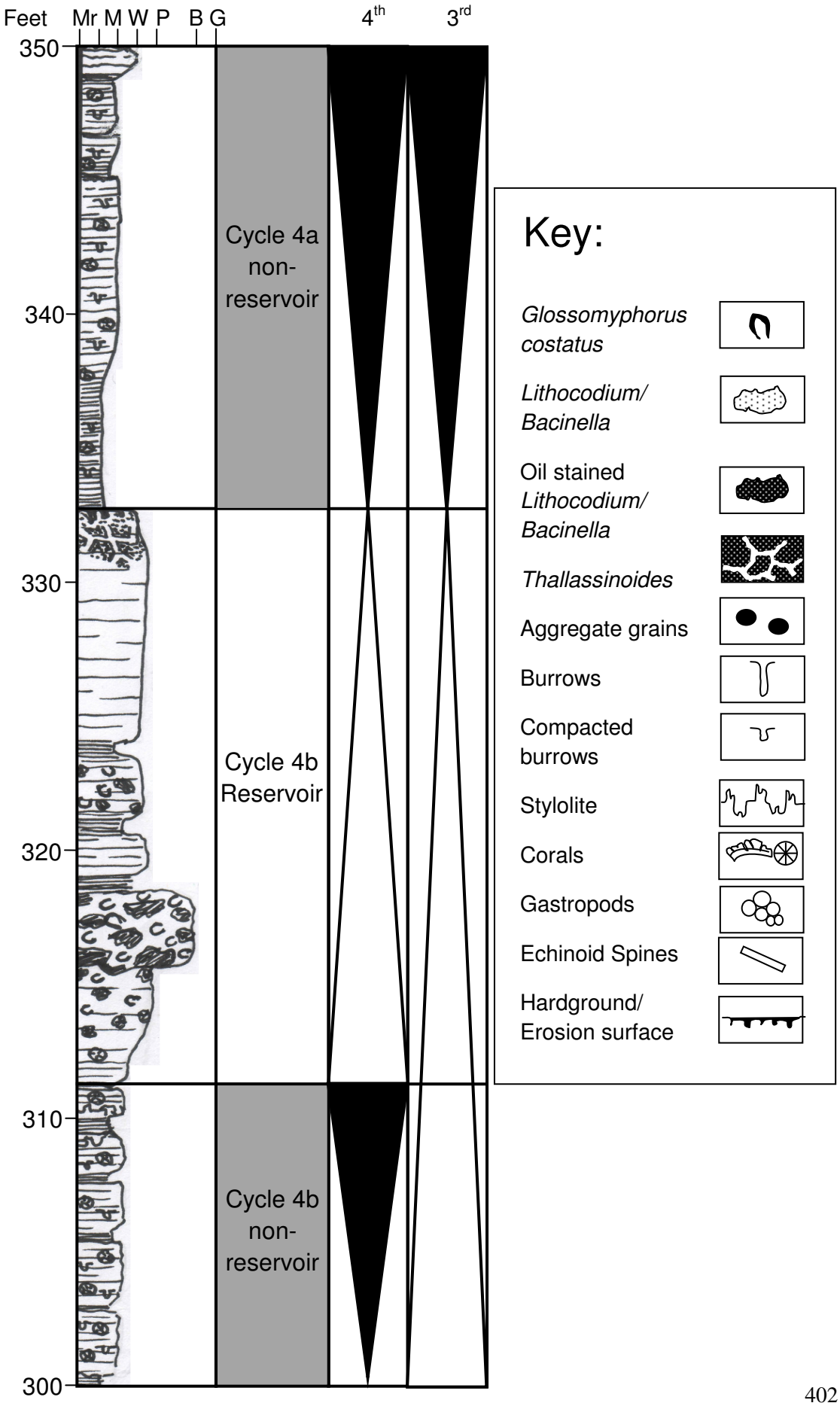
Feet
Mr M W P B G
4th
3rd
350
340
330
320
310
300
Cycle 4a non-reservoir
Cycle 4b Reservoir
Cycle 4b non-reservoir
Key:
Glossomyphorus costatus
Lithocodium/ Bacinella
Oil stained Lithocodium/ Bacinella
Thallassinoides
Aggregate grains
Burrows
Compacted burrows
Stylolite
Corals
Gastropods
Echinoid Spines
Hardground/ Erosion surface

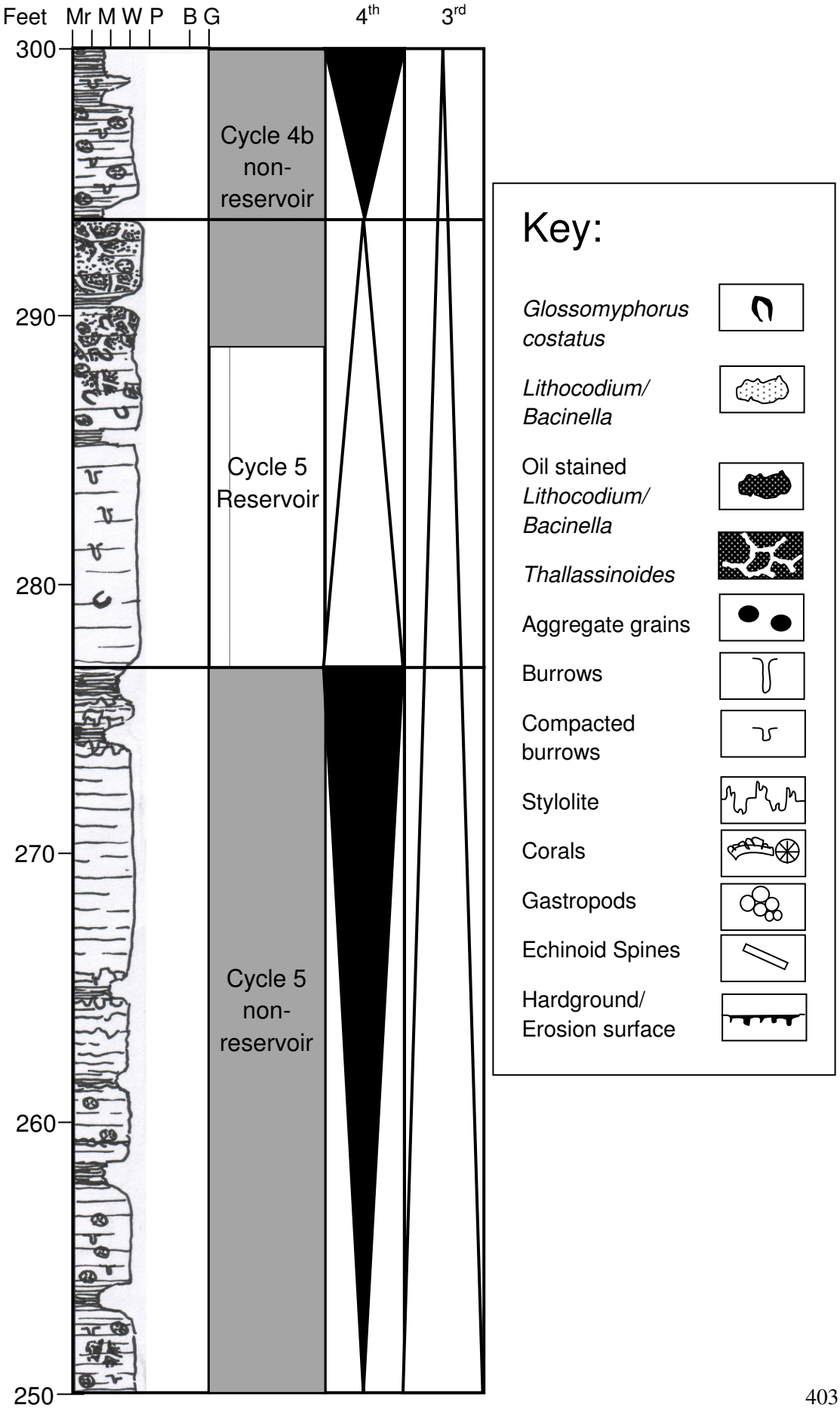
Feet
Mr M W P B G
4th
3rd
300
290
280
270
260
250
Cycle 4b non-reservoir
Cycle 5 Reservoir
Cycle 5 non-reservoir
Key:
Glossomyphorus costatus
Lithocodium/ Bacinella
Oil stained Lithocodium/ Bacinella
Thallassinoides
Aggregate grains
Burrows
Compacted burrows
Stylolite
Corals
Gastropods
Echinoid Spines
Hardground/ Erosion surface

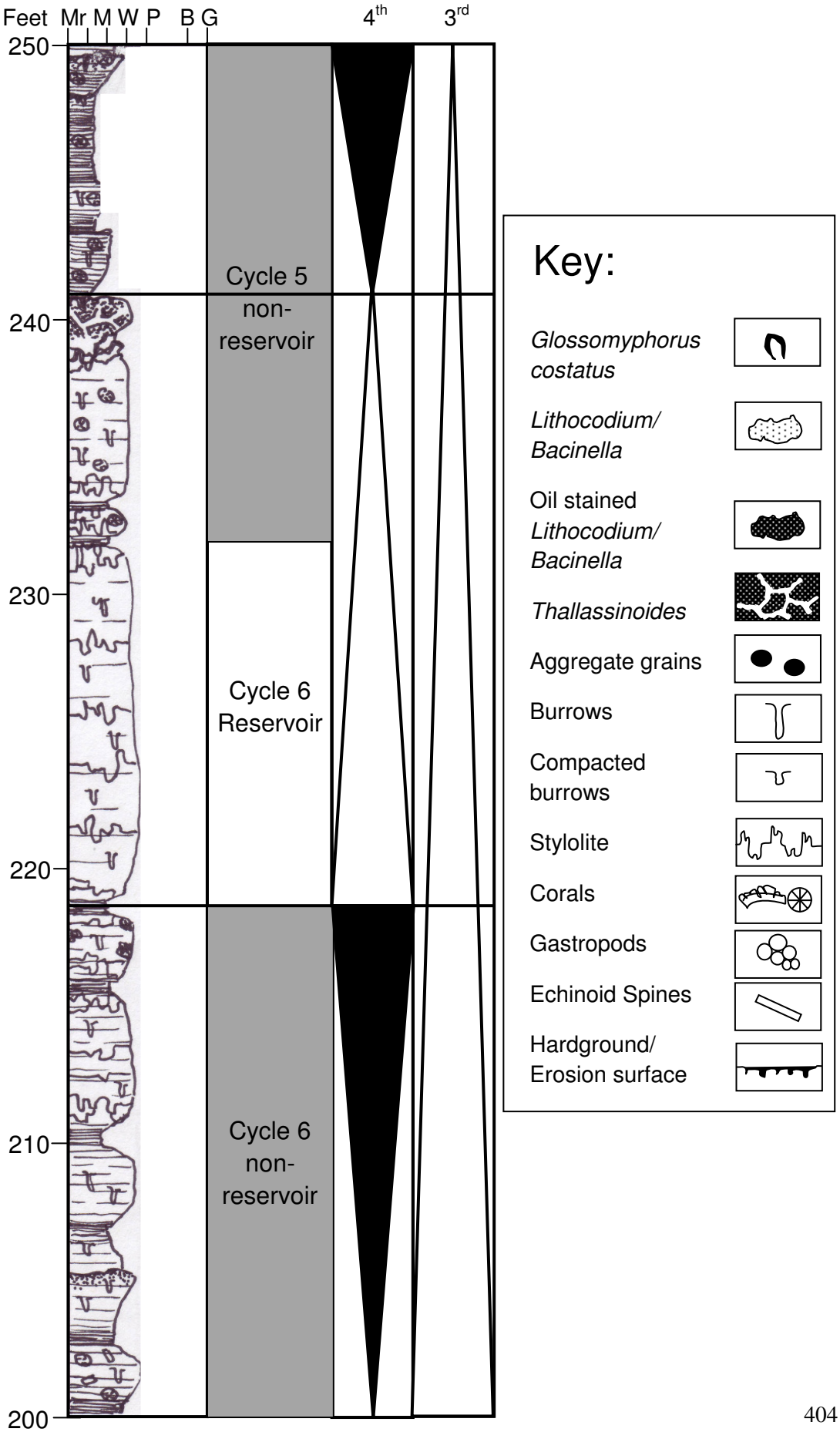
Feet
Mr
M
W
P
B
G
4th
3rd
250
240
230
220
210
200
Cycle 5
non-
reservoir
Cycle 6
Reservoir
Cycle 6
non-
reservoir
Key:
Glossomyphorus costatus
Lithocodium/ Bacinella
Oil stained Lithocodium/ Bacinella
Thallassinoides
Aggregate grains
Burrows
Compacted burrows
Stylolite
Corals
Gastropods
Echinoid Spines
Hardground/ Erosion surface

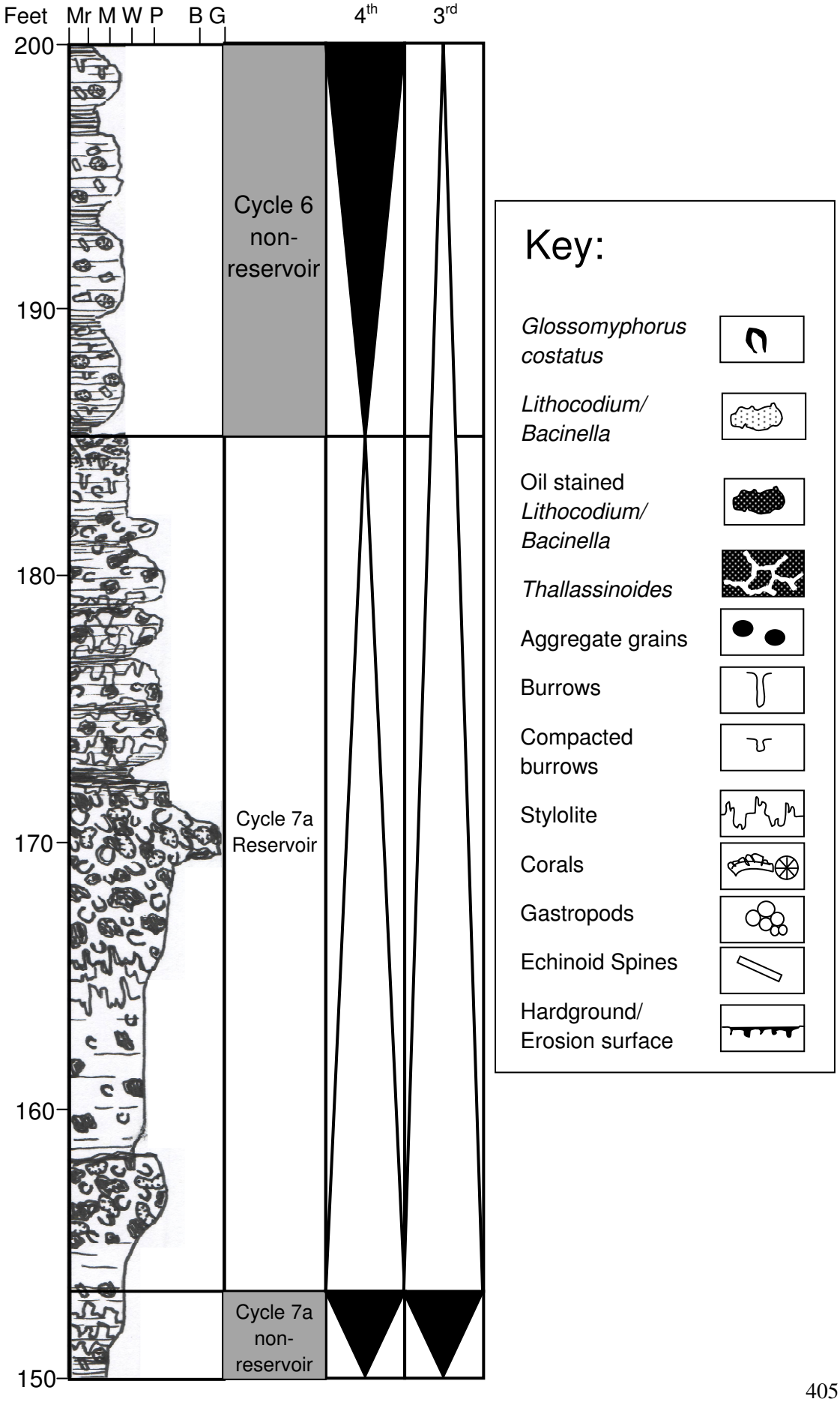
Feet
Mr M W P B G
4th
3rd
200
190
180
170
160
150
Cycle 6 non-reservoir
Cycle 7a Reservoir
Cycle 7a non-reservoir
Key:
Glossomyphorus costatus
Lithocodium/ Bacinella
Oil stained Lithocodium/ Bacinella
Thallassinoides
Aggregate grains
Burrows
Compacted burrows
Stylolite
Corals
Gastropods
Echinoid Spines
Hardground/ Erosion surface

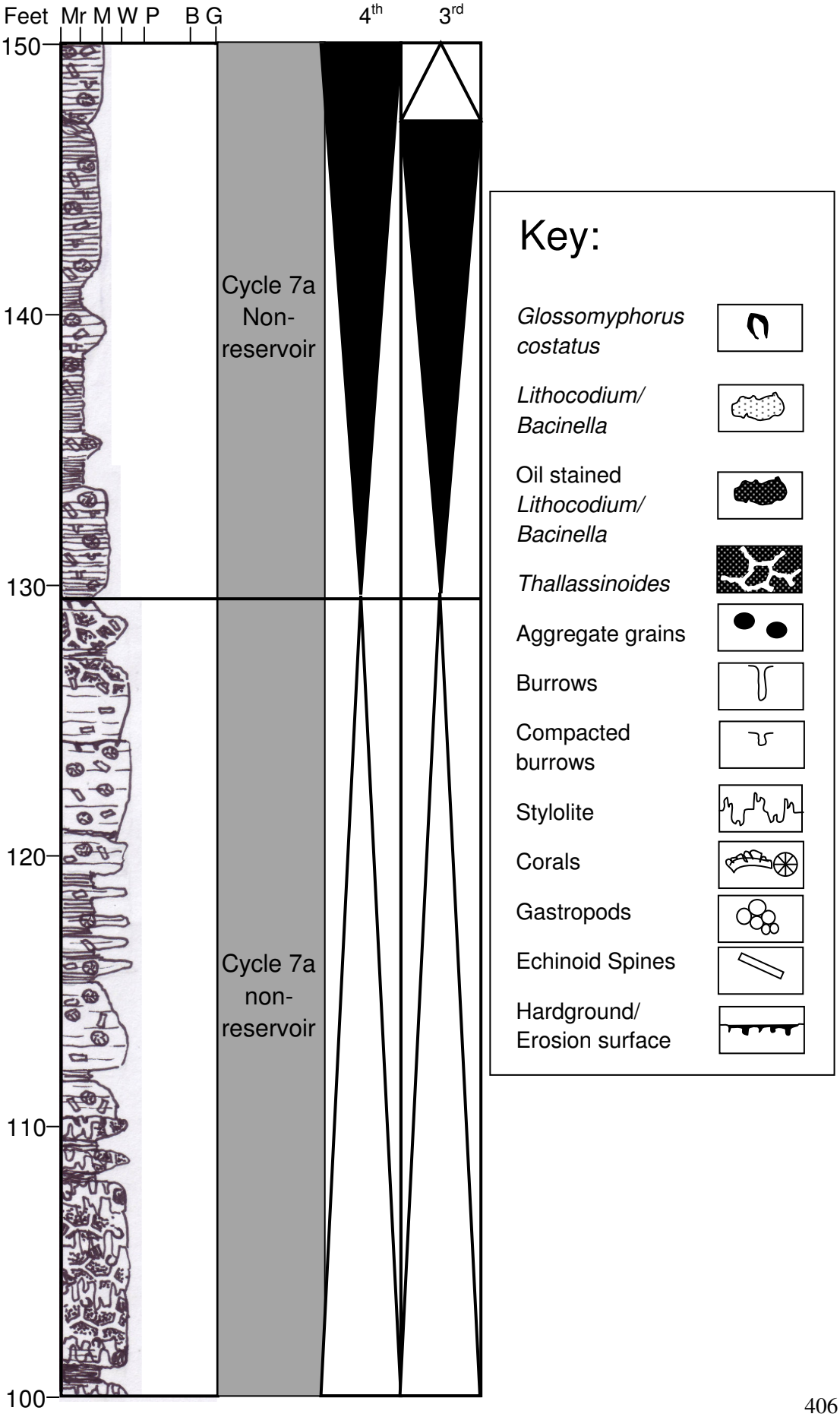
Feet
Mr
M
W
P
B
G
4th
3rd
150
140
130
120
110
100
Cycle 7a
Non-
reservoir
Cycle 7a
non-
reservoir
Key:
Glossomyphorus costatus
Lithocodium/ Bacinella
Oil stained Lithocodium/ Bacinella
Thallassinoides
Aggregate grains
Burrows
Compacted burrows
Stylolite
Corals
Gastropods
Echinoid Spines
Hardground/ Erosion surface

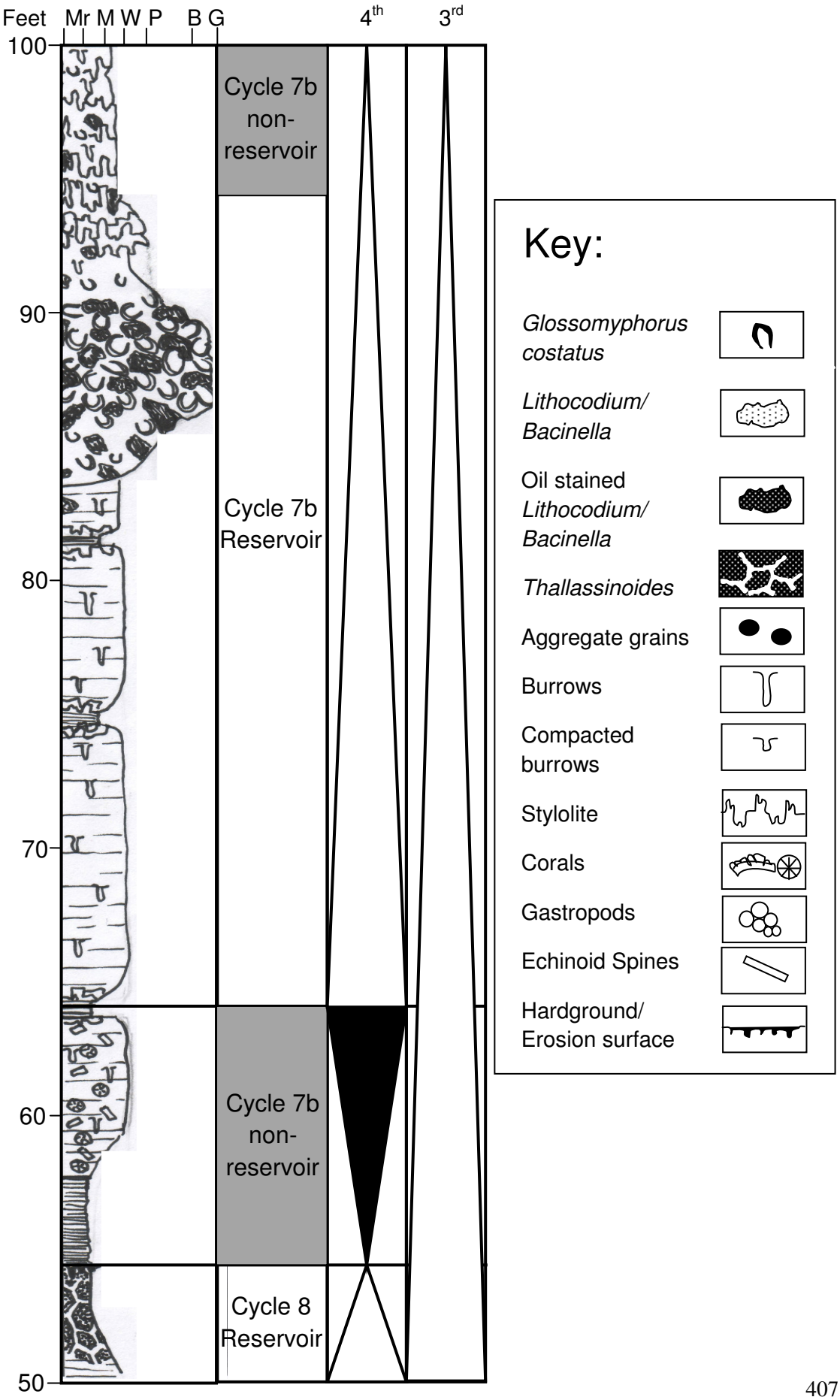
Feet
Mr M W P B G
4th
3rd
100
90
80
70
60
50
Cycle 7b non-reservoir
Cycle 7b Reservoir
Cycle 7b non-reservoir
Cycle 8 Reservoir
Key:
Glossomyphorus costatus
Lithocodium/ Bacinella
Oil stained Lithocodium/ Bacinella
Thallassinoides
Aggregate grains
Burrows
Compacted burrows
Stylolite
Corals
Gastropods
Echinoid Spines
Hardground/ Erosion surface

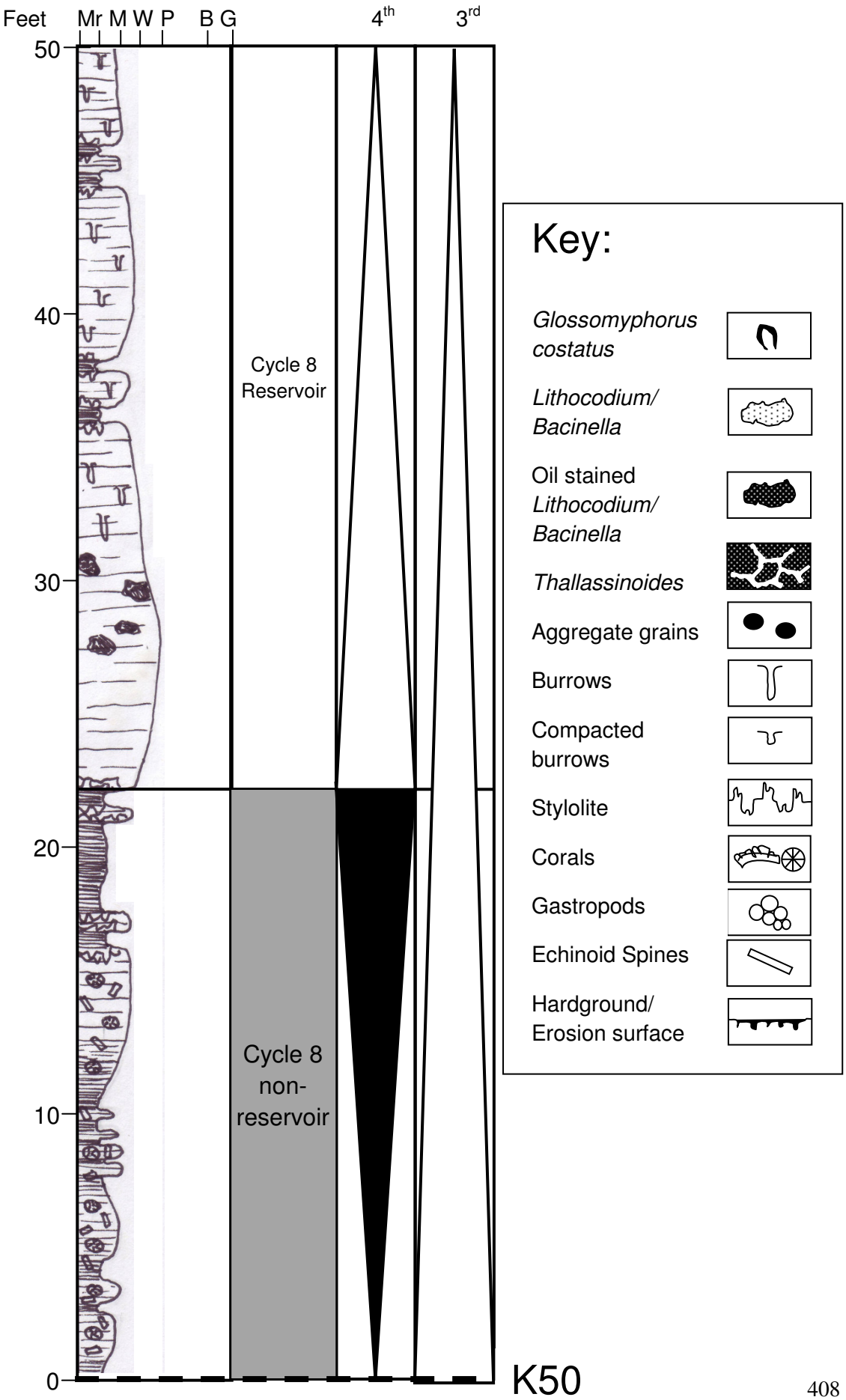
Feet
Mr M W P B G
4th
3rd
50
40
30
20
10
0
Cycle 8
Reservoir
Cycle 8
non-
reservoir
Key:
Glossomyphorus costatus
Lithocodium/ Bacinella
Oil stained Lithocodium/ Bacinella
Thallassinoides
Aggregate grains
Burrows
Compacted burrows
Stylolite
Corals
Gastropods
Echinoid Spines
Hardground/ Erosion surface

K50

Appendix 2C

Well 3, core log

These are the core logs from Well 3. The scale is based on Dunham's classification scheme with Mr meaning Micrite, M meaning Mudstone, W meaning Wackestone, P meaning Packstone, B meaning boundstone and G meaning grainstone. The depths shown on these logs are the deviated core depths (angles of deviation can be seen in Section 1.2: Table 1.1). Each page shows 50ft of core with the first page showing the top 50ft which leads progressively towards the bottom 50ft in the last page. Each page has a key that describes the symbols used within the logs. The logs are accompanied by the reservoir and non-reservoir sections, which are coloured white and grey, respectively. The black triangles represent the TST's and the white triangles representing the HST's. The 4^{th} order SB's and MFS's are also shown. This data relates to Sections 3.4.1 and 4.6.

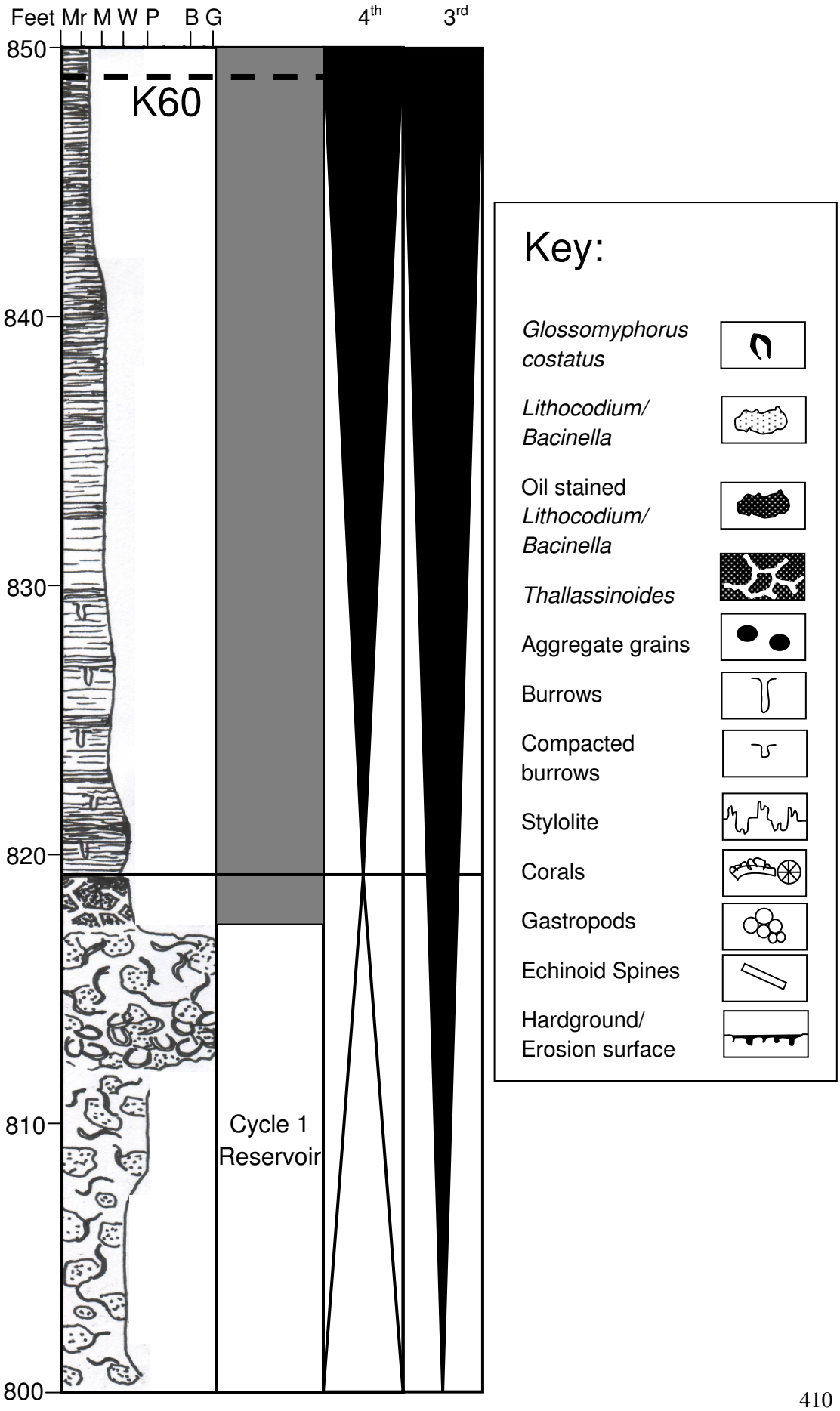
Feet Mr M W P B G
4th
3rd
850
840
830
820
810
800
K60
Cycle 1
Reservoir
Key:
Glossomyphorus costatus
Lithocodium/ Bacinella
Oil stained Lithocodium/ Bacinella
Thallassinoides
Aggregate grains
Burrows
Compacted burrows
Stylolite
Corals
Gastropods
Echinoid Spines
Hardground/ Erosion surface

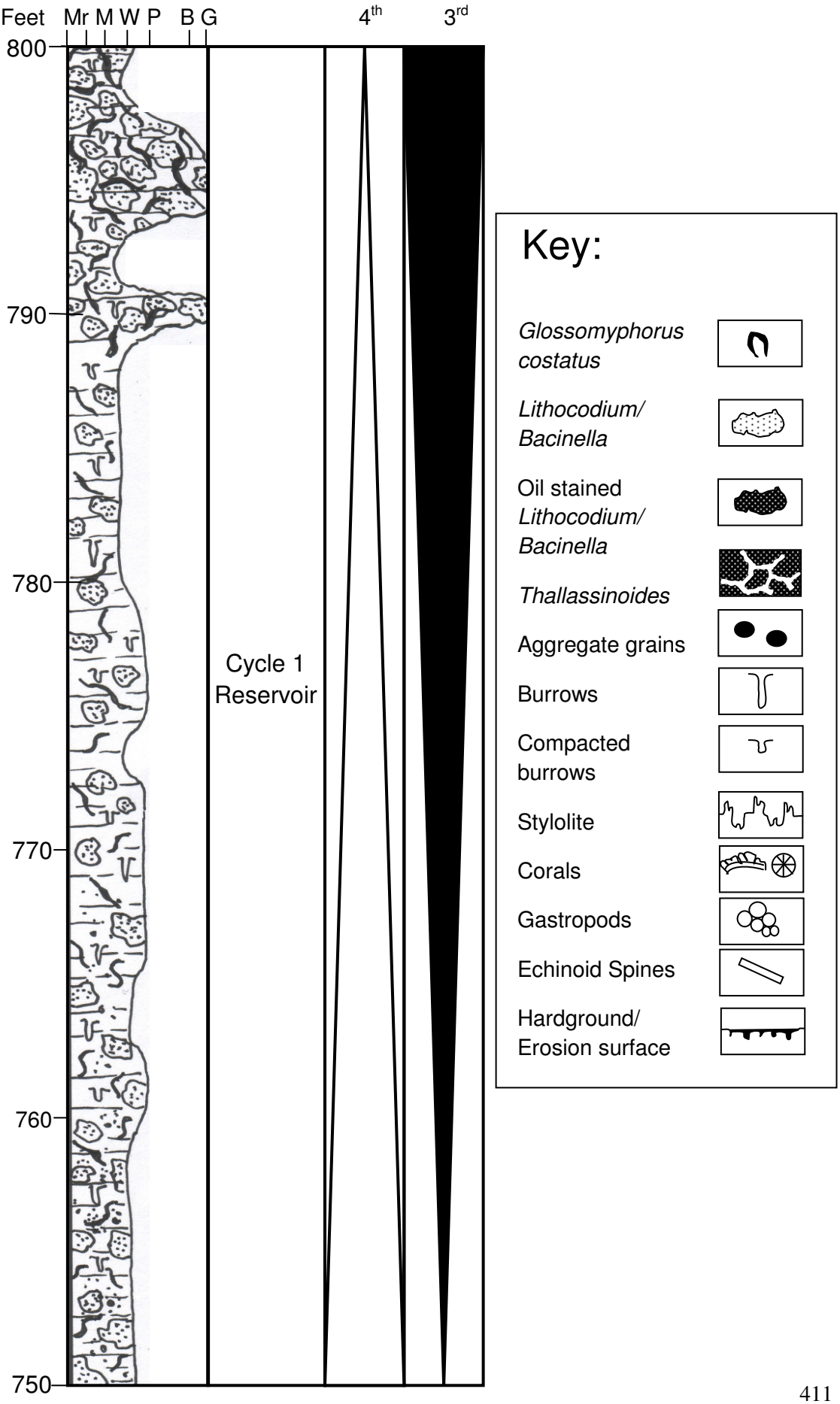
Feet
Mr M W P B G
4th
3rd
800
790
780
770
760
750
Cycle 1
Reservoir
Key:
Glossomyphorus costatus
Lithocodium/ Bacinella
Oil stained Lithocodium/ Bacinella
Thallassinoides
Aggregate grains
Burrows
Compacted burrows
Stylolite
Corals
Gastropods
Echinoid Spines
Hardground/ Erosion surface

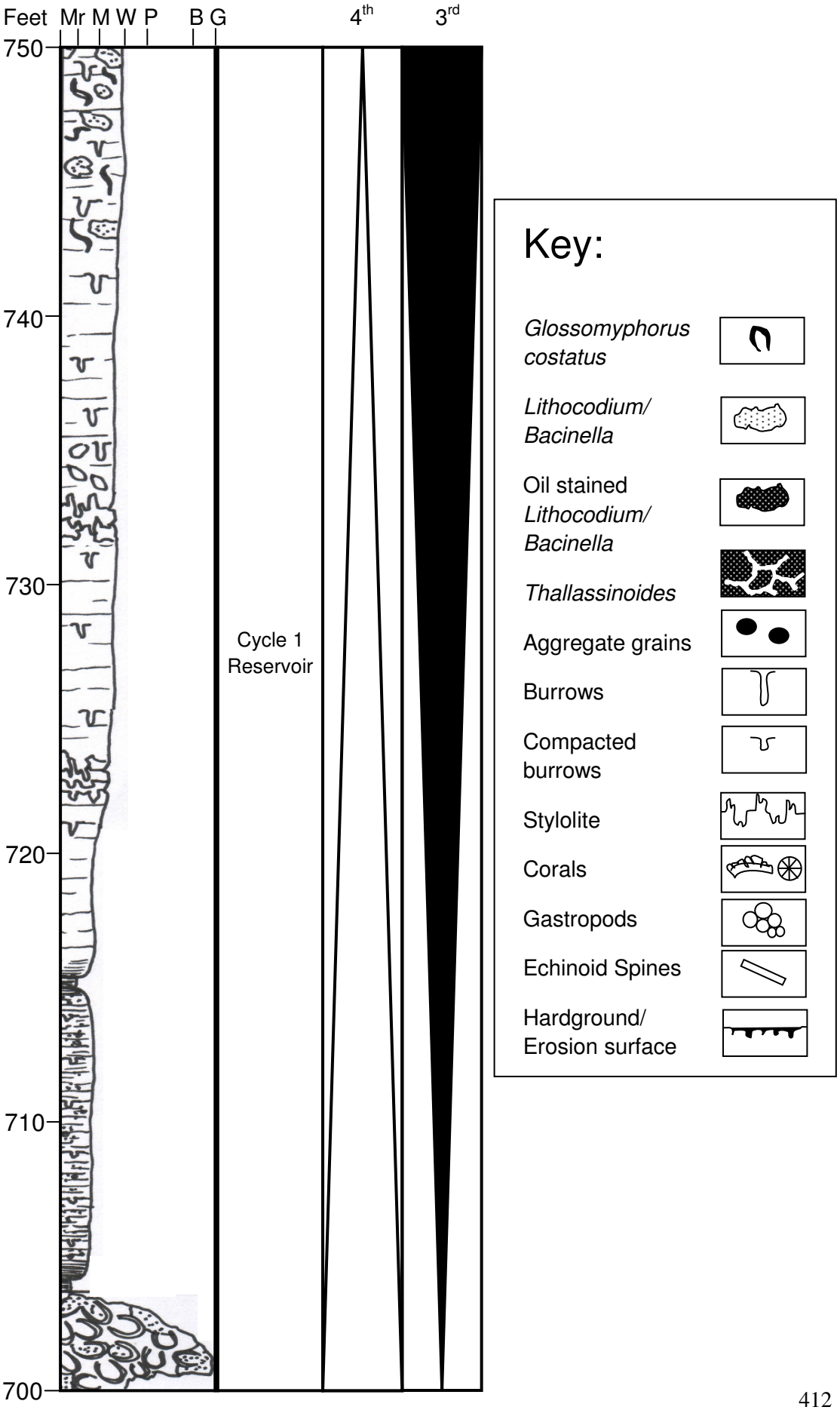
Feet
Mr
M
W
P
B
G
4th
3rd
750
740
730
720
710
700
Cycle 1
Reservoir
Key:
Glossomyphorus costatus
Lithocodium/ Bacinella
Oil stained Lithocodium/ Bacinella
Thallassinoides
Aggregate grains
Burrows
Compacted burrows
Stylolite
Corals
Gastropods
Echinoid Spines
Hardground/ Erosion surface

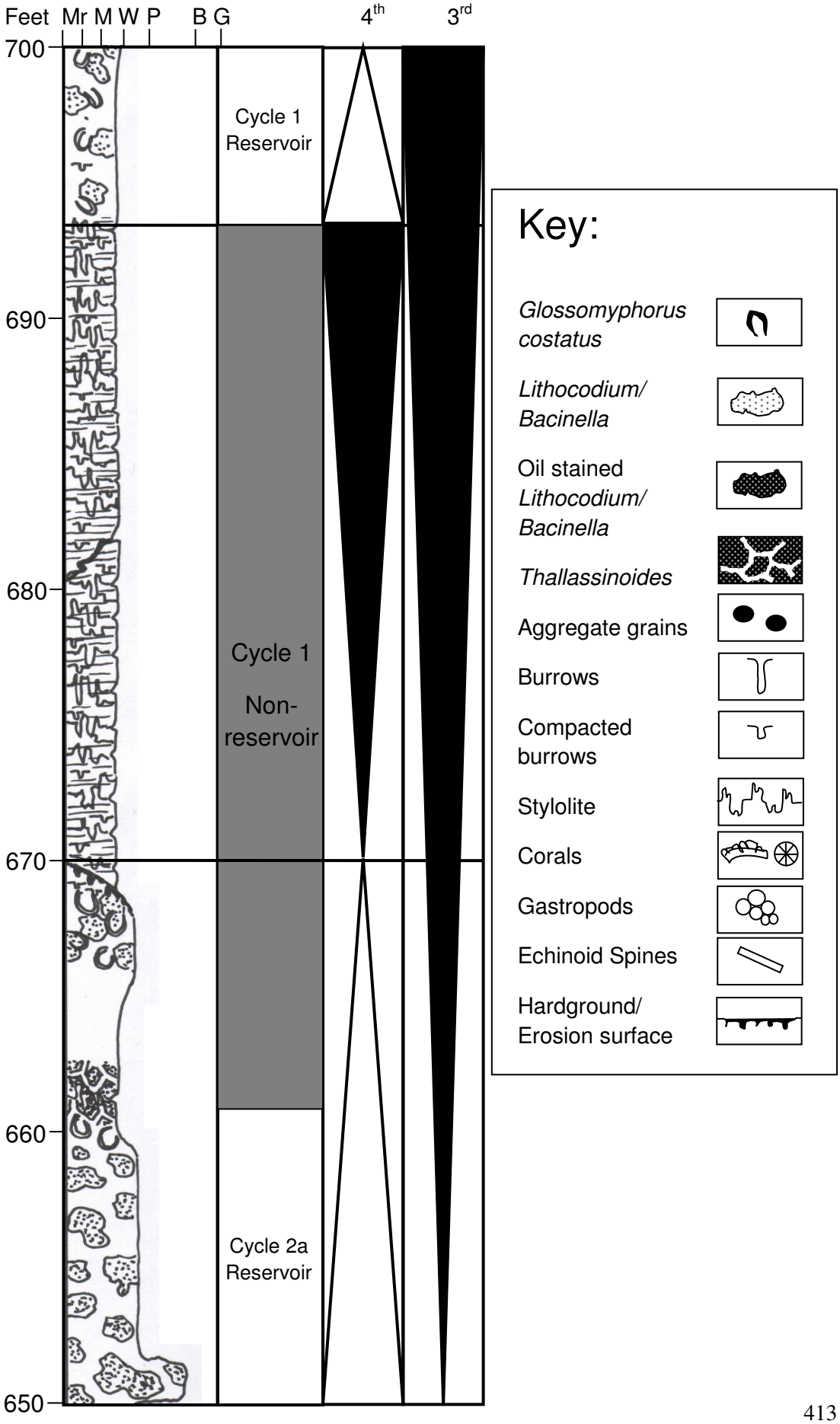
Feet
Mr
M
W
P
B
G
4th
3rd
700
690
680
670
660
650
Cycle 1
Reservoir
Cycle 1
Non-
reservoir
Cycle 2a
Reservoir
Key:
Glossomyphorus costatus
Lithocodium/ Bacinella
Oil stained Lithocodium/ Bacinella
Thallassinoides
Aggregate grains
Burrows
Compacted burrows
Stylolite
Corals
Gastropods
Echinoid Spines
Hardground/ Erosion surface

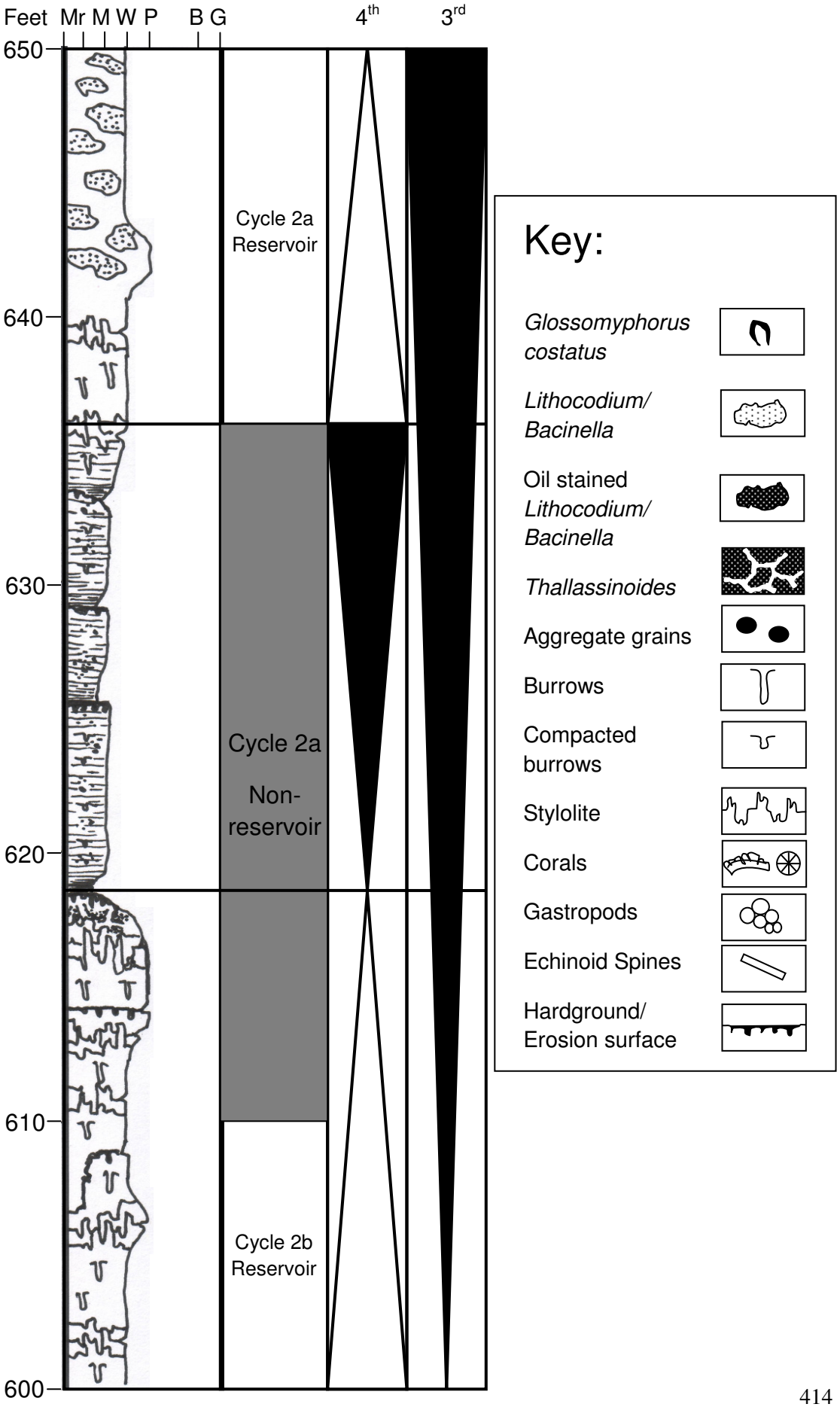
Feet
Mr
M
W
P
B
G
4th
3rd
650
640
630
620
610
600
Cycle 2a
Reservoir
Cycle 2a
Non-
reservoir
Cycle 2b
Reservoir
Key:
Glossomyphorus costatus
Lithocodium/ Bacinella
Oil stained Lithocodium/ Bacinella
Thallassinoides
Aggregate grains
Burrows
Compacted burrows
Stylolite
Corals
Gastropods
Echinoid Spines
Hardground/ Erosion surface

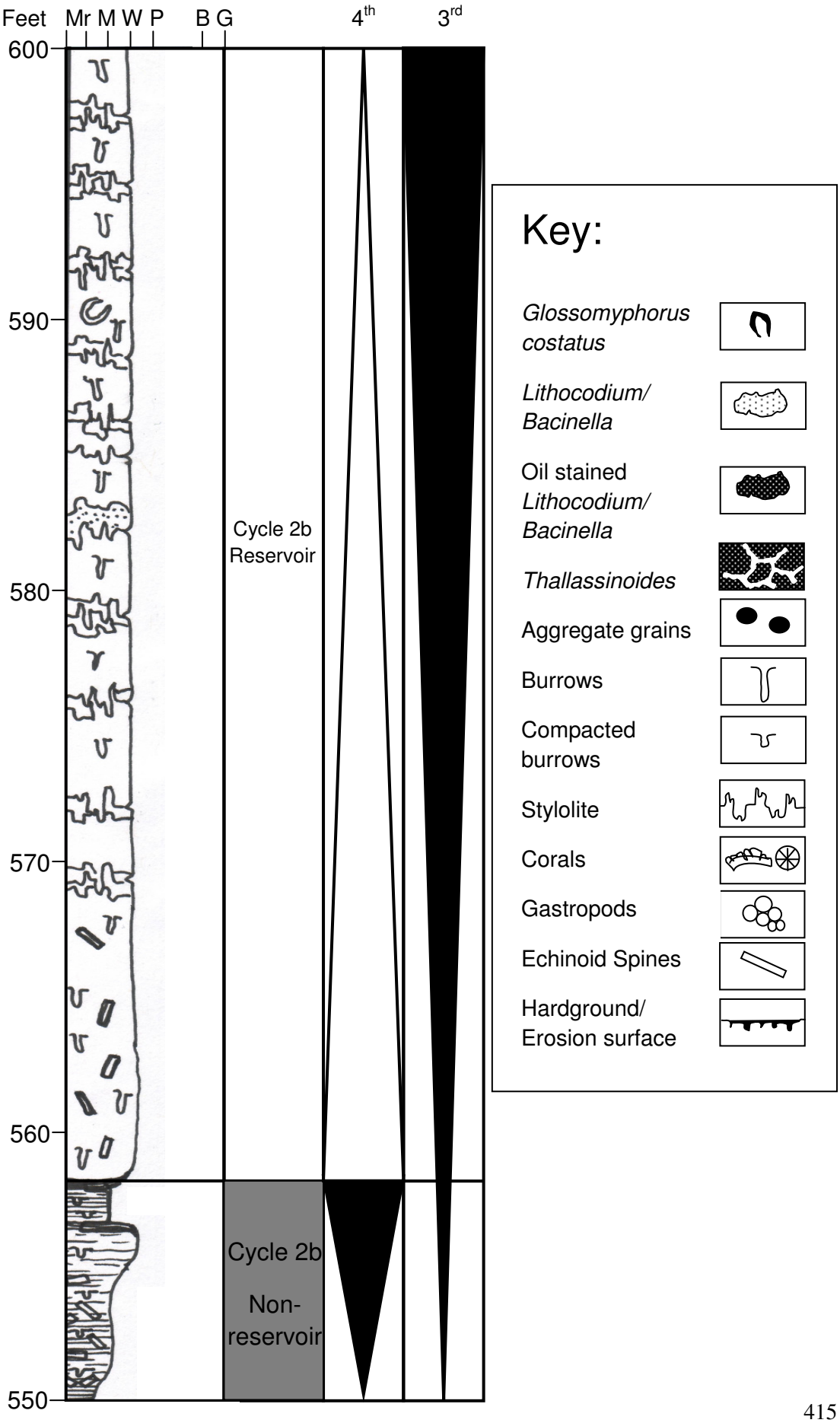
Feet
Mr M W P
B G
4th
3rd
600
590
580
570
560
550
Cycle 2b Reservoir
Cycle 2b Non-reservoir
Key:
Glossomyphorus costatus
Lithocodium/ Bacinella
Oil stained Lithocodium/ Bacinella
Thallassinoides
Aggregate grains
Burrows
Compacted burrows
Stylolite
Corals
Gastropods
Echinoid Spines
Hardground/ Erosion surface

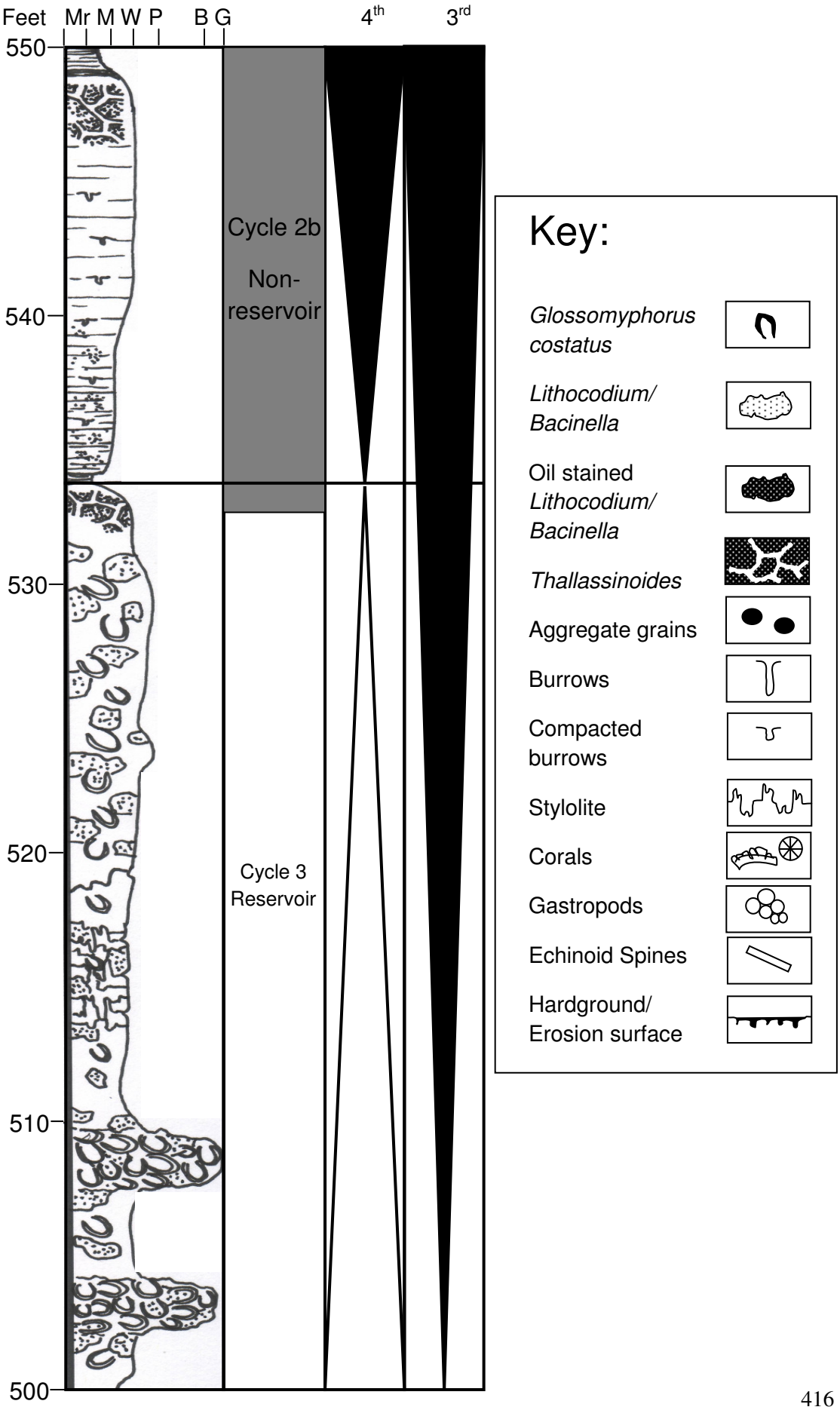
Feet
Mr M W P B G
4th
3rd
550
540
530
520
510
500
Cycle 2b
Non-reservoir
Cycle 3
Reservoir
Key:
Glossomyphorus costatus
Lithocodium/ Bacinella
Oil stained Lithocodium/ Bacinella
Thallassinoides
Aggregate grains
Burrows
Compacted burrows
Stylolite
Corals
Gastropods
Echinoid Spines
Hardground/ Erosion surface

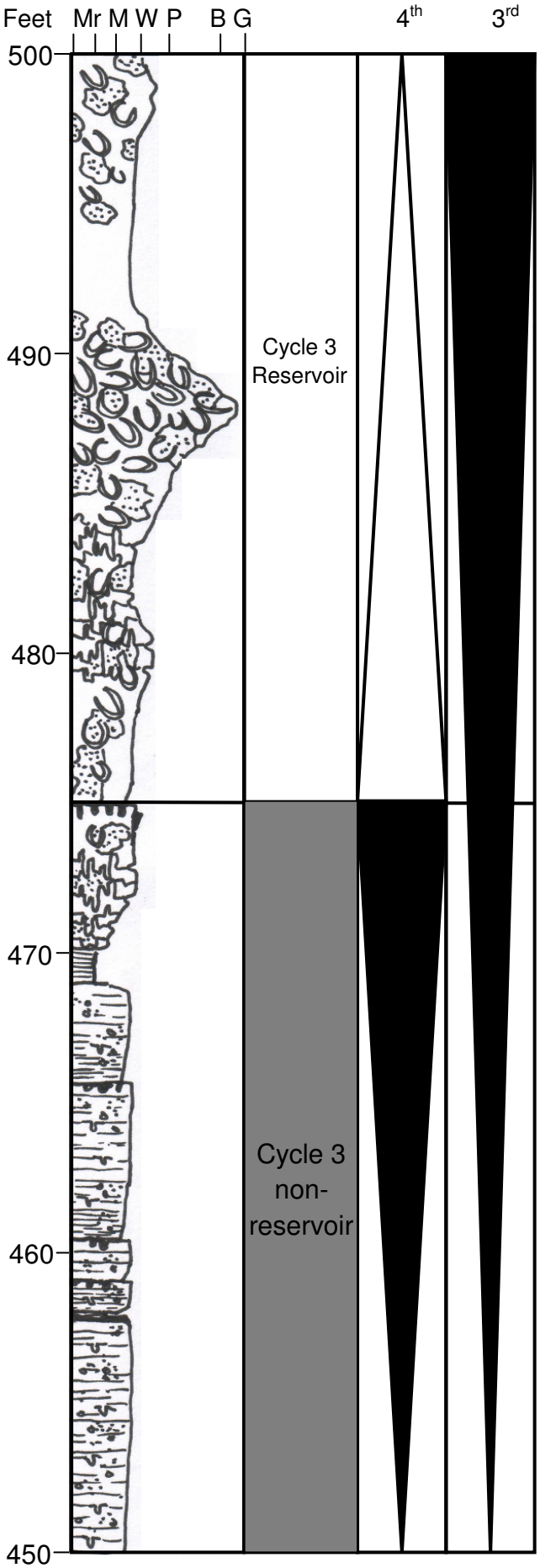

Key:

- *Glossomyphorus costatus*
- *Lithocodium/ Bacinella*
- Oil stained *Lithocodium/ Bacinella*
- *Thallassinoides*
- Aggregate grains
- Burrows
- Compacted burrows
- Stylolite
- Corals
- Gastropods
- Echinoid Spines
- Hardground/ Erosion surface

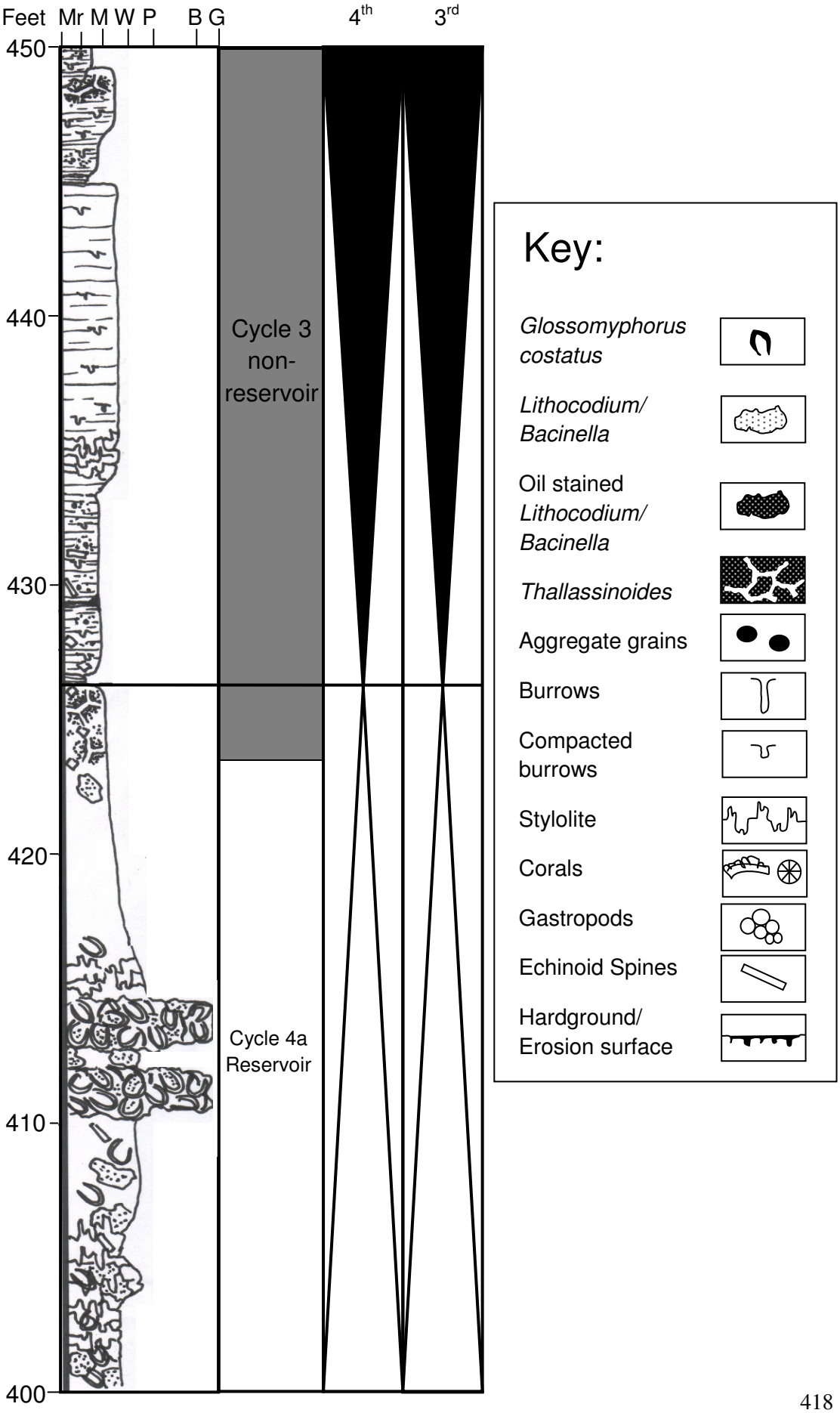
Feet
Mr
M
W
P
B
G
4th
3rd
450
440
430
420
410
400
Cycle 3
non-
reservoir
Cycle 4a
Reservoir
Key:
Glossomyphorus costatus
Lithocodium/ Bacinella
Oil stained Lithocodium/ Bacinella
Thallassinoides
Aggregate grains
Burrows
Compacted burrows
Stylolite
Corals
Gastropods
Echinoid Spines
Hardground/ Erosion surface

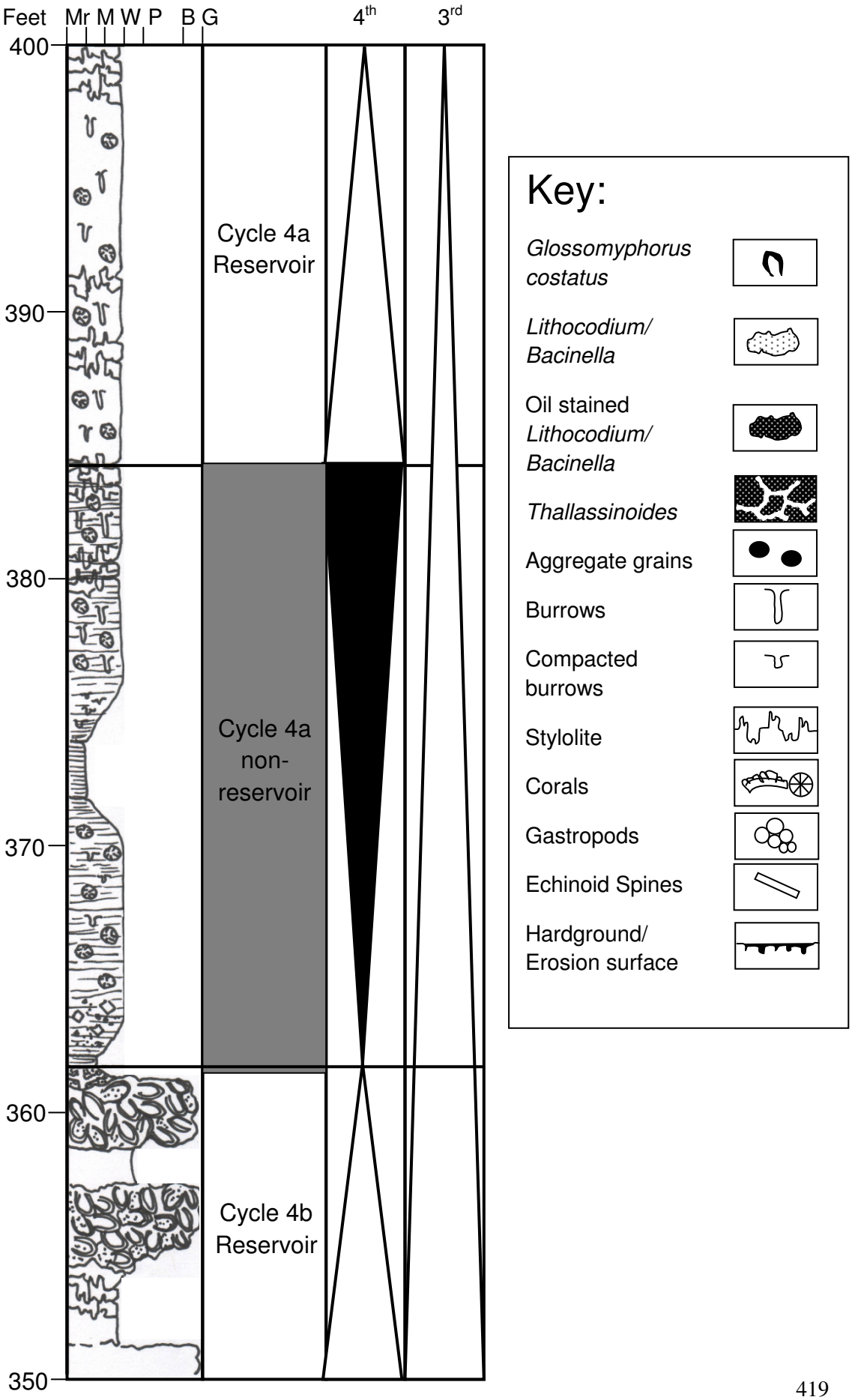
Feet
Mr M W P B G
4th
3rd
400
390
380
370
360
350
Cycle 4a Reservoir
Cycle 4a non-reservoir
Cycle 4b Reservoir
Key:
Glossomyphorus costatus
Lithocodium/ Bacinella
Oil stained Lithocodium/ Bacinella
Thallassinoides
Aggregate grains
Burrows
Compacted burrows
Stylolite
Corals
Gastropods
Echinoid Spines
Hardground/ Erosion surface

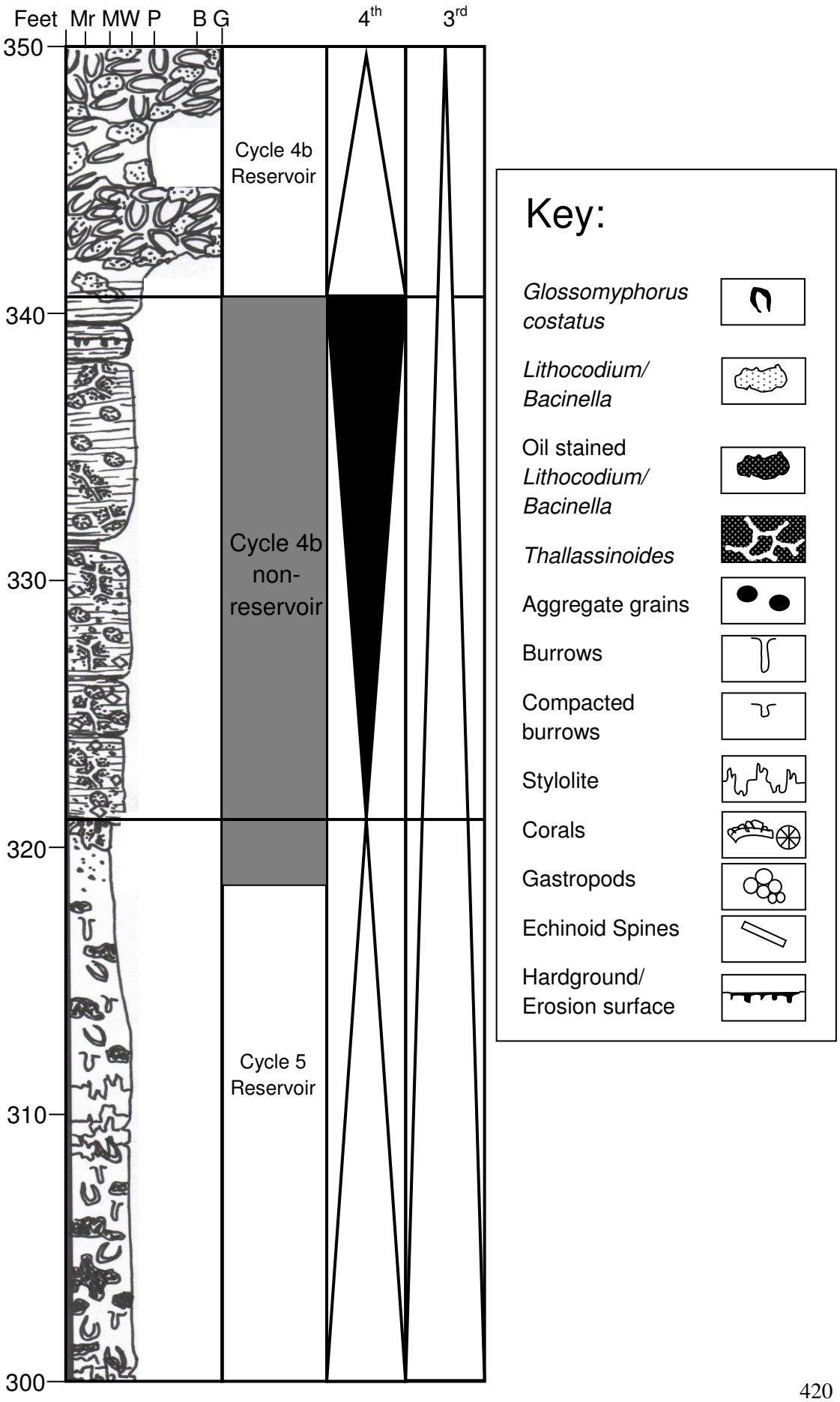
Feet
Mr
MW
P
B
G
4th
3rd
350
340
330
320
310
300
Cycle 4b Reservoir
Cycle 4b non-reservoir
Cycle 5 Reservoir
Key:
Glossomyphorus costatus
Lithocodium/ Bacinella
Oil stained Lithocodium/ Bacinella
Thallassinoides
Aggregate grains
Burrows
Compacted burrows
Stylolite
Corals
Gastropods
Echinoid Spines
Hardground/ Erosion surface

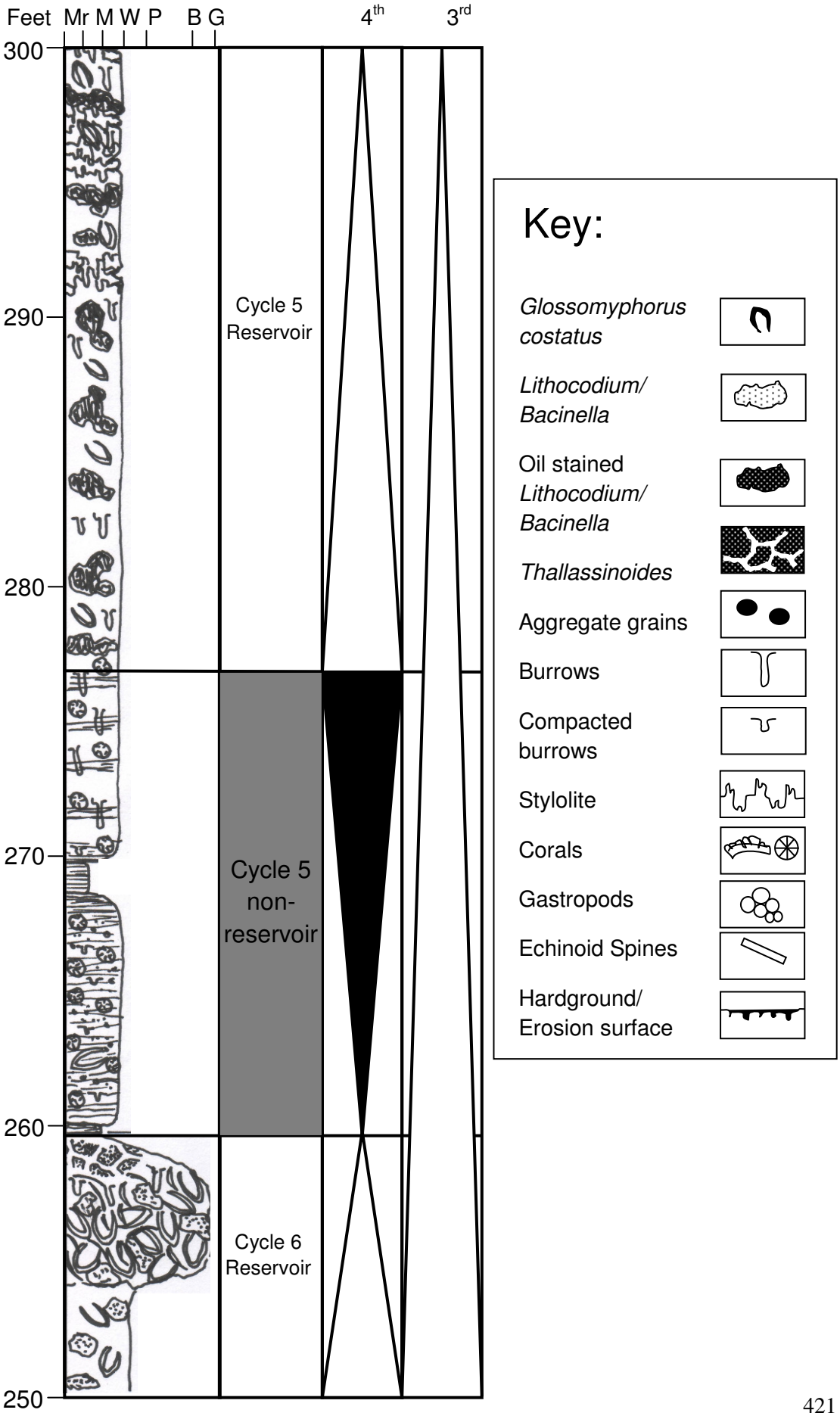
Feet
Mr
M
W
P
B
G
4th
3rd
300
290
280
270
260
250
Cycle 5 Reservoir
Cycle 5 non-reservoir
Cycle 6 Reservoir
Key:
Glossomyphorus costatus
Lithocodium/ Bacinella
Oil stained Lithocodium/ Bacinella
Thallassinoides
Aggregate grains
Burrows
Compacted burrows
Stylolite
Corals
Gastropods
Echinoid Spines
Hardground/ Erosion surface

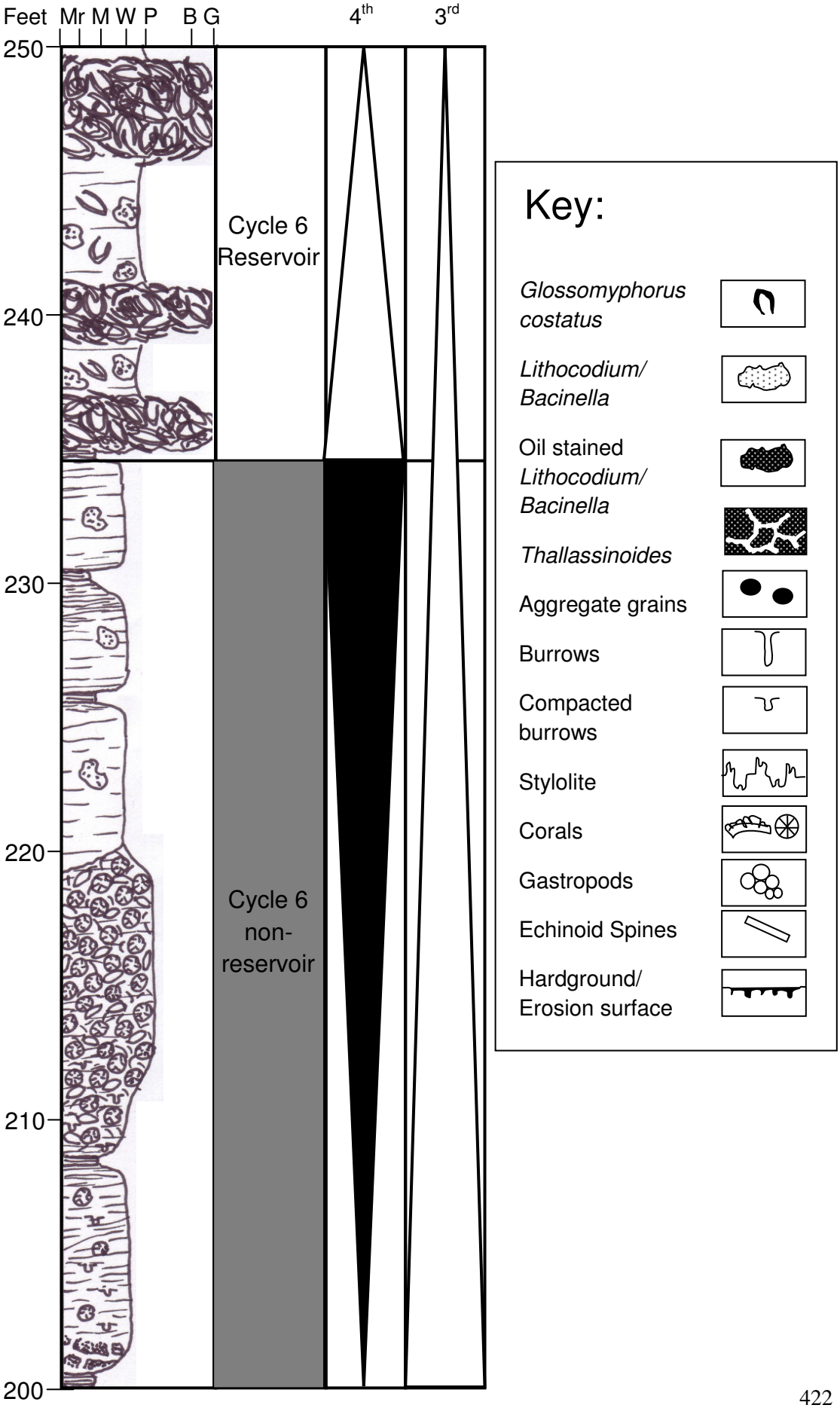
Feet
Mr
M
W
P
B
G
4th
3rd
250
240
230
220
210
200
Cycle 6
Reservoir
Cycle 6
non-
reservoir
Key:
Glossomyphorus costatus
Lithocodium/ Bacinella
Oil stained Lithocodium/ Bacinella
Thallassinoides
Aggregate grains
Burrows
Compacted burrows
Stylolite
Corals
Gastropods
Echinoid Spines
Hardground/ Erosion surface

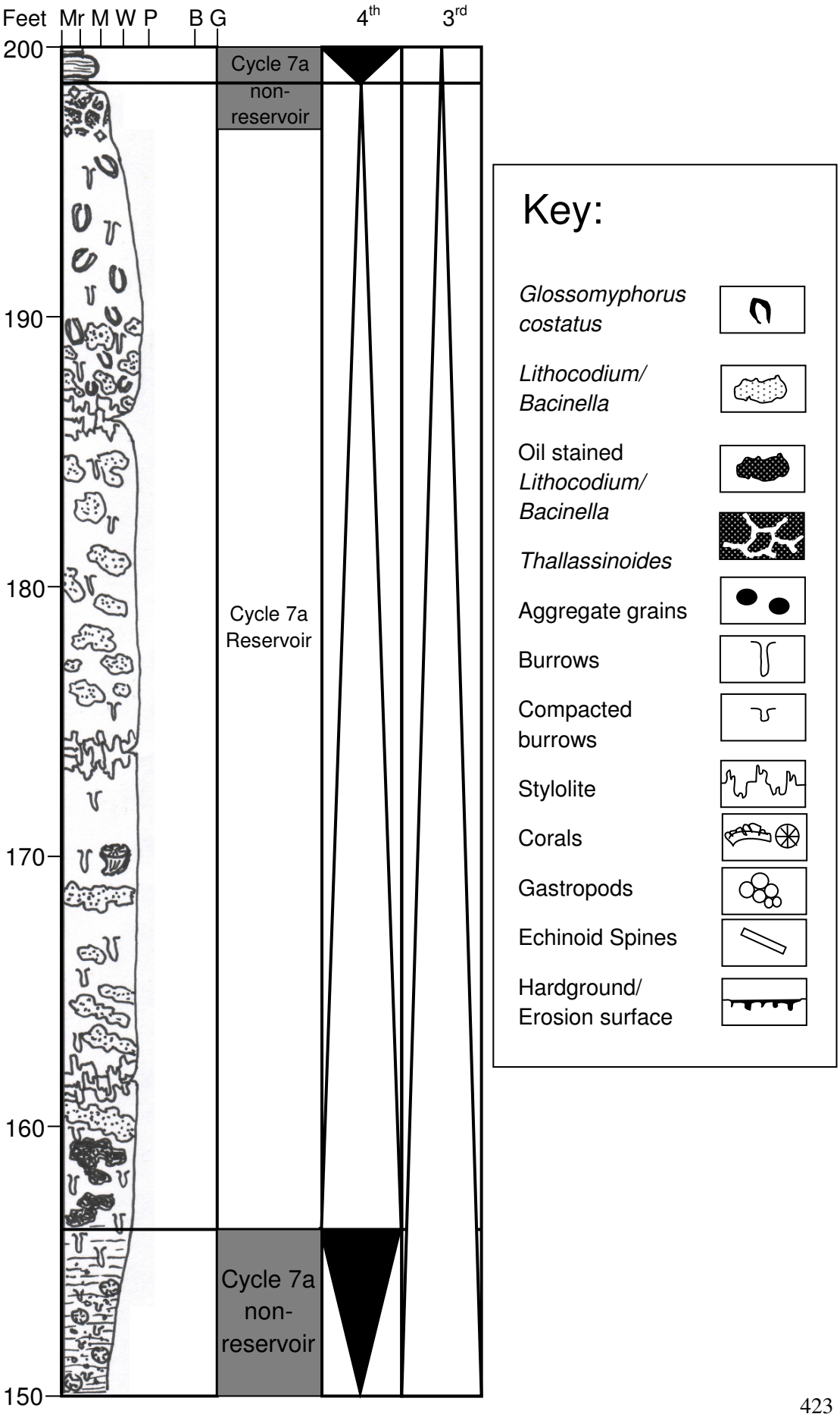
Feet
Mr
M
W
P
B
G
4th
3rd
200
190
180
170
160
150
Cycle 7a non-reservoir
Cycle 7a Reservoir
Cycle 7a non-reservoir
Key:
Glossomyphorus costatus
Lithocodium/ Bacinella
Oil stained Lithocodium/ Bacinella
Thallassinoides
Aggregate grains
Burrows
Compacted burrows
Stylolite
Corals
Gastropods
Echinoid Spines
Hardground/ Erosion surface

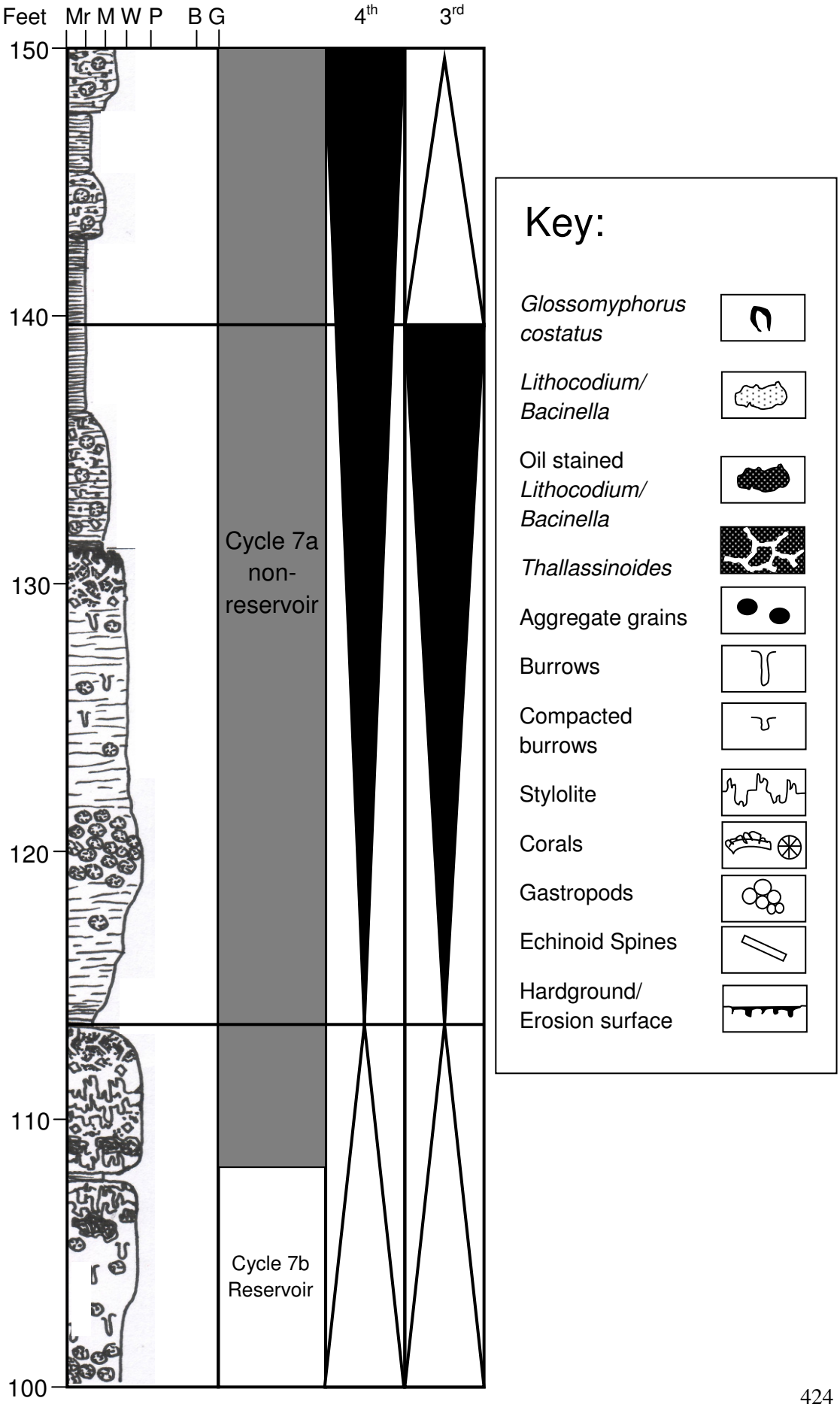
Feet
Mr
M
W
P
B
G
4th
3rd
150
140
130
120
110
100
Cycle 7a non-reservoir
Cycle 7b Reservoir
Key:
Glossomyphorus costatus
Lithocodium/ Bacinella
Oil stained Lithocodium/ Bacinella
Thallassinoides
Aggregate grains
Burrows
Compacted burrows
Stylolite
Corals
Gastropods
Echinoid Spines
Hardground/ Erosion surface

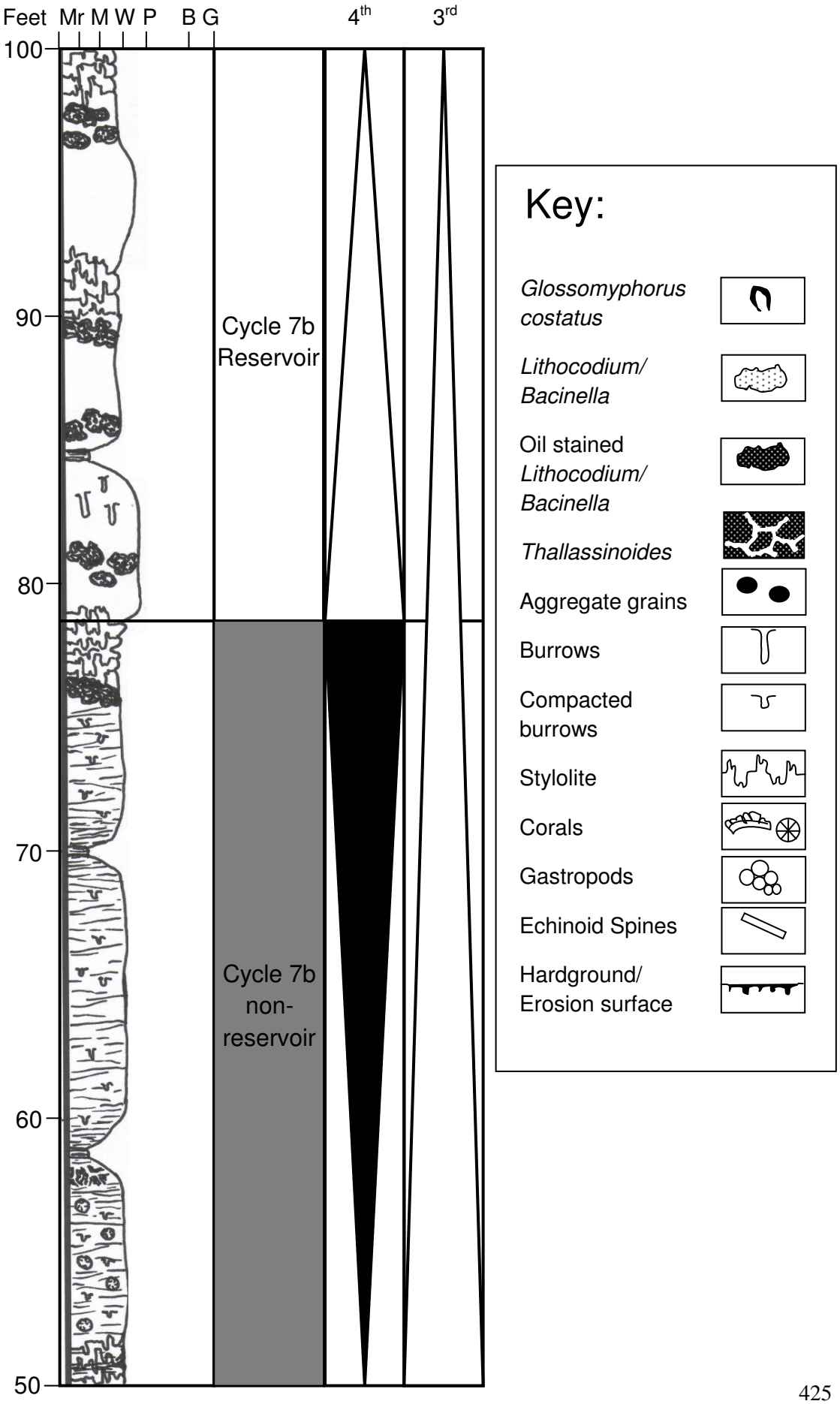
Feet
Mr
M
W
P
B
G
4th
3rd
100
90
80
70
60
50
Cycle 7b Reservoir
Cycle 7b non-reservoir
Key:
Glossomyphorus costatus
Lithocodium/ Bacinella
Oil stained Lithocodium/ Bacinella
Thallassinoides
Aggregate grains
Burrows
Compacted burrows
Stylolite
Corals
Gastropods
Echinoid Spines
Hardground/ Erosion surface

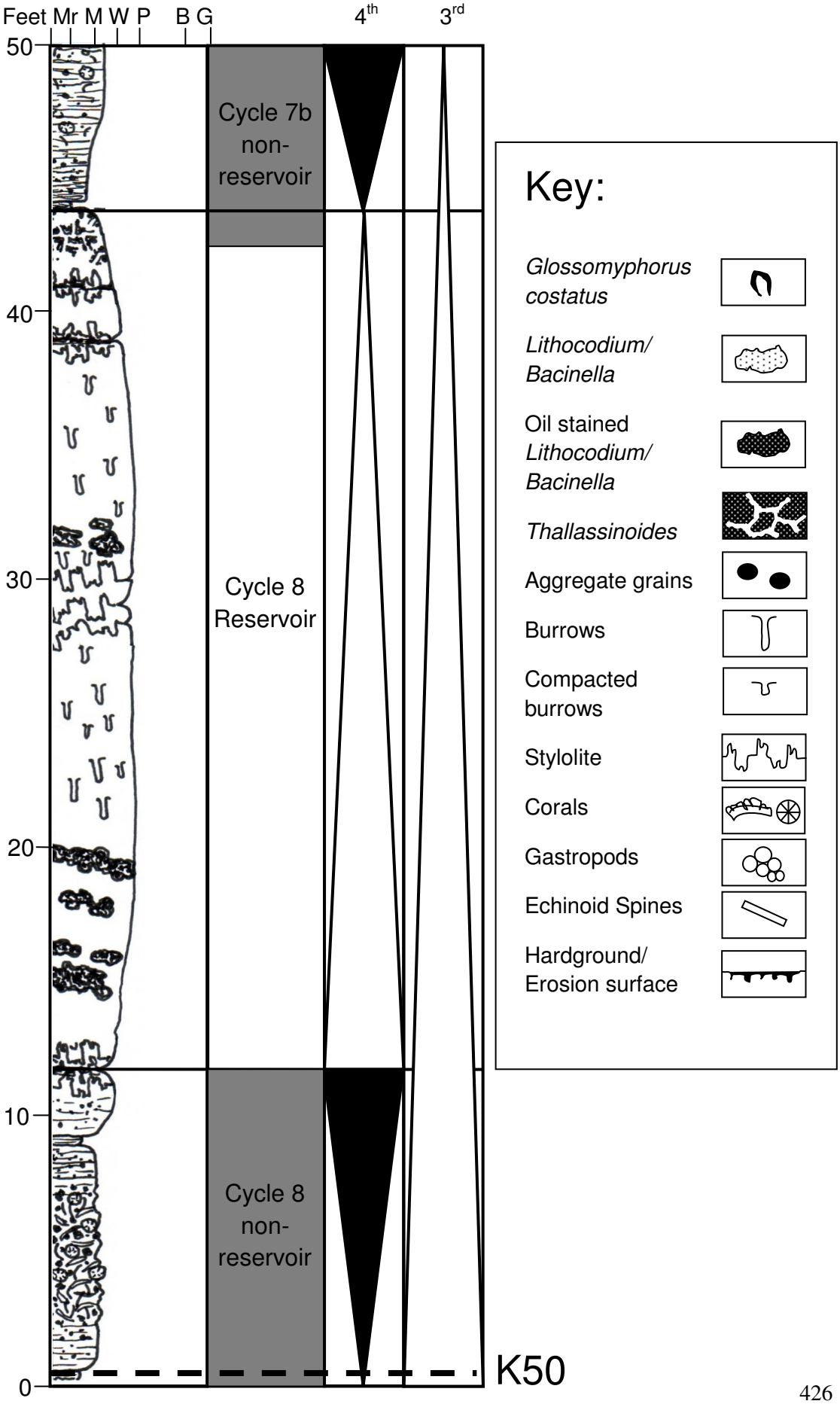
Feet Mr M W P B G
4th
3rd
50
40
30
20
10
0
Cycle 7b non-reservoir
Cycle 8 Reservoir
Cycle 8 non-reservoir
K50
Key:
Glossomyphorus costatus
Lithocodium/ Bacinella
Oil stained Lithocodium/ Bacinella
Thallassinoides
Aggregate grains
Burrows
Compacted burrows
Stylolite
Corals
Gastropods
Echinoid Spines
Hardground/ Erosion surface

Appendix 2D

Well 4, core log

These are the core logs from Well 4. The scale is based on Dunham's classification scheme with Mr meaning Micrite, M meaning Mudstone, W meaning Wackestone, P meaning Packstone, B meaning boundstone and G meaning grainstone. The depths shown on these logs are the deviated core depths (angles of deviation can be seen in Section 1.2: Table 1.1). Each page shows 50ft of core with the first page showing the top 50ft which leads progressively towards the bottom 50ft in the last page. Each page has a key that describes the symbols used within the logs. The logs are accompanied by the reservoir and non-reservoir sections, which are coloured white and grey, respectively. The black triangles represent the TST's and the white triangles represent the HST's. The 4^{th} order SB's and MFS's are also shown. This data relates to Sections 3.4.1 and 4.6.

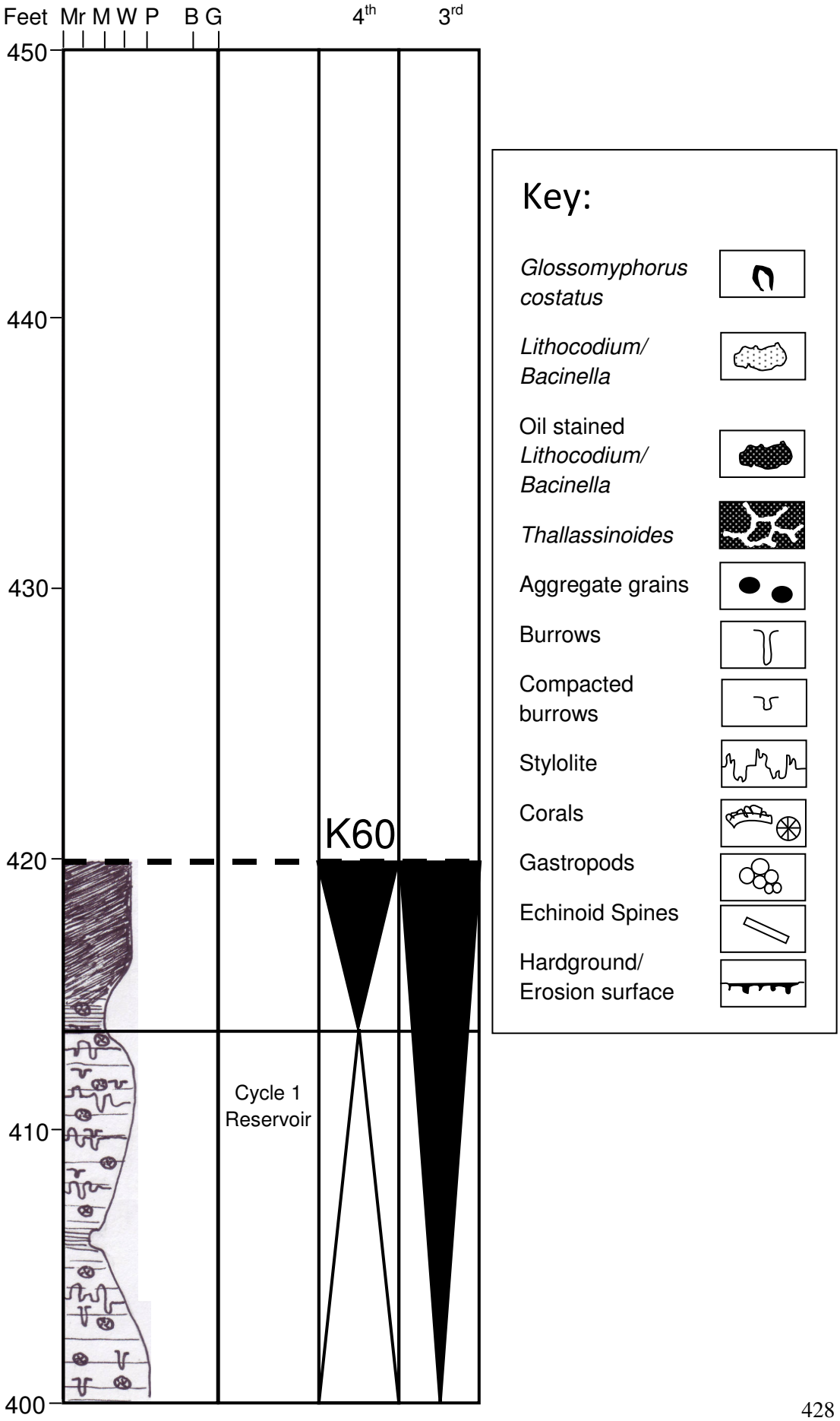
Feet
Mr
M
W
P
B
G
4th
3rd
450
440
430
420
410
400
K60
Cycle 1
Reservoir
Key:
Glossomyphorus costatus
Lithocodium/ Bacinella
Oil stained Lithocodium/ Bacinella
Thallassinoides
Aggregate grains
Burrows
Compacted burrows
Stylolite
Corals
Gastropods
Echinoid Spines
Hardground/ Erosion surface

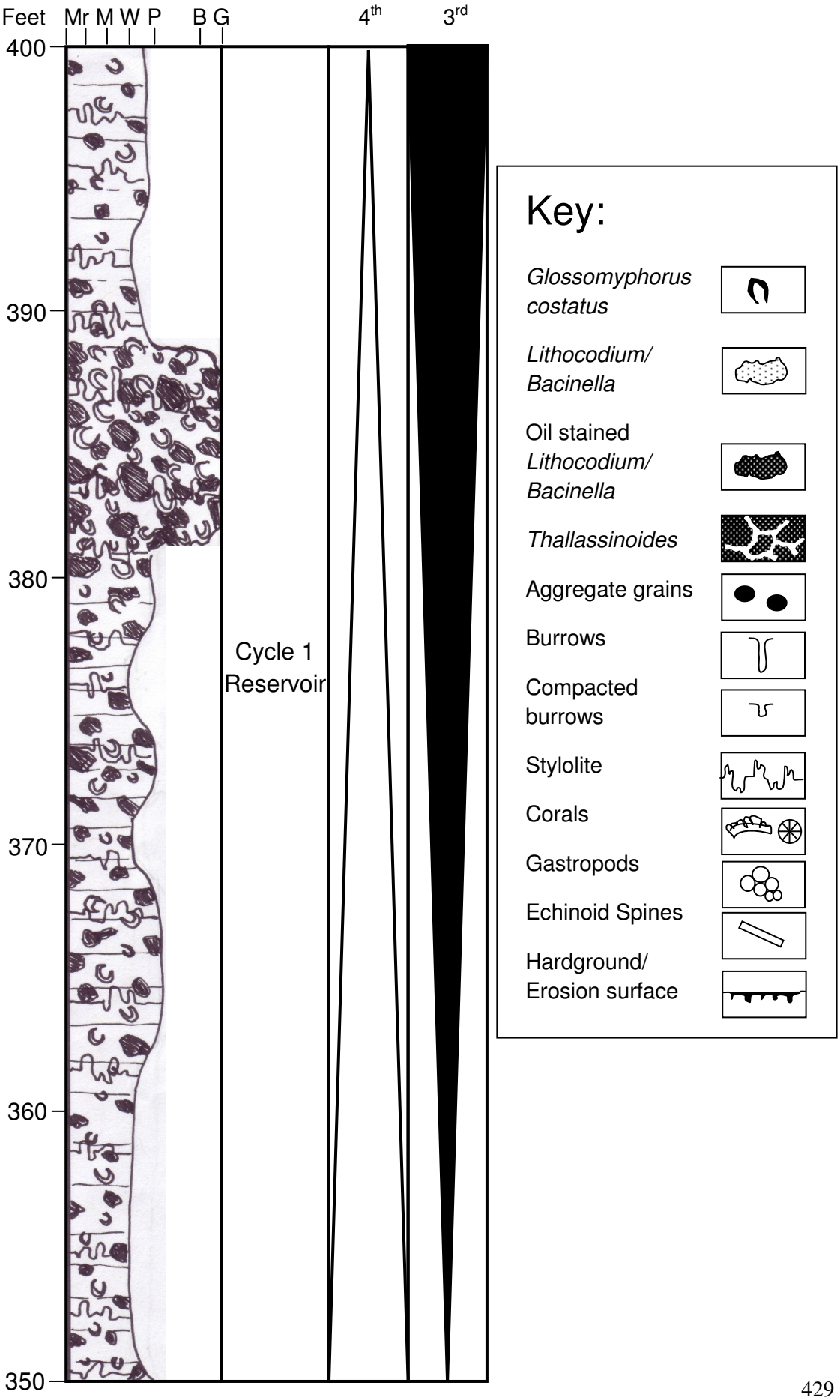
Feet
Mr
M
W
P
B
G
4th
3rd
400
390
380
370
360
350
Cycle 1
Reservoir
Key:
Glossomyphorus costatus
Lithocodium/ Bacinella
Oil stained Lithocodium/ Bacinella
Thallassinoides
Aggregate grains
Burrows
Compacted burrows
Stylolite
Corals
Gastropods
Echinoid Spines
Hardground/ Erosion surface

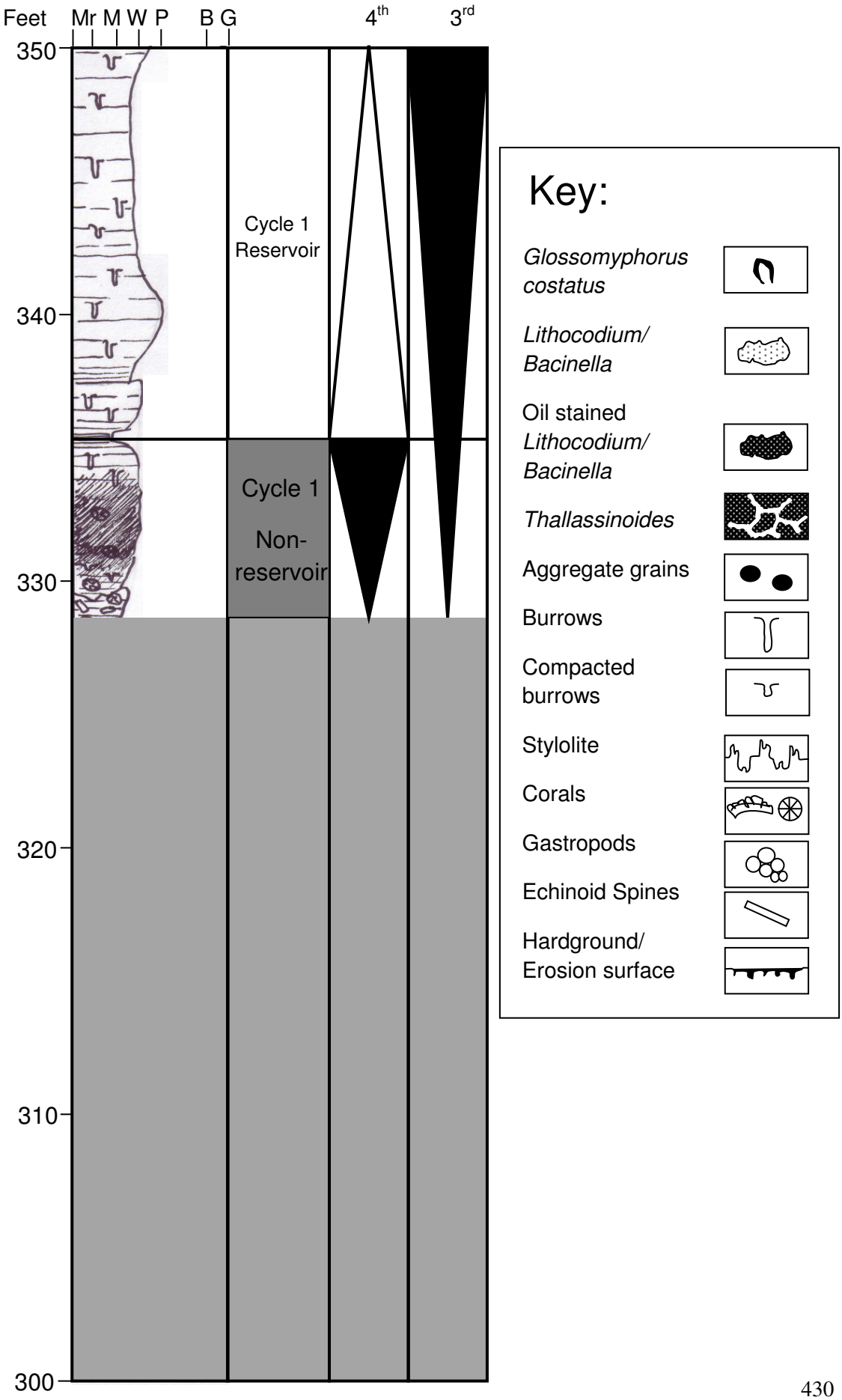
Feet
Mr M W P
B G
4th
3rd
350
340
330
320
310
300
Cycle 1
Reservoir
Cycle 1
Non-
reservoir
Key:
Glossomyphorus costatus
Lithocodium/ Bacinella
Oil stained Lithocodium/ Bacinella
Thallassinoides
Aggregate grains
Burrows
Compacted burrows
Stylolite
Corals
Gastropods
Echinoid Spines
Hardground/ Erosion surface

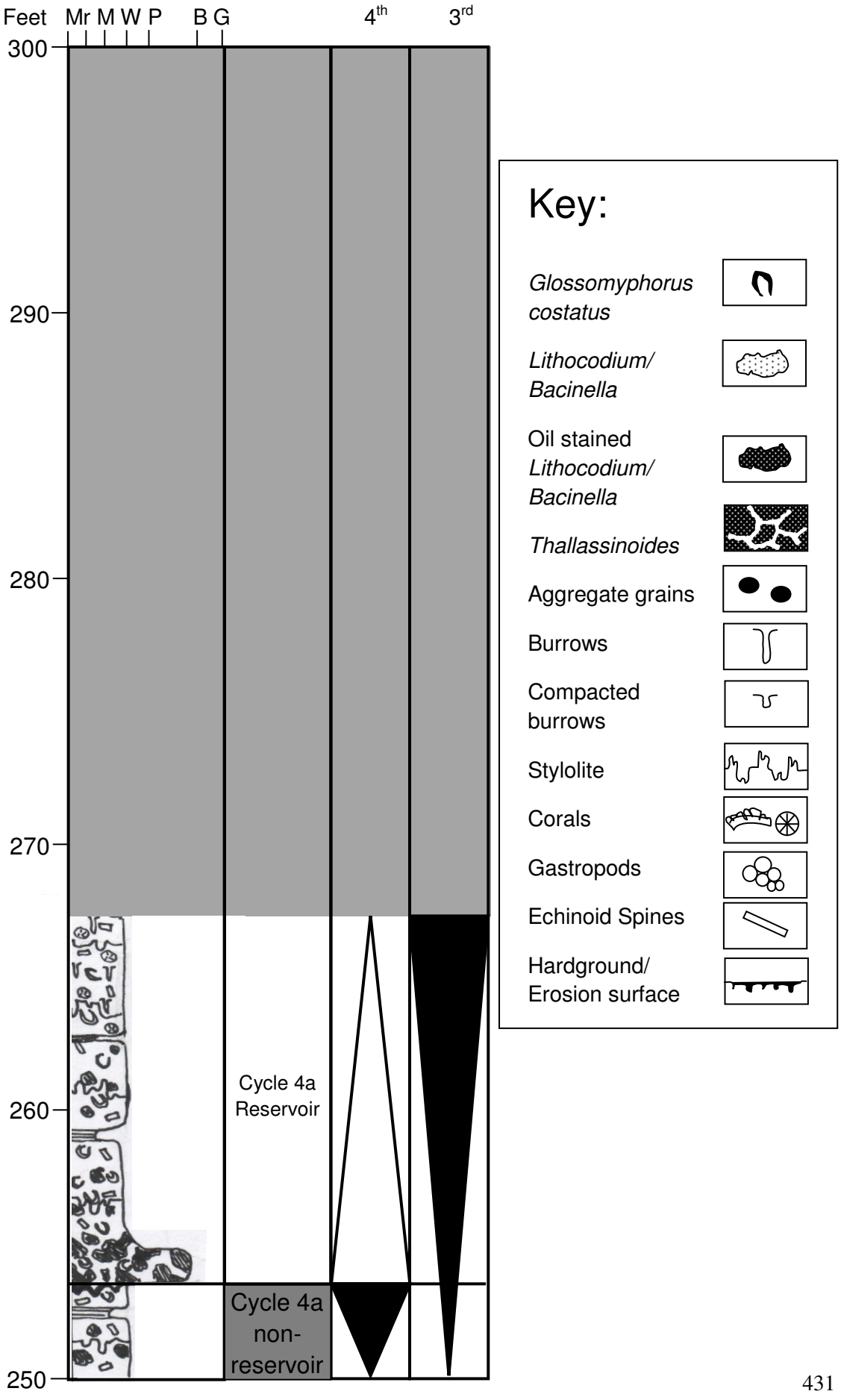
Feet
Mr M W P
B G
4th
3rd
300
290
280
270
260
250
Cycle 4a Reservoir
Cycle 4a non-reservoir
Key:
Glossomyphorus costatus
Lithocodium/ Bacinella
Oil stained Lithocodium/ Bacinella
Thallassinoides
Aggregate grains
Burrows
Compacted burrows
Stylolite
Corals
Gastropods
Echinoid Spines
Hardground/ Erosion surface

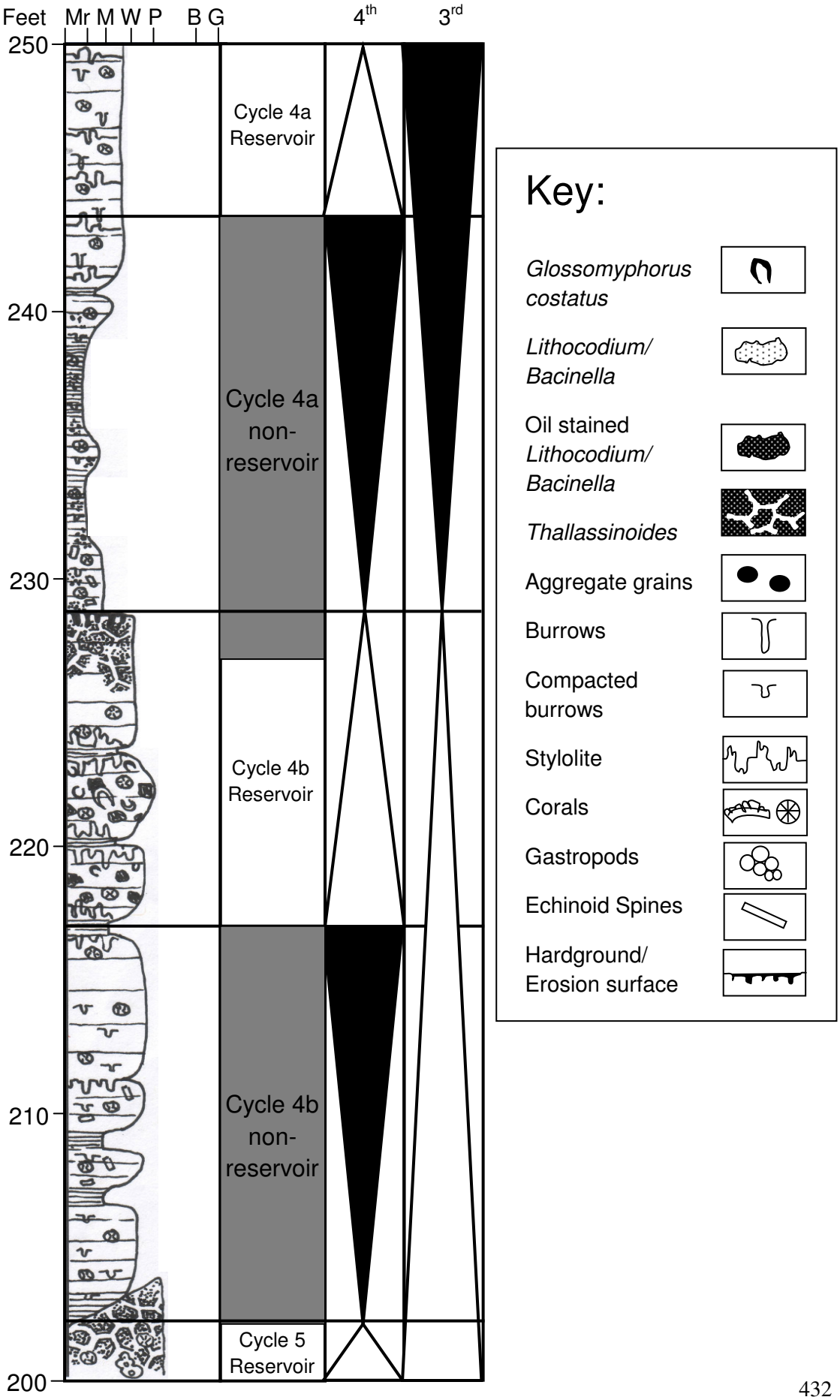
Feet
Mr M W P B G
4th
3rd
250
240
230
220
210
200
Cycle 4a Reservoir
Cycle 4a non-reservoir
Cycle 4b Reservoir
Cycle 4b non-reservoir
Cycle 5 Reservoir
Key:
Glossomyphorus costatus
Lithocodium/ Bacinella
Oil stained Lithocodium/ Bacinella
Thallassinoides
Aggregate grains
Burrows
Compacted burrows
Stylolite
Corals
Gastropods
Echinoid Spines
Hardground/ Erosion surface

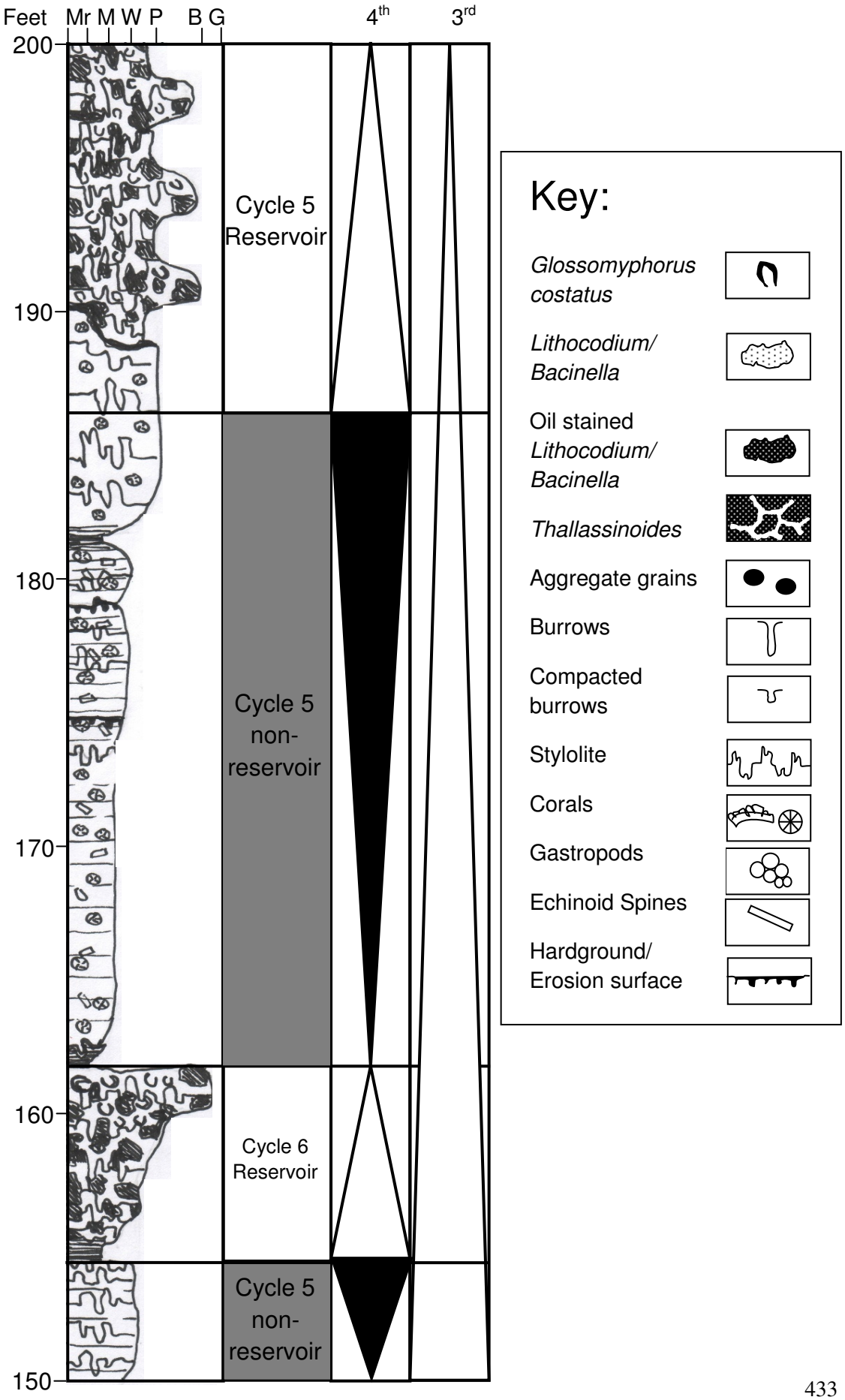
Feet
Mr M W P B G
4th
3rd
200
190
180
170
160
150
Cycle 5 Reservoir
Cycle 5 non-reservoir
Cycle 6 Reservoir
Cycle 5 non-reservoir
Key:
Glossomyphorus costatus
Lithocodium/ Bacinella
Oil stained Lithocodium/ Bacinella
Thallassinoides
Aggregate grains
Burrows
Compacted burrows
Stylolite
Corals
Gastropods
Echinoid Spines
Hardground/ Erosion surface

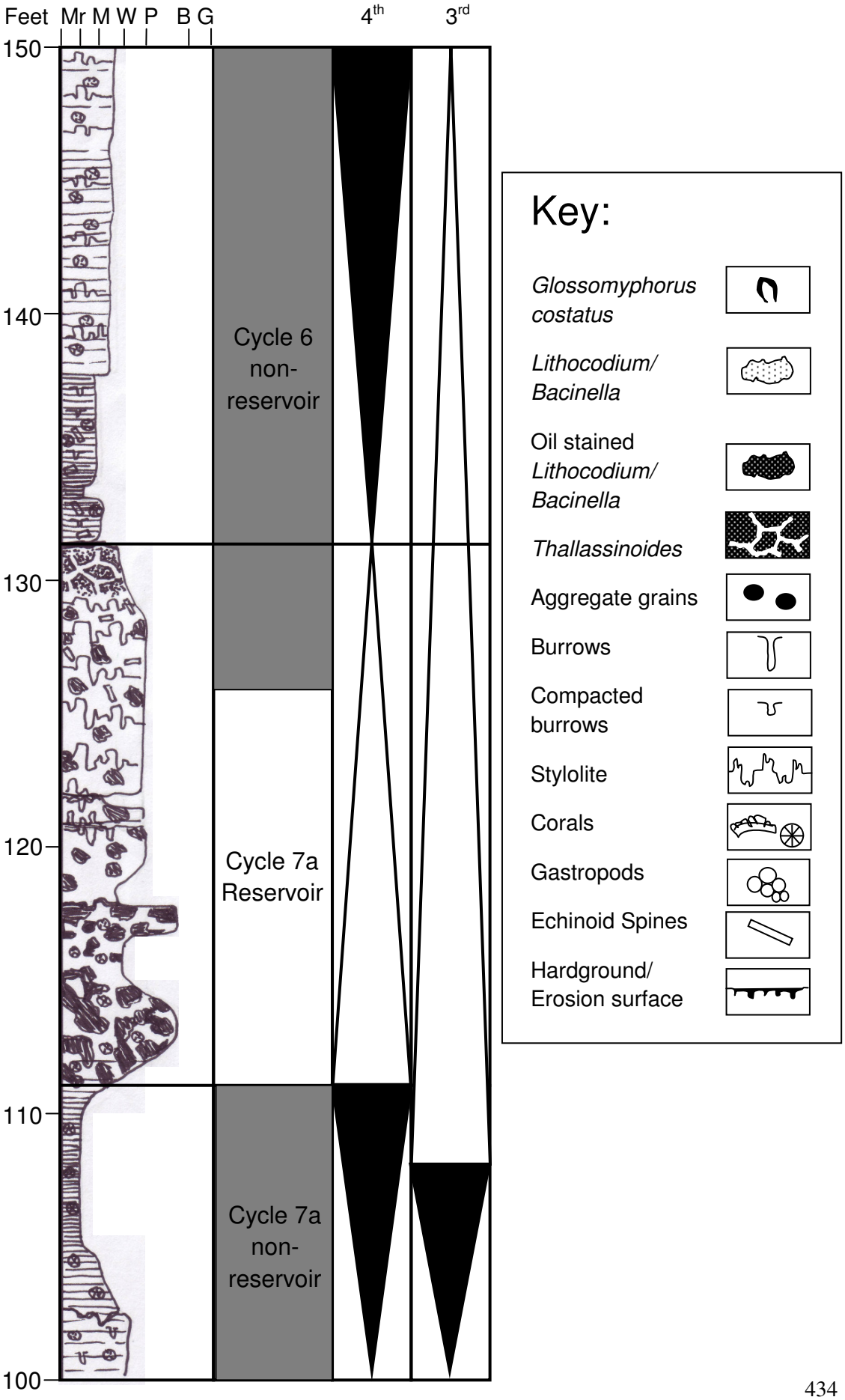
Feet
Mr
M
W
P
B
G
4th
3rd
150
140
130
120
110
100
Cycle 6 non-reservoir
Cycle 7a Reservoir
Cycle 7a non-reservoir
Key:
Glossomyphorus costatus
Lithocodium/ Bacinella
Oil stained Lithocodium/ Bacinella
Thallassinoides
Aggregate grains
Burrows
Compacted burrows
Stylolite
Corals
Gastropods
Echinoid Spines
Hardground/ Erosion surface

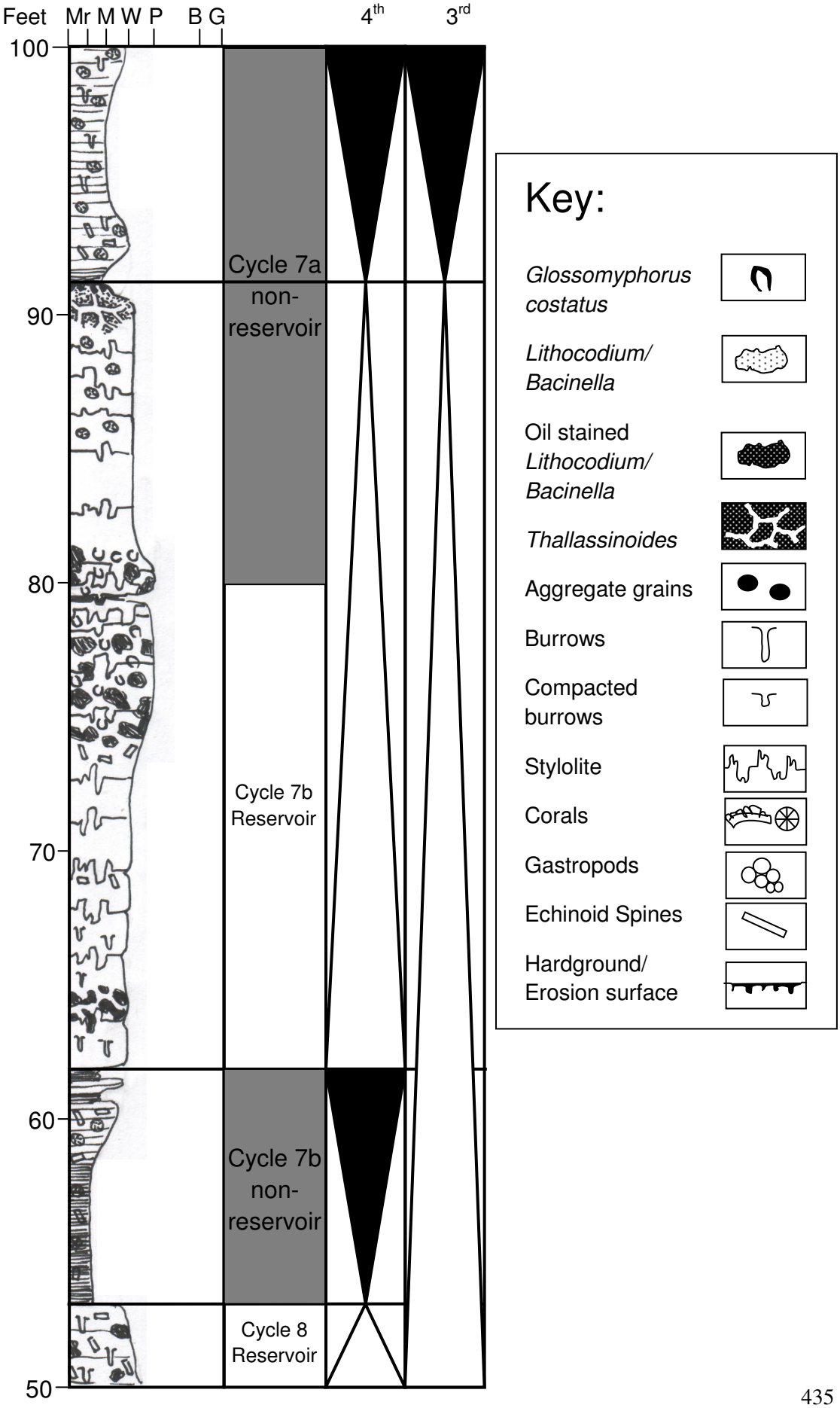
Feet
Mr M W P B G
4th
3rd
100
90
80
70
60
50
Cycle 7a non-reservoir
Cycle 7b Reservoir
Cycle 7b non-reservoir
Cycle 8 Reservoir
Key:
Glossomyphorus costatus
Lithocodium/ Bacinella
Oil stained Lithocodium/ Bacinella
Thallassinoides
Aggregate grains
Burrows
Compacted burrows
Stylolite
Corals
Gastropods
Echinoid Spines
Hardground/ Erosion surface

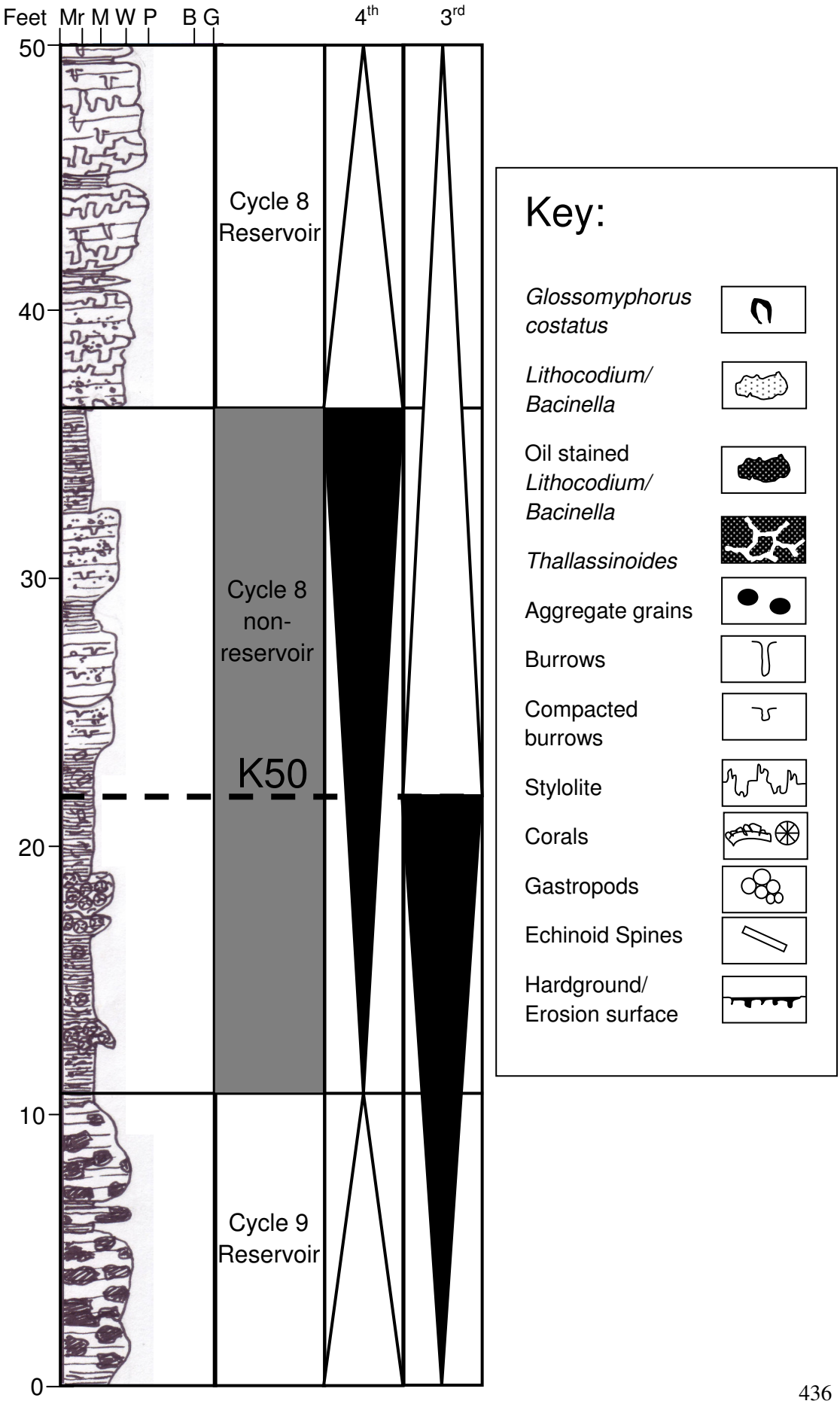
Feet
Mr
M
W
P
B
G
4th
3rd
50
40
30
20
10
0
Cycle 8
Reservoir
Cycle 8
non-
reservoir
K50
Cycle 9
Reservoir
Key:
Glossomyphorus costatus
Lithocodium/ Bacinella
Oil stained Lithocodium/ Bacinella
Thallassinoides
Aggregate grains
Burrows
Compacted burrows
Stylolite
Corals
Gastropods
Echinoid Spines
Hardground/ Erosion surface

Appendix 2E

Well 5, core log

These are the core logs from Well 5. The scale is based on Dunham's classification scheme with Mr meaning Micrite, M meaning Mudstone, W meaning Wackestone, P meaning Packstone, B meaning boundstone and G meaning grainstone. The depths shown on these logs are the deviated core depths (angles of deviation can be seen in Section 1.2: Table 1.1). Each page shows 50ft of core with the first page showing the top 50ft which leads progressively towards the bottom 50ft in the last page. Each page has a key that describes the symbols used within the logs. The logs are accompanied by the reservoir and non reservoir-sections, which are coloured white and grey, respectively. The black triangles represent the TST's and the white triangles representing the HST's. The 4^{th} order SB's and MFS's are also shown. This data relates to Sections 3.4.1 and 4.6.

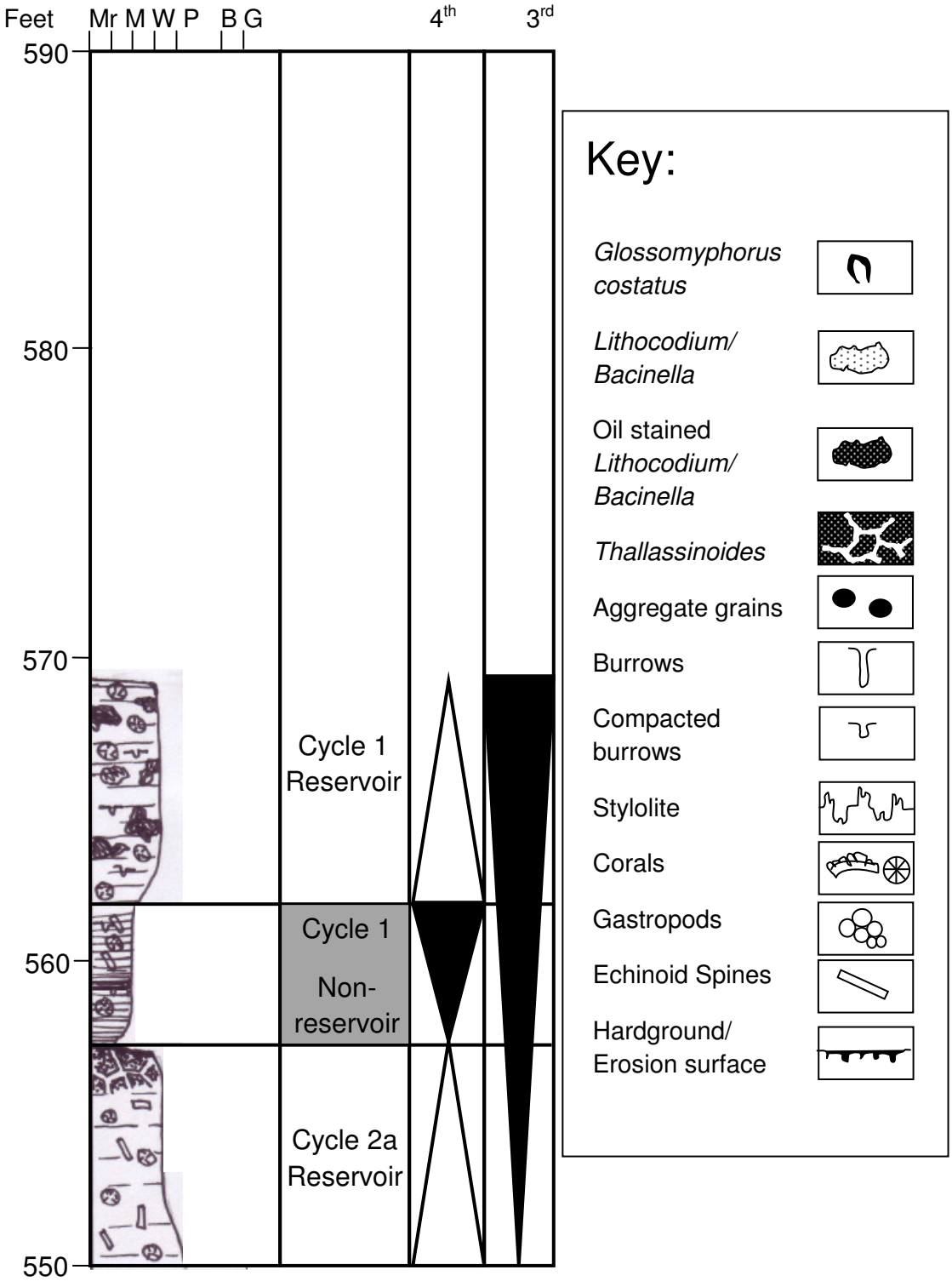
Feet
Mr M W P B G
4th
3rd
590
580
570
560
550
Cycle 1
Reservoir
Cycle 1
Non-
reservoir
Cycle 2a
Reservoir
Key:
Glossomyphorus costatus
Lithocodium/ Bacinella
Oil stained Lithocodium/ Bacinella
Thallassinoides
Aggregate grains
Burrows
Compacted burrows
Stylolite
Corals
Gastropods
Echinoid Spines
Hardground/ Erosion surface

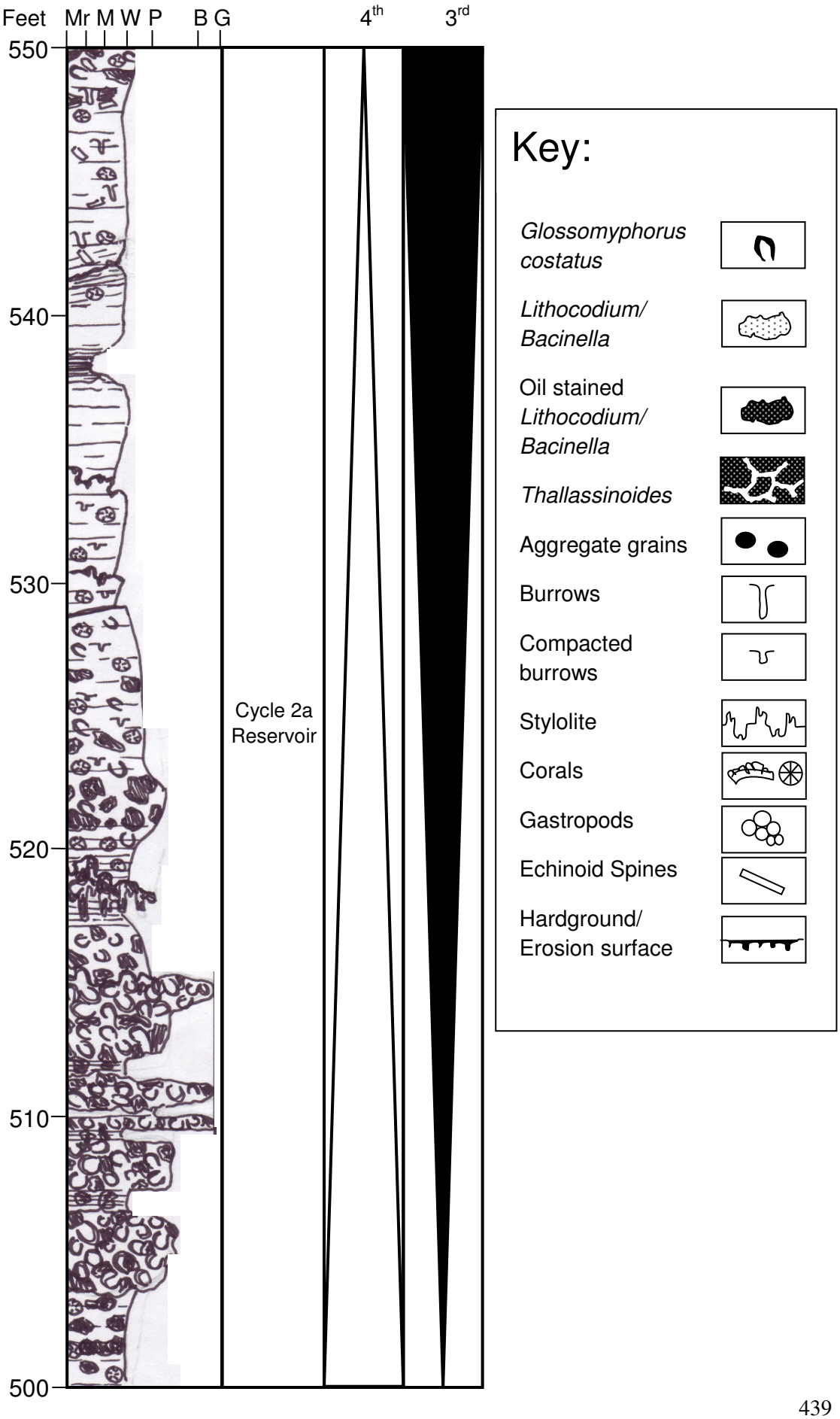
Feet
Mr M W P B G
4th
3rd
550
540
530
520
510
500
Cycle 2a
Reservoir
Key:
Glossomyphorus costatus
Lithocodium/ Bacinella
Oil stained Lithocodium/ Bacinella
Thallassinoides
Aggregate grains
Burrows
Compacted burrows
Stylolite
Corals
Gastropods
Echinoid Spines
Hardground/ Erosion surface

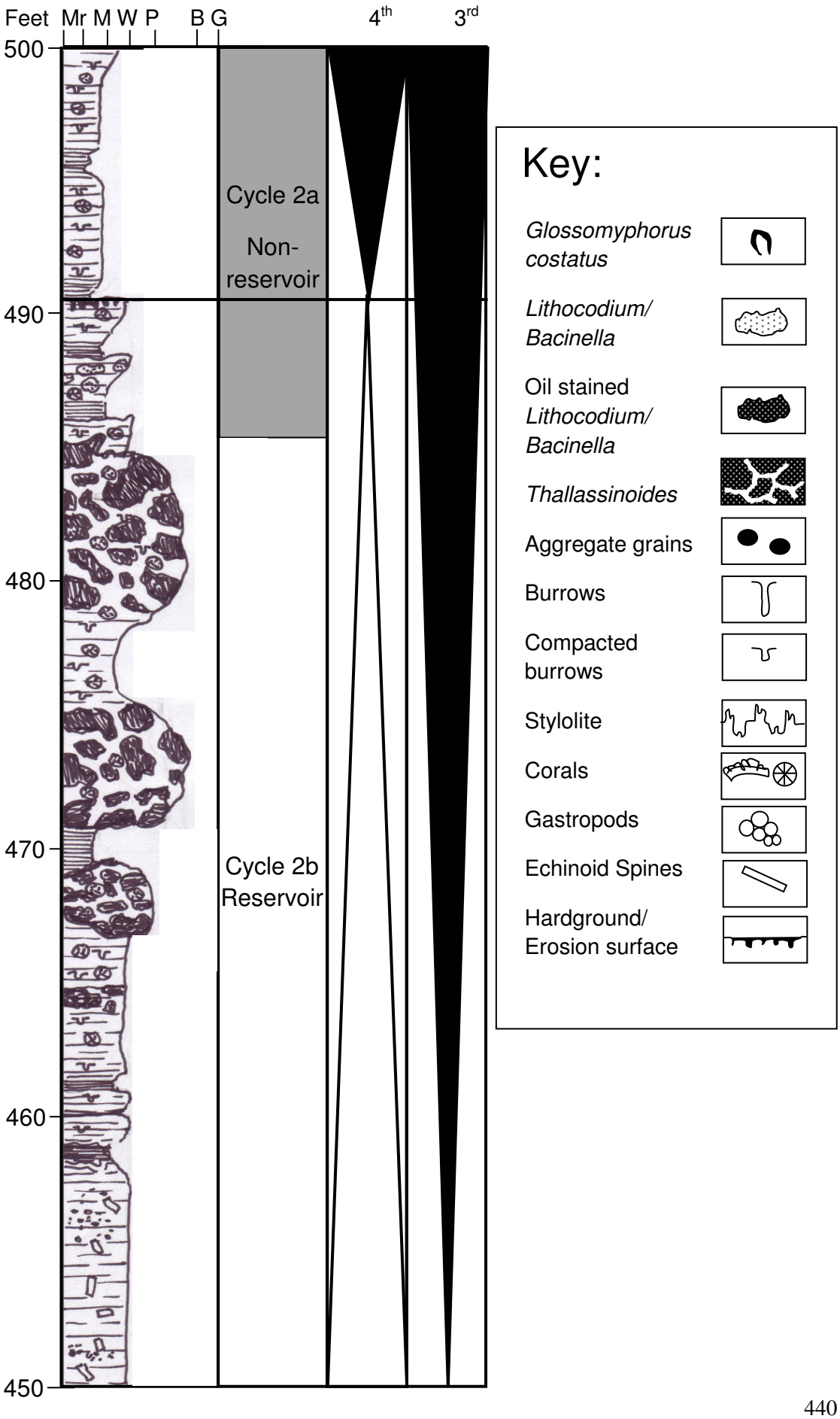
Feet
Mr M W P
B G
4th
3rd
500
490
480
470
460
450
Cycle 2a
Non-reservoir
Cycle 2b
Reservoir
Key:
Glossomyphorus costatus
Lithocodium/ Bacinella
Oil stained Lithocodium/ Bacinella
Thallassinoides
Aggregate grains
Burrows
Compacted burrows
Stylolite
Corals
Gastropods
Echinoid Spines
Hardground/ Erosion surface

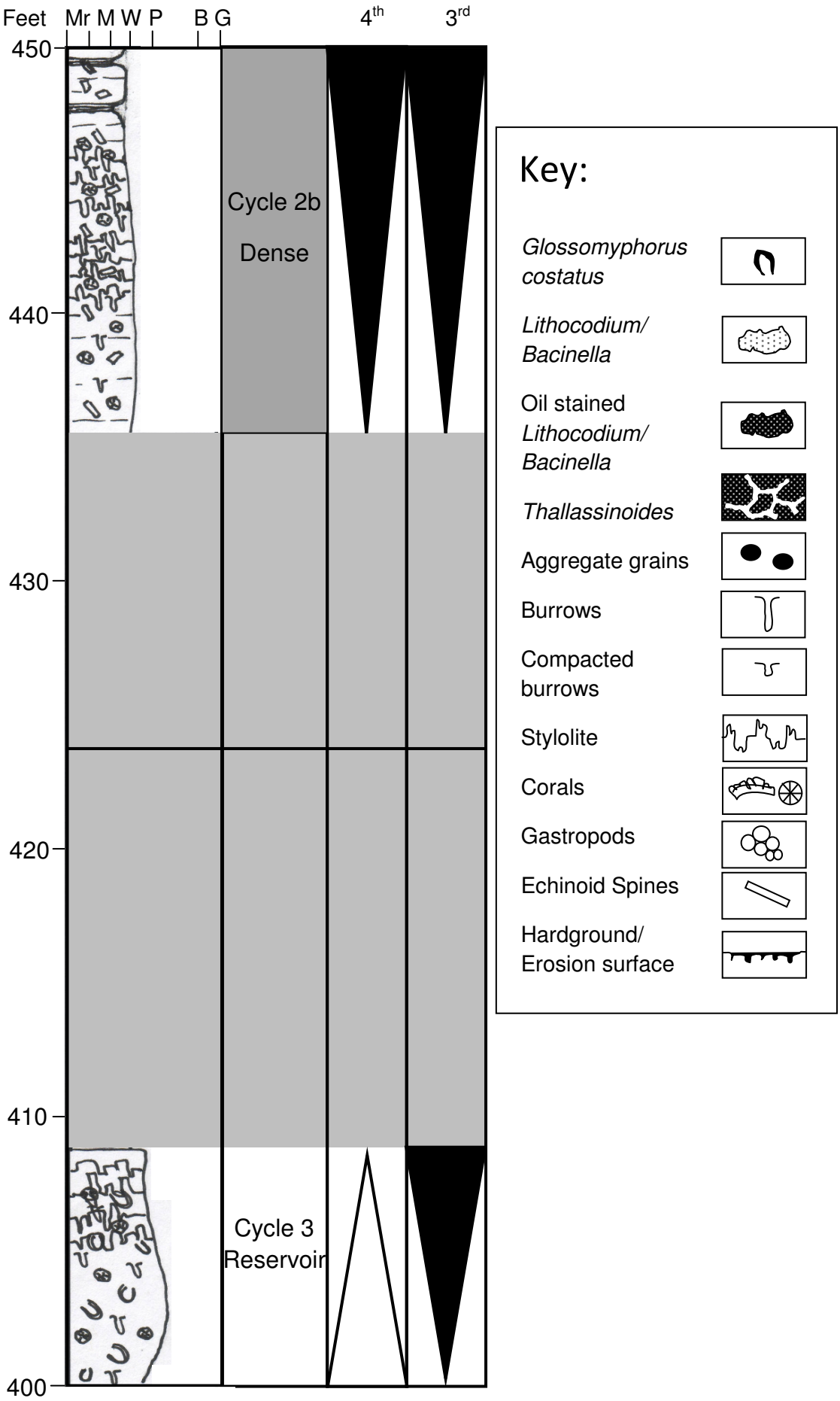
Feet
Mr M W P
B G
4th
3rd
450
440
430
420
410
400
Cycle 2b
Dense
Cycle 3
Reservoir
Key:
Glossomyphorus costatus
Lithocodium/ Bacinella
Oil stained Lithocodium/ Bacinella
Thallassinoides
Aggregate grains
Burrows
Compacted burrows
Stylolite
Corals
Gastropods
Echinoid Spines
Hardground/ Erosion surface

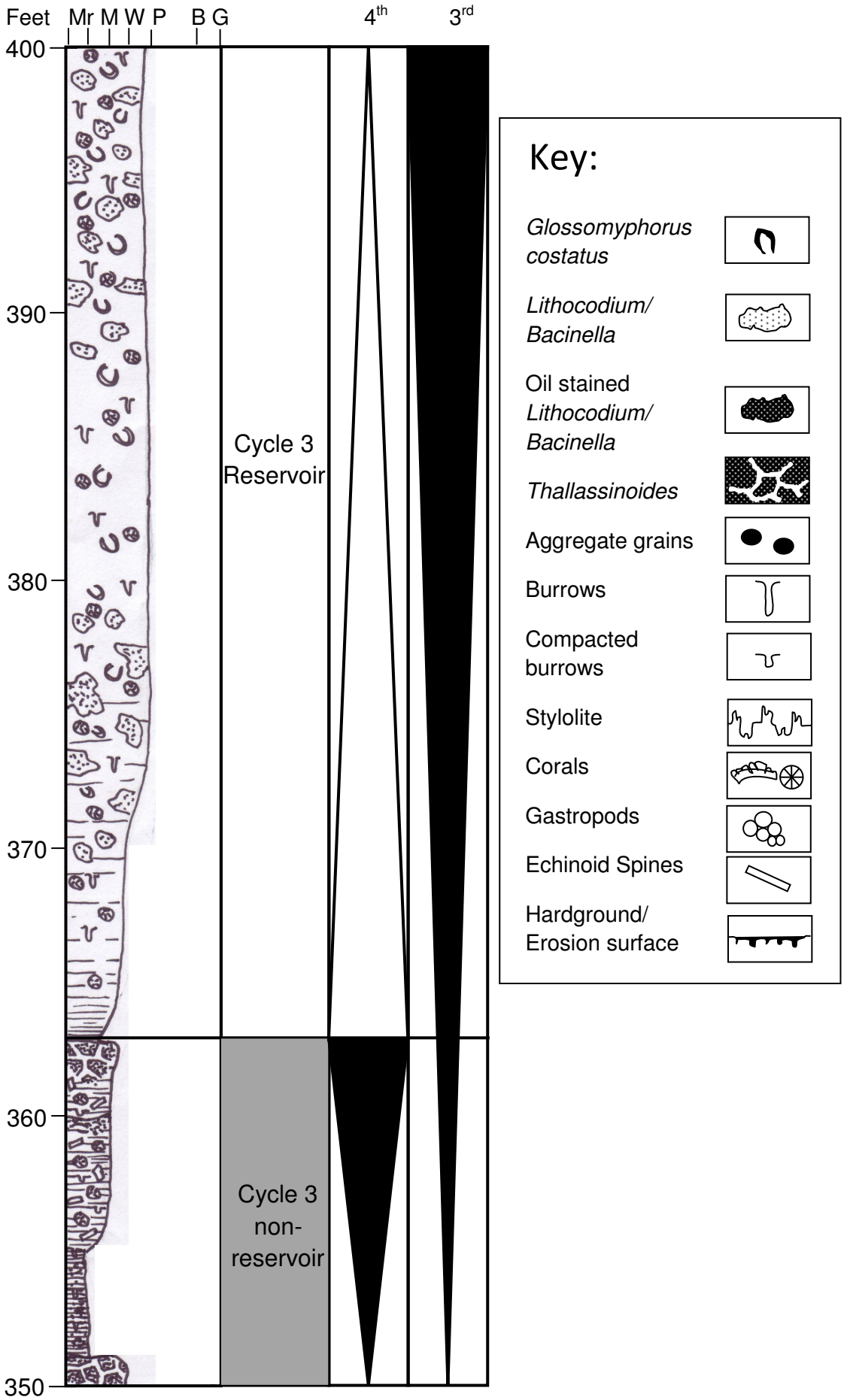
Feet
Mr
M
W
P
B
G
4th
3rd
400
390
380
370
360
350
Cycle 3
Reservoir
Cycle 3
non-
reservoir
Key:
Glossomyphorus costatus
Lithocodium/ Bacinella
Oil stained Lithocodium/ Bacinella
Thallassinoides
Aggregate grains
Burrows
Compacted burrows
Stylolite
Corals
Gastropods
Echinoid Spines
Hardground/ Erosion surface

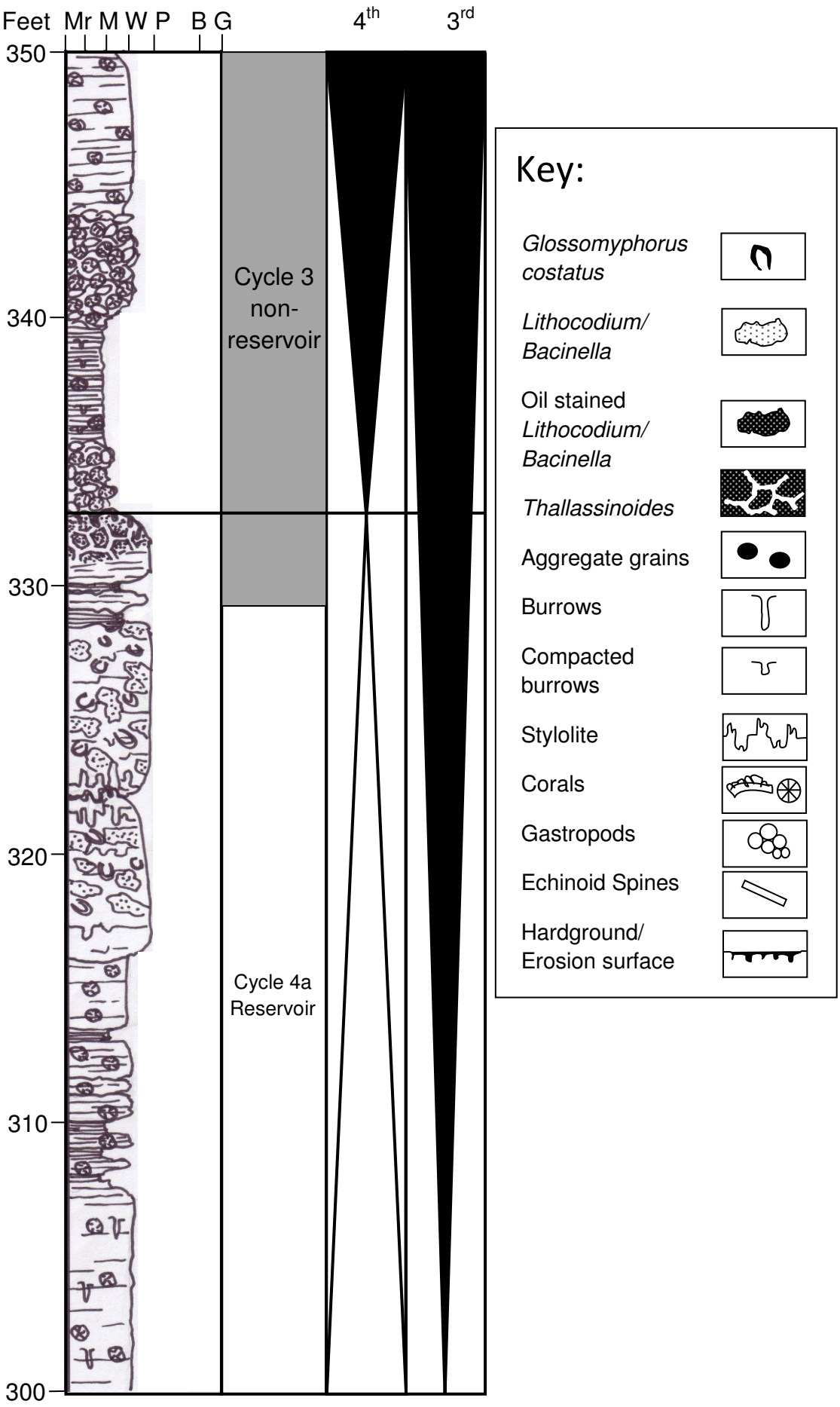
Feet
Mr
M
W
P
B
G
4th
3rd
350
340
330
320
310
300
Cycle 3 non-reservoir
Cycle 4a Reservoir
Key:
Glossomyphorus costatus
Lithocodium/ Bacinella
Oil stained Lithocodium/ Bacinella
Thallassinoides
Aggregate grains
Burrows
Compacted burrows
Stylolite
Corals
Gastropods
Echinoid Spines
Hardground/ Erosion surface

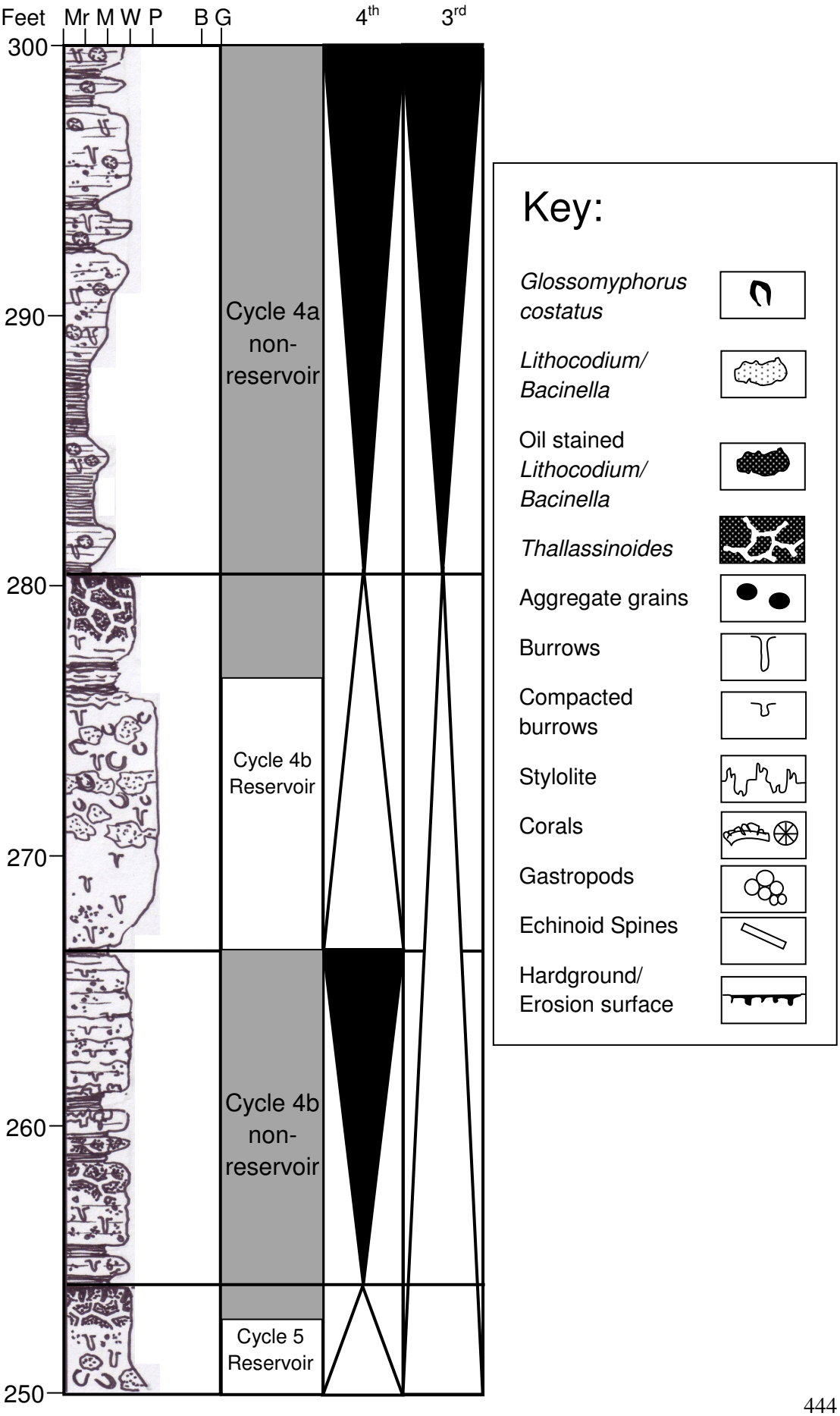
Feet
Mr M W P B G
4th
3rd
300
290
280
270
260
250
Cycle 4a non-reservoir
Cycle 4b Reservoir
Cycle 4b non-reservoir
Cycle 5 Reservoir
Key:
Glossomyphorus costatus
Lithocodium/ Bacinella
Oil stained Lithocodium/ Bacinella
Thallassinoides
Aggregate grains
Burrows
Compacted burrows
Stylolite
Corals
Gastropods
Echinoid Spines
Hardground/ Erosion surface

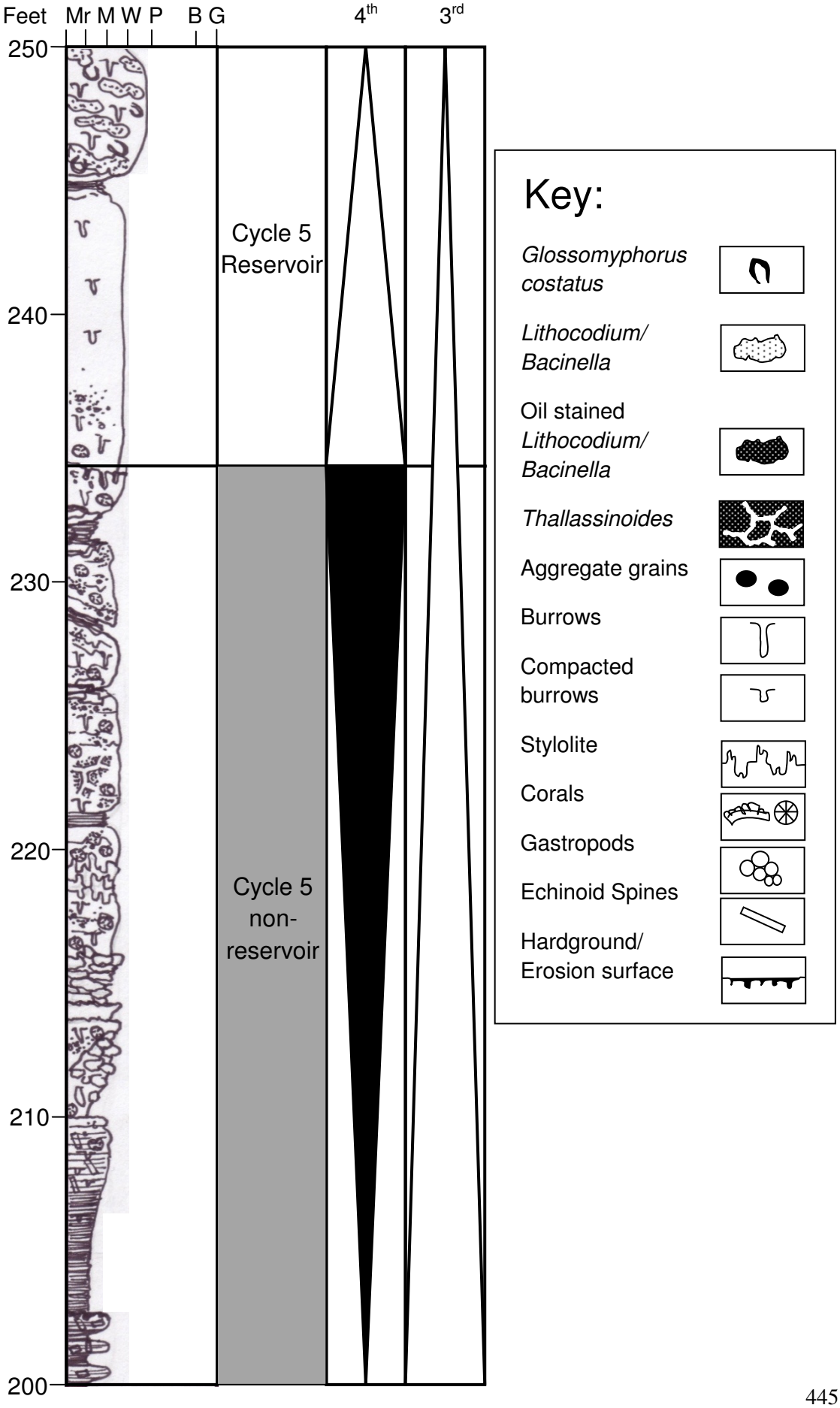
Feet
Mr M W P B G
4th
3rd
250
240
230
220
210
200
Cycle 5 Reservoir
Cycle 5 non-reservoir
Key:
Glossomyphorus costatus
Lithocodium/ Bacinella
Oil stained Lithocodium/ Bacinella
Thallassinoides
Aggregate grains
Burrows
Compacted burrows
Stylolite
Corals
Gastropods
Echinoid Spines
Hardground/ Erosion surface

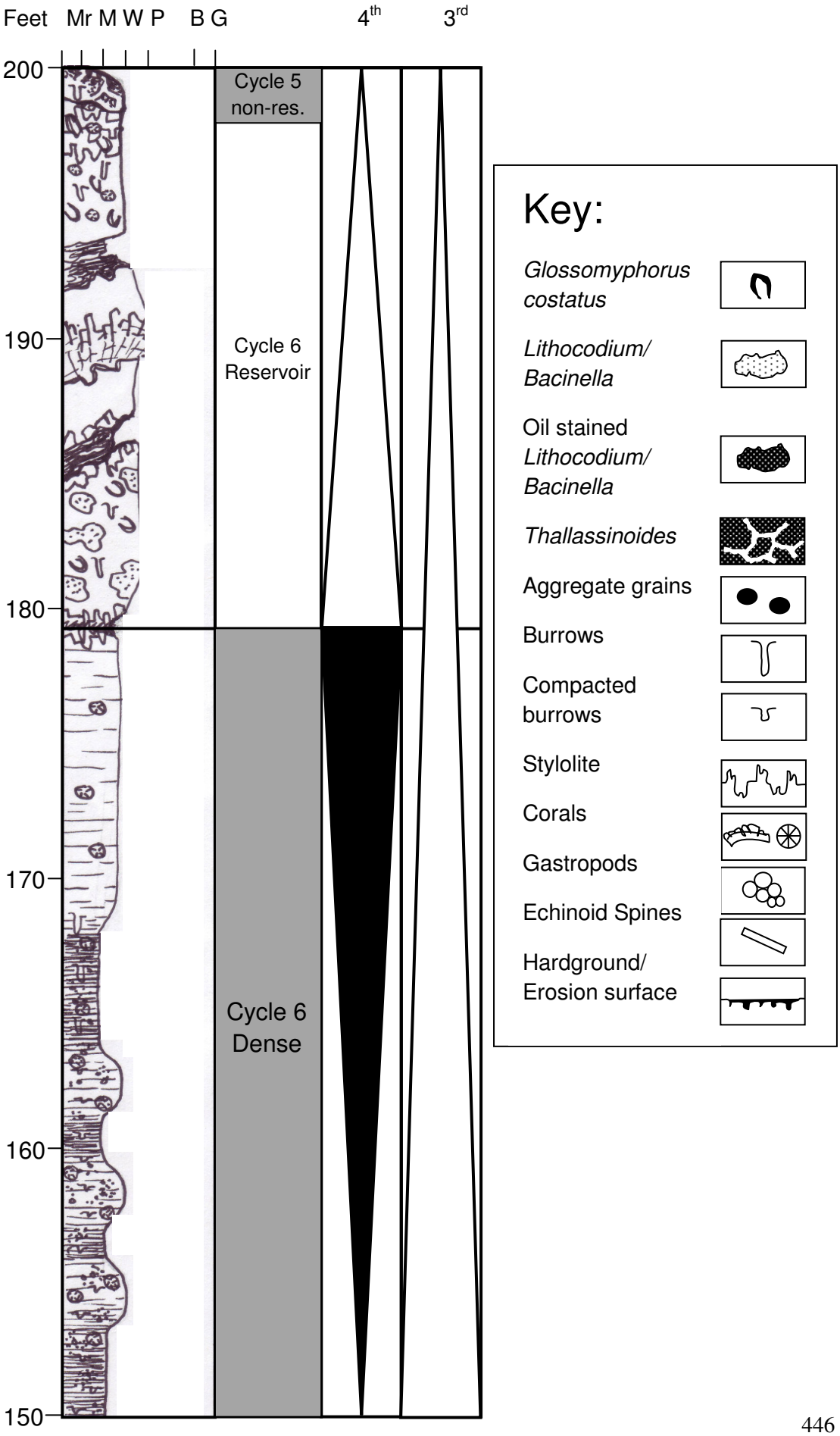
Feet
Mr M W P
B G
4th
3rd
200
190
180
170
160
150
Cycle 5
non-res.
Cycle 6
Reservoir
Cycle 6
Dense
Key:
Glossomyphorus costatus
Lithocodium/ Bacinella
Oil stained Lithocodium/ Bacinella
Thallassinoides
Aggregate grains
Burrows
Compacted burrows
Stylolite
Corals
Gastropods
Echinoid Spines
Hardground/ Erosion surface

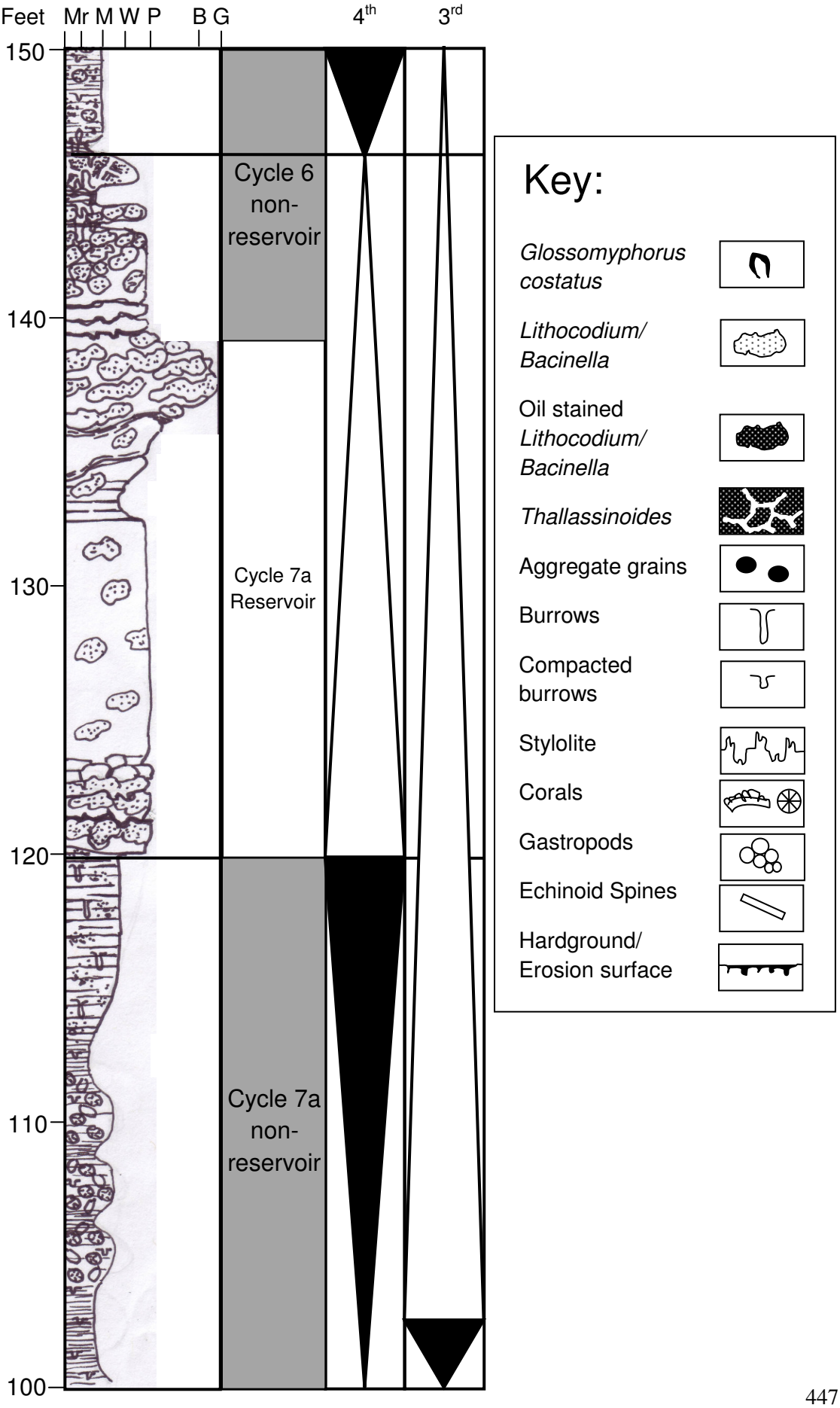
Feet
Mr M W P
B G
4th
3rd
150
140
130
120
110
100
Cycle 6 non-reservoir
Cycle 7a Reservoir
Cycle 7a non-reservoir
Key:
Glossomyphorus costatus
Lithocodium/ Bacinella
Oil stained Lithocodium/ Bacinella
Thallassinoides
Aggregate grains
Burrows
Compacted burrows
Stylolite
Corals
Gastropods
Echinoid Spines
Hardground/ Erosion surface

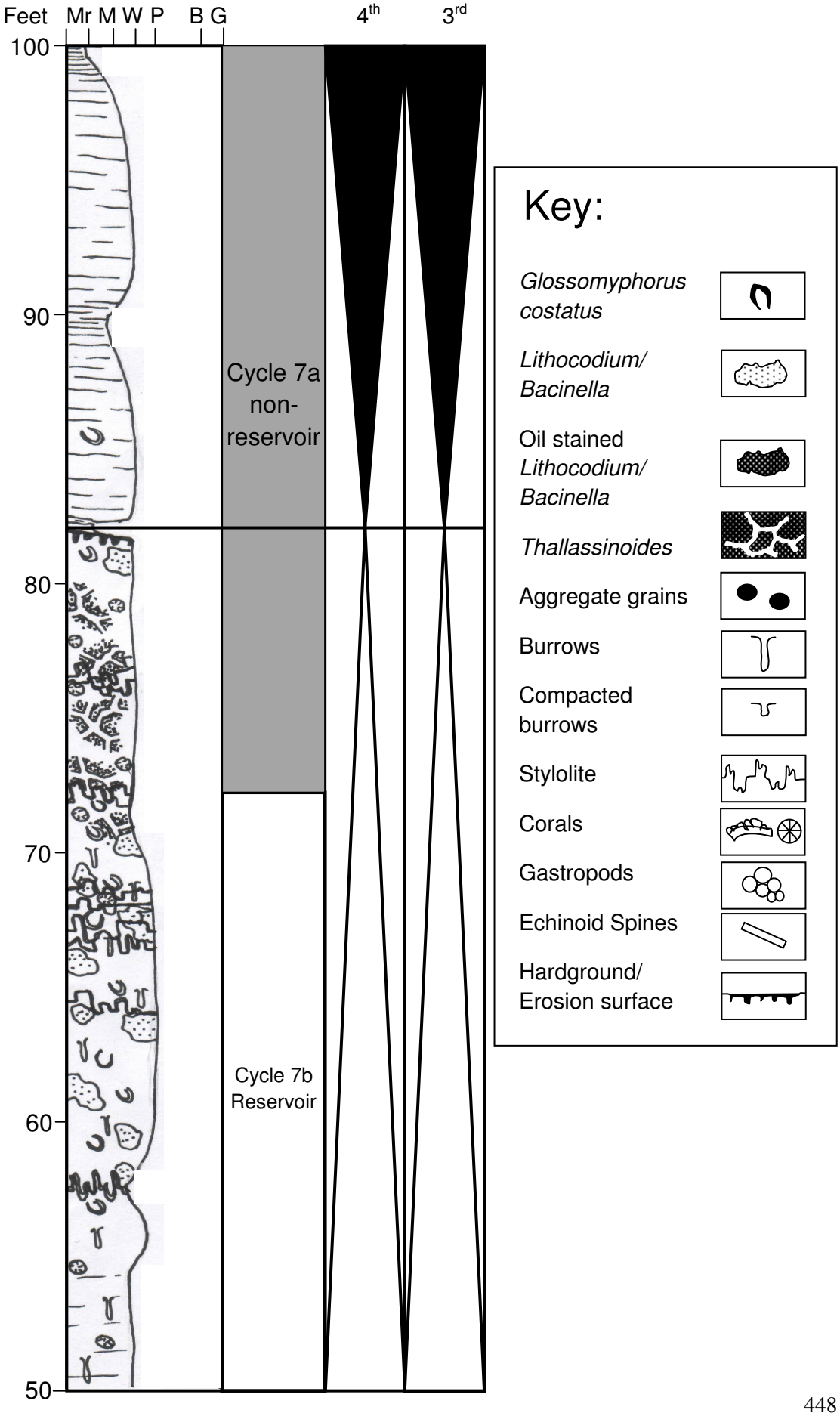
Feet
Mr M W P B G
4th
3rd
100
90
80
70
60
50
Cycle 7a non-reservoir
Cycle 7b Reservoir
Key:
Glossomyphorus costatus
Lithocodium/ Bacinella
Oil stained Lithocodium/ Bacinella
Thallassinoides
Aggregate grains
Burrows
Compacted burrows
Stylolite
Corals
Gastropods
Echinoid Spines
Hardground/ Erosion surface

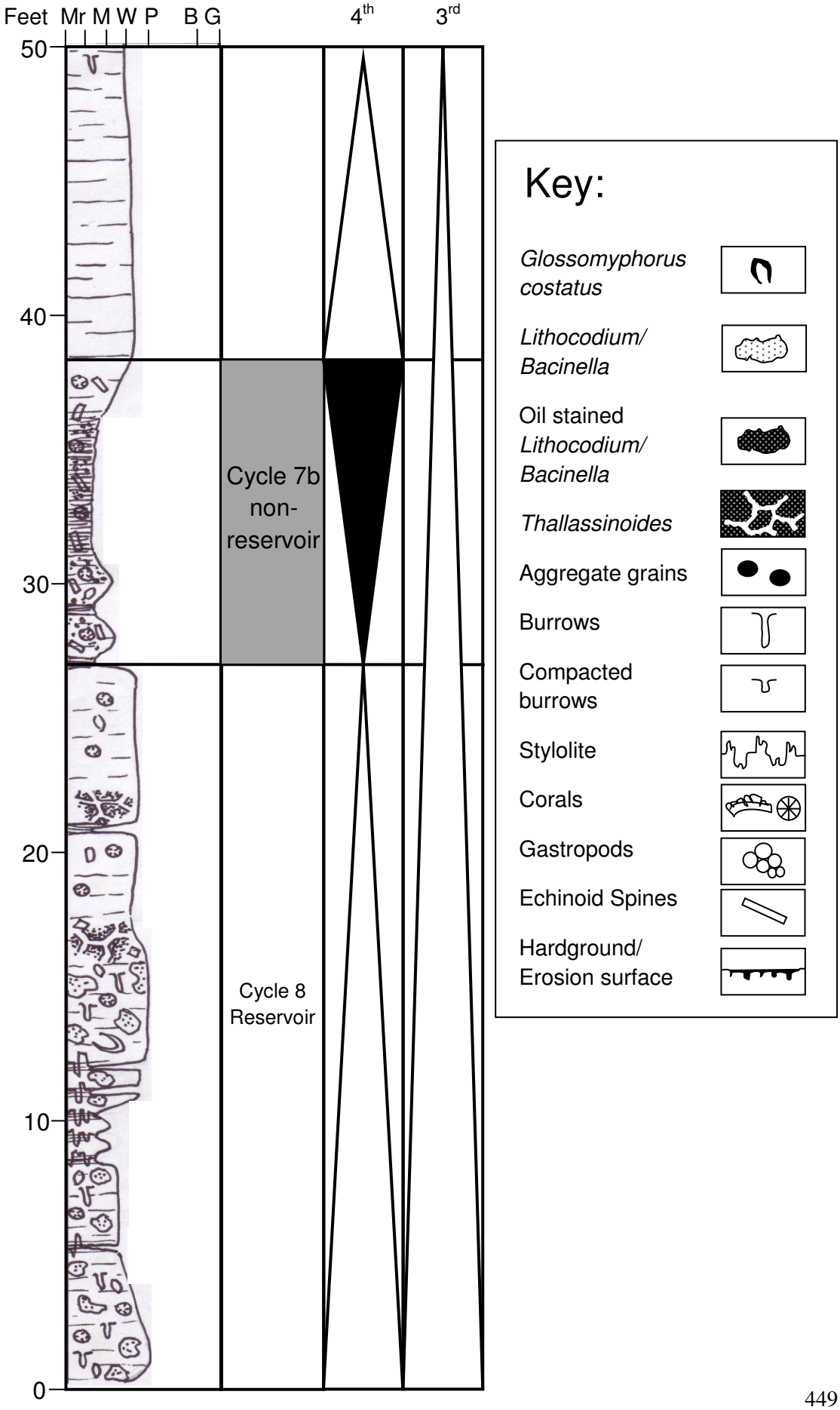
Feet
Mr
M
W
P
B
G
4th
3rd
50
40
30
20
10
0
Cycle 7b non-reservoir
Cycle 8 Reservoir
Key:
Glossomyphorus costatus
Lithocodium/ Bacinella
Oil stained Lithocodium/ Bacinella
Thallassinoides
Aggregate grains
Burrows
Compacted burrows
Stylolite
Corals
Gastropods
Echinoid Spines
Hardground/ Erosion surface

Appendix 3A

Manual macropore count data tables

The data in these tables relates to the manual counts of open macropore space in column 3, along with the counts of occluded (cemented) macropore space in column 4 (only from the reservoir horizons). Column 1 shows which 4th order HFC the thin sections are from and column 2 shows the specific depth in feet of each thin section. For Well 2-5 the depths were calculated by using the depth of Cycle 8 hardground (SB) as the base of the scale, whereas for Well 1, the depths were calculated using the base of the core as the base of the scale, which is close to Cycle 2a hardground (SB). Columns 5-8 show the manual counts of intra-skeletal pores, the amount of vugs, the amount of interparticle pores and the amount of fracture pore space, respectively. This data relates to Section 5.3.1, 5.3.2 and 5.3.4.

Cycle	Depth (ft)	A.	B.	C.	I. S.	S. M.	S. V.	L. V.	I. P.	F.
1	64	35.8	64.2	4867	6.1	0	0	0	93.9	0
1	62	19.9	80.1	3533	3.5	0	0	0	96.5	0
1	56	29.1	70.9	5636	0.06	0	1.54	0.2	98.2	0
1	45	36.7	63.3	7008	3.4	0.1	0	0	96.5	0
1	40	4.8	95.2	392	95.6	0	1.9	0.7	1	0.8
1	38	12.9	87.1	2407	48.4	0.2	0	0	51.3	0.1
1	28	6.6	93.4	348	40.2	2.9	16.7	0	40.2	0
1	27	22.8	77.2	1405	34.1	0.4	0	0	65.5	0.1
1	26	4.7	95.3	941	4.5	0.4	0	1.5	93.6	0
1	0	22.5	77.5	967	54.1	0	0	0	45.7	0.2

Table 3A.1: Well 1: % open macroporosity and amount of macropore types. A represents the percentage of open macropores, B represents the percentage of occluded macropores and C represents the total number of macropores counted. The initials I. S. represents Intra-Skeletal pores, S. M. represents Small Moulds, S. V. represents Small Vugs, L. V. represents Large Vugs, I. P. represents Interparticle pores and F. represents Fractures.

Cycle	Depth (ft)	A.	B.	C.	I. S.	S. M.	S. V.	L. V.	I. P.	F.
4a	238	26.8	73.2	712	22.2	0	0	0	77.8	0
4a	234	0	100	353	59.7	0	0	0	40.3	0
4a	231	9	91	789	56.9	0	0	0	43.1	0
4a	231	66.3	33.7	463	66.6	0	0	0	33.4	0
4a	229	15.9	84.1	646	6.6	0.2	10.4	1.7	81.1	0
4a	227	34.3	65.7	300	80.6	2.4	0	0	17	0
4a	227	42.7	57.3	232	89.3	0.4	1.7	0	8.6	0
4a	202	0	100	546	30.8	0.3	53.8	2.6	12.3	0.2
4b	198	38.1	61.9	580	100	0	0	0	0	0
4b	194	2.9	97.1	206	97.1	1	0	0	0	1.9
4b	191	45.6	54.4	590	81.5	0.2	0	0	18.3	0
7a	92	71.5	28.5	1188	34.1	0	0	0.1	65.7	0.1
7a	83	62.9	37.1	793	92.9	0	0	0	7.1	0
7a	82	69.9	30.1	1048	88.3	0	0	0.3	11.4	0
7a	75	92.8	7.2	1357	88.1	0	0	0	11.9	0
7a	74	96.8	3.2	650	66.8	1.7	0	0	31.5	0
7b	25	73.3	26.7	609	83.1	0.7	0	0	16.2	0
7b	24	92.4	7.6	1059	80	0.8	0.3	0.1	18.8	0

Table 3A.2: Well 2: % open macroporosity and amount of macropore types. A represents the percentage of open macropores, B represents the percentage of occluded macropores and C represents the total number of macropores counted. The initials I. S. represents Intra-Skeletal pores, S. M. represents Small Moulds, S. V. represents Small Vugs, L. V. represents Large Vugs, I. P. represents Interparticle pores and F.

Cycle	Depth (ft)	A.	B.	C.	I. S.	S. M.	S. V.	L. V.	I. P.	F.
4a	232	81.8	18.2	303	42.9	1	0	0	56.1	0
4a	231	77.5	22.5	720	81	0.8	0	0	18.2	0
4a	227	77.5	22.5	1663	5.8	0.3	0	14.6	79.1	0.2
4a	227	94.8	5.2	1135	10.8	0.2	0	3.2	85.8	0
4a	224	82.8	17.2	64	78.2	0	0	0	21.8	0
4b	196	7	93	776	61.1	0.8	0	0	37.9	0.2
4b	191	63	37	884	12	0	0	0	88	0
4b	186	10.2	89.8	235	69.7	0	0.5	0	29.8	0
4b	177	77.6	22.4	920	72.1	0	0	0	27.9	0
7a	91	81.4	18.6	781	74.2	1.3	0	2.2	22.3	0
7a	90	62	38	716	79	1.5	0	0	19.5	0
7a	90	0.3	99.7	610	55.2	0	0	0	44.8	0
7a	87	68	32	972	36.8	0	0	1.3	61.5	0.4
7a	83	71.3	28.7	878	78.9	0.2	0	0	20.9	0

Table 3A.3: Well 3: % open macroporosity and amount of macropore types. A represents the percentage of open macropores, B represents the percentage of occluded macropores and C represents the total number of macropores counted. The initials I. S. represents Intra-Skeletal pores, S. M. represents Small Moulds, S. V. represents Small Vugs, L. V. represents Large Vugs, I. P. represents Interparticle pores and F. represents Fractures.

Cycle	Depth (ft)	A.	B.	C.	I. S.	S. M.	S. V.	L.V.	I. P.	F.
1	448	87.4	12.6	2508	45.4	4.2	0	0	50.4	0
1	445	96.9	3.1	2000	22.8	6.3	0	0	70.9	0
1	434	44.5	55.5	1266	3.6	0.8	0	0	95.6	0
1	431	92.7	7.3	328	78	22	0	0	0	0
1	416	78.8	21.2	231	0	0	0	12.9	87.1	0
1	398	39.5	60.5	114	0	0	0	3.4	96.6	0
1	389	98	2	53	0	0	100	0	0	0
1	381	12.8	87.2	55	85.7	1.8	0	0	12.5	0
4a	203	25.9	74.1	147	42.4	0	0	0	57.6	0
4a	195	0	100	22	15.3	0	0	0	84.7	0
4b	170	3.5	96.5	352	28.6	0	0	0	71.1	0.3
4b	168	0	100	283	7.1	0	0	92.9	0	0
4b	166	0	100	170	34.1	0	0	25.9	40	0
5	141	79.8	20.2	109	87.1	0	5	0	7.2	0.7
6	75	0	100	193	55	44.5	0	0	0	0.5
7a	69	0	100	195	0	4.1	0	95.9	0	0
7a	67	98.9	1.1	848	98.8	0	0	0.1	1	0.1
7a	62	70	30	773	36.8	0	0	1.3	61.5	0.2
7a	59	8.1	91.9	591	78.9	0	0	0.1	21	0

Table 3A.4: Well 4: % open macroporosity and amount of macropore types. A represents the percentage of open macropores, B represents the percentage of occluded macropores and C represents the total number of macropores counted. The initials I. S. represents Intra-Skeletal pores, S. M. represents Small Moulds, S. V. represents Small Vugs, L. V. represents Large Vugs, I. P. represents Interparticle pores and F. represents Fractures.

Cycle	Depth (ft)	A.	B.	C.	I. S.	S. M.	S. V.	L. V.	I. P.	F.
1	457	10.1	89.9	2249	2.9	0	0	0	96.8	0.3
1	451	44.5	55.5	524	12	0	2.5	1.1	84	0.4
1	401	86.2	13.8	80	18.8	0	0	0	81.2	0
4a	228	86.2	13.8	1091	95.6	1.8	2.3	0	0	0.3
4a	225	62.4	37.6	771	99.7	0	0.2	0	0	0
4a	222	53.8	46.2	208	72.6	0.5	26.5	0	0	0.4
4a	216	0	100	152	100	0	0	0	0	0
4a	212	60.3	39.7	284	31.3	0	14.8	0	52.4	1.5
4b	186	0	100	226	27.4	9.7	0	0	62	0.9
4b	183	72.8	27.2	946	5.3	0	0	0	94.7	0
4b	180	0.9	99.1	112	99.1	0	0.9	0	0	0
6	90	15.3	84.7	456	33.3	0.3	0	0	65.1	1.3
7a	88	59.1	40.9	993	41.1	0	0	1.3	57.6	0
7a	85	0	100	801	97.4	0	2.5	0.1	0	0
7a	82	26.1	73.9	1408	100	0	0	0	0	0
7a	80	92.9	7.1	1970	84.1	0	0	0	15.9	0
7a	72	94.4	5.6	1408	84.5	1.3	0	0	14.2	0
7a	69	35.6	64.4	1029	71	0.3	0	0	28.3	0.4

Table 3A.5: Well 5: % open macroporosity and amount of macropore types. A represents the percentage of open macropores, B represents the percentage of occluded macropores and C represents the total number of macropores counted. The initials I. S. represents Intra-Skeletal pores, S. M. represents Small Moulds, S. V. represents Small Vugs, L. V. represents Large Vugs, I. P. represents Interparticle pores and F.

Appendix 3B

Macropore type graphs (Wells 1, 2, 3 & 5)

These graphs show the manually counted macropore types from the same 2" by 3" thin sections used for petrographic analysis. The data is plotted as percentages. The y-axis relates to the individual depths in feet of each thin section. For Well 2-5 the depths were calculated by using the depth of Cycle 8 hardground (SB) as the base of the scale, whereas for Well 1, the depths were calculated using the base of the core as the base of the scale, which is close to Cycle 2a hardground (SB). This data relates to Section 5.3.4, where the data table for Well 4 is shown.

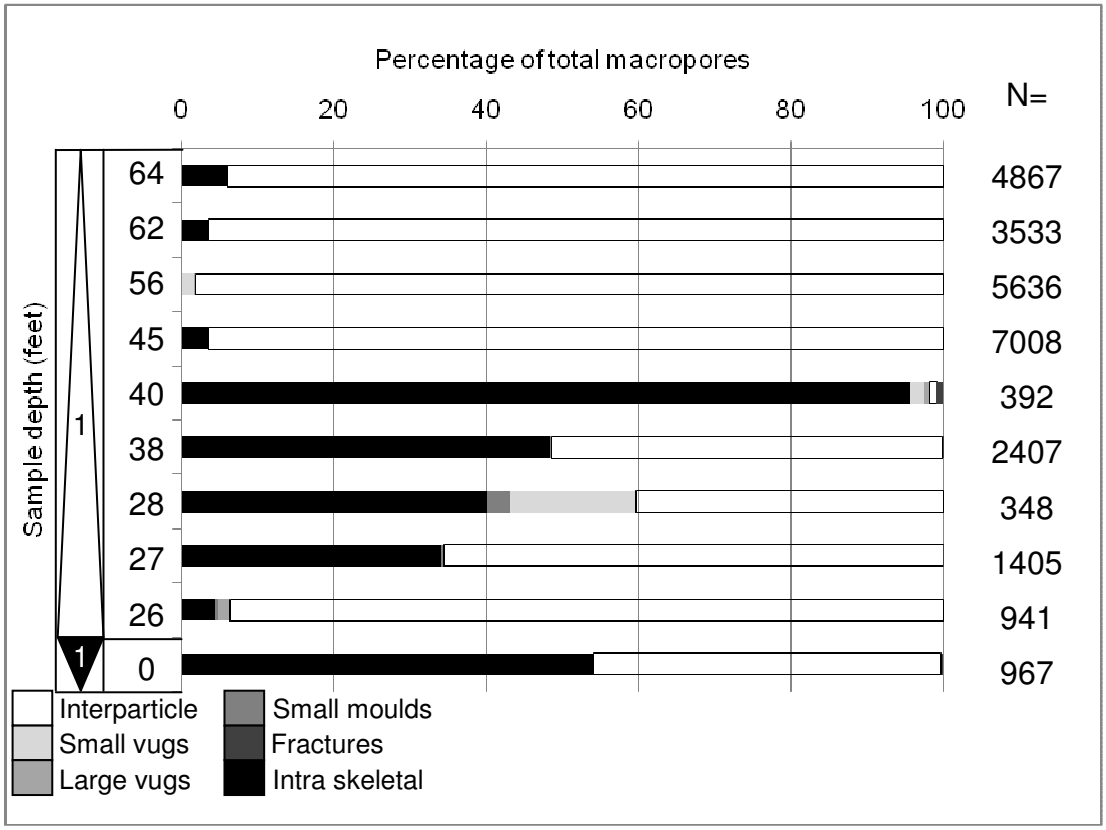

Graph 3B.1: Macropore type data for Well 1

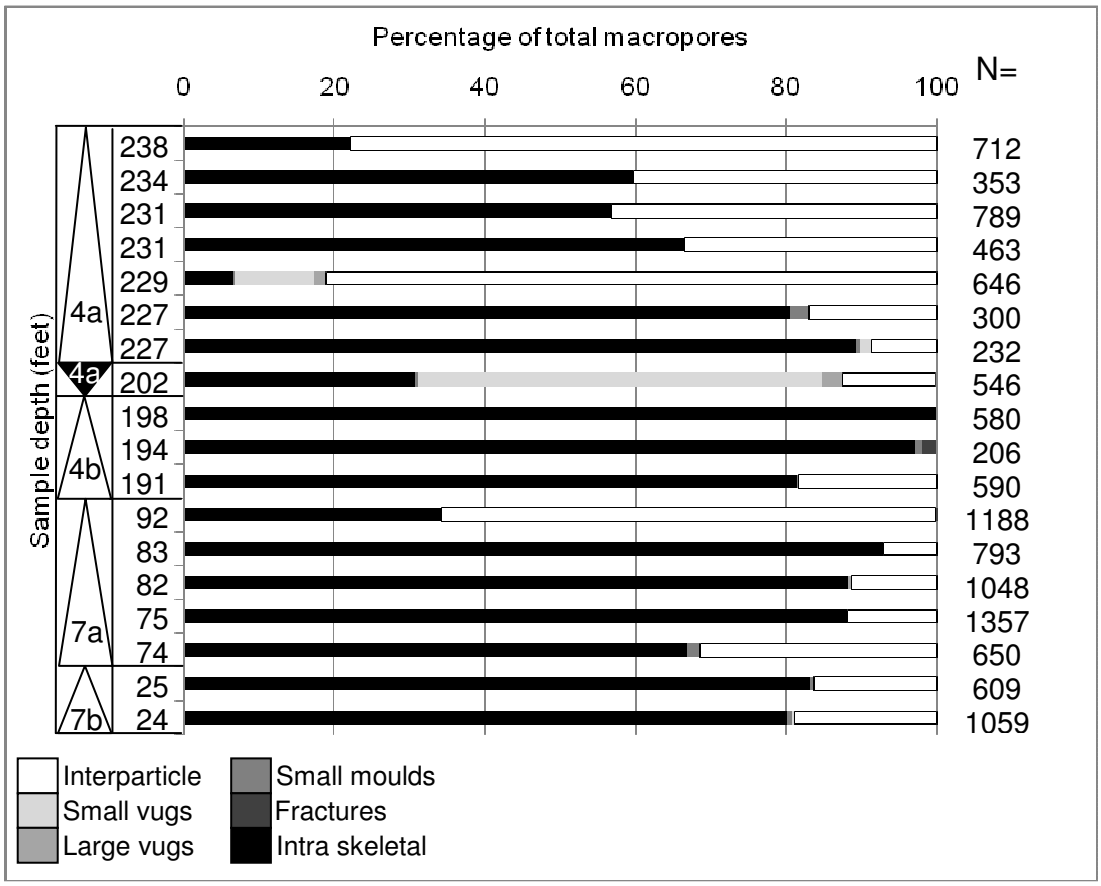

Graph 3B.2: Macropore type data for Well 2

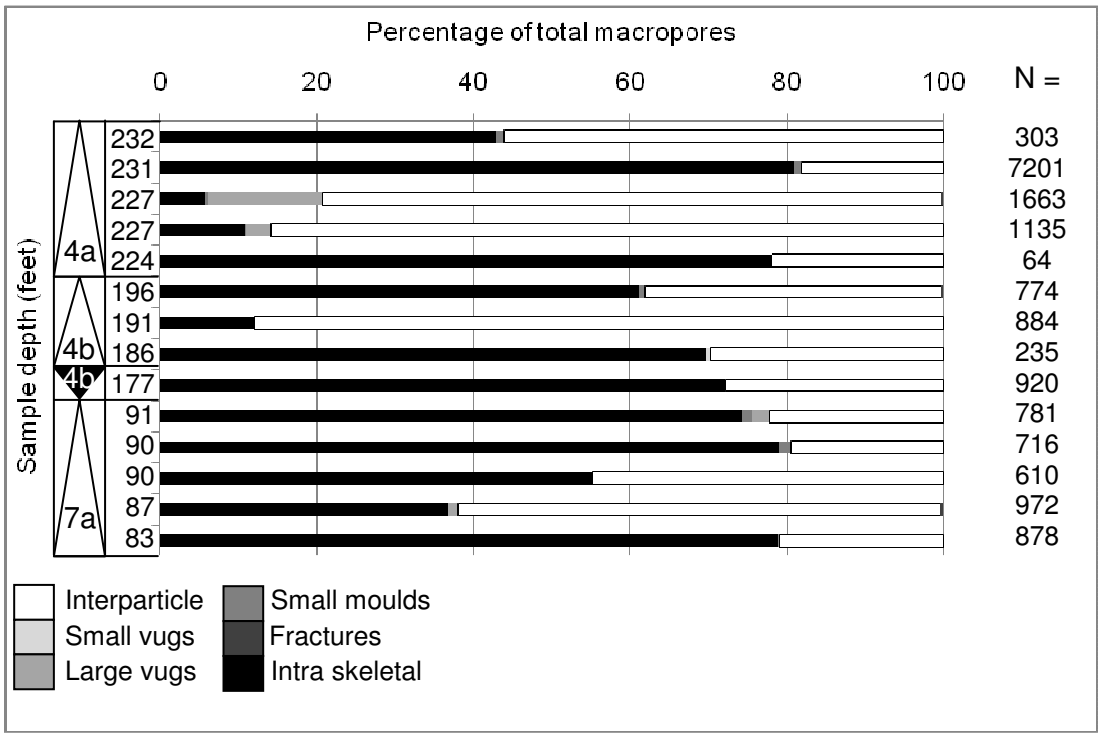

Graph 3B.3: Macropore type data for Well 3

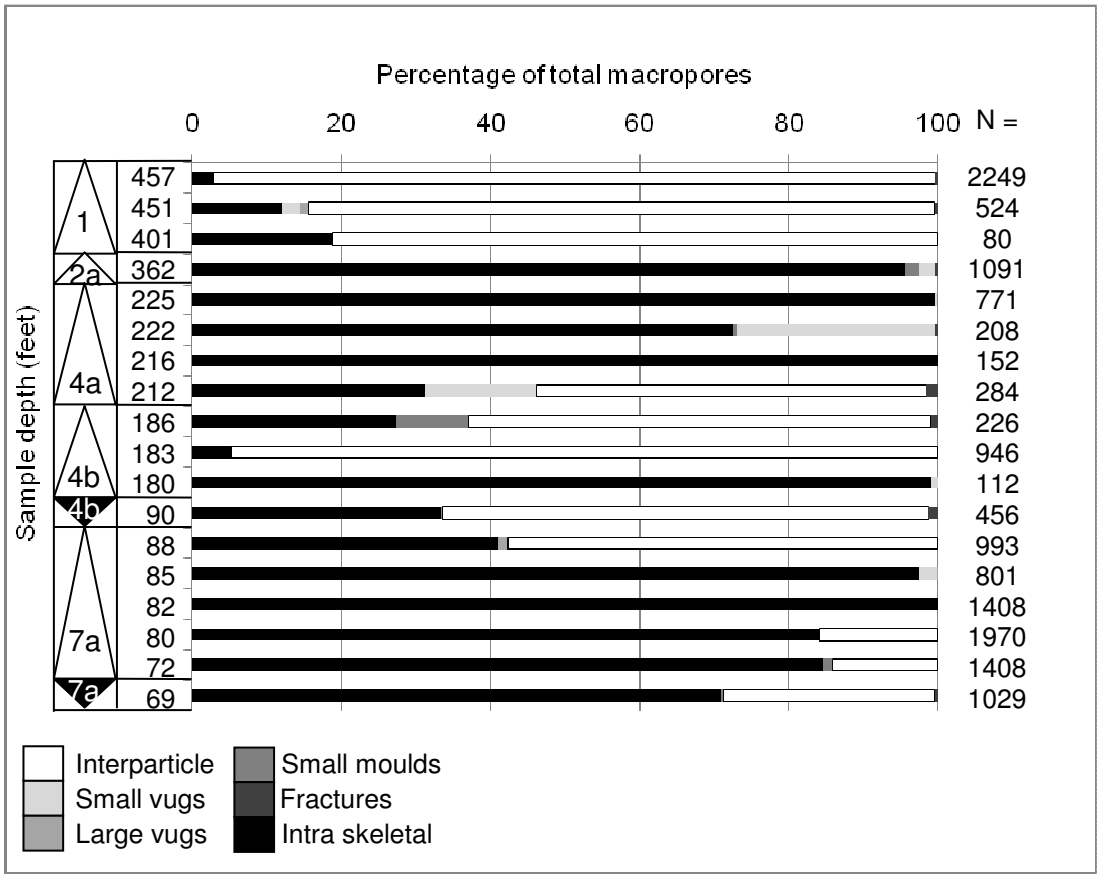

Graph 3B.4: Macropore type data for Well 5

Appendix 4

Stable $\delta^{18}O_{VPDB}$ and $\delta^{13}C_{VPDB}$ data tables

The stable $\delta^{13}C_{VPDB}$ and $\delta^{18}O_{VPDB}$ data is displayed in these tables, which was collected manually using a steel handpick. Column 1 shows the depths in feet where the data was collected from: for Wells 2-5, the depths are calculated using Cycle 8 hardground (SB) as the base of the scale, whereas for Well 1 the depths are calculated from the base of the core, which is close to Cycle 2a hardground (SB). Column 2 shows the $\delta^{13}C$ data whereas column 3 shows the $\delta^{18}O$ data. This data is shown in Sections 6.2.1 and 6.2.2.

HFC	Sample depth	$\delta^{13}C$	$\delta^{18}O$
4a	232	2	-3.7
4a	232	2.7	-4.0
4a	231	2.4	-4.2
4a	227	2.2	-3.7
4a	227	2.3	-3.8
4a	224	2.6	-4.6
4a	218	2.9	-5.0
4a	210	2.2	-5.0
4a	198	1.3	-3.3
4b	196	1.9	-3.6
4b	191	2.1	-4.0
4b	186	1.8	-5.2
6	109	0.4	-4.4
6	101	0.8	-3.8
6	96	1.4	-4.1
7a	91	1.9	-3.5
7a	90	2.1	-4.5
7a	90	2.1	-4.2
7a	87	1.9	-4.9
7a	83	2.1	-3.7
7a	83	2.1	-3.9
7a	75	2.1	-4.7

Table 4.1: Well 3: Oil leg bulk micrite

HFC	Sample depth	$\delta^{13}C$	$\delta^{18}O$
1	513	3.4	-5.5
1	459	2.9	-5.5
1	448	2.9	-5.9
1	445	3	-6.9
1	434	3.2	-6.6
1	431	2.9	-7.0
1	416	3.1	-6.7
1	398	3.2	-6.7
1	389	3.3	-6.4
1	379	3.4	-4.7
1	206	2.1	-7.1
4a	195	2.3	-5.5
4a	185	2.1	-4.7
4a	178	1.5	-3.2
4a	175	1.4	-3.4
4b	170	1.9	-6.1
4b	168	2	-5.6
4b	166	1.8	-6.8
5	97	1.7	-5.8
6	89	1.1	-3.9
6	81	0.9	-3.6
6	75	1.8	-6.1
7a	69	2	-6.1
7a	69	1.9	-5.7
7a	69	1.8	-6.5
7a	67	1.9	-7.0
7a	62	1.9	-6.4
7a	59	1.9	-5.8
7a	58	1.8	-5.3
7a	57	1.8	-4.0
7a	56	1	-5.6
7a	54	-0.1	-3.6

Table 4.2: Well 4: Oil leg bulk micrite

HFC	Sample depth	$\delta^{13}C$	$\delta^{18}O$
3	244	1.5	-4.1
3	243	1.5	-4.2
4a	241	1.5	-3.1
4a	241	2.5	-3.2
4a	238	2.7	-3.2
4a	234	2.5	-5.0
4a	231	2.7	-3.5
4a	231	2.8	-3.7
4a	229	2.7	-4.0
4a	227	2.5	-3.3
4a	227	2.5	-4.4
4a	224	2.2	-4.6
4a	222	2.3	-3.9
4a	220	2.3	-5.2
4a	219	1.9	-4.4
4a	218	2.3	-4.0
4a	216	2.3	-4.6
4a	214	2.1	-3.9
4a	213	1.9	-4.0
4a	213	2.2	-3.4
4a	213	1.5	-4.2
4a	211	1.1	-4.3
4a	207	1.4	-3.5
4a	204	0.6	-3.6
4a	203	0.7	-2.4
4a	202	1	-2.7
4b	198	1.6	-4.3
4b	194	2.1	-4.6
4b	186	1.9	-3.9
4b	181	0.1	-3.1
4b	177	0	-2.8
6	110	1.3	-4.3
6	107	1.1	-4.2
6	104	0.3	-3.2
6	104	0.4	-3.7
7a	92	2.2	-3.2
7a	83	2.1	-3.9
7a	82	2.1	-4.5
7a	75	2	-4.3
7a	74	2	-4.3
7b	25	1.9	-3.5
7b	24	1.8	-5.1

Table 4.3: Well 2: Transition zone bulk micrite

HFC	Sample depth	$\delta^{13}C$	$\delta^{18}O$
1	64	2.6	-7.3
1	62	2.8	-7.9
1	56	3	-7.5
1	45	3.2	-7.3
1	40	3.1	-7.7
1	38	3.3	-7.5
1	28	4.3	-7.5
1	27	2.8	-7.4
1	26	3.2	-7.4
1	0	3.3	-6.1

Table 4.4: Well 1: Water leg bulk micrite

HFC	Sample depth	$\delta^{13}C$	$\delta^{18}O$
1	457	3	-7.0
1	451	3.1	-6.6
1	401	3	-6.1
3	251	1.7	-4.6
3	246	1.2	-3.5
3	242	1.3	-3.5
3	235	1.8	-4.0
4a	228	2.7	-4.0
4a	225	2.7	-4.5

Table 4.5: Well 5: Transition zone bulk micrite

HFC	Sample depth	$\delta^{13}C$	$\delta^{18}O$
1	448	2.3	-8
1	448	2.9	-8
1	445	2.9	-8.4
1	445	2	-9.8
1	431	3.3	-5.8
1	185	1.5	-8.8
4b	168	1.5	-9.5
4b	166	1.8	-7.6
4b	166	1.7	-7.5
4b	166	1.3	-8.5
6	81	1.2	-9.3
6	75	1	-9.3

Table 4.6: Well 4: Oil leg LMC cements

HFC	Sample depth	$\delta^{13}C$	$\delta^{18}O$
4a	231	1.6	-8.8
4a	231	1.7	-8.3
4a	231	2.1	-8.8
4a	231	1.7	-8.3
4a	227	1.5	-9.3
4a	227	2	-8.3
4a	227	2.3	-8.3
4a	227	2.3	-8.2
4a	227	1.7	-9.3
4b	196	1	-9.7
7a	91	0.9	-8.6

Table 4.7: Well 3: Oil leg LMC cements

HFC	Sample depth	$\delta^{13}C$	$\delta^{18}O$
4a	241	2.4	-5.6
4a	241	1.9	-5.5
4a	231	2.4	-7.9
4a	231	1.7	-8.8
4a	229	2.1	-8.3
4a	229	1.8	-8.2
4a	227	1.8	-8.8
4a	219	2	-8.5
4b	181	1.2	-9.0
6	107	1.2	-9.0
7a	83	1.5	-8.2
7a	83	1.5	-8.3

Table 4.8: Well 2: Transition zone LMC cements

HFC	Sample depth	$\delta^{13}C$	$\delta^{18}O$
1	62	2.9	-8.6
1	56	2.9	-8.5
1	40	2.3	-5.9
1	38	3	-8.7
1	38	2.7	-8.7
1	28	2.8	-8.4
1	28	3.2	-8.3
1	28	2.4	-8.9
1	28	2.7	-8.6
1	28	2.6	-8.6

Table 4.9: Well 1: Water leg LMC cements

HFC	Sample depth	$\delta^{13}C$	$\delta^{18}O$
7a	58	1.2	-9.3
7a	57	1.3	-9.9
7a	57	1.1	-9.4
7a	56	1.4	-8.7
7a	58	1	-9.0
7a	56	1.1	-8.9
7a	57	1.5	-8.5
7a	58	1.4	-8.8
7a	58	1.1	-9.7
7a	56	0.9	-9.9
7a	54	0.8	-9.7
7a	57	1.4	-9.5

Table 4.10: Fault LMC cements: Well 4

Well	HFC	Sample depth	$\delta^{13}C$	$\delta^{18}O$
4	1	389	4.1	-5.4
4	1	389	4.1	-5.5
4	1	389	3	-6.4
2	4a	202	2.4	-4.1
2	4a	202	2.2	-3.9
2	4a	202	2.1	-5.2
4	4a	178	1.7	-2.9
4	4a	175	1.7	-3.1
5	7a	80	1.6	-2.5
5	3	251	2.8	-5.1

Table 4.11: Dolomite rhomb cements within Thallassinoides *(grey rows) and the matrix (white rows).*

Well	HFC	Sample depth	$\delta^{13}C$	$\delta^{18}O$
4	4b	170	2.3	-6.1
4	4b	170	2	-7.6
4	4b	170	2.5	-6.9
4	6	75	2.2	-6.8
4	6	75	2.1	-7.3
4	6	75	2	-7.3
2	7b	25	1.5	-8.4
3	7a	91	1.6	-6.4
3	7a	83	2.5	-5.3

Table 4.12: Saddle dolomite cements

Appendix 5

Microporosity data tables

The data tables show the amount of microporosity that was calculated by the method outlined in Section 1.2. Column 1 shows the depth in feet that related to the individual 2" by 2" thin sections (same ones used for petrographic analysis) that the percentage of microporosity was calculated. For Well 2-5 the depths were calculated by using the depth of Cycle 8 hardground (SB) as the base of the scale, whereas for Well 1, the depths were calculated using the base of the core as the base of the scale, which is close to Cycle 2a hardground (SB). Column 2 shows the percentage of open porosity calculated from mercury injection commercially. Column 3 shows the percentage of microporosity attributed to each thin section. This data relates to Section 7.2.

Depth (feet)	Total porosity (%)	Microporosity (%)
64	2.3	2
62	12.6	12.6
56	21	21
45	19.4	19.4
40	17.3	17.3
38	20.58	20.3
28	20.6	20.6
27	20.6	20.6
26	20.9	20.9
0	20.3	20.3

Table 5.1: microporosity data for Well 1. The percentages were calculated with respect to the total core plug volume.

Depth (feet)	Total porosity (%)	Microporosity (%)
229	14.5	1.1
219	5.9	5.4
213	2.6	2.6
194	1.1	0.9
191	7.3	6.5
186	1.8	1.5
181	2.2	0.8
177	0.9	0.9
110	0.4	0.4
107	1.5	1.5
104	5	5
104	5	4.4
92	14.1	13.6
83	10.7	4.3
75	17.3	16.7
74	17.4	16.3

Table 5.2: microporosity data for Well 2. The percentages were calculated with respect to the total core plug volume.

Depth (feet)	Total porosity (%)	Microporosity (%)
231	5.89	1.8
227	14.56	10.8
227	18.46	17.2
224	17.73	16.6
210	9	8.9
198	9	9
196	9	8.2
191	13.35	12.4
186	16.86	9.4
91	15.58	14.4
90	19.21	18.8
90	9.18	8.7
83	13.88	12.2
75	28.19	10.1

Table 5.3: microporosity data for Well 3. The percentages were calculated with respect to the total core plug volume.

Depth (feet)	Total porosity (%)	Microporosity (%)
513	6.9	5.9
459	3.5	2.1
448	3.9	0.2
434	32.3	31.9
431	24.1	14.7
416	28.7	15.2
398	27	17.6
389	32.1	3.8
381	23.2	16.9
379	15.2	15.2
195	1.4	0.8
185	0.1	0.1
178	3.9	3.9
175	6.4	4.7
170	0.8	0.7
168	2.6	1.7
166	10.2	7.1
97	0.4	0.4
89	0.3	0.3
81	0.1	0.1

Table 5.4: microporosity data for Well 4. The percentages were calculated with respect to the total core plug volume.

Depth (feet)	Total porosity (%)	Microporosity (%)
246	1.3	0.8
242	1	0.5
235	2.1	1.6
231	2.2	2.2
228	2.6	1.8
225	8.4	7.9
222	9.1	6.7
216	15	14.4
212	2	2
199	0.7	0.1
193	2.8	2.3
183	10.1	8.8
104	0.9	0.4
99	1.3	0.8
91	2.2	2.2
90	1.1	0.3
88	8.1	0.7
85	1.6	0.5
82	10	5.7
80	17.3	16.1
72	20.6	19.9
69	8.3	7.8

Table 5.5: microporosity data for Well 5. The percentages were calculated with respect to the total core plug volume

Appendix 6

Porosity and Permeability plots

The scatter plots labelled A in Figures 6.1-6.34 show the porosity data plotted against stratigraphic depth (in feet) from the SB of Cycle 8 in the Lower Lekhwair Formation.

The scatter plots labelled B in Figures 6.1-6.34 show the permeability data plotted against stratigraphic depth (in feet) from the SB of Cycle 8 in the Lower Lekhwair Formation. Both A and B scatter plots have a column to the left of each plot displaying the HST (white triangles) and the TST (black triangles) sequences.

The scatter plots labelled C in Figures 6.1-6.34 shows the porosity and permeability data plotted according to the different lithologies. These general lithologies are described in Section 3.4.1 and also displayed in the summary diagrams in Section 8.2.2. The lithologies are colour coded: the AM are black diamonds, the PM are black squares, the *o*SH are white triangles, the BW are white diamonds, the *gl*WP are white squares, the *l*B are white triangles and the *gl*PG are black stars.

The scatter plots labelled D in Figures 6.1-6.34 shows the porosity and permeability data plotted according to the reservoirs and non-reservoirs. The data representing the reservoirs are white diamonds whereas the data representing the non -reservoirs are black diamonds. The dashed lines represent the 4^{th} order SB's bounding the individual 4^{th} order HFC's.

Well 1

Cycle 1

Well 1 only covers the Lower Kharaib Formation in the water leg. The porosity throughout Cycle 1 is 10-22% while the permeability is 0.1-9.5mD (Figs. 6.1A & 6.1B). This HFC mainly consists of BW, and *gl*WP, which are dominantly concentrated in micrite grains (Figs. 6.1C & 6.1D). There is abundance in interparticle porosity. This produces a well connected interparticle pore system which is reflected in the porosity and permeability data.

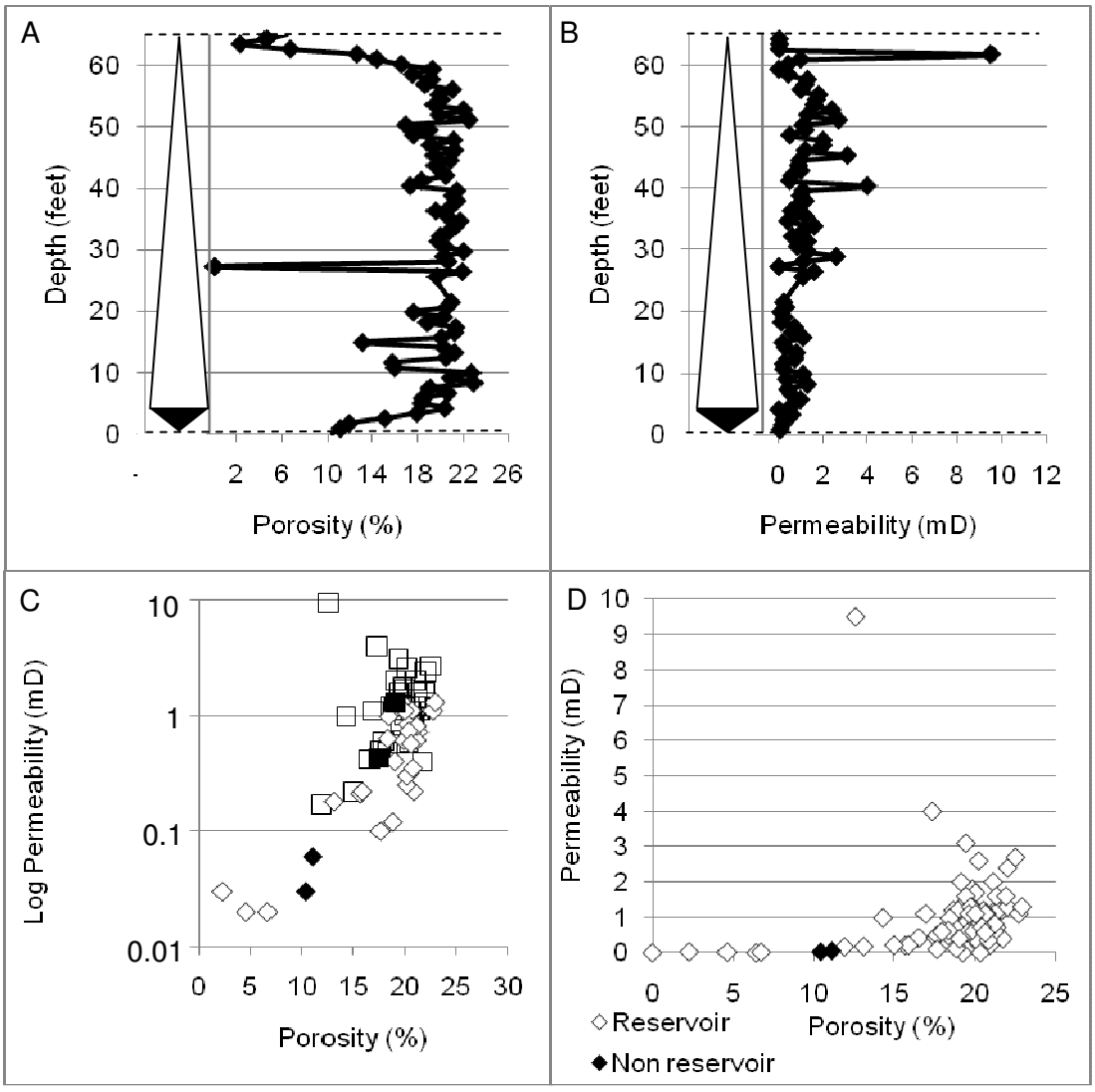

Figure 6.1: porosity and permeability data for Cycle 1, Well 1: A) porosity data against depth, B) the permeability data against depth, C) porosity and permeability relationships with respect to the lithologies and D) the porosity and permeability relationships with respect to the reservoirs and non-reservoirs.

Well 2

Cycle 4a

Within Cycle 4a there are three separate horizons with the first two measuring ~10ft in thickness with porosity of 15-11% and 15-8% and a maximum permeability of 16mD and 10mD, respectively (Figs. 6.2A & 6.2B). The third porosity high is at the base of the HST, measuring ~5ft in thickness with porosity of 5-7%. The permeability spikes are localised to a couple of feet in thickness and only correspond to the top two porosity highs. These two horizons are associated with the BW, just below the firmground assemblage, and the *glPG* within the mid-late HST and the reservoir (Figs. 6.2C & 6.2D). The horizon separating the two porosity highs is comparable to the non-reservoirs of the firmgrounds above and the TST micrites/mudstones below with porosity of 0.5% and a permeability of 0.8-0.01mD (Figs. 6.2A & 6.2D).

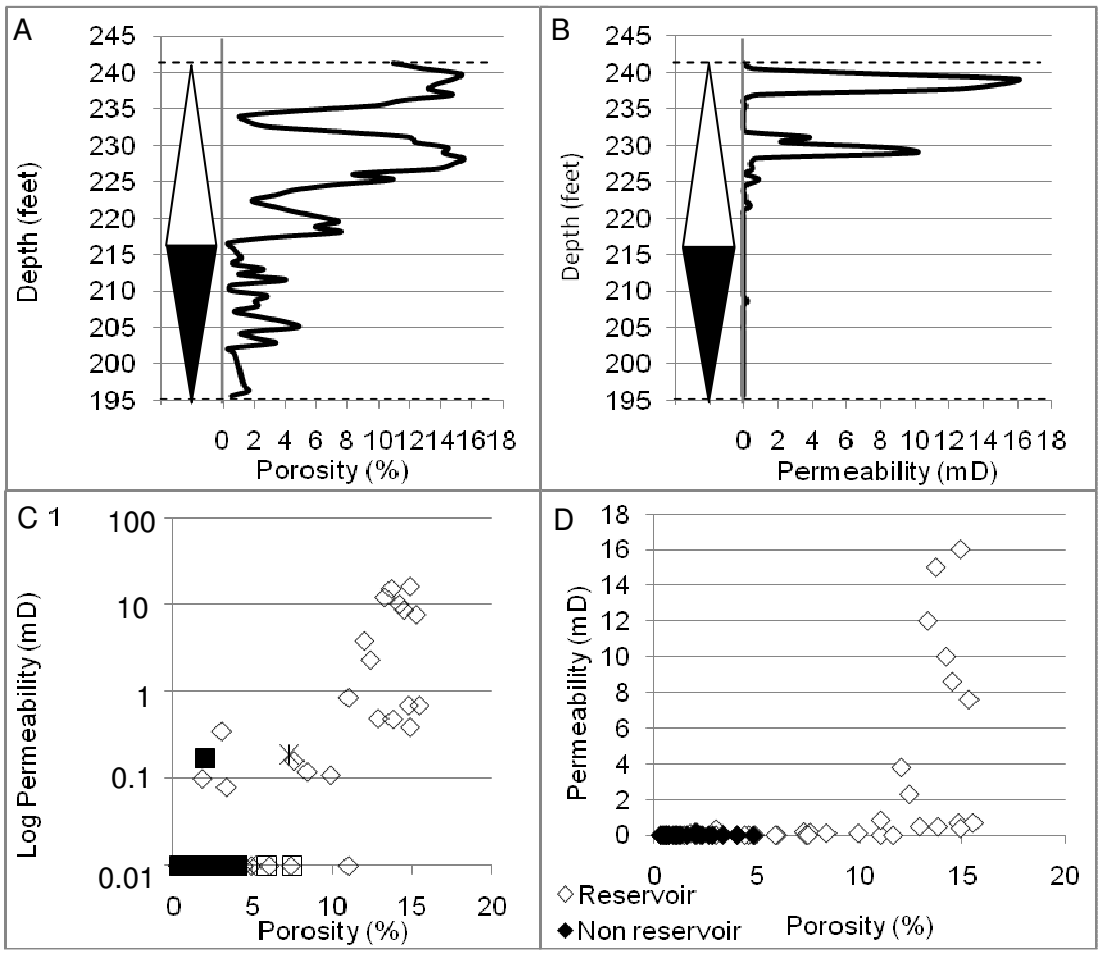

Figure 6.2: porosity and permeability data for Cycle 4a, Well 2: A) porosity data against depth, B) permeability data against depth, C) the porosity and permeability relationships with respect to the lithologies and D) the porosity and permeability relationships with respect to the reservoirs and non-reservoirs.

Cycle 4b

Cycle 4b contains one high porosity horizon measuring 7ft in thickness with values of 6%-17% and a permeability maximum of 11mD (Figs. 6.3A t& 6.3B). The remaining parts have a much lower porosity of 4-0.4% and a permeability of 0.01mD (Figs. 6.3A & 6.3B). The highest porosity and permeability relationships exist within the BW and the *l*B lithologies and the reservoir (Figs. 6.3C & 6.3D).

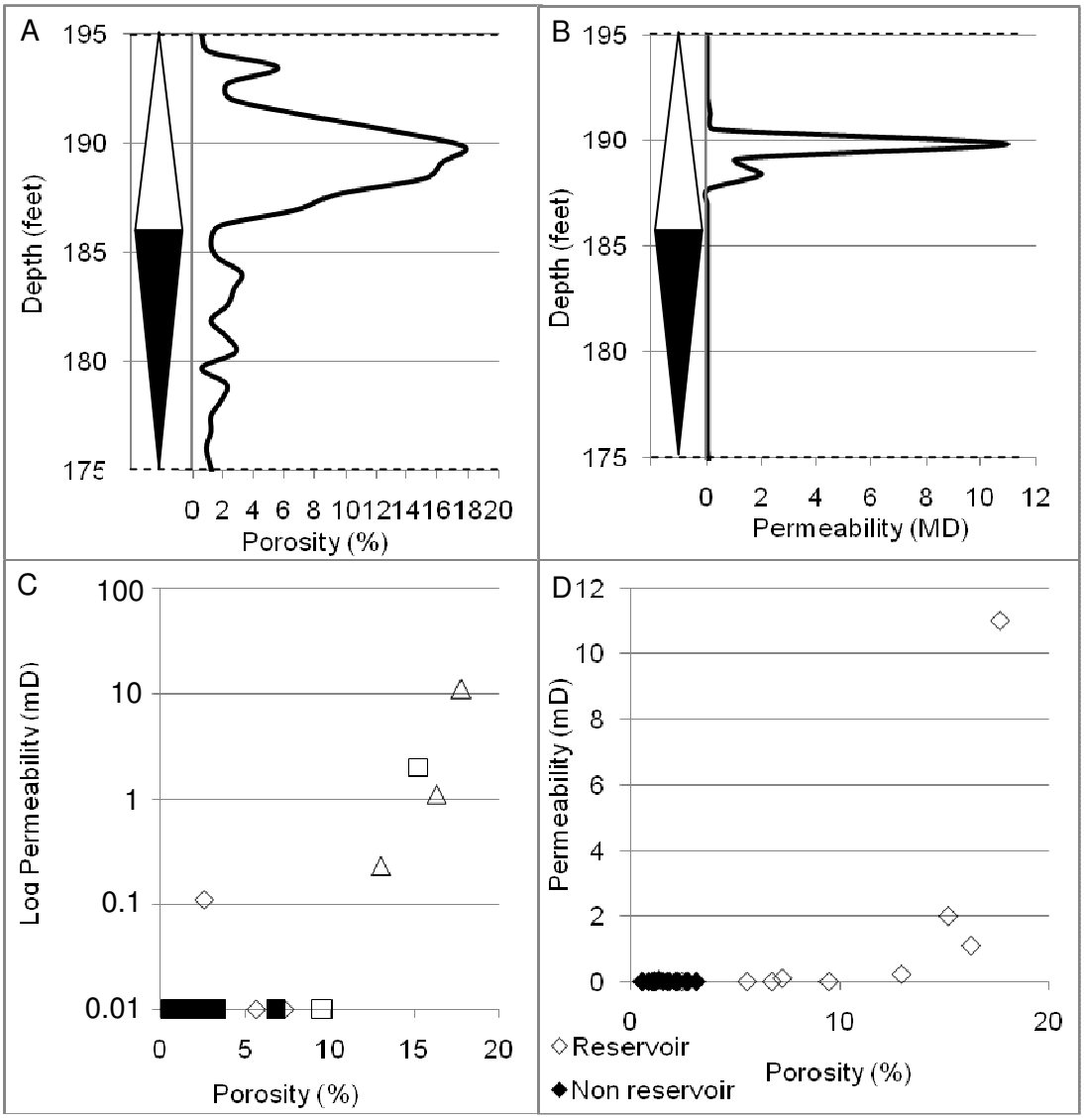

Figure 6.3: porosity and permeability data for Cycle 4b, Well 2: A) porosity data against depth, B) permeability data against depth, C) the porosity and permeability relationships with respect to the lithologies and D) the porosity and permeability relationships with respect to the reservoirs and non-reservoirs.

Cycle 5

The reservoir horizon in Cycle 5 is very thin measuring 12ft and has a porosity of 5-15% and a permeability of 0.1-0.5mD (Figs. 6.4A & 6.4B). The remaining HFC has much lower porosity of 6-0.3% and a permeability of 0.01-0.04mD (Figs. 6.4A & 6.4B) .The highest porosity and permeability relationships exclusively exist within the BW lithology and mostly within the reservoir (Figs. 6.4C & 6.4D).

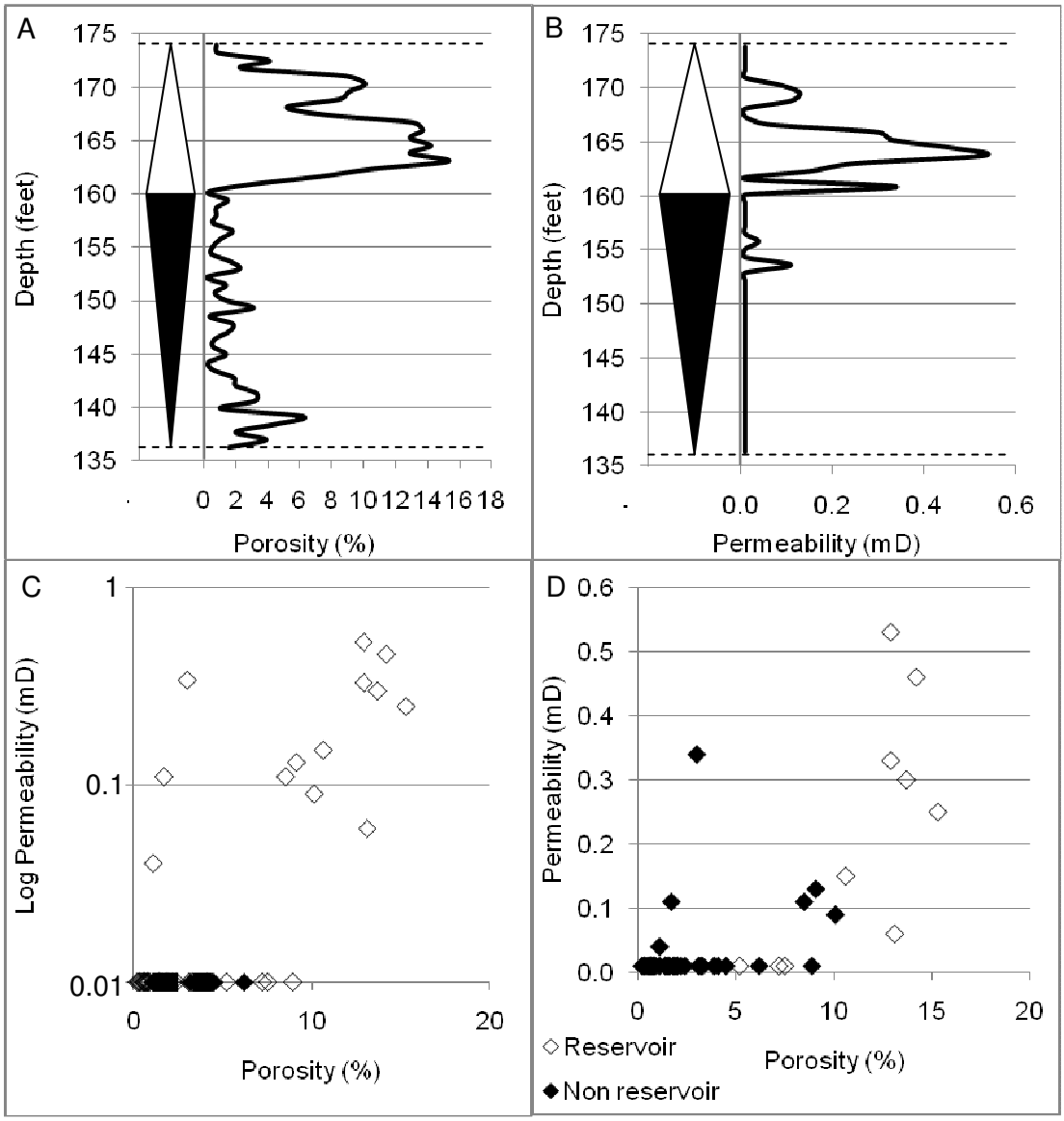

Figure 6.4: porosity and permeability data for Cycle 5, Well 2: A) porosity data against depth, B) permeability data against depth, C) the porosity and permeability relationships with respect to the lithologies and D) the porosity and permeability relationships with respect to the reservoirs and non-reservoirs.

Cycle 6

Cycle 6 has one reservoir horizon measuring 10ft thick with a porosity of 7-21% and a permeability of 1-25mD (Figs. 6.5A & 6.5B). Only one foot of the entire reservoir horizon records 25mD while the remaining 12ft of the reservoir has a permeability of 1-9mD. The remaining parts of the HFC have a porosity of 5-1% and a permeability of 0.01-4mD (Figs. 6.5A & 6.5B). The highest porosity and permeability relationships exist within the BW lithology and the reservoir (Figs. 6.5C & 6.5D).

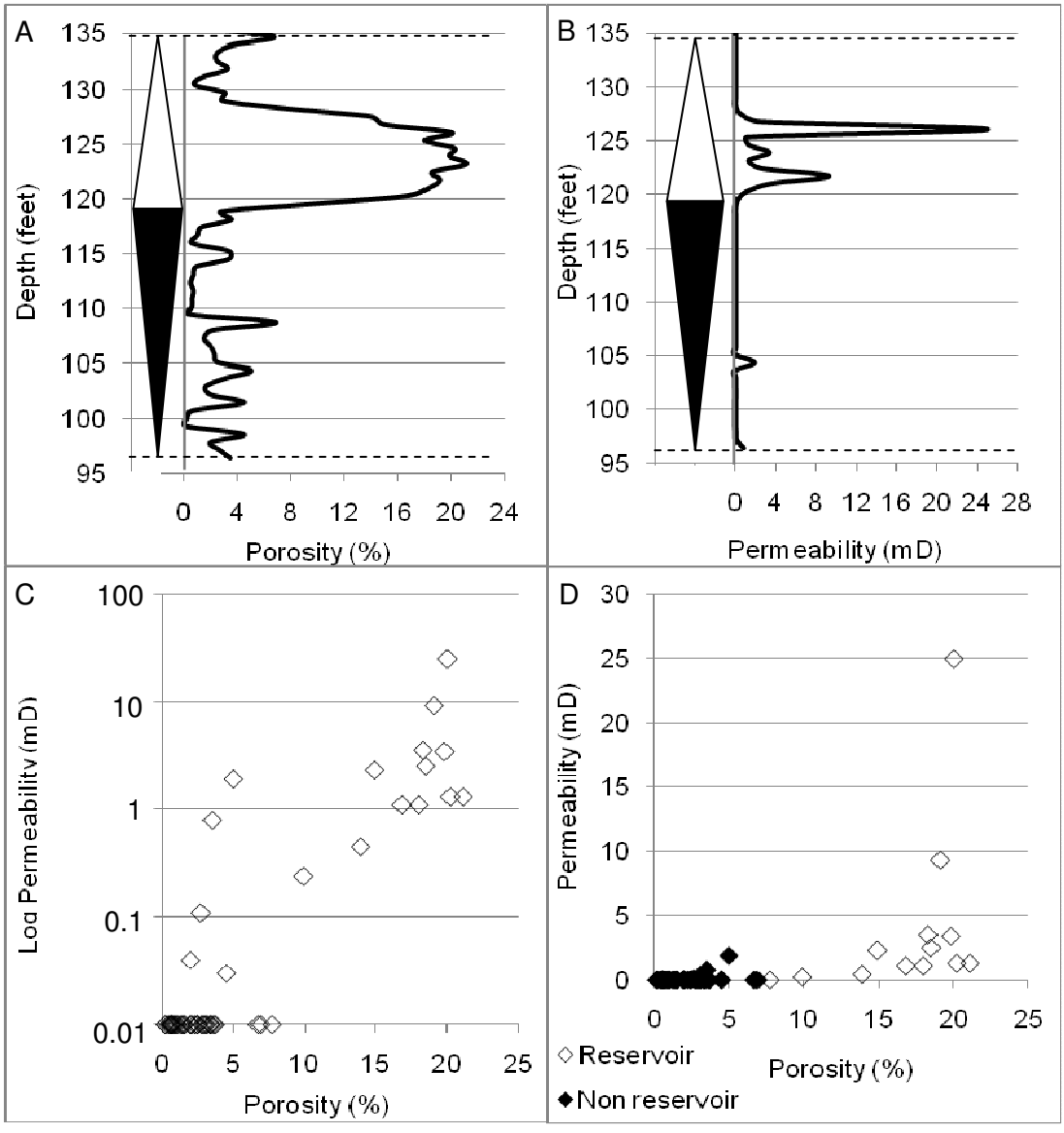

Figure 6.5: porosity and permeability data for Cycle 6, Well 2: A) porosity data against depth, B) permeability data against depth, C) porosity and permeability relationships with respect to the lithologies and D) the porosity and permeability relationships with respect to the reservoirs and non-reservoirs.

Cycle 7a

Cycle 7a has two reservoir units; the first measures 5ft in thickness, it encompasses the topmost 5ft of the entire HFC, it has porosity ranging from 6-16% and permeability of 11-0.03mD (Figs. 6.6A & 6.6B). The second reservoir measures 17ft in thickness, has a porosity of 9-25% and a permeability of 21-0.1mD (Figs. 6.6A & 6.6B). The intermediate zone has a porosity of 1-3% and a permeability of 0.01mD (Figs. 6.6A & 6.6B). The remaining HFC has a porosity of 9-0.5% and a permeability of 0.01-1.2mD: there is an anomalous result of 7mD in the TST micrites/mudstones (Figs. 6.6A & 6.6B). The second reservoir unit with the highest porosity and permeability relationships is associated with the BW. The remaining reservoir is associated with the *gl*WP (Figs. 6.6C & 6.6D).

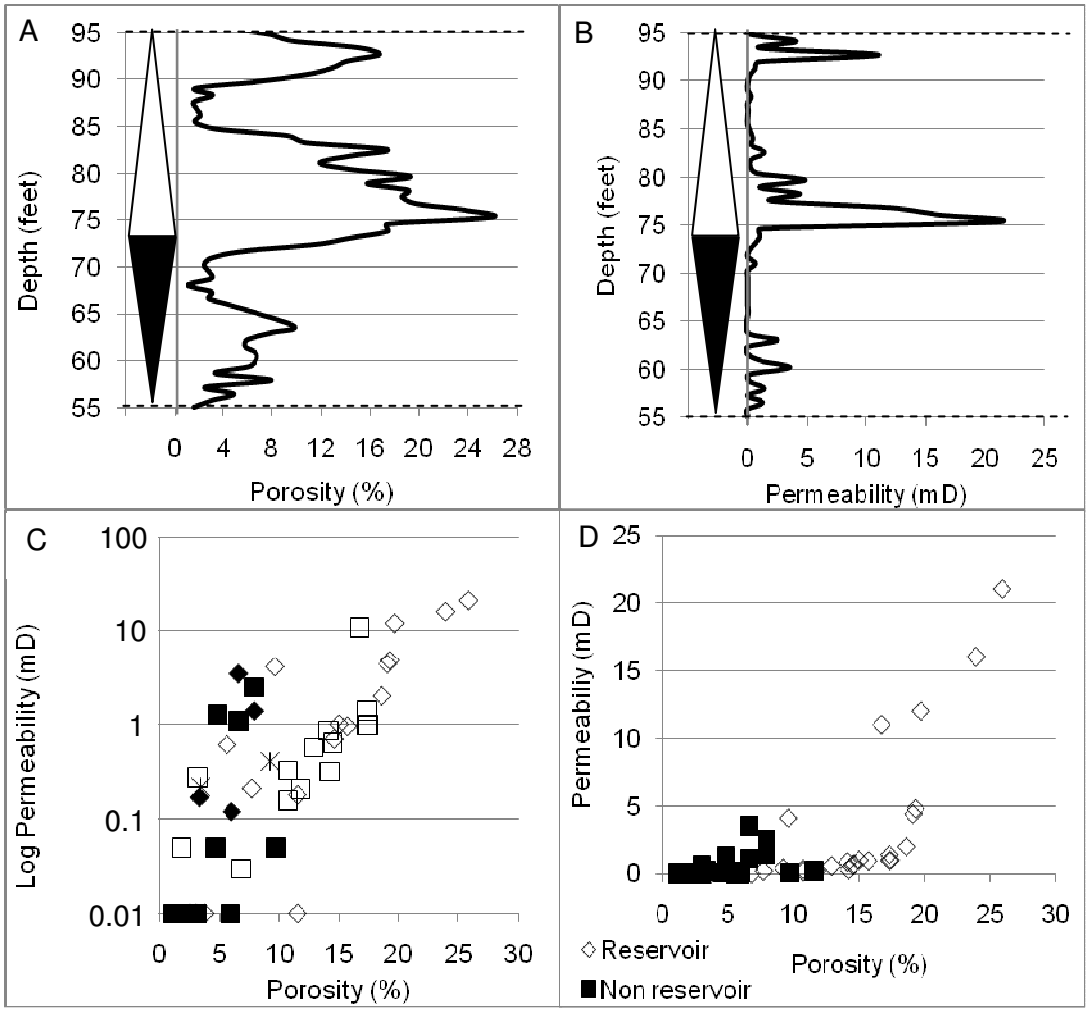

Figure 6.6: porosity and permeability data for Cycle 7a Well 2: A) porosity data against depth, B) permeability data against depth, C) porosity and permeability relationships with respect to the lithologies and D) the porosity and permeability relationships with respect to the reservoirs and non-reservoirs.

Cycle 7B

Cycle 7b has two reservoir horizons; the first measures 8ft with a porosity range of 9-16% and a permeability range of 0.2-6.3mD (Figs. 6.7A & 6.7B). The second horizon measures 8ft in thickness, has a porosity range of 7-12% and a permeability range of 0.3-0.1mD (Figs. 6.7A & 6.7B). The lower porosity unit separating the two reservoir measures 9-10ft in thickness and has a porosity range of 7-1% and a permeability of 0.01mD (Figs. 6.7A & 6.7B). Within this less permeable horizon these is a 3ft horizon with porosity of 8-10% with a permeability of 0.05mD (Figs. 6.7A & 6.7B). The remaining HFC contains porosity of 0.1-6% with a permeability of 0.01-2mD (Figs. 6.7A & 6.7B). The highest porosity and permeability relationships exist within the *gl*WP and the *gl*PG lithologies and mostly the reservoir (Figs. 6.7C & 6.7D).

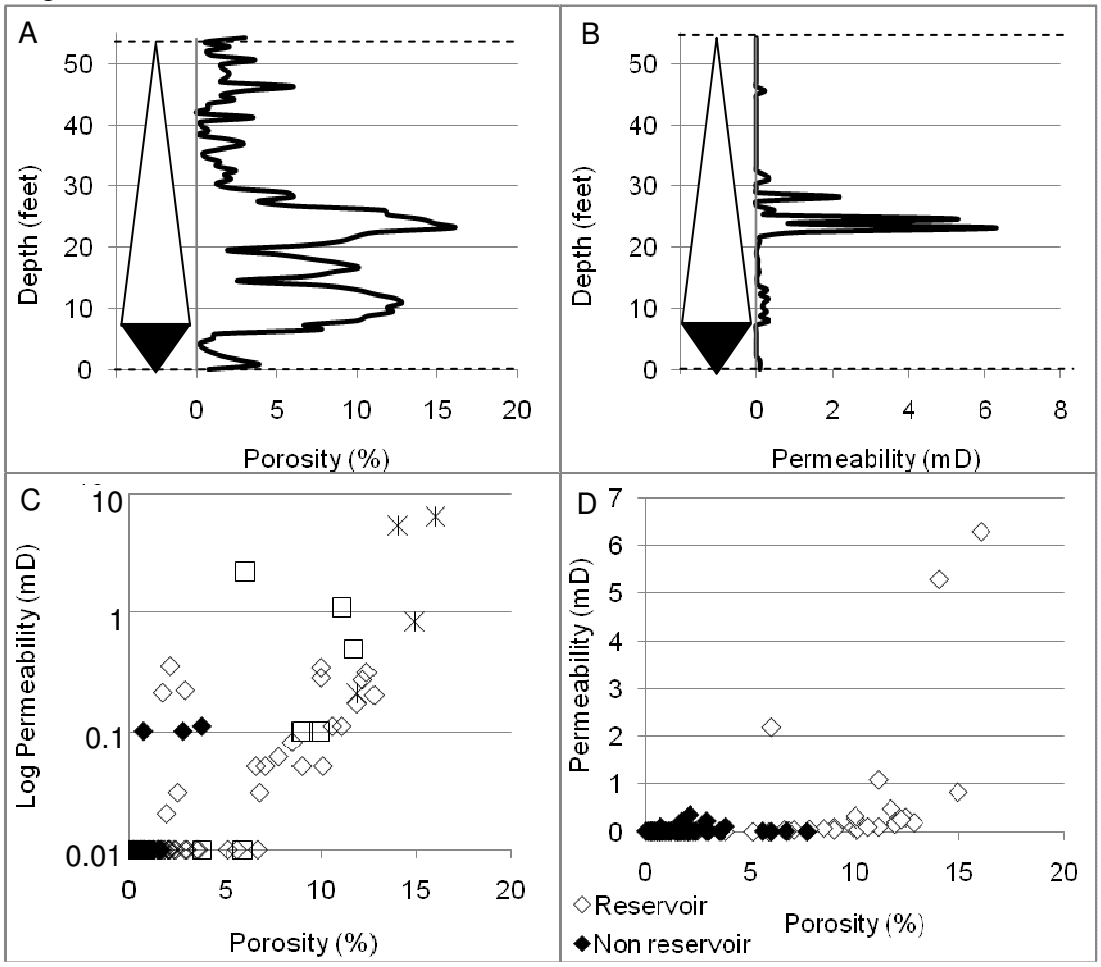

Figure 6.7: porosity and permeability data for Cycle 7b, Well 2: A) porosity data against depth, B) permeability data against depth, C) porosity and permeability relationships with respect to the lithologies and D) the porosity and permeability relationships with respect to the reservoirs and non-reservoirs.

Well 3

Cycle 1

Cycle 1 has a very uniform porosity range throughout this HFC of 24-37%, with a permeability that is less uniform but has a range of 6-20mD (Figs. 6.8A & 6.8B). There is a permeability spike that does not correspond to any particular porosity spike, which extends over 5-6ft with values of 75mD (Figs. 6.8A & 6.8B). One foot in particular shows a permeability of 127mD. Only the few feet at the bottom and top of this HFC show slightly lower porosities of 21-18%, with permeability range of 5-0.001mD (for the bottommost 10ft and the topmost 5ft of Cycle 1) (Figs. 6.8A & 6.8B). The highest porosity and permeability relationships are within the BW, the *gl*WP, and the *gl*PG lithologies within the reservoirs (Figs. 6.8C & 6.8D).

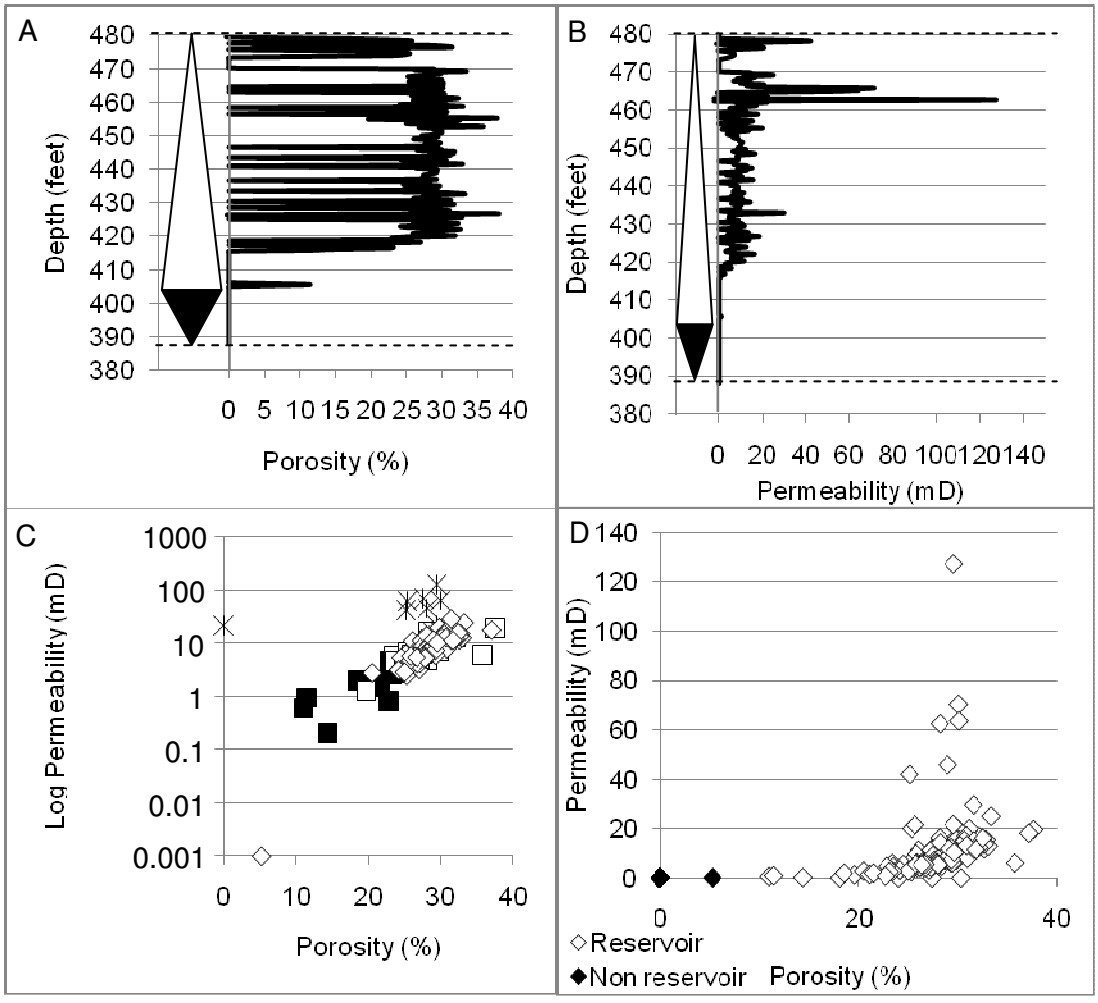

Figure 6.8: porosity and permeability data for Cycle 1, Well 3: A) porosity data against depth, B) permeability data against depth, C) porosity and permeability relationships with respect to the lithologies and D) the porosity and permeability relationships with respect to the reservoirs and non-reservoirs.

Cycle 2a

Cycle 2a has two reservoir horizons; one is very small and measures 4ft in thickness while the second reservoir horizon below is much thicker at 15ft (Figs. 6.9A & 6.9B). The reservoir horizons have porosity ranging from 15-21% and 8-26%, respectively, and permeability for the first reservoir ranges from 0.4-6.7mD and for the second reservoir it ranges from 0.1-26mD (Figs. 6.9A & 6.9B). The intermediate zone has lower porosity measuring 8-2% with a permeability of 0.001-2.3mD (Figs. 6.9A & 6.9B). The remaining HFC, representing the lower TST has porosity of 10-7% with permeability of 0.001-0.1mD (Figs. 6.9A & 6.9B). The majority of the topmost and bottommost portions of Cycle 2a have no data. The highest porosity and permeability relationships exist mostly within the reservoir and the *gl*WP (Figs. 6.9C & 6.9D).

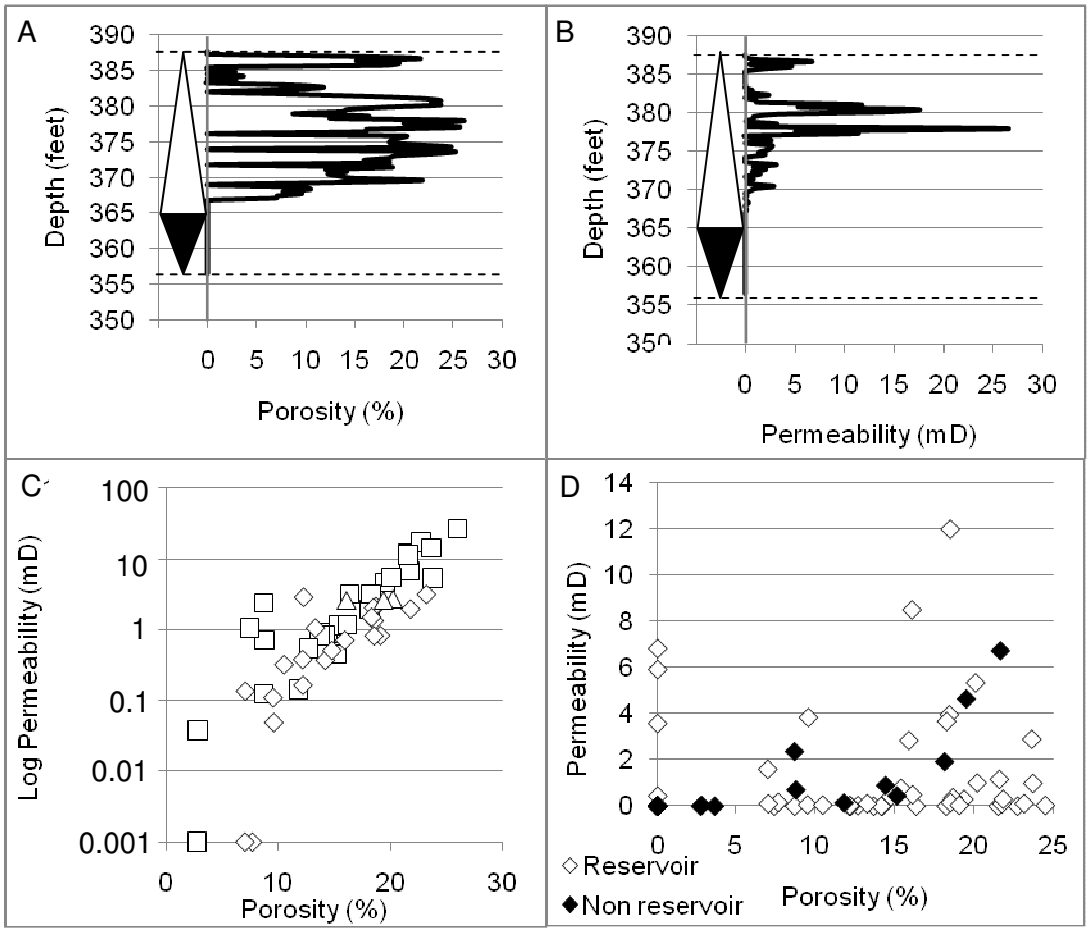

Figure 6.9: porosity and permeability data for Cycle 2a, Well 3: A) porosity data against depth, B) permeability data against depth, C) porosity and permeability relationships with respect to the lithologies and D) the porosity and permeability relationships with respect to the reservoirs and non-reservoirs.

Cycle 2b

Cycle 2b has two separate reservoir horizons measuring, from the top, 30ft and 13ft, respectively. The uppermost reservoir has porosity ranging from 10-20% with a permeability ranging from 0.2-8.4mD and the lowermost reservoir having porosity ranging from 10-24% and a permeability ranging from 0.1-8mD (Figs. 6.10A & 6.10B). The intermediate zones have lower porosity which ranges from 3-5% with permeability of 0.001-0.1mD (Figs. 6.10A & 6.10B). The majority of the lower portion of this HFC, which falls within the TST, has very low porosity and permeability apart from a 5ft thick porosity spike of 10% (Figs. 6.10A & 6.10B). The highest porosity and permeability relationships mostly exist within the BW, with one data point within PM (Figs. 6.10C & 6.10D).

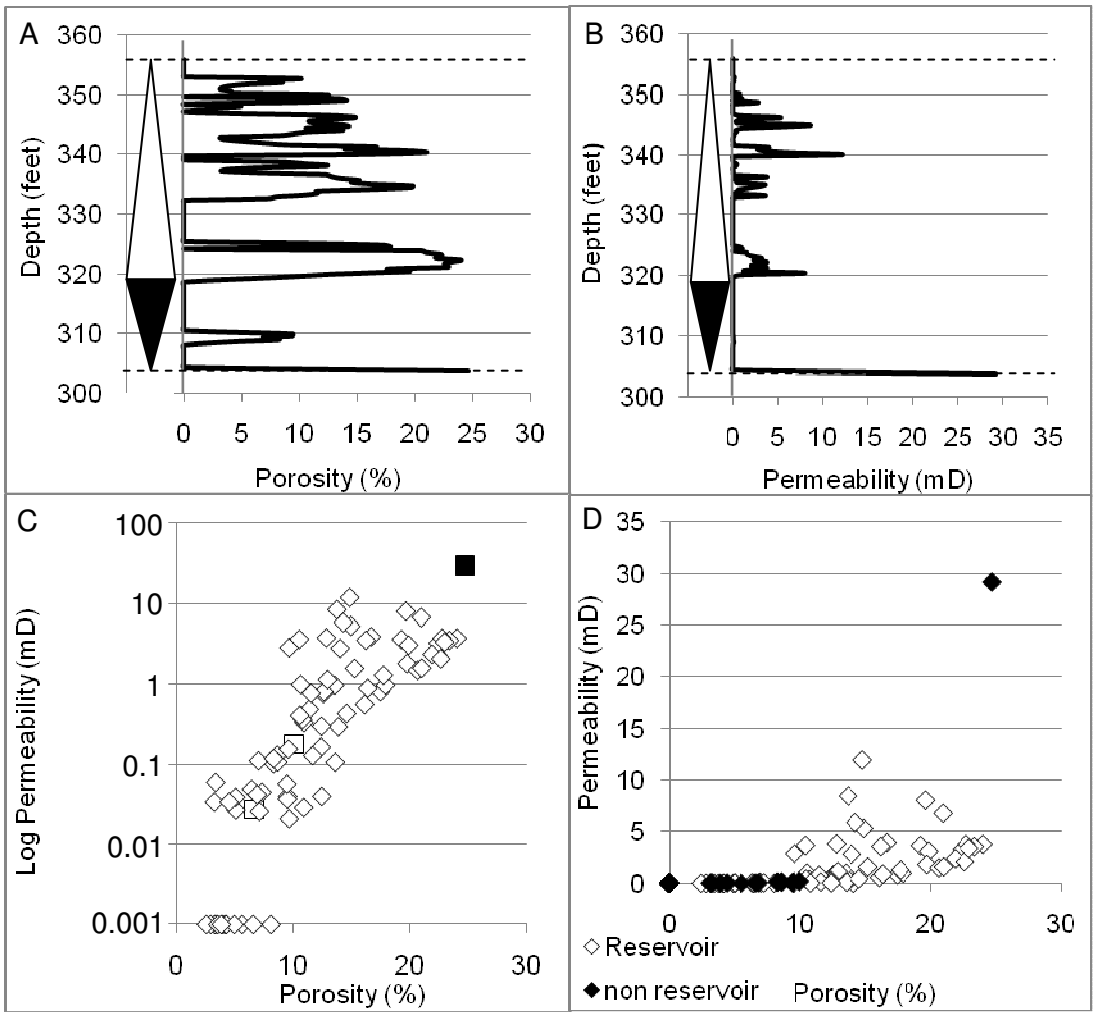

Figure 6.10: porosity and permeability data for Cycle 2b, Well 3: A) porosity data against depth, B) permeability data against depth, C) porosity and permeability relationships with respect to the lithologies and D) the porosity and permeability relationships with respect to the reservoirs and non-reservoirs.

Cycle 3

All the HST and the topmost few feet of the TST have porosity that is moderately variable with a range of 17-35% and permeability of 2-100mD (Figs. 6.11A & 6.11B). Within the HST there is a permeability high lasting for 4-5ft with measurements ranging between 237-372mD (Figs. 6.11A & 6.11B). The remaining lower TST has no data. The highest porosity and permeability data exists within reservoir and the BW, the *gl*WP and the *gl*PG (Figs. 6.11C & 6.11D).

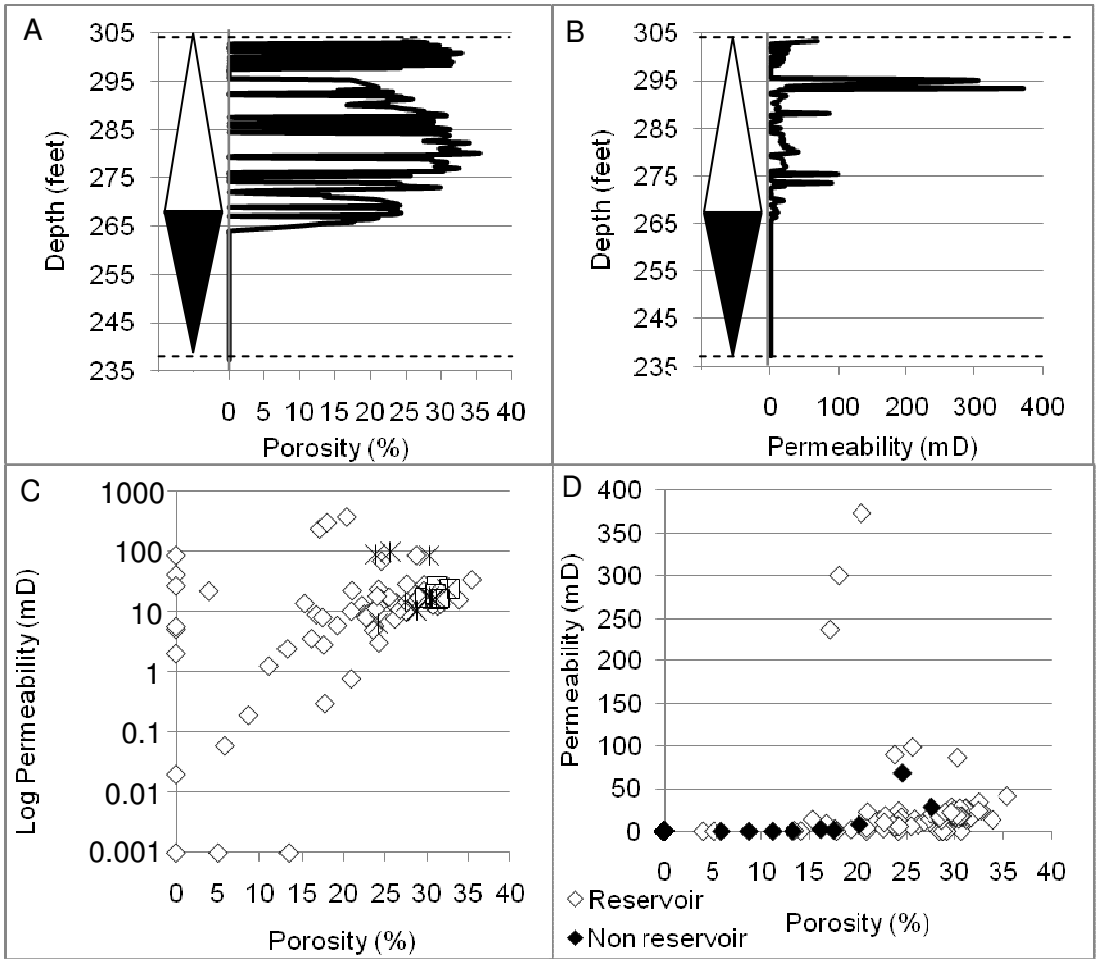

Figure 6.11: porosity and permeability data for Cycle 3, Well 3: A) porosity data against depth, B) permeability data against depth, C) porosity and permeability relationships with respect to the lithologies and D) the porosity and permeability relationships with respect to the reservoirs and non-reservoirs.

Cycle 4a

Cycle 4a has two reservoir horizons, measuring 15ft and 4ft thick. The top reservoir has porosity ranging from 10-21%, with the bottom reservoir having 8-10% porosity (Figs. 6.12A & 6.12B). The top reservoir contains the highest value for a single foot of core with 28% (Figs. 6.12A & 6.12B). The permeability for the entire HFC is relatively low ranging from 0.001-8mD (Figs. 7.20A & 7.20B). There are three permeability spikes ranging over a foot in thickness; all three exist within the top reservoir with measurements of 26mD, 97mD and 31mD (Figs. 6.12A & 6.12B). The highest porosity and permeability relationships are present within reservoir, the BW and the *gl*PG (Figs. 6.12C & 6.12D).

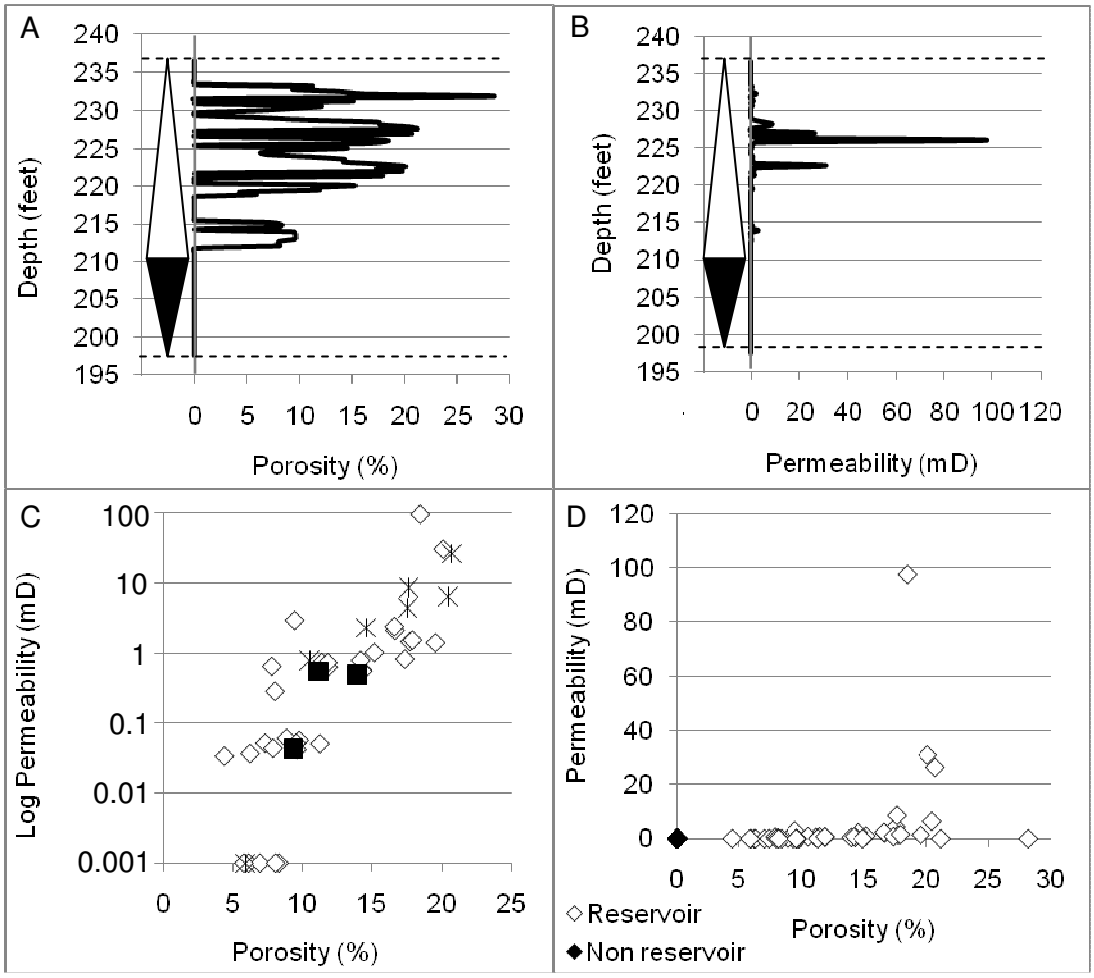

Figure 6.12: porosity and permeability data for Cycle 4a, Well 3: A) porosity data against depth, B) permeability data against depth, C) porosity and permeability relationships with respect to the lithologies and D) the porosity and permeability relationships with respect to the reservoirs and non-reservoirs.

Cycle 4b

Cycle 4b only has one reservoir horizon measuring 10ft in thickness with porosity values ranging from 8-26% and uniform permeability between 0.05-4mD (Figs. 6.13A & 6.13B). There are two permeability spikes that range for one foot in thickness, with measurements of 98-52mD (Figs. 6.13A & 6.13B). The remaining HFC has no data. The highest porosity and permeability relationships exist within the reservoir, the BW and the *gl*PG (Figs. 6.13C & 6.13D).

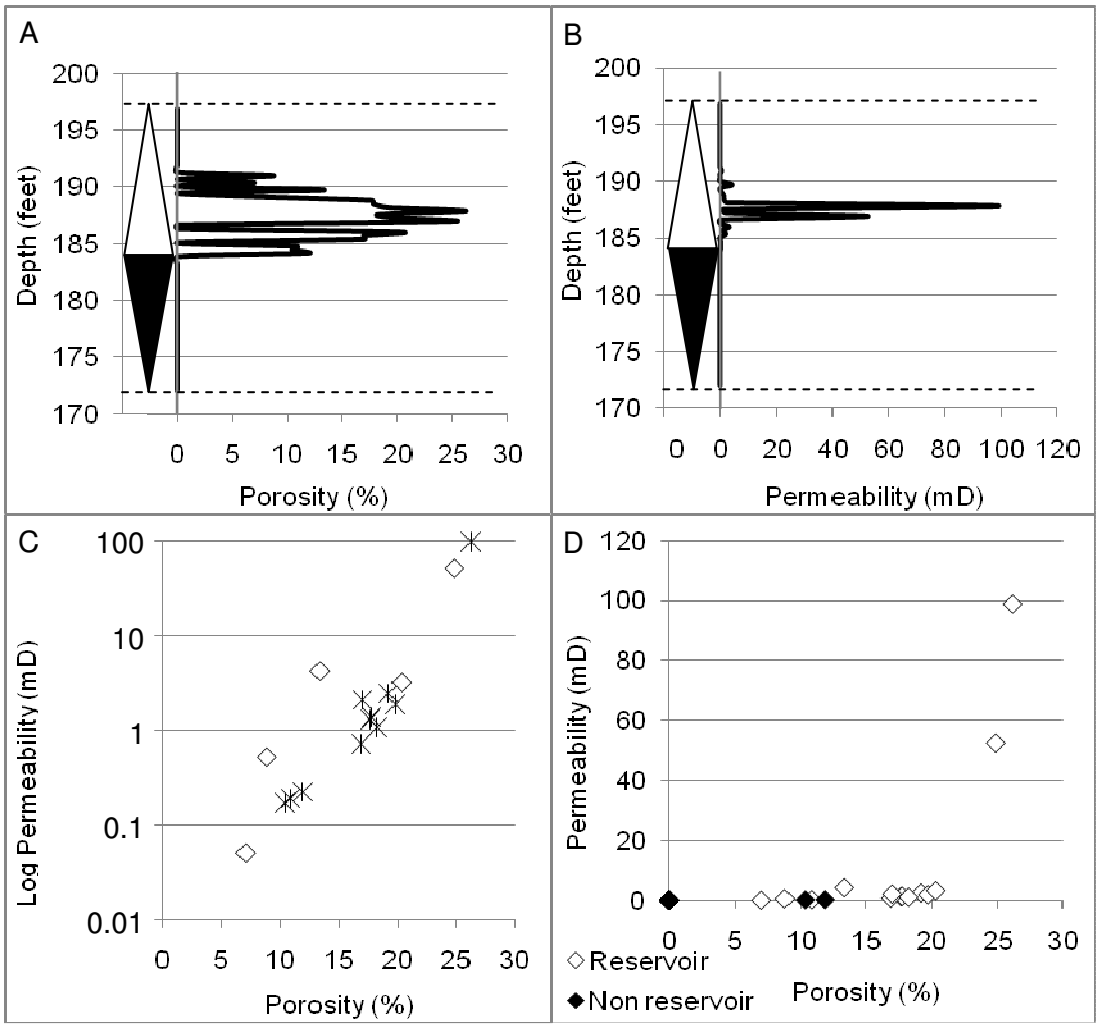

Figure 6.13: porosity and permeability data for Cycle 4b, Well 3: A) porosity data against depth, B) permeability data against depth, C) porosity and permeability relationships with respect to the lithologies and D) the porosity and permeability relationships with respect to the reservoirs and non-reservoirs.

Cycle 5

Cycle 5 has three reservoir horizons, one measuring 8ft thick, the second measuring 17ft thick and the third measuring 5ft thick. All three reservoirs have porosity ranges of 10-18%, with permeability of 0.19-9mD for the first, 0.05-23mD for the second and 0.05-9mD for the third (Figs. 6.14A & 6.14B). The two intermediate zones both only measure a few feet in thickness and have slightly lower porosities of 4-9% with permeability ranging 0.001mD to 1mD (Figs. 6.14A & 6.14B). The lower TST has no data (Figs. 6.14A 6.14B). The highest porosity and permeability relationships exist within the reservoir, the BW and the PM (Figs. 6.14C & 6.14D).

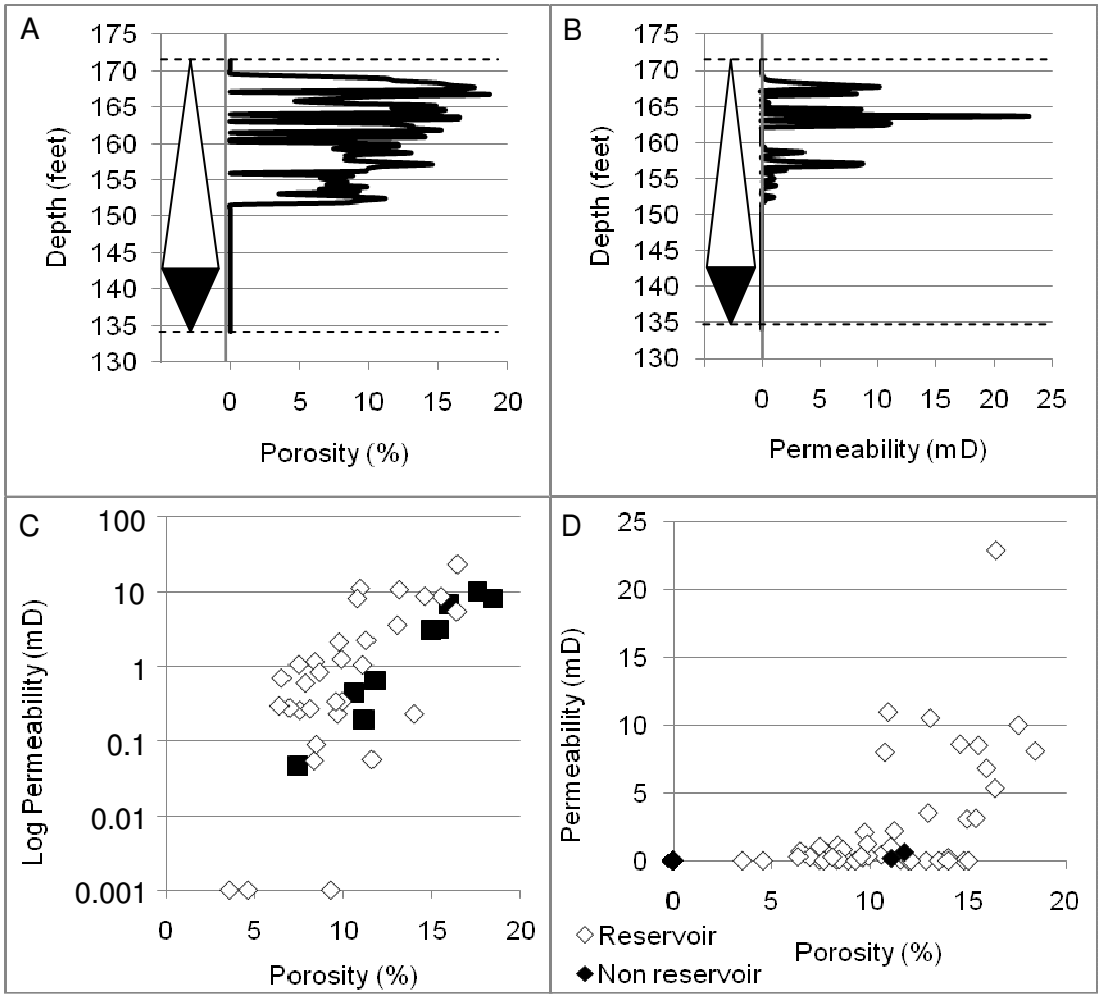

Figure 6.14: porosity and permeability data for Cycle 5, Well 3: A) porosity data against depth, B) permeability data against depth, C) porosity and permeability relationships with respect to the lithologies and D) the porosity and permeability relationships with respect to the reservoirs and non-reservoirs.

Cycle 6

Cycle 6 has only one reservoir horizon measuring 12ft thick. It has a porosity range of 15-34% and a permeability range of 0.5-21mD (Figs. 6.15A & 6.15B). There are three permeability spikes each one foot in thickness with measurements of 32mD, 35mD and 83mD (Figs. 6.15A & 6.15B). Only a few feet above the reservoir potion has data with porosity of 6% and a permeability of 0.02mD (Figs. 6.15A & 6.15B). The remaining HFC has no data. The highest porosity and permeability relationships exist mainly within the BW (Figs. 6.15C & 6.15D).

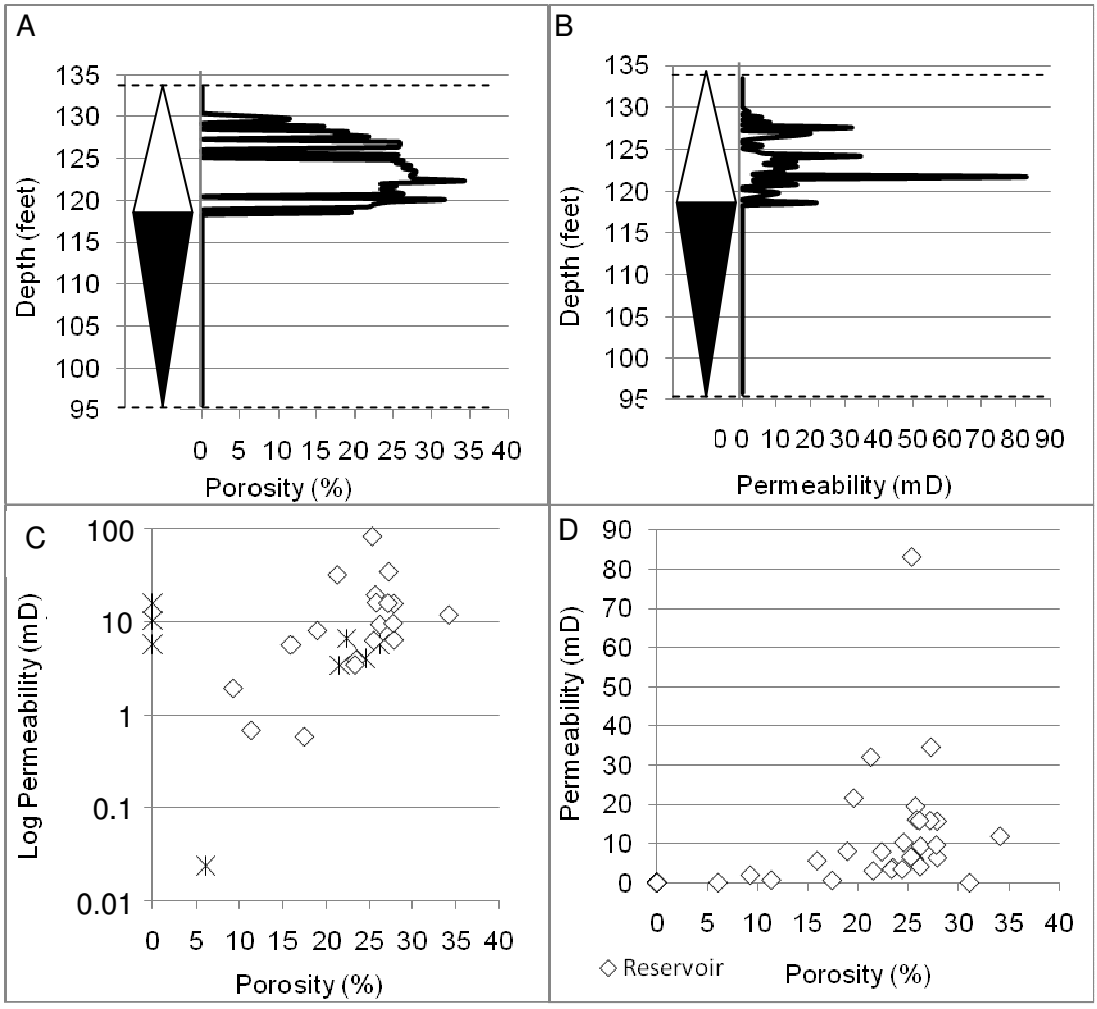

Figure 6.15: porosity and permeability data for Cycle 6, Well 3: A) porosity data against depth, B) permeability data against depth, C) porosity and permeability relationships with respect to the lithologies and D) the porosity and permeability relationships with respect to the reservoirs and non-reservoirs.

Cycle 7a

Cycle 7a has two reservoir horizons measuring 10ft and 15ft, respectively. The porosity for both reservoirs ranges from 9-30% and permeability ranges from 0.1-22mD (Figs. 6.16A & 6.16B). The HST does have a section of no data measuring 8ft in thickness. Within the first reservoir the permeability spikes to 181mD; the highest values in this HFC (Figs. 6.16A & 6.16B). Within the second reservoir there are three permeability spikes of 68-65mD, 98mD and 83mD, respectively (Figs. 6.16A & 6.16B). The TST has no data. The highest porosity and permeability relationships exist within the *gl*WP (Figs. 6.16C & 6.16D).

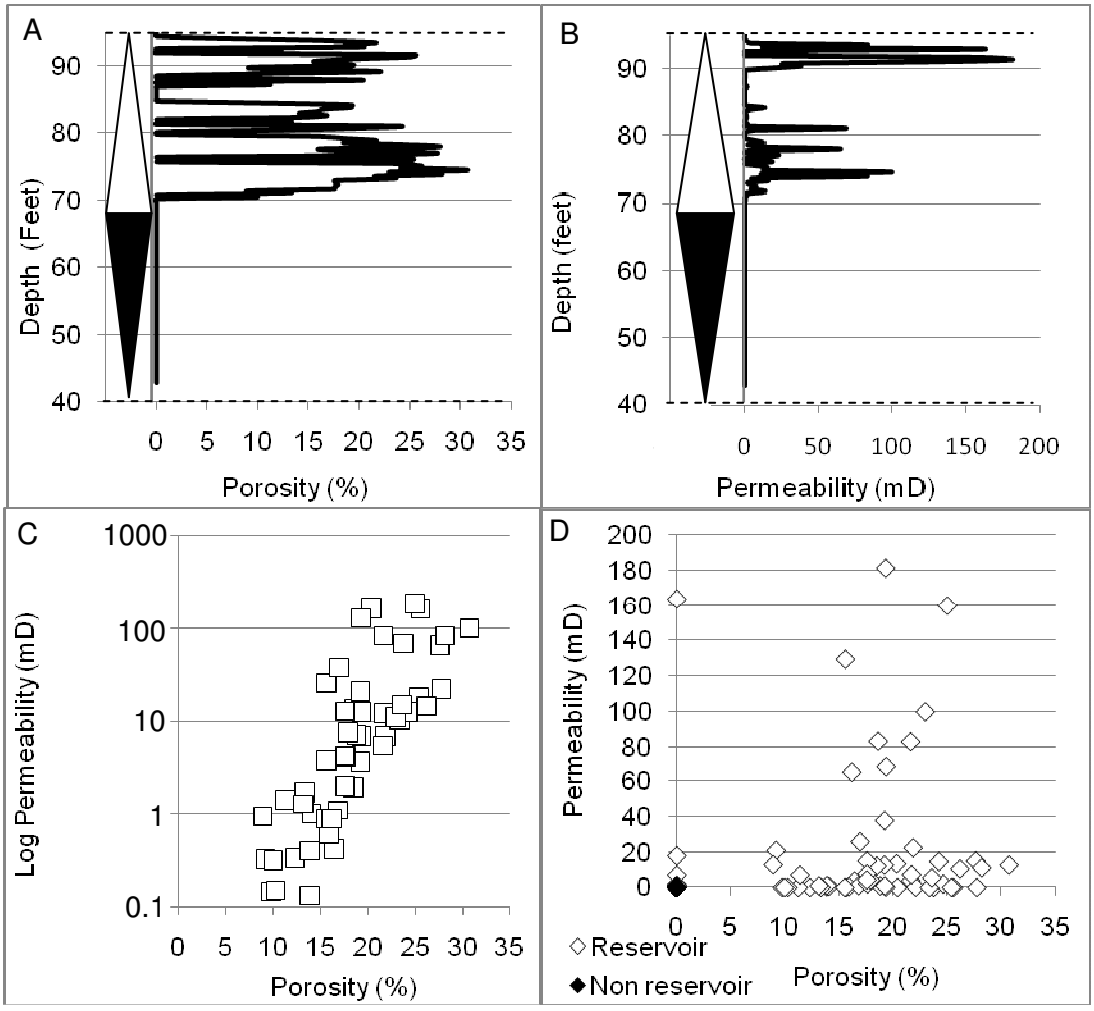

Figure 7.16: porosity and permeability data for Cycle 7a, Well 3: A) porosity data against depth, B) permeability data against depth, C) porosity and permeability relationships with respect to the lithologies and D) the porosity and permeability relationships with respect to the reservoirs and non-reservoirs.

Cycle 7b

Cycle 7b has very little data for the HST and shows a porosity range of 12-19% and a permeability range of 0.001-2mD which covers the early HST and the late TST (Figs. 6.17A & 6.17B). There is a small permeability spike of 14mD within the non - reservoir TST (Figs. 6.17A & 6.17B). The highest porosity and permeability data exists within the BW and the PM (Figs. 6.17C & 6.17D). The HST has little data.

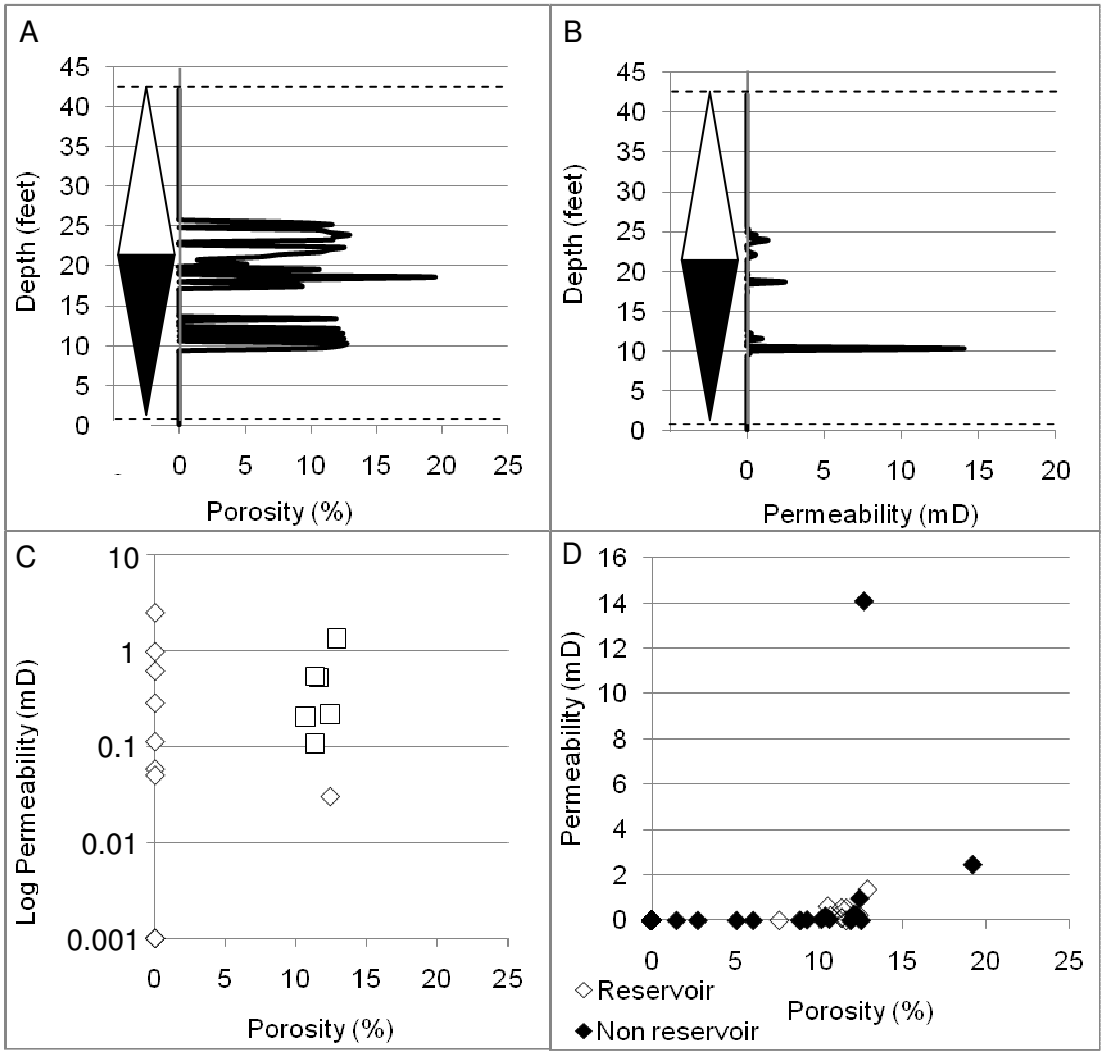

Figure 6.17: porosity and permeability data for Cycle 7b, Well 3: A) porosity data against depth, B) permeability data against depth, C) porosity and permeability relationships with respect to the lithologies and D) the porosity and permeability relationships with respect to the reservoirs and non-reservoirs.

Well 4

Cycle 1

Cycle 1 has porosity ranging from 14-39% and the permeability ranging from 5-30mD (Figs. 6.18A & 6.18B). The topmost portion of the reservoir shows two permeability spikes that both measure 6-7ft in thickness. The first ranges from 34-670mD while the second ranges from 57-830mD (Figs. 6.18A & 6.18B). Only the bottommost 30ft and the topmost 5ft show permeability values of 0.001-1mD (Figs. 6.18A & 6.18B). Porosity is only much lower in the topmost and bottommost few feet with values at 0.5-3% (Figs. 6.18A & 6.18B). The highest porosity and permeability relationships exist within the reservoir, the *gl*WP and the *gl*PG (Figs. 6.18C & 6.18D).

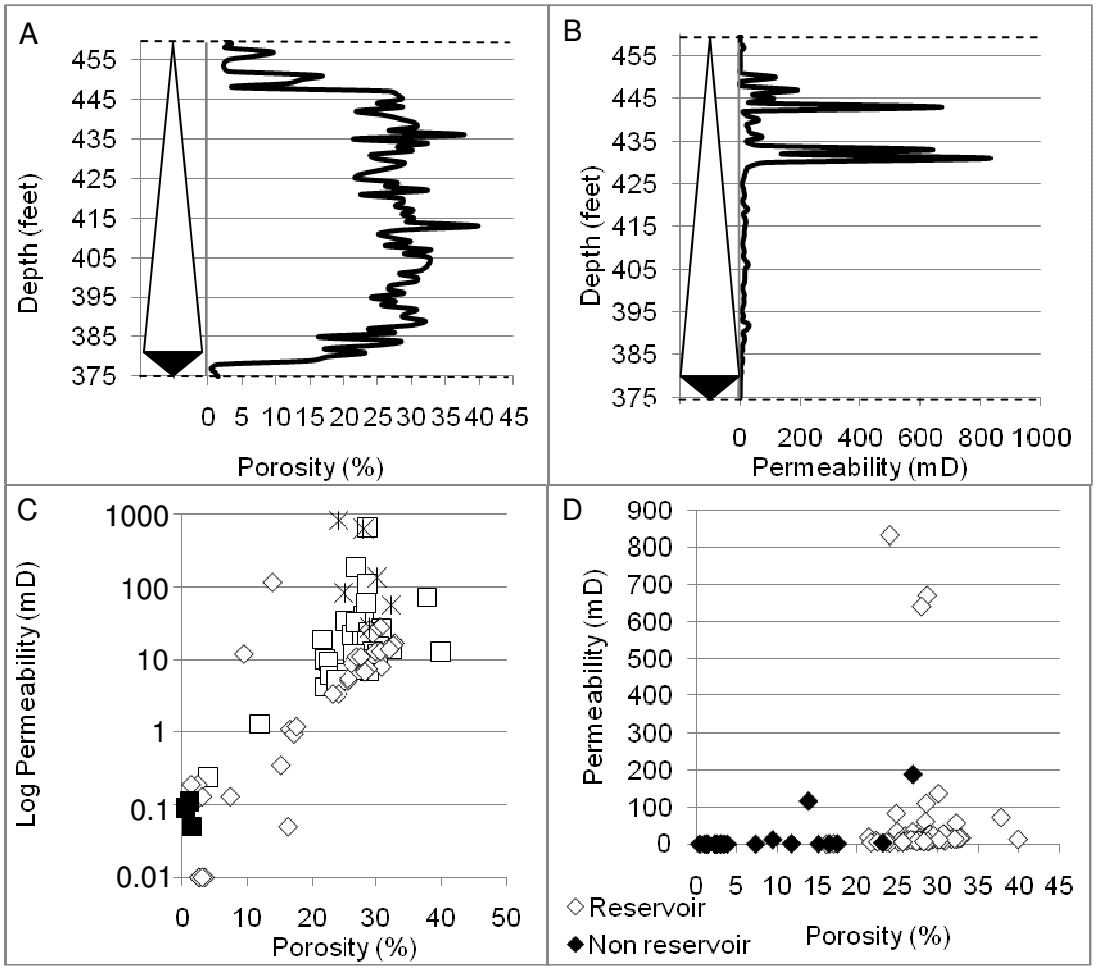

Figure 6.18: porosity and permeability data for Cycle 1, Well 4: A) porosity data against depth, B) permeability data against depth, C) porosity and permeability relationships with respect to the lithologies and D) the porosity and permeability relationships with respect to the reservoirs and non-reservoirs.

Cycle 4a

Cycle 4a has a relatively low porosity of 0.2-10% and a permeability of 0.01-7mD (Figs. 6.19A & 6.19B). There are no significant permeability spikes with respect to Cycle 1 above. The highest porosity and permeability relationships are present within the BW and the PM (Figs. 6.19C & 6.19D).

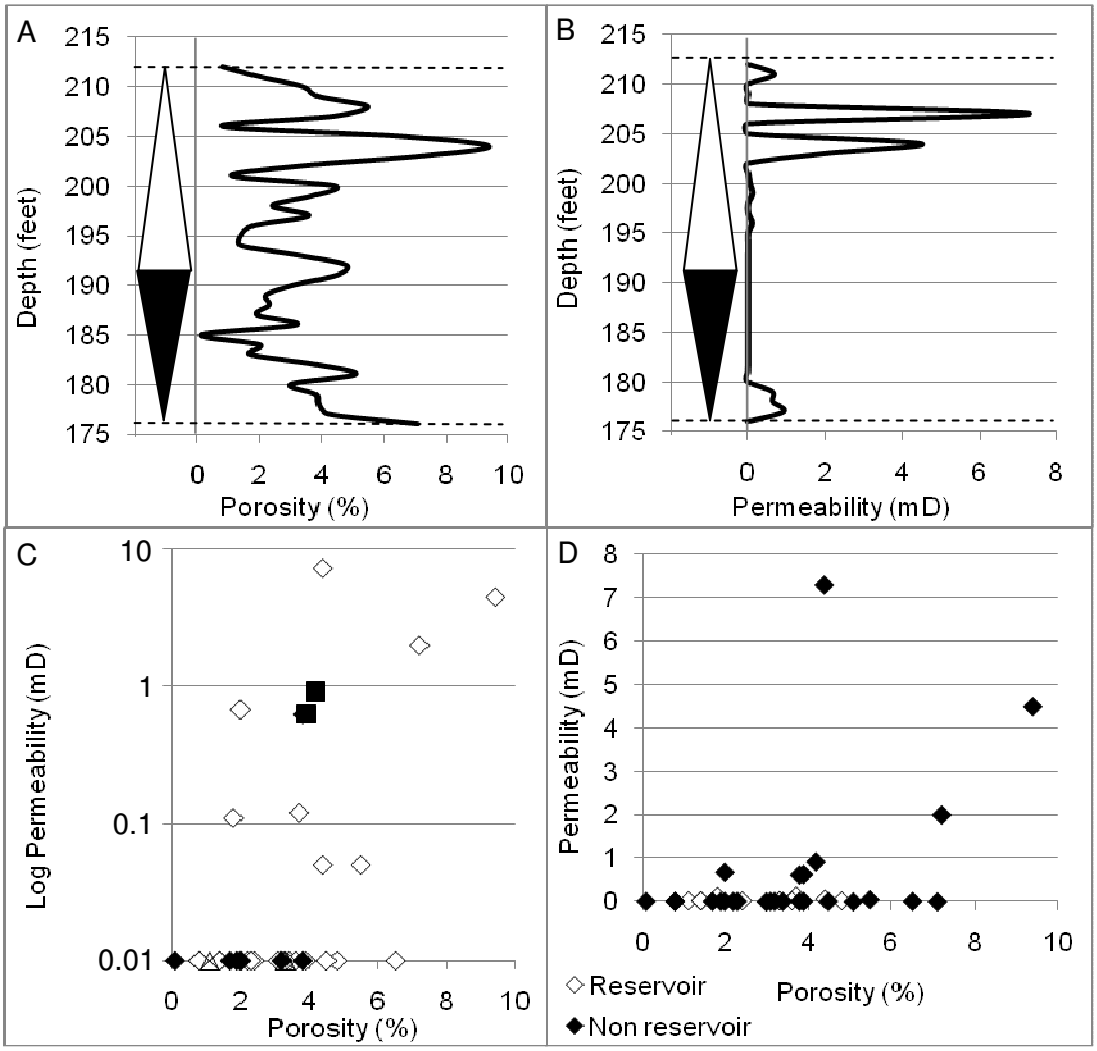

Figure 6.19: porosity and permeability data for Cycle 4a, Well 3: A) porosity data against depth, B) permeability data against depth, C) porosity and permeability relationships with respect to the lithologies and D) the porosity and permeability relationships with respect to the reservoirs and non-reservoirs.

Cycle 4b

For Cycle 4b there are two porosity spikes of 10% within the HST and another spike of 16% in the base of the TST. The only permeability spike exists at the bottom of the HFC within the base of the TST with a value of 38mD (Figs. 6.20A & 6.20B). The highest porosity and permeability relationships are within the BW and the *glWP* (Figs. 6.20C & 6.20D).

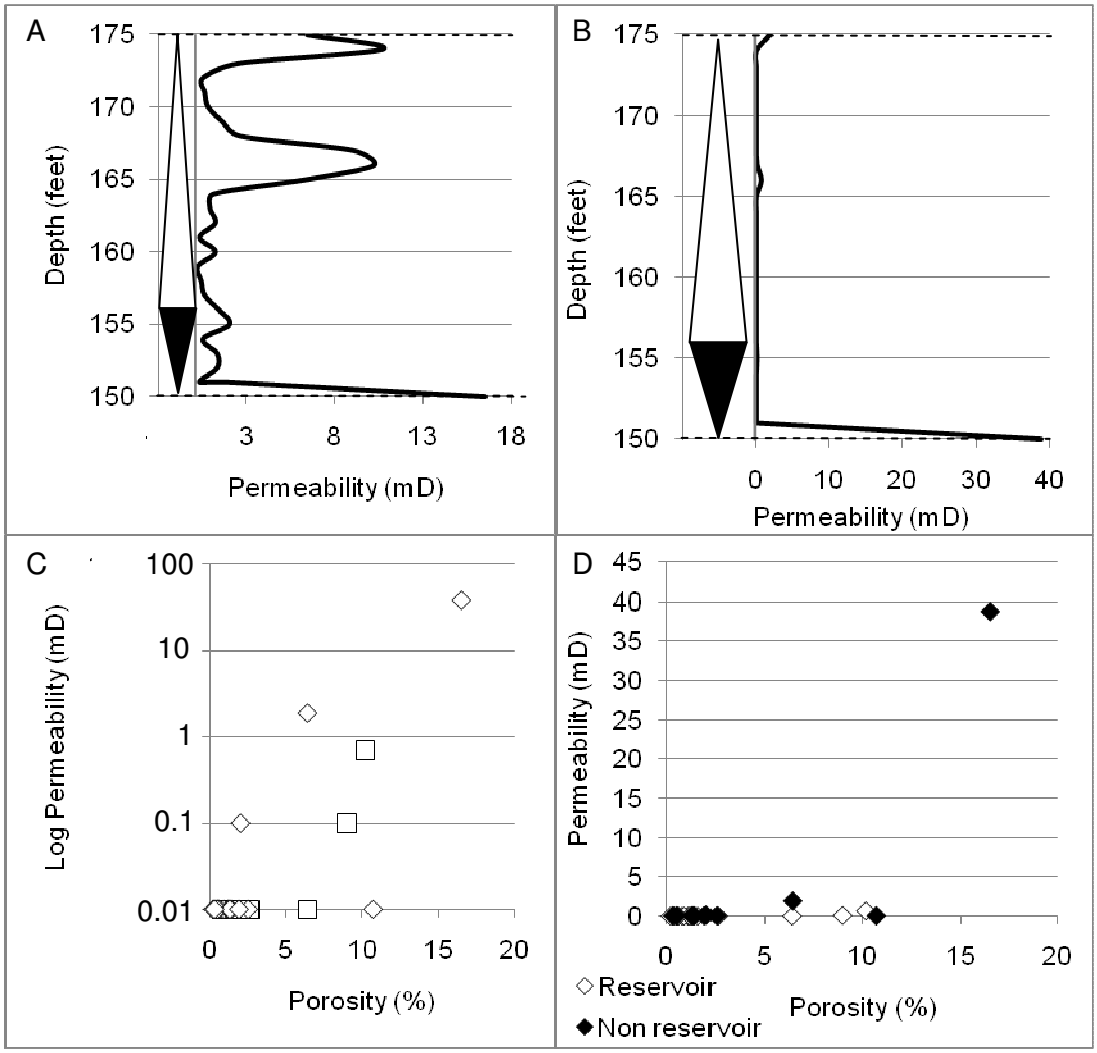

Figure 7.20: porosity and permeability data for Cycle 4b, Well 4: A) porosity data against depth, B) permeability data against depth, C) porosity and permeability relationships with respect to the lithologies and D) the porosity and permeability relationships with respect to the reservoirs and non-reservoirs.

Cycle 5

Cycle 5 has a porosity range of 0.3-13% and a permeability range of 0.01-6mD (Figs. 6.21A & 6.21B). The TST has lower porosity of 1-5% and permeability of 0.001-1.5mD (Figs. 6.21A & 6.21B). The highest porosity and permeability relationships exist within the *gl*WP and *l*B (Figs. 6.21C & 6.21D).

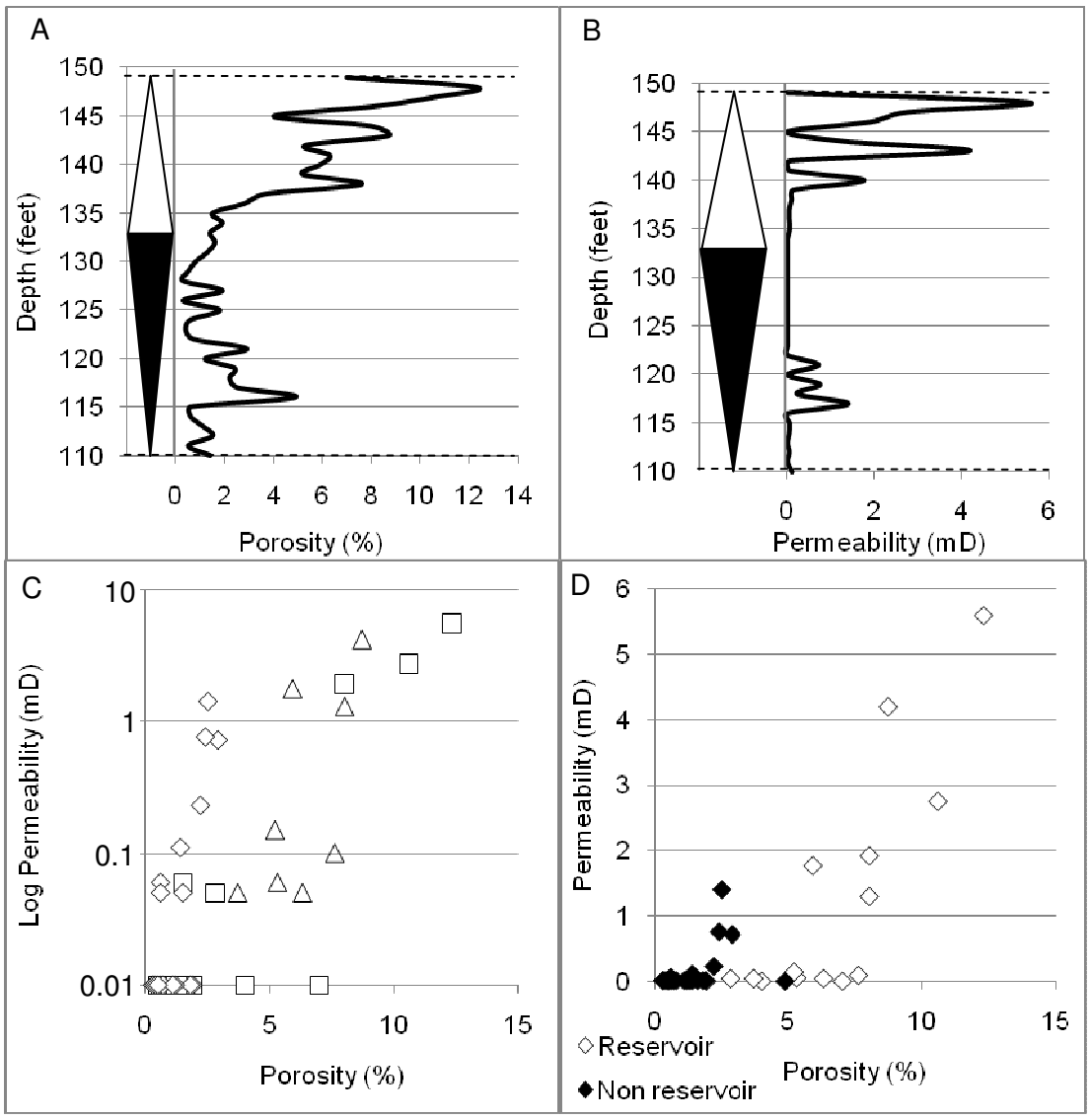

Figure 7.21: porosity and permeability data for Cycle 5, Well 4: A) porosity data against depth, B) permeability data against depth, C) porosity and permeability relationships with respect to the lithologies and D) the porosity and permeability relationships with respect to the reservoirs and non-reservoirs.

Cycle 6

Cycle 6 has a porosity range of 0.2-12% and a permeability range of 0.01-2.5mD (Figs. 6.22A & 6.22B). There is no significant porosity of permeability spikes within this HFC. Cycle 6 has a thin reservoir measuring only a few feet at the top of the HFC. It is within the HST and the late TST that porosity values get above 10% (Figs. 6.22A & 6.22B). The remainder of the HFC has porosity ranging from 0.2-2%. The permeability for the entire HFC ranges from 0.01-0.5mD (Figs. 6.22A & 6.22B). The highest porosity and permeability relationships are associated with the reservoir, the *gl*WP and the *gl*PG (Figs. 6.22C & 6.22D).

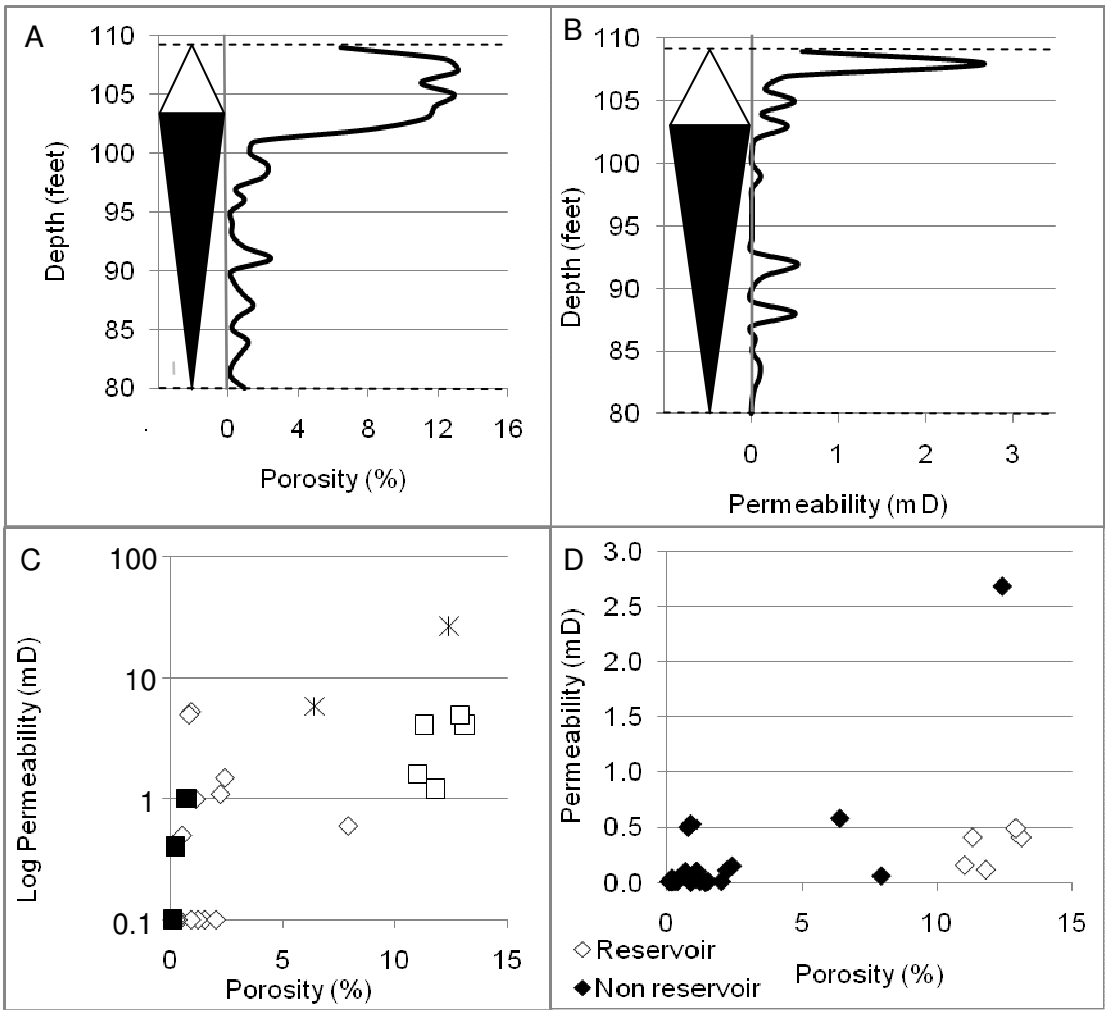

Figure 7.22: porosity and permeability data for Cycle 6, Well 4: A) porosity data against depth, B) permeability data against depth, C) porosity and permeability relationships with respect to the lithologies and D) the porosity and permeability relationships with respect to the reservoirs and non-reservoirs.

Cycle 7a

Cycle 7a has two porosity and permeability highs measuring 3ft and 6ft thick. Both have porosity of ~12%, with the top spike having permeability of 33mD and the lower spike having 3mD. The remainder of the HFC has porosity ranging from 5-6% with permeability ranging from 0.01-10mD (a small permeability spike exists within the TST) (Figs. 6.23A & 6.23B). The highest porosity and permeability relationships exist within the reservoir, the mid-late HST and the BW (Figs. 6.23C & 6.23D).

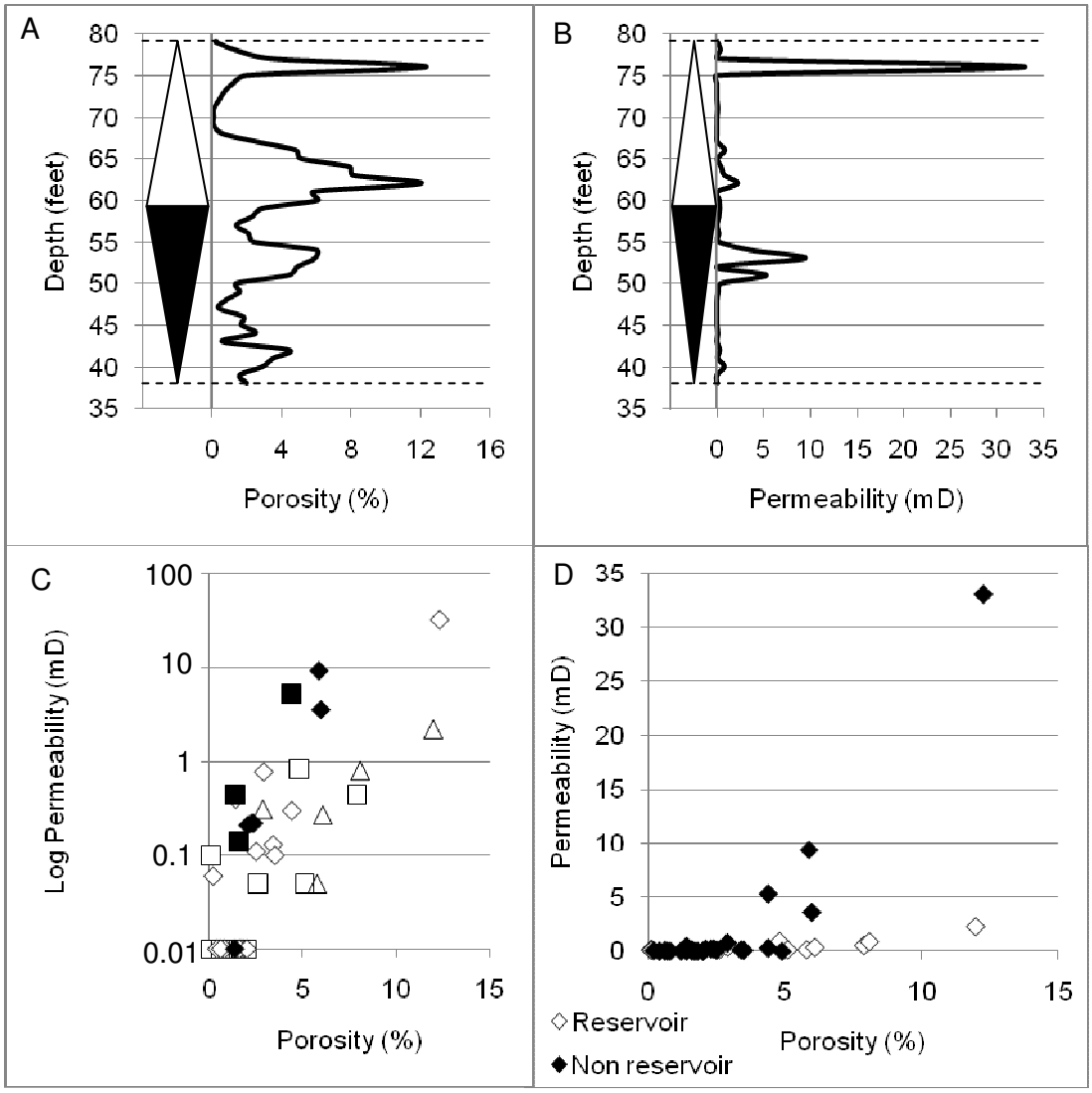

Figure 6.23: porosity and permeability data for Cycle 7a, Well 4: A) porosity data against depth, B) permeability data against depth, C) porosity and permeability relationships with respect to the lithologies and D) the porosity and permeability relationships with respect to the reservoirs and non-reservoirs.

Cycle 7b

The HST of Cycle 7b has a 20ft thick reservoir with porosity ranging from 0.2-10% and a permeability ranging of 0.01-1.5mD (Figs. 6.24A & 6.24B). A permeability spike exists within the base of the HST of 10mD (Figs. 6.24A & 6.24B). The late HST and the TST have lower porosity and permeability relationships of 0.1-3% porosity and 0.001-1mD permeability. The *gl*WP and the *gl*PG coincides with the highest porosity and permeability values (Figs. 7.33C & 7.33D).

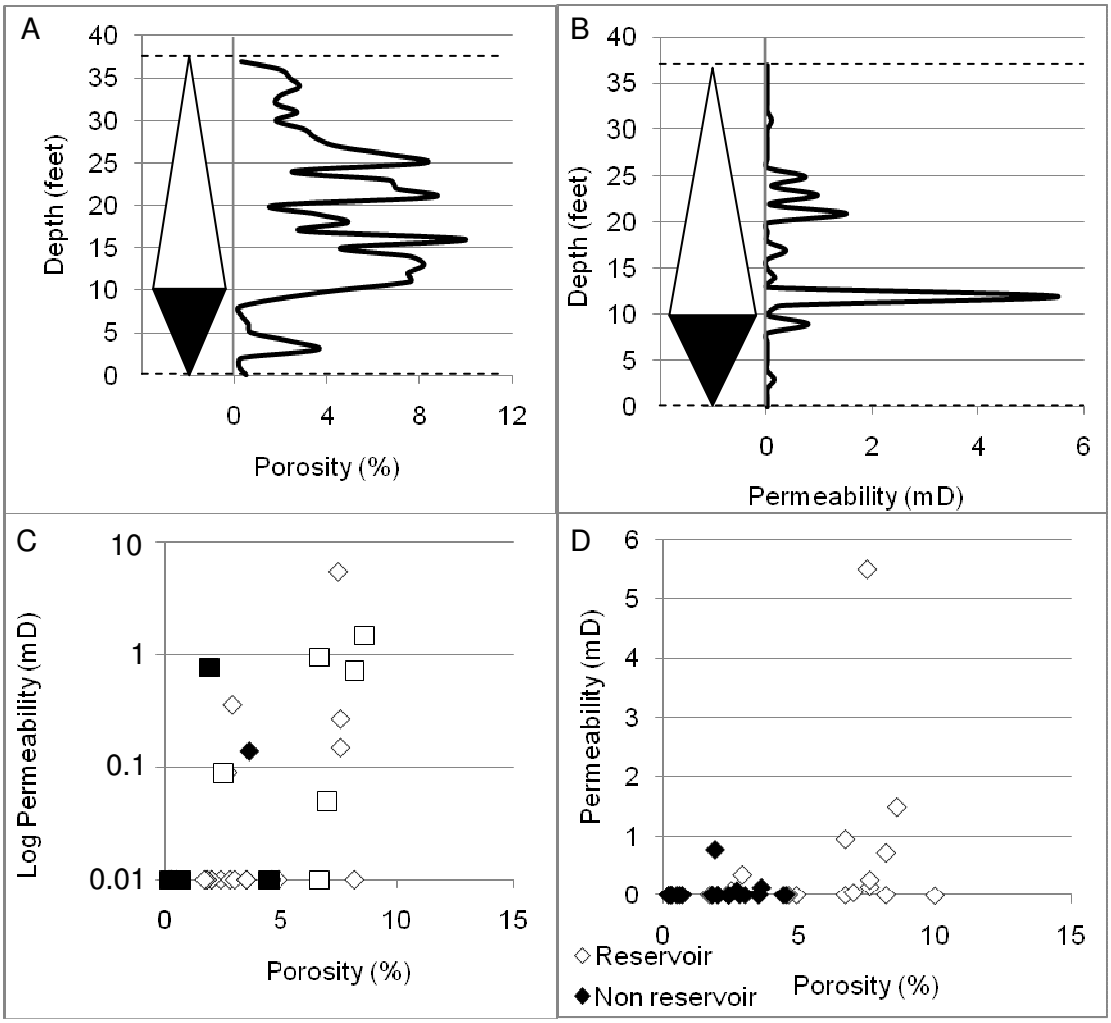

Figure 6.24: porosity and permeability data for Cycle 7b, Well 4: A) porosity data against depth, B) permeability data against depth, C) porosity and permeability relationships with respect to the lithologies and D) the porosity and permeability relationships with respect to the reservoirs and non-reservoirs.

Well 5

Cycle 1

There is more extensive porosity and permeability data in comparison with the core section which measures 12ft (Appendix 2E). The porosity values range from 2-20% and permeability of 0.4-4mD, with a spike of 6mD (Figs. 6.25A & 6.25B). The bottommost 4ft of this HFC has 1-8% porosity and 0.1-0.8mD permeability (Figs. 6.25A & 6.25B). The highest porosity and permeability relationships are in the BW and the reservoir (Figs. 6.35C & 6.25D).

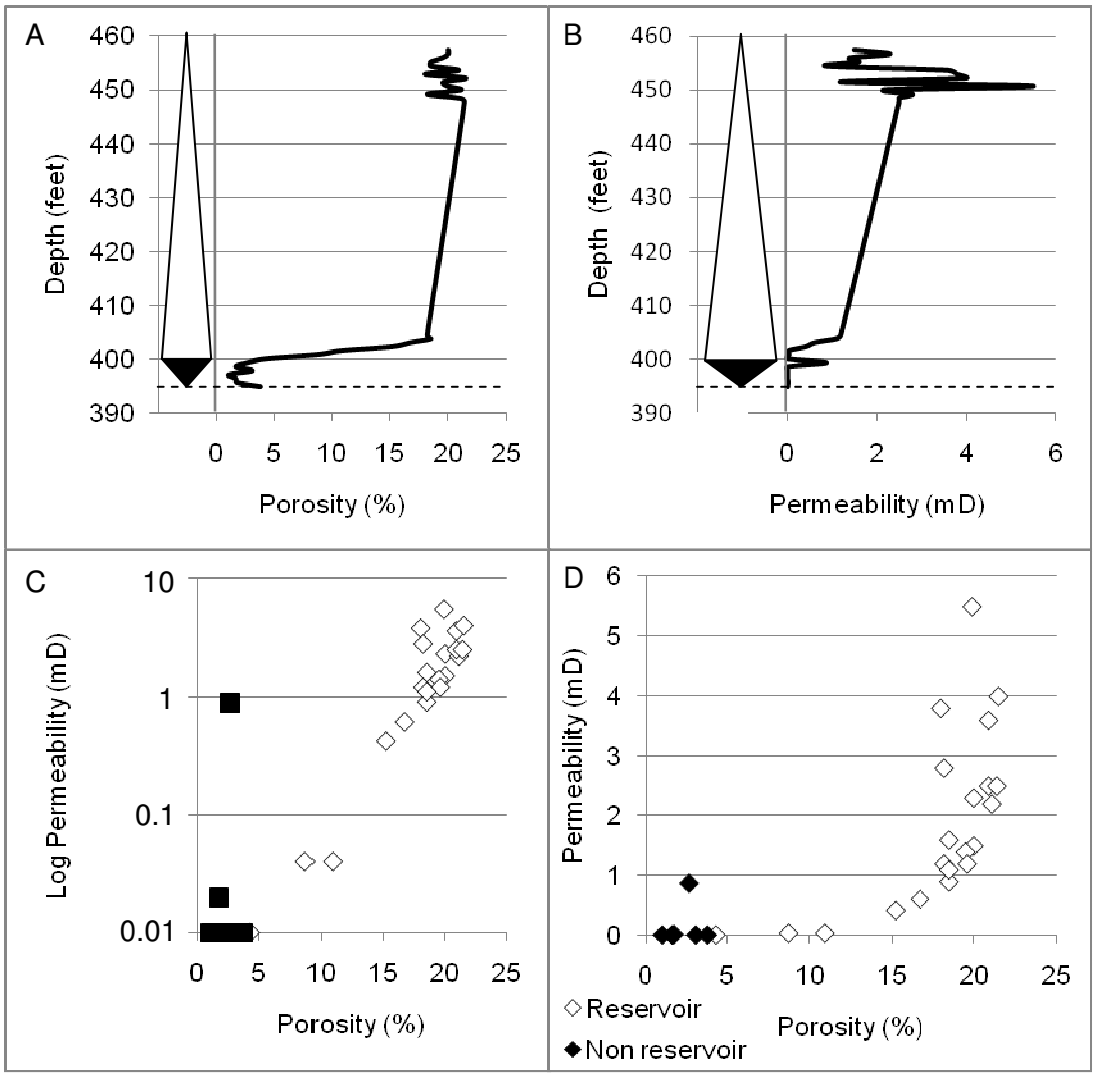

Figure 6.25: porosity and permeability data for Cycle 1, Well 5: A) porosity data against depth, B) permeability data against depth, C) porosity and permeability relationships with respect to the lithologies and D) the porosity and permeability relationships with respect to the reservoirs and non-reservoirs.

Cycle 2a

Cycle 2a has two areas where the porosity gets above 10%: one measuring 3ft at the top of this HFC with the other measuring 15ft at the bottom of the HST (Figs. 6.26A & 6.26B). The top reservoir roughly coincides with a small permeability spike of 2mD, whereas the second reservoir coincides with many larger permeability spikes of 3-5mD. The porosity for the remaining portions of the HFC ranges from 1-9% with permeability of 0.001-1mD. The highest porosity and permeability relationships mostly exist within the *gl*PW (Figs. 6.26A & 6.26B).

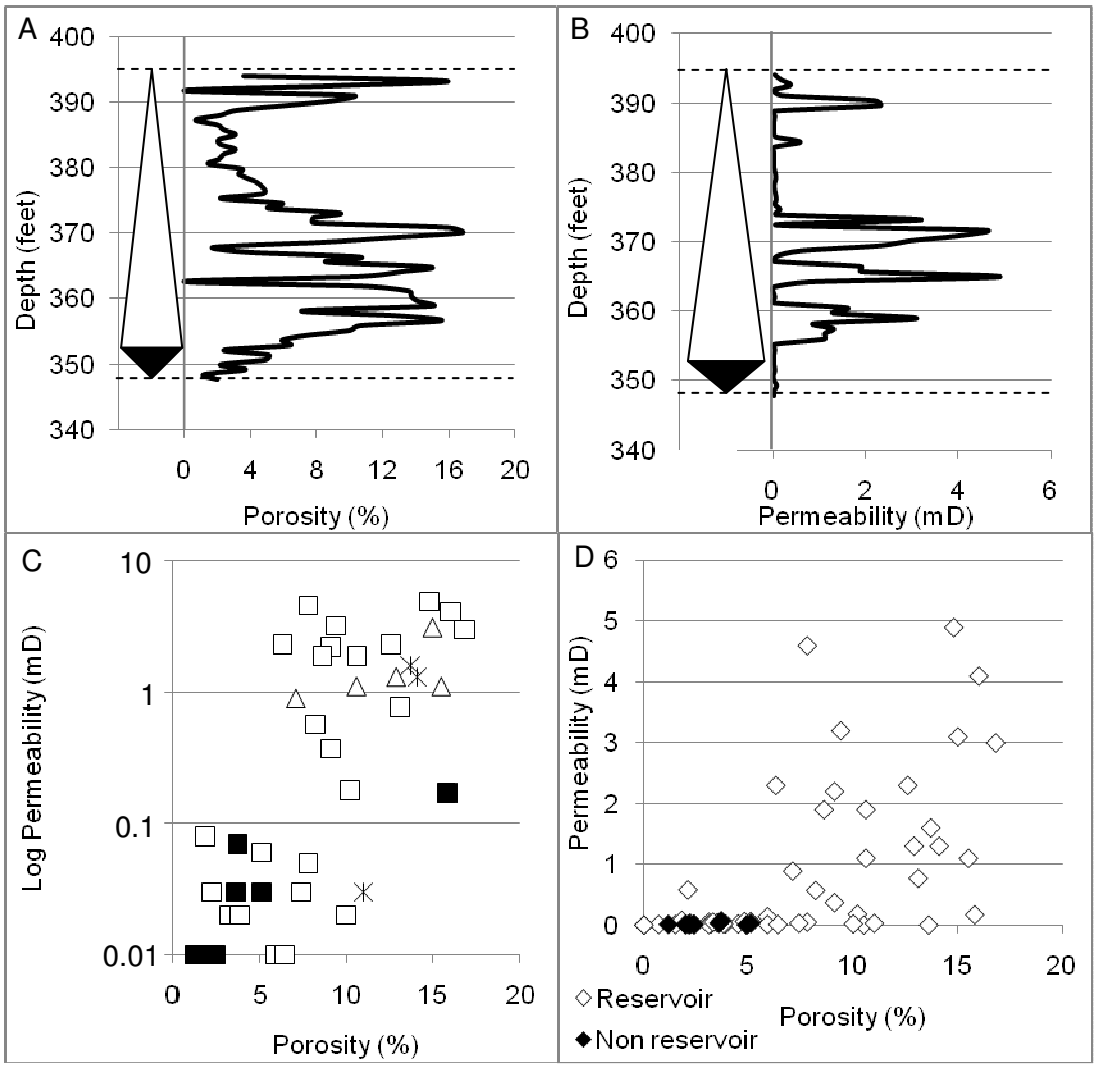

Figure 6.26: porosity and permeability data for Cycle 2a, Well 5: A) porosity data against depth, B) permeability data against depth, C) porosity and permeability relationships with respect to the lithologies and D) the porosity and permeability relationships with respect to the reservoirs and non-reservoirs.

Cycle 2b

Cycle 2b has very variable porosity for both the HST and the TST, ranging from 1-10% (Figs. 6.27A and 6.27B). There are two single foot thick zones: one within the late HST with 16% porosity and the second within the early TST at the base of the HCF of 14% porosity (Figs. 6.27A & 6.27B). The permeability for the entire HFC is very low and ranges from 0.01-1.5mD (Figs. 6.27A & 6.27B). The highest porosity and permeability relationships are within the BW and the *l*B (Figs. 6.27C & 6.27D).

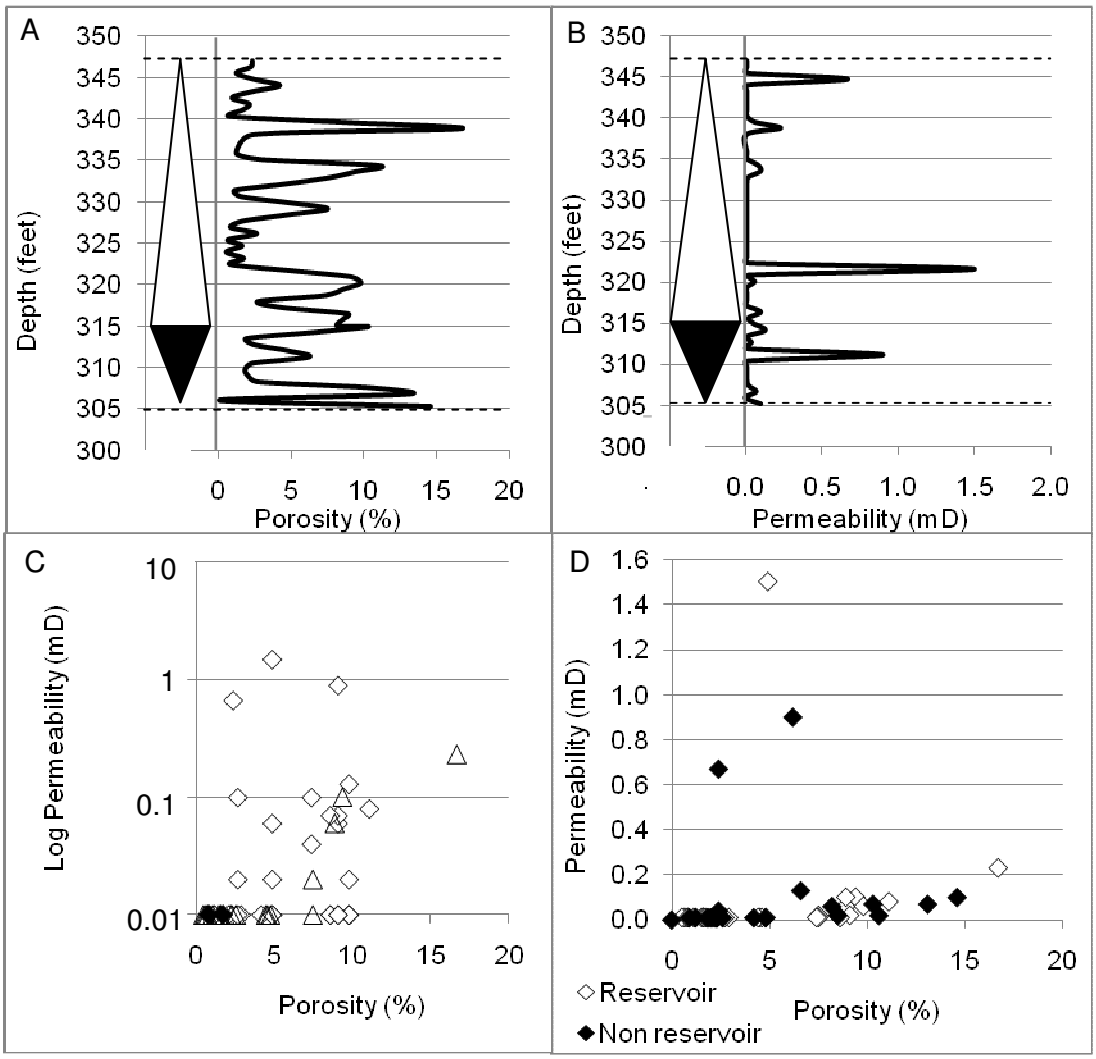

Figure 6.27: porosity and permeability data for Cycle 2b, Well 5: A) porosity data against depth, B) permeability data against depth, C) porosity and permeability relationships with respect to the lithologies and D) the porosity and permeability relationships with respect to the reservoirs and non-reservoirs.

Cycle 3

Cycle 3 HST has two high porosity and permeability areas. The first is ~20ft thick and has porosity ranging from 15-28% with permeability ranging from 1-25mD (Figs. 6.28A & 6.28B). The second lasts for 6ft, has a porosity range of 10-17% and a permeability of 2-24mD (Figs. 6.28A & 6.28B). All the permeability spikes coincide with porosity highs. The TST has consistently lower porosity of 0.35-7% and a permeability of 0.01-0.3mD (Figs. 6.28A & 6.28B). The highest porosity and permeability relationships exist within the *gl*WP and the reservoir (Figs. 6.28C & 6.28D).

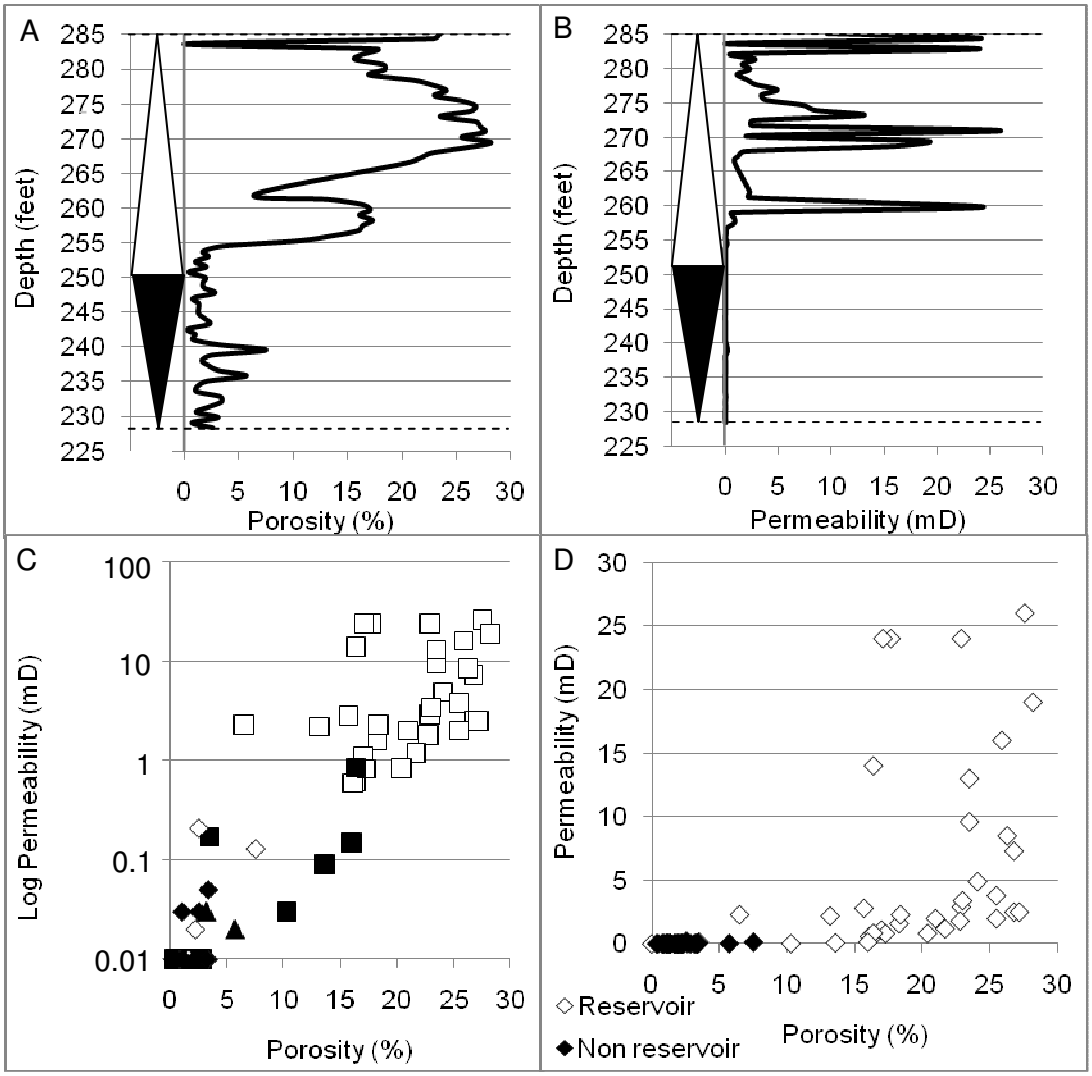

Figure 6.28: porosity and permeability data for Cycle 3, Well 5: A) porosity data against depth, B) permeability data against depth, C) porosity and permeability relationships with respect to the lithologies and D) the porosity and permeability relationships with respect to the reservoirs and non-reservoirs.

Cycle 4a

Cycle 4a HST has two reservoir sections measuring 10ft and 5ft thick. The first has a porosity range of 10-19% and coincides with the highest permeability of 8mD (Figs. 6.29A & 6.29B). The TST has consistently lower porosity of 0.3-10% and a permeability of 0.01-0.1mD (Figs. 6.29A & 6.29B). The highest porosity and permeability relationships exist within the *gl*WP (Figs. 6.29C & 6.29D).

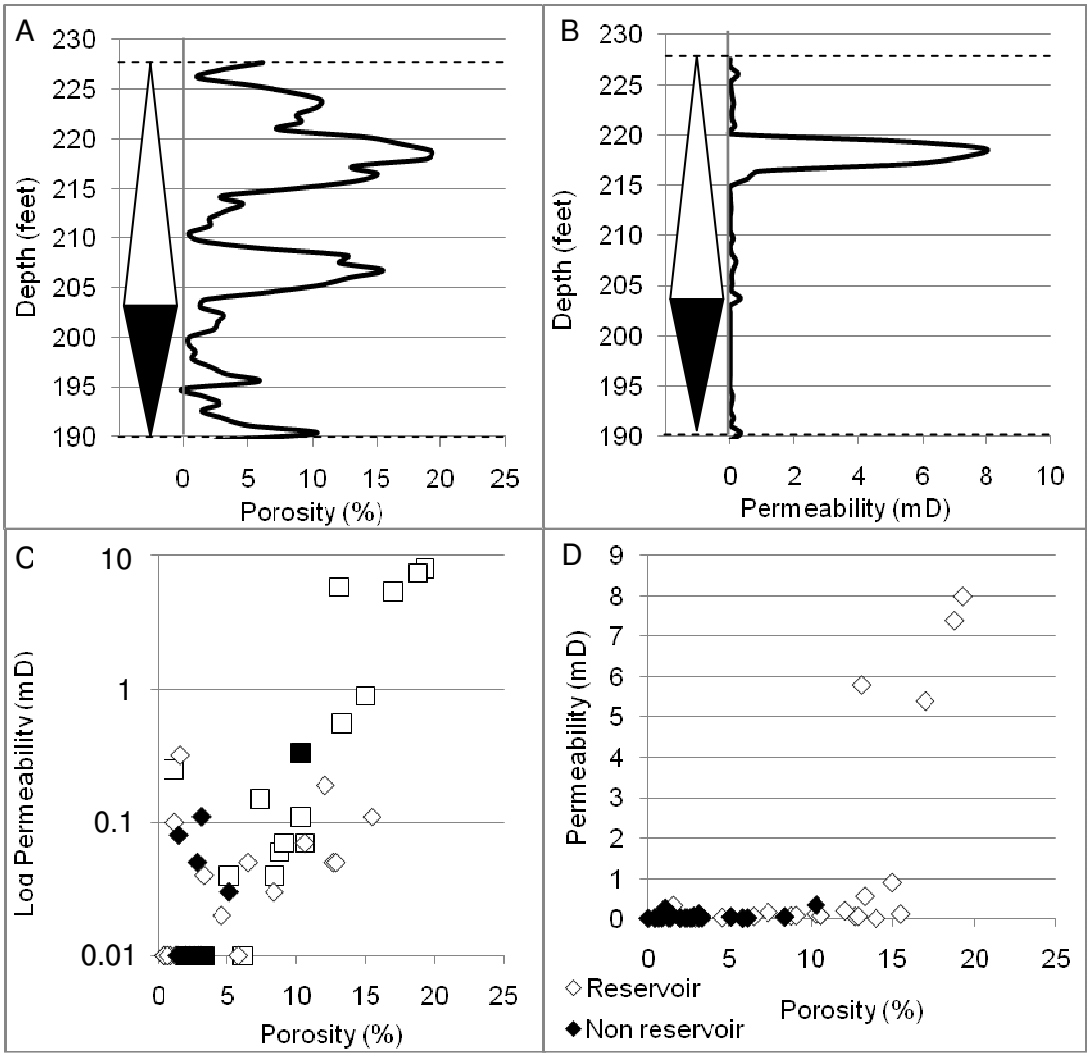

Figure 6.29: porosity and permeability data for Cycle 4a, Well 5: A) porosity data against depth, B) permeability data against depth, C) porosity and permeability relationships with respect to the lithologies and D) the porosity and permeability relationships with respect to the reservoirs and non-reservoirs.

Cycle 4b

Cycle 4b has one reservoir measuring 5ft thick with porosity range of 10-13% (Figs. 6.30A & 6.30B). . This coincides with the highest permeability values of 0.2-0.5mD: the permeability is very low for the entire HFC (Figs. 6.30A & 6.30B). The TST has much lower porosity and permeability of 1-2% and 0.001-0.2mD, respectively. The highest porosity and permeability relationships correspond with the early HST and within the *gl*WP (Figs. 6.30C & 6.30D).

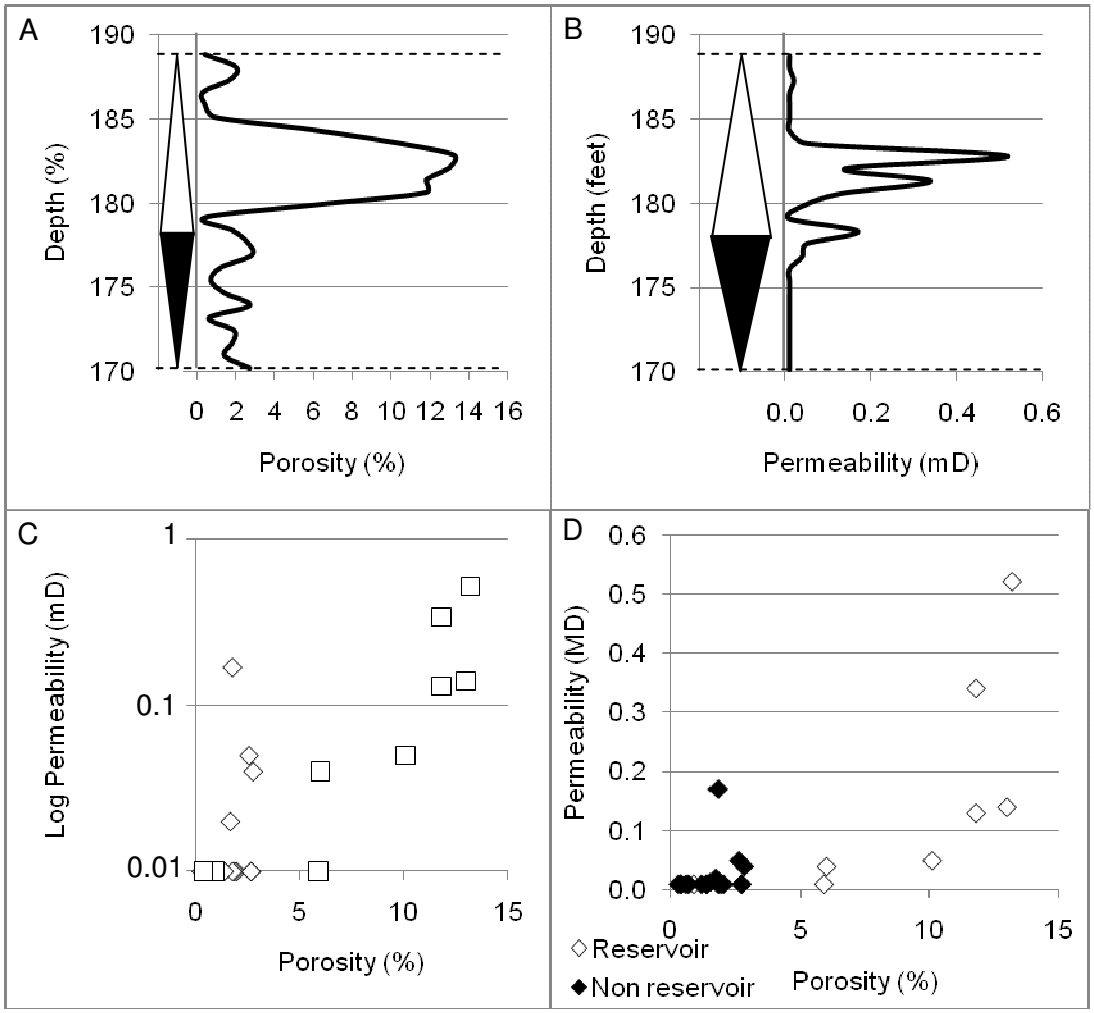

Figure 6.30: porosity and permeability data for Cycle 4b, Well 5: A) porosity data against depth, B) permeability data against depth, C) porosity and permeability relationships with respect to the lithologies and D) the porosity and permeability relationships with respect to the reservoirs and non-reservoirs.

Cycle 5

Cycle 5 has two reservoir horizons measuring 3ft and 7ft thick. The top reservoir has a porosity of 8% and a permeability of 0.1mD, while the second has a porosity range of 12-14% and a permeability range of 0.05-0.3mD. The highest permeability of 0.5mD within the HST corresponds to a porosity low between the two reservoirs. The TST has lower porosity of 0.3-7% with permeability of 0.01-0.7mD (Figs. 6.31A & 6.31B). The highest porosity and permeability relationships mostly exist within the HST, the reservoir and the BW (Figs. 6.31C & 6.31D).

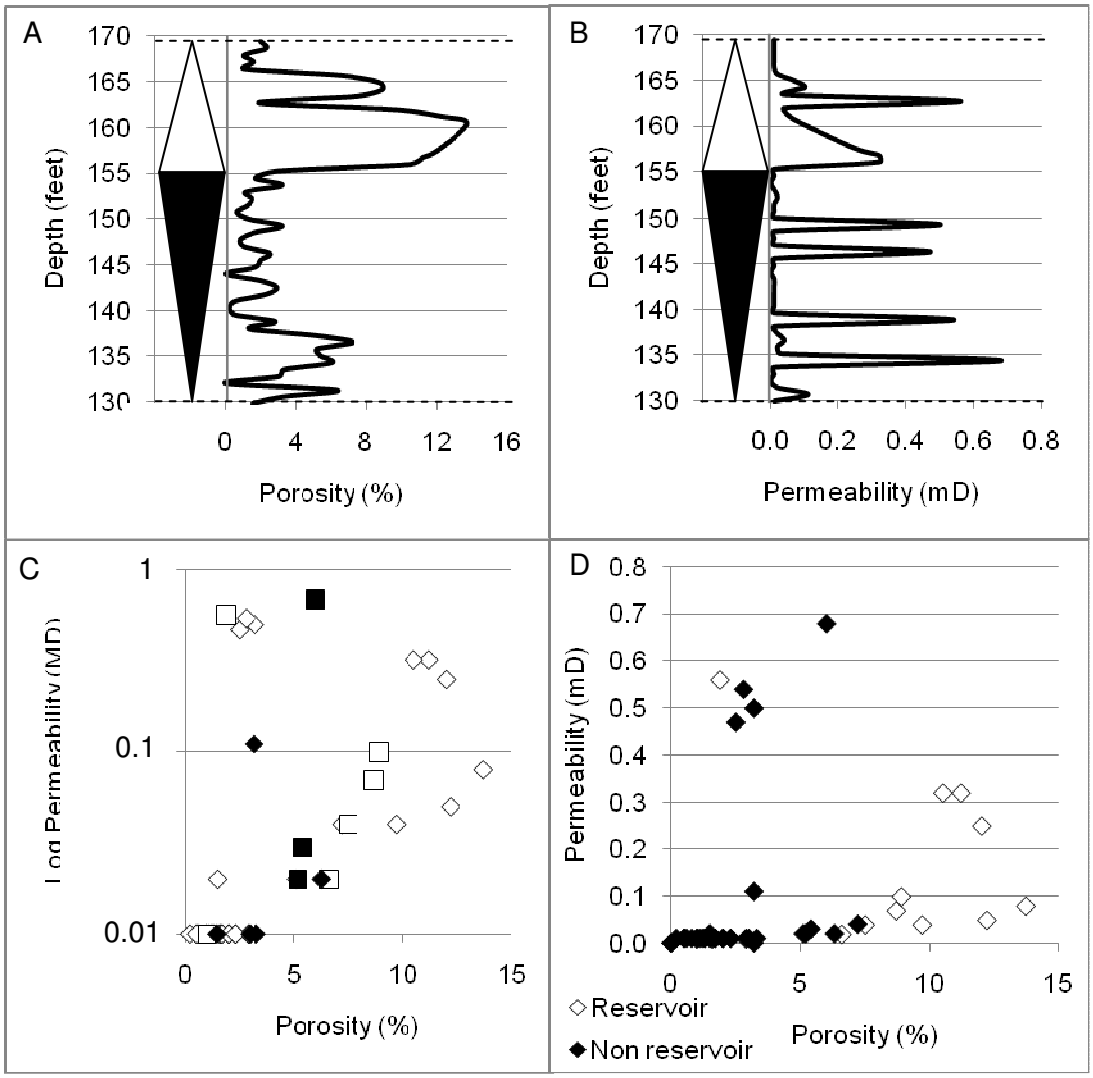

Figure 6.31: porosity and permeability data for Cycle 5, Well 5: A) porosity data against depth, B) permeability data against depth, C) porosity and permeability relationships with respect to the lithologies and D) the porosity and permeability relationships with respect to the reservoirs and non-reservoirs.

Cycle 6

Cycle 6 has one reservoir section measuring 9-10ft thick. It has 5-20% porosity and 1-3.5mD permeability. This horizon covers the first few feet at the top of the TST. The remainder of the HFC has lower porosity and permeability of 0.1-9% and 0.001-3mD (Figs. 6.32A & 6.32B). The highest porosity and permeability relationships exist within the PM and the *gl*WP (Figs. 6.32C & 6.32D).

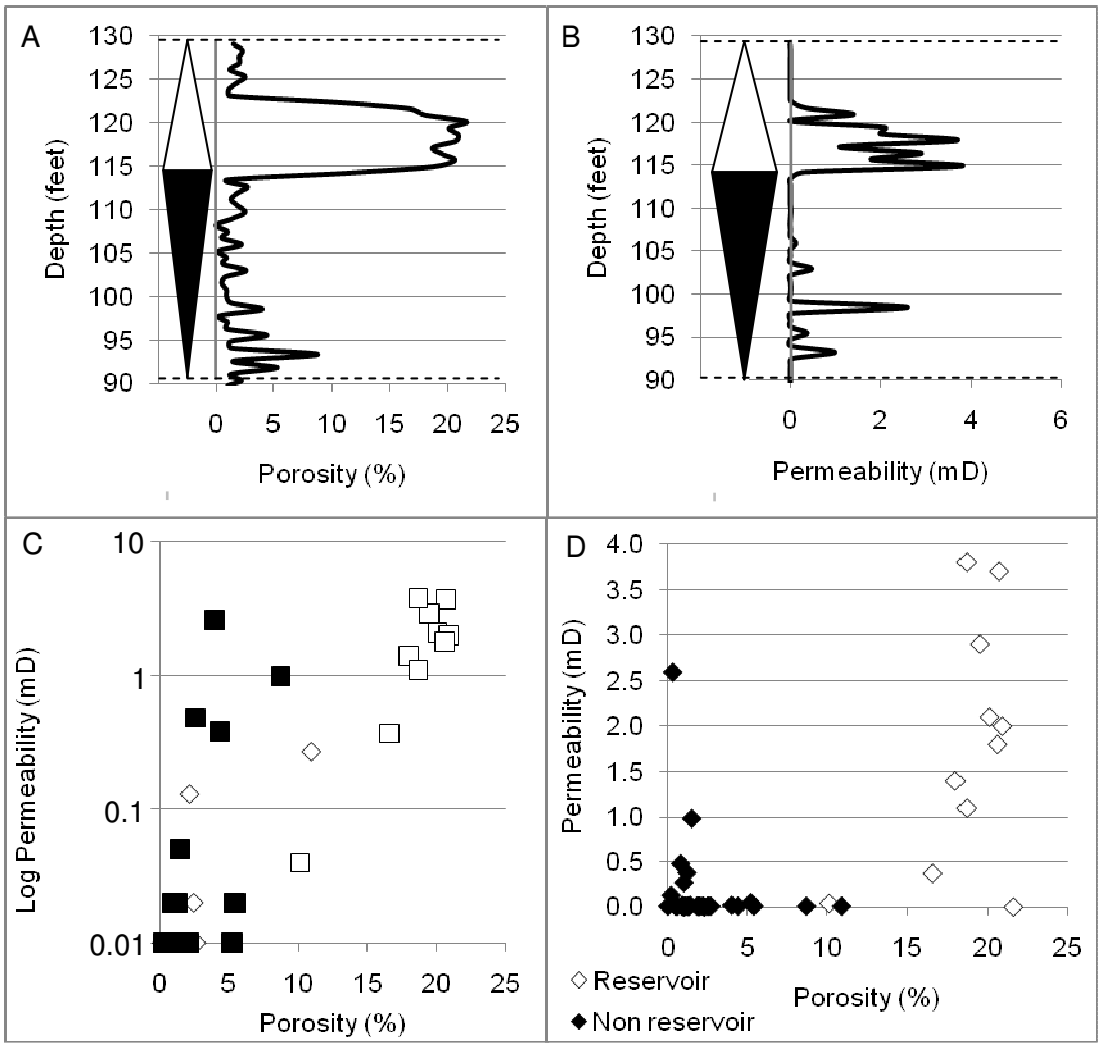

Figure 6.32: porosity and permeability data for Cycle 6, Well 5: A) porosity data against depth, B) permeability data against depth, C) porosity and permeability relationships with respect to the lithologies and D) the porosity and permeability relationships with respect to the reservoirs and non-reservoirs.

Cycle 7a

Cycle 7a has two reservoir sections, the first measuring 3ft and the second measuring 7ft thick. The first reservoir has 10-17% porosity and 0.01-3mD permeability, while the second reservoir has 15-28% porosity and 15-35mD permeability (Figs. 6.33A & 6.33B). The highest permeability values coincide with the highest porosity values and the second reservoir which overlaps into the topmost portions of the TST (Figs. 6.33A & 6.33B). The TST has porosity ranging from 0.1-10% and permeability ranging from 0.01-35mD (Figs. 6.33A & 6.33B). Within the TST the highest porosity also coincides with the highest permeability (Figs. 6.33A & 6.33B). The highest porosity and permeability relationships are mostly in the *gl*WP (Figs. 6.33C & 6.33D).

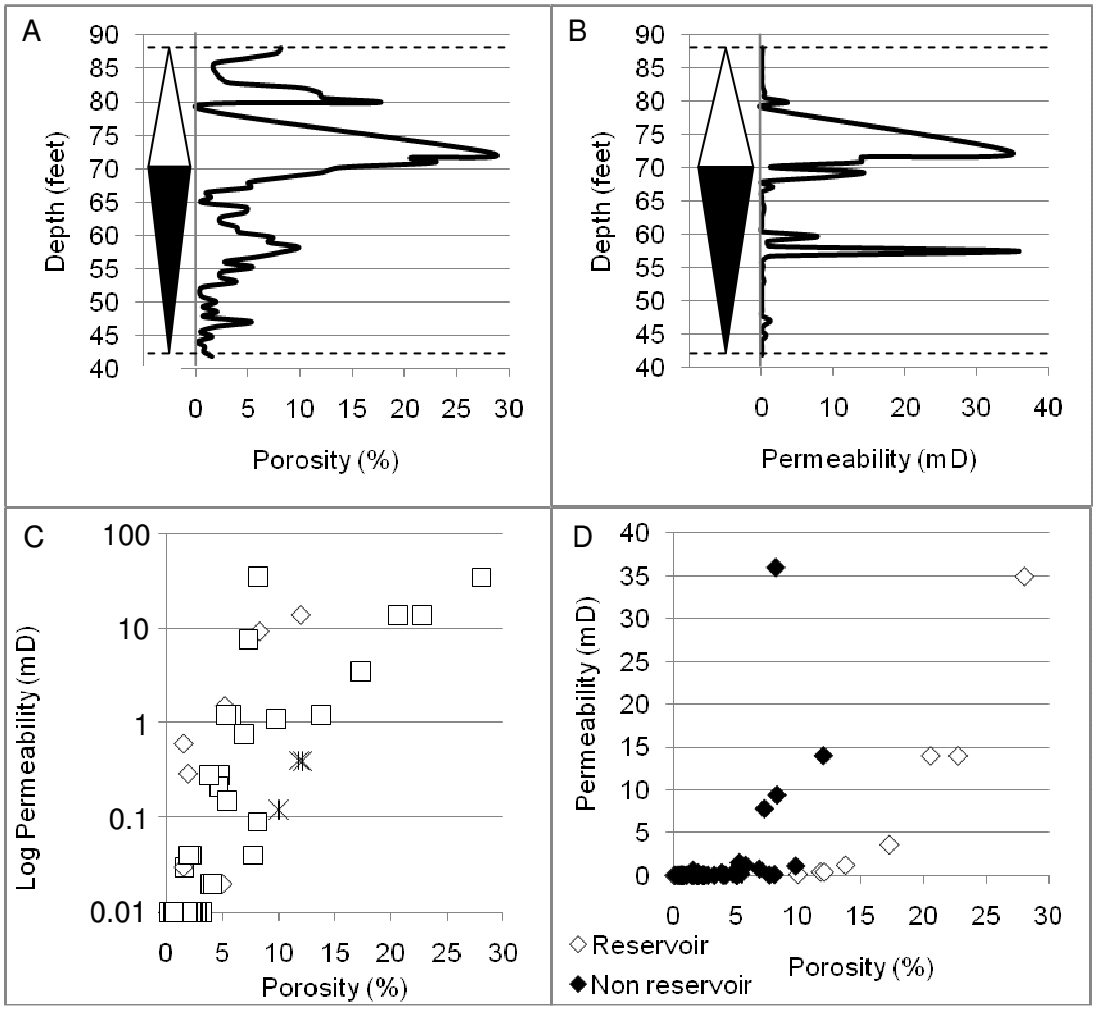

Figure 6.33: porosity and permeability data for Cycle 7a, Well 5: A) porosity data against depth, B) permeability data against depth, C) porosity and permeability relationships with respect to the lithologies and D) the porosity and permeability relationships with respect to the reservoirs and non-reservoirs.

Cycle 7b

Cycle 7b has three reservoir horizons: the first measuring 10ft thick, the second measuring 5ft thick and the third measuring 5ft thick. The porosity ranges from 10-23% in the first, 8-10% in the second and 10-16% in the third (Figs. 6.34A & 6.34B). Only the first reservoir has permeability ranging from 6-23mD, the lower two reservoirs have 0.01mD permeability (Figs. 6.34A & 6.34B). The permeability spike coincides with the highest porosity values within the top reservoir section (Figs. 6.34A & 6.34B). The remaining HFC has lower porosity values of 0.1-5% and permeability ranging from 0.01-4mD (Figs. 6.34A & 6.34B). The highest porosity and permeability relationships exist within the reservoir and the *gl*WP (Figs. 6.34C & 6.34D).

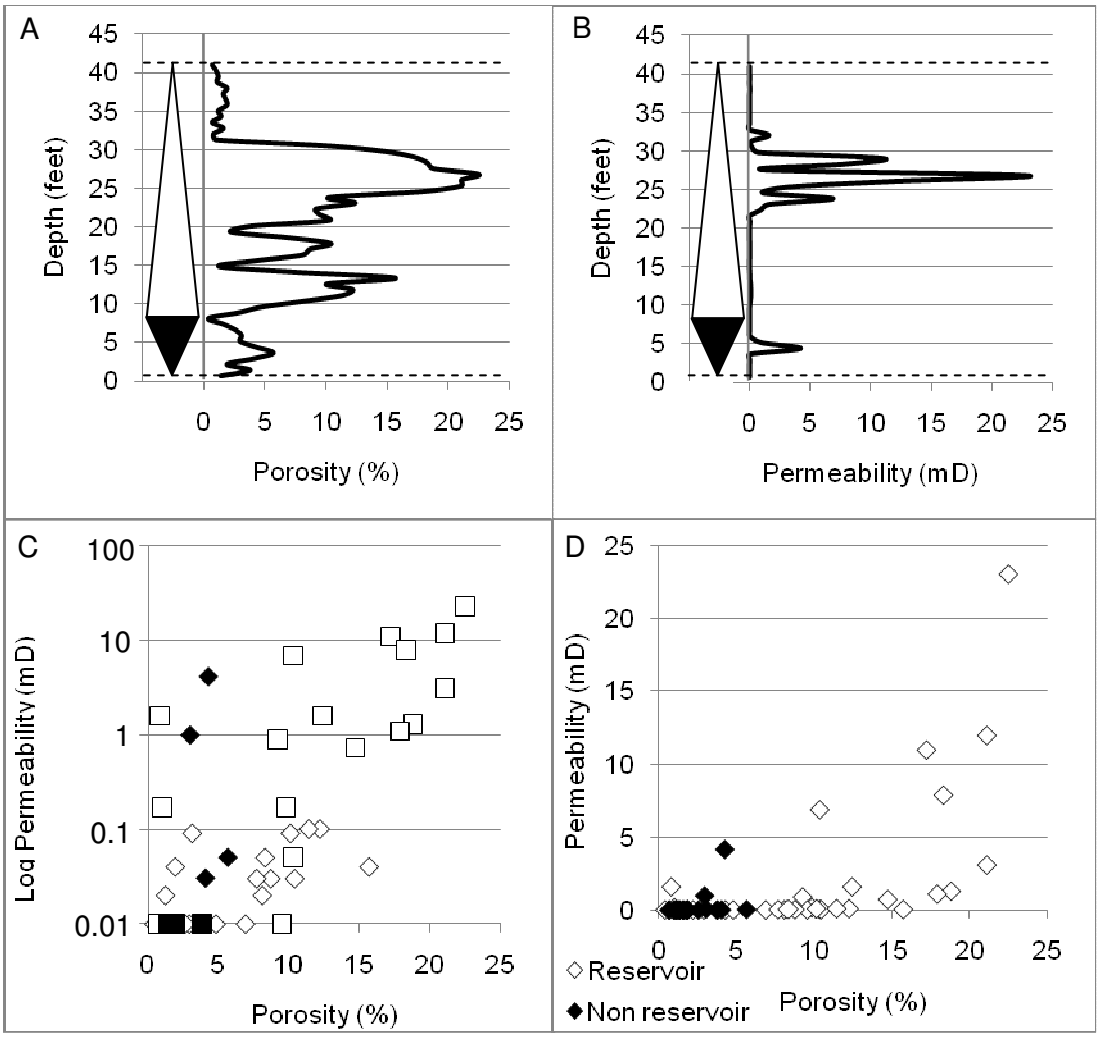

Figure 6.34: porosity and permeability data for Cycle 7b, Well 5: A) porosity data against depth, B) permeability data against depth, C) porosity and permeability relationships with respect to the lithologies and D) the porosity and permeability relationships with respect to the reservoirs and non-reservoirs.